

ADVANCES IN POLYMER SCIENCE

233

Volume Editors A.M. van Herk • K. Landfester

# Hybrid Latex Particles

Preparation with (Mini)emulsion Polymerization

 Springer

**Editorial Board:**

**A. Abe · A.-C. Albertsson · K. Dušek · W.H. de Jeu  
H.-H. Kausch · S. Kobayashi · K.-S. Lee · L. Leibler  
T.E. Long · I. Manners · M. Möller · E.M. Terentjev  
M. Vicent · B. Voit · G. Wegner · U. Wiesner**

# Advances in Polymer Science

Recently Published and Forthcoming Volumes

## **Hybrid Latex Particles**

Volume Editors: van Herk, A.M.,  
Landfester, K.  
Vol. 233, 2010

## **Biopolymers**

Volume Editors: Abe, A., Dušek, K.,  
Kobayashi, S.  
Vol. 232, 2010

## **Polymer Materials**

Volume Editors: Lee, K.-S., Kobayashi, S.  
Vol. 231, 2010

## **Polymer Characterization**

Volume Editors: Dušek, K., Joanny, J.-F.  
Vol. 230, 2010

## **Modern Techniques for Nano- and Microreactors/-reactions**

Volume Editor: Caruso, F.  
Vol. 229, 2010

## **Complex Macromolecular Systems II**

Volume Editors: Müller, A.H.E.,  
Schmidt, H.-W.  
Vol. 228, 2010

## **Complex Macromolecular Systems I**

Volume Editors: Müller, A.H.E.,  
Schmidt, H.-W.  
Vol. 227, 2010

## **Shape-Memory Polymers**

Volume Editor: Lendlein, A.  
Vol. 226, 2010

## **Polymer Libraries**

Volume Editors: Meier, M.A.R., Webster, D.C.  
Vol. 225, 2010

## **Polymer Membranes/Biomembranes**

Volume Editors: Meier, W.P., Knoll, W.  
Vol. 224, 2010

## **Organic Electronics**

Volume Editors: Meller, G., Grasser, T.  
Vol. 223, 2010

## **Inclusion Polymers**

Volume Editor: Wenz, G.  
Vol. 222, 2009

## **Advanced Computer Simulation Approaches for Soft Matter Sciences III**

Volume Editors: Holm, C., Kremer, K.  
Vol. 221, 2009

## **Self-Assembled Nanomaterials II**

Nanotubes  
Volume Editor: Shimizu, T.  
Vol. 220, 2008

## **Self-Assembled Nanomaterials I**

Nanofibers  
Volume Editor: Shimizu, T.  
Vol. 219, 2008

## **Interfacial Processes and Molecular Aggregation of Surfactants**

Volume Editor: Narayanan, R.  
Vol. 218, 2008

## **New Frontiers in Polymer Synthesis**

Volume Editor: Kobayashi, S.  
Vol. 217, 2008

## **Polymers for Fuel Cells II**

Volume Editor: Scherer, G.G.  
Vol. 216, 2008

## **Polymers for Fuel Cells I**

Volume Editor: Scherer, G.G.  
Vol. 215, 2008

## **Photoresponsive Polymers II**

Volume Editors: Marder, S.R., Lee, K.-S.  
Vol. 214, 2008

## **Photoresponsive Polymers I**

Volume Editors: Marder, S.R., Lee, K.-S.  
Vol. 213, 2008

# Hybrid Latex Particles

Preparation with (Mini)emulsion  
Polymerization

Volume Editors: Alex M. van Herk  
Katharina Landfester

With contributions by

S.A.F. Bon · E. Bourgeat-Lami · B. Charleux · F. D'Agosto  
G. Delaittre · A. Elaissari · A.M. van Herk · K. Landfester  
M. Lansalot · Md M. Rahman · R.F.A. Teixeira · C.K. Weiss

*Editors*

Prof. Alex M. van Herk  
Eindhoven University of Technology  
Chemical Engineering and Chemistry  
PO Box 513, Helix STO 1.42  
5600 MB Eindhoven  
The Netherlands  
a.m.v.herk@tue.nl

Prof. Katharina Landfester  
Max-Planck-Institute for Polymer Research  
Ackermannweg 10  
55128 Mainz  
Germany  
landfester@mpip-mainz.mpg.de

ISSN 0065-3195 e-ISSN 1436-5030  
ISBN 978-3-642-16059-2 e-ISBN 978-3-642-16060-8  
DOI 10.1007/978-3-642-16060-8  
Springer Heidelberg Dordrecht London New York

Library of Congress Control Number: 2010936198

© Springer-Verlag Berlin Heidelberg 2010

This work is subject to copyright. All rights are reserved, whether the whole or part of the material is concerned, specifically the rights of translation, reprinting, reuse of illustrations, recitation, broadcasting, reproduction on microfilm or in any other way, and storage in data banks. Duplication of this publication or parts thereof is permitted only under the provisions of the German Copyright Law of September 9, 1965, in its current version, and permission for use must always be obtained from Springer. Violations are liable to prosecution under the German Copyright Law.

The use of general descriptive names, registered names, trademarks, etc. in this publication does not imply, even in the absence of a specific statement, that such names are exempt from the relevant protective laws and regulations and therefore free for general use.

*Cover design:* WMXDesign GmbH, Heidelberg

Printed on acid-free paper

Springer is part of Springer Science+Business Media ([www.springer.com](http://www.springer.com))

---

## Volume Editors

Prof. Alex M. van Herk

Eindhoven University of Technology  
Chemical Engineering and Chemistry  
PO Box 513, Helix STO 1.42  
5600 MB Eindhoven  
The Netherlands  
*a.m.v.herk@tue.nl*

Prof. Katharina Landfester

Max-Planck-Institute for Polymer Research  
Ackermannweg 10  
55128 Mainz  
Germany  
*landfester@mpip-mainz.mpg.de*

## Editorial Board

Prof. Akihiro Abe

Professor Emeritus  
Tokyo Institute of Technology  
6-27-12 Hiyoshi-Honcho, Kohoku-ku  
Yokohama 223-0062, Japan  
*aabe.34@xc4.so-net.ne.jp*

Prof. Hans-Henning Kausch

Ecole Polytechnique Fédérale de Lausanne  
Science de Base  
Station 6  
1015 Lausanne, Switzerland  
*kausch.cully@bluewin.ch*

Prof. A.-C. Albertsson

Department of Polymer Technology  
The Royal Institute of Technology  
10044 Stockholm, Sweden  
*aila@polymer.kth.se*

Prof. Shiro Kobayashi

R & D Center for Bio-based Materials  
Kyoto Institute of Technology  
Matsugasaki, Sakyo-ku  
Kyoto 606-8585, Japan  
*kobayash@kit.ac.jp*

Prof. Karel Dušek

Institute of Macromolecular Chemistry  
Czech Academy of Sciences  
of the Czech Republic  
Heyrovský Sq. 2  
16206 Prague 6, Czech Republic  
*dusek@imc.cas.cz*

Prof. Kwang-Sup Lee

Department of Advanced Materials  
Hannam University  
561-6 Jeonmin-Dong  
Yuseong-Gu 305-811  
Daejeon, South Korea  
*kslee@hnu.kr*

Prof. Dr. Wim H. de Jeu

Polymer Science and Engineering  
University of Massachusetts  
120 Governors Drive  
Amherst MA 01003, USA  
*dejeu@mail.pse.umass.edu*

Prof. L. Leibler

Matière Molle et Chimie  
Ecole Supérieure de Physique  
et Chimie Industrielles (ESPCI)  
10 rue Vauquelin  
75231 Paris Cedex 05, France  
*ludwik.leibler@espci.fr*

Prof. Timothy E. Long

Department of Chemistry  
and Research Institute  
Virginia Tech  
2110 Hahn Hall (0344)  
Blacksburg, VA 24061, USA  
*telong@vt.edu*

Maria Jesus Vicent, PhD

Centro de Investigacion Principe Felipe  
Medicinal Chemistry Unit  
Polymer Therapeutics Laboratory  
Av. Autopista del Saler, 16  
46012 Valencia, Spain  
*mjvicent@cipf.es*

Prof. Ian Manners

School of Chemistry  
University of Bristol  
Cantock's Close  
BS8 1TS Bristol, UK  
*ian.manners@bristol.ac.uk*

Prof. Brigitte Voit

Institut für Polymerforschung Dresden  
Hohe Straße 6  
01069 Dresden, Germany  
*voit@ipfdd.de*

Prof. Martin Möller

Deutsches Wollforschungsinstitut  
an der RWTH Aachen e.V.  
Pauwelsstraße 8  
52056 Aachen, Germany  
*moeller@dwf.rwth-aachen.de*

Prof. Gerhard Wegner

Max-Planck-Institut  
für Polymerforschung  
Ackermannweg 10  
55128 Mainz, Germany  
*wegner@mpip-mainz.mpg.de*

Prof. E.M. Terentjev

Cavendish Laboratory  
Madingley Road  
Cambridge CB 3 OHE, UK  
*emt1000@cam.ac.uk*

Prof. Ulrich Wiesner

Materials Science & Engineering  
Cornell University  
329 Bard Hall  
Ithaca, NY 14853, USA  
*ubw1@cornell.edu*

---

## **Advances in Polymer Sciences**

### **Also Available Electronically**

*Advances in Polymer Sciences* is included in Springer's eBook package *Chemistry and Materials Science*. If a library does not opt for the whole package, the book series may be bought on a subscription basis. Also, all back volumes are available electronically.

For all customers who have a standing order to the print version of *Advances in Polymer Sciences*, we offer free access to the electronic volumes of the Series published in the current year via SpringerLink.

If you do not have access, you can still view the table of contents of each volume and the abstract of each article by going to the SpringerLink homepage, clicking on "Browse by Online Libraries", then "Chemical Sciences", and finally choose *Advances in Polymer Science*.

You will find information about the

- Editorial Board
- Aims and Scope
- Instructions for Authors
- Sample Contribution

at [springer.com](http://springer.com) using the search function by typing in *Advances in Polymer Sciences*.

*Color figures* are published in full color in the electronic version on SpringerLink.



## Aims and Scope

The series *Advances in Polymer Science* presents critical reviews of the present and future trends in polymer and biopolymer science including chemistry, physical chemistry, physics and material science. It is addressed to all scientists at universities and in industry who wish to keep abreast of advances in the topics covered.

Review articles for the topical volumes are invited by the volume editors. As a rule, single contributions are also specially commissioned. The editors and publishers will, however, always be pleased to receive suggestions and supplementary information. Papers are accepted for *Advances in Polymer Science* in English.

In references *Advances in Polymer Sciences* is abbreviated as *Adv Polym Sci* and is cited as a journal.

Special volumes are edited by well known guest editors who invite reputed authors for the review articles in their volumes.

Impact Factor in 2009: 4.600; Section "Polymer Science": Rank 4 of 73

# Preface

In this volume of “Advances in Polymer Science,” the topic of hybrid latexes is covered.

A hybrid latex particle is either a latex comprising of a high molar mass polymer and an oligomer (or an alkyd resin) or a latex particle that contains both organic and inorganic material phases.

Hybrid latex particles find their applications in coatings, adhesives, plastics, and specialty applications like medical diagnostics. In the last 10 years, an increased interest in hybrid latex particles in both scientific communities and industry can be observed. Especially the incorporation of clay platelets and nanosilica particles in latexes can be regarded as main areas of interest in the field of polymer colloids at the moment. Scientific meetings over the past 3 years have featured many contributions in this direction from all over the world.

We mainly focus on the use of emulsion polymerization and miniemulsion polymerization techniques to prepare hybrid latex particles containing both organic and inorganic materials, because the scope of these kind of materials in applications is much broader than that of, for example, the alkyd resin containing latex particles.

The number of methods and approaches to produce hybrid latexes has increased dramatically in the last 10 years. Not only molecules and latex particles but also surfactant assemblies, block copolymers, and inorganic particles are used as building blocks to create hybrid latex particles. Conventional emulsion polymerization has been studied for the preparation of hybrid latexes already since the early 1980s. In the last decade miniemulsion polymerization turned out to be a valuable alternative for emulsion polymerization. The use of controlled radical polymerization increased the efficiency of the encapsulation process tremendously and added new possibilities to the chain architectures used in the polymeric part of the hybrid latexes.

In Chap. 1, a small overview of emulsion polymerization and miniemulsion polymerization is given, followed by some history of preparation of hybrid latex particles.

In Chap. 2, physical methods for the preparation of hybrid latex particles are covered. In Chap. 3, the use of emulsion polymerization, mainly in combination

with free-radical polymerization, is covered, whereas in Chap. 4 an emphasis on the use of controlled radical polymerization is given. Chapter 5 covers the use of miniemulsion polymerization, and in the final chapter preparation of magnetic hybrid latex particles and the interesting specialty applications of these particles are treated.

Summer 2010

*Katharina Landfester and Alex M. van Herk*

# Contents

<b>Historical Overview of (Mini)emulsion Polymerizations and Preparation of Hybrid Latex Particles .....</b>	<b>1</b>
A.M. van Herk	
<b>Physical Methods for the Preparation of Hybrid Nanocomposite Polymer Latex Particles .....</b>	<b>19</b>
Roberto F.A. Teixeira and Stefan A.F. Bon	
<b>Organic/Inorganic Composite Latexes: The Marriage of Emulsion Polymerization and Inorganic Chemistry .....</b>	<b>53</b>
Elodie Bourgeat-Lami and Muriel Lansalot	
<b>Preparation of Hybrid Latex Particles and Core–Shell Particles Through the Use of Controlled Radical Polymerization Techniques in Aqueous Media .....</b>	<b>125</b>
Bernadette Charleux, Franck D’Agosto, and Guillaume Delaittre	
<b>Miniemulsion Polymerization as a Means to Encapsulate Organic and Inorganic Materials .....</b>	<b>185</b>
Clemens K. Weiss and Katharina Landfester	
<b>Organic–Inorganic Hybrid Magnetic Latex .....</b>	<b>237</b>
Md Mahbubor Rahman and Abdelhamid Elaissari	
<b>Index .....</b>	<b>283</b>

# Historical Overview of (Mini)emulsion Polymerizations and Preparation of Hybrid Latex Particles

A.M. van Herk

**Abstract** In this introductory chapter, a brief overview of emulsion polymerization and miniemulsion polymerization principles is given in relation to preparation of hybrid latex particles. An account is presented of the early history of preparation of hybrid latex particles with an emphasis on the hybrid lattices containing organic and inorganic material phases. The two approaches for obtaining encapsulated inorganic particles are discussed: the chemical method in which polymerization takes place in the presence of inorganic particles, and the physical method whereby latex particles are deposited on the surface of inorganic particles by heterocoagulation.

A new classification scheme for the preparation of hybrid latex particles and corresponding higher-order nanostructures is given in this paper. This classification is partially based on a discussion during the International Polymer Colloids Group meeting in Italy in 2009.

**Keywords** Emulsion polymerization · Encapsulation · Hybrid latex particles · Miniemulsion polymerization · Nanocomposites · Nanosyntheses

## Contents

1	Introduction .....	2
2	Emulsion Polymerization .....	5
2.1	General Aspects of Emulsion Polymerization .....	5
2.2	Principles of the Emulsion Polymerization Process .....	6
2.3	Particle Nucleation .....	6
2.4	Particle Morphologies .....	7
3	Miniemulsion and Microemulsion Polymerization .....	9

4	Encapsulation of Inorganic Particles .....	10
4.1	Early Accounts of Encapsulation Through Emulsion Polymerization.....	10
4.2	Encapsulation of Inorganic Particles with Emulsion Polymerization.....	12
5	Conclusions .....	16
	References .....	17

## 1 Introduction

In this special issue of *Advances in Polymer Science*, the topic of hybrid lattices is covered. According to the IUPAC “Terminology of polymers and polymerization processes in dispersed systems” a hybrid latex particle is either a latex comprising a high molar mass polymer and an oligomer (or an alkyd resin), or a latex particle that contains both organic and inorganic material phases [1].

We will focus on the use of emulsion polymerization and miniemulsion polymerization techniques for the preparation of hybrid latex particles. Also, more emphasis will be put on the preparation of hybrid lattices containing organic and inorganic materials, because the scope of these kinds of materials in applications is much broader than that of, for example, latex particles containing alkyd resin.

In this introductory chapter, a brief overview of emulsion polymerization and miniemulsion polymerization is given, followed by some history of the preparation of hybrid latex particles, with an emphasis on the hybrid lattices containing organic and inorganic material phases.

The number of methods and approaches for the production of hybrid lattices has increased dramatically in the last 10 years. Not only molecules and latex particles but also surfactant assemblies, block copolymers and inorganic particles are used as building blocks to create hybrid latex particles. Recognizing the general classification scheme introduced by Bourgeat Lami in 2002 [2], a new classification scheme for the preparation of hybrid latex particles and corresponding higher-order nanostructures will be given in this introduction. This classification is partially based on a discussion during the International Polymer Colloids Group meeting in Italy in 2009 [3].

The building blocks for preparing the hybrid latex particles will be referred to as synthons or nanosynthons. The word “synthon” was introduced by E.J. Corey as being a fragment in a molecule related to a possible synthetic operation [4] In this paper, we refer to synthons as being reactive molecules that are building blocks for higher-order structures. A monomer is typically a synthon that leads to a higher-order structure, the polymer. Dissolved polymer molecules can also act as synthons, for example in the sense that they can combine to higher-order structures like gels or can be used in encapsulation by building a polymer shell by the layer-by-layer approach using oppositely charged polyelectrolytes [5].

The nanosynthon is a particle (not a molecule) that can create hybrid structures and/or suprastructures [6]. Figure 1 shows how hybrid latex particles can be produced and how hybrid particles can lead to suprastructures and functionalities.

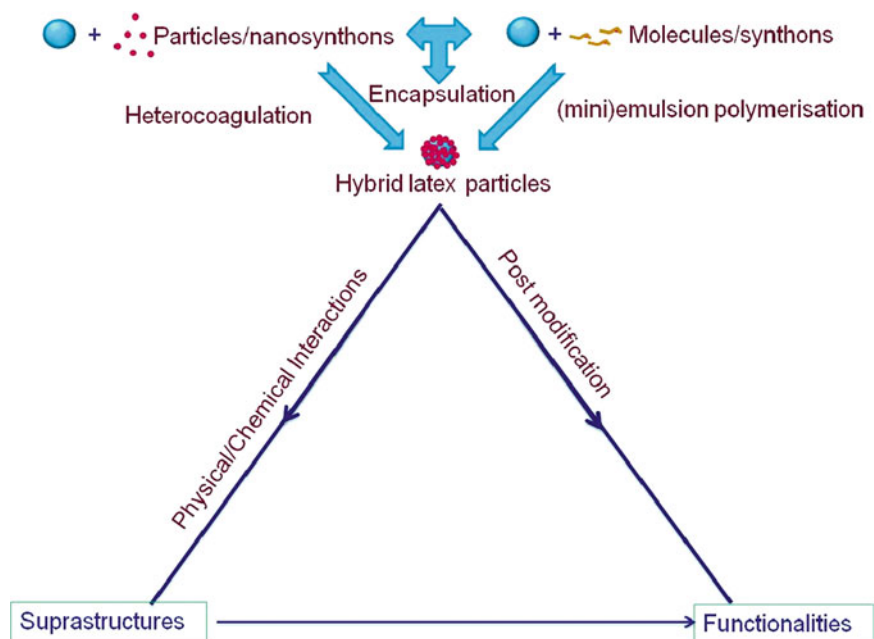


**Fig. 1** Preparation methods for hybrid latex particles and subsequent formation of suprastructures and functionalities

The hybrid latex particle is created out of molecules (synths) and/or particles (nanosynths). If we use only particles to create a hybrid latex particle we refer to the process as heterocoagulation (lefthand side of Fig. 1). Heterocoagulation is the process by which different types of particles (different in composition and/or size) coagulate in a controlled way. In using heterocoagulation to prepare hybrid latex particles the different particles often have different charge. If for example a positively charged inorganic particle is slowly added to a surplus of negatively charged latex particles immediate charge reversal of the inorganic particle takes place and the systems remains stable. If the core particle is a liquid or a void, the particle is also called a colloidosome (see [7]).

Hybrid latex particles can also be produced by reacting molecules (monomers) via (mini)emulsion polymerization on the surface of an inorganic particle (nanosynthon); this process is usually referred to as encapsulation (righthand side of Fig. 1). Inorganic/organic hybrid latex particles can also be produced by only using synths, for example by combining synths for inorganic material with synths for polymers. If the two types of synths are reacted simultaneously an interpenetrating network of the organic and inorganic material can be obtained. If the two synths are reacted consecutively more structured materials can be obtained. An example is the vesicle-directed growth of silica where the bilayer of the vesicles contains polydivinylbenzene obtained after photopolymerization (dioctadecyl

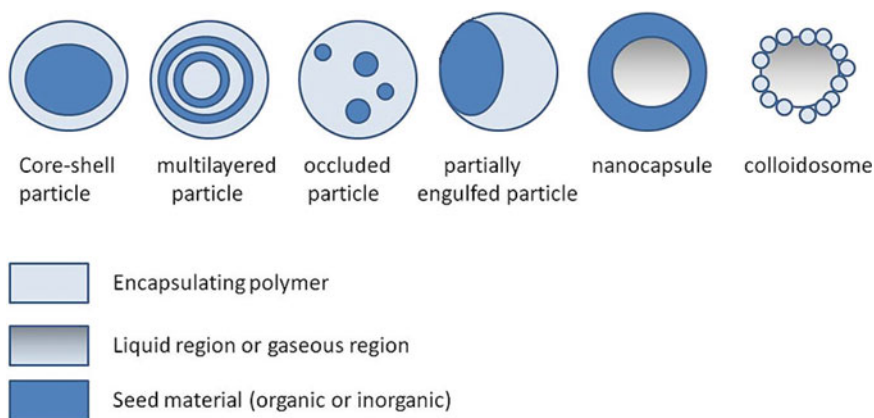


**Fig. 2** Different morphologies that can be obtained during preparation of hybrid latex particles

ammonium bromide and divinylbenzene are the synthons respectively). The outside of the structure is produced from siloxanes to produce a layer of silica. In this way a hollow structure with an organic/inorganic shell is obtained [8] and the polymer and inorganic material are separated. A hybrid latex particle can intrinsically contain the desired functionality (for example an encapsulated pigment particle that is more compatible with the binder system in a coating) or can obtain its final functionality after post-modification (for example a magnetic core-shell particle that is functionalized with certain proteins to target certain organs in the human body [9]). Hybrid latex particles can construct blocks (nanosynthons) for suprastructures that then contain the desired functionalities (for example an encapsulated clay particle that leads to a film with better barrier properties).

The resulting structures of hybrid latex particles are shown in (Fig. 2) and can be described as follows: In encapsulating, for example, an inorganic nanoparticle, the expected outcome is the core-shell particle. In some cases, more than one core particle is encapsulated in the resulting hybrid particle, which could be called an occluded particle. Combining synthons for preparation of a polymeric phase and an inorganic phase, one might also produce occluded particles or multilayered particles. Depending on the surface tensions between the seed material and the polymer and each of the two materials with the water phase, one might obtain partially engulfed particles. Encapsulating a liquid or creating a void inside a particle leads to a nanocapsule. If the particles contain a solid core that is supposed to be released later, these are also called nanocapsules. Depositing particles on a droplet or on a void leads to colloidosomes.

The polymerization techniques applied in encapsulation of nanosized structures are usually emulsion or miniemulsion polymerization. In heterocoagulation, the nanosynthons are often also prepared by emulsion polymerization (Fig. 1).



## 2 Emulsion Polymerization

The emulsion polymerization technique is a heterophase polymerization technique in which three phases can be distinguished: the water phase, the latex particle phase and the monomer droplet phase (the latter is usually present during part of the polymerization reaction). The product of an emulsion polymerization is a latex: a submicrometer dispersion of polymer particles in water. Non-aqueous dispersions of latex particles also exist.

The emulsion polymerization technique usually contains a micelle-forming surfactant and a water-soluble initiator in combination with a water-insoluble monomer. Polymerization takes place in the monomer-swollen micelles and latex particles. Therefore, the term “emulsion polymerization” is a misnomer; the starting point is an emulsion of monomer droplets in water, and the product is a dispersion of latex particles. In the case of microemulsion polymerization, the monomer droplets are made very small (typical particle radius is 10–30 nm) and they become the locus of polymerization. In order to obtain such small droplets, a co-surfactant (e.g. hexanol) is usually applied. A microemulsion is thermodynamically stable [10]. A similar polymerization technique is miniemulsion polymerization in which the thermodynamically unstable droplets have a radius of between 30 and 500 nm [11]. It is also possible to perform inverse emulsion polymerizations whereby the continuous phase is organic, in combination with a water-soluble monomer in small water droplets.

### 2.1 General Aspects of Emulsion Polymerization

Emulsion polymerization involves the emulsification of monomers in an aqueous phase, and stabilization of the droplets by a surfactant. Usually, a water-soluble initiator is used to start the free-radical polymerization. The final product is a dispersion of submicrometer polymer particles, which is called latex. The locus of polymerization is the micelle. Typical applications are paints, coatings, adhesives, paper coatings and carpet backings. The latex particles can have different structures (see Fig. 2). Excellent text books on the applications and structure–property relationships exist [11–15]. Besides a full description of the kinetics and mechanism of emulsion polymerization [16], a textbook adapted for use as material for people entering the field is also available [17].

In emulsion polymerization, one can achieve relatively high rates of polymerization and high molar masses as compared to, for example, solution polymerization.

One of the first major applications of latex was the replacement of natural rubber latex by synthetic rubber latex during the Second World War. From there, a continuing interest in the preparation of lattices has evolved. At the end of the twentieth century, environmental aspects are starting to play a role in the further introduction of emulsion polymerization techniques, replacing solvent-based polymerization processes.

## 2.2 Principles of the Emulsion Polymerization Process

The physical picture of emulsion polymerization is based originally on the qualitative picture of Harkins [18] and the quantitative treatment of Smith and Ewart [19], followed by other contributions. Gilbert shaped the qualitative and quantitative picture of the emulsion polymerization process as it is now generally accepted [16]. The main components of an emulsion polymerization recipe are the monomer(s), dispersing medium (usually water), surfactant and initiator.

During the progress of the polymerization, three distinct intervals can be observed. Interval I is the initial stage, during which particle nucleation takes place. The mechanisms of particle nucleation will be discussed in Sect. 2.3.

Interval II is characterized by a constant particle number, while polymerization in the particles proceeds in the presence of a separate monomer phase. The beginning of interval II is usually taken as the conversion, when the surfactant concentration drops below its critical micelle concentration (CMC). The monomer-swollen particles grow and increase their surface area and consume the monomer droplets. The end of interval II is characterized by the disappearance of monomer droplets. From the beginning of interval III, no monomer droplets are present and the monomer concentration in the particles and water phase continuously decreases.

## 2.3 Particle Nucleation

The nucleation stage (interval I) is the stage during which the particles are formed and therefore the final particle number (and thus particle size) is determined. In micellar nucleation, an oligomer produced from the initiator-derived radical grows until it is surface-active and then enters the micelle (surfactant–cosurfactant system). The number of particles increases in this interval and therefore also the rate of polymerization. When the particle formation is finished and, in the ideal situation, from then on the number of polymer particles remains constant, interval I is finished and interval II starts.

This nucleation mechanism is elegantly quantified by Smith and Ewart [19], who stated that particle nucleation will stop when the surfactant concentration drops below its CMC due to adsorption of surfactant onto the surface of the newly formed polymer particle.

Two weaknesses of the Smith–Ewart nucleation model are: (1) particles are formed even when no micelles are present; and (2) more water-soluble monomers do not fit the theory.

A homogeneous nucleation model was proposed [20, 21] in which radicals react in the aqueous phase with solubilized monomer to form growing oligomeric species (Fig. 3). These species will form particles when the critical water solubility length is reached ( $j_{\text{crit-mer}}$ ). The consequence is that in cases where homogeneous nucleation is the dominating regime of particle nucleation, the water solubility of the monomer, the initiator concentration, and the water solubility of the initiator become important parameters in the emulsion polymerization process.

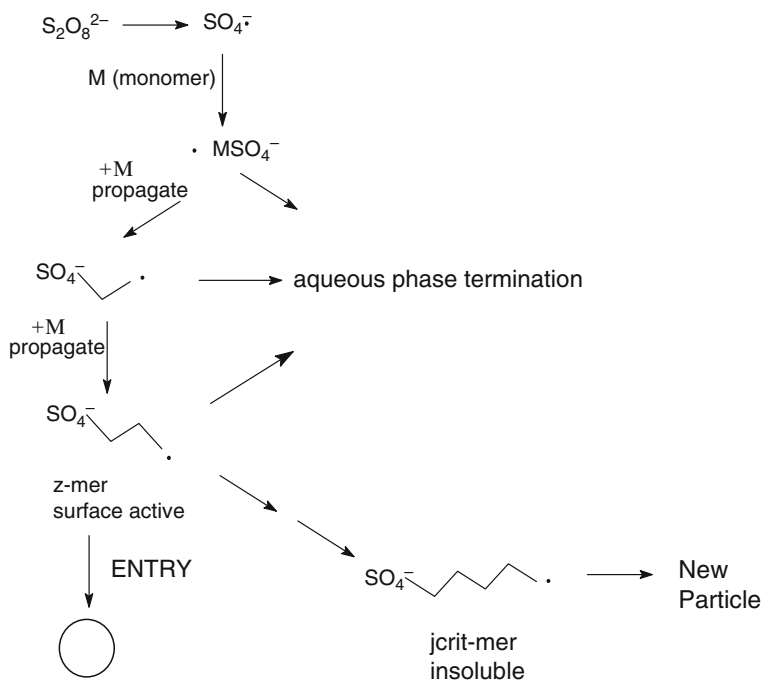


**Fig. 3** Model of homogeneous nucleation related to entry for persulphate-derived radicals

In this special issue, we aim to relate the mechanism of polymerization to the production of hybrid latex particles. In general, encapsulation of inorganic particles is achieved by performing an emulsion polymerization in the presence of the inorganic particles. The encapsulation efficiency is determined by the amount of polymer formed exclusively on the surface of the inorganic particles as opposed to the formation of a second crop of particles (called secondary nucleation) that do not contain inorganic particles. In the light of the nucleation mechanism, we are dealing with a so-called seeded emulsion polymerization that starts in interval II of the emulsion polymerization process.

## 2.4 Particle Morphologies

As mentioned before, hybrid latex particles are usually prepared by seeded emulsion polymerization. In the first stage, well-defined inorganic or organic particles are prepared, while in the second stage a monomer is polymerized in the presence of these well-defined particles. Multistage emulsion polymerization produces structures such as core-shell, “inverted” core-shell structures, and phase-separated structures such as sandwich structures, hemispheres, “raspberry-like” and void

particles (see also Fig. 2). Control of the composite latex particle morphology is important for many latex applications, such as adhesives and coatings [22], and for impact modification and toughening of polymer matrices [23]. The morphology of the particle has a big influence on the properties. The particle morphology can be affected by many of the polymerization parameters. Examples are: water solubility of the monomers; type, amount and addition mode of other ingredients such as surfactant; initiator; chain transfer agent; crosslinking agents; degree of compatibility of polymers; viscosity of the polymerization loci (through swelling of the core particle with monomer and the molar mass of the polymer); degree of grafting of the second stage polymer onto the core particle; polarity of the polymers; interfacial tension at the polymer–polymer and polymer–water interphases; degree of crosslinking; methods of monomer addition; and polymerization temperature.

Particle morphology in emulsion polymerizations with more than one monomer (consecutive homo- and or copolymerization) is governed by thermodynamics and kinetics.

The thermodynamics are mainly controlled by the interfacial tensions between the two polymers and between each of the polymers and water. Calculations of the latex particle morphology on the basis of minimization of the interfacial energy change have been reported by Sundberg et al. [24] and Chen et al. [25, 26]. The interfacial tension seems to be one of the main parameters controlling particle morphology in composite latexes. Depending on the type of initiator and surfactant, the surface polarity can be different. Therefore, the particle surface polarity, rather than the polymer bulk properties, could be the controlling parameter in determining which phase will be inside or outside in composite particles.

It is possible that equilibrium morphology is not obtained because the movement of the polymer chains is not fast enough to reach that equilibrium within the time-frame of the reaction; this is kinetic control of morphology. The kinetic parameters influence the rate of formation of a certain morphology [27, 28], which is basically determined by the interfacial tensions [29]. The parameters of importance are the rate of formation of the polymer (parameters are propagation rate coefficient, and the local monomer and radical concentrations) and the rate of diffusion of the polymer chains (parameters are viscosity in the locus of polymerization, molar mass and topology of the polymer chain). Both the rate of formation and the rate of diffusion of a polymer chain are, for example, affected by the mode of addition of the monomer and initiator. An increased rate of addition of the monomer will lead to a lower instantaneous conversion and thus a lower viscosity in the particle, which in turn increases the rates of diffusion and leads to different morphologies.

Asua et al. [30, 31] also developed a mathematical model for the development of particle morphology in emulsion polymerization. This model is based on the migration of clusters. The clusters are formed if the newly formed polymer chain is incompatible with the polymer existing at the site where it is formed, thus inducing phase separation. The equilibrium morphology is reached when the clusters migrate to an equilibrium situation in order to minimize the Gibbs free energy. The motion of the clusters is due to the balance between the van der Waals forces and the viscous forces.

### 3 Miniemulsion and Microemulsion Polymerization

From a synthetic point of view, emulsion polymerization is not suitable for all monomers. For monomers that are highly water-soluble or, on the other hand, almost insoluble in water, the standard emulsion polymerization technique is not suitable. For water-soluble monomers, besides emulsion polymerization, aqueous phase polymerization can also occur, in which case one could resort to inverse emulsion polymerization, whereby water droplets containing the monomer are polymerized in an oil phase.

In the case of monomers with low water solubility, another problem arises. In emulsion polymerizations, transport of monomer from monomer droplets to the growing polymer particles is needed, which demands a minimum water solubility of the monomer. For example dodecylmethacrylate (water solubility of 0.065 mmol/L) cannot be polymerized by conventional emulsion polymerization. Another reason for hydrophobic monomers to polymerize slowly in emulsion polymerization could be that entry of radicals is slow because the oligomers do not grow to their critical chain length [32]. Another solution to this problem is to directly polymerize within the monomer droplets, which have to be very small in order to keep the benefits of producing polymer in the form of latex. In contrast to emulsion polymerization, where the droplets are of the same size as those in suspension polymerization (10–100  $\mu\text{m}$ ), in mini- and microemulsion polymerization the droplets are very much smaller and enable the polymerization to take place directly within the monomer droplets.

In miniemulsion polymerization, the droplets are in the range from 50 to 500 nm. A combination of a surfactant (e.g. SDS) and a hydrophobe or costabilizer (for example, a long chain alkane or alcohol) is used. The droplets are formed using devices like ultrasonifiers, homogenizers or even static mixers. The miniemulsions are thermodynamically unstable and therefore are only stable for a limited period of time, ranging from hours to days.

In principle, polymerization proceeds in the monomer droplets and the final particle number is close to the initial number of monomer droplets. However, in many cases not all droplets are initiated to become polymer particles, but only a fraction ( $\leq 20\%$ ) of the initial number of monomer droplets. This effect is related to Ostwald ripening and often a hydrophobe is added in the recipes to prevent this from happening.

The miniemulsion process is also very suitable for the preparation of hybrid latex particles. One can have the inorganic particles already present in the droplets, then the polymerization reaction results in encapsulated nanoparticles (see [33]).

In microemulsions, the droplets are even smaller (5–20 nm) and the microemulsion is thermodynamically stable. Here also, a mixed emulsifier system is used [10].

## 4 Encapsulation of Inorganic Particles

### 4.1 *Early Accounts of Encapsulation Through Emulsion Polymerization*

Encapsulation is the process of obtaining small solid nanoparticles, liquid nanodroplets or gas nanobubbles with a polymeric coating. We will give a historic account of some of the early work on encapsulating inorganic pigments and fillers with a polymer through (mini)emulsion polymerization.

The encapsulation of pigment and filler particles is an important area of research, both in the academic world and in industrial laboratories. At present, emphasis is given to the incorporation of clay in polymeric materials, including polymeric nanoparticles. Such systems are expected to exhibit properties other than the sum of the properties of the individual components. In general, several benefits from this encapsulation step can be expected when the obtained particles will be applied in a polymeric matrix (e.g., plastics or emulsion paints) as compared to physical blends:

- Improved barrier properties of a paint film
- Improved mechanical properties
- Better particle dispersion in the polymeric matrix and, as a consequence, improved effectiveness in light scattering in a paint film
- Protection of the filler or pigment from outside influences
- Protection of the matrix polymer from interaction with the pigment

The applications of these encapsulated particles can be found in filled plastics, paints, inks, paper coatings etc. In solid polymeric materials and films, the interaction between filler or pigment and polymer is very important for mechanical properties like fracture toughness [34, 35].

The treatment of inorganic particles with hydrophobizing or coupling agents like silanes, titanates, zirconates etc. is aimed at improving the compatibility with the matrix polymer and it is shown that indeed many rheological and mechanical properties can benefit from this step [36]. However it is also clear that this relatively simple treatment is not sufficient to produce a composite with improved properties as compared to those of the unfilled polymer. The search for even better properties has initiated the process of encapsulation of inorganic particles where an intermediate layer, which interacts strongly with both the filler surface and the matrix polymer, would provide the required improvement. Similar conclusions were reached by Dekkers and Heikens [37] in their study on the effect of interfacial adhesion on tensile behavior of polystyrene–glass-bead composites. They state that obviously a more drastic modification (than surface modification with silanes) near the surface of the glass beads is required in order to obtain a composite both stiffer and tougher than the matrix material polystyrene; for instance, encapsulation of the glass beads within a layer of low-modulus material.

If there is good interaction between the inorganic material and the polymer, the polymer chains directly in contact with the surface are very difficult to remove,

even without the presence of covalent bonds between the surface and the polymer layer. This bound polymer does not necessarily lead to reinforcement of a filled polymer and, in some cases, this layer can degrade the tear strength of the material by allowing failure at a weak second interface between bound and matrix polymer. This degradation can be alleviated by crosslinking the polymer or by increasing the molecular weight to force either chemical or physical links across the weak second interface [38]. Processing these particles at higher temperatures and high shear necessitates high molecular weights or crosslinking, in which case covalent bonding with the surface is superfluous.

Ono [39] showed in 1986 that carbon powders coated with polymethylmethacrylate were directly moldable into sheets that had excellent thermal properties and could also be used as electric conductive plastics.

One of the most important applications of encapsulated pigment and filler particles is in emulsion paints. One of the more expensive components of water-borne paints is the white pigment, usually titanium dioxide (rutile form). The pigment is added to obtain hiding power. The hiding power or opacity depends on the occurrence of light absorption and light scattering. For pigments with a high refractive index, like titanium dioxide, light scattering is the main contribution to the hiding power. The light scattering effectiveness of the pigment particles depends on the particle size and on the interparticle distance. Agglomerates of pigment, already present in the wet paint film or formed by flocculation during the drying process, will reduce the scattering effectiveness of the expensive dispersed pigment particles. One of the earlier papers in the field of encapsulation originates from 1980 by Laible et al. who stated that by encapsulating the pigment particles it would be expected that the chance of flocculation is reduced and that the dispersion in the final paint film is improved [40]. It has been suggested that the layer thickness could be optimized to obtain optimum spacing between titanium dioxide particles to achieve maximum light scattering [41].

Most titanium dioxide pigments are already surface-modified with other inorganic oxides to deal with the generation of radicals in titanium dioxide under the influence of UV light. These radicals can lead to degradation of the matrix polymer and, subsequently, to chalking. With the proper choice of the polymer layer, the durability might be improved further. Other advantages are improved block resistance, less dirt pick-up, better adhesion [34, 42] and improved chemical resistance [34].

Besides inorganic pigment and filler particles, there is also early work (from 1978) on encapsulation of organic pigments, e.g. copper-phthalocyanine and azo pigments [43]. For further reading on encapsulation of different materials see [44].

When the inorganic particles are magnetically responsive, this opens pathways to special applications like coupling of enzymes and antibodies to the surface of the magnetic particles after which drug targeting becomes possible. Also, these particles can be used in biochemical separations [45]. Furthermore, early accounts (from 1983) can be found where these magnetic particles are applied in magnetic recording media, oil spill clean-up and moldable magnetic powders [46]. In 1986, Cohen

described the precipitation of iron hydroxides in swollen polymer particles, which were converted to the oxide by means of a heat treatment [47]. For further developments see [9].

Although some papers on encapsulation of inorganic particles can be found before 1980, most of the early work begins in the mid-1980s and, on average, about 50 papers per year were published on the topic of encapsulation using the emulsion polymerization technique.

All this work has been done in the early days of encapsulation study. Although a lot of success has been obtained, a general deficiency in the approaches mentioned is the irregular structure of the encapsulating polymer layer. Besides polymerization from the surface, there is also often formation of secondary polymer particles, which heterocoagulate on the surface and can create an irregular polymer layer. One solution is to use controlled radical polymerization from the surface in order to have regular growth, and often secondary nucleation is suppressed (see Sect. 4.2.3).

An increased interest in this approach was created when clay encapsulation was attempted. Furthermore, the miniemulsion polymerization technique proved to be another versatile route towards encapsulated materials (see [33]). In the past decade, about 100 papers per year are published (excluding the many papers on clay nanocomposites produced by techniques other than (mini)emulsion polymerization).

## ***4.2 Encapsulation of Inorganic Particles with Emulsion Polymerization***

### **4.2.1 General Principles**

Emulsion polymerization is the technique that is used most often because of the many applications of encapsulated pigment particles that are related to water-based coatings.

In order to encapsulate an inorganic particle, one can resort to physical or chemical methods and use molecules or particles as the building blocks (see Fig. 1). A physical approach in which one uses molecules and inorganic particles is the layer-by-layer approach, initially developed by Möhwald and Caruso [5]. In this approach, polyelectrolytes are deposited on the surface of inorganic particles and an alternating charge of the polyelectrolytes is applied for each consecutive layer (see Fig. 4). Using monomers to build up polymer chains that encapsulate the particles is the principle of (mini)emulsion polymerization that we are discussing here. The driving force for the layer-by-layer approach is dominantly physical (e.g. electrostatic attraction), whereas in the emulsion polymerization approach the driving force is the insolubility of the formed polymer chains in water. In the emulsion approach, the inorganic particles (usually after some hydrophobization) are dispersed with the normal surfactants and an emulsion polymerization is performed, where the locus of polymerization is the hemi- or admicelle around the inorganic particle (Fig. 4).



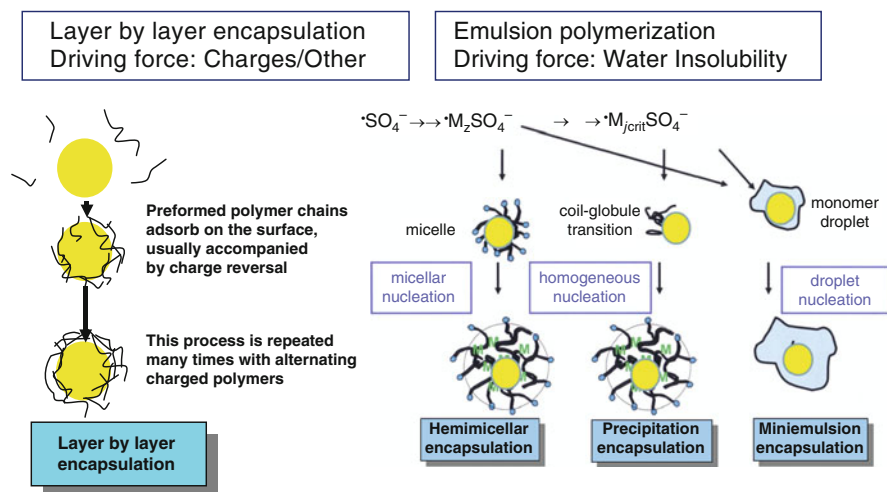


**Fig. 4** Representation of encapsulation of inorganic (submicrometer) particles through the layer-by-layer approach (*left*) or (mini)emulsion polymerization (*right*)

Usually “maximum” properties are obtained when the inorganic particles are distributed evenly and as single (primary) particles in the matrix. This means that in the steps towards obtaining the final product, keeping the particles well dispersed is of major importance. Initially, the particles should be well dispersed in the aqueous phase and (partial) coagulation during the emulsion polymerization must be avoided because this leads to irreversible fixation of the coagulates.

Depending on the conditions, one can distinguish three different mechanisms (Fig. 4):

1. Formation of a hemimicelle on the surface of the inorganic particle where, after swelling with monomer, the encapsulating polymer is formed.
2. Precipitation of polymer chains initiated in the aqueous phase.
3. Formation of polymer inside the particle containing monomer droplet (mini-emulsion polymerization approach).

Examples of early work on the hemimicelle approach include the study of  $\text{TiO}_2$  [48–50] as one of the obvious candidates to benefit from encapsulation. In this work, the so-called coupling agents were applied, which usually contain at least one smaller alkoxy group that can react with a hydroxyl group on the surface. The other groups can contain functionalities that can interact physically or chemically with the surrounding polymer matrix, thereby aiding dispersion of the filler.

Other additives that are used to make the surface hydrophobic are, for example, a combination of methacrylic acid and aluminum nitrate as a coupling agent [51] or groups like stearic acid. Without chemical modification of the surface, one can also use bilayers of adsorbed surfactant as a locus of polymerization [52]. The first step is the formation of a so-called hemimicelle, a bilayer of the surfactant molecules at

the solid–aqueous interface (Fig. 4). A hemimicelle can be considered as the surface analogue of a micelle, and therefore this approach can be compared to the emulsion polymerization approach.

Early examples of the precipitation approach include the aqueous solution polymerizations reported by Chaimberg et al. [53] for the graft polymerization of polyvinylpyrrolidone onto silica. The nonporous silica particles were modified with vinyltriethoxysilane in xylene, isolated and dispersed in an aqueous solution of vinylpyrrolidone. The reaction was performed at 70°C and initiated by hydrogen peroxide, after which precipitation on the surface occurred, leading to encapsulation. Nagai et al. [54] in 1989 reported on the aqueous polymerization of the quaternary salt of dimethylaminoethyl methacrylate with lauryl bromide, a surface-active monomer, on silica gel. Although the aim was to polymerize only on the surface, separate latex particles were also formed.

The miniemulsion approach is extensively discussed in the contribution of Weiss and Landfester [33].

## 4.2.2 Efficiency of Encapsulation

Polymerization on the surface is in competition with the process of new particle formation. Depending on the amount of surfactant, the type of monomer and the monomer droplet size any of the three nucleation mechanisms shown in Fig. 4 (micellar, homogeneous or droplet nucleation) can occur. In order to prevent micellar nucleation, the net surfactant concentration, after correction for the adsorbed amount on the surfaces, should be below the CMC. The presence of conventional surfactants in encapsulation reactions introduces the problem that a delicate balance between the stabilization of polymer particles and inorganic particles and the formation of new particles has to be maintained.

However, homogeneous nucleation can also occur, which will be more substantial with more water-soluble monomers present. Therefore, more free polymer will be formed and the efficiency will drop. The efficiency seems to depend on the water solubility of the monomer. Also, lowering the monomer addition rate can slow down production of new particles, as described below.

According to Hergeth and coworkers [55], a minimum surface of the inorganic particles is needed to prevent secondary nucleation. To estimate this amount, a formula was derived for seeded emulsion polymerization with spherical particles and a water-soluble initiator [55]. This formula was based on the observation that primary particles are produced by a collapse and micellization process of oligomeric chains. An upper limit for the particle size was estimated to be 100 nm for the encapsulation of silica with polyvinyl acetate. A relatively water-soluble monomer is applied here; for more hydrophobic monomers this upper limit will be higher. Because the surface area needed to prevent secondary nucleation is proportional to the monomer conversion per unit of time, the encapsulation efficiency can be improved by using monomer-starved conditions. So far, mainly submicrometer particles have been encapsulated with this method. The encapsulation of the larger filler particles

(>1  $\mu\text{m}$ ) is more difficult because the low surface area of the particles does not suffice to capture all the formed oligomers and, therefore, secondary nucleation is almost unavoidable in the normal emulsion polymerization approach. However, the process of heterocoagulation can also occur during an emulsion polymerization and in many instances is the main mechanism of encapsulation. This mechanism leads to non-uniform polymer layers, but the resulting encapsulated particles can still improve the filler properties [56].

In general, a strong interaction of the first layer of encapsulating polymer with the surface of the inorganic particle can lead to an increase in the glass transition temperature,  $T_g$  [57].

Using less water-soluble monomers in combination with a nonionic initiator, the formation of surface-active oligomers in the aqueous phase can be minimized, thus increasing the efficiency of encapsulation.

In summary, highest efficiencies are obtained from using small particles at a high concentration, a hydrophobic initiator, low surfactant concentration and monomers with low water solubility (added semi-continuously).

#### 4.2.3 Special Approaches

Besides emulsion polymerization with a separate monomer phase, emulsions consisting of diluted monomer droplets together with inorganic particles were also polymerized by the group of Ruckenstein [58]. They created emulsions of decane, a monomer and silica in an aqueous solution of surfactant, which were polymerized to latexes containing uniformly distributed inorganic particle clusters of submicrometer size.

Inverse emulsions were also prepared, and (the otherwise difficult) encapsulation with water-soluble monomers like acrylamide was performed [58]. In a first step, a colloidal dispersion was prepared by dispersing the silica particles in an aqueous solution of acrylamide containing a water-soluble dispersant, a crosslinking agent like *N,N*-methylene bisacrylamide and an initiator. The colloidal system was dispersed in decane containing a suitable surfactant.

Another possibility, which has not fully been explored yet, is the use of vesicles (which intrinsically can form bilayers) as a locus of polymerization on the surface of inorganic particles. Both the adsorption of vesicles (on, for example, glass beads) [59] as well as the polymerization within vesicle structures has been described [60–62].

In the past, many groups have tried to encapsulate clay platelets inside latex particles. This encapsulation poses some extra challenges because of the tendency of the clay platelets to form stacks and card-house structures. Most of the attempts resulted in the so-called armored latex particles, i.e. clay platelets in the surface of the latex. Recently, natural and synthetic clays were successfully encapsulated. The anisotropy of the clay resulted in non-spherical latex particles (Figs. 5 and 6), either peanut-shaped [63] or flat [64]. Clay platelets also turned out to be good stabilizing agents for inverse Pickering emulsion polymerizations [65].

**Fig. 5** Cryo-TEM picture of peanut-shaped encapsulated montmorillonite. The clay has been edge-modified with a reactive titanate and the surrounding polymer created by a starved-fed emulsion polymerization of methylmethacrylate [63]

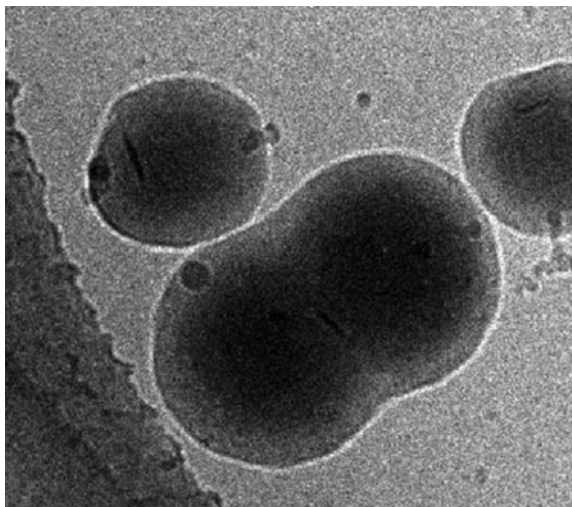
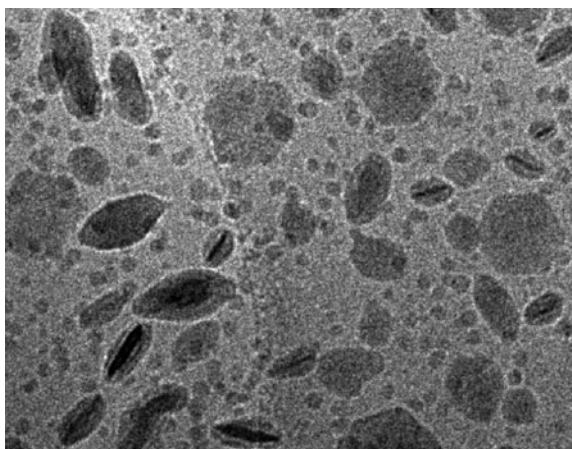


**Fig. 6** Cryo-TEM picture of flat encapsulated gibbsite platelets. The polymerization has been performed from the surface with amphipatic RAFT agents. Note that some of the flat latex particles are seen from the face and some from the side. Secondary nucleation is also visible in this image [64]



## 5 Conclusions

Encapsulation of organic and inorganic pigment and filler particles has been achieved in the laboratory for many different materials. The number of commercial applications of encapsulated particles is limited. BASF has one of the first coatings on the market with nanocomposite particles containing high levels of silica [66]. For submicrometer particles, the emulsion and miniemulsion polymerization approaches seem the most promising. For larger particles, this method is less suitable and one has to resort to other techniques like suspension polymerization, or heterocoagulation with small latex particles. The main problems are to obtain and maintain primary particles during the encapsulation reaction and, at the same time, have high encapsulation efficiency.

## References

1. Slomkowski S et al (2003) IUPAC terminology of polymerization processes and polymers in dispersed systems
2. Bourgeat-Lami E (2002) *J Nanosci Nanotechnol* 2:1–24
3. Polymer Colloids Group (2009) Polymer colloids – quo vadis? 1st international polymer colloids group conference, Lucca, Italy, 6–11 July 2009
4. Corey EJ (1967) *Pure Appl Chem* 14:19–37
5. Caruso F, Möhwald H (1999) *Langmuir* 15:8276–8281
6. Cronin L, Beugholt C, Krickemeyer E, Schmidtman M, Bögge H, Kögerler P, Luong K, Müller A (2002) *Angew Chem Int Ed* 41:2805–2808
7. Teixeira RFA, Bon SAF (2010) Physical methods for the preparation of hybrid nanocomposite polymer latex particles. *Adv Polym Sci*. doi:10.1007/12\_2010\_65
8. Hubert DHW, Jung M, Frederik PM, Bomans PHH, Meuldijk J, German AL (2000) *Adv Mater* 12:1286–1289
9. Rahman MM, Elaissari A (2010) Organic–inorganic hybrid magnetic latex. *Adv Polym Sci*. doi:10.1007/12\_2010\_59
10. Guo JS, Sudol ED, Vanderhoff JW, El-Aasser MS (1992) In: Daniels ES, Sudol ED, El-Aasser MS (eds) ACS symposium series: polymer latexes – preparation, characterization and applications, vol 492. American Chemical Society, Washington, DC, p 99
11. Tang H-I, Sudol ED, Adams ME, Silebi CA, El-Aasser MS (1992) In: Daniels ES, Sudol ED, El-Aasser MS (eds) ACS symposium series: polymer latexes – preparation, characterization and applications, vol 492. American Chemical Society, Washington, DC, p 72
12. Lovell PA, El-Aasser MS (eds) (1996) *Emulsion polymerization and emulsion polymers*. Wiley, Chichester
13. Blackley DC (1997) *Polymer latices, science and technology*. Chapman & Hall, London
14. Warson H, Finch CA (2001) *Applications of synthetic resin latices*. Wiley, Chichester
15. Urban D, Takamura A (2002) *Polymer dispersions and their industrial applications*. Wiley, Weinheim
16. Gilbert RG (1995) *Emulsion polymerization, a mechanistic approach*. Academic, London
17. van Herk AM (2005) *Chemistry and technology of emulsion polymerization*. Blackwell, Oxford
18. Harkins WD (1947) *J Am Chem Soc* 69:1428–1430
19. Smith WV, Ewart RW (1948) *J Chem Phys* 16:592–596
20. Goodall AR, Wilinon MC, Hearn JJ (1977) *Polym Sci* 15:2193–2198
21. Fitch RM, Tsai CH (1971) In: Fitch RM (ed) *Polymer colloids*. Plenum, New York, p 73
22. Vandezande GA, Rudin A (1994) *J Coat Technol* 66:99–108
23. Lovell PA (1995) *Macromol Symp* 92:71–92
24. Sundberg DC, Casassa AP, Pantazopoulos J, Muscato MR, Kronberg B, Berg J (1990) *J Appl Polym Sci* 41:1425–1442
25. Chen YC, Dimonie VL, El-Aasser MS (1991) *J Appl Polym Sci* 42:1049–1063
26. Chen YC, Dimonie VL, El-Aasser MS (1992) *Pure Appl Chem* 64:1691–1696
27. Chern CS, Poehlein GW (1990) *J Polym Sci Polym Chem Ed* 28:3073–3099
28. Mills MF, Gilbert RG, Napper DH (1990) *Macromolecules* 23:4247–4257
29. Chen YC, Dimonie VL, Shaffer OL, El-Aasser MS (1993) *Polym Int* 30:185–189
30. González-Ortiz LJ, Asua JM (1996) *Macromolecules* 28:3135–3145
31. González-Ortiz LJ, Asua JM (1996) *Macromolecules* 29:383–389
32. Maxwell IA, Morrison BR, Gilbert RG, Napper DH (1991) *Macromolecules* 24:1629–1640
33. Weiss CK, Landfester K (2010) Miniemulsion polymerization as a means to encapsulate organic and inorganic materials. *Adv Polym Sci*. doi:10.1007/12\_2010\_61
34. Godard P, Wertz JL, Biebuyck JJ, Mercier JP (1989) *Pol Eng Sci* 29:127–133
35. Kendall K (1978) *Br Polym J* 10:35–38
36. Hawthorne DG, Hodgkin JH, Loft BC, Solomon DH (1974) *J Macromol Sci Chem* A8:649–657

37. Dekkers MEJ, Heikens D (1983) *J Appl Polym Sci* 28:3809–3815
38. Kendall K, Sherliker FR (1980) *Br Polym J* 12:85–88
39. Ono T (1986) *Org Coat* 18:279–296
40. Laible R, Hamann K (1980) *Adv Colloid Interface Sci* 13:65–99
41. Templeton-Knight RL (1990) *J Oil Colour Chem Assoc* 1:459–464
42. Hoy KL, Smith OW (1991) *Polymeric material science and engineering. Abstracts of ACS Fall Meeting 1991, New York* 65:78–79
43. Kroker R, Hamann K (1978) *Angew Makromol Chemie* 13:1–22
44. van Herk AM, German AL (1998) Microencapsulated pigments and fillers. In Arshady R (ed) *Microspheres, microcapsules & liposomes, vol 1. Preparation & chemical applications*, Citus Books, London
45. Arshady R (1993) *Biomaterials* 14:5–15
46. Buske N, Goetze T (1983) *Acta Polym* 34:184–185
47. Cohen B, Wong TK, Hargitay B (1986) Magnetically responsive reagent carrier. *Eur Pat.* 180384 A2, CA 105 P 75418n.
48. Caris CHM, van Elven LPM, van Herk AM, German AL (1989) *Br Polym J* 21:133–140
49. Caris CHM, Kuijpers RPM, van Herk AM, German AL (1990) *Makromol Chem Makromol Symp* 35/36:535–548
50. Janssen RQF, van Herk AM, German AL (1993) *J Oil Colour Chem Assoc* 11:455–461
51. Lorimer JP, Mason TJ, Kershaw D, Livsey I, Templeton-Knight R (1991) *Colloid Polym Sci* 269:392–397
52. Meguro K, Yabe T, Ishioka S, Kato K, Esumi K (1986) *Bull Chem Soc Jpn* 59:3019–3021
53. Chaimberg M, Parnas R, Cohen Y (1989) *J Appl Polym Sci* 37:2921–2931
54. Nagai K, Ohishi Y, Ishiyama K, Kuramoto N (1989) *J Appl Polym Sci* 38:2183–2189
55. Hergeth W, Starre P, Schmutzler K, Wartewig S (1988) *Polymer* 29:1323–1328
56. Janssen EAWG, van Herk AM, German AL (1993) *Polym Prepr Am Chem Soc Div Polym Chem* 34:532–533
57. Rittigstein P, Torkelson JM (2006) *J Polym Sci B Polym Phys* 44:2935–2943
58. Park JS, Ruckenstein E (1990) *Polymer* 31:175–179
59. Jackson S, Reboiras MD, Lyle IG, Jones MN (1986) *Faraday Discuss Chem Soc* 85:291–301
60. Jung M, Hubert DHW, Bomans PHH, Frederik PM, Meuldijk J, van Herk AM, Fischer H, German AL (1997) *Langmuir* 13:6877–6880
61. Jung M, Hubert DHW, Bomans P, Frederik PM, van Herk AM, German AL (2000) *Adv Mater* 12:210–213
62. Jung M, den Ouden I, Montoya-Goñi A, Hubert DHW, Frederik PM, van Herk AM, German AL (2000) *Langmuir* 16:4185–4195
63. Voorn DJ, Ming W, Van Herk AM (2006) *Macromolecules* 39:4654–4656
64. Ali SI, Heuts JPA, Hawke BS, van Herk AM (2009) *Langmuir* 25:10523–10533
65. Voorn DJ, Ming W, van Herk AM (2006) *Macromolecules* 39:2137–2143
66. Xue Z, Wiese H (2004) *US patent* 6833401 B1

# Physical Methods for the Preparation of Hybrid Nanocomposite Polymer Latex Particles

Roberto F.A. Teixeira and Stefan A.F. Bon

**Abstract** In this chapter, we will highlight conceptual physical approaches towards the fabrication of nanocomposite polymer latexes in which each individual latex particle contains one or more “hard” nanoparticles, such as clays, silicates, titanates, or other metal(oxides). By “physical approaches” we mean that the “hard” nanoparticles are added as pre-existing entities, and are not synthesized in situ as part of the nanocomposite polymer latex fabrication process. We will narrow our discussion to focus on physical methods that rely on the assembly of nanoparticles onto the latex particles after the latex particles have been formed, or its reciprocal analogue, the adhesion of polymer onto an inorganic nanoparticle. First, will discuss the phenomenon of heterocoagulation and its various driving forces, such as electrostatic interactions, the hydrophobic effect, and secondary molecular interactions. We will then address methods that involve assembly of nanoparticles onto or around the more liquid precursors (i.e., swollen/growing latex particles or monomer droplets). We will focus on the phenomenon of Pickering stabilization. We will then discuss features of particle interaction with soft interfaces, and see how the adhesion of particles onto emulsion droplets can be applied in suspension, miniemulsion, and emulsion polymerization. Finally, we will very briefly mention some interesting methods that make use of interface-driven templating for making well-defined assembled clusters and supracolloidal structures.

**Keywords** Colloids · Heterocoagulation · Nanocomposites · Pickering stabilization · Polymer latex · Self-assembly · Supracolloidal structures

---

S.A.F. Bon (✉) and R.F.A. Teixeira  
Department of Chemistry, University of Warwick, Coventry CV4 7AL, UK  
e-mail: [S.Bon@warwick.ac.uk](mailto:S.Bon@warwick.ac.uk); [R.F.Teixeira@warwick.ac.uk](mailto:R.F.Teixeira@warwick.ac.uk)



## Contents

1	Assembly of Nanoparticles onto Prefabricated “Larger” Particles via Heterocoagulation .	20
1.1	Electrostatic Interactions .....	21
1.2	Hydrophobic Interactions .....	25
1.3	Secondary Molecular Interactions.....	30
2	Assembly of Nanoparticles onto Prefabricated Larger Particles via Repetitive Heterocoagulation: the Layer-by-Layer Technique.....	33
3	Assembly of Nanoparticles onto Emulsion Monomer Droplets and their Subsequent Polymerization.....	34
3.1	Pickering Stabilization: Adhesion of Particles to “Soft” Interfaces .....	34
3.2	Polymerization of Emulsion Droplets Armored with Inorganic Nanoparticles: Pickering Suspension and Miniemulsion Polymerization .....	38
4	Assembly of Nanoparticles onto the Surface of Polymer Colloids Throughout Emulsion Polymerization: Solids-Stabilized, or Pickering, Emulsion Polymerization .....	42
5	Hybrid Polymer Colloids Through Assembly of Colloidal Building Blocks via Interface-Driven Templating.....	44
6	Outlook .....	46
	References .....	46

## 1 Assembly of Nanoparticles onto Prefabricated “Larger” Particles via Heterocoagulation

Heterocoagulation is the mutual adhesion of particles of a dissimilar nature upon collision, as a result of their individual Brownian motion. Brownian motion is a stochastic, or random, movement of colloidal particles suspended in a fluid (or gas) as a result of the internal thermal energy of the system, and thus of collisions with the solvent (or gas) molecules, as pointed out independently by Einstein and Smoluchowski. Derjaguin pointed out that the term “heteroadagulation” should be used for adhesion of small particles that move through Brownian motion onto much larger objects, whose Brownian motion can be neglected, such as fibers [1]. For example, Jachowicz and Berthiaume [2] reported the deposition of cationic, anionic, and neutral silicon oil droplets in the form of oil-in-water emulsions on native or cationically modified human hair fibers, driven by electrostatic forces.

Since heterocoagulation is a stochastic process, great care needs to be taken not to end up with large fractal clusters or flocks of the two colloidal components. Driving forces to promote adhesion of inorganic nanoparticles onto the surface of polymer latex particles, or vice versa, can be based on a variety of forces, such as electrostatic attraction, hydrophobic interactions, and secondary molecular interactions such as (multiple) hydrogen bond interactions and specific molecular recognition (e.g. complementary proteins like avidin–biotin).



## 1.1 *Electrostatic Interactions*

When an inorganic nanoparticle has the opposite charge to a larger polymer latex particle, they will attract each other on the basis of Coulomb's law. The range in which this attractive force is felt depends on the charge densities and, more importantly, on the extent of the diffuse double layers of the two interacting colloids. If one wants to adhere more than one nanoparticle onto a polymer latex sphere, the small particles already present on the surface of the latex particle will influence the adsorption behavior of the next-to-be-adsorbed nanoparticle. The spatial distribution for sorption of the nanoparticles on the surface is logically influenced, and a close encounter can even locally be of a repulsive nature. This charge inversion is also the reason why typically only a single layer of nanoparticles can adhere onto the surface of the central particle.

The attraction between oppositely charged colloids can be understood and modeled using the DLVO theory [3–6]. The DLVO theory links the van der Waals attraction between particles with the electrostatic effects resulting from the presence of a double layer of counterions. A detailed theoretical discussion lies outside the scope of this chapter. One of the difficulties of the DLVO theory is that an exact analytical description of interaction of overlapping double layers is only known for flat, infinite parallel surfaces. For spherical double layers, approximations need to be made or numerical theoretical simulations need to be performed.

Hogg, Healy, and Fuerstenau [7] developed their HHF theory to describe the interactions of two particles of different size. In 1985, Matijevic and Barouch [8] evaluated the validity of the HHF theory for the electrostatic interaction between two surfaces of different sizes for both unlike particles with potentials opposite in sign, and for particles with same sign potentials. The computational calculations overcame the problem of the accuracy in the evaluation of incomplete elliptic integrals of the first kind, which is a direct consequence of a non-linearity of the Poisson–Boltzmann equation. They concluded that for systems with dissimilar particles with either opposite signs or the same sign, the approximation of the HHF theory achieved good results. However, when potential differences increased, marked deviations from the HHF theory were found.

In 1976, Bleier and Matijevic [9] reported the interaction, in aqueous solution, of two different monodisperse hydrous chromium(III) oxide sols of approximate radii of 110 and 186 nm with poly(vinyl chloride) latexes of ca. 169 and 255 nm in radius and of relatively narrow particle size distribution. Zeta-potential measurements of the chromium(III) oxide sols as a function of pH in a 8.9 mM background electrolyte solution of  $\text{NaNO}_3$  showed an isoelectric point (IEP) of pH 7.2–7.6. Below the IEP, the sols were positively charged and negatively charged above the IEP. Dispersions of the inorganic sols were stable below pH 4.6 and above pH 9.0. Both PVC latexes were stable and negatively charged throughout the pH range (3.0–11.0) investigated. They found that rapid coagulation of mixtures of the inorganic sol with the polymer latex occurred between pH 3.0 and 4.6. Because both individual dispersions were stable, this was therefore directly ascribed to mutual coagulation of

oppositely charged particles. These experimental observations were in agreement with the earlier predictions by the HHF theory [7]. Obviously, bulk coagulation needs to be avoided. A logical parameter therefore is the geometric ratio of the sizes of the two different colloids involved: the larger the size, the easier it would be to avoid mass coagulation. Note that Vincent et al. [10–12] showed that small particles, in the presence of a low electrolyte concentration, can act as bridging flocculants of large particles of opposite charge.

Vincent and coworkers described the adsorption–desorption behavior of small positively charged polystyrene latex particles onto much larger negatively charged polystyrene spheres [13, 14]. In addition to surface charges, both sets of particles had a layer of adsorbed poly(vinyl alcohol) so that the influence of the extent of the diffuse double layer upon variation of the electrolyte concentration could be investigated. At low electrolyte concentration, the diffuse double layers are extended and the small particles adhere in a way that shows a relatively large spatial distance between them on the surface of the large sphere. The extended double layers effectively cause a strong and irreversible adsorption. The lateral repulsion force and the electrostatic adsorption force both decrease when the electrolyte concentration is increased. The spatial arrangement of the small particles may now experience a lateral net attractive rather than repulsive force, which leads to clustering of the nanoparticles on the surface. The adsorption behavior also can become reversible, being a direct function of the thickness of the sterically stabilizing poly(vinyl alcohol) layers around both the small particles and the larger latex spheres, and of the volume fractions of the particles in the system.

Hansen and Matijević [15] studied the adsorption of negatively charged (carboxylic acid functionality) poly(methyl methacrylate) (PMMA) latex of average particle radius of 40 nm onto to much larger positive inorganic sols made from either hydrated aluminum oxide (particle radius 250 nm) or hematite (radius 272–276 nm). The polymer latex showed an IEP of pH 3.8, the hydrated aluminum hydroxide particles an IEP of pH 8.7, and the hematite had a value of pH 7.2, all measured in 0.01 M  $\text{KNO}_3$  background electrolyte. Above the IEPs of these dispersions, the latex and the solids were negatively charged. The adsorption process of the smaller latex particles proceeded in a reversible manner, implying equilibrium conditions. The maximum number of small particles adsorbed onto a large particle was shown to increase with increasing  $\text{KNO}_3$  concentration, reaching practically a “fully covered” monolayer. This is in agreement with the findings by Vincent [13, 14]. It was possible to compare the interactions energies obtained from the adsorption isotherm of the latex poly(methyl methacrylate *co*-methacrylic acid) onto positive oxide (alumina or hematite) to the calculated values according to the derived expression based on the two-dimensional Poisson–Boltzmann equation [16].

Furusawa and Anzai investigated the heterocoagulation of a highly monodisperse amphoteric polymer latex (particle diameter 250 nm, IEP ca. pH 6.8 in 5.0 mM KCl background electrolyte, positively charged at low pH) onto various silica spheres (diameters 240, 460, 960, and 1590 nm; IEP ca. pH 3.0) dispersed in pure water or upon addition of various hydroxypropyl celluloses (HPCs) [17, 18]. Stable dispersions for both individual particles under the condition that they had opposite

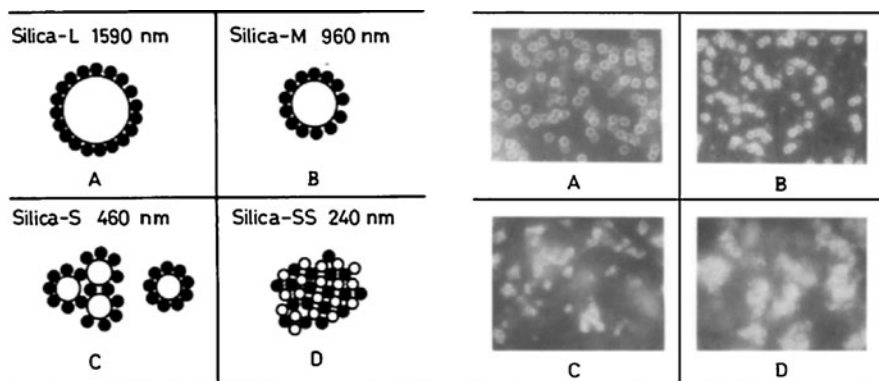


**Fig. 1** *Left: (a–d)* Different morphologies of heterocoagulate particles that can be obtained when the relative sizes of the two colloids are varied. *Right: Micrographs* obtained from heterocoagulation of an amphoteric latex (diameter 250 nm) at pH 5.6, at which it has a cationic surface charge, with negatively charged silica particles of various diameters: 1590 (a), 960 (b), 460 (c), and 240 (d) nm. Reproduced from Figs. 2 and 3 from [17]

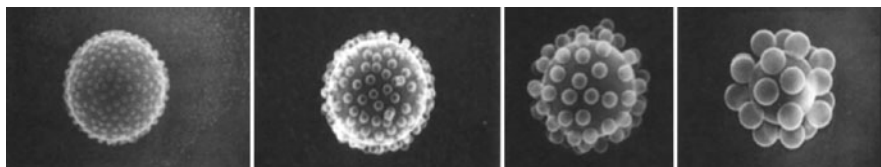


**Fig. 2** TFFDSEM images of various anionic polymer latexes of different sizes. From *left to right*: poly(vinylidene chloride) latex of 116 nm, and polystyrene particles of 180, 320, and 696 nm in diameter, assembled onto a large cationic polystyrene latex of 2170 nm via heterocoagulation in 0.5 mM KCl background electrolyte. Images reproduced from Fig. 7 from [20]

surface charge only occurred in the narrow pH window between pH 5 and 6. Stable raspberry-like heterocoagulates were obtained when the ratio of the diameter of the silica to latex particle was greater than 3. For ratios of a lower value, larger irregular aggregates were obtained (see Fig. 1).

Harley, Thomson, and Vincent used thin-film freeze-drying scanning electron microscope (TFFDSEM) [19] as a visualization method to study the heterocoagulation of monodisperse anionic polymer latexes of various diameters made using potassium persulfate as initiator (i.e., polystyrene spheres of 696, 320, and 180 nm and a poly(vinylidene chloride) latex of 116 nm) onto a large cationic polystyrene latex of 2170 nm in diameter, using azobis(isobutylamide) dihydrochloride as initiator [20]. Adsorption isotherms of the four sets of negatively charged particles onto the large cationic microspheres were of the “high-affinity” type, in 0.5 mM KCl background electrolyte. This was logical and ascribed directly to extended interacting double layers. The particles packed beautifully symmetrically onto the surface (see Fig. 2), implying that lateral electrostatic repulsion between neighboring adhered particles plays a key role.

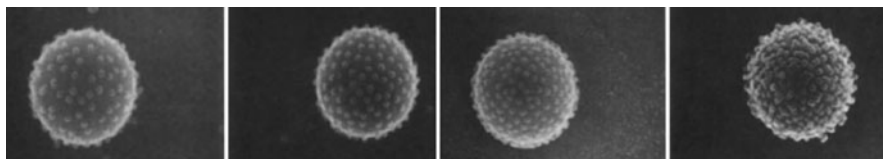


**Fig. 3** TFFDSEM images of an anionic poly(vinylidene chloride) latex of 116 nm, assembled onto a large cationic polystyrene latex of 2170 nm via heterocoagulation at various background electrolyte concentrations of KCl: from *left to right*, 0.01, 0.1, 0.5, and 5.0 mM. Images reproduced from Fig. 9 from [20]

The influence of the concentration of the background electrolyte was beautifully captured in a series of images using the anionic poly(vinylidene chloride) latex of 116 nm, at KCl concentrations of 0.01, 0.1, 0.5, and 5.0 mM (see Fig. 3). Increasing the background electrolyte concentration and thus effectively reducing the thickness of the double layer led to closer spatial arrangements of the particles onto the surface of the central microsphere. At the highest electrolyte concentration, one could even argue the onset of an attractive rather than repulsive force between neighboring particles.

Ottewill and coworkers used heterocoagulation as a route to hard core/soft shell polymer composites. Small cationic latex particles of poly(butyl methacrylate) were adhered onto the surface of larger anionic polystyrene latex particles [21]. Upon raising the temperature of the assembled colloidal dispersion, the poly(butyl methacrylate) latex particles underwent film formation leading to a smooth shell. Okubo examined the reciprocal concept of using heterocoagulation as a method for preparation of soft core/hard shell polymer composites. The source for hard particles, however, was not inorganic nanoparticles but cationic polystyrene spheres of 103 nm in diameter, assembled onto soft poly(ethyl acrylate-*co*-ethyleneglycol dimethacrylate-*co*-methacrylic acid) latex spheres of 714 nm [22].

Xu et al. heterocoagulated cationic PMMA latex particles of an estimated 150–200 nm in diameter with various clays, Montmorillonite (GelWhite GP and Cloisite Na<sup>+</sup>) and (fluoro)hectorites (Laponite RD, RDS, B, S, JS), having plate dimensions between 25 and 600 nm. No details on the stable colloidal armored structures were reported. Mass coagulation was induced in order to obtain a nanocomposite bulk material, which was further analyzed [23]. Chen et al. [24] added TiO<sub>2</sub> and SiO<sub>2</sub>/TiO<sub>2</sub> nanoparticles with a positive surface charge at a very low pH of 0–2 to both anionic and cationic latexes based on PMMA. A bulk nanocomposite blend was analyzed.

Voorn et al. heterocoagulated both anionic “hard” polystyrene and “soft” poly(*iso*-butyl methacrylate) latex particles onto large positively charged gibbsite clay platelets. The soft latex was allowed to spread and wet the surface of the clay platelets to form a more uniform layered film by curing at 80°C [25] (see Fig. 4). At low number ratios of latex particles to clay platelets (i.e., <180) multi-layered aggregates were formed. Increasing the amount of latex particles resulted in coverage of isolated clay particles. The use of small latex particles at low ionic strength proved beneficial to warrant overall colloidal stability [26].

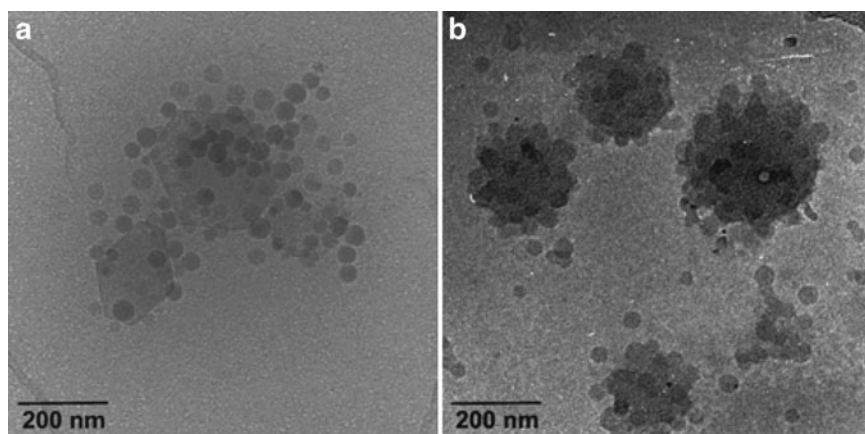


**Fig. 4** Cryo-TEM micrographs of cationic gibbsite with anionic poly(*iso*-butyl methacrylate) latex particles at different NaCl concentrations: (a)  $3.1 \times 10^{-4}$  M and (b)  $9.1 \times 10^{-4}$  M. The image is a reproduction of Fig. 8 from [25]

## 1.2 Hydrophobic Interactions

It is common knowledge that amphiphilic molecules, such as sodium dodecyl sulfate, above a certain critical concentration in water form assembled structures in which the hydrophobic units are clustered together. The notice of a “hydrophobic effect” was brought to light by Walter Kauzmann, whilst studying forces that influenced protein denaturation [27]. An excellent critical review on interfaces and the driving forces of hydrophobic assembly was written by Chandler in 2005 [28].

The hydrophobic effect is the tendency of nonpolar species to cluster in water in order to decrease the overall interfacial area between the hydrophobic species and water. It can be seen as predominantly driven by the large cohesive energy of water. Clustering of a set of individual hydrophobic particles into an agglomerate structure initially looks entropy driven. However, one should look at the overall change in free energy, and thus also at enthalpy. The latter is a measure of the average potential energy of interaction between molecules. Assembly processes that involve considerable changes in the number of molecular interactions, therefore could (also) be enthalpy driven.

There have been numerous attempts to define hydrophobic interactions, but there is no single one that can explain all experimental results [29]. In 1989, Eriksson [30] postulated that the long-range hydrophobic interactions (LRHFs) occurred due to structural changes on the boundary layers of water when in contact with hydrophobic surfaces. Attard [29] pointed out that the likely origin of the long-range hydrophobic forces is the formation of nanobubbles. Stillinger has suggested that the interface of liquid water near a large hydrophobic particle can be modeled analogously to a water–vapor interface [31].

Yaminsky et al. [32] evaluated theoretically a hydrophobic surface in water with a contact angle of more than  $90^\circ$  and concluded that the water–vapor cavity is thermodynamically favored at small separations.

The existence of such a hydrophobic “gap” between liquid water and the hydrophobic surface has been experimentally confirmed by, for example, Mezger and coworkers using high-resolution X-ray studies at the water–octadecyltrichlorosilane interface [33]. The reason is that the persistence of a hydrogen-bonded network of water molecules is geometrically impossible on a “large” (in excess of  $\sim 1$  nm) interface, and therefore leads to drying. This dewetting effect can lead to very strong interactions between hydrophobic objects, as seen for example in surface force measurements. When two hydrophobic objects approach each other, water is depleted from the region between the two objects [34].

These hydrophobic interactions are reported to be “long-range” commonly covering distances of 1–100 nm [35], greatly exceeding the interaction range of van der Waals forces. Singh and coworkers [36] investigated the hydrophobic effect between naturally occurring superhydrophobic rough surfaces (water contact angle of  $170^\circ$ ) beneath a water surface, using force measurements in which a superhydrophobic tip was placed in contact with a flat superhydrophobic substrate, both immersed in water, the tip being subsequently retracted. They found a very-long-range hydrophobic interaction that was due to out-of-contact “cavitation” of the intervening water at tip-to-substrate separations ranging from  $0.8\mu\text{m}$  to an impressive  $3.5\mu\text{m}$ . Cavitation is a first-order phase transition, which was the reason for the observed sudden, strong attractive force identified as a vapor bridge spanning the tip-to-substrate gap.

Nagai and coworkers reported a study of heterocoagulation driven by the hydrophobic effect of cationically charged “hard” poly[styrene-*co*-(methacryloyloxyphenyl-dimethylsulfonium methylsulfate)], or “soft” poly[styrene-*co*-(butyl acrylate)-*co*-(methacryloyloxyphenyl-dimethylsulfonium methylsulfate)] latex particles of ca. 220–240 nm in diameter onto neutral microspheres of crosslinked polystyrene ( $8.5\mu\text{m}$  in diameter) [37]. A separate study on the small cationic latex particles showed that their interface was hydrophobic, as the cationic surfactant cetyltrimethylammonium bromide (CTAB) adsorbed onto the surface, clearly driven by a hydrophobic effect [38]. The assembly of the cationic latex particles onto the larger microspheres was studied against increasing NaCl concentrations, which influenced the packing patterns from individually spaced to clusters (see Fig. 5).

### 1.2.1 Self-Assembly of Amphiphilic Particles Driven by the Hydrophobic Effect

An interesting “molecular” approach using the hydrophobic effect to assemble gold nanoparticles was taken by Zubarev and coworkers who attached V-shaped (twin-tailed) amphiphilic polystyrene-*block*-poly(ethylene oxide) with a central carboxylic acid moiety (which binds to the gold nanoparticle), effectively giving biphasic, Janus-type characteristics [39]. Self-assembly led to wormlike aggregates (see Fig. 6).



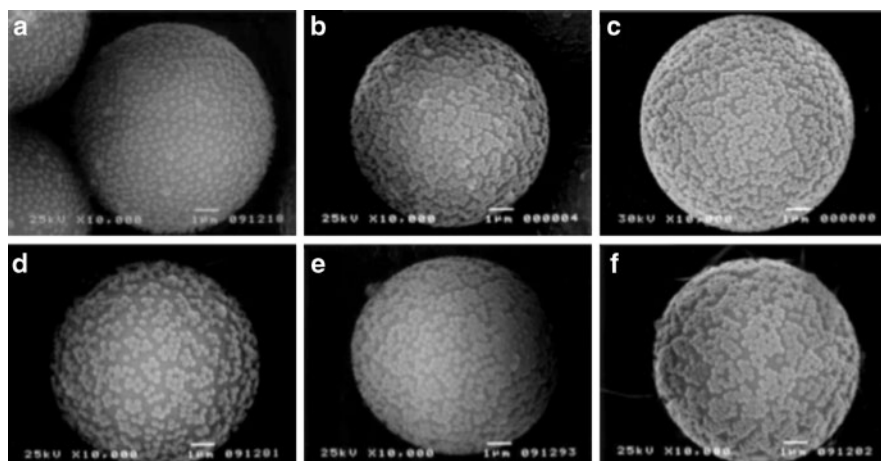


**Fig. 5** SEM photographs of cationic polymer latex particles heterocoagulated onto the surface of crosslinked polystyrene microspheres driven by the hydrophobic effect, against increasing NaCl concentrations. “Hard” poly[styrene-*co*-(methacryloyloxyphenyl-dimethylsulfonium methylsulfate)] particles at (a) 0.5, (b) 50, and (c) 200 mM of NaCl. “Soft” poly[styrene-*co*-(butyl acrylate)-*co*-(methacryloyloxyphenyl-dimethylsulfonium methylsulfate)] latex particles at (d) 0.5, (e) 50, and (f) 200 mM of NaCl

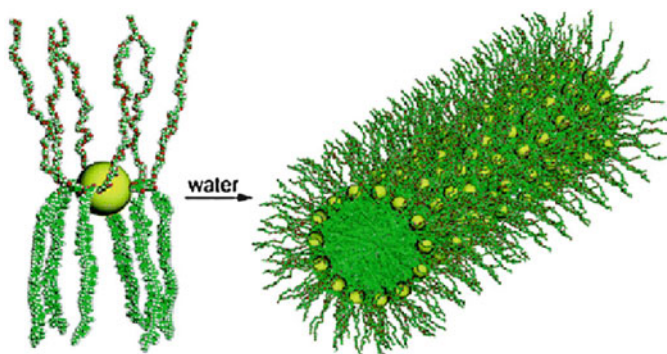


**Fig. 6** Representation of the amphiphilicity-driven self-assembly of Au-(PS-PEO)<sub>n</sub> nanoparticles (for simplicity reasons only six PS-PEO molecules are shown). This figure is a reproduction of Fig. 1A from [39]

Along this line of using amphiphilic features of particles to drive assembly using a hydrophobic effect, there has been a recent surge of interest in the fabrication and behavior of anisotropic “patchy” or Janus-type colloidal particles as a promising route to innovative nanocomposite materials [40, 41]. Whereas a thorough review lies outside our scope, we would like to highlight a few examples. Müller and coworkers prepared disc-like polymer Janus particles from assem-

bled films of polystyrene-*block*-poly(butadiene)-*block*-PMMA triblock copolymer (SBM) [42], selective crosslinking of the poly(butadiene) block, and dissolution via sonication, and then assembled them into supracolloidal Janus micelles. They revisited this in another paper and described the hydrolysis of the PMMA into poly(methacrylic acid) [43]. Again, assembly into supracolloidal micelles was driven by the hydrophobic effect. Chen and coworkers prepared polymeric Janus particles from divinylbenzene (DVB) and *N*-isopropylacrylamide (NIPAM) via an yttrium hydroxide nanotube (YNT)-supported route. On removal from their support, these asymmetric particles assembled into flower-like supracolloidal structures (see Fig. 7) [44].

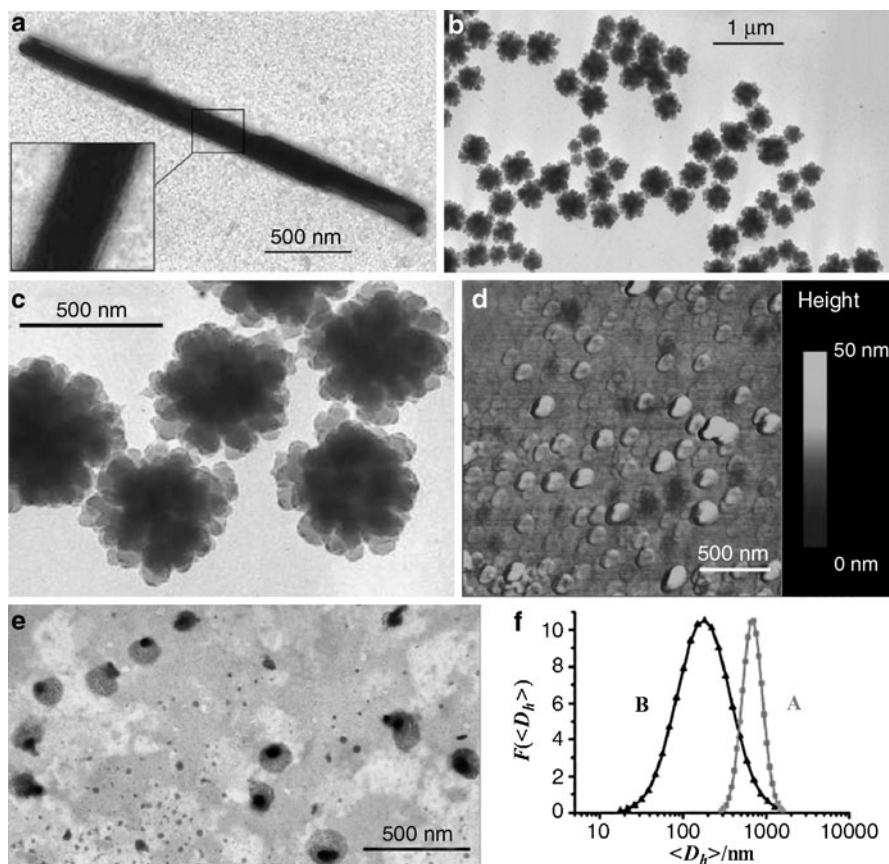


**Fig. 7** (a) TEM image of a hybrid nanotube. *Inset* at higher magnification shows the polymer layer surrounding the yttrium hydroxide nanotube (YNT). (b) TEM image of the supermicelles. (c) TEM image of the supermicelles at a larger magnification. (d) AFM image of petal-like (Janus) particles that result from the dissociation of the supermicelles on mica. (e) TEM image of the Janus particles stained with RuO<sub>4</sub>. (f) Distribution of the hydrodynamic diameter  $\langle D_h \rangle$  of the supermicelles (A) and the Janus particles (B). This figure is reproduced from Fig. 2 in [44]



Granick and coworkers studied, both experimentally and by Monte Carlo simulations, the assembly of amphiphilic colloidal microspheres into clusters [45]. Not only supracolloidal spherical micellar structures were observed, but also wormlike strings. Fluorescent carboxylated polystyrene microspheres were partially coated (hemisphere) with a thin gold layer, the latter subsequently being modified with octadecanethiol to promote a hydrophobic nature. The hemisphere with the free carboxylate groups was occasionally made more hydrophilic by grafting of DNA oligomers onto the surface of the microsphere. With increasing salt concentration ( $\text{KNO}_3$ ), a transition from unimers, spherical clusters, and wormlike strings was observed in both simulations and experiments.

Recently, Miller and Cacciuto explored the self-assembly of spherical amphiphilic particles using molecular dynamics simulations [46]. They found that, as well as spherical micellar-type structures and wormlike strings, also bilayers and faceted polyhedra were possible as supracolloidal structures. Whitelam and Bon [47] used computer simulations to investigate the self-assembly of Janus-like peanut-shaped nanoparticles and found phases of clusters, bilayers, and non-spherical and spherical micelles, in accordance with a packing parameter that is used conventionally and in analogy to predict the assembled structures for molecular surfactants. They also found faceted polyhedra, a structure not predicted by the packing parameter (see Fig. 8). In both studies, faceted polyhedra and bilayers coexist, a phenomenon that is still unexplained.

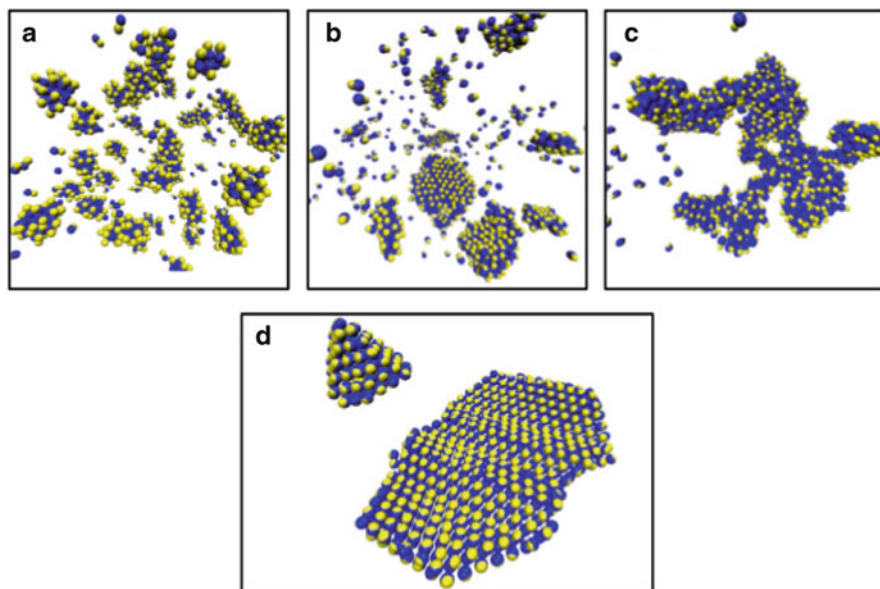


**Fig. 8** Various configurations for assembled peanut-shaped amphiphilic nanoparticles of variable particle geometry. (a) Micelles of various morphologies; (b) coexisting bilayers and micelles, (c) disordered wormlike micelle, and (d) coexisting polygon and bilayer. This figure is reproduced from Fig. 6 in [47]

### 1.3 Secondary Molecular Interactions

Beyond electrostatic and hydrophobic forces, the heterocoagulation process could be controlled by secondary molecular interactions. We will briefly highlight with some examples the hydrogen bonding,  $\pi$ - $\pi$  interactions, and specific molecular interactions obtained from complementary DNA strands, and biotin-avidin complexation.

#### 1.3.1 Hydrogen Bonding

Hydrogen bonding is one of the most common interactions that can aid the assembly process of colloidal particles. Hydrogen bonding is an attractive interaction of a hydrogen atom with an electronegative atom (typically oxygen, nitrogen, or fluorine) and, strengthwise, typically lies between van der Waals and ionic attractions. We restrict ourselves to mentioning some typical examples.

Armes and coworkers studied the preparation of polypyrrole particles in the presence of silica sols [48, 49]. Hydrogen bonding between the silica surface and the polypyrrole particles, in addition to electrostatic and hydrophobic interactions, led to raspberry-shaped nanocomposite colloids.

Yang and coworkers [50] assembled particles of poly(ethylene glycol dimethacrylate-*co*-acrylic acid) [poly(EGDMA-*co*-AA)] onto larger poly(ethylene glycol dimethacrylate-*co*-4-vinylpyridine) [poly(EGDMA-*co*-VPy)] microspheres to form a core-corona structure with a raspberry-like polymer composite. They used a hydrogen interaction mechanism through an affinity complex between the carboxylic acid group and pyridine group.

Li et al. [51] prepared monodisperse microspheres by distillation precipitation polymerization of DVB and NIPAM with 2,2-azobisisobutyronitrile (AIBN) as initiator in acetonitrile, in the absence of any surfactant. Next, latex particles of poly(EGDMA-*co*-AA) were assembled onto the microspheres to afford a core-corona composite polymer particle with a raspberry-like morphology, strengthened by hydrogen-bonding interaction.

#### 1.3.2 $\pi$ - $\pi$ Interactions

Li and coworkers [52] described the formation of supracolloidal balls with a mean diameter of  $148 \pm 5$  nm by self-assembly of  $\text{Fe}_3\text{O}_4$  nanoparticles ( $6.0 \pm 1.3$  nm) that were functionalized with 2-carboxyterthiophene (TTP-COOH). The driving force behind self-assembly in DMF was shown to be  $\pi$ - $\pi$  stacking of the thiophene units (see Fig. 9).

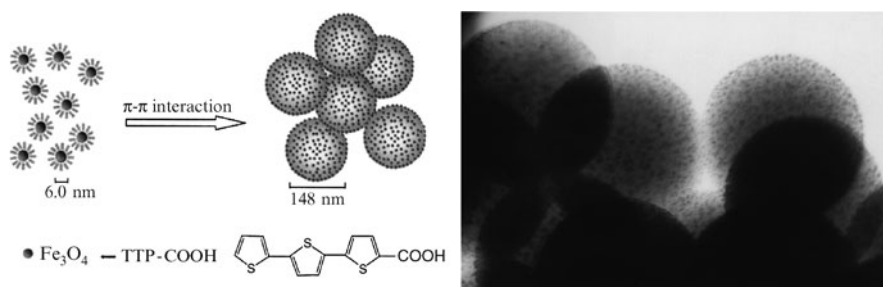


**Fig. 9** Structure model proposed for the self-assembly process of individual nanoparticles to form microspheres through  $\pi$ - $\pi$  interactions (*left*). The sizes of individual nanoparticles and microspheres can be determined directly from TEM images (*right*). Figure reproduced from Figs. 2 and 3 from [52]

### 1.3.3 Specific Recognition of Complementary DNA Strands

An interesting approach using specific multiple hydrogen-bond recognition is the functionalization of nanoparticles with DNA-based oligonucleotides. Mirkin and coworkers [53] functionalized two batches of Au colloids of 13 nm diameter dispersed in water with separate non-complimentary oligonucleotides, i.e., 3'-thiol-TTTGCTGA and 3'-thiol-TACCGTTG. Combination of the two separate functionalized gold nanoparticles led to a stable colloidal sol, the grafted oligonucleotides providing steric stabilization and thereby improving the stability of the sol to increasing temperature and/or electrolyte concentration. Aggregation of the gold nanoparticles was achieved by addition of a duplex consisting of 5'-ATGGCAACTATACGCGCTAG and 3'-ATATGCGCGATCTCAGCAA, containing eight-base-pair sticky ends, complementary to the gold sols.

Valignat [54] demonstrated that this powerful assembly method could be used to lock reversibly directed assembled (with optical tweezers) microspheres grafted with complementary polymer brushes into a prearranged suprastructure (see Fig. 10).

### 1.3.4 Avidin-Biotin Recognition

There are alternatives to complementary DNA strand recognition, for example the strong interaction between avidin (or its related streptavidin) and biotin. Avidin is a tetrametric glycoprotein that has the ability to interact strongly with up to four biotin units. Biotin, also known as vitamin H or B7, is a soluble B complex of ureido(tetrahydroimidazole) ring fused with a tetrahydrothiophene ring. The interaction between avidin and biotin is widely explored. An interesting example related to heterocoagulation of small polystyrene particles on larger silica microspheres was

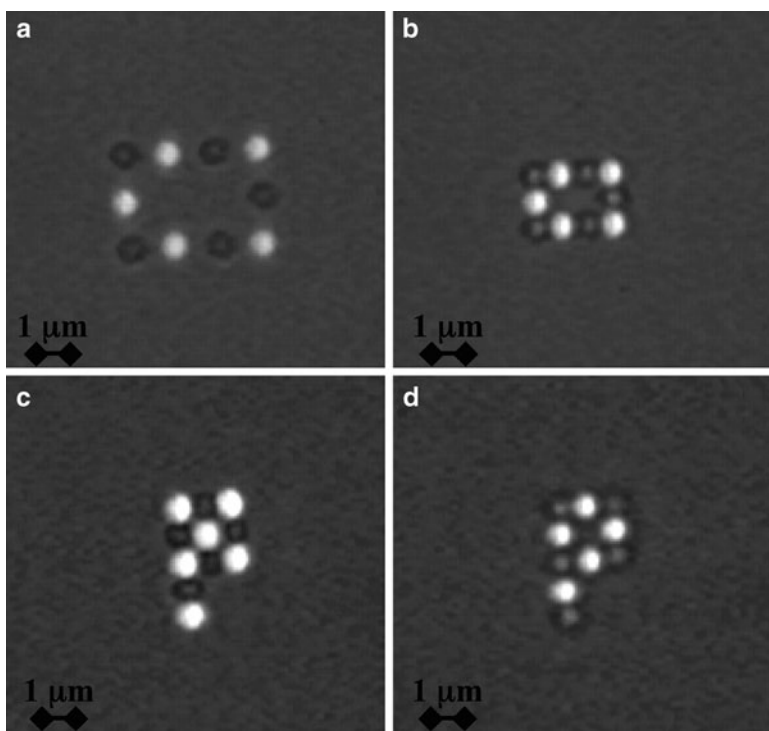


**Fig. 10** Directed assembly of particles. Fluorescent and nonfluorescent particles bear complementary strands of DNA. **(a)** Particles are first captured in discrete time-shared traps induced by laser tweezers. **(b–d)** Particles are moved in contact to promote hybridization between the DNA strands and form the following rigid structures: a rectangle **(b)**, a “full” P **(c)**, and an “empty” P **(d)**. This figure is reproduced from Fig. 4 in [54]

reported by Fleming and coworkers [55]. Amine-functionalized silica microspheres of 5  $\mu\text{m}$  diameter were either treated with biotin sulfosuccinimide ester, or reacted with avidin after activation of the silica spheres with glutaraldehyde. Biotin-labeled polystyrene particles of ca. 200 nm in diameter were made in a similar manner. However, avidin-labeled polystyrene particles were obtained by treatment of the biotin-labeled ones with excess amounts of avidin. Upon mixing the complementary colloids, strong adhesion of the polystyrene particles onto the surface of the silica spheres was observed. From earlier work by Chern [56], it should be noted that avidin is not able to induce flocculation of biotin-labeled particles (diameter  $\sim 549$  nm), because its size ( $\sim 4$  nm) is not large enough to bridge the overlapping double layers of the particles. The armored structure obtained by Fleming [57] is strengthened by the biotin–avidin interaction, although the heterocoagulation process itself is not induced by it.

## 2 Assembly of Nanoparticles onto Prefabricated Larger Particles via Repetitive Heterocoagulation: the Layer-by-Layer Technique

The layer-by-layer (LbL) technique for the assembly of nanoparticles onto a substrate can be seen as a repetitive extension of heterocoagulation. Driving forces for adhesion can in theory be based on the same interactions, i.e., electrostatic, hydrophobic, and secondary molecular interactions. For example, in the case of LbL assembly driven by electrostatic interactions, alternating layers of positively and negatively charged particles and/or (macro)molecules are deposited sequentially onto the underlying substrate, the latter obviously also undergoing surface charge-inversion in inverse alternating fashion [58]. Hydrogen bonding as a driving force to LbL self-assembly was investigated by Rubner et al. [59] and Zhang et al. [60, 61]. The LbL technique based on biotin–avidin recognition was described by Osa [62, 63].

The excess amount of material used is removed between steps. The LbL technique is easy to carry out and very versatile. Because of this, a great range of polyelectrolytes, biopolymers (proteins and nucleic acids), lipids, and inorganic particles have been used as building blocks in the preparation of multilayer composite films [64, 65], and in the fabrication of micro- and nanometer-sized capsules, the latter introduced in 1998 by Donath and Caruso [66–68].

Caruso et al. [69] reported the preparation of negatively charged polystyrene latex particles (640 nm diameter) armored with a nanocomposite multilayer of SiO<sub>2</sub> nanoparticles (Ludox TM-40;  $26 \pm 4$  nm diameter) and poly(diallyldimethylammonium chloride) (PDADMAC). These two components were sequentially adsorbed onto the surface of the polystyrene latex spheres (see Fig. 11), after adsorption of a precursor polyelectrolyte multilayer film of PDADMAC/

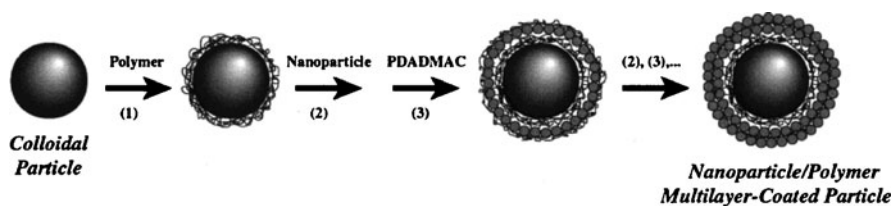


**Fig. 11** Preparation of multilayer-coated particles. The first stage involves the formation of a three-layer polyelectrolyte multilayer film [PDADMAC/poly(sodium 4-styrenesulfonate)/PDADMAC], formed by the sequential adsorption of PDADMAC and poly(sodium 4-styrenesulfonate) under conditions where they are oppositely charged (*step 1*). The outermost layer, PDADMAC, positively charged, aids the subsequent adsorption of negatively charged SiO<sub>2</sub> nanoparticles. SiO<sub>2</sub>/PDADMAC multilayer shells on the polystyrene latexes are then formed by the sequential adsorption of SiO<sub>2</sub> (*step 2*) and PDADMAC (*step 3*). Additional SiO<sub>2</sub> and PDADMAC cycles result in further growth of the multilayer shell thickness on the PS latexes. The excess/unadsorbed polyelectrolyte and nanoparticles are removed by a series of centrifugation/water wash/redispersion cycles before additional layers are deposited. Figure and legend taken from [69]

poly(sodium 4-styrenesulfonate)/PDADMAC, which provided a uniformly charged surface and facilitated subsequent  $\text{SiO}_2$  nanoparticle adsorption. The process was driven by electrostatic interactions. Using electrophoretic mobility (EPM) measurements, reversal of the  $\zeta$ -potential after each deposition step was shown. Single-particle light scattering (SPLS) measurements showed the linear increase of the particle dimensions upon increasing  $\text{SiO}_2$ /PDADMAC multilayer number. Electron microscopy showed the evidence of a stepwise multilayer growth, with TEM data yielding an average diameter increment of ca. 65 nm, corresponding to a layer thickness of approximately  $32 \pm 5$  nm for each  $\text{SiO}_2$ /PDADMAC layer pair. A similar approach was undertaken using nanoparticles of  $\text{Fe}_3\text{O}_4$  (diameter 10–15 nm) [69].

### 3 Assembly of Nanoparticles onto Emulsion Monomer Droplets and their Subsequent Polymerization

In the previous section, we have seen that “hard” inorganic nanoparticles can adhere onto the surface of polymer latex particles via a stochastic process of collisions, which was referred to as heterocoagulation. Once deposited onto the surface of the latex particles, the strength of adhesion governed by attractive forces such as electrostatic attraction, the hydrophobic effect, and hydrogen bond interactions needs to outbalance repulsive forces and the entropy gain achieved when nanoparticles detach. This potential detachment of nanoparticles from the surface of the polymer latex particle is typically induced by the thermal energy of the system,  $k_B T$  (where  $k_B$  is the Boltzmann constant and  $T$  is temperature).

What happens if we replace the polymer latex particle with a monomer droplet onto which we had first assembled the “hard” nanoparticles and then polymerized the now-armored droplet?

#### 3.1 *Pickering Stabilization: Adhesion of Particles to “Soft” Interfaces*

The phenomenon whereby solid particles adhere onto an emulsion droplet (i.e., a liquid–liquid interface) was first observed and reported by Ramsden [70] and Pickering [71] in the 1900s. They found that these emulsion droplets were stable against coalescence, because the adhered solid particles effectively provided a barrier. Emulsions stabilized by adhered solid particles were coined Pickering emulsions [72, 73]. Hildebrand et al. [74] suggested that the reason the particles place themselves in the liquid–liquid interface is that they partially wet the two liquid phases. In line with the Bancroft rule for emulsification, which links whether a water-in-oil or oil-in-water emulsion is preferred for a certain type of emulsifying agent, the authors suggested that the type of emulsion produced by a solid powder

is determined by the contact angle between the solid and the liquid–liquid interface: “In order for the powder to remain in the interface the angle must be finite, and unless the angle is  $90^\circ$ , the interface will be on one side or the other of the points of contact of the particles, and its tension will cause the film to be concave on that side” [74].

The observations by Ramsden and Pickering that emulsion droplets armored with solid particles were “stable” against coalescence suggests that the particles are in essence trapped and cannot leave the interface to re-enter one of the two liquid phases.

### 3.1.1 Interaction of a Single Spherical Particle with a “Soft” Interface

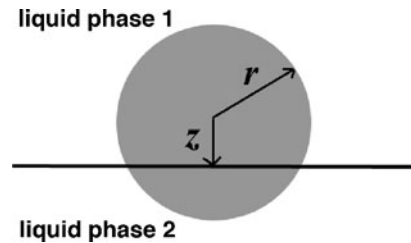
Pieranski [75] developed a simple macroscopic model to calculate the free energy as a function of the position of a spherical particle with respect to the “soft” liquid–liquid (or, as was the case in his manuscript, a liquid–air interface). In this macroscopic continuous model, three interfacial energy ( $E$ ) contributions can be derived as the product of the interfacial tension and the respective contact areas (see Fig. 12 for illustration of  $r$  and  $z$ ):

$$\begin{aligned} E_{p1} &= \gamma_{p1} 2\pi r^2 \left(1 + \frac{z}{r}\right) \\ E_{p2} &= \gamma_{p2} 2\pi r^2 \left(1 - \frac{z}{r}\right) \\ E_{12} &= -\gamma_{12} \pi r^2 \left(1 - \left(\frac{z}{r}\right)^2\right) \end{aligned}$$

$\gamma_{p1}$ ,  $\gamma_{p2}$ , and  $\gamma_{12}$  are the interfacial tensions between the particle and liquid phase 1, the particle and liquid phase 2, and the two liquid interfaces. When we define the following dimensionless numbers:

$$z_0 = \frac{z}{r}; \sigma_1 = \frac{\gamma_{p1}}{\gamma_{12}}; \sigma_2 = \frac{\gamma_{p2}}{\gamma_{12}}; E_0 = \frac{E_{p1} + E_{p2} + E_{12}}{k_B T}$$

**Fig. 12** Interaction of a sphere with a liquid–liquid interface on a macroscopic scale and in a continuous fashion.  $r$  radius of the sphere;  $z$  distance from the centre of the sphere to the interface



we find for the relative free energy  $E_0$ :

$$E_0 = \left[ \frac{\gamma_{12}\pi r^2}{k_B T} \right] (z_0^2 + 2(\sigma_1 - \sigma_2)z_0 + 2\sigma_1 + 2\sigma_2 - 1)$$

The equilibrium position for the particle can easily be found from:

$$\begin{aligned} \frac{dE_0}{dz_0} &= 2z_0 + 2(\sigma_1 - \sigma_2) = 0 \\ z_0^{\min} &= \sigma_2 - \sigma_1 \end{aligned}$$

For values of  $z_0^{\min}$  between  $-1$  and  $1$ , the particle adheres to the liquid–liquid interface. The energy it will take to remove the particle from the interface into either the bulk of phase 1 or phase 2 can easily be obtained from:

$$\begin{aligned} \Delta E_1 &= E_0(z_0 = 1) - E_0(z_0^{\min}) \\ \Delta E_2 &= E_0(z_0 = -1) - E_0(z_0^{\min}) \end{aligned}$$

Whereas this model gives a good feel for the order of magnitude of the energy well in which the particles are trapped, it is rather crude and thus a simplification of reality. It does ignore surface charges (chemical heterogeneity of the surface, or “patchiness”) and potential morphological surface roughness of the spherical particle, and as previously mentioned it assumes absence of external fields (such as gravity), or flow. A problem also ignored is the three-phase interaction at the contact line between the two liquids and the particle. Gibbs already suggested qualitatively that this three-phase contact line should be treated as a one-dimensional “line tension”, in analogy with the two-dimensional surface tension between the interphase of two bulk phases. An expression for the free energy as a function of particle–interface separation for a spherical particle of radius  $R$ , extended to account for line tension ( $\tau$ ), was given by Aveyard and Clint [76], in which they basically added one extra term to the Pieranski equation:

$$E_0 = \left[ \frac{\gamma_{12}\pi r^2}{k_B T} \right] (z_0^2 + 2(\sigma_1 - \sigma_2)z_0 + 2\sigma_1 + 2\sigma_2 - 1) + \frac{2\pi r\tau}{k_B T} \sqrt{(1 - z_0^2)}$$

As can be seen from this expression, the effect of line tension becomes increasingly important for smaller spherical particles as it scales linearly with the radius of the particle, whereas contributions arising from interfacial tensions scale quadratically. A debate on experimentally realistic values of line tension is ongoing, especially when the spherical particles become of nanoscale dimensions and line tension may become important.



One key question that remains is what is the validity of these macroscopic models when we scale the size of our spherical particle down to nanoscale dimensions? The liquid–liquid interface can no longer be modeled as flat (capillary waves need to be considered), and additional small-scale effects, such as discrete rather than continuous wetting of the spherical nanoparticle by the liquid molecules, need to be taken into account. Can this be reflected in line tension?

Cheung and Bon [77] used molecular simulations to investigate the behavior of a non-charged nanoparticle in proximity and adhered to an ideal liquid–liquid interface. In the model, a two-component Widom-Rowlinson (WR) fluid [78] was used to generate the two phase-separated bulk liquids and the corresponding soft interface, thereby neglecting electrostatic and attractive van der Waals forces. Calculated free energy profiles as function of the distance of the nanoparticle from the soft liquid–liquid interface confirmed that macroscopic models, such as the Pieranski model [75], gave a poor description of the energy well. The energy well was considerably wider, and thus the distance of interaction greater, between the particle and the interface. The reason for this is most probably due to the existence of capillary waves (the liquid–liquid interface can no longer be considered flat). Moreover, the smaller the nanoparticle, the larger the underestimation of the depth of the energy well by the Pieranski model, with deviations of up to 50%. The binding energy was found to increase quadratically with the radius of the nanoparticle, with an additional linear dependency (which could plausibly be seen as line tension). The overall good news from these simulations is that nanoparticles adhere considerably stronger to, and are trapped over a longer range by, the liquid–liquid interface than predicted by macroscopic models.

A question often asked is whether the parabolic energy wells as predicted by Pieranski have an activation barrier that prevents the particle from “falling” in spontaneously. One can argue that, especially for a large spherical particle, upon its approach to the soft interface, the interface needs to deform and liquid has to drain. This event adds an activation barrier that needs to be overcome for the particle not to bounce off the interface, and clearly the interfacial tension between the two soft bulk phases (liquid–liquid and liquid–air) and the viscosity of both phases play key roles. Note that a potential hydrophobic effect [28] can counterbalance such a barrier because the dewetting of the liquid between a hydrophobic particle and the hydrophobic liquid phase, or air, stimulates long-range attraction and eases the adhesion process.

Obviously one also should take into account the shape of the particle, as often the particles used will differ from spheres. This can clearly have dramatic effects on where and how the particle adheres to the interface when it tries to minimize energy from interfacial as well as line tensions. The three-point contact angle needs to be constant, which means that the contact line must undergo curvature in order to accommodate this. This has a pronounced influence on the interaction (of a long-range nature) between adhered particles on the surface. An in-depth discussion lies outside the scope of this review, but the interested reader is referred to (as a starting point) work by Vermant and coworkers [79, 80].

### 3.1.2 Droplets Armored with a Layer of Adhered Particles

The above discussion only considers the existence of a single isolated particle on a liquid–liquid interface. Experimentally, however, the number of nanoparticles adhered to a single monomer droplet or growing polymer particle will be greater than unity. This means that particle–particle interactions, both attractive and/or repulsive in nature, need to be taken into account. An elegant example confirming the existence of attractive particle–particle interactions can be found in work reported by Russell and coworkers [81]. They prepared a dispersion of 2.8 nm (diameter) tri-*n*-octylphosphine (TOPO)-covered cadmium selenide (CdSe) nanoparticles in toluene. Upon introduction of a water droplet, the nanoparticles organized themselves onto the toluene–water interface. Introduction of 4.6 nm (diameter) CdSe nanoparticles led to displacement of the smaller ones from the liquid–liquid interface. A clear phase-separation was seen on the surface of the water droplet, showing distinct regions of the 2.8 and 4.6 nm CdSe nanoparticles, respectively.

When particles of a narrow particle size distribution (monodisperse) adhere to the interface of a spherical droplet, 2D crystallization can occur. As a direct result of the curved surface of the droplet, packing into infinite hexagonal 2D arrays is no longer possible. The determination of the packing geometry is often referred to as the Thomson problem [82], generalized by Tammes. In short, there are 12 packing defects, either in the form of point dislocations or grain boundary scars (the latter for large droplets, which have a greater number of particles on the surface). Bausch et al. [83, 84] showed that for large droplets onto which thousands of microspheres were assembled, this rule of 12 defects prevailed in the form of five- and seven-neighbor line defects, or grain boundary scars. Bon and coworkers [85] studied a system of intermediate size (tens to hundreds of particles on a sphere), i.e., the packing patterns of silica nanoparticles on polystyrene latex particles made via Pickering miniemulsion polymerization [86, 87]. They found an excellent correlation between the experimental morphology and the nearest-neighbor distribution using metropolis Monte Carlo simulations, using a 12–24 Lennard–Jones potential. Moreover, they addressed the effect of the polydispersity of the nanoparticles used in preparing the armored droplets. They found that upon broadening of the particle size distribution, the packing geometry could no longer be described in terms of 12-point dislocations or grain boundary scars [85].

## 3.2 *Polymerization of Emulsion Droplets Armored with Inorganic Nanoparticles: Pickering Suspension and Miniemulsion Polymerization*

We have seen from the above discussion that solid particles can adhere to a “soft” interface, and thus to monomer droplets. The effect of Pickering stabilization protects the droplets from coalescence. The use of solid particles as stabilizers in emulsion-based polymerization techniques was first described in open literature by

Hohenstein [88, 89] for suspension polymerizations in the 1940s. Winslow and Martreyek [90] investigated the influence of both solid inorganic particles such as bentonite and  $\text{Ca}_3(\text{PO})_4$  and organic stabilizers on the suspension polymerization of mixtures of DVB with ethylvinylbenzene. Wiley [91], in 1954, showed that monomer droplets of styrene dispersed in water in the presence of Dowex-50 ion-exchange resin beads or bentonite clay led to adhesion of the solid particles onto the surface of the droplets. The Pickering-stabilized droplets underwent so-called limited coalescence, a process that after a certain time period effectively yielded a stable set of solids-armored liquid droplets. Pickering stabilization could be promoted upon addition of, for example, gelatin and/or inorganic salts. Assuming monolayer adsorption of the colloid onto the surface of the monomer liquid droplets, Wiley was able to predict the average droplet size by assuming cubic (square) packing of spherical solid particles onto a spherical monomer droplet. This yielded the following equation, after a slight addition from Bon et al. to account for coverage:

$$R_{\text{mon}} = C\pi \left( \frac{m_{\text{mon}}}{m_{\text{part}}} \right) \left( \frac{\rho_{\text{part}}}{\rho_{\text{mon}}} \right) R_{\text{part}}$$

in which  $R_{\text{mon}}$  is the radius of the monomer droplet,  $R_{\text{part}}$  the radius of the spherical Pickering stabilizer,  $C$  accounts for coverage (for full monolayer coverage following 2D square or cubic packing  $C = 1$ ), and  $m$  and  $\rho$  stand for the masses and densities, respectively.

In suspension polymerization, inorganic solids such as hydroxyapatite [ $3 \text{ Ca}_3(\text{PO}_4)_2 \cdot \text{Ca}(\text{OH})_2$ ] are often used in conjunction with (polymeric) surfactants. Deslandes [92] reported in 1987 a study in which he investigated the morphology of the beads obtained in the suspension copolymerization of styrene and butadiene. A thin layer composed of very uniformly distributed hydroxyapatite particles was adhered to the surface of the polymer bead, and surrounded by a thicker and flakier layer of loosely packed agglomerates of hydroxyapatite and small polymer beads, which were also covered by a monolayer of inorganic matter. Despite this paper, studies on the use of solid particles in suspension polymerization remained focused on their effective use as stabilizers.

A shift of interest in the area of Pickering suspension polymerization towards the morphologies of the polymerized emulsion droplets was reported by Bon and coworkers [93–96]. They demonstrated that microgels of poly(methyl methacrylate-*co*-divinylbenzene) could be used to stabilize emulsion droplets composed of various monomers, i.e., styrene, DVB, and *n*-butylacrylate [93]. A substantial amount of hexadecane was added as porogen. Upon Pickering suspension polymerization, the in situ generated polymer phase separated towards the interface and formed an interpenetrating network with the microgel particles. A variety of microcapsules with a raspberry-type morphology were synthesized. They showed the fabrication of  $\text{TiO}_2$  nanoparticle (ca. 150 nm in diameter) armored microspheres and capsules made via Pickering suspension polymerization of styrene and DVB. For the capsules hexadecane was used as non-solvent for the polymer [95]. Upon polymerization, the polymer phase-separated at the interface of the

droplet. The average size of the capsules could be varied by altering the amount of  $\text{TiO}_2$  nanoparticles. The polymer wall thickness could be controlled by variation of the monomer to hexadecane ratio. They also reported on the fabrication of complex silica-based microcapsules via a two-stage templating route [97] in which nanocomposite polystyrene latex particles armored with Laponite clay discs (made via Pickering miniemulsion polymerization) were used as Pickering stabilizer of emulsion droplets containing poly(diethoxysilane) and oil. Upon hydrolysis and sol-gel reaction of the poly(diethoxysilane), hollow capsules were obtained. The organic components could be removed via an additional calcination step. The capsule walls could be decorated on either the outside or inside with nanocapsules composed of Laponite clay.

A variety of other nanoparticles have been used in Pickering suspension polymerizations, including magnetic  $\text{Fe}_3\text{O}_4$  [98–100] and CdS nanoparticles stabilized by poly(ethylene glycol-*block*-styrene-*block*-2-(dimethylamino) ethyl methacrylate) [101].

Wu and coworkers [102] reported on the inverse Pickering suspension polymerization of N-isopropyl acrylamide (NIPAM). They used various sizes of silica particles, ranging from 53 to 962 nm in diameter, as solids stabilizer. Suspension polymerizations were successful for the silica particles of diameter <500 nm. Similar work was reported by Wang and coworkers. [103].

Bon and Kumacheva and coworkers [104] demonstrated that monodisperse solids-stabilized droplets could be generated in a microfluidic flow focusing device, whereby the solid particles were initially present in the dispersed phase. Polymerization of the monomer droplets led to hybrid polymer microspheres. They also showed that non-spherical particles could be obtained by geometric confinement of the droplets in the channel [104, 105].

A logical extension from Pickering suspension polymerization would be to miniaturize the size of the droplets into the regime of miniemulsion polymerization. Landfester and coworkers [106] described miniemulsion copolymerizations of styrene with 4-vinylpyridine in presence of Ludox TMA silica nanoparticles. The use of 4-vinylpyridine was required to warrant the fabrication of armored latex particles. Bon and coworkers [87] described the Pickering miniemulsion polymerization of styrene using Laponite RD clay discs as solids stabilizer in the absence of any auxiliary comonomer or surfactant. In a detailed mechanistic study [86], they reported that this Pickering miniemulsion polymerization using Laponite clay discs (ca. 25 nm in diameter and 1 nm in height) was successful and yielded armored polymer latexes for a variety of hydrophobic monomers, including styrene, lauryl(meth)acrylate, butyl(meth)acrylate, octylacrylate, and 2 ethylhexylacrylate. Studying the polymerization rates, they found a pronounced retardation effect up to intermediate conversion, which was more prominent for smaller particles. A model was presented that allowed for prediction of the average particle sizes of the latexes produced as function of the amounts of monomer and clay discs used. A linear relationship between the number of clay discs used and the total surface area of the latex particles was shown. Key herein was that the sonication process to prepare the armored miniemulsion droplets warranted reversible adhesion of the Laponite

clay discs throughout the emulsification step. Bon and coworkers [85] also performed Pickering miniemulsion polymerizations of styrene using spherical silica nanoparticles of approximately 25 nm in diameter (Ludox TM-40), in which the packing arrangements of the silica nanoparticles on the surface were investigated and modeled with the aid of Monte Carlo simulations. Zhang and coworkers used organically modified silica nanoparticles to carry out a Pickering miniemulsion polymerization of styrene [107]. The co-use of sodium dodecyl sulfate (SDS) and 2-(methacryloyl) ethyltrimethylammonium chloride (MTC) as auxiliary monomer was also reported in the Pickering miniemulsion polymerization of styrene stabilized by silica nanoparticles [108].

Bon, Keddy, and coworkers [109] demonstrated that “soft” armored polymer latex made via Pickering miniemulsion polymerization [i.e., poly(lauryl acrylate) armored with Laponite clay discs] could be used as a nanocomposite additive in standard poly(butyl acrylate-*co*-acrylic acid) waterborne pressure-sensitive adhesives (PSAs), leading to marked mechanical property enhancements (see Fig. 13).

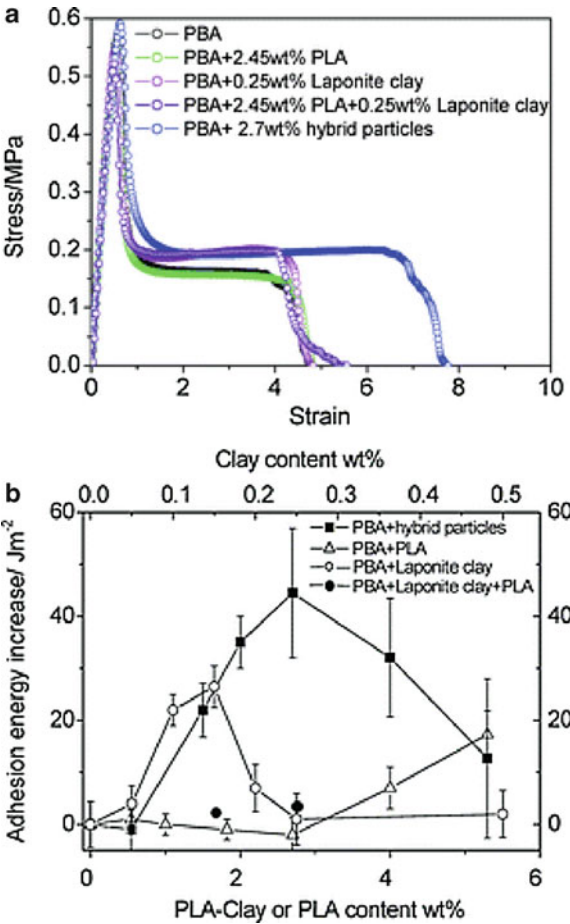


**Fig. 13** (a) Comparison of the probe-tack stress–strain curves for the model PBA adhesive in the presence of 2.7 wt% clay-armored soft–hard hybrid particles with the equivalent amount of non-armored PLA (2.45 wt%), Laponite clay discs (0.25 wt%), and a blend of non-armored PLA (2.45 wt%) and Laponite clay (0.25 wt%). (b) Synergistic effect of PLA–nanoclay hybrid particles on the tack energy of the model PSA. The increase in the tack energy above PBA is given as a function of the nanofiller content. Figure and legend are taken from [109]

A maximum tack energy enhancement of  $45\text{Jm}^{-2}$  was found in nanocomposite PSAs containing 2.7 wt% hybrid particles, which was about 70% greater than found for the PBA adhesive alone. In comparison, the tack energy for nanocomposites containing an equivalent amount of non-armored PLA, Laponite clay discs, or both did not lead to increases of the same magnitude, therefore showing a synergistic effect as a direct result of the supracolloidal armored structure of the clay poly(lauryl acrylate) additive.

Voorn and coworkers demonstrated the inverse Pickering miniemulsion polymerization of aqueous acrylamide and 2-hydroxyethyl methacrylate in cyclohexane using hydrophobically modified Montmorillonite platelets (cloisite 20A) as solids stabilizer [110].

#### **4 Assembly of Nanoparticles onto the Surface of Polymer Colloids Throughout Emulsion Polymerization: Solids-Stabilized, or Pickering, Emulsion Polymerization**

The use of a high-energy homogenization step to prepare the submicrometer-sized monomer droplets for the Pickering miniemulsion process could be a drawback for industrial scale-up. A better outcome could be achieved by the equivalent emulsion polymerization process in which solid nanoparticles were used as solids stabilizer.

Müller and coworkers prepared disc-like polymer Janus particles from assembled films of the triblock copolymer SBM and, after hydrolysis of the ester groups into methacrylic acid units, used these as Pickering stabilizer in the soap-free emulsion polymerization of styrene and butyl acrylate [111]. Armes and coworkers described the synthesis of PMMA/silica nanocomposite particles in aqueous alcoholic media using silica nanoparticles as stabilizer [112], extending this method to operate in water with a glycerol-modified silica sol [113, 114]. Sacanna showed that methacryloxypropyltrimethoxysilane [115] in the presence of nanosized silica led to spontaneous emulsification in water, which upon a two-step polymerization procedure afforded armored particles with an outer shell of PMMA [116]. Bon and coworkers demonstrated the preparation of armored hybrid polymer latex particles via emulsion polymerization of methyl methacrylate and ethyl methacrylate stabilized by unmodified silica nanoparticles (Ludox TM-40) [117]. Performance of an additional conventional seeded emulsion polymerization step provided a straightforward route to more complex multilayered nanocomposite polymer colloids (see Fig. 14).

The use of either styrene or butyl methacrylate as monomer led to stable latexes that were not covered by silica particles. Bon and coworkers proposed a mechanism for the solids-stabilized, or Pickering, emulsion polymerization that effectively combines coagulative nucleation with heterocoagulation throughout the polymerization process. The growing latex particles become unstable and collide irreversibly with the nanoparticles that are dispersed in the water phase. The key to successful polymerization is that this collision process is fast with respect to the timescales of particle nucleation and growth.

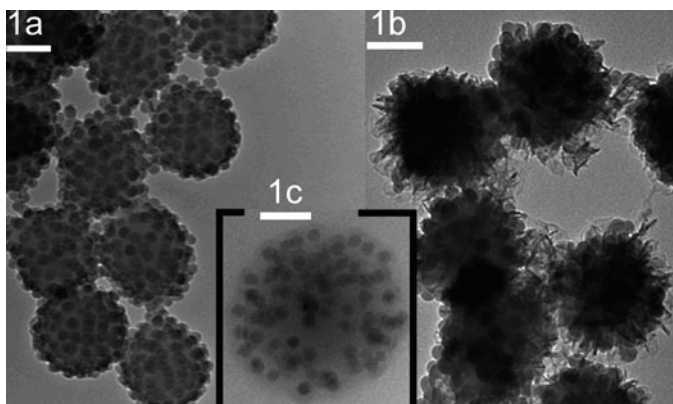


**Fig. 14** TEM images of (a) PMMA latex armored with silica nanoparticles obtained by Pickering emulsion polymerization. Multilayered nanocomposite polymer colloids with (b) a “hairy” outer-layer of poly(acrylonitrile) and (c) a soft shell of poly(*n*-butyl acrylate). Scale bars: 100 nm. Figure and legend are taken from [117]

Wu and coworkers studied the silica-nanoparticle-stabilized emulsion polymerization of vinyl acetate, with the aid of a small amount of anionic reactive surfactant, 3-allyloxy-2-hydroxy-1-propanesulfonic acid sodium salt (HAPS) [118]. They argued that hydrogen bond interactions allowed for strong adhesion, and also commented on the mechanism of solids-stabilized emulsion polymerization.

Bon and coworkers carried out a study on the fate of the nanoparticles throughout solids-stabilized emulsion polymerization [119]. A quantitative method based on disk centrifugation was developed to monitor the amount of nanoparticles present in the water phase in solids-stabilized emulsion polymerizations of vinyl acetate, methyl methacrylate, and butyl acrylate. The concentration profile of nanoparticles in the water phase as a function of monomer conversion agreed with theoretical models developed for the packing densities in these systems [120]. Noteworthy was that in the case of silica-nanoparticle-stabilized emulsion polymerization of vinyl acetate, the event of late-stage limited coalescence, leading to small armored non-spherical clusters, could be predicted and explained on the basis of the concentration profiles and particle size measurements. Adjusting the amount of silica nanoparticles prevented this phenomenon.

Ma and Dai [121] reported the synthesis of polystyrene latexes armored with silica nanoparticles (10–15 nm in diameter, PA-ST silica sol, Nissan Chemicals) via solids-stabilized emulsion polymerization. They used VA-086, 2,2'-azobis[2-methyl-*N*-(2-hydroxyethyl)propionamide], as nonionic initiator. Whereas we found that Pickering emulsion polymerization of styrene using Ludox TM-40 and a low flux of radicals generated from potassium persulfate did not result in an armored latex, the hydroxyethyl groups probably enhance the wettability of the surface of the latex particles to promote silica adhesion. This was confirmed by a



study undertaken by Bourgeat-Lami [122], who showed that poly(ethylene glycol) monomethylether methacrylate (PEGMA) macromonomer aided the adhesion of silica nanoparticles in the surfactant-free solids-stabilized emulsion polymerization of styrene. They also noticed a reduced overall rate of polymerization due to the presence of the nanoparticles on the surface of the growing latex particles, which was earlier observed by Bon and Colver [123] in Pickering miniemulsion polymerizations. Similar results of reduced polymerization rates were reported by Zhang and coworkers, who studied the silica-nanoparticle-stabilized emulsion polymerization of methyl methacrylate in presence of hydroxyethyl methacrylate [124]. Song and coworkers performed photocatalytic emulsion copolymerizations of styrene and EGDMA with auxiliary monomers of acrylic acid or sodium styrene sulfonate, and in the presence of a cationic titania hydrosol. They found that the auxiliary monomers greatly promoted adhesion of the titania nanoparticles onto the polymer latexes [125, 126].

## 5 Hybrid Polymer Colloids Through Assembly of Colloidal Building Blocks via Interface-Driven Templating

Mixtures of polymer latexes and inorganic colloids can be assembled into supracolloidal clusters with controlled spatial organization of the particles via geometric or interfacial-energy-driven confinement.

Pine and coworkers [127] confined particles to the interface of emulsion droplets, after which the fluid was evaporated, leading to specific packing arrangements that depended on the original number of spheres per liquid droplet (see Fig. 15). Clusters of colloidal spheres included doublets, triangles, tetrahedral and more exotic polyhedra. This was extended using various combinations of two different colloids with several size ratios in water-in-oil emulsions: monodisperse silica or polystyrene microspheres for larger particles, and silica or titania nanoparticles for smaller particles. Not only the size but also the adhesion behavior of the individual colloids at the water-oil interface played an important role. Packing predictions were carried out with Surface Evolver and corresponded to the experimentally observed structures [128]. A third paper addressed formation of composite colloids in toluene-in-water emulsions in which polystyrene was added as macromolecular glue [129].

Lee and Weitz showed that confinement of particles in the middle phase of double emulsion droplets and subsequent evaporation of this phase led to nanoparticle supracolloidal capsules [130], also referred to as colloidosomes [131].

Velegol used a so-called particle lithography technique in which colloids were deposited on a flat solid surface, after which heterocoagulation of macromolecules and or particles could take place on the exposed areas [132–135]. Anisotropic assemblies of colloids can be manufactured via this route.

Xia and coworkers demonstrated the assembly of colloids into well-defined clusters by dewetting of aqueous dispersions of monodisperse particles across surfaces patterned with two-dimensional arrays of templates or relief structures [136].



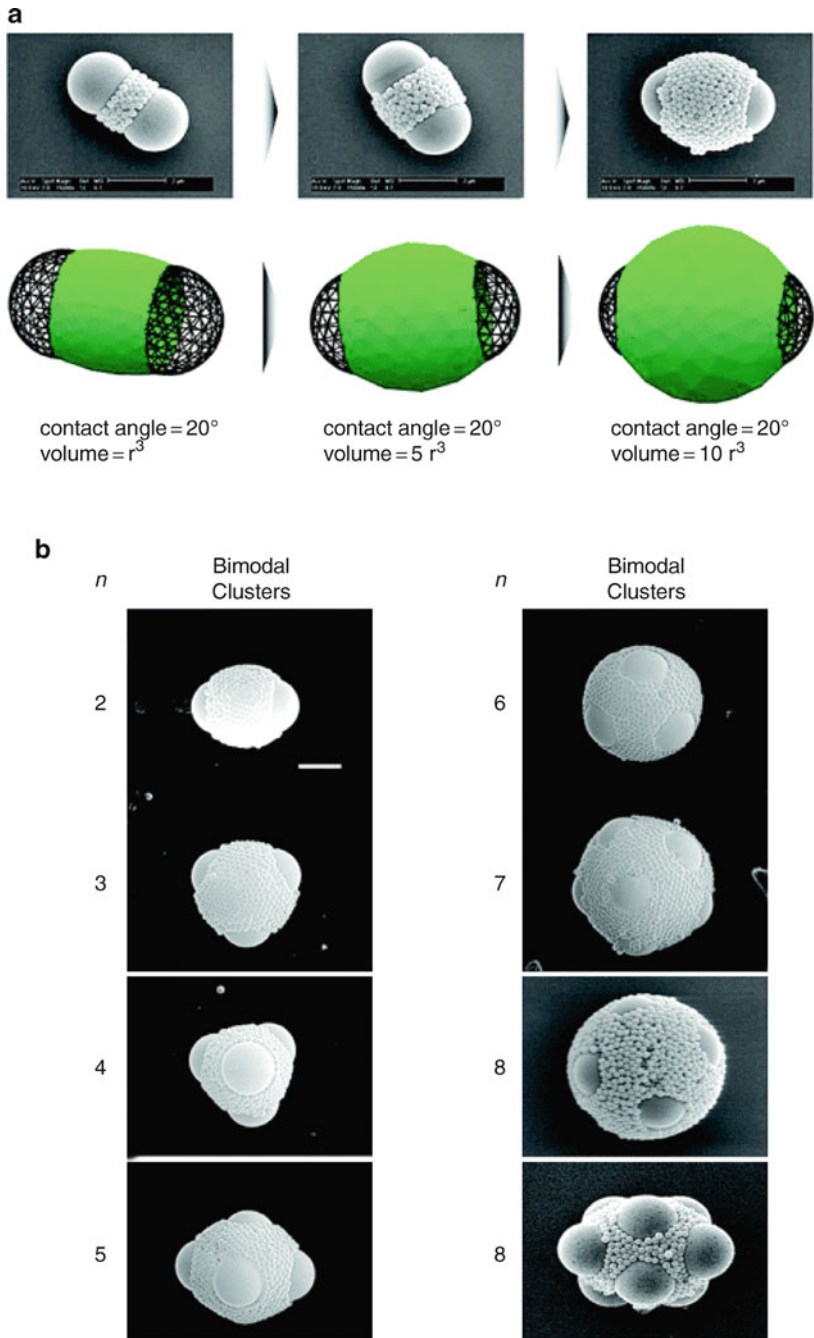


**Fig. 15** (a) *Top*: SEM images for the structural evolution of bimodal colloidal clusters of silica microspheres and nanospheres for  $n = 2$ . *Bottom*: Surface Evolver simulated structural evolution for  $n = 2$  as a function of the amount of silica nanospheres. (b) SEM images of silica–silica composite clusters for  $n = 2 - 8$ . Scale bar:  $2\mu\text{m}$ . The size ratio of large and small silica particles was fixed at 10. Figure and legend are taken from Fig. 3 from [128]

## 6 Outlook

We have seen in this review that there are a vast array of physical methods that we can make use of in the design of nanocomposite polymer colloids. The classical approach of heterocoagulation can undergo a renaissance by exploring driving forces such as the hydrophobic effect and secondary molecular interactions. Self-assembly of complex anisotropic colloidal particles is already creating a whole new direction in the fabrication of supracolloidal structures.

The behavior of nanoparticles at soft interfaces and their ability to adhere to these strongly has great potential for further studies, especially in the area of solids-stabilized emulsion polymerization. The ability to control and understand mechanistically this process will allow the design of innovative hybrid polymer colloids.

Creative methods of templating, whether in droplets or on hard patterned surfaces, together with advances in lithography and colloid visualization methods, will also contribute greatly to a wealth of innovative supracolloidal structures.

## References

1. Derjaguin BV (1954) A theory of the heterocoagulation, interaction and adhesion of dissimilar particles in solutions of electrolytes. *Discuss Faraday Soc* 18:85–98
2. Jachowicz J, Berthiaume MD (1989) Heterocoagulation of silicon emulsions on keratin fibers. *J Colloid Interface Sci* 133(1):118–134
3. Derjaguin BV, Landau L (1941) Theory of stability of strongly charged lyophobic sols of the adhesion of strongly charged particles in solution electrolytes. *Acta Physicochim USSR* 14:633–662
4. Verwey EJW, Overbeek JTG (1948) *Theory of the stability of lyophobic colloids*. Elsevier, Amsterdam
5. Hamaker HC (1937) The London-van der Waals attraction between spherical particles. *Phys Rev Lett* 4:1058
6. Visser J (1972) Hamaker constants. comparison between Hamaker constants and Lifshitz-van der Waals constants. *Adv Colloid Interface Sci* 3: 331
7. Hogg R, Healy TW, Fuerstenau DW (1966) Mutual coagulation of colloidal dispersions. *Trans Faraday Soc* 62:1638
8. Barouch E, Matijevic E, Wright TH (1985) Double-layer interactions of unlike spheres. Part 2. Numerical analysis of electrostatic interaction energy. *J Chem Soc Faraday Trans* 81(1): 1819–1832
9. Bleier A, Matijevic E (1976) Heterocoagulation. I. Interactions of monodispersed chromium hydroxide with polyvinyl chloride latex. *J Colloid Interface Sci* 55(3):510–524
10. Luckham PF, Vincent B, McMahon J, Tadros TF (1983) The controlled flocculation of particulate dispersions using small particles of opposite charge. II. Investigation of floc structure using a freeze-fracture technique. *Colloids Surf* 6(1):83–95
11. Luckham PF, Vincent B, Tadros TF (1983) The controlled flocculation of particulate dispersions using small particles of opposite charge. III. Investigation of floc structure using rheological techniques. *Colloids Surf* 6(2):101–118
12. Luckham PF, Vincent B, Tadros TF (1983) The controlled flocculation of particulate dispersions using small particles of opposite charge. IV. Effect of surface coverage of adsorbed polymer on heteroflocculation. *Colloids Surf* 6(2):119–133

13. Vincent B, Young CA, Tadros TF (1978) Equilibrium aspects of heteroflocculation in mixed sterically stabilised dispersions. *Faraday Discuss Chem Soc* 65:296
14. Vincent B, Jafelicci M, Luckham PF, et al. (1980) Adsorption of small, positive particles onto large, negative particles in the presence of polymer. Part 2. Adsorption equilibrium and kinetics as a function of temperature. *J Chem Soc Faraday Trans 1: Physical Chemistry in Condensed Phases* 76:674–682
15. Hansen FN, Matijević E (1980) Heterocoagulation Part 5. Adsorption of a carboxylated polymer latex on monodispersed hydrated metal oxides. *J Chem Soc Faraday Trans 1: Physical Chemistry in Condensed Phases* 76:1240–1262
16. Barouch E, Matijević E, Ring TA, Finlan JM (1978) Heterocoagulation II. Interaction energy of two unequal spheres. *J Colloid Interface Sci* 67(1):1–9
17. Furusawa K, Anzai C (1992) Heterocoagulation behaviour of polymer latices with spherical silica. *Colloids Surf* 63(1–2):103–111
18. Furusawa K, Anzai C (1987) Preparation of composite fine particles by heterocoagulation. *Colloid Polym Sci* 265:882–888
19. Harley S (1990) Ph.D. dissertation thesis, University of Bristol
20. Harley S, Thompson DW, Vincent B (1992) The adsorption of small particles onto larger particles of opposite charge – direct electron-microscope studies. *Colloids Surf* 62(1–2):163–176
21. Ottewill RH, Schofield AB, Waters JA, Williams NSJ (1997) Preparation of core-shell polymer colloid particles by encapsulation. *Colloid Polym Sci* 275:274–283
22. Okubo M, Lu Y, Wang Z (1999) Analysis of stepwise heterocoagulation for the preparation of soft core/hard shell composite polymer particles. *Colloid Polym Sci* 277:77–82
23. Xu Y, Brittain WJ, Xue C, Eby RK (2004) Effect of clay type on morphology and thermal stability of PMMA-clay nanocomposites prepared by heterocoagulation method. *Polymer* 45(11):3735–3746
24. Chen J-H, Dai C-A, Chen H-J, Chien P-C, Chiu W-Y (2007) Synthesis of nano-sized TiO<sub>2</sub>/poly(AA-co-MMA) composites by heterocoagulation and blending with PET. *J Colloid Interface Sci* 308(1):81–92
25. Voorn DJ, Ming W, van Herk AM, Bomans PHH, Frederik PM, Gasemjit P, Johanssmann D (2005) Controlled heterocoagulation of platelets and spheres. *Langmuir* 21(15):6950–6956
26. Voorn DJ, Ming W, Laven J, Meuldijk J, de With G, van Herk AM (2007) Plate-sphere hybrid dispersions: heterocoagulation kinetics and DLVO evaluation. *Colloids Surf A Physicochemical Eng Asp* 294(1–3):236–246
27. Kauzmann W (1959) Some forces in the interpretation of protein denaturation. *Adv Protein Chem* 14:1–63
28. Chandler D (2005) Interfaces and the driving force of hydrophobic assembly. *Nature* 437:640–647
29. Attard P (2003) Nanobubbles and the hydrophobic attraction. *Adv Colloid Interface Sci* 104(1–3):75–91
30. Eriksson JC, Ljunggren S, Claesson PM (1989) A phenomenological theory of long-range hydrophobic attraction forces based on a square-gradient variational approach. *J Chem Soc Faraday Trans 2: Molecular and Chemical Physics* (85):163–176
31. Stillinger FH (1982) Capillary waves and the inherent density profile for the liquid-vapor interface. *J Chem Phys* 76:1087–1091
32. Yaminsky VV, Yushchenko VS, Amelina EA, Shchukin ED (1983) Cavity formation due to a contact between particles in a nonwetting liquid. *J Colloid Interface Sci* 96(2):301–306
33. Mezger M, Reichert H, Schoeder S, Okasinski J, Schroeder H, Dosch H, Palms D, Ralston J, Honkimaeki V (2006) High-resolution in situ X-ray study of the hydrophobic gap at the water-octadecyl-trichlorosilane interface. *PNAS* 103(49):18401–18404
34. Lum K, Chandler D, Weeks JD (1999) Hydrophobicity at small and large length scales. *J Phys Chem B* 103:4570–4577
35. Pashley RM, McGuiggan PM, Ninham BW, Evans DF (1985) Attractive forces between uncharged hydrophobic surfaces: direct measurements in aqueous solution. *Science* 229(4718):1088–1089

36. Singh S, Houston J, van Swol F, Brinker CJ (2006) Superhydrophobicity: drying transition of confined water. *Nature* 442:526
37. Yamaguchi K, Ito M, Taniguchi T, Kawaguchi S, Nagai K (2004) Preparation of core-shell composite polymer particles by a novel heterocoagulation based on hydrophobic interaction. *Colloid Polym Sci* 282(4):366–372
38. Yamaguchi K, Taniguchi T, Kawaguchi S, Nagai K (2001) Fabrication of polymer particle monolayer onto alkylated glass plates. *Chem Lett* 7:658
39. Zubarev ER, Xu J, Sayyad A, Gibson DJ (2006) Amphiphilic-driven organization of nanoparticles into discrete assemblies. *J Am Chem Soc* 128(47):15098–15099
40. Walther A, Mueller AHE (2008) Janus particles. *Soft Matter* 4(4):663–668
41. Wurm F, Kilbinger AFM (2009) Polymeric Janus asymmetric particles. *Angew Chem, Int Ed* 48(45):8412–8421
42. Erhardt R, Boeker A, Zettl H, Kaya H, Pyckhout-Hintzen W, Krausch G, Abetz V, Mueller AHE (2001) Janus micelles. *Macromolecules* 34(4):1069–1075
43. Erhardt R, Zhang M, Boeker A, Zettl H, Abetz C, Frederik P, Krausch G, Abetz V, Mueller AHE (2003) Amphiphilic Janus micelles with polystyrene and poly(methacrylic acid) hemispheres. *J Am Chem Soc* 125(11):3260–3267
44. Nie L, Liu S, Shen W, Chen D, Jiang M (2007) One-pot synthesis of amphiphilic polymeric Janus particles and their self-assembly into supermicelles with a narrow size distribution. *Angew Chem Int Ed* 46:6321–6324
45. Hong L, Cacciuto A, Luijten E, Granick S (2008) Clusters of amphiphilic colloidal spheres. *Langmuir* 24:621–625
46. Miller W, Cacciuto A (2009) *Phys Rev E* 80:21404
47. Whitlam S, Bon SAF (2010) Self-Assembly of amphiphilic peanut-shaped nanoparticles. *J Chem Phys* 132:074901
48. Maeda S, Armes SP (1993) Preparation of novel polypyrrole-silica colloidal nanocomposites. *J Colloid Interface Sci* 159(1):257–259
49. Maeda S, Armes SP (1994) Preparation and characterization of novel polypyrrole-silica colloidal nanocomposites. *J Mater Chem* 4(6):935–942
50. Li R, Yang X, Li G, Li S, Huang W (2006) Core-corona polymer composite particles by self-assembled heterocoagulation based on a hydrogen-bonding interaction. *Langmuir* 22(19):8127–8133
51. Li GL, Song YY, Yang XL, Huang WQ (2007) Preparation of poly(divinylbenzene-co-N-isopropylacrylamide) microspheres and their hydrogen-bonding assembly behavior for raspberry-like core-corona polymer composite. *J Appl Polym Sci* 104(2):1350–1357
52. Jin J, Iyoda T, Cao C, Song Y, Jiang L, Li TJ, Zhui DB (2001) Self-assembly of uniform spherical aggregates of magnetic nanoparticles through pi-pi interactions. *Angew Chem Int Ed* 40(11):2135–2138
53. Mirkin CA, Letsinger RL, Mucic RC, Storhoff JJ (1996) A DNA-based method for rationally assembling nanoparticles into macroscopic materials. *Nature* 382(6592):607–609
54. Valignat M-P, Theodoly O, Crocker JC, Russel WB, Chaikin PM (2005) Reversible self-assembly and directed assembly of DNA-linked micrometer-sized colloids. *Proc Natl Acad Sci USA* 102(12):4225–4229
55. Fleming MS, Mandal TK, Walt DR (2001) Nanosphere–microsphere assembly: methods for core–shell materials preparation. *Chem Mater* 13(6):2210–2216
56. Chern CS, Lee CK, Chen CY (1996) Biotin-modified submicron latex particles for affinity precipitation of avidin. *Colloids Surf B Biointerfaces* 7(1–2):55–64
57. Fleming MS, Mandal TK, Walt DR (2001) Nanosphere–microsphere assembly: methods for core-shell materials preparation. *Chem Mater* 13(6):2210–2216
58. Decher G (1997) Fuzzy nanoassemblies: toward layered polymeric multicomposites. *Science* 277(5330):1232
59. Stockton WB, Rubner MF (1997) Molecular-level processing of conjugated polymers. 4. Layer-by-Layer manipulation of polyaniline via hydrogen-bonding interactions. *Macromolecules* 30(9):2717–2725

60. Wang L, Wang Z, Zhang X, Shen J, Chi L, Fuchs H (1997) A new approach for the fabrication of an alternating multilayer film of poly(4-vinylpyridine) and poly(acrylic acid) based on hydrogen bonding. *Macromol Rapid Commun* 18(6):509–514
61. Zhang H, Wang D, Wang Z, Zhang X (2007) Hydrogen bonded layer-by-layer assembly of poly(2-vinylpyridine) and poly(acrylic acid): influence of molecular weight on the formation of microporous film by post-base treatment. *Eur Polym J* 43(7):2784–2791
62. Hoshi T, Anzai J-I, Osa T (1995) Controlled deposition of glucose oxidase on platinum electrode based on an avidin/biotin system for the regulation of output current of glucose sensors. *Anal Chem* 67(4):770–774
63. Anzai J-I, Kobayashi Y, Nakamura N, Nishimura M, Hoshi T (1998) Layer-by-layer construction of multilayer thin films composed of avidin and biotin-labeled poly(amine)s. *Langmuir* 15(1):221–226
64. Decher G, Lehr B, Lowack K, Lvov Y, Schmitt J (1994) New nanocomposite films for biosensors: layer-by-layer adsorbed films of polyelectrolytes, proteins or DNA. *Biosens Bioelectron* 9(9–10):677–684
65. Sukhorukov GB, Möhwald H, Decher G, Lvov YM (1996) Assembly of polyelectrolyte multilayer films by consecutively alternating adsorption of polynucleotides and polycations. *Thin Solid Films* 284–285:220–223
66. Caruso F, Caruso RA, Möhwald H (1998) Nanoengineering of inorganic and hybrid hollow spheres by colloidal templating. *Science* 282(5391):1111
67. Donath E (1998) Novel hollow polymer shells by colloid-templated assembly of polyelectrolytes. *Angew Chem Int Ed* 37:2202
68. Johnston APR, Cortez C, Angelatos AS, Caruso F (2006) Layer-by-layer engineered capsules and their applications. *Curr Opin Colloid Interface Sci* 11(4):203–209
69. Caruso F, Möhwald H (1999) Preparation and characterization of ordered nanoparticle and polymer composite multilayers on colloids. *Langmuir* 15(23):8276–8281
70. Ramsden W (1903) Separation of solids in the surface-layers of solutions and ‘suspensions’ (observations on surface-membranes, bubbles, emulsions, and mechanical coagulation). – Preliminary account. *Proc R Soc Lond Sect A* 72:156–164
71. Pickering SU (1907) CXCVI. – Emulsions. *J Chem Soc Trans* 91:2001–2021
72. Aveyard R, Binks BP, Clint JH (2003) Emulsions stabilised solely by colloidal particles. *Adv. Colloid Interface Sci* 100–102:503–546
73. Binks BP (2002) Particles as surfactants – similarities and differences. *Curr Opin Colloid Interface Sci* 7(1,2):21–41
74. Finkle P, Draper HD, Hildebrand JH (1928) The theory of emulsification. *J Am Chem Soc* 45:2780–2788
75. Pieranski P (1980) Two-dimensional interfacial colloidal crystals. *Phys Rev Lett* 45(7):569–572
76. Aveyard R, Clint JH (1996) Particle wettability and line tension. *J Chem Soc Faraday Trans* 92:85–89
77. Cheung DL, Bon SAF (2009) Interaction of nanoparticles with ideal liquid-liquid interfaces. *Phys Rev Lett* 102(6):066103
78. Widom B, Rowlinson JS (1970) New model for the study of liquid-vapor phase transitions. *J Chem Phys* 52:1670–1684
79. Madivala B, Franssaer J, Vermant J (2009) Self-assembly and rheology of ellipsoidal particles at interfaces. *Langmuir* 25(5):2718–2728
80. Madivala B, Vandebril S, Franssaer J, Vermant J (2009) Exploiting particle shape in solid stabilized emulsions. *Soft Matter* 5(8):1717–1727
81. Lin Y, Skaff H, Emrick T, Dinsmore AD, Russell TP (2003) Nanoparticle assembly and transport at liquid-liquid interfaces. *Science* 299, (5604), 226–229
82. Thomson JJ (1904) On the structure of the atom: an investigation of the stability and periods of oscillation of a number of corpuscles arranged at equal intervals around the circumference of a circle; with application of the results to the theory of atomic structure. *Philos Mag* 7(39):237–265

83. Bausch AR, Bowick MJ, Cacciuto A, Dinsmore AD, Hsu MF, Nelson DR, Nikolaides MG, Travesset A, Weitz DA (2003) Grain boundary scars and spherical crystallography. *Science* 299(5613):1716–1718
84. Lipowsky P, Bowick MJ, Meinke JH, Nelson DR, Bausch AR (2005) Direct visualization of dislocation dynamics in grain-boundary scars. *Nat Mater* 4(5):407–411
85. Fortuna S, Colard CAL, Troisi A, Bon SAF (2009) Packing patterns of silica nanoparticles on surfaces of armored polystyrene latex particles. *Langmuir* 25(21):12399–12403
86. Bon SAF, Colver PJ (2007) Pickering miniemulsion polymerization using Laponite clay as a stabilizer. *Langmuir* 23(16):8316–8322
87. Cauvin S, Colver PJ, Bon SAF (2005) Pickering stabilized miniemulsion polymerization: preparation of clay armored latexes. *Macromolecules* 38(19):7887–7889
88. Hohenstein WP (1945) The method of polymerization in suspension *Polym Bull* 1(1):13–16
89. Hohenstein WP, Mark H (1946) Polymerization of olefins and diolefins in suspension and emulsion. I. *J Polym Sci* 1:127–45
90. Winslow FH, Matreyek W (1951) Particle size in suspension polymerization. *J Ind Eng Chem* 43:1108–1112
91. Wiley RM (1954) Limited coalescence of oil droplets in coarse oil-in-water emulsions. *J Colloid Sci* 9:427–437
92. Deslandes Y (1987) Morphology of hydroxyapatite as suspension stabilizer in the polymerization of poly(styrene-co-butadiene). *J Appl Polym Sci* 34(6):2249–2257
93. Bon SAF, Cauvin S, Colver PJ (2007) Colloidosomes as micron-sized polymerisation vessels to create supracolloidal interpenetrating polymer network reinforced capsules. *Soft Matter* 3(2):194–199
94. Bon Stefan AF, Chen T (2007) Pickering stabilization as a tool in the fabrication of complex nanopatterned silica microcapsules. *Langmuir* 23(19):9527–9530
95. Chen T, Colver PJ, Bon SAF (2007) Organic-inorganic hybrid hollow spheres prepared from TiO<sub>2</sub>-stabilized Pickering emulsion polymerization. *Adv Mater* 19(17):2286–2289
96. Colver PJ, Chen T, Bon SAF (2006) Supracolloidal structures through liquid-liquid interface driven assembly and polymerization. *Macromol Symp* 245:34–41
97. Bon SAF, Chen T (2007) Pickering stabilization as a tool in the fabrication of complex nanopatterned silica microcapsules. *Langmuir* 23(19):9527–9530
98. Wang C, Zhang C, Li Y, Chen Y, Tong Z (2009) Facile fabrication of nanocomposite microspheres with polymer cores and magnetic shells by Pickering suspension polymerization. *React Funct Polym* 69(10):750–754
99. Hasell T, Yang J, Wang W, Li J, Brown PD, Poliakoff M, Lester E, Howdle SM (2007) Preparation of polymer-nanoparticle composite beads by a nanoparticle-stabilised suspension polymerisation. *J Mater Chem* 17:4382–4386
100. Yang J, Hasell T, Wang W, Li J, Brown PD, Poliakoff M, Lester E, Howdle SM (2008) Preparation of hybrid polymer nanocomposite microparticles by a nanoparticle stabilized dispersion polymerization. *J Mater Chem* 18:998–1001
101. Chen K, Yang Y, Sa Q, Shi L, Zhao H (2008) Suspension polymerization stabilized by triblock copolymer with CdS nanoparticles. *Polymer* 49(11):2650–2655
102. Duan L, Chen M, Zhou S, Wu L (2009) Synthesis and characterization of poly(N-isopropylacrylamide)/silica composite microspheres via inverse Pickering suspension polymerization. *Langmuir* 25(6):3467–3472
103. Gao Q, Wang C, Liu H, Wang C, Liu X, Tong Z (2009) Suspension polymerization based on inverse Pickering emulsion droplets for thermo-sensitive hybrid microcapsules with tunable supracolloidal structures. *Polymer* 50(12):2587–2594
104. Nie Z, Park JI, Li W, Bon SAF, Kumacheva E (2008) An “inside-out” microfluidic approach to monodisperse emulsions stabilized by solid particles. *J Am Chem Soc* 130(49):16508–16509
105. Bon SAF, Mookhoek SD, Colver PJ, Fischer HR, van der Zwaag S (2007) Route to stable non-spherical emulsion droplets. *Eur Polym J* 43(11):4839–4842
106. Tiarks F, Landfester K, Antonietti M (2001) Silica nanoparticles as surfactants and fillers for latexes made by miniemulsion polymerization. *Langmuir* 17(19):5775–5780



107. Zhang K, Wu W, Meng H, Guo K, Chen JF (2009) Pickering emulsion polymerization: Preparation of polystyrene/nano-SiO<sub>2</sub> composite microspheres with core-shell structure. *Powder Technol* 190(3):393–400
108. Zhang Y, Chen H, Shu X, Zou Q, Chen M (2009) Fabrication and characterization of raspberry-like PS/SiO<sub>2</sub> composite microspheres via miniemulsion polymerization. *Colloids Surf A Physicochem Eng Asp* 350(1–3):26–32
109. Wang T, Colver PJ, Bon SAF, Keddle JL (2009) Soft polymer and nano-clay supracolloidal particles in adhesives: synergistic effects on mechanical properties. *Soft Matter* 5(20):3842–3849
110. Voorn DJ, Ming W, Van Herk AM (2006) Polymer-clay nanocomposite latex particles by inverse Pickering emulsion polymerization stabilized with hydrophobic montmorillonite platelets. *Macromolecules* 39(6):2137–2143
111. Walther A, Hoffmann M, Mueller AHE (2008) Emulsion polymerization using Janus particles as stabilizers. *Angew Chem Int Ed* 47(4):711–714
112. Percy MJ, Amalvy JL, Randall DP, Armes SP, Greaves SJ, Watts JF (2004) Synthesis of vinyl polymer-silica colloidal nanocomposites prepared using commercial alcoholic silica sols. *Langmuir* 20(6):2184–2190
113. Schmid A, Tonnar J, Armes SP (2008) A new highly efficient route to polymer-silica colloidal nanocomposite particles. *Adv Mater* 20(17):3331–3336
114. Schmid A, Armes SP, Leite CAP, Galembeck F (2009) Efficient preparation of polystyrene/silica colloidal nanocomposite particles by emulsion polymerization using a glycerol-functionalized silica sol. *Langmuir* 25(4):2486–2494
115. Sacanna S, Philipse AP (2007) A generic single-step synthesis of monodisperse core/shell colloids based on spontaneous Pickering emulsification. *Adv Mater* 19(22):3824–3826
116. Sacanna S, Kegel WK, Philipse AP (2007) Thermodynamically stable Pickering emulsions. *Phys Rev Lett* 98(15):158301
117. Colver PJ, Colard CAL, Bon SAF (2008) Multilayered nanocomposite polymer colloids using emulsion polymerization stabilized by solid particles. *J Am Chem Soc* 130(50):16850–16851
118. Wen N, Tang Q, Chen M, Wu L (2008) Synthesis of PVAc/SiO<sub>2</sub> latices stabilized by silica nanoparticles. *J Colloid Interface Sci* 320(1):152–158
119. Colard Catheline AL, Teixeira RFA, Bon Stefan AF (2010) Unraveling mechanistic events in solids-stabilized emulsion polymerization by monitoring the concentration of nanoparticles in the water phase. *Langmuir* ASAP, doi:10.1021/1a904817f
120. Fortuna S, Colard Catheline AL, Troisi A, Bon Stefan AF (2009) Packing patterns of silica nanoparticles on surfaces of armored polystyrene latex particles. *Langmuir ACS J surf colloids* 25(21):12399–12403
121. Ma H, Dai LL (2009) Synthesis of polystyrene-silica composite particles via one-step nanoparticle-stabilized emulsion polymerization. *J Colloid Interface Sci* 333(2):807–811
122. Sheibat-Othman N, Bourgeat-Lami E (2009) Use of silica particles for the formation of organic-inorganic particles by surfactant-free emulsion polymerization. *Langmuir* 25(17):10121–10133
123. Bon Stefan AF, Colver Patrick J (2007) Pickering miniemulsion polymerization using Laponite clay as a stabilizer. *Langmuir* 23(16):8316–8322
124. Yu C-L, Kang J-S, Zhang F-A (2009) The effect of nano-SiO<sub>2</sub> colloid on soap-free emulsion polymerization of methyl methacrylate and hydroxyethyl methacrylate. *J Macromol Sci A Pure Appl Chem* 46(9):870–875
125. Song X, Yin G, Zhao Y, Wang H, Du Q (2009) Effect of an anionic monomer on the Pickering emulsion polymerization stabilized by titania hydrosol. *J Polym Sci A Polym Chem* 47(21):5728–5736
126. Song X, Zhao Y, Wang H, Du Q (2009) Fabrication of polymer microspheres using titania as a photocatalyst and Pickering stabilizer. *Langmuir* 25(8):4443–4449
127. Manoharan VN, Elssesser MT, Pine DJ (2003) Dense packing and symmetry in small clusters of microspheres. *Science* 301(5632):483–487

128. Cho Y-S, Yi G-R, Lim J-M, Kim S-H, Manoharan Vinothan N, Pine David J, Yang S-M (2005) Self-organization of bidisperse colloids in water droplets. *J Am Chem Soc* 127(45):15968–15975
129. Cho Y-S, Yi G-R, Kim S-H, Jeon S-J, Elsesser MT, Yu HK, Yang S-M, Pine DJ (2007) Particles with coordinated patches or windows from oil-in-water emulsions. *Chem Mater* 19(13):3183–3193
130. Lee D, Weitz DA (2008) Double emulsion-templated nanoparticle colloidosomes with selective permeability. *Adv Mater* 20(18):3498–3503
131. Dinsmore AD, Hsu Ming F, Nikolaides MG, Marquez M, Bausch AR, Weitz DA (2002) Colloidosomes: selectively permeable capsules composed of colloidal particles. *Science* 298(5595):1006–1009
132. Jerri HA, Dutter RA, Velegol D (2009) Fabrication of stable anisotropic microcapsules. *Soft Matter* 5(4):827–834
133. Chaturvedi N, Jerri H, Velegol D (2008) Design and characterization of randomly speckled spheres. *Langmuir* 24(14):7618–7622
134. Yake AM, Snyder CE, Velegol D (2007) Site-specific functionalization on individual colloids: size control, stability, and multilayers. *Langmuir* 23(17):9069–9075
135. Snyder CE, Yake AM, Feick JD, Velegol D (2005) Nanoscale functionalization and site-specific assembly of colloids by particle lithography. *Langmuir* 21(11):4813–4815
136. Xia Y, Yin Y, Lu Y, McLennan J (2003) Template-assisted self-assembly of spherical colloids into complex and controllable structures. *Adv Funct Mater* 13(12):907–918



# Organic/Inorganic Composite Latexes: The Marriage of Emulsion Polymerization and Inorganic Chemistry

Elodie Bourgeat-Lami and Muriel Lansalot

**Abstract** This review article describes recent advances in the synthesis and properties of waterborne organic/inorganic colloids elaborated through conventional emulsion polymerization, a well-established technology. These materials can be defined as aqueous suspensions of composite latex particles made up of organic and inorganic domains organized into well-defined core–shell, multinuclear, raspberry-like, multipod-like, or armored morphologies. Particular emphasis is placed on the synthetic strategies for fabrication of these colloidal materials. Two main approaches are described: the polymerization of organic monomers in the presence of preformed inorganic particles, and the reverse approach by which inorganic materials are synthesized in the presence of preformed polymer latexes. The list of examples provided in this review is by no means exhaustive but rather intends to give an overview of synthetic methods for selected inorganic compounds (e.g., silica, iron oxide, pigments, clays, quantum dots, and metals), and briefly reports on potential applications of the resulting materials.

**Keywords** Clays · Emulsion polymerization · Iron oxide · Metals · Organic/inorganic composite colloids · Particle morphology · Pigments · Quantum dots · Silica · Surface modification

## Contents

1	Introduction and Scope .....	56
2	Polymer–Silica Nanocomposite Particles .....	58
2.1	Emulsion Polymerization in the Presence of Silica Particles .....	59
2.2	Coating of Polymer Latexes with a Silica Shell .....	70

3	Synthesis of Magnetic Latex Particles .....	72
3.1	Encapsulation of Iron Oxide Nanoparticles by Emulsion Polymerization .....	74
3.2	Synthesis of Iron Oxide Nanoparticles in the Presence of Preformed Polymer Particles .....	87
4	Pigmented Latexes .....	89
4.1	Polymer Encapsulation of TiO <sub>2</sub> Pigments .....	90
4.2	Titania-Coated Polymer Spheres and Hollow Titania Shells .....	92
4.3	Other Pigments .....	93
5	Polymer–Clay Nanocomposite Latexes .....	95
5.1	PCNs Elaborated by Conventional Emulsion Polymerization .....	96
5.2	Soap-Free Latexes Stabilized by Clay Platelets .....	100
6	Synthesis of Quantum Dot Tagged Latex Particles .....	102
6.1	Encapsulation of QDs Through Emulsion Polymerization .....	103
6.2	Synthesis of Quantum Dots in the Presence of Polymer Particles .....	106
7	Synthesis of Metallic Latex Particles .....	109
7.1	Polymer Encapsulation of Metallic Particles Through Emulsion Polymerization ..	109
7.2	Polymer Particles as Template for the Synthesis of Metallic Shells and Metallic Nanoparticles .....	110
8	Summary and Outlook .....	114
	References .....	115

## Abbreviations

1VID	1-Vinylimidazole
2VPy	2-Vinylpyridine
4VPy	4-Vinylpyridine
AA	Acrylic acid
AAEM	Acetoacetoxyethyl methacrylate
AAm	Acrylamide
ACPA	4,4'-Azobis(4-cyanopentanoic acid)
AEMH	2-Aminoethylmethacrylamide hydrochloride
AFM	Atomic force microscopy
AIBA	2,2'-Azobis(2-amidinopropane) dihydrochloride
AIBN	2,2'-Azobis(isobutyronitrile)
AOA	12-Acryloxy-9-octadecenoic acid
BA	<i>n</i> -Butyl acrylate
BMA	<i>n</i> -Butyl methacrylate
CMC	Critical micelle concentration
CS	Chitosan
CTAB	Cetyltrimethyl ammonium bromide
DMAEMA	2-(Dimethylamino)ethyl methacrylate
DSC	Differential scanning calorimetry
DVB	Divinyl benzene
EGDMA	Ethylene glycol dimethacrylate
GA	Gluteraldehyde

GMA	Glycidyl methacrylate
HEMA	2-Hydroxyethyl methacrylate
KPS	Potassium persulfate
MA	Maleic anhydride
MAA	Methacrylic acid
MADQUAT	2-Methacryloyloxy ethyl trimethyl ammonium chloride
MBA	<i>N,N'</i> -Methylene bisacrylamide
MMA	Methyl methacrylate
MMT	Montmorillonite
MPDES	Methacryloxy propyl dimethyl ethoxysilane
MPDMS	Methacryloxy propyl dimethoxysilane
MPTMS	Methacryloxy propyl trimethoxysilane
MTC	2-(Methacryloyl) ethyl trimethyl ammonium chloride
Ms	Saturation magnetization
NaSS	Sodium styrene sulfonate
NIPAM	<i>N</i> -Isopropylacrylamide
NVCL	<i>N</i> -Vinylcaprolactam
OA	Oleic acid
O/I	Organic/inorganic
P4VPy	Poly(4-vinylpyridine)
P2VPy	Poly(2-vinylpyridine)
PCN	Polymer–clay nanocomposites
PDMAEMA	Poly[2-(dimethylamino)ethyl methacrylate]
PDVB	Poly(divinyl benzene)
PEG	Poly(ethylene glycol)
PEGMA	Poly(ethylene glycol) monomethyl ether methacrylate
PMMA	Poly(methyl methacrylate)
PS	Polystyrene
PSD	Particle size distribution
PVA	Polyvinyl alcohol
PVC	Polyvinyl chloride
PVP	Poly( <i>N</i> -vinylpyrrolidone)
QDs	Quantum dots
SDBS	Sodium dodecylbenzene sulfonate
SDS	Sodium dodecyl sulfate
SEM	Scanning electron microscopy
TALH	Titanium(IV) bis(ammonium lactate) di-hydroxyde
TEM	Transmission electron microscopy
TEOS	Tetraethyl orthosilicate
$T_g$	Glass transition temperature
TGA	Thermogravimetric analysis
TOPO	Tri- <i>n</i> -octylphosphine oxide
VDAC	Vinylbenzyl dimethyl dodecyl ammonium chloride

## 1 Introduction and Scope

The incorporation of inorganic materials into polymers is of significant theoretical and experimental interest, with a rich history in the polymer and engineering communities. Mineral fillers and extenders such as calcium carbonate, fumed silica, kaolin, and ceramic fibers have been used as additives in polymers for more than a century. Not only can these inorganic solids provide enhanced physical properties such as stiffness, mechanical strength, chemical inertness, thermal resistance, and optical properties (transparency, opacity), but they can also significantly contribute to cost reduction. Although the addition of minerals to enhance polymer performance and impart physical and rheological properties is common in the production of modern plastics and in many industrial formulations (foods, inks, paints, adhesives, paper coatings, textiles, photographic films, pharmaceutical and cosmetic preparations), the remarkable scientific progress in the ability to fabricate, manipulate, and assemble organic and inorganic compounds at the nanometer scale has revolutionized the way such composite materials are envisaged and elaborated.

Organic/inorganic (O/I) composite latexes are typical examples of nanocomposite materials that combine the best attributes of inorganic solids with the processing and handling advantages of organic polymers. The huge breakthroughs that have been achieved in inorganic chemistry now allow the synthesis of nanoparticles of noble metals, metal oxides, and semiconductors with outstanding electronic, optical, magnetic, or catalytic properties in large quantities using thermal decomposition, hydrolysis, reduction and other soft-chemistry processes in solution [1, 2]. On the other hand, synthetic latexes have raised increasing interest in the last century, and large quantities of commodity polymers [polystyrene (PS), polyvinyl chloride (PVC), styrene–butadiene or polychloroprene rubbers] are manufactured as aqueous dispersions. Combining both materials into a unique nanostructured composite particle is of obvious benefit for both the academic and industrial communities. Given the extensive variety of inorganic materials now commercially accessible [clays, quantum dots (QDs), metals, silica, titania, alumina, zirconia, iron oxides and so on], the potential combinations of organic polymers and inorganic nanoparticles, and thus the tailorability of their properties and performances, is essentially endless. Furthermore, the properties of these two-phase colloidal materials not only depend on the chemical nature of the constitutive organic and inorganic components, but may also greatly benefit from the ability to design particle nanostructures. For example, if the organic polymer is located at the outer particle surface (in the so-called core–shell morphology), it can protect the core from environmental aggressions, or provide functional groups to improve interactions with the surrounding medium, or impart specific sensing and colloidal properties. By contrast, when the polymer is surrounded by the mineral, and thus plays the role of a template, hollow particles can be produced by subsequent removal of the core. The structures obtained are of particular interest for encapsulation technologies, drug delivery, or as pigments for the paint industry. Therefore, by controlling the composite particle morphology through appropriate routes and reaction conditions, synergetic behaviors and completely new properties can potentially emerge. Many strategies have been reported

for the elaboration of such colloidal nanocomposites including heterocoagulation, layer-by-layer assembly techniques, and in situ polymerization. The reader is referred to recent reviews and text books for a comprehensive description of these methods [3–15].

In order to avoid overlapping with these previous reviews, we will mainly focus in this article on the synthesis and properties of O/I composite latexes elaborated by emulsion polymerization, a process that is extensively employed industrially to manufacture a variety of products such as paints, adhesives, impact modifiers and so on. Composite particles elaborated through miniemulsion polymerization or controlled radical polymerization, are reviewed elsewhere in this special issue and will not be considered here. As both the synthetic strategies and properties of the resulting materials depend on the type of inorganic particles, this review is organized around the nature of the inorganic phase, namely metal oxides, metals, non-oxide semi-conductors (QDs), and aluminosilicates (clays). A list of inorganic particles of interest is given in Table 1.

For the sake of clarity, the different types of inorganic materials will be discussed separately. For each of them (except for clays), we will distinguish between two synthetic approaches (Fig. 1). In the first approach, the composite colloid is elaborated by in situ emulsion polymerization in the presence of preformed inorganic particles, usually used as seeds but which can also play the role of stabilizers. In the second approach, polymer latexes elaborated through conventional emulsion polymerization are used as templates to grow inorganic domains either within or at the surface of the particles. Given the rapidly expanding body of literature in the field, the intent in the following sections is not to provide an exhaustive list of examples but rather to

**Table 1** Some inorganic particles of interest and examples of their potential end-use application

Inorganic material	Chemical formula	Potential application
<i>Oxides</i>		
Silica	SiO <sub>2</sub>	Paints, plastics
Titanium dioxide	TiO <sub>2</sub>	Paints
Iron oxide	Fe <sub>3</sub> O <sub>4</sub> /Fe <sub>2</sub> O <sub>3</sub>	Biomedical, catalysis
Zinc oxide	ZnO	Paints, electronics
Alumina	Al <sub>2</sub> O <sub>3</sub>	Coatings
<i>Metals</i>		
Gold	Au	Optics, biomedical
Silver	Ag	Optics, biomedical
Palladium	Pd	Catalysis
Copper	Cu	Catalysis
<i>Non-oxide semiconductors</i>		
Cadmium selenide	CdSe	Optics, biomedical
Cadmium sulfide	CdS	Optics, biomedical
<i>Aluminosilicates</i>		
Montmorillonite	–	Plastics, paints
Laponite	–	Plastics, paints

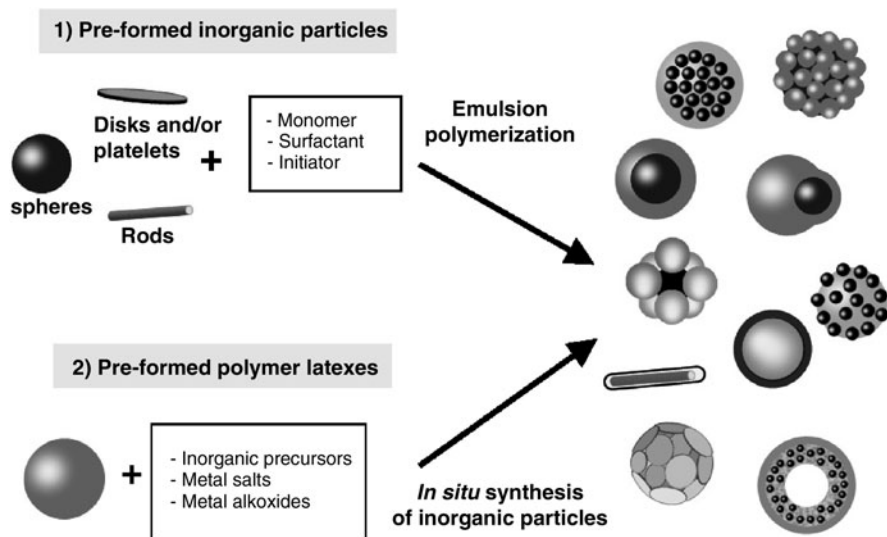


**Fig. 1** Two main different approaches to fabrication of O/I particles: (1) organic polymerization in the presence of preformed inorganic particles and (2) inorganic formation at the surface or inside the internal volume of preformed polymer latex particles

give an overview of the various synthetic methods, with emphasis on the techniques that have been developed to control the surface chemistry of the inorganic or organic materials and the morphology of the resulting composite particles.

## 2 Polymer–Silica Nanocomposite Particles

To date, silica has been the focus of the majority of studies on oxide-based nanostructured materials. One of the major reasons for this is its easy processability, high chemical inertness and exceptional colloidal stability. Moreover, silica can be processed as a thin film with controllable porosity and optical transparency. All these properties make silica ideal for use in model systems, and it is widely used in many industrial areas ranging from paints and drug delivery to composite materials. Zou et al. have recently published a detailed review on the preparation, characterization, properties, and applications of polymer/silica nanocomposites and the reader is referred to this review for in-depth description of the various synthetic routes [16].

Silica particles used in emulsion polymerization are of different origin and, consequently, their sizes and surface properties significantly vary. Although the large majority of works involve the use of anionic silica sols, cationic silica has also been used on some occasions. Silica particles are most often amorphous colloidal silicas of commercial origin with diameters in the range of 10–80 nm. Silica particles of larger diameters are prepared by controlled hydrolysis and precipitation

of tetraethyl orthosilicate (TEOS) from alcohol/water mixtures according to the well-established Stöber process [17]. In this technique, TEOS is introduced into a mixture of alcohol, ammonia, and water to form dense (compact) monodisperse silica spheres through base-catalyzed hydrolysis and condensation reactions. The technique affords a relatively good control over the particle size and size distribution for low solid contents. However, the breadth of the distribution broadens, and the particles become less spherical, for solid contents higher than typically 5 wt%. Numerous methods inspired from the original Stöber process have been therefore developed to increase both particle size and solid content while maintaining narrow particle size distributions (PSDs) [18].

Regardless of the nature of the silica particles, synthetic strategies need to be established in order to increase the chemical affinity with hydrophobic polymers and to control the morphology of the resulting composite colloid. All these methods share a common feature in the sense that they all aim at creating significant interactions at the silica–polymer interface by using suitable primers (adsorbed or grafted on the silica surface) capable of participating in the polymerization reaction or to impart the required compatibility. An overview of these methods is given in the following section.

## ***2.1 Emulsion Polymerization in the Presence of Silica Particles***

### **2.1.1 Silica Particles Functionalized by Methacryloxy Propyl Trimethoxysilane**

Silane coupling agents have been used for decades in order to provide enhanced adhesion between a variety of inorganic substrates and organic resins. They are organometallic derivatives of the type  $R_nSiX_{4-n}$ , where X is an alkoxy group and R is a functional organic group. Organosilane compounds are known to react with hydroxylated surfaces to form mono- or multilayer coverages, depending on the number of alkoxy groups and the amount of water.

The use of organosilane molecules to generate silica-based composite particles was first demonstrated by Guyot and coworkers in the mid-1990s. The authors reported successful encapsulation of silica particles functionalized by methacryloxy propyl trimethoxysilane (MPTMS) with poly(ethyl acrylate), through emulsion polymerization. The films cast from the composite suspensions were shown to exhibit remarkable mechanical properties, similar to those of vulcanized elastomers reinforced by solid particles [19–21]. It was argued at that time that polymer chains grafted on the silica surface via the silane coupling agent formed a succession of tight loops into which the free polymer chains were entangled, thereby leading to a physical network of silica beads responsible for the unusually high mechanical properties. The strategy was next extended with success to non-aqueous dispersion polymerization [22–24] and later applied by several groups to the synthesis of polymer/silica composite particles of various morphologies (Fig. 2) [25–32].

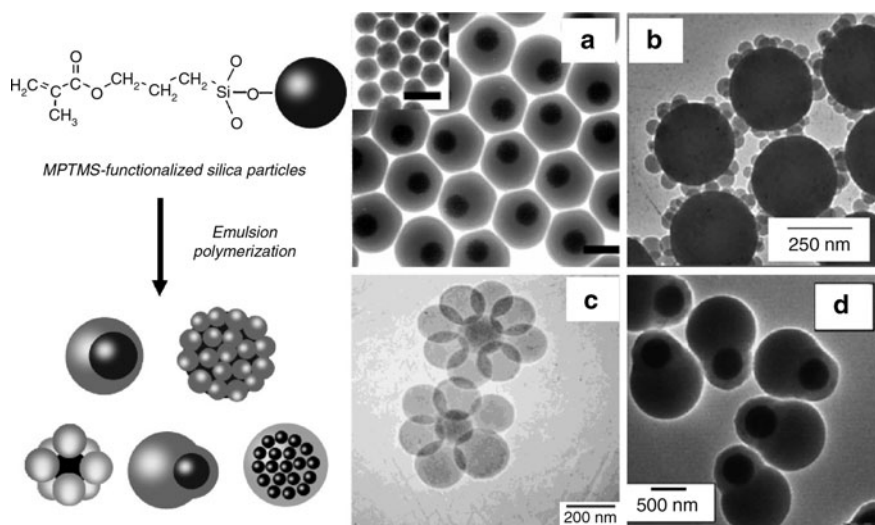


**Fig. 2** *Left*: Silica/polystyrene composite particles elaborated through emulsion polymerization using MPTMS as silane coupling agent. *Right*: TEM images reproduced (a) from [25] (scale bars: 200 nm) with permission of Wiley-VCH, (b) from [26] with permission of Springer, (c) from [27] with permission of American Chemical Society, and (d) from [28] with permission of Wiley-VCH

Many factors can influence particle morphology. Among them, the size and concentration of the silica particles and the grafting density of MPTMS appeared to be predominant parameters. As described in [33] and illustrated in Fig. 3, the mechanism of particle formation can be summarized as follows. The initiator starts to decompose in the water phase, giving rise to the formation of radicals. These radicals propagate with aqueous phase monomers until they undergo one of the following fates: (1) aqueous phase termination or (2) entry into a micelle or precipitation (depending on the surfactant concentration), creating somehow a new particle. Aqueous-phase oligomers of all degrees of polymerization can also undergo frequent collision with the surface of the silica seed particles, and therefore have a high probability of copolymerizing with the double bonds of silica, thus generating chemisorbed polymer chains in the early stages of polymerization. These discrete polymer loci are preferred for adsorption of further oligomers or radicals compared with the bare seed surface. As a result, they become discrete loci of polymerization. Provided that the seed develops a sufficient surface area and contains enough double bonds to enable efficient capture of the growing radicals, polymerization exclusively takes place at the silica surface. High MPTMS grafting density thus allows core-shell formation through the efficient capture of a large number of oligoradicals or primary particles in the earlier stage of the reaction. The shell may result from the collapsing of the growing polymer chains on the functionalized silica surface or from the coalescence of freshly nucleated primary particles, the latter situation being promoted by the close proximity of the precursor particles and the low surface energy. For low MPTMS grafting densities, the polymer chains form



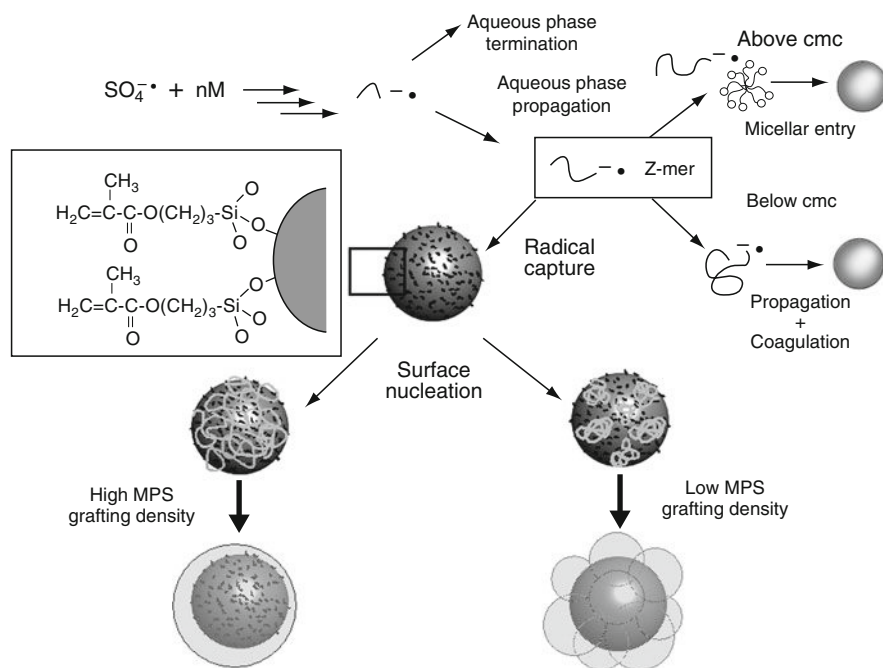


**Fig. 3** Main features of the formation of silica/polymer nanocomposite particles through emulsion polymerization using MPS as silane coupling agent. Reproduced from [33] with permission of American Scientific Publishers

segregated domains around the silica particles because the high interfacial energy (due to the presence of unreacted silanol groups) promotes neither spreading of the polymer chains on the surface nor interparticle coalescence.

In agreement with the mechanism of composite particle formation depicted above, multipod-like morphologies with five, six, or eight PS nodules per silica particle were obtained with success using silica seeds treated with small amounts of MPS (in the range  $0.1\text{--}1\text{ molecule nm}^{-2}$ ) [27, 33]. It was subsequently reported that the geometry of such binary polymer/silica colloidal clusters could be finely tuned by varying the diameter of the silica seed (Fig. 4) [34]. The resulting complex colloidal assemblies displayed polyhedral arrangements that shared some common aspects with the space-filling models of simple binuclear molecules. To this respect, they could be regarded as “colloidal molecules”, a concept first introduced by van Blaaderen [35], which consists in considering that spherical colloids can be treated as if there were atoms and that molecules can form more complex materials that atoms can. Besides their potential interest as model systems for the physicist community, these colloidal clusters can be used as building blocks for the elaboration of ordered arrays of non-spherical colloids with potential applications in photonic crystals. It is foreseen, for example, that the controlled assembly of tetrapod-like colloids should result in colloidal crystals with a full photonic bandgap.

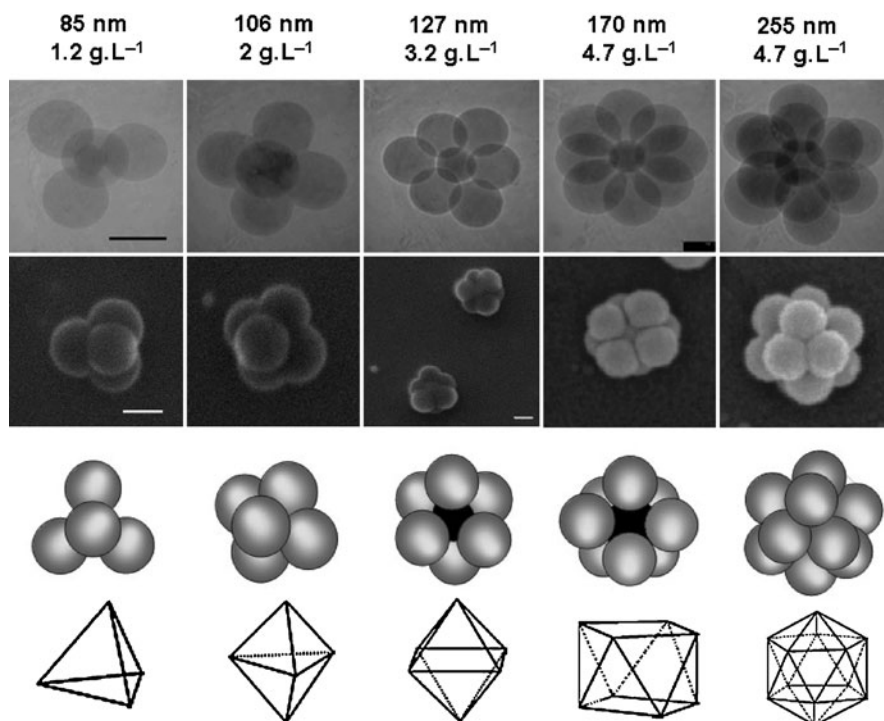


**Fig. 4** *Top*: TEM and SEM micrographs of silica/polystyrene binary clusters obtained by emulsion polymerization of styrene ( $100 \text{ g.L}^{-1}$ ) using  $\text{NP}_{30}$  as surfactant ( $3 \text{ g.L}^{-1}$ ) and MPTMS-functionalized silica seeds of different diameters. *Scale bars*: 200 nm. The silica particle size and concentration are given above the images. *Bottom*: Sphere configurations, and polyhedra formed by drawing lines from the center of each PS nodule to its neighbors. Adapted from [34] with permission of Wiley-VCH

When the ratio of the number of silica seed particles to the number of PS nodules was equal to one, original silica/PS dumbbell-like or snowman-like morphologies were obtained [36, 37]. Anisotropic colloids have recently gained increasing interest due to their unique properties and performances. Moreover, these dissymmetrical colloids could be further processed into Janus particles (e.g., particles whose surfaces of both hemispheres are different from a chemical point of view). In a typical procedure, the mineral part of the snowman-like particles was selectively functionalized to anchor desirable groups. Then, the protecting PS mask was removed in a subsequent step by ultracentrifugation to allow further selective modification of the freshly generated new hemisphere (Fig. 5) [38]. Although several methods have been developed in the recent literature to synthesize Janus colloids, as reviewed by Perro and coworkers [39], none of them allows the production of large amounts of particles. In this context, the process depicted in Fig. 5, which is potentially amenable to industrial scale-up, offers a versatile methodology for fabrication of large quantities of nanometric Janus structures.

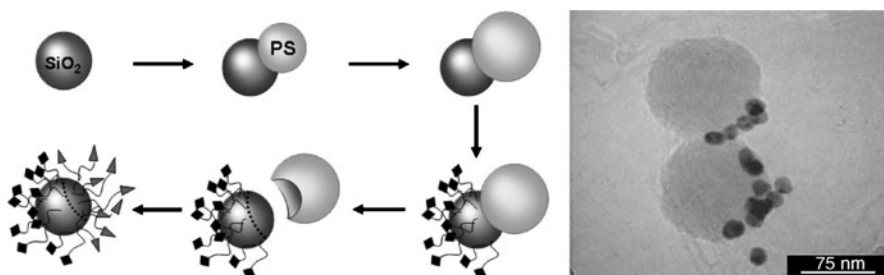


**Fig. 5** *Left*: Consecutive stages involved in the formation of Janus nanoparticles through a protection–deprotection route. *Right*: TEM image of Janus nanoparticles. Reproduced from [38] with permission of the Royal Society of Chemistry

Following a slightly different approach, but still based on emulsion polymerization, Nagao et al. also recently reported the synthesis of anisotropic polymer particles composed of silica, poly(methyl methacrylate) (PMMA) and PS in two steps [28]. First, core–shell particles with a silica core and a crosslinked PMMA–PMPTMS copolymer shell were synthesized by emulsion copolymerization of methyl methacrylate (MMA) and MPTMS in the presence of MPTMS-grafted silica particles. The crosslinked polymer-coated silica particles were then used as seeds to grow protruding PS nodules on their surface, resulting in snowman-shaped composite particles (Fig. 2d).

It would be too simplistic to consider that the amount of grafted MPTMS is the only parameter that allows the control of particle morphology. Because interfacial tensions are heavily involved, the nature of the emulsion stabilizer, its concentration, the suspension pH, or the type of monomer could also significantly influence the final morphology [25, 29]. For example, by simply changing the type of surfactant used in the polymerization recipe, the particle morphology can change from multipod to excentered core–shell [33]. In addition, when the number of silica particles is significantly higher than the number of latex particles, composite colloids with internal occluded domains of several silica particles and “inverted” raspberry-like morphologies (the silica particles being located at the surface of the latex spheres) can also be obtained. The latter morphology is observed for low MPTMS grafting densities and is mainly a consequence of the surfactant-like behavior of the inorganic particles in this specific situation.

### 2.1.2 Macromonomer-Mediated Synthesis of Polymer–Silica Colloidal Clusters

Apart from the use of organosilanes that form covalent bonds with silica surfaces, chemical modification can also be performed through physicochemical adsorption of appropriate molecules (or macromolecules) active in the polymerization process. For instance, Reculosa et al. reported the synthesis of silica/PS raspberry-like

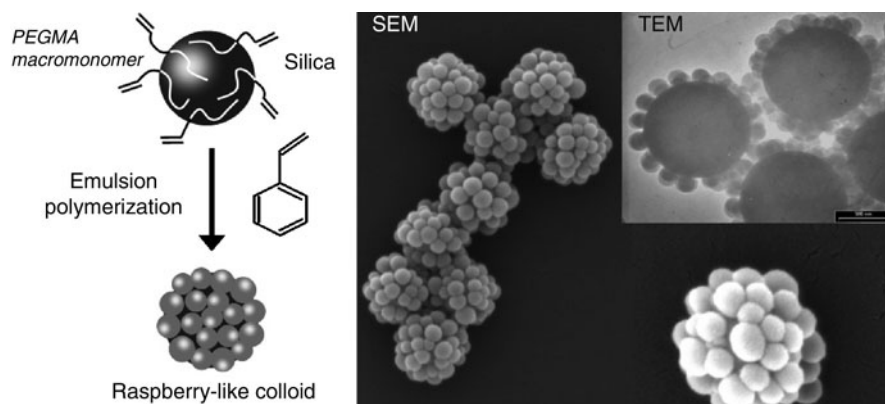


**Fig. 6** *Left:* Elaboration of silica/polystyrene raspberry-like colloids through emulsion polymerization using a MMA-terminated poly(ethylene oxide) macromonomer (PEGMA) as coupling agent. *Right:* SEM and TEM pictures of the raspberry-like particles. Adapted from [40] with permission of American Chemical Society

colloids through emulsion polymerization using a MMA-terminated poly(ethylene oxide) macromonomer (PEGMA) [40]. Here, strong cooperative hydrogen bonding interaction between ethylene oxide units and surface silanols replaces covalent bonding, while copolymerization with the methacrylate group enables anchoring of the PS nodules on the silica seed (Fig. 6).

As previously, the morphology strongly depends on the ratio between the number of silica seeds and the number of growing nodules. Dissymmetrical, snowman-like and multipod-like colloids were obtained by varying these respective numbers [36, 41]. But, in contrast to MPTMS, which forms strong covalent bonds with the silica surface, PEO-based macromonomers display only weak, reversible interactions. Taking advantage of this feature, Perro et al. recently demonstrated the possibility of generating planar daisy-shaped, super-triangle and super-square colloidal clusters upon drying of composite suspensions containing silica particles surrounded by six and eight PS nodules, respectively (Fig. 7) [42]. It was shown that the binary clusters had a polyhedral shape in suspension and that the planar arrangement resulted from the falling-in of the PS nodules on the TEM grid. Electronic tomography experiments strongly supported the hypothesis and provided good evidence for the suspected underlying mechanism.

Alternative approaches involving molecules that combine the properties of a monomer with those of a surfactant (so-called polymerizable surfactants) have also been reported. For example, quaternary alkyl salts of dimethyl aminoethyl methacrylate (CnBr) surfactants were used to promote polymer encapsulation of silica gels in aqueous suspension [43, 44]. The polymerizable surfactant formed a bilayer on the silica surface, the configuration of which enabled the formation of core-shell particles. The CnBr amphiphilic molecule was either homopolymerized or copolymerized with styrene adsorbed in the reactive surfactant bilayer. This concept of admicellar polymerization is detailed in Sect. 3.1. In the recent

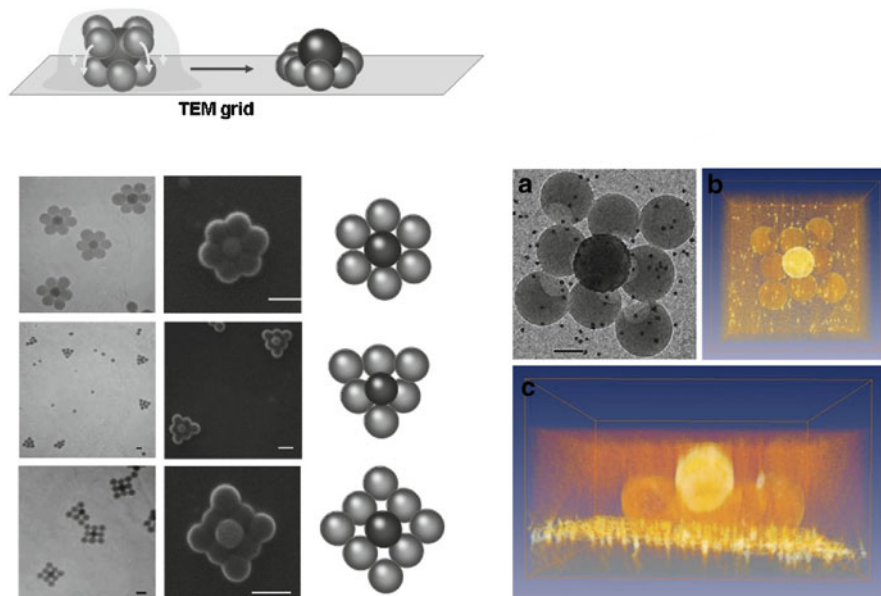


**Fig. 7** *Left:* Daisy-shape, super-triangle and super-square colloidal binary clusters obtained by drying a suspension of hexapod- and octopod-like PS/silica particles elaborated through emulsion polymerization using PEGMA as compatibilizer. TEM images are shown next to the corresponding structures. *Scale bars:* 200 nm. *Right:* Super-square colloidal cluster as obtained after an octopod-like PS–silica cluster has fallen in on a copper grid coated with a carbon membrane. (a) TEM micrograph as observed in the direction perpendicular to the grid plane. *Scale bar:* 100 nm. (b) The same view in the form of a 3D reconstruction calculated from 60 TEM images acquired at different tilt angles (the brighter sphere is the silica seed). (c) The same 3D reconstruction observed in a direction parallel to the grid plane. Adapted from [42] with permission of The Royal Society of Chemistry

work of Qu et al., an anionic reactive surfactant was used in combination with a non-ionic surfactant to encapsulate silica particles through emulsion polymerization [32]. For low silica concentrations, and therefore low amounts of adsorbed surfactant, a “rough” shell was observed that was composed of homogeneously distributed polymer protrusions, which presumably originated from the coalescence of polymer nodules formed in the earlier stages of the polymerization. This result is fairly consistent with previous literature involving MPTMS as coupling agent and suggests that both processes follow similar reaction mechanisms.

Another relevant system involves oleic acid (OA) adsorption at the silica–water interface. This method was first demonstrated by Ding et al. [45] and was next used by Mahdavian and coworkers to encapsulate very small silica nanoparticles [46]. In the latter case, a core–shell structure with a core composed of aggregated silica particles and a shell made of MMA, styrene and acrylic acid (AA), was formed. The authors suggest that the polymerization proceeds through oligoradical entry into the OA admicelles.

### 2.1.3 Utilization of Auxiliary Comonomers

The strategy of using auxiliary (co)monomers exhibiting strong interaction with the surface of silica was first reported by Armes and coworkers, who described the homopolymerization of 4-vinylpyridine (4VPy) in the presence of an ultrafine aqueous silica sol [47]. Here, acid–base interactions between the silanol groups and the pyridine group of the poly(4VPy) chains promoted nanocomposite formation. The polymerization was performed at 60°C under soap-free conditions using ammonium persulfate as initiator, and led to the formation of nanocomposite particles with a “current-bun” morphology. The strategy was further extended to copolymers of 4VPy with MMA, styrene, *n*-butyl acrylate (BA) or *n*-butyl methacrylate (BMA) [48, 49]. In the case of BA, the resulting films showed a high gloss and a good transparency (even for high silica contents), as well as unusually low water uptake. These water-borne colloidal nanocomposites are of potential interest for the elaboration of fire-retardant or abrasion-resistant coatings. More recently, lightly crosslinked silica/P4VPy composite particles were successfully used to stabilize oil-in-water emulsion droplets at pH 8. The emulsion was destabilized upon decreasing the pH, thereby highlighting the pH-responsive properties of this new type of Pickering emulsifier [50, 51].

In addition to 4VPy, 1-vinyl imidazole (1VID) and 2-(methacryloyl) ethyl trimethyl ammonium chloride (MTC) were also shown to be efficient auxiliary comonomers by Chen and coworkers [52, 53]. Both strategies allowed the preparation of silica/PMMA raspberry-like composite particles, provided that enough comonomer was used. Although for 1VID, the composite particle size decreased with increasing silica content as expected, surprisingly the final particle size was independent of the silica concentration in the case of MTC. The overall synthetic scheme is illustrated in Fig. 8 for 1VID. These composite colloids are of potential interest for electrocoating applications, as recently reported by Kammona et al. [54].

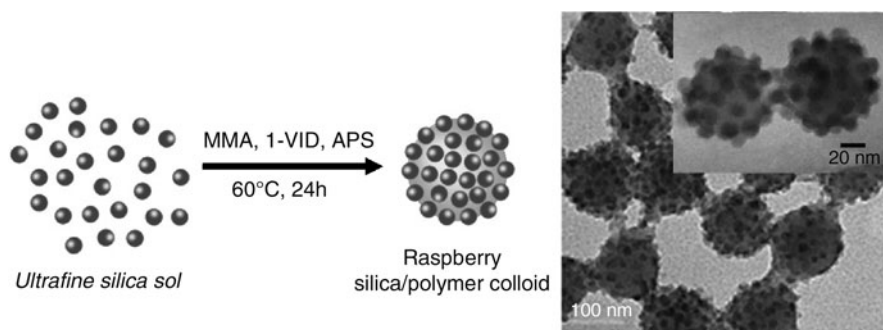


**Fig. 8** *Left*: Reaction scheme for the formation of silica/PMMA raspberry-like colloids prepared using 1VID as auxiliary comonomer. *Right*: TEM images of obtained nanocomposite particles. Reproduced from [52, 54] with permission of American Chemical Society and Elsevier, respectively



All the above-mentioned nanocomposite colloid syntheses involving an auxiliary comonomer were performed in the absence of surfactant, the composite particles being stabilized by the nanosized silica particles (below 20 nm in diameter) adhering on their surface. The auxiliary comonomer method can also be extended to larger silica particles provided that some surfactant is used to stabilize the composite latex. Following this strategy, Cheng et al. reported the elaboration of silica/PMMA composite particles through conventional emulsion polymerization using silica particles with diameters of 60, 250, and 500 nm as seeds and 4VPy as auxiliary comonomer [55]. Raspberry-like or core-shell morphologies were obtained depending on the surfactant concentration, the monomer to silica ratio, and the type of monomer addition (either at once or semi-continuously).

#### 2.1.4 Cationic Initiators

Another efficient synthetic route to the formation of polymer/silica nanocomposite colloids is through electrostatic adsorption of the cationic 2,2'-azobis (2-amidinopropane) dihydrochloride (AIBA) initiator. Pioneering works in this field were reported in 2001 by Luna-Xavier et al., who described the synthesis of silica/PMMA nanocomposite latexes by emulsion polymerization using AIBA in combination with a non-ionic surfactant [56–58]. The role of the suspension pH and the influence of the monomer, silica, and initiator concentrations on nanocomposite formation was investigated in depth and analyzed in a quantitative way [57]. Although electrostatic attraction between the cationic polymer end groups and the negatively charged silica surface was shown to be the driving force of composite particle formation at high pH, polymerization in adsorbed surfactant bilayers appeared to be the predominant mechanism at lower pH. Depending on the diameter of the silica beads, either strawberry-like (the silica being inside the particles) or core-shell morphologies (the latex forming the shell) were produced by this method. The approach was extended later by Qi and coworkers to nanometric silica and soft polymers [59]. Under such conditions, the silica particles were mainly located at the polymer surface. The raspberry-like colloids produced in this way were further encapsulated by a PMMA shell.

As shown in the recent work of Dupin et al., AIBA can also be advantageously combined with 2VPy to synthesize polymer/silica composite particles by soap-free emulsion polymerization [60]. Here, strong electrostatic interaction of the cationic initiator with the anionic silica ensured the formation of raspberry-like silica/polymer colloids with high silica aggregation efficiency as compared to the anionic persulfate initiator originally used by the same group (Sect. 2.1.3). Getting almost complete silica incorporation in such syntheses is essential because the excess silica sol may compromise the performance of the nanocomposite material in certain applications. The approach was next extended to a commercially available glycerol-modified silica sol in the absence of any added auxiliary comonomer [61–63]. The authors pointed out the importance of using the cationic AIBA initiator in combination with the glycerol-functionalized silica to achieve the desirable

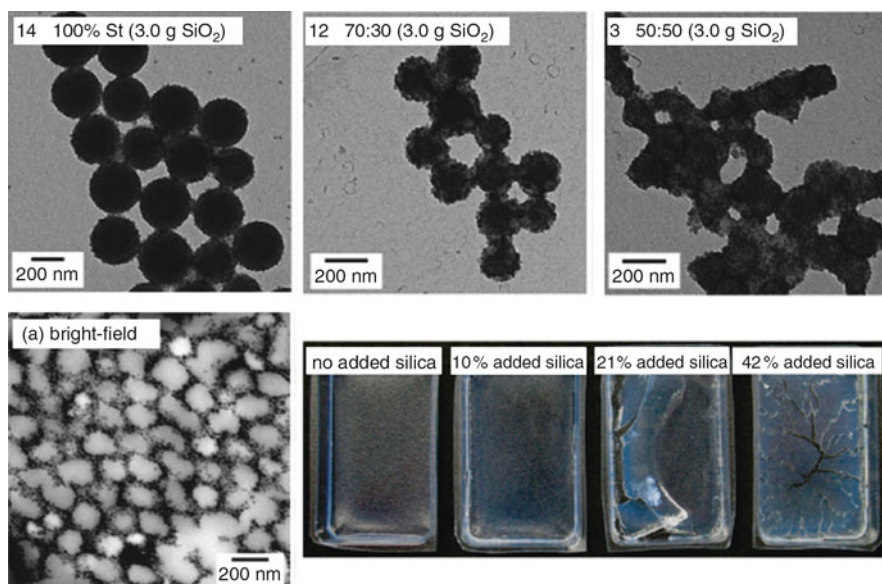


**Fig. 9** *Top row*: TEM images of a series of nanocomposite particles synthesized by emulsion copolymerization of styrene and BA of varying mass ratios in the presence of a cationic azo initiator and a commercial ultrafine glycerol-modified silica sol. *Bottom row*: TEM of an ultramicrotomed section of nanocomposite particles obtained for a 50:50 styrene:BA mass ratio (*bottom left*). Digital photographs of nanocomposite films deliberately contaminated by increasing amounts of silica, showing significant embrittlement and illustrating the detrimental effect of excess silica on film properties (*bottom right*). Reproduced from [63] with permission of American Chemical Society

morphology in very high yields. This optimized protocol was further extrapolated to film-forming poly(styrene-*co*-BA) copolymers [63]. Figure 9 illustrates the morphological variations observed with increasing BA content and the resulting film nanostructure. As highlighted by the authors, these nanocomposites offer great advantages in coating applications compared to composite films prepared by simply mixing the silica sol with a film-forming latex suspension.

### 2.1.5 Soap-Free Latexes

As mentioned above, almost all polymerizations performed in the presence of an auxiliary comonomer were conducted without surfactant [47–55, 60]. Since these early works, several groups have demonstrated that silica particles can stabilize polymer latexes provided that wetting of the nanoparticles with the polymer chains is favorable [64–68]. The overall process, often referred to as Pickering stabilization by reference to the stabilization of two immiscible liquids by solid particles [69], has



recently found a resurgence of interest as illustrated by the numerous examples provided throughout this review. More details on Pickering emulsions can be found in the review article by Bon [70].

Although the aforementioned articles are relevant to this section, the intent of the following is to complement – rather than repeat – a discussion on these papers. For instance, Zhang et al. have reported the synthesis of latexes with 40% solid content through emulsifier-free emulsion polymerization of BA, hydroxyethyl methacrylate (HEMA), and AA in the presence of a nanometric colloidal silica suspension [65]. Although the mechanism of composite particle formation was not discussed, this is to our knowledge the first example of the synthesis of high-solid-content, film-forming polymer/silica composite particles in the absence of surfactant. Another particular example of interest is the recent work of Colver et al. on the synthesis of PMMA latexes armored with 25-nm diameter Ludox silica nanoparticles [66]. Here, the suspension pH was the key to the process and was maintained around 5.5 to ensure the formation of raspberry-like particles that were uniformly distributed in size without any coagulation. Although the authors did not discuss this point in detail, they stressed that the solid content could be increased up to 45%. Unfortunately, for unclear reasons, the strategy was unsuccessful for both styrene and butyl acrylate, which illustrates that there is still a lot of work to do before getting a clear picture of particle nucleation and stabilization in such systems. Multilayered composite colloids with a hairy outer layer of polyacrylonitrile or a soft shell of poly(*n*-butyl acrylate) were obtained by feeding the armored colloids with the corresponding monomers in the presence of an anionic surfactant. Interestingly, the silica nanoparticles were found to migrate and expand through the soft shell (Fig. 10).

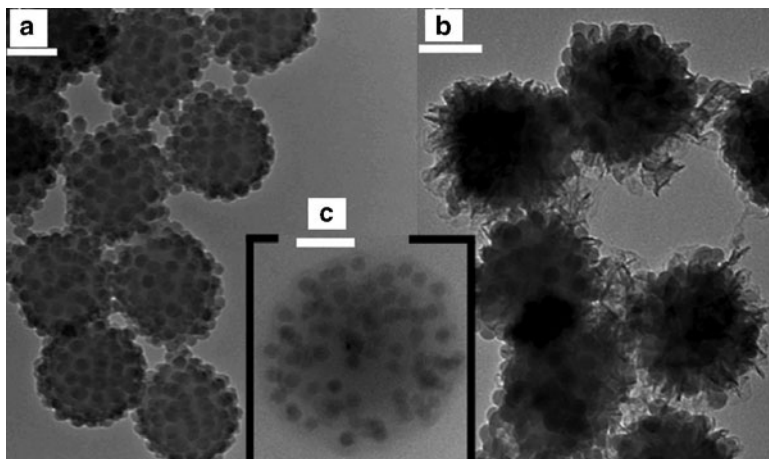


**Fig. 10** TEM images (scale bars: 100 nm) of (a) PMMA latex armored with Ludox silica nanoparticles. Multilayered nanocomposite polymer colloids with (b) a “hairy” outer layer of polyacrylonitrile, and (c) a soft shell of poly(*n*-butyl acrylate). Reproduced from [66] with permission of American Chemical Society

Also relevant to this section is the very recent work of Sheibat-Othmann and Bourgeat-Lami on the synthesis of PS latex particles stabilized by Klebosol and Ludox silica particles in the presence of a PEGMA macromonomer [68]. In contrast to the previous work of Colver et al., polymerizations performed under basic conditions provided colloiddally stable latexes using Ludox silica and styrene monomer. The PEGMA macromonomer probably plays a determinant role that makes both systems quite different from the physico-chemical point of view, although similar ingredients were used. Even if it can be argued that polymerization into monomer droplets is unlikely in such “Pickering” polymerizations due to the large size of the emulsion droplets compared to the size of the composite particles, the authors showed that the monomer droplets could efficiently compete for silica adsorption, leading to some temporary instability during polymerization. Besides these physico-chemical aspects, the study highlighted the importance of stirring on the reaction rate and particle stability and also showed that, under certain conditions, the silica particles formed a barrier to radical absorption and decreased the polymerization rate.

Finally, it is also worth mentioning the BASF patent on the synthesis of high-solid-content polyacrylate/silica latexes incorporating a high amount of silica [71]. The silica particles appear to be glued together by the polymer, thereby forming some kind of heterocoagulated polymer/silica beads with a rough surface [71]. These latexes have found a commercial application as transparent, flame retardant, scratch-resistant coatings [72]. To our knowledge, this is one of the first and rare examples of commercial polymer/silica nanocomposites.

## 2.2 *Coating of Polymer Latexes with a Silica Shell*

Core-shell particles have attracted much research attention in recent years because of their great potential in the protection, modification, and functionalization of the core with suitable shell materials to achieve specific physical or chemical performances. For instance, the optical, electrical, thermal, mechanical, magnetic, and catalytic properties of core particles can be finely tuned by coating them with a thin mineral shell [73, 74]. Silica shells are produced by a variety of methods that can be divided into two groups: (1) the layer-by-layer self-assembly of preformed silica nanoparticles on oppositely charged templates, and (2) seeded polycondensation techniques involving sol-gel precursors. The former method is outside the scope of this article and only the second method will be discussed.

Although many inorganic surfaces can be directly coated with silica because of the significant affinity between both materials, latex particles must be functionalized by grafting or adsorption of appropriate compounds that can enhance the coupling (and thus deposition) of the silica precursor on their surface. These molecules are either groups capable of undergoing a chemical reaction with the sol-gel precursor or ionic molecules capable of promoting electrostatic attraction between the latex core and the inorganic shell.

For instance, Tissot et al. reported the successful incorporation of silanol groups on the surface of PS latex particles using MPTMS as a functional (co)monomer [75–77]. These surface silanols enabled the subsequent growth of a silica shell onto the PS seed by addition of TEOS and ammonia to the colloidal suspension, either in water or in a mixture of ethanol and water. No secondary-nucleated silica particles were formed, indicating strong affinity of the sol–gel precursor for the polymer surface. Burning of the latex core resulted in the formation of hollow silica spheres. One main advantage of this method is that the nature and the size of the polymeric core can be tuned by conventional polymer colloid chemistry, while the shell thickness can be accurately controlled by the silica-to-polymer weight ratio and the diameter of the latex core. The technique was also successfully applied to the synthesis of core–shell latexes made of a soft poly(BA) core coated by a rigid silica shell. Such soft/hard core–shell particles can find applications as nanofillers for impact resistance improvement.

Following a related approach, Castelvetro et al. reported the formation and properties of hybrid latex films resulting from the coalescence of low  $T_g$  poly(BA-*co*-MMA-*co*-MPTMS) terpolymer latex particles coated by a silica shell [78]. The latex was synthesized at neutral pH by semi-continuous emulsion polymerization under starved-feed conditions in order to protect the MPTMS monomer from premature hydrolysis and condensation reactions. A substantial amount of free silanols were therefore available for further reaction with the silica precursor. In order to avoid the formation of a densely crosslinked silica network around the latex core, which may significantly alter film formation, the pH was kept at around 2 (at this pH, hydrolysis is promoted and condensation is significantly retarded). TEM and AFM studies of the nanocomposite film indicated that the silica shell formed a continuous percolating network throughout the polymer matrix. A porous film of interconnected hollow silica spheres was next elaborated by thermo-oxidative decomposition of the organic phase.

It is also possible to grow silica shells without functionalizing the latex core. In this case, the opposite charges developed on the core and shell materials promote shell formation through electrostatic attraction. For example, Hotta and coworkers reported the deposition of a thin silica film onto PS spheres by the addition of an acidic hydro-alcoholic solution of pre-hydrolyzed TEOS [79]. The final silica film thickness was optimum at pH below the isoelectric point of silicic acid, at which the electrostatic attraction between the silica precursors and the negatively charged PS spheres was maximized. Ordered macroporous materials were subsequently formed by centrifuging the silica-coated PS particles and removing the latex core by calcination. In a related approach, Cornelissen [80] and Lu [81] used amino-functionalized PS spheres to promote charge attraction between the PS beads and the silica shell. Above pH 10, the amine-functionalized template is slightly positively charged and, consequently, the silica sols could easily nucleate on the surface of each PS bead and eventually merge and grow into a thin uniform silica shell. A similar approach was recently followed by Yang et al., who adsorbed poly-L-lysine (a polyamino acid) on amino-functionalized PS spheres [82]. It was found that poly-L-lysine promoted the growth of a continuous shell without the concurrent formation of secondary nucleated silica particles (Fig. 11).

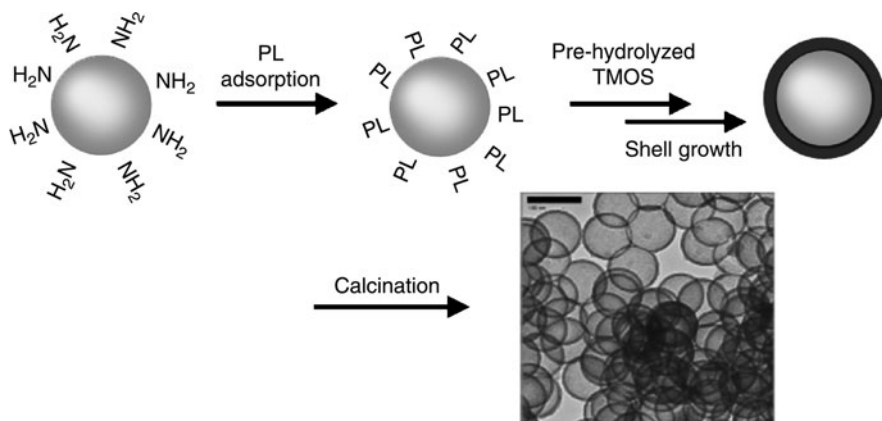


**Fig. 11** Representation of the coating of polymer colloids with silica using poly-L-lysine as compatibilizer, with TEM image of the resulting hollow silica spheres. Scale bar: 100 nm Adapted from [82] with permission of American Chemical Society

Graf and coworkers reported a general strategy to coat polymer particles with silica that provided uniform and smooth coatings without the use of silane coupling agents or electrostatic attraction [83]. Here, the deposition was assisted by the addition of poly(*N*-vinyl pyrrolidone) (PVP). Depending on whether PVP was adsorbed flat on the surface or in the form of trains (which in turn depends on PVP molecular weight), either rough or smooth silica coatings were obtained. PVP was also used by Kobayashi et al. with the aim of suppressing the formation of free-standing silica particles and improving shell uniformity [84]. However, the strategy was less successful in this case, as judged from the TEM images. This last example and many other nonconclusive works show that controlling the homogeneity and the thickness of the silica shell without forming rough surfaces and/or plain colloids requires a set of experimental conditions to be fulfilled and is particularly challenging. Although some approaches were undoubtedly successful, there is no universal method to date that allows the formation of high-solid-content suspensions of silica-coated particles with thick, smooth, and uniform shells. There is still much work to be done in this field before one can envisage commercial applications of such products.

### 3 Synthesis of Magnetic Latex Particles

During the last few years, different synthetic procedures have been reported for the synthesis of magnetic nanoparticles. These methods include co-precipitation, thermal decomposition and/or reduction, microemulsion synthesis, and hydrothermal synthesis. Despite poor shape control and quite polydisperse particles, co-precipitation is probably the simplest synthetic route. By contrast, thermal decomposition is experimentally more demanding but affords the best results in

terms of size and shape control of the nanoparticles. To date, these two routes are the most explored, and they provide magnetic nanoparticles on a large scale. This probably explains why iron oxides used in emulsion polymerization are, in most cases, obtained by co-precipitation. This consists of aqueous solutions of iron salts ( $\text{Fe}^{2+}/\text{Fe}^{3+}$ ) precipitated by the addition of a base, usually under inert atmosphere, at room or elevated temperatures. Various parameters can influence the size, morphology, and composition of the magnetic nanoparticles:  $\text{Fe}^{2+}$  to  $\text{Fe}^{3+}$  initial ratio, temperature, pH, and ionic strength. Stable aqueous or organic dispersions of the magnetic nanoparticles (3–30 nm in size) are obtained by the use of surface-active species capable of generating repulsive interactions between the particles. These species could be: (1) charged molecules (e.g., citrate or tetramethyl ammonium ions), (2) surfactant (e.g., OA), or (3) polymer [e.g., poly(acrylic acid) (PAA) or polyvinyl alcohol (PVA)]. The obtained stable dispersions are often called “ferrofluids”. Indeed, the strong interactions between the solvent molecules and the iron oxide nanoparticles ensure a uniform magnetic behavior of the whole fluid, which behaves like a single-phase system when a magnetic field is applied [85]. Regarding their magnetic properties, these nanoparticles are superparamagnetic, which means that they respond to a magnetic field but lose their magnetization when the field is removed. Readers who are interested in a detailed review on the synthesis, properties, and applications of magnetic nanoparticles are referred to the recent paper from Lu et al. [86].

Bare magnetic nanoparticles are sensitive to oxidation in air therefore it is necessary to develop efficient strategies to avoid any stability issues. This can be achieved by the production of a polymer shell, which will not only protect the inorganic component, but will also provide the nanoparticles with selective functionalities needed for further applications. The nanoparticles can also be gathered into one larger polymer particle. Indeed, polymer particles incorporating magnetic iron oxide nanoparticles such as magnetite ( $\text{Fe}_3\text{O}_4$ ) or maghemite ( $\gamma\text{-Fe}_2\text{O}_3$ ) find a wide range of applications, notably in catalysis, environment and food analysis, water treatment, and biotechnology, for which the magnetic properties of the particles are sought for effective separation steps [86–88]. To date, the major field of interest remains the biomedical field, in which the magnetic nanoparticles have been successfully used as solid support for the purification, extraction, and concentration of biomolecules in biomedical diagnostics, as contrast agents in magnetic resonance imaging, as mediators in hyperthermia, and as carriers for guided drug delivery [86, 89–92].

Whatever the targeted applications, the PSD has to be narrow to ensure a uniform response to an external magnetic field, and the magnetic material has to be homogeneously distributed and properly encapsulated in order to avoid any leakage of iron oxide. Moreover, appropriate surface functionalities should allow further selective binding with (bio)molecules. Finally, the size of the magnetic particles must be finely tuned according to the targeted application. Those in the submicrometer range are particularly interesting because of their low sedimentation rate, large specific surface area for immobilization of (bio)molecules, and potential integration in microfluidic-based technologies.

Instead of presenting an exhaustive survey of all the literature, which would by far exceed the scope of this review, we will present typical and representative

examples of the synthesis of magnetic latex particles using emulsion polymerization as one of the key step of their synthesis. In addition, this article will focus on iron oxide nanoparticles such as magnetite  $\text{Fe}_3\text{O}_4$  and maghemite  $\gamma\text{-Fe}_2\text{O}_3$ , which are the most-described magnetic nanoparticles for the synthesis of magnetic latex particles. Besides, they are currently the only accepted non-toxic magnetic materials for medical applications [93]. The literature also offers a few examples using cobalt [94], cobalt ferrite ( $\text{CoFe}_2\text{O}_4$ ) [95], nickel or cobalt metal [96–98],  $\text{Ni}_{0.5}\text{Zn}_{0.5}\text{Fe}_2\text{O}_4$  [99], and NiS [100].

### ***3.1 Encapsulation of Iron Oxide Nanoparticles by Emulsion Polymerization***

The preparation of magnetic latex particles using emulsion polymerization in the presence of a freshly prepared ferrofluid was first reported in the late 1970s and at the beginning of the 1980s but was not investigated in detail [101–103]. Since then, a great number of studies have been published in the literature, and magnetic nanoparticles are one of the most documented types of inorganic particle being used to form composite colloids. Most of the reported works rely on the synthesis of polymer particles through conventional emulsion polymerization methods carried out in the presence of colloidal iron oxides (most often used as magnetic seeds). An overview of the various methods reported in the literature is given in the following sections.

#### **3.1.1 Surfactant Bilayer (Admicellar Polymerization)**

One of the basic requirements for efficient encapsulation of inorganic nanoparticles is to enhance the interfacial affinity between the nanoparticles and the monomer. One frequently encountered strategy for achieving this is to create hydrophobic loci inside a bilayer of surfactant(s). Indeed, the primary surfactant is the one coating the nanoparticles after their synthesis and allowing dispersion of the nanoparticles in nonpolar solvents. Once the excess of the primary surfactant is removed, the nanoparticles are coated with a secondary surfactant to form a self-organized bilayer of the two surfactants on the surface of the nanoparticles, thus allowing their dispersion in water [104–106]. The hydrophobic interlayer thus formed between the two surfactants can solubilize the monomer and finally promote the polymerization close to/at the vicinity of the surface of the nanoparticles, according to the so-called admicellar polymerization mechanism (Fig. 12).

Meguro et al. were among the first to explore this method for the encapsulation of non-magnetic iron oxide ( $\alpha\text{-Fe}_2\text{O}_3$ ) and titanium dioxide through emulsion polymerization of styrene adsolubilized into adsorbed bilayers of sodium dodecyl sulfate (SDS) [107]. Using the same concept, magnetic PS and PMMA particles were obtained by Yanase et al. [108, 109] using a commercial ferrofluid with magnetite particles covered by sodium oleate and sodium dodecylbenzenesulfonate

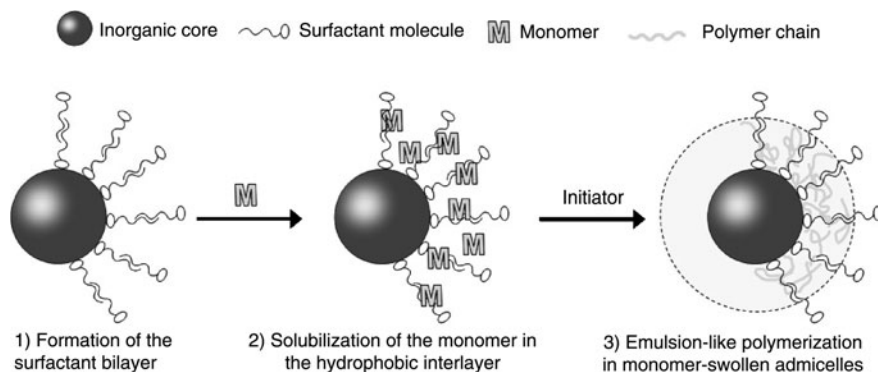


**Fig. 12** Pigment encapsulation through an emulsion-like polymerization reaction. The process involves (1) formation of surfactant bilayers, (2) solubilization of monomer, and (3) free radical polymerization

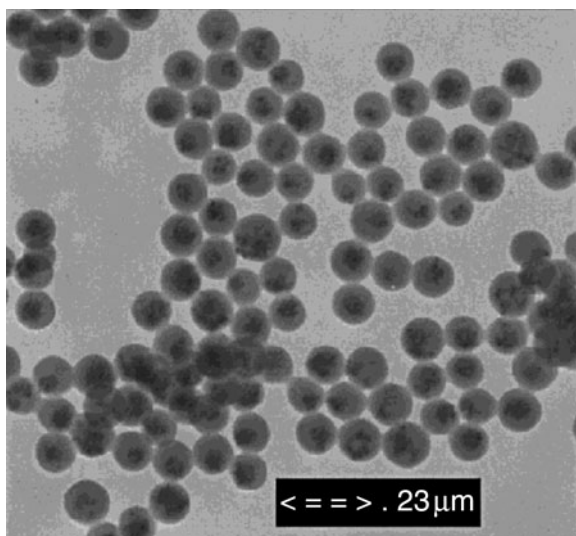


**Fig. 13** TEM image of PS-iron oxide composite particles. Reprinted from [110] with permission of the American Chemical Society

(SDBS). The process yielded PS particles with up to 20 wt% of encapsulated  $\text{Fe}_3\text{O}_4$ . However, the latex yield was generally low and the PSD quite broad, leading to an inhomogeneous distribution of magnetite from one particle to another. Still using the bilayer procedure with OA and SDBS-coated  $\gamma\text{-Fe}_2\text{O}_3$ , highly charged and monodisperse superparamagnetic latex particles of poly[styrene-*co*-MMA-*co*-sodium styrene sulfonate (NaSS)] were prepared (Fig. 13). These were then assembled into colloidal crystals, which were found particularly suitable for the creation of unique magnetically induced photonic bandgap materials [110, 111].



Magnetic latex particles of PMMA (in the range of  $100 \pm 50$  nm) were obtained by soapless seeded emulsion polymerization performed in the presence of 10-nm  $\text{Fe}_3\text{O}_4$  nanoparticles coated with a bilayer of lauric acid [112]. This work shed light on the importance of keeping a good balance between the amount of iron oxide nanoparticles (and hence the surfactant bilayer) and the initial amount of MMA: too high an amount of monomer (higher than the bilayer could accommodate, thus leading to destruction of the bilayer) led to the expected seeded emulsion polymerization but also to a crop of particles generated by self-nucleation (including either homogeneous or micellar nucleation) (Fig. 14). The particle size was consequently larger in this case. Kinetic modeling of this system was also established [113]. In an approach very similar to Wang's work,  $\gamma\text{-Fe}_2\text{O}_3$  modified by myristic acid and soluble in octane was dispersed in SDS solution [114]. Subsequent polymerization of styrene, divinylbenzene (DVB) and NaSS provided composite particles, but iron oxide nanoparticles were confined to the surface of the polymer particles. These particles nevertheless easily aligned in the presence of a magnetic field and could find potential applications in proton-exchange membranes. Another related work reports the soapless emulsion polymerization of styrene/BA/methacrylic acid (MAA) in the presence of sodium dodecylsulfonate- $\text{Fe}_3\text{O}_4$  [115]. The influence of various parameters on particle size and PSD was discussed, in particular the effect of the polarity medium (through the addition of a polar solvent).

The admicellar polymerization concept was also applied to the synthesis of thermosensitive magnetic latex particles based on *N*-isopropylacrylamide (NIPAM). In this case, however, the polymerization could be better defined as seeded precipitation polymerization owing to the water solubility of this monomer. Kondo et al. [116] were among the first to synthesize PNIPAM particles using  $\text{Fe}_3\text{O}_4$  nanoparticles covered with two layers of OA and SDBS. *N,N'*-Methylene bisacrylamide

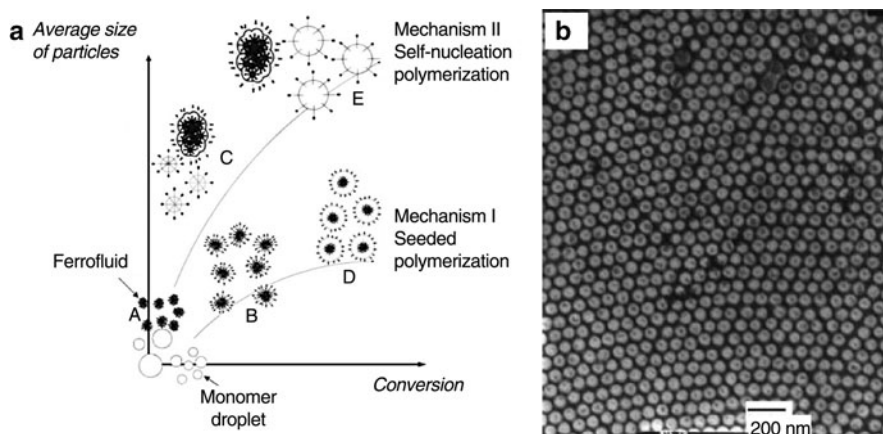


**Fig. 14** (a) Mechanisms proposed in [112] for particle nucleation and growth in the case of MMA soapless emulsion polymerization in the presence of  $\text{Fe}_3\text{O}_4$  coated with a bilayer of lauric acid. (b) TEM image of an example of composite magnetic particles obtained. Adapted from [112] with permission of Wiley Periodicals



(MBA) was used as a crosslinker, and MAA allowed the introduction of carboxyl groups for the subsequent covalent immobilization of proteins. Monodisperse magnetic and thermosensitive particles loaded with up to 10 wt% of magnetic material were obtained and successfully used for enzyme immobilization. The thermosensitivity of the particles could be varied by introducing styrene [117]. First, magnetite nanoparticles modified by a double layer of OA and SDBS were encapsulated inside PS particles using surfactant-free emulsion polymerization. These particles were then used as seeds for the emulsion copolymerization of NIPAM and MAA. The surface of the obtained submicrometer particles (loaded with up to 10 wt% of magnetic material) were then functionalized via covalent immobilization of bovine serum albumin (BSA) using carbodiimide chemistry, and successfully used in anti-BSA antibody purification. In some cases, NIPAM was polymerized in the presence of a few percent of AA in order to impart pH sensitivity [118].

More recently, Lee et al. [119, 120] described the synthesis of the same kind of particles (without, however, referring to the previous work of Kondo). The difference lies in the coverage of  $\text{Fe}_3\text{O}_4$  nanoparticles, which were in this case coated with either a bilayer of lauric acid or with PAA oligomers. For each surface treatment, the influence of the initiator (either potassium persulfate (KPS) [119] or AIBA [120]) on the mechanism of particle formation, PSD, and particle morphologies was discussed. PSD was generally quite broad and the iron oxide nanoparticles were either located in the PS core or adsorbed at the surface. Further encapsulation with poly(NIPAM-*co*-MAA) provided core-shell particles.

In many of the works described above, a functional monomer such MAA, AA, or NaSS was introduced to provide the particles with chemical groups that allowed their utilization in specific applications. A variety of functional magnetic particles were prepared for various purposes. For instance, carboxyl-functionalized magnetic PS particles were produced from 10-nm  $\text{Fe}_3\text{O}_4$  coated with a bilayer of OA and sodium 10-undecenoate as primary and secondary surfactants, respectively [121]. The authors discussed the influence of the initiator on the morphology of the final particles (homogeneous encapsulation with KPS, not with benzoyl peroxide). Up to 42 wt% of magnetic material could be encapsulated (with a corresponding saturation magnetization,  $M_s$ , of  $30\text{ emu g}^{-1}$ ). Successive immobilization of proteins such as BSA was achieved. In the same way, chaperone protein was immobilized on carboxyl-functionalized magnetic particles to assist the *in vitro* refolding of a lipase (i.e., *B. cepacia* lipase) [122].

$\beta$ -Diketone groups were introduced on the surface of magnetic particles through the emulsion copolymerization of styrene and acetoacetoxyethyl methacrylate (AAEM) in the presence of sodium-oleate-modified 10-nm  $\gamma\text{-Fe}_2\text{O}_3$  nanoparticles [123]. Varying the initial iron oxide to monomer ratio or initial AAEM concentration led to composite particles incorporating up to 15 wt% of maghemite ( $M_s$  ca.  $16\text{ emu g}^{-1}$ ) and displaying various morphologies, including raspberry-like particles. The PSD was, however, quite broad, whatever the final particle size (600–200 nm, depending on the initial recipe). In another relevant work, Pd catalysts were immobilized onto superparamagnetic polymer nanoparticles consisting of a  $\gamma\text{-Fe}_2\text{O}_3$  core and a poly[styrene-*co*-DVB-*co*-4-vinylbenzene chloride (VBC)]

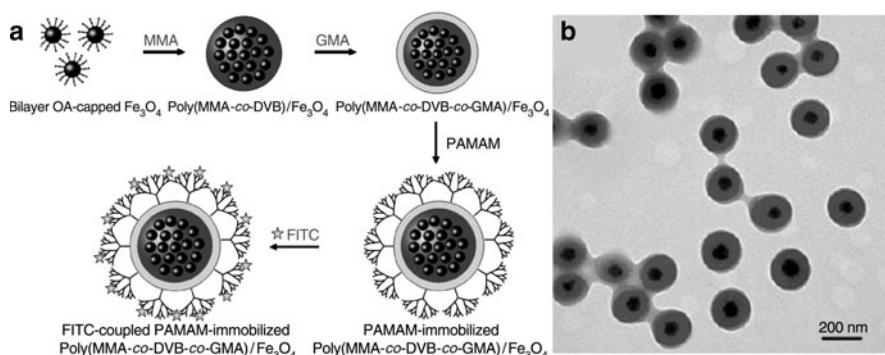


**Fig. 15** (a) Preparation of dendritic PAMAM-immobilized magnetic poly(MMA-*co*-DVB-*co*-GMA) particles and coupling with FITC. (b) TEM image of the magnetic poly(MMA-*co*-DVB-*co*-GMA) microspheres with 10 wt% of DVB. Adapted from [126] with permission of the American Chemical Society

shell [124]. The chloro group was used to introduce N-heterocyclic carbenes that could form strong complexes with Pd catalysts. The obtained Pd-supported nanoparticles successfully promoted Suzuki cross-coupling reactions. Acrylamide (AAm) was recently used as a functional monomer in the emulsion polymerization of styrene carried out in the presence of Fe<sub>3</sub>O<sub>4</sub> coated by OA/SDS bilayer [125]. Using microwave irradiation to initiate the polymerization, monodisperse magnetic particles of poly(styrene-*co*-acrylamide) were formed with up to 46 wt% of magnetite. The aim of the authors was to use amidocyanogen groups for further covalent binding of biomolecules; however, this was not demonstrated. Magnetic particles with an increased degree of functionality were recently produced through the attachment of poly(amidoamine) (PAMAM) dendrimers using the epoxy groups available at the surface of poly[MMA-*co*-DVB-*co*-glycidyl methacrylate (GMA)] magnetic particles obtained using bilayer-OA-coated Fe<sub>3</sub>O<sub>4</sub> nanoparticles (Fig. 15) [126]. Highly fluorescent particles were then obtained through the covalent coupling of fluorescein isothiocyanate (FITC).

As illustrated by the studies detailed above, admicellar polymerization can lead to various morphologies and very often not to the expected core-shell ones. Nevertheless, despite the variety of obtained morphologies, the aforementioned particles (when properly functionalized) have found applications in various fields such as catalysis, optoelectronics, or biotechnology. Some of the works presented so far show very interesting and promising results, with an effective and homogeneous distribution of iron oxide nanoparticles inside the synthesized polymer particles, together with a high magnetic content. But, most suffer from one or several of the following drawbacks: the PSD can be quite broad, the magnetic content is not systematically high, the distribution of iron oxide may be inhomogeneous from one particle to another and inside the particle (in the core versus at the periphery), or the solid content of the final latex can be quite low. To circumvent some of these limitations (but unfortunately not all of them at the same time), alternative procedures have been developed.

### 3.1.2 Other Surface Coatings of Iron Oxide Nanoparticles

The surfactant bilayer strategy is obviously not the only method that has been developed to favor polymerization at the surface of iron oxide nanoparticles. Thus, other (macro)molecules have been employed to this aim. Recently, various polymers such as PAA [119, 120], PMAA [127], chitosan [128], or dextran derivatives [129–131] have been used as steric stabilizers to form aqueous dispersions of iron oxide nanoparticles for use in emulsion polymerization. In the case of PMAA [127], the cationic AIBA azo initiator was first adsorbed on PMAA-coated  $\text{Fe}_3\text{O}_4$  to favor monomer polymerization in the vicinity of the nanoparticles. The magnetic nuclei thus formed aggregated and yielded magnetic PS particles with a raspberry-like morphology. Dextran derivatives were used for the synthesis of PGMA magnetic particles.

Poly(ethylene glycol) (PEG) was also used to modify the surface of iron oxide nanoparticles. For instance, fluorescent and magnetic polysaccharide-based particles were prepared in three steps [132]. First, commercial magnetite powder and europium phthalate complex (fluorescent) were blended and dispersed in a PEG solution to obtain fluorescent magnetite colloid particles (FMCPs). Copolymerization of styrene and maleic anhydride in the presence of FMCPs seeds led to magnetite europium phthalate/poly(styrene-*co*-maleic anhydride) core-shell composite microspheres. Finally, heparin was conjugated with the surface anhydrides to form FMCPs/SMA heparin glycoconjugate core-shell composite particles. In another work, commercial  $\text{Fe}_3\text{O}_4$  was modified with PEG for the synthesis of azidocarbonyl-functionalized magnetic particles via a two-step procedure [133]. First, magnetic poly(styrene-*co*-AAm-*co*-AA) particles were obtained through emulsion polymerization performed in water/ethanol mixture in the presence of PEG-modified  $\text{Fe}_3\text{O}_4$  and a small amount of SDS. Azidocarbonyl groups were then converted into amido groups and successfully used for covalent protein immobilization. Margel's group very recently reported the use of gelatin-modified  $\gamma\text{-Fe}_2\text{O}_3$  in the emulsion polymerization of two particular monomers: (1) an iodinated methacrylate, allowing the synthesis of radio-opaque magnetic core-shell nanoparticles for X-ray imaging applications [134], and (2) a fluorinated acrylate, leading to the formation of magnetic core-shell nanoparticles used for inhibition of insulin amyloid fibril formation [135]. Using the same polymerization procedure, the formation of poly(divinyl benzene) (PDVB)-coated maghemite nanoparticles was also studied [136]. Air-stable carbon-coated iron ( $\alpha\text{-Fe/C}$ ) crystalline nanoparticles were obtained by annealing the PDVB-coated maghemite nanoparticles to form magnetic particles with higher Ms ( $83 \text{ emu g}^{-1}$  versus  $33 \text{ emu g}^{-1}$  for  $\gamma\text{-Fe}_2\text{O}_3$  based particles).

### 3.1.3 Emulsion Polymerization-Related Procedures

Some of the works depicted in the literature cannot be rigorously classified as emulsion polymerization methods. These strategies, sometimes quite original and innovative, usually imply multiple steps (one of them being emulsion polymerization).

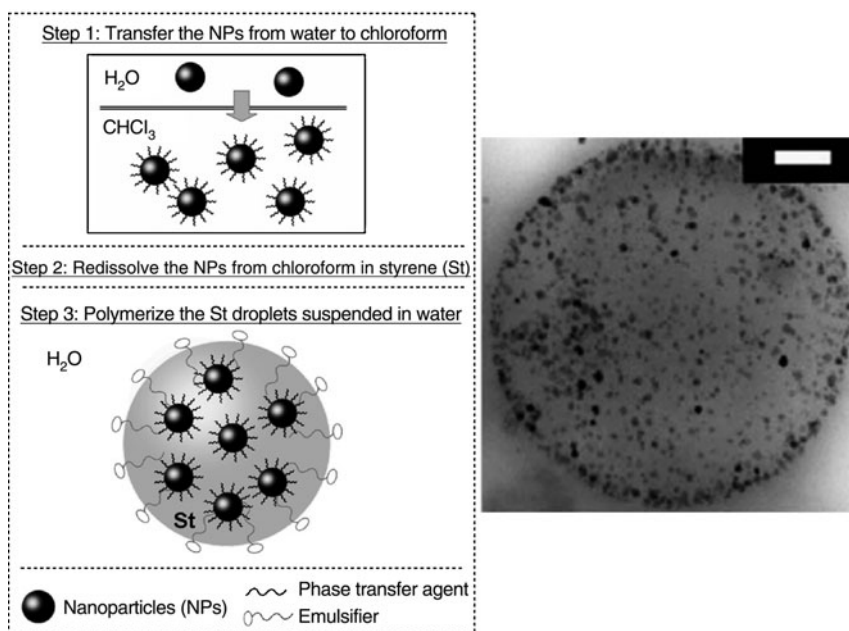


**Fig. 16** Synthesis of Fe<sub>3</sub>O<sub>4</sub>/PS particles. *Left*: Scheme of the process. *Right*: TEM photo of Fe<sub>3</sub>O<sub>4</sub>/PS particle (scale bar: 100 nm). From [137] with permission of the Royal Society of Chemistry

They rely on vigorous stirring or ultrasonication, either to help the dispersion of iron oxides in water or in the monomer, or to achieve a fine dispersion of the monomer droplets before starting the polymerization. They also imply an intermediate step consisting in the encapsulation of several iron oxides in a silica particle, or the use of a magnetic emulsion as a seed instead of iron oxide nanoparticles. These processes are described below.

Yang et al. [137] described a very nice approach (though inadequately termed “mini-emulsion polymerization”) for efficient encapsulation of aqueous nanoparticles such as Fe<sub>3</sub>O<sub>4</sub>, Au, and CdTe (Fig. 16). The nanoparticles were first transferred from water to chloroform using a polymerizable surfactant as phase transfer agent. The solid NPs obtained after chloroform evaporation were then dissolved in styrene containing 2,2'-azobis(isobutyronitrile) (AIBN). An aqueous solution of a polymerizable emulsifier and a co-emulsifier (Triton X-100) was added to the styrene solution and the resulting mixture was submitted to mechanical stirring for 30 min. Polymerization was then carried out at 80°C for 6 h. The resulting magnetic polymer particles showed a very homogeneous distribution of Fe<sub>3</sub>O<sub>4</sub> inside the polymer particles of a few micrometers (typically 3 μm, with broad PSD). Bifunctional (magnetic with Fe<sub>3</sub>O<sub>4</sub> and fluorescent with CdTe) particles were also reported by the same team [138]. Better results in terms of fluorescence were obtained if the magnetic NPs were first coated with silica and functionalized with MPTMS. In addition, use of ultrasonication instead of mechanical stirring allowed decreasing particle size (from a few micrometers to 136 nm) and narrowing of the PSD.

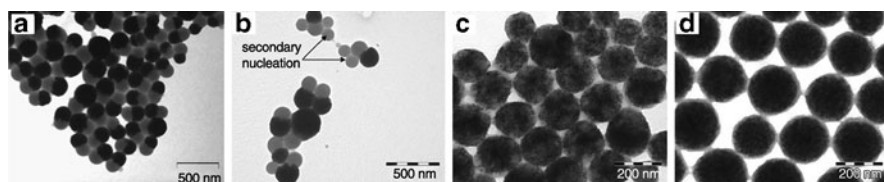


**Fig. 17** TEM images of PS magnetic particles obtained with (a) AIBN only, (b) KPS only, (c) AIBN/DVB, and (d) KPS/DVB. Adapted from [139] with permission of Wiley Periodicals

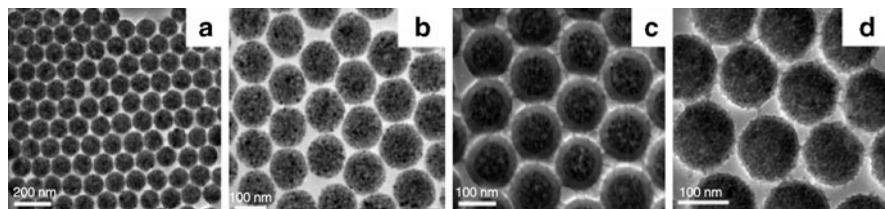


**Fig. 18** (a, b) TEM images of as-synthesized magnetic  $\text{Fe}_3\text{O}_4/\text{PS}$  nanospheres, and (c, d) silica-coated magnetic  $\text{Fe}_3\text{O}_4/\text{PS}$  nanospheres. From [140] with permission of the American Chemical Society

Instead of using stable aqueous dispersions of iron oxides, Montagne et al. [139] successfully synthesized highly magnetic latex particles (60 wt% of magnetic material), starting from a commercial oil-in-water magnetic emulsion. Depending on the initial conditions, various morphologies could be obtained (Fig. 17). The desired core-shell structure was effectively obtained with a given styrene to DVB ratio, KPS as the initiator, and an amphiphilic functional copolymer as the stabilizer of the starting magnetic emulsion. The use of this copolymer not only provided the latex with a high degree of functionalization but also ensured its colloidal stability in media of high ionic strength.

A multistep procedure combining modified miniemulsion/emulsion polymerization and the sol-gel technique was implemented by Xu et al. [140] to obtain monodisperse, nanoscale (100 nm), superparamagnetic  $\text{Fe}_3\text{O}_4/\text{PS}$  spheres coated with an adjustable silica shell (2–30 nm thick) (Fig. 18).  $\text{Fe}_3\text{O}_4/\text{PS}$  particles incorporated a very high magnetite content (86 wt%). This amount obviously decreased with the presence of the silica shell (the thicker the shell, the lower the Ms). The influence of the following parameters was studied in detail for the synthesis of  $\text{Fe}_3\text{O}_4/\text{PS}$  particles: (1) type of initiator on composite morphology, (2) feed ratio of the magnetite-containing miniemulsion and styrene macroemulsion on magnetite content, and (3) hydrophobic agent or amount of surfactant on size and size distribution. The obtained conversions were, however, low [141].

Another strategy (which could be related to seeded emulsion polymerization) was recently developed by Ding et al. [142, 143] to promote the formation of polymer chains close to the surface of iron oxides. The procedure, based on the formation of polymer-monomer pairs, was the following: PVA-coated  $\text{Fe}_3\text{O}_4$  nanoparticles were mixed with chitosan (CS) and AA polymer-monomer pair to form micelles

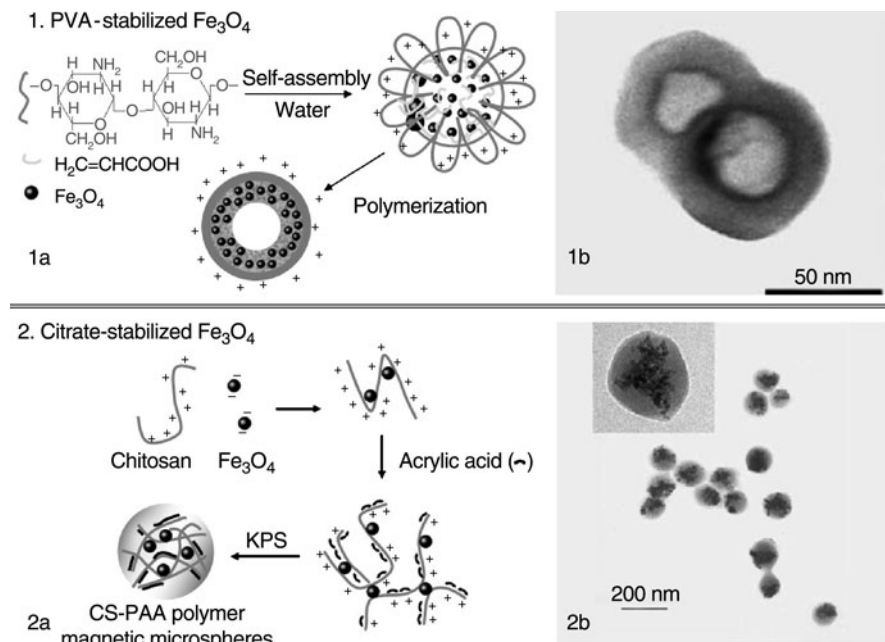


**Fig. 19** Strategy based on polymer–monomer pair with (1) PVA-stabilized  $\text{Fe}_3\text{O}_4$ : preparation of hollow magnetic particles (1a), and example of particle (cut-section TEM photo) (1b). (2) Citrate-stabilized  $\text{Fe}_3\text{O}_4$ : preparation of plain magnetic particles (2a), and example of particle (TEM photo) (2b). Adapted from [142] with permission of Wiley-VCH and from [144] with permission of Elsevier

loaded with  $\text{Fe}_3\text{O}_4$ . The cores consisted of the polyionic complexes of CS and AA (i.e., positively charged protonated CS chains and negatively charged dissociated AA), and the shells consisted of protonated CS chains. The polymerization of AA was then initiated by KPS, and followed by crosslinking of the shells with glutaraldehyde (GA) at the end of polymerization to form magnetic hollow  $\text{Fe}_3\text{O}_4$ /polymer hybrid nanospheres (ca. 80 nm in size) (Fig. 19-1). By adjusting the initial amount of CS, AA, and GA, the size could be increased to 200 nm [143]. In addition, high Ms could be attained ( $M_s = 41 \text{ emu g}^{-1}$ ). The PVA-stabilized  $\text{Fe}_3\text{O}_4$  nanoparticles interacted with AA (or PAA) via hydrogen bonds. In a second approach, citrate/ $\text{Fe}_3\text{O}_4$  nanoparticles were used [144] to form an electrostatic assembly. As a result, plain instead of hollow magnetic particles were obtained with 36 wt% of magnetite (corresponding to  $M_s = 23 \text{ emu g}^{-1}$ ) (Fig. 19-2). Their capacity to act as drug carriers was also shown. Finally, the concept was recently extended to the preparation of CS–PMAA magnetic particles [145]. In this last case, the particles were not only magnetic but also luminescent through the incorporation of negatively charged CdTe QDs.

Another valuable approach, which was detailed in Sect. 2 for silica particles, is based on the use of silane derivatives carrying vinyl groups (such as MPTMS)



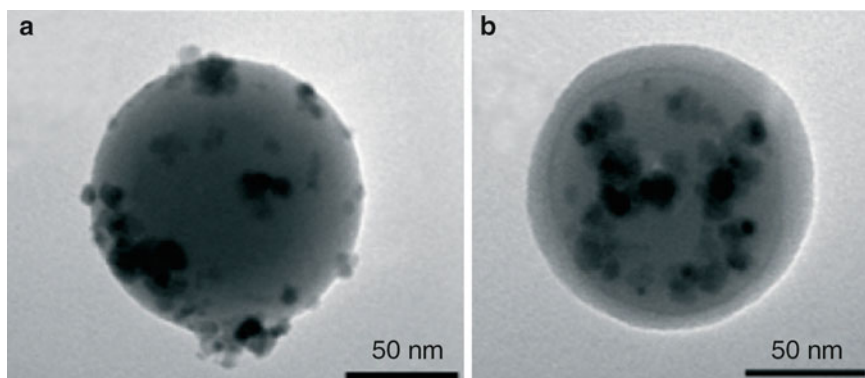


**Fig. 20** Examples of composite core-shell colloids without (a) and with (b) PMMA outer shell. The particle core consists of polymerized MPTMS-droplets stabilized by magnetite (a). Adapted from [147] with permission of Wiley-VCH

that are attached to the nanoparticles via the surface hydroxyl groups of iron oxide. Using MPTMS as a coupling agent, Sacanna et al. [146, 147] successfully obtained magnetic PMMA nanoparticles. The key step relied on the condensation of MPTMS on iron oxide nanoparticles in conditions leading to the formation of a nanoparticle-stabilized emulsion (referred to as a Pickering emulsion [148]), which was then further “frozen” by MPTMS polymerization. Because the magnetite was exposed on the surface, the obtained stable composite particles were coated with a PMMA shell through seeded emulsion polymerization (Fig. 20). The controlled magnetic moment of the resulting magnetic polymer particles was exploited for field-induced colloidal crystallization and (dipolar) chain formation.

Very original morphologies were obtained using silica-coated  $\text{Fe}_3\text{O}_4$  core-shell nanoparticles, subsequently functionalized with MPTMS [149]. Indeed, when used in styrene emulsion polymerization, anisotropic structures could be obtained by adjusting the interfacial tension (excentric spherical particles), crosslinking (concentric spherical particles), crosslinking and a large amount of styrene (anisotropic ellipsoids), or pre-swelling of concentric particles (asymmetric doublets) (Fig. 21). Using the same kind of MPTMS-grafted  $\text{Fe}_3\text{O}_4/\text{SiO}_2$  as seeds in styrene emulsion polymerization in the presence of pyrene, composite particles with a magnetic silica core and a fluorescent polymer shell were recently reported [150].

In a closely related work using silica-coated iron oxide nanoparticles, thermoresponsive and magnetic latex particles were produced through colloid-template polymerization, which consists in a three-step procedure [151]. Magnetite nanoparticles of 10 nm were obtained by co-precipitation and stabilized by citrate groups, and subsequently covered by a silica layer via a modified Stöber method. The surface of the resulting 100-nm silica-coated magnetite nanoparticles aggregates was then modified with MPTMS to introduce polymerizable groups onto the surface. These template cores were finally used as seeds in the polymerization of NIPAM in

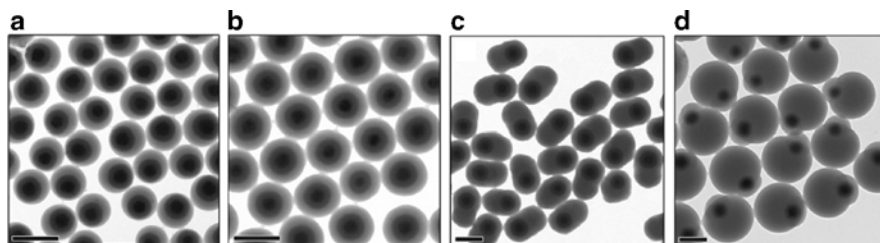


**Fig. 21** TEM images of a series of  $\text{Fe}_3\text{O}_4/\text{SiO}_2/\text{PS}$  composite colloids with complex structures and shapes produced by emulsion polymerization of styrene using MPTMS grafted  $\text{Fe}_3\text{O}_4/\text{SiO}_2$  particles as seeds. **(a, b)** Spherical colloids produced in one-step emulsion polymerization **(a)** without and **(b)** with DVB as crosslinker. **(c)** Ellipsoids formed by swelling and phase separation in one-step emulsion polymerization. **(d)** Doublets produced by separated steps of swelling and phase separation. Scale bars: 400 nm. Reprinted from [149] with permission of the American Chemical Society

the presence of MBA as a crosslinker. The crosslinking density appeared to play an important role in the encapsulation process: for a MBA to NIPAM weight ratio lower than 10%, the silica-coated magnetic particles were not efficiently encapsulated by PNIPAM, and for values over 30% some particles would adhere to each other. The shell thickness could be tailored by varying the initial amount of NIPAM, and the size or concentration of the template cores. The obtained particles effectively showed thermosensitivity (the higher the amount of MBA, the lower the swelling ratio) with a slightly higher volume phase transition temperature ( $37^\circ\text{C}$ , versus  $32^\circ\text{C}$  for pure and lightly crosslinked PNIPAM), and superparamagnetic behavior. This increase in the volume phase transition temperature could be explained by the presence of the magnetic nanoparticles, which acted as additional physical crosslinkers. Cai et al. [152] described a very similar approach consisting in the use of  $\text{Fe}_3\text{O}_4/\text{silica}$  particles modified with MPTMS (ca. 100 nm in size), which were subsequently used as seeds for the copolymerization of NIPAM and 2-(dimethylamino)ethyl methacrylate (DMAEMA).

Using a very similar procedure, magnetite/silica nanoassemblies were produced to serve as magnetically recoverable catalyst supports [153]. In detail, 100-nm silica-coated  $\text{Fe}_3\text{O}_4$  nanoparticles were functionalized with MPTMS and then used as seeds in NIPAM/MBA precipitation polymerization. After swelling these  $\text{Fe}_3\text{O}_4/\text{silica}/\text{PNIPAM}$  colloids in an aqueous solution of  $\text{AgNO}_3$ , Ag nanoparticles were directly synthesized inside the polymer network through in situ reduction with  $\text{NaBH}_4$ . This “ $\text{Ag}^+$  absorption–reduction” process can be repeated to increase the number density of Ag particles embedded in the polymer shells. An additional sol–gel process was performed to form satellite silica by using Ag nanoparticles as templates, producing  $\text{Fe}_3\text{O}_4/\text{SiO}_2/\text{PNIPAM}/\text{SiO}_2$  assemblies (Fig. 22). The use of these assemblies as recoverable catalyst supports was further evidenced in the case of Au-catalyzed reduction of 4-nitrophenol in the presence of  $\text{NaBH}_4$ .



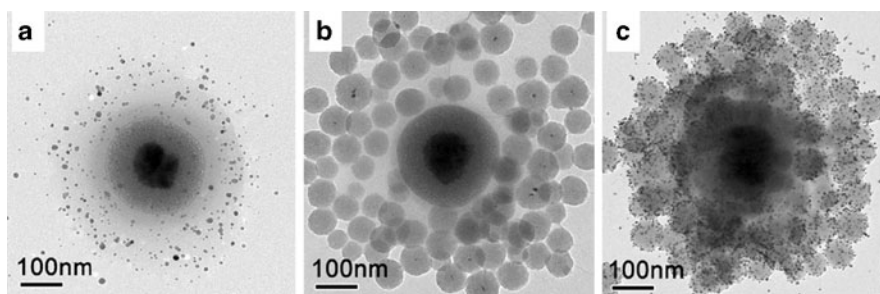


**Fig. 22** TEM images showing the evolution of hierarchical assemblies: (a)  $\text{Fe}_3\text{O}_4/\text{SiO}_2/\text{PNIPAM}/\text{Ag}$ , (b)  $\text{Fe}_3\text{O}_4/\text{SiO}_2/\text{PNIPAM}/\text{SiO}_2$ , and (c)  $\text{Fe}_3\text{O}_4/\text{SiO}_2/\text{PNIPAM}/\text{SiO}_2\text{-Au}$ . Adapted from [153] with permission of the American Chemical Society

### 3.1.4 Heterocoagulation Followed by Emulsion Polymerization

Another strategy involving emulsion polymerization is based on the heterocoagulation of inorganic nanoparticles arranged on a polymer particle as a magnetic surface layer. The heterocoagulation is an electrostatically driven interaction between colloids of opposite charges, so the pH has to be carefully chosen. Then, a compound is added to improve the hydrophobicity of the heterocoagulates (through the formation of a surfactant–bilayer–admicellar polymerization). This ensures the formation of a third layer through emulsion polymerization using the heterocoagulates as seeds, and finally provides a composite particle with a trilayer morphology (Fig. 23).

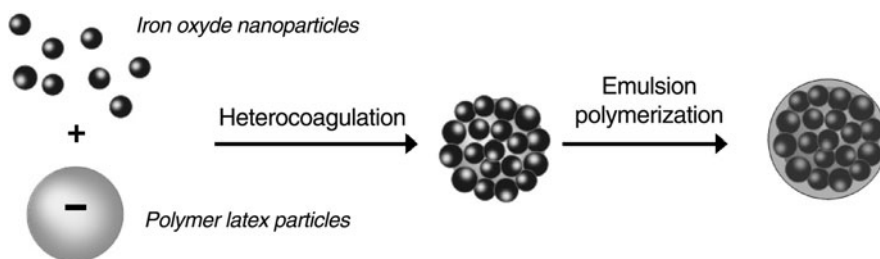
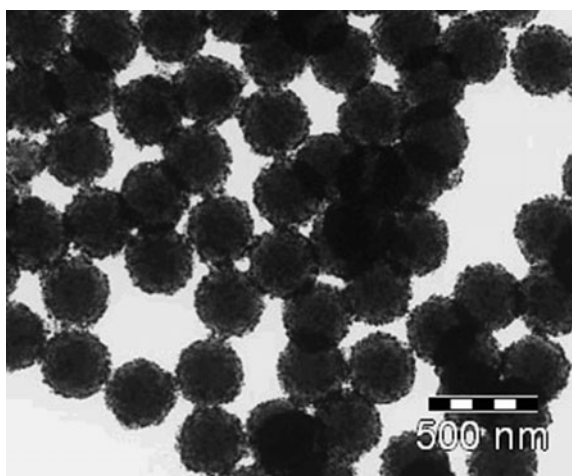


**Fig. 23** Encapsulation of iron oxide nanoparticles in a two-step procedure: electrostatic-driven adsorption of iron oxide nanoparticles onto polymer particles, followed by encapsulation of the obtained heterocoagulates by emulsion polymerization

The first work describing this procedure was published by Furusawa et al. [154] using  $\text{NiO} \cdot \text{ZnO} \cdot \text{Fe}_2\text{O}_3$  as the magnetic component and PS latexes as the particulate support (with 40 wt% of magnetic material). After the addition of sodium oleate, efficient encapsulation of the heterocoagulates by a PS layer was effectively observed, providing spherical magnetic particles with a smooth surface. The same kind of trilayer composite particles were obtained by first adsorbing  $\gamma\text{-Fe}_2\text{O}_3$  on a poly(styrene-*co*-BA-*co*-AA) core. After addition of sodium methacrylate, a third

**Fig. 24** TEM image of composite particles with a trilayer morphology using poly[styrene-*co*-(*N*-isopropylacrylamide)] as cationic seed. Adapted from [158] with permission of Springer



layer of poly(styrene-*co*-BA-*co*-AA) was formed [155]. The photovoltaic properties of the composite particles were also evaluated [156].

Still using the same two-step procedure, monodisperse and thermoresponsive magnetic latex particles based on PNIPAM were prepared [157, 158]. Anionic iron oxide nanoparticles were first adsorbed onto preformed cationic particles of various compositions [PS, poly(styrene-*co*-NIPAM) core-shell, or PNIPAM]. The obtained heterocoagulates were then encapsulated with crosslinked PNIPAM through seeded precipitation polymerization (Fig. 24). The magnetic content varied from 6 to 23 wt%. These particles were successfully used for the covalent immobilization of antibodies, and the resulting conjugates were tested as solid phases in immunoassays [159].

A slightly different procedure was depicted by Gu et al. [160]. Negatively charged PS particles were first formed in the presence of a silane coupling agent. After a given reaction time, silane-modified magnetic nanoparticles were continuously supplied into the reactor under acidic conditions, inducing the heterocoagulation of these cationic nanoparticles onto the anionic polymer particles. The morphology of the magnetic particles was strongly dependent on the silane coupling reagents. Trifunctional MPTMS led to disk-like or concave-like shapes, whereas difunctional methacryloxy propyl methyl dimethoxy silane (MPDMS) produced spherical particles. Addition of NaSS improved the colloidal stability of the magnetic polymer particles [161]. However, the amount of incorporated  $\text{Fe}_3\text{O}_4$  remained quite low (5 wt%), therefore resulting in low  $M_s$  ( $<0.5 \text{ emu g}^{-1}$ ).

### 3.1.5 Miscellaneous

A few systems that do not follow any of the procedures described so far are detailed below. Lee and Senna [162] described the synthesis of magnetic PS microparticles of the core-shell type prepared by emulsion polymerization of styrene in the presence of PS seed microspheres and magnetite coated with a bilayer of sodium oleate.

Small composite nanoparticles were produced in the continuous phase through emulsion polymerization. These nanoparticles were shown to adhere to the seed surface, giving rise to the formation of large PS microspheres covered with a layer of smaller nanocomposite particles. Owing to the complexity of the initial system (micrometric PS seeds, sodium oleate-coated- $\text{Fe}_3\text{O}_4$ , SDS micelles), the mechanisms leading to the formation of the particles was unclear, probably combining seeded, micellar, and admicellar emulsion polymerization.

In another work,  $\text{Fe}_3\text{O}_4$  nanoparticles were covered by poly(MMA-*co*-MAA) using very high surfactant to monomer ratios [163]. The best results in terms of magnetic properties and colloidal features were obtained using KPS and SDS, with magnetite to monomer ratio of 25 wt% ( $M_s = 3.2 \text{ emu g}^{-1}$ ). However, there were neither TEM photos to illustrate the obtained morphologies nor indication of the weight fraction of magnetic particles to evaluate the success of the synthesis.

A final example implies no surface modification. Using magnetite nanoparticles as seeds, Sun et al. [164] described the synthesis of magnetic core–poly(AAm) shell particles obtained by UV irradiation of an aqueous solution of  $\text{Fe}_3\text{O}_4$ , AAm, and MBA. The surface of the particles was then modified to introduce amino groups, subsequently linked to L-histidine labeled with  $^{188}\text{Re}$ , one of the most efficient radioisotopes for cancer radiotherapy.

Although out of the main focus of this paper, it is worth mentioning the case of inverse emulsion. This involves the polymerization of water-soluble monomers such as AAm or NIPAM [165, 166]. Only a few studies report on the synthesis of magnetic particles using this process [167–172].

### 3.2 *Synthesis of Iron Oxide Nanoparticles in the Presence of Preformed Polymer Particles*

All the studies detailed in the previous section rely on the use of preformed iron oxide nanoparticles, in the presence of which emulsion polymerization has been carried out. By contrast, this section focuses on the synthesis of iron oxide nanoparticles inside or onto the surface of preformed polymer particles. The studies using this strategy are by far less numerous and are detailed below.

This approach was pioneered in the work of Ugelstad et al. [173, 174] (Fig. 25). In their method, magnetic iron oxides were formed in situ inside preformed micrometric polymer particles. The pores of monodisperse, porous PS particles contained oxidizing surface groups and were filled with a solution of  $\text{FeCl}_2$ . Increasing the pH and the temperature induced the formation of superparamagnetic iron oxides in the pores. The composite particles were finally coated by a polymer shell to avoid any desorption of the magnetic nanoparticles. The diameter of the particles ranged from 1 to  $30 \mu\text{m}$ , with iron oxide loading up to 30 wt% and various surface-reactive groups (hydroxyl, carboxylic, amine, and aldehyde). These particles are currently marketed under the trade name Dynabeads®.

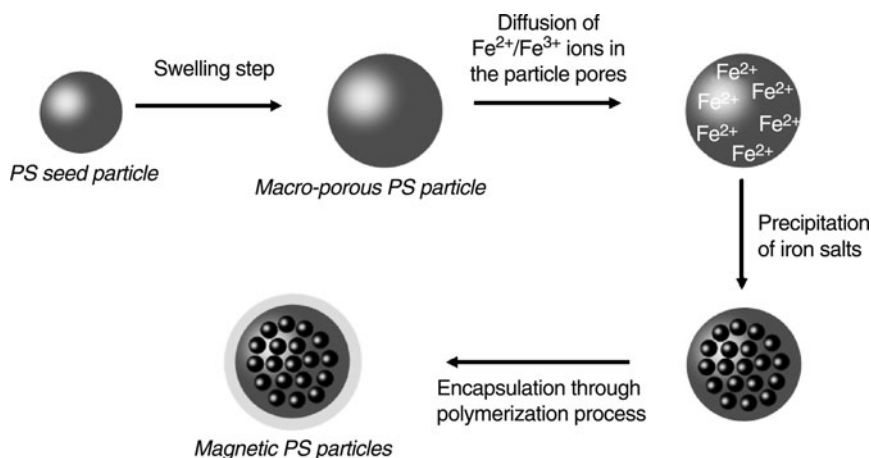


**Fig. 25** Synthesis of magnetic polymer particles according to the process developed by Ugelstad et al. [173, 174]

Using a similar procedure, smaller magnetic particles (400–700 nm in diameter) were produced by Lindlar et al. [175]. Polymer particles of poly(MMA-*co*-GMA) were first synthesized by surfactant-free emulsion polymerization. Ethylene diamine was then added to obtain internal anchor groups able to favor the subsequent impregnation and hydrolysis of iron salts inside the particles. The final composite particles were monodisperse in size and the magnetic loading was close to 25 wt%.

Related studies report on the formation of iron oxides onto the surface of polymer particles adequately functionalized to chelate precursor metal ions. Pich et al. [176] prepared  $\beta$ -diketone-functionalized PS latexes through surfactant-free emulsion copolymerization of styrene and AAEM. Solutions of  $\text{FeCl}_2$  and  $\text{FeCl}_3$  were added to the dispersion, followed by the dropwise addition of  $\text{NH}_4\text{OH}$ . After washing, up to 14 wt% of iron oxides could be deposited on the particles but the Ms remained low ( $<1 \text{ emu g}^{-1}$ ). Temperature-sensitive and magnetic hybrid hydrogels of *N*-vinylcaprolactam (VCL) and AAEM incorporating up to 15 wt% of  $\text{Fe}_3\text{O}_4$  were reported by the same group [177]. Emulsion polymerization of GMA was performed in the presence of seeds of PS particles (2.4  $\mu\text{m}$ , obtained by dispersion polymerization) to afford core-shell latexes functionalized with a thin layer of epoxy groups [178].  $\text{Fe}_3\text{O}_4$  nanoparticles were then synthesized onto the surface of PS/PGMA core-shell particles by nucleation and controlled growth mechanisms. The obtained magnetic particles contained about 6 wt% of  $\text{Fe}_3\text{O}_4$ , corresponding to a Ms value of  $3 \text{ emu g}^{-1}$ .

Another work describes the synthesis of magnetic nanocontainers (i.e., hollow spheres) of magnetite formed using PS particles obtained by emulsion polymerization as sacrificial core [179]. The coating procedure involved the controlled hydrolysis of aqueous solution of  $\text{FeCl}_3$  in the presence of the PS latex, urea, and PVP. The particles coated with hematite (non-magnetic) that were obtained after aging at  $95^\circ\text{C}$  were then heated to  $500^\circ\text{C}$  to provide hollow hematite spheres.

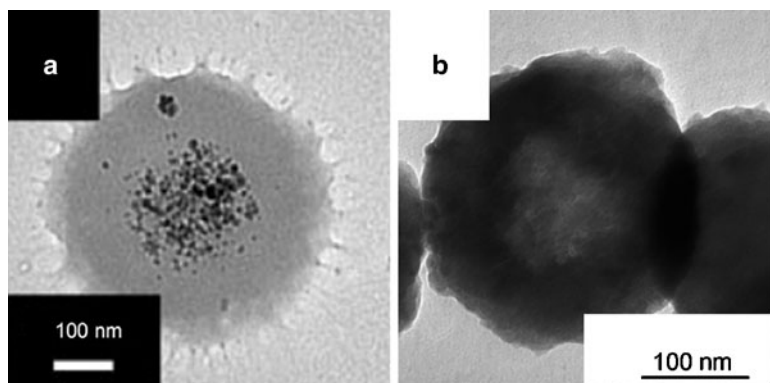


**Fig. 26** Examples of iron oxide nanoparticles synthesized inside PNIPAM particles. (a) Sulfonate-functionalized particles based on poly(NIPAM-*co*-GMA). Reprinted from [180] with permission of Springer. (b) Poly(NIPAM-*co*-sodium acrylate) particles. Reprinted from [181] with permission of the American Chemical Society

Further heating at 350°C for 1 h under hydrogen atmosphere finally led to hollow magnetite spheres displaying superparamagnetic behavior, with  $M_s$  close to that of bulk material ( $67 \text{ emu g}^{-1}$ ).

A substantial amount of work has been dedicated to the in situ synthesis of iron oxide nanoparticles inside microgel particles (i.e., crosslinked latex particles), generally obtained by precipitation polymerization. Although not strictly speaking in the scope of this review article, which focuses on emulsion polymerization, it is worth mentioning the synthesis of these particles, which actually find many applications in various fields. For instance,  $\text{Fe}_3\text{O}_4$  nanoparticles could be synthesized within preformed PNIPAM-based particles (Fig. 26) [180–183]. Of particular interest is the recent work of Brugger et al. [184], who used PNIPAM-based magnetic microgel particles as stimuli-responsive emulsifiers for oil-in-water emulsions, allowing controlled breaking of such emulsions.

## 4 Pigmented Latexes

Pigments (and extenders) are the main and most important constituents of water-based coatings and play a crucial role in, for instance, the papermaking and paint industries. A proper pigmentation drives not only the aesthetics of the film (such as gloss, opacity, and color) but also ensures long-term protection against environmental aggression and preserves the mechanical and performance properties of the film. In the paint industry, high quality coatings with a high gloss and color strength are generally required. In gloss and semi-gloss paints, the pigment is predominantly titanium dioxide ( $\text{TiO}_2$ ), whilst in matte paints significant quantities of extenders (such as calcium carbonate, China clay and silica) are included in the paint formulation.

Adequate formulations depend not only upon the selection of raw materials, but also on accurate calculation and optimization of the amounts of its constituents. To achieve the optimum visual and economic benefits of a pigment, it is essential that the surface is uniformly and completely covered by the coating formulation. Opacity is therefore an essential requirement of latex paints. Opacity is most readily achieved by using a pigment of high refractive index,  $\text{TiO}_2$  being the most widely used although  $\text{ZnO}$  or  $\text{SbO}_2$  can also be employed. Whatever the paint composition, high quality coatings are obtained for optimal pigment dispersion, which is to say for optimum particle size and stability. To improve and to stabilize paint dispersions, it is common to use polymeric dispersants [185, 186]. However, this is generally not sufficient and a lot of pigments need a surface treatment to maximize their efficiency. Indeed, a problem of paint formulation is not only to promote pigment dispersion in the latex blend but also to maintain a minimum distance between individual pigment particles in the dried film. In practice, this never occurs. This issue can be solved by coating the inorganic pigment with a thin polymer layer. This way, optimal disposition of the inorganic particles within the polymeric film can be achieved, resulting in optimal light scattering and hence better opacity and good film properties [187]. Some of these methods are described in the following section for  $\text{TiO}_2$  and a few other selected pigments.

#### ***4.1 Polymer Encapsulation of $\text{TiO}_2$ Pigments***

Owing to the major technological importance of  $\text{TiO}_2$  pigments in the paint industry, it is not surprising that most published works in this field are found in the patent literature [188–196]. Among the various approaches, emulsion polymerization is by far the technique the most frequently reported. In a typical procedure, the pigment particles are dispersed into water under high shear in the presence of surfactant to help dissociate the pigment agglomerates [197–199]. Then, a monomer or a mixture of monomers is introduced into the suspension medium, and a water-soluble free radical initiator is subsequently added to start polymerization. In most examples, the coating takes place through the admicellization/adpolymerization mechanism described in Sect. 3.1.1 for iron oxide encapsulation. This process is highly dependent on the geometry of the bilayer structure and on the surfactant packing density, which in turn are functions of the soap concentration. Emulsifier concentrations that are too low can lead to incomplete pigment coverage, whereas too large a concentration can result in the formation of free polymer particles that do not participate in the coating. The nature of the surfactant also plays an important role in the coating mechanism. For instance, Solc [190, 193] and Hasegawa [200, 201] claimed the use of water-soluble anionic surfactants, while Martin [191, 195] recommended the use of non-ionic oxyethylenic amphiphiles. As shown by Hoy and Smith, it can also be advantageous to use a combination of surfactants. For example, they demonstrated that more uniform coverages and better coating efficiencies could be achieved by using an amphipathic polymer in combination with a companion surfactant [194, 202].

The fundamental aspects of polymer encapsulation of  $\text{TiO}_2$  pigments were widely studied in the 1990s by the group of German and van Herk [203–209] with the successive Ph.D. theses of Caris [210] and Janssen [211]. With the intention of achieving high coating efficiencies, Caris used a polymerizable titanate coupling agent (diisopropyl methacryl isostearoyl titanate) to covalently attach polymer chains onto the surface of the  $\text{TiO}_2$  pigments according to the coupling strategy previously described for silica. A similar strategy was also recently reported by Yang et al. [212]. Preventing secondary nucleation is essential because newly formed particles may compete for surfactant adsorption and consequently lead to pigment coagulation. Maintaining a good stability of the encapsulated powders is also critical for pigment encapsulation through emulsion polymerization. Soap deficiency can be determined by following the evolution of the surfactant concentration through on-line conductivity measurements. Secondary nucleated particles lead to a decrease of the conductivity signal due to surfactant adsorption from the continuous phase, whereas severe coagulation is identified by an increase of conductivity consequent to surfactant desorption. It is therefore possible to use this technique to optimize the surfactant concentration in order to obtain the best encapsulation efficiency with maximum stability of the encapsulated pigment.

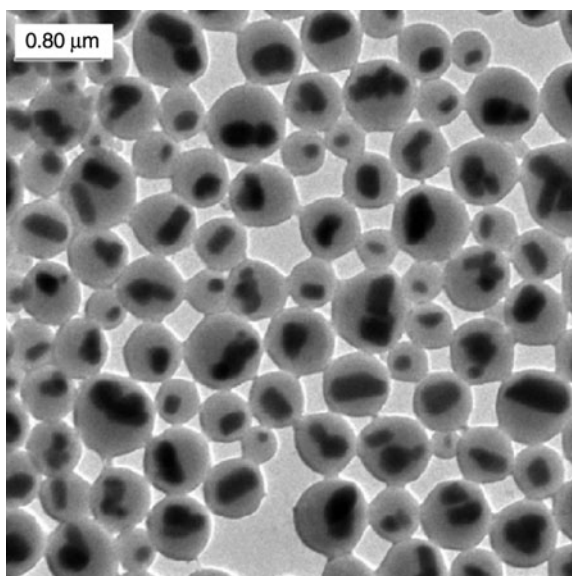
With the objective of promoting polymer formation at the surface of  $\text{TiO}_2$  pigments and prevent secondary nucleation, Haga et al. used a diazoic amidinium initiator previously anchored on the mineral surface [213], whereas Janssen used redox initiators [208]. Although real benefit was taken from the nature of the initiator, in particular in the case of hydrophilic monomers like MMA, there was still a competition between the formation of surface polymer and free latex particles in these systems. In both cases, better results were obtained when the monomer was introduced under starved-feed conditions, which enabled a significant decrease in the extent of secondary nucleation.

It is worth mentioning the recent work of Nguyen et al. [214], who succeeded in  $\text{TiO}_2$  encapsulation through controlled radical polymerization via the Reversible Addition-Fragmentation chain Transfer (RAFT) process (Fig. 27). Encapsulation of  $\text{TiO}_2$  using RAFT polymerization was also recently reported by Daigle et al. [215]. In this case, the method was also applied to metals (Mo, Zn) or other metal oxides ( $\text{ZrO}_2$ , CuO,  $\text{BaTiO}_3$ ,  $\text{Al}_2\text{O}_3$ ). In both studies, the use of macro-RAFT copolymers displaying a strong affinity for the pigment surface first enabled the formation of stable dispersion of the inorganic pigments. In a second step, the active chain end of the copolymer could be reactivated for the polymerization of hydrophobic monomers, thus leading to the formation of an encapsulating polymeric shell. More details on the use of controlled radical polymerization techniques for the synthesis of composite colloids can be found in the review article by Charleux et al. [216].

When successful, polymer encapsulation of  $\text{TiO}_2$  pigments provides an efficient way to control pigment interparticle spacing and enables better paint performances, such as higher hiding power, tinting strength, gloss, scrub resistance, or stability, compared to conventional paint formulations. As illustrated in recent articles, these materials are also of potential interest for the elaboration of electrophoretic displays [217–219] and lithium ion batteries [220].



**Fig. 27** Encapsulation of  $\text{TiO}_2$  pigment particles by a poly(BA-*co*-MMA) shell using a poly(BA<sub>5</sub>-*co*-AA<sub>10</sub>) macro-RAFT agent as dispersant. Reprinted from [214] with permission of the American Chemical Society



Apart from encapsulation reactions, a few groups also attempted to use  $\text{TiO}_2$  particles to stabilize polymer microspheres. For instance, Liu et al. reported a two-step procedure in which composite latex particles, coated with HEMA-functionalized  $\text{TiO}_2$  nanoparticles synthesized in a first step, were used in a second step as Pickering stabilizer to form micron-size beads through a suspension-like process [221]. Chen and coworkers also reported a method (which looks closer to suspension than to emulsion polymerization) for fabrication of hollow spheres through Pickering stabilization of emulsions microdroplets [222]. Another particular example that deserves attention is the synthesis of polyacrylate core- $\text{TiO}_2$  shell nanocomposite particles by in situ emulsion polymerization [223]. The authors argued that the core-shell structure resulted from the judicious combination of a cationic surfactant with an anionic persulfate initiator under controlled pH conditions. The exact mechanism for the formation of these core-shell particles remains nevertheless unclear.

## 4.2 Titania-Coated Polymer Spheres and Hollow Titania Shells

The high refractive index and photocatalytic properties of  $\text{TiO}_2$  make titania particles of great interest for various applications, including coatings, photonic crystals, and photovoltaic devices [224–226]. In particular, hollow titania spheres with a low-index core and a high-index shell are suitable building blocks for colloidal crystals, provided that the spheres are monodisperse in size with a smooth surface. However, since titania precursors are highly reactive, avoiding the formation of free-standing titania particles and rough coatings, is highly challenging. Therefore,



over the past 10 years, a number of groups have explored methods to address this challenge and to generate hollow titania spheres with smooth shells. The success of these methods relies on several parameters and requires precise optimization of the reaction conditions, as briefly described below.

In 2001, Shisho and Kawahashi reported the first successful formation of uniform  $\text{TiO}_2$  coatings on the surface of 420-nm diameter PS latexes by hydrolysis of titanium tetrabutoxide in ethanolic solutions in the presence of PVP [227]. The shell thickness was controlled by adjusting the concentration of the precursor solution, and a 30-nm-thick  $\text{TiO}_2$  coating was achieved without formation of separate inorganic particles under optimized conditions. A very similar procedure was followed some years later by Li [228], Syoufian [229], and Wang [230] (using albeit slightly different experimental conditions). In 2001, Imhof demonstrated the possibility of generating very thin and homogeneous titania coatings using cationic latexes as the seed, and titanium isopropoxyde as inorganic precursor [231]. The coating was again performed in ethanol media, and PVP was used to help stabilize the particles. The positive groups ensured quick deposition of the titania precursors on the latex seed and enabled the formation of 7- to 50-nm-thick titania shells without formation of secondary particles. Crystalline hollow spheres were further obtained by calcination of the  $\text{TiO}_2$ -coated particles at elevated temperatures. Increasing the temperature up to  $600^\circ\text{C}$  yielded hollow crystalline anatase titania particles, whereas the rutile form of  $\text{TiO}_2$  was obtained by calcining at  $900\text{--}1000^\circ\text{C}$  (Fig. 28).

Using the layer-by-layer method, Caruso and coworkers reported in the same period that PS colloidal particles coated with polyelectrolyte multilayers can be used as templates to produce hybrid hollow spheres by infiltration with a water-soluble and stable  $\text{TiO}_2$  precursor, namely titanium(IV) bis(ammonium lactate) di-hydroxyde (TALH) [232]. In virtue of the high chemical stability of the TALH precursor, a highly uniform coating was produced without the undesirable formation of titania particles in solution, which often occurs using more conventional precursors. Refluxing the TALH-coated particles at  $100^\circ\text{C}$  converted TALH to titania anatase nanoparticles, whereas calcination at  $450^\circ\text{C}$  gave hollow titania spheres. Macroporous titania spheres of the rutile phase were produced at a higher temperature ( $950^\circ\text{C}$ ). Eiden and Maret also described the successful formation of hollow spheres of rutile by templating negatively charged PS beads with  $\text{Ti}(\text{OEt})_4$  from absolute ethanol, followed by calcination at elevated temperatures under an oxygen atmosphere [233]. Unfortunately, no TEM images for evaluating the quality of the coating were provided in this article.

### 4.3 Other Pigments

Besides  $\text{TiO}_2$ , a few other pigments like aluminum [234–236], zinc oxide [237, 238], and calcium carbonate [207, 239–241] have also been reported. Some of them will be briefly discussed below.

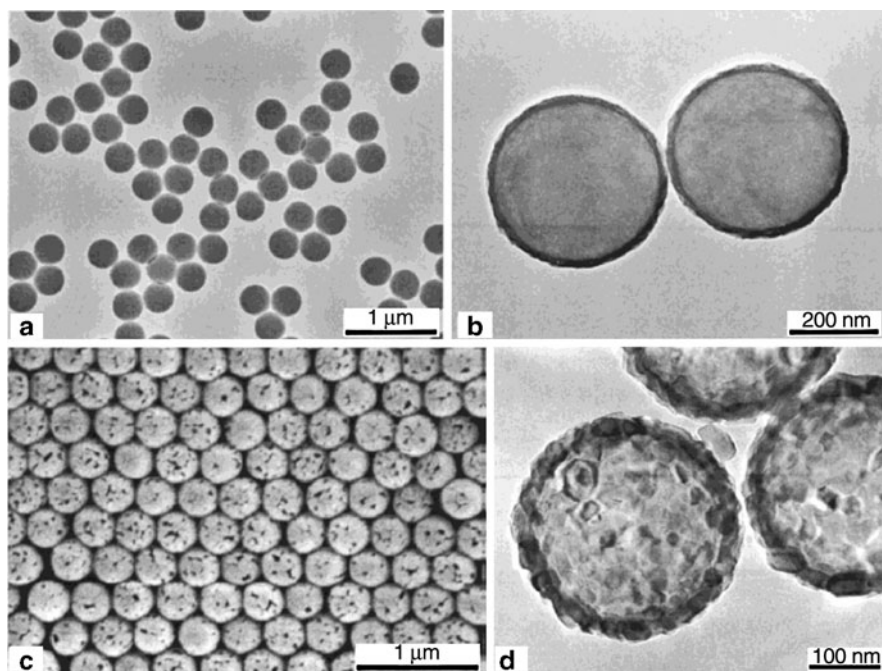


**Fig. 28** TEM images of (a) the polystyrene latex spheres used as the core and (b) the same particles coated with a thin 25 nm titania shell. (c) SEM image of hollow titania spheres obtained by calcination of the polystyrene/TiO<sub>2</sub> core-shell particles at 600°C under air. (d) Enlarged TEM view of some hollow titania particles showing the small anatase crystallites that compose the shell. Reproduced from [231] with permission of the American Chemical Society

For example, Batzilla and co-authors described the encapsulation reaction of commercial aluminum pigments through an emulsion-like polymerization process [242]. They reported the use of phosphorous-containing protecting agents to provide a good dispersion of the Al pigment and control its reactivity. They also recommended using monomers with strong adhesion with the metal surface (e.g., carboxylic acid derivatives).

Another class of extender widely used in coating applications is calcium carbonate (CaCO<sub>3</sub>). Despite potential interest in polymer encapsulation of CaCO<sub>3</sub> powders, only few studies can be found in the literature. Janssen et al. employed emulsion polymerization to encapsulate titanate-functionalized CaCO<sub>3</sub> pigments with PS [207]. Thermogravimetric analysis (TGA) showed that only 10% of PS was tightly bound to the inorganic surface, the remaining 90% polymer being extractable with toluene. Yang et al. [239] also described CaCO<sub>3</sub> encapsulation by PS using soap-free polymerization, while Yu et al. [240] reported the preparation of CaCO<sub>3</sub>/PS composite particles using a polymerizable silane derivative previously attached on the mineral surface. The pretreated CaCO<sub>3</sub> particles were shown to act as comonomers during the emulsion polymerization process in a similar way to that discussed in Sect. 2.1.1 for silica. More recently, Wu and coworkers

observed an increase of polymerization rate with increasing  $\text{CaCO}_3$  concentration during the preparation of  $\text{CaCO}_3$ /PMMA composite particles by soap-free emulsion polymerization [241]. TEM studies of the nanocomposite particles indicated successful pigment encapsulation, whereas TGA and X-ray photoelectron spectroscopy suggested PMMA grafting on the nano- $\text{CaCO}_3$  surface.

## 5 Polymer–Clay Nanocomposite Latexes

In addition to spherical particles, anisotropic fillers such as layered aluminosilicates (commonly called clays) have received much attention in recent literature. Indeed, because of their high aspect ratio, clay platelets of a few nanometers thick and several hundred nanometers long allow a substantial improvement in strength, elastic modulus, and toughness whilst retaining optical transparency. Additional benefits are enhanced resistance to tear, radiation, and fire as well as a lower thermal expansion and a lower permeability to gases. It is generally admitted that end-use properties of polymer–clay nanocomposites (PCNs) heavily depend on their nanostructure. Three main morphologies are usually reported: segregated, intercalated, and exfoliated. The exfoliated morphology consists of individual silicate layers dispersed in the polymer matrix as a result of extensive polymer penetration and delamination of the silicate crystallites, whereas a finite expansion of the clay layers produces intercalated nanocomposites (Fig. 29). In general, the greatest property enhancements are observed for exfoliated nanocomposites, which could be regarded as the “ideal” morphology, although in practice many systems fall short of this idealized nanostructure.

As outlined in a considerable number of texts and reviews covering the synthesis, characterization, and properties of PCNs [243–246], many parameters can

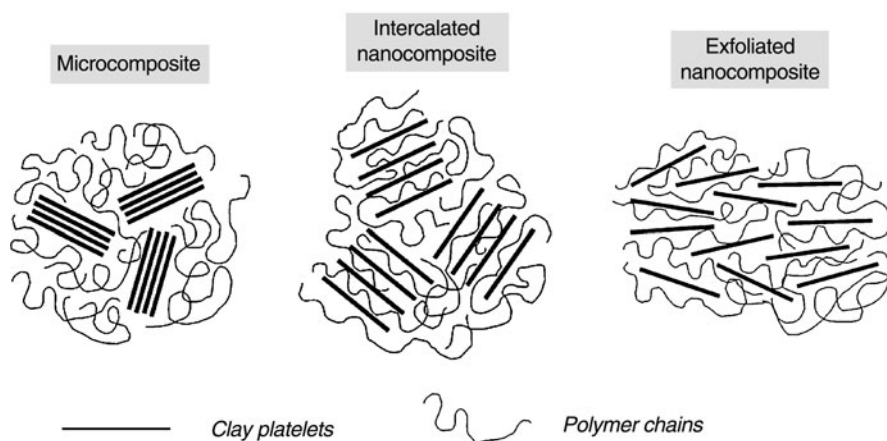


**Fig. 29** Different morphologies encountered in polymer-layered silicate nanocomposites: phase segregated (*left*), intercalated (*middle*), and exfoliated nanocomposites (*right*)

influence the nanostructure, such as the type of clay, the nature of the polymer, and the polymerization process (e.g., bulk, solution, suspension, miniemulsion or emulsion polymerization). However, so far there is no clear general consensus as to which process is the best suited to provide the requested exfoliated morphology for a given set of conditions (given type of clay and monomer composition). This is due in part to the high complexity of these systems and the multiple parameters involved. Compared to more traditional solvent-borne or melt-processing approaches, waterborne processes in general and emulsion polymerization in particular nevertheless offer some obvious advantages, as detailed in the following section. The reader is referred to the recent review of Paulis and Leiza for complementary information [247].

### ***5.1 PCNs Elaborated by Conventional Emulsion Polymerization***

Although both natural and synthetic aluminosilicates have long been reported to be effective free radical initiators for the aqueous polymerization of vinylic monomers [248–251], their utilization in nanocomposite materials was reported only recently.

The first papers on the synthesis of PCNs through emulsion polymerization were published in the 1990s by Lee et al. [252–255]. Intercalated nanocomposites based on Bentonite [which consists of 70 wt% montmorillonite (MMT)] and PMMA [252], PS [253], or styrene/acrylonitrile copolymers [254, 255] were successfully obtained using pristine clays as seeds, KPS as initiator, and SDS as surfactant. Confinement of the polymer chains in the interlayer gallery space was evidenced by differential scanning calorimetry (DSC) and TGA, and was suspected to originate from ion–dipole interactions between the organic polymer and the MMT surface. Unfortunately, since the latex was coagulated before characterization, no information was given at that time on particle morphology. In every case, it was shown that a non-negligible part of the polymer was adsorbed on the clay surface after extraction of the pulverized product in hot toluene, indicating significant polymer–clay interaction. However, it remains unclear whether such interactions occurred in suspension or were induced by the coagulation process.

Following a very similar procedure involving KPS as initiator and SDS as surfactant, Tong et al. reported *in situ* emulsion polymerization of ethyl acrylate in the presence of pristine Bentonite [256]. Drying of the latex suspension produced films exhibiting enhanced mechanical and thermal properties as well as reduced permeability to water vapor. Generally speaking, and regardless of synthetic procedures, nanoscale dispersion of layered silicates in plastics produces glassy modulus enhancements of one to two times and rubbery modulus increases of five- to 20-fold. Improved thermal properties are also observed in many systems, including intercalated nanocomposites obtained by emulsion polymerization. Such improvements are mainly due to the nanometric dimensions of the platelets. TEM analysis of an ultramicrotomed section of the film indicated, in the case described above, an intercalated (partially exfoliated) morphology as shown in Fig. 30. Recently, Pan et al. also showed enhanced mechanical properties for PVC/MMT nanocomposites elaborated in a similar way [257], and Kim et al. observed a shift

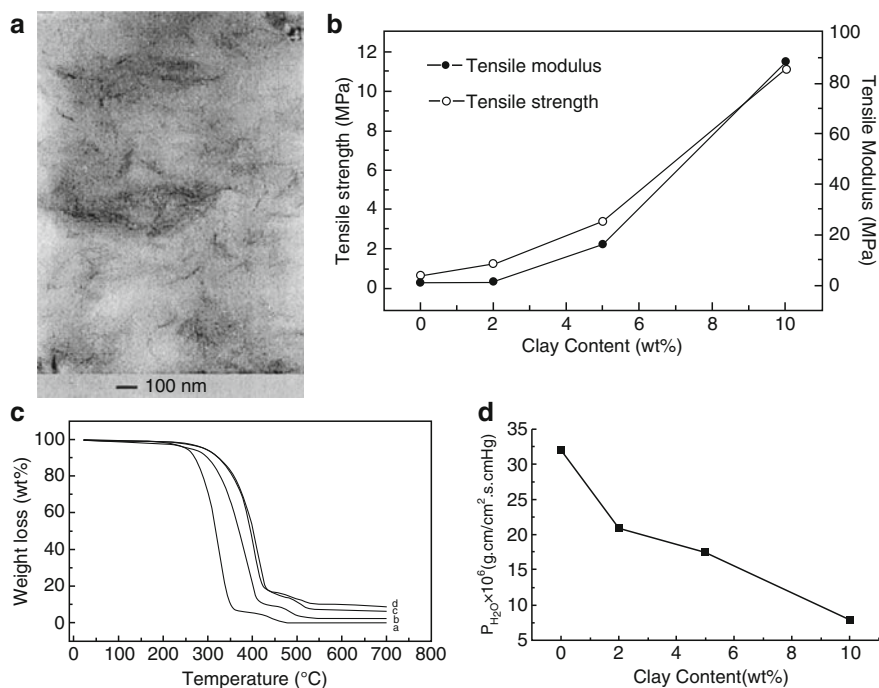


**Fig. 30** (a) Representative TEM image of exfoliated-intercalated clay in a poly(ethyl acrylate) matrix containing 5 wt% of clay. Dependence of mechanical (b), thermal (c), and permeation (d) properties with clay loading. Adapted from [256] with permission of Wiley Periodicals

of the onset of the thermal degradation toward higher temperatures as a function of clay content in exfoliated PS/MMT nanocomposites [258]. Bandyopadhyay et al. synthesized PMMA/MMT nanocomposites through emulsion polymerization with SDS as the emulsifier and showed enhanced thermal stability and an increase in  $T_g$  of 6°C [259].

Although a straight comparison between these different systems would be appealing, a comprehensive discussion on structure–property relationships will not be attempted in this review. Indeed, the diversity of systems in terms of type of clay, surface modification, and polymerization methods renders this exercise quite risky. Therefore, we will not try to compare the properties of the different systems described, and only discuss those whose properties bring a clear “added-value” to the nanocomposite material.

Besides properties (which are usually enhanced by adding clay), another crucial factor of PCN materials elaborated through emulsion polymerization is their solid content. Although this point is less frequently addressed, most of the polymer/clay composite latexes reported in literature have solid contents below 20%. However, solid contents between 40% and 60% and sometimes higher are required for industrial applications. Using a seeded semi-batch emulsion polymerization process and a procedure otherwise very similar to that described above for Bentonite,

Diaconu et al. recently reported the successful preparation of poly(BA-*co*-MMA)/MMT latexes of 45% solids with moderate viscosities and containing 3 wt% of clay [260, 261]. This is to our knowledge one of the first and rare examples of “high solids” PCN latex in the literature. A further increase of the solid content to meet the requirements of industrial recipes remains a real challenge.

The very simple methods depicted above show that, in virtue of their high swelling capabilities in water, pristine clays are valuable candidates for the elaboration of exfoliated nanocomposites through in situ emulsion polymerization. In spite of that, a number of groups have performed organic modification of clay particles with the objective of increasing interfacial interactions and controlling particle morphology. These works are presented below.

Quite a lot of studies have dealt with the use of organoclays in emulsion polymerization. In most of these studies, the organoclay is dispersed in water and the polymerization proceeds as in conventional emulsion polymerization by monomer diffusion from the droplets to the organophilic clay surface, where propagation of polymer chains takes place. However, in a few examples, the organoclay is dispersed in the monomer phase. This monomer clay suspension is next emulsified (sometimes with the aid of ultrasound to help dispersion and promote clay exfoliation) and the resulting droplets are polymerized [262–267]. The latter processes look closer to suspension or miniemulsion (depending on the nature of the initiator) than emulsion polymerization and will not be discussed further.

Organic modifiers are generally used to render clay surfaces hydrophobic and to promote monomer penetration in the interlayer space. Organic modifiers carrying suitable reactive end groups can also react with the polymer matrix and further strengthen the interfacial polymer–clay interaction, as reported by many groups. For instance, Qutubuddin et al. have incorporated vinylbenzyl dimethyl dodecyl ammonium chloride (VDAC) in MMT using cation exchange [268]. The amount of VDAC was kept well below the cation exchange capacity of the clay in order to preserve clay colloidal stability (an issue that is surprisingly neglected in the literature). A partially exfoliated nanocomposite was obtained upon polymerization of styrene in the presence of the organoclay, but the latex colloidal stability was only moderate because there was no surfactant to stabilize the resulting particles. Very recently, Sedlakova and coworkers followed a similar approach using the cationic 2-(acryloyloxy) ethyl trimethyl ammonium chloride monomer [269]. Choi et al. also reported the preparation of PS/MMT nanocomposites through in situ emulsion polymerization using SDBS as surfactant and 2-acrylamido-2-methyl-1-propanesulfonic acid (AMPS) as functional comonomer to promote adhesion at the polymer–clay interface [270]. Exfoliated nanocomposites with clay contents of up to 20 wt% with respect to polymer were successfully achieved by this method. It was speculated that the hydrogen ions of sulfonic acid protonated the amido group of the AMPS comonomer, which could then undergo exchange reactions with the clay counter-ions. The method was further extended to acrylonitrile [271], styrene/MMA [272], and acrylonitrile–butadiene–styrene [273] (co)polymers. However, no mention was made in these papers of particle size or latex colloidal stability. It should be noted here that AMPS was also used by Li et al. in the synthesis of poly(BA-*co*-AA)/MMT latexes by semi-batch emulsion polymerization for pressure-sensitive



adhesives [274]. It is worth mentioning the recent work of Greesh and coworkers, who systematically investigated the effect of the nature of the organic modifier on the microstructure and thermomechanical properties of poly(styrene-*co*-BA)/MMT composite films containing 10 wt% of clay [275]. The ability of the clay modifier to efficiently interact with the clay surface, its compatibility with the monomer, and its reactivity were all found to be determinant parameters for achieving fully exfoliated morphologies. AMPS was shown to fulfill all these requirements.

Besides reactive organic modifiers, a few groups have also reported the use of “simple” surfactants to promote clay exfoliation [276, 277]. For instance, Meneghetti and Qutubuddin synthesized partially exfoliated PMMA/MMT nanocomposites using SDS as regular surfactant and a zwitterionic octadecyl dimethyl betaine as organic modifier [278]. It was shown that the zwitterionic modifier provided better colloidal stability as compared to a cationic surfactant. This can be interpreted in terms of charge neutralization of the SDS-stabilized latex particles by the cationic surfactant (although this was not discussed in the paper). Li et al. also found that emulsion polymerization of styrene, conducted in the presence of MMT functionalized by a zwitterionic surfactant, produced exfoliated nanocomposites as proved by TEM and by the disappearance of the  $d_{001}$  peak in the X-ray diffraction pattern [279].

All the examples of PCN latexes described thus far involved MMT as the clay. Although MMT is by far the most commonly used layered silicate in PCN syntheses, other types of clays have also been reported.

For instance, Herrera et al. recently conducted a series of experiments on Laponite [280–283]. Laponite is a synthetic clay that is similar in structure to MMT, except for the nature of the interlayer cation ( $Mg^{2+}$  for Laponite and  $Al^{3+}$  for MMT) and the clay dimensions. Each elementary Laponite disk has a thickness of around 1 nm and a diameter of 30–40 nm. In addition, Laponite also has the advantage over natural clays of being chemically pure and free from external contaminations. All these properties make Laponite a valuable candidate for use in PCN synthesis.

Following strategies similar to those mentioned in Sect. 1.1 for silica, film-forming poly(styrene-*co*-BA)/Laponite composite particles were synthesized in batch through conventional emulsion polymerization using organically modified Laponite as seed. The clay particles were functionalized either through ion exchange of a cationic initiator (AIBA) or a cationic monomer [2-methacryloyloxy ethyl trimethyl ammonium chloride (MADQUAT)], or through the reaction of the edge-hydroxyls with suitable polymerizable organosilane molecules (such as methacryloxy propyl dimethyl ethoxysilane). The so-obtained organoclays were further suspended in water, which required the use of ultrasound. For organoclays functionalized by cation exchange, a small amount of tetra-sodium pyrophosphate was introduced in the suspension to reverse the edge positive charges and promote clay–clay repulsions. Then, emulsion polymerization was carried out in batch in the presence of the organoclay (10 wt% based on monomer) using SDS as surfactant and KPS or 4,4'-azobis(4-cyanopentanoic acid) (ACPA) as initiators, except when AIBA was used as organic modifier. The overall process is illustrated in Fig. 31.



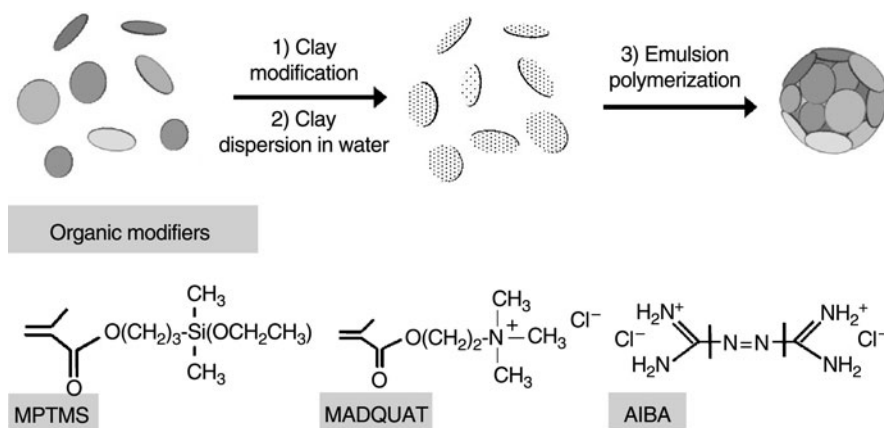


**Fig. 31** Procedure used for the synthesis of polymer/Laponite composite particles through emulsion polymerization

Regardless of the nature of the organic modifier, colloiddally stable composite latexes with diameters in the range 50–150 nm were successfully obtained, provided that the original clay suspension was sufficiently stable and un-aggregated. All three methods produced clay-armored composite particles characterized by a polymer core surrounded by an outer shell of clay platelets, as evidenced by cryo-TEM. Transparent films that exhibited remarkable mechanical and thermal properties were produced upon drying of the composite latexes. Cryo-microtomy revealed a honeycomb distribution of Laponite within the film, consistent with the armored morphology (Fig. 32). Quite recently, Ruggerone et al. also reported a similar morphology for PS/Laponite films containing up to 20% of clay and investigated the resulting mechanical properties [284].

A similar strategy involving Laponite or MMT platelets grafted with polymerizable organotitanate and organosilane molecules was recently reported by Voorn et al. [285, 286]. Here, starved-feed soap-free emulsion polymerization of MMA conducted in the presence of the organoclay led to clay encapsulation. However the solid content was quite low (typically around 7%).

## 5.2 Soap-Free Latexes Stabilized by Clay Platelets

Very recently, a number of groups have explored methods of preparing clay-armored latexes by soap-free emulsion polymerization (referred to as “Pickering polymerization” [69] by analogy with the stabilization of emulsions by inorganic solids). In this process, the monomer is simply emulsified in a water dispersion of clay platelets that ultimately stabilize the hybrid particles by adhering on their surface and forming a protecting armor.

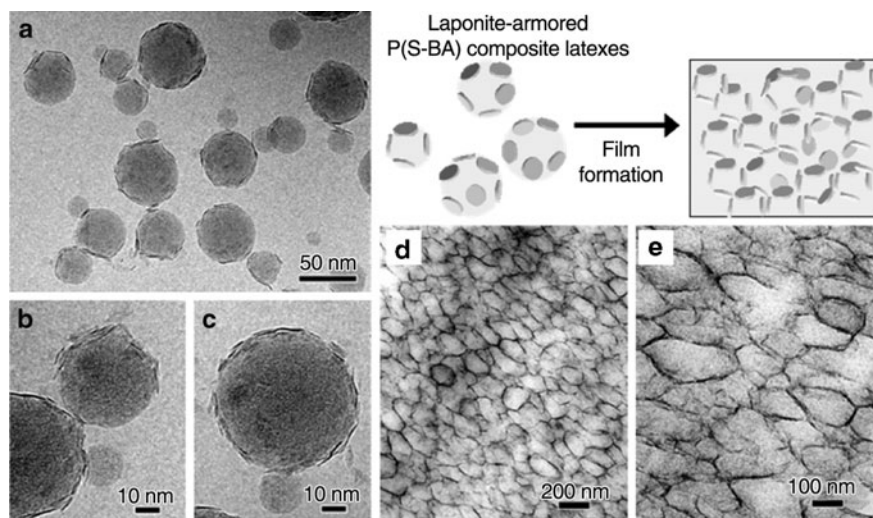


**Fig. 32** (a–c) Cryo-TEM images of poly(styrene-*co*-BA)/Laponite nanocomposite particles prepared through emulsion polymerization using MADQUAT as reactive compatibilizer. The nanoparticles are seen embedded in a film of vitreous ice. (d, e) Electron micrographs at intermediate and high magnifications of an ultrathin cryosection of a film prepared from the composite latex suspension. The thin dark layer covering the surface of the polymer particles corresponds to 1-nm thick diffracting clay platelets that are oriented edge-on with respect to the direction of observation. Adapted from [283] with permission of Wiley-VCH

For instance, using the afore-cited AMPS comonomer (un-correctly defined as reactive surfactant in a subsequent paper), Choi et al. reported the preparation of PMMA/MMT nanocomposites through in situ soap-free emulsion polymerization [287]. However, at that time, the authors did not stress the role of the clay as stabilizer. Park et al. synthesized PMMA/MMT nanocomposites for optical applications by soap-free emulsion polymerization, but again the article focused on the properties and there was no mention of colloidal aspects [288]. In the same period, Lin and coworkers reported the formation of 300–600 nm diameter PMMA latex particles initiated by KPS and stabilized by MMT platelets [289]. The authors argued that KPS intercalation inside the clay galleries was the driving force that enabled the polymerization to take place at the clay surface. Although the solid content was quite low and the amount of MMT rather high, this article remains nevertheless very instructive.

Using an original approach, Zhang and coworkers recently reported the synthesis of PMMA latex particles stabilized by MMT platelets tethered with poly[2-(dimethylamino)ethyl methacrylate] (PDMAEMA) brushes (Fig. 33) [290]. The PDMAEMA polyelectrolyte brush was synthesized by atom transfer radical polymerization using a cationic initiator previously introduced in the clay galleries. The PDMAEMA-functionalized clay platelets were further used to stabilize the emulsion polymerization of MMA initiated by the remaining free radical initiator present on the clay surface.

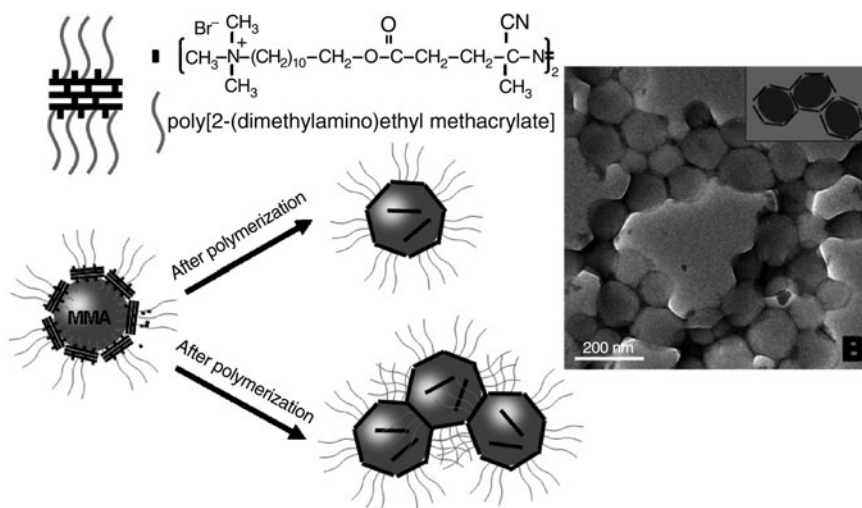


**Fig. 33** *Left*: Synthesis of clay-armored PMMA latexes through soap-free emulsion polymerization using PDMAEMA-tethered clay as stabilizer. *Right*: TEM image of the so-obtained PMMA/clay composite colloid. Reproduced from [290] with permission of Wiley Periodicals

Recently, a number of groups have also reported the Pickering stabilization of monomer-containing lipid droplets by clays, and their subsequent free radical polymerization [291]. As these articles fall outside the scope of this review, they will not be discussed further. Although not strictly speaking in the scope of the present review, it is also worth mentioning the recent work of Voorn et al. on the first surfactant-free inverse emulsion polymerization stabilized with hydrophobic MMT platelets [292].

## 6 Synthesis of Quantum Dot Tagged Latex Particles

QDs are semiconductor nanoparticles typically 1–10 nm in size that show unique luminescence properties due to 3D size-confinement effects [293–295]. Regardless of the excitation wavelength, a narrow emission peak is observed, the wavelength of the emitted light being size-dependent. Furthermore, QDs show excellent photostability, and different-sized QDs can be simultaneously excited by a single wavelength because each type of QD exhibits a specific emission peak. Due to their outstanding optical and electronic properties, QDs have found increasing applications in the fields of biotechnologies (e.g., diagnostic, imaging, optical tracking), optoelectronics (e.g., light emitted diodes) and photonics (e.g., photonic crystals) [295].

The most often encountered inorganic semiconductors in the literature are those from groups II–VI, i.e., ZnO, ZnS, ZnSe, CdTe, CdS and CdSe, the last two being the most studied and documented. QDs are in most cases made as colloidal solutions

[294, 296]. In this approach, precursors of the material are reacted in the presence of a stabilizing agent that will restrict the growth of the particle and keep its dimensions within the limits of the quantum-size effect that gives the QDs their outstanding properties. The most popular route is based on the pyrolysis of organometallic precursors in a hot coordinating solvent that mediates nanoparticle growth and stabilizes the inorganic surface [297–299]. For instance, a typical synthesis of CdSe is the following: dimethyl cadmium  $\text{Cd}(\text{CH}_3)_2$  and trioctyl phosphide selenide are initially dissolved in the organic solvent tri-*n*-octylphosphine and injected into a hot coordinating solvent of tri-*n*-octylphosphine oxide (TOPO) at 350°C under argon atmosphere. The temperature is lowered to 300°C by the injection. The rapid introduction of the reagent mixture produces a yellow/orange solution that is characteristic of CdSe nanocrystal formation. The growth of the QDs after the injection is then carried out at a given temperature in the range of 250–300°C. Since the growth of the QDs is dependent on the process of Ostwald ripening, the size of the QDs can be tuned by the temperature. Careful control of the reaction conditions produces CdSe QDs that are relatively homogeneous in size, and tunable in the 2–8 nm range. However, because the organometallic precursors are extremely toxic, expensive, and explosive, alternative procedures using metallic oxides (e.g., CdO) and organic stabilizing agents have been developed [300, 301]. For instance, less experimentally demanding procedures can be carried out using aqueous solutions of Cd(II) salts [for instance  $\text{Cd}(\text{ClO}_4)_2$  or  $\text{Cd}(\text{NO}_3)_2$ ] mixed with anionic or Lewis basic polymers such as sodium polyphosphate or polyamines [302, 303], or a polymerizable stabilizer [304]. The subsequent addition of a sulfide source (such as  $\text{H}_2\text{S}$  or  $\text{Na}_2\text{S}$ ) produces CdS nanoparticles that are in the 1–10 nm size range. The size of the nanocrystals depends on a large number of experimental conditions, such as the relative concentrations of the precursors and rates of addition.

The stability of the QDs, and hence their luminescence, can be improved by coating the QDs with an additional layer of another semiconductor material with a wider band gap energy (e.g., CdSe coated with ZnS [305, 306]). Other strategies have also been envisioned to improve their stability, their compatibility with various media, and their functionality. Ligand exchange, encapsulation by phospholipids, polymers or silica, or coating by biological molecules (proteins, DNA, antibodies) are a few examples of such modifications. Obviously, incorporating QDs in polymer particles using emulsion polymerization is a very attractive challenge for many scientists targeting applications in the biomedical field (diagnosis, image tracking, bar-coding) or in photonics (photonic crystals).

## 6.1 Encapsulation of QDs Through Emulsion Polymerization

### 6.1.1 Conventional Emulsion Polymerization

Only a few papers report on the encapsulation of QDs inside polymer particles through conventional emulsion polymerization. Indeed, at the end of the most popular routes used for QDs synthesis, the obtained nanocrystals are usually

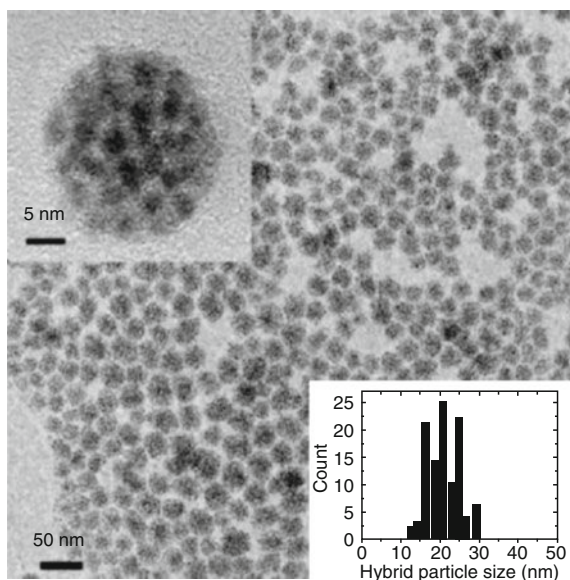
hydrophobic. Thus, the incorporation of hydrophobic QDs into polymer particles via a proper emulsion polymerization may be very challenging owing to the poor aqueous-phase transport of these species. Various synthetic strategies related to emulsion polymerization have been developed to improve the compatibility between the QDs and the reagents.

In one of the reported works, TOPO-coated CdSe QDs were dispersed in a micellar solution of surfactant, which could be subsequently swollen by monomer [307]. In detail, a toluene solution of CdSe was first added dropwise to a micellar solution of cetyltrimethyl ammonium bromide (CTAB). Then, a mixture of styrene, DVB, AA, and AIBN was added dropwise at 0°C. Finally, the system was heated to 70°C for 20 h. Submicrometer particles were prepared with an effective incorporation of hydrophobic TOPO-coated CdSe into carboxylic functionalized and crosslinked PS particles. The QD-tagged PS particles were then coated with a fluorescent silica shell through TEOS addition. Particle sizes ranging from 300 nm to 20 µm were produced, depending on the recipe used for the synthesis. However, the solid content was quite low and there was no information about the amount of QDs incorporated.

Another strategy consists in the use of QDs coated with a cysteine acrylamide, a polymerizable stabilizer [304]. Successful incorporation of hydrophilic cysteine-acrylamide-stabilized QDs into 80–200 nm fluorescent latexes was achieved via emulsion polymerization, as reported by Sherman et al. [308], using two different procedures. In the first, a two-step shot growth surfactant-free emulsion polymerization of styrene and NaSS was performed in the presence of a solution of hydrophilic cysteine-acrylamide-stabilized CdS or CdSe/CdS QDs. In the second approach, CdSe/CdS QDs were first electrostatically modified by vinylbenzyl(trimethyl)–ammonium chloride and subsequently copolymerized with styrene in the presence of SDS. A third approach was also described in this paper: coating of cationic PS particles with anionic poly(cysteine acrylamide)-coated QDs through electrostatic-driven interactions.

Using a procedure that probably relies on admicellar polymerization, Lee et al. [309] successfully entrapped CdSe or CdSe/ZnS QDs in various polymer particles. TOPO-coated QDs were first dissolved in chloroform in the presence of a large amount of sodium bis(2-ethylhexyl)sulfosuccinate (AOT). The waxy solid obtained after solvent evaporation was then dissolved in water at 80°C (probably stabilized by a bilayer of TOPO and AOT). After centrifugation and dialysis, and dilution in water, monomer was added to the reaction mixture, stirred for 1 h and heated to 60°C. Polymerization was initiated with KPS, and 20 nm hybrid particles containing a few tens of QDs each were successfully obtained (Fig. 34). This procedure was, however, limited to QDs smaller than 5 nm in size. The versatility of the process was demonstrated by the successful synthesis of hybrid colloids using various monomer(s): pure styrene or a mixture of styrene/DVB (1:1), pure P4VPy or a mixture of P4VPy/DVB, or pure PMAA. The pure PDVB particles showed, however, better robustness to post-synthesis treatments. The main drawback of the process was the quenching of the photoluminescence of the QDs. This problem was circumvented by the use of CdSe coated with a protective ZnS shell.

**Fig. 34** TEM images of hybrid colloidal nanoparticles of CdSe and PDVB. The *upper inset* is a high magnification image showing individual CdSe nanocrystals within the PDVB colloidal particle. The *lower inset* shows the PSD. Reprinted from [309] with permission of the Royal Society of Chemistry



### 6.1.2 Emulsion Polymerization-Related Procedures

Using the procedure described above for the synthesis of magnetic particles and depicted in Fig. 16 (see Sect. 3.1.3), CdTe QDs of different size (and thus different emission wavelength) were embedded in PS particles using emulsion polymerization [137, 310]. The obtained micrometric particles showed good photoluminescence properties and the photostability of the QDs was even enhanced when encapsulated in the PS particles, compared to an aqueous solution of CdTe. In addition, the labeling of PS particles with both green- and red-emitting QDs was demonstrated, showing the possible application of this approach to the synthesis of multiplexed optical coding (Fig. 35). Bifunctional (magnetic with  $\text{Fe}_3\text{O}_4$  and fluorescent with CdTe) particles were also reported by the same team [138] (see Sect. 3.1.3).

The concept of polymer–monomer pairs depicted above for the synthesis of magnetic particles also proved to be efficient for QDs encapsulation (see Sect. 3.1.3, Fig. 19) [145]. CdTe QDs coated with mercapto propionic acid (MPA) were first embedded in CS/PMAA particles providing raisin-bun or core–shell morphologies, depending on the initial ratio of  $[-\text{COOH}]$  to  $[-\text{NH}_2]$ . The photoluminescence properties of the core–shell morphology were found to be pH-dependent. CdTe QDs were then encapsulated together with magnetic  $\text{Fe}_3\text{O}_4$  nanoparticles to afford multifunctional particles that were able to act as imaging agents. The magnetic content could be varied from 11 to 32 wt%, but it was found that too high a magnetic content led to a decrease or quenching of the QD fluorescence. Finally, these particles were evaluated for magnetically enhanced cellular uptake.



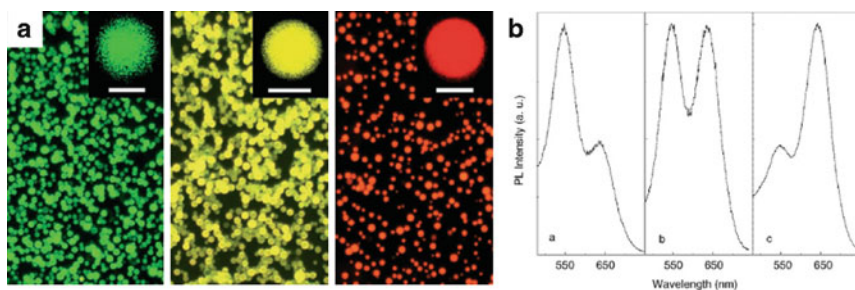


**Fig. 35** (a) Fluorescence images of PS particles loaded with green (*left*), yellow (*middle*), and red CdTe dots (*right*). The *insets* are the corresponding confocal fluorescence images. *Scale bars*: 2  $\mu\text{m}$ . (b) Fluorescence spectra of PS beads incorporated with both green and red CdTe dots with their photoluminescence (PL) peak-intensity ratio being 2:1 (a), 1:1 (b), and 1:2 (c). The initial input ratio of green to red dots was 1:0.3 (a), 1:0.6 (b), and 1:1.2 (c). Reprinted from [310] with permission of Wiley-VCH

### 6.1.3 Miscellaneous

A recent work reported the inverse (mini)emulsion polymerization of NIPAM in paraffin oil using water-soluble CdSe/ZnS QDs coated with a polymerizable amphiphilic copolymer [311]. The QDs were homogeneously distributed inside the obtained particles (ca. 1  $\mu\text{m}$  in size, broadly distributed), which effectively displayed photoluminescence properties. In addition, the presence of QDs did not interfere with the thermosensitive behavior of PNIPAM.

Finally, as in the case of iron oxides, a few studies report the incorporation of QDs inside microgel particles obtained by precipitation polymerization. For instance, hydrosoluble CdTe nanocrystals capped with thioglycolic acid could be reversibly incorporated inside poly(NIPAM-*co*-4VPy) copolymer particles by varying the pH [312]. The entrapment of QDs was dominated by the physical entanglement of the collapsed network and electrostatic interactions between the loaded QDs and the gel network. In another study from the same group, CdTe QDs co-stabilized by both thioglycerol and thioglycolic acid were incorporated inside PNIPAM microspheres through hydrogen bonding [313]. Finally, CTAB-modified CdTe QDs were entrapped into poly(NIPAM-*co*-AA) microgels through electrostatic interactions [314].

## 6.2 Synthesis of Quantum Dots in the Presence of Polymer Particles

As mentioned above, different synthetic procedures have been developed for the formation of QDs, and each of them has its own advantages and drawbacks. When envisioning the synthesis of QDs inside or at the surface of polymer particles obtained by emulsion polymerization, aqueous-based procedures will be logically favored.



One of the first examples of QDs synthesis onto the surface of latex particles was reported by Zhang et al. [315, 316], who recently described the synthesis of monodisperse nanocomposite particles with inorganic CdS nanocrystals deposited onto poly(MMA-*co*-MAA) latex particles (varying from 150 to 600 nm) obtained by emulsion polymerization (Fig. 36). In a first step, latex particles were ion-exchanged with a  $\text{Cd}(\text{ClO}_4)_2$  solution. The  $\text{Cd}^{2+}$  ions thus introduced into the electrical double layer were further reduced into CdS by addition of a  $\text{Na}_2\text{S}$  solution. By adjusting the initial MMA to MAA ratio and consequently the density of surface  $\text{COO}^-$ , as well as adjusting the ratio of  $\text{Cd}^{2+}$  to surface  $\text{COO}^-$ , the size of CdS nanoparticles could be varied from 3 to 8 nm and the surface coverage could reach 40%. Colloidal arrays with interesting optical properties were obtained when the nanocomposite particles were sedimented under gravity [316]. The CdS-loaded nanocomposite particles could be subsequently recovered by a film-forming polymer shell by reacting MMA and BA monomers. The resulting colloidal nanocomposites were finally assembled into 3D periodic arrays consisting of rigid poly(MMA-*co*-MAA)/CdS core particles regularly distributed within the soft polymer matrix. In contrast to what was anticipated in Fig. 36, QDs were uniformly mixed with the shell-forming polymer, leading to the doping of the poly(MMA-*co*-BA) matrix [315].

Using a similar procedure, poly[styrene-*co*-(2-methacrylic acid 3-(bis-carboxy methylamino)-2-hydroxypropyl ester)] [poly(styrene-*co*-GMA-IDA)] latex particles (70–130 nm in size) obtained by surfactant-free emulsion polymerization were successfully coated with CdS nanoparticles [317]. The GMA-IDA groups offered coordination sites for chelating metal ions, at which CdS nanoparticles were grown. The density and size of CdS nanoparticles could be varied by adjusting the ionic content and concentration of chelating groups, providing nanocomposite particles

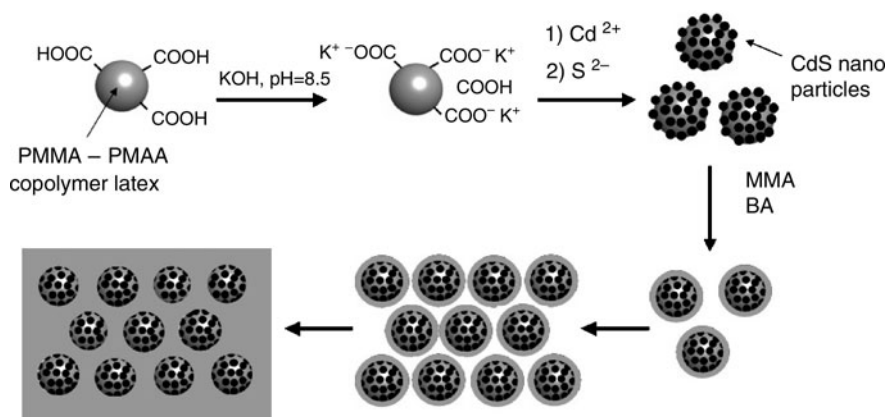


**Fig. 36** Synthesis of poly(MMA-*co*-MAA)/CdS/poly(MAA-*co*-BA) multilayered hybrid particles with a periodic structure. Redrawn and adapted from [315] with permission of the American Chemical Society

with luminescent properties. The same study was then carried out with poly(MMA-*co*-MA-*co*-GMA-IDA) particles displaying various  $T_g$  to investigate the influence of this parameter on CdS formation [318]. The addition of a protective ZnS shell on CdS nanoparticles provided hybrid particles with enhanced photoluminescence properties [319].

Particles of poly(styrene-*co*-DMAEMA) have also been reported for the effective synthesis of luminescent CdS/polymer composite particles [320]. The difference in this case was that surfactant-free emulsion copolymerization was performed in the presence of  $\text{Cd}^{2+}$  ions that were coordinated to DMAEMA.

Alternatively, QDs can be synthesized inside preformed microgels particles (200–600 nm) obtained by the copolymerization of NIPAM, AA, and 2-hydroxyethyl acrylate in the presence of MBA [182]. An aqueous solution of  $\text{Cd}(\text{ClO}_4)_2$  (the  $\text{Cd}^{2+}$  source) was first added to the particles to induce ion exchange between the cations of the microgels and  $\text{Cd}^{2+}$ . After dialysis, slow addition of  $\text{Na}_2\text{S}$  solution induced the formation of CdS nanocrystals. The optical properties of the embedded QDs (versus free QDs) were maintained and only slightly affected (e.g., red-shift or broader emission peak). The microgels could be further coated by a polymeric shell, and the resulting hydrophobic QD-doped particles were used as building blocks for the fabrication of photonic crystals (Fig. 37) [321].

Optical detection of glucose by CdS QDs immobilized inside microgels was very recently reported [322]. This original approach relies on the formation of copolymer microgels constituted of poly(*N*-isopropylacrylamide-*co*-acrylamide-*co*-phenyl boronic acid). These particles were obtained in two steps: synthesis of poly(NIPAM-*co*-AAm-*co*-AA) microgels, and coupling of 3-aminophenylboronic acid to the  $-\text{COOH}$  groups of the AA units. Then,  $\text{Cd}^{2+}$  complexation was achieved by the PAAm segments through the addition of  $\text{Cd}(\text{ClO}_4)_2$ . After removal of excess  $\text{Cd}^{2+}$ , a thioacetamide solution was added dropwise and the dispersion heated to  $85^\circ\text{C}$  for 1 h to afford CdS-embedded microgels. Phenyl boronic acid is known to

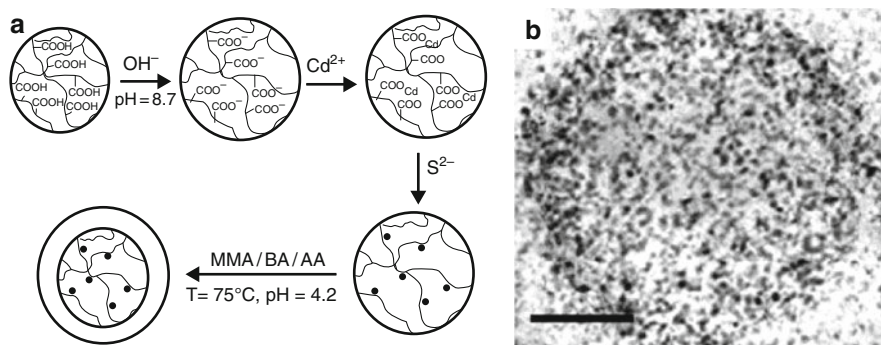


**Fig. 37** (a) Synthesis of hybrid core-shell particles doped with CdS quantum dots. Reprinted from [321] with permission of Wiley-VCH. (b) TEM photo of the core microgels. Scale bar: 50 nm. Reprinted from [182] with permission of the American Chemical Society

strongly bond to glucose, allowing the fluorescence of the in situ synthesized QDs to be reversibly quenched and anti-quenched when the microgels undergo swelling and deswelling in response to the changes in glucose concentration.

## 7 Synthesis of Metallic Latex Particles

The strong interest in the incorporation of metallic nanoparticles into polymer latexes arises from the outstanding optical, magnetic, and catalytic properties of metal nanoclusters with potential uses in electronic and optical devices, magnetic recording media, biological labeling, and catalysis. The formation of metal colloids or clusters by the controlled reduction, nucleation, and growth of metal salts in aqueous solution has been investigated for over a century. Nevertheless, studies dealing with the preparation of metallic polymer particles through emulsion polymerization are scarce.

### 7.1 *Polymer Encapsulation of Metallic Particles Through Emulsion Polymerization*

In 1999, Quaroni and coworkers reported for the first time the elaboration of polymer-coated silver nanoparticles through emulsion polymerization [323]. The silver colloids (around 100 nm diameter and irregular in shape) were previously modified by adsorption of a double layer of OA. Then, a uniform layer of poly(styrene-co-MAA) copolymers was formed on the hydrophobized inorganic seed particles, providing a protective organic and functional shell to the metal particle. Whereas thin coatings (<10 nm) were shown to follow the shape of the metal core, thicker coatings assumed more globular shapes. As the authors noted, the polymer shell induced only minor changes in spectral properties under conditions where the particles were un-aggregated. The plasmon resonance underwent only a small red shift, which was ascribed to an increase of the dielectric constant in the particle environment. A similar approach was described by Bao et al. who used 100 nm silver nanoparticles onto which was adsorbed an azo initiator (ACPA) [324]. Emulsion copolymerization of styrene and NaSS was performed in the presence of PAA as a steric stabilizer in a water/ethanol mixture. A thin polymeric shell (5–10 nm) was thus formed onto the silver nanoparticles, protecting them from dissolution when nitric acid was added to the medium. Non-spherical metallic particles could also be encapsulated, as reported by Obare et al. CTAB-coated gold nanorods were covered by a PS shell, which induced only slight modifications of the optical properties of the nanorods [325], as previously observed by Quaroni et al. for silver particles [323]. The Au core was then dissolved by KCN to provide hollow PS nanotubes.

In a related approach, Gu et al. reported the synthesis of multilayered gold/silica/PS core-shell particles through seeded emulsion polymerization. In this

study, silica-coated gold colloids were encapsulated by PS using MPTMS as silane coupling agent according to the procedure previously described for silica (see Sect. 2.1.1). These particles were subsequently transformed into hollow spheres by chemical etching of the silica core in acidic medium [326].

Metal/polymer hybrid particles displaying an eccentric structure were very recently reported [327, 328]. The key parameter for the formation of such morphologies was the addition of the metal nanoparticles after the polymerization was started. The reaction was performed in a water/ethanol mixture (40/60 by weight), ethanol playing a key role in the reduction of charge effects. Each hybrid particle contained only one metal nanoparticle anchored on the poly(styrene-*co*-DVB-*co*-NaSS) polymer particle. The strategy proved to be successful for gold, palladium, and platinum.

Finally, even if microgels are out of the scope of the present review, it is worth mentioning that gold nanoparticles have also been encapsulated inside thermo- and pH-responsive poly(NIPAM-*co*-AA) microgel particles using 60 nm OA-coated nanoparticles as seeds [329, 330].

## 7.2 *Polymer Particles as Template for the Synthesis of Metallic Shells and Metallic Nanoparticles*

Polymer particles can serve as colloidal templates for the in situ synthesis of either metallic nanoparticles or metallic shells. This is achieved by the reaction of the metal salt precursors previously adsorbed on their surface through ion exchange or complexation chemistry. The colloidal templates must contain surface groups with strong affinity for the metal precursors. Functional groups issued from carboxyl ( $-\text{COOH}$ ), hydroxyl ( $-\text{OH}$ ), thiol ( $-\text{SH}$ ), amino ( $-\text{NH}_2$ ), cyano ( $-\text{CN}$ ), or pyridino derivatives can be easily introduced into polymer latexes by copolymerization of the corresponding monomer. In this method, the surface-complexed metal salts are then directly transformed into metal colloids by the addition of reducing agents. For instance, polymer particles with a PS core and a P4VPy shell were used as template for the synthesis of noble metal (including palladium, gold and silver) nanoparticles in the shell layer (Fig. 38) [331]. The Pd-functionalized composite particles were successfully used as catalysts in Suzuki cross-coupling reactions.

Similarly, using the same particles as those used for the synthesis of CdS QDs (see Sect. 6.2, Fig. 36), silver nanoparticles could be deposited onto carboxylated poly(MMA-*co*-MAA) particles using silver salts as precursors [315, 316]. As for the case of CdS, periodic structures of polymer/silver hybrid colloids were elaborated. The method obviously opens a new avenue for production of optically responsive materials with a controlled periodicity. In another work using commercial 110 nm carboxylate-functionalized PS particles as templates, Hao et al. reported the synthesis of silver nanodisks formed through chemical reduction of silver salts in DMF [332]. The composite particles obtained (Fig. 39) exhibited an intense electronic spectrum differing markedly from those of spheres. Still using

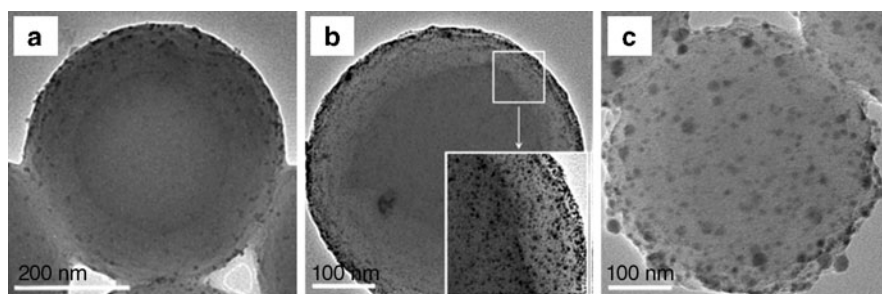


**Fig. 38** TEM images of (a) poly(styrene-*co*-4VPy)/Pd, (b) poly(styrene-*co*-4VPy)/Au, and (c) poly(styrene-*co*-4VPy)/Ag composite particles produced via chemical reduction of the corresponding metal salts previously adsorbed on the surface of poly(styrene-*co*-4VPy) core-shell particles. Adapted from [331] with permission of the American Chemical Society

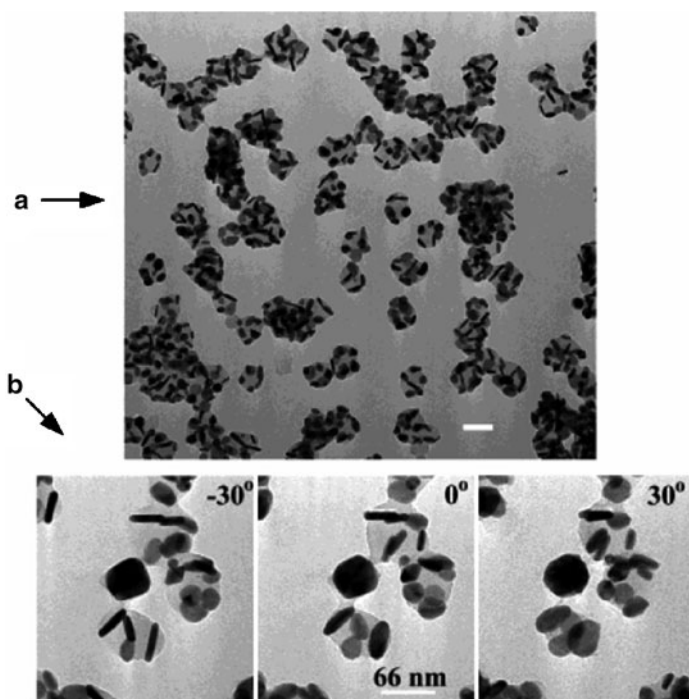


**Fig. 39** (a) TEM image of a fresh Ag/PS sample. Scale bar: 100 nm. (b) TEM images of Ag/PS, tilting the sample plane from  $-30^\circ$  through  $0^\circ$  to  $+30^\circ$ . Reproduced from [332] with permission of the American Chemical Society

carboxylated particles, different in situ chemical reduction methods were studied by Mayer et al. to form silver-latex composites using commercial PS latexes [333]. By adjusting the latex surface properties, the reduction method and conditions, or the silver precursor type, various composite materials could be prepared.

In other works, palladium [334–337] and rhodium [335–337] nanoparticles were formed onto the surface of PS-based polymer particles functionalized through the copolymerization of styrene with AA, MAA, and acrylonitrile. The resulting composite colloids were evaluated as catalysts for the hydrogenation of alkenes, the Rh-based composite showing activities close to commercially available products [336]. Using the obtained Pd-functionalized polymer particles, nickel [338], nickel/cobalt [339], or cobalt [340] nanoparticles were anchored onto the surface through chemical metal deposition (electroless plating) [341].

Sulfate-functionalized PS particles (of 710 and 580 nm) obtained by emulsion polymerization were coated with silver or gold nanoparticles through the adsorption of their corresponding metal salts in an ethanol/acetone mixture. This was followed by chemical reduction and a seeding growth step (both performed in ethanol) [342]. The obtained core-shell colloids were able to crystallize into long-range ordered structures with photonic bandgaps (Fig. 40). As well as potential applications as photonic crystals, the ordered structures may find applications as substrates for SERS (surface enhanced Raman spectroscopy) studies.

More recently, noble metals such as gold, silver, platinum, and palladium were deposited onto sulfate-functionalized PS particles through the addition of their respective metal salts in the absence of extra reducing agent [343]. The sulfate groups were supposed to be involved in a redox reaction with the metal salts, eventually leading to the formation of the metal nanoparticles (Fig. 41).

A last example of particular interest that also relies on the adsorption of metal salts was recently proposed for the synthesis of silver nanoparticles inside the

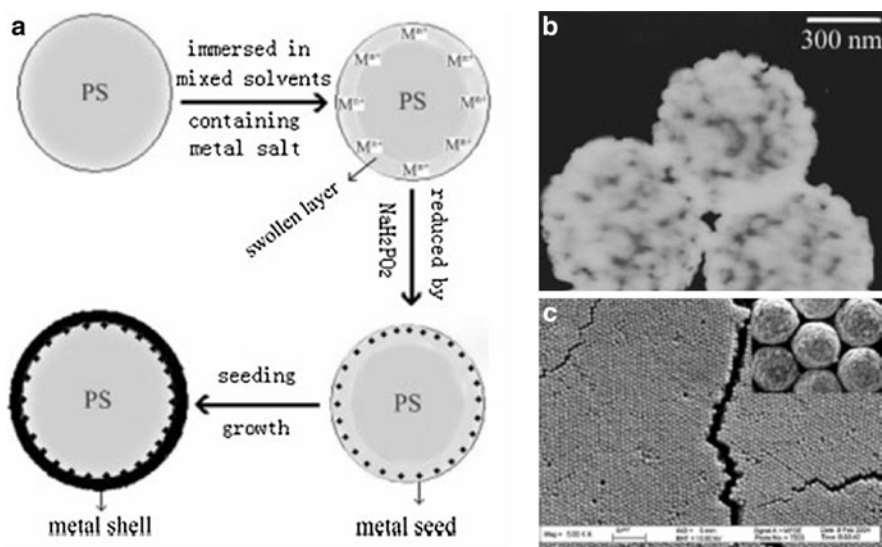
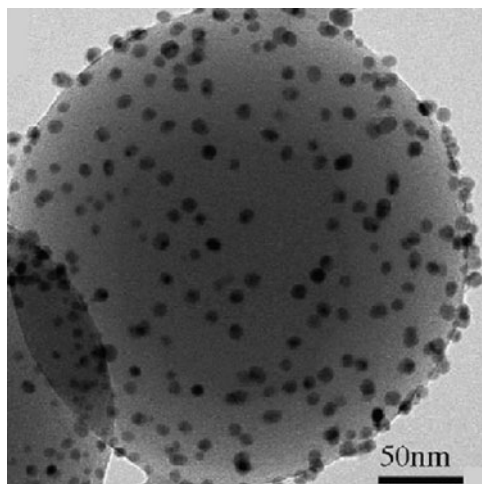


**Fig. 40** (a) Procedure for coating PS colloids with gold or silver. (b) TEM image of 580 nm PS colloids coated with gold. (c) SEM image of opals made of gold-coated PS composite colloids. Reproduced from [342] with permission of Wiley-VCH



**Fig. 41** TEM image of nanosize-dot-arrayed Ag-PS composite fabricated by means of the redox reaction method. Reprinted from [343] with permission of Elsevier



outer layer of “nano-tree”-type core-shell particles, i.e., particles with a PS core surrounded by regularly branched chains of PEG [344]. Similarly, Mei et al. showed that palladium nanoparticles could be synthesized inside the hairy layer of PS-PNIPAM core-shell particles [345]. In both cases, the composite particles were subsequently used as catalyst in the reduction reaction of 4-nitrophenol in the presence of sodium borohydride.

Instead of precursor metal salts, metal oxides could also be used. Silver-PS core-shell particles were thus recently synthesized using a two-step procedure [346]. First, hydrogen reduction of a saturated silver(I) oxide solution at elevated temperature was carried out in the presence of commercial sulfate-functionalized PS particles (200 nm) used as support for the reduction of Ag salt into silver. The formed Ag nanoparticles were attached to the PS particles (Fig. 42a). Subsequent acetone treatment led to the encapsulation of the silver nanoparticles inside the PS spheres (Fig. 42b), accompanied by a red-shift of the characteristic plasmon resonance frequency of the particles (Fig. 42c).

In alternative procedures, the coating can also be produced by the controlled hydrolysis of metal salts into metal oxides, followed by reduction of the oxide into the corresponding metal. Submicrometer-sized composite spheres of yttrium and zirconium compounds and hollow metallic spheres have been prepared this way by coating cationic PS latex particles with basic yttrium carbonate and basic zirconium sulfate, respectively, followed by calcination of the coated latexes at elevated temperatures [347, 348]. Uniform coatings of copper compounds have been formed in a similar procedure by aging (at high temperature) the aqueous solutions of the metal salt in the presence of urea, PVP, and anionic PS latexes [349]. The coating was shown to proceed by in situ heterocoagulation of the precipitating metal colloids on the organic seed surface. Voids were produced in a subsequent step by complete thermal oxidative decomposition of the polymer core.



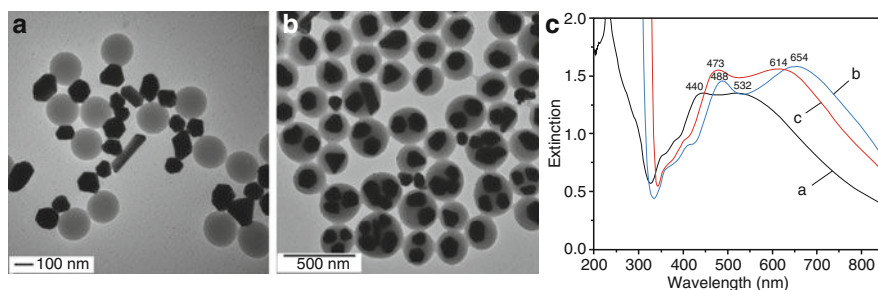


**Fig. 42** TEM images of (a) Ag nanoparticles adsorbed onto PS particles, and (b) Ag-PS core-shell particles. (c) Extinction spectra of as-prepared Ag-PS particles (curve *a*), Ag-PS particles dispersed in acetone (curve *b*), and redispersed back in water (curve *c*). Adapted from [346] with permission of the American Chemical Society

Finally, similarly to magnetic nanoparticles or QDs, microgel particles have been used as template for the synthesis of metallic nanoparticles such as silver [182, 321].

## 8 Summary and Outlook

This review article highlights the synthesis and properties of O/I particles elaborated through emulsion polymerization, which is a well-established technology. The relatively recent advances in the synthesis of these particles have paved the way to a huge range of new materials with outstanding properties. In this article, we have reported selected examples of O/I colloids prepared from either preformed minerals or preformed latex particles. When minerals are used as seeds, suitable interactions of the growing polymer with their surface are provided by the previous adsorption and/or reaction of molecules that can be either inactive or active in the subsequent polymerization process. Such molecules include conventional surfactants, organosilanes and titanates, macromonomers and surfmers, ionic initiators, and ionic monomers. The overall strategy provides an accurate control over the composite particle nanostructure, leading to a multitude of morphologies (core-shell, multinuclear, multipod-like, snowman-like, armored-like, etc.). Furthermore, the strategy affords the opportunity to precisely design the surface properties of the polymer-coated mineral particles by selecting appropriate functional monomers.

In another approach, metallic particles, semiconductors, or metal oxides are generated at the surface or inside polymer colloids used as templates. Again, the seed particle surface must carry suitable functionalities to promote interaction (and thus deposition) of the inorganic precursor. Inorganic nanoparticles are obtained in a subsequent step by thermal decomposition, hydrolysis, chemical reduction or other soft-chemistry processes. These strategies allow selective nucleation and growth of the inorganic particles at the surface or inside the latex particles, which eventually protect them from agglomeration.

Although a general chemical approach to the fabrication of these polymer/inorganic composite particles in a precisely controlled manner is not yet available, impressive progress has been made towards the designed synthesis of colloidal particles made of organic and inorganic domains assembled into unique and well-defined structures. These simple methods will most probably open the way to the fabrication of large amounts of original assemblies.

In practice, an infinite variety of polymer/inorganic particle combinations can be envisaged. This article has attempted to summarize the most important issues to be considered for successful formation of such nanocomposite colloids. The ability to tailor the affinity between the organic and inorganic parts is the key to a happy marriage between these two naturally incompatible compounds. However, despite the considerable advances, excitement, and promise of O/I composite latexes, substantial fundamental research is still necessary to provide a deeper understanding of current synthetic methods, develop new processes, and enable further exploitation of these materials.

We hope that the general concepts and principles reviewed in this article will provide the reader with the necessary background to develop deeper expertise and to create novel O/I hybrid particles and nanocomposites with outstanding characteristics and properties.

## References

1. Moriarty P (2001) *Rep Prog Phys* 64:297
2. Cao G (2004) *Nanostructures and nanomaterials – synthesis, properties and applications*. Imperial College Press, London
3. Hofman-Caris CHM (1994) *New J Chem* 18:1087
4. van Herk AM (1997) In: Asua JM (ed) *Polymeric dispersions: principles and applications*, NATO ASI series E: applied sciences, vol 335. Kluwer Academic, Dordrecht, p 435
5. van Herk AM, German AL (1999) In: Arshady R (ed) *Microspheres microcapsules & liposomes*, vol 1. Preparation and chemical applications. Citus Books, London, chap 17, p 457
6. Pomogalio AD (2000) *Russ Chem Rev* 69:53
7. Bourgeat-Lami E (2002) In: R. Arshady, A. Guyot (eds) *Dendrimers, assemblies and nanocomposites*, MML series 5. Citus Books, London, chap 5, p 149
8. Bourgeat-Lami E (2002) *J Nanosci Nanotechnol* 2:1
9. Bourgeat-Lami E (2004) In: Nalwa HS (ed) *Encyclopedia of nanoscience and nanotechnology*, vol 8. American Scientific, Los Angeles, p 305
10. Bourgeat-Lami E, Duguet E (2006) In: Ghosh (ed) *Functional coatings by polymer microencapsulation*. Wiley-VCH, Weinheim, chap 4, p 85
11. Bourgeat-Lami E (2007) In: Kickelbick G (ed) *Hybrid materials, synthesis, characterization and applications*. Wiley-VCH, Weinheim, p 87
12. Castelvetro V, De Vita C (2004) *Adv Colloid Interface Sci* 108/109:167
13. Hussain F, Hojjati M, Okamoto M, Gorga RE (2006) *J Comp Mater* 40:1511
14. Balmer JA, Schmid A, Armes SP (2008) *J Mater Chem* 18:5722
15. Wang T, Keddie JL (2009) *Adv Colloid Interface Sci* 147/148:319
16. Zou H, Wu S, Shen J (2008) *Chem Rev* 108:3893
17. Stöber W, Fink A, Bohn E (1968) *J Colloid Interface Sci* 26:62
18. Kang S, Hong SI, Choe CR, Park M, Rim S, Kim J (2001) *Polymer* 42:879
19. Bourgeat-Lami E, Espiard P, Guyot A (1995) *Polymer* 36:4385

20. Espiard P, Guyot A (1995) *Polymer* 36:4391
21. Espiard P, Guyot A, Perez J, Vigier G, David L (1995) *Polymer* 36:4397
22. Bourgeat-Lami E, Lang J (1998) *J Colloid Interface Sci* 197:293
23. Bourgeat-Lami E, Lang J (1999) *J Colloid Interface Sci* 210:281
24. Corcos F, Bourgeat-Lami E, Novat C, Lang J (1999) *Colloid Polym Sci* 277:1142
25. Zhang K, Chen H, Chen X, Chen Z, Cui Z, Yang B (2003) *Macromol Mater Eng* 288:380
26. Nagao D, Ueno T, Oda D, Konno M (2009) *Colloid Polym Sci* 287:1051
27. Reculusa S, Mingotaud C, Bourgeat-Lami E, Duguet E, Ravaine S (2004) *Nano Lett* 4:1677
28. Nagao D, Hashimoto M, Hayasaka K, Konno M (2008) *Macromol Rapid Commun* 29:1484
29. Zhang K, Zheng L, Zhang X, Chen X, Yang B (2006) *Colloids Surf A Physicochem Eng Asp* 277:145
30. Zeng Z, Yu J, Guo Z (2004) *Macromol Chem Phys* 205:2197
31. Zeng Z, Yu J, Guo Z (2005) *J Polym Sci Part A Polym Chem* 43:2826
32. Qu A, Wen X, Pi P, Cheng J, Yang Z (2008) *J Colloid Interface Sci* 317:62
33. Bourgeat-Lami E, Insulaire M, Reculusa S, Perro A, Ravaine S, Duguet E (2006) *J Nanosci Nanotechnol* 6:432
34. Perro A, Duguet E, Lambert O, Taveau J-C, Bourgeat-Lami E, Ravaine S (2009) *Angew Chem Int Ed Engl* 48:361
35. Van Blaaderen A (2003) *Science* 301:470
36. Reculusa S, Poncet-Legrand C, Perro A, Duguet E, Bourgeat-Lami E, Mingotaud C, Ravaine S (2005) *Chem Mater* 17:3338
37. Reculusa S, Poncet-Legrand C, Ravaine S, Duguet E, Bourgeat-Lami E, Mingotaud C (2004) Nanometric or mesoscopic dissymmetric particles, and method for preparing same. French Patent FR2846572, WO 2004/044061
38. Perro A, Reculusa S, Pereira F, Delville MH, Mingotaud C, Duguet E, Bourgeat-Lami E, Ravaine S (2005) *Chem Commun* 5542
39. Perro A, Reculusa S, Ravaine S, Bourgeat-Lami E, Duguet E (2005) *J Mater Chem* 15:3745
40. Reculusa S, Poncet-Legrand C, Ravaine S, Mingotaud C, Duguet E, Bourgeat-Lami E (2002) *Chem Mater* 14:2354
41. Perro A, Reculusa S, Bourgeat-Lami E, Duguet E, Ravaine S (2006) *Colloids Surf A Physicochem Eng Asp* 284/285:78
42. Perro A, Nguyen D, Ravaine S, Bourgeat-Lami E, Lambert O, Taveau J-C, Duguet E (2009) *J Mater Chem* 19:4225
43. Nagai K, Ohishi Y, Ishiyama K, Kuramoto N (1989) *J Appl Polym Sci* 38:2183
44. Nagai K (1994) *Macromol Symp* 84:29
45. Ding XF, Zhao JZ, Liu YH, Zhang HB, Wang ZC (2004) *Mater Lett* 58:3126
46. Mahdavian AR, Ashjari M, Makoo AB (2007) *Eur Polym J* 43:336
47. Barthet C, Hickey AJ, Cairns DB, Armes SP (1999) *Adv Mater* 11:408
48. Percy MJ, Barthet C, Lobb JC, Khan MA, Lascelles SF, Vamvakaki M, Armes SP (2000) *Langmuir* 16:6913
49. Amalvy JI, Percy MJ, Armes SP (2001) *Langmuir* 17:4770
50. Fujii S, Read ES, Binks BP, Armes SP (2005) *Adv Mater* 17:1014
51. Fujii S, Armes SP, Binks BP, Murakami R (2006) *Langmuir* 22:6818
52. Chen M, Wu L, Zhou S, You B (2004) *Macromolecules* 37:9613
53. Chen M, Zhou S, You B, Wu L (2005) *Macromolecules* 38:6411
54. Kammona O, Kotti K, Kiparissides C, Celis J-P, Franssaer J (2009) *Electrochim Acta* 54:2450
55. Cheng X, Chen M, Zhou S, Wu L (2006) *J Polym Sci Part A Polym Chem* 44:3807
56. Luna-Xavier JL, Bourgeat-Lami E, Guyot A (2001) *Colloid Polym Sci* 279:947
57. Luna-Xavier JL, Guyot A, Bourgeat-Lami E (2002) *J Colloid Interface Sci* 250:82
58. Luna-Xavier JL, Guyot A, Bourgeat-Lami E (2004) *Polym Int* 53:609
59. Qi D-M, Bao Y-Z, Huang Z-M, Weng Z-X (2006) *J Appl Polym Sci* 99:3425
60. Dupin D, Schmid A, Balmer JA, Armes SP (2007) *Langmuir* 27:11812
61. Schmid A, Tonnar J, Armes SP (2008) *Adv Mater* 20:3331
62. Schmid A, Armes SP, Leite CAP, Galembeck F (2009) *Langmuir* 25:2486
63. Schmid A, Scherl P, Armes SP, Leite CAP, Galembeck F (2009) *Macromolecules* 42:3721

64. Lee J, Hong CK, Choe S, Shima SE (2007) *J Colloid Interface Sci* 310:112
65. Zhang F-A, Yu C-L (2007) *Eur Polym J* 43:1105
66. Colver PJ, Colard CA L, Bon SAF (2008) *J Am Chem Soc* 130:16850
67. Hu J, Ma J, Deng W (2008) *Mater Lett* 62:2931
68. Sheibat-Othman N, Bourgeat-Lami E (2009) *Langmuir* 25:10121
69. Binks BP, Horozov TS (eds) (2006) *Colloidal particles at liquid interfaces*. Cambridge University Press, Cambridge
70. Teixeira RFA, Bon SAF (2010) Physical methods for the preparation of hybrid nanocomposite polymer latex particles. *Adv Polym Sci* doi:10.1007/12\_2010\_65
71. Xue Z, Wiese H (2006) US patent US7094830B2
72. Tiarks F, Leuninger J, Wagner O, Jahns E, Wiese H (2007) *Surf Coat Intern* 90:221
73. Kalele S, Gosavi SW, Urban J, Kulkarni SK (2006) *Curr Sci* 91:1038
74. Kickelbick G, Liz-Marzan LM (2004) In: Nalwa HS (ed) *Encyclopedia of nanoscience and nanotechnology*, vol 2 American Scientific, Los Angeles, p 199
75. Tissot I, Novat C, Lefebvre F, Bourgeat-Lami E (2001) *Macromolecules* 34:5737
76. Bourgeat-Lami E, Tissot I, Lefebvre F (2002) *Macromolecules* 35:6185
77. Tissot I, Reymond JP, Lefebvre F, Bourgeat-Lami E (2002) *Chem Mater* 14:1325
78. Castelvetro V, Manariti A, De Vita C, Ciardelli F (2002) *Macromol Symp* 187:165
79. Hotta Y, Alberius PCA, Bergstro L (2003) *J Mater Chem* 13:496
80. Cornelissen JJLM, Connor EF, Kim H-C, Lee VY, Magibitang T, Rice PM, Volasen W, Sundberg LK, Millar RD (2003) *Chem Commun* 1010
81. Lu Y, McLellan J, Xia Y (2004) *Langmuir* 20:3464
82. Yang J, Lind JU, Trogler WC (2008) *Chem Mater* 20:2875
83. Graf C, Vossen D, Imhof A, Van Blaaderen A (2003) *Langmuir* 19:6693
84. Kobayashi Y, Misawa K, Kobayashi M, Takeda M, Konno M, Satake M, Kawazoe Y, Ohuchi N, Kasuya A (2004) *Colloids Surf A Physicochem Eng Asp* 242:47
85. Rosensweig RE (1985) *Ferrohydrodynamics*. Cambridge University Press, Cambridge
86. Lu A-H, Salabas EL, Schüth F (2007) *Angew Chem Int Ed Engl* 46:1222
87. Pyle BH, Broadaway SC, McFeters GA (1999) *Appl Environ Microbiol* 65:1966
88. Cumbal L, Greenleaf J, Leun D, SenGupta AK (2003) *React Funct Polym* 54:167
89. Mornet S, Vasseur S, Grasset F, Veverka P, Goglio G, Demourgues A, Portier J, Pollert E, Duguët E (2006) *Prog Solid State Chem* 34:237
90. Pankhurst QA, Connolly J, Jones SK, Dobson J (2003) *J Phys D Appl Phys* 36:R167
91. Elaissari A, Sauzedde F, Montagne F, Pichot C (2003) In: Elaissari A (ed) *Colloidal polymers: synthesis and characterization*. Marcel Dekker, New York, p 285
92. Arshady R, Pouliquen D, Halbreich A, Roger J, Pons J-N, Bacri J-C, Da Silva MdF, Häfeli U (2002) In: Arshady R, Guyot A (eds) *Dendrimers, assemblies, nanocomposites*, MML series 5. Citus Books, London, p 283
93. Vatta LL, Sanderson RD, Koch KR (2006) *Pure Appl Chem* 78:1793
94. Charmot D (1989) *Prog Colloid Polym Sci* 79:94
95. Lin C-R, Wang C-C, Chen IH (2006) *J Magn Magn Mater* 304:e34
96. Wang Y, Feng L, Pan C (1998) *J Appl Polym Sci* 70:2307
97. Wang PH, Pan CY (2000) *Colloid Polym Sci* 278:245
98. Wang PH, Pan CY (2002) *Colloid Polym Sci* 280:152
99. Jiang J (2007) *Eur Polym J* 43:1724
100. Liu W-J, He W-D, Wang Y-M, Wang D, Zhang Z-C (2005) *Polymer* 46:8366
101. Molday RS, Yen SPS, Rembaum A (1977) *Nature* 268:437
102. Kwon O, Solc J (1986) *J Magn Magn Mater* 54–57:1699
103. Solc J (1983) Colloidal size hydrophobic polymers particulate having discrete particles of an inorganic material dispersed therein. US Patent 4,421,660
104. Wooding A, Kilner M, Lambrick DB (1991) *J Colloid Interface Sci* 144:236
105. Wooding A, Kilner M, Lambrick DB (1992) *J Colloid Interface Sci* 149:98
106. Shen L, Laibinis PE, Hatton TA (1999) *Langmuir* 15:447
107. Meguro K, Yabe T, Ishioka S, Kato K, Esumi K (1986) *Bull Chem Soc Jpn* 59:3019
108. Yanase N, Noguchi H, Asakura H, Suzuta T (1993) *J Appl Polym Sci* 50:765

109. Noguchi H, Yanase N, Uchida Y, Suzuta T (1993) *J Appl Polym Sci* 48:1539
110. Xu X, Friedman G, Humfeld KD, Majetich SA, Asher SA (2002) *Chem Mater* 14:1249
111. Xu X, Friedman G, Humfeld KD, Majetich SA, Asher SA (2001) *Adv Mater* 13:1681
112. Wang P-C, Chiu W-Y, Lee C-F, Young T-H (2004) *J Polym Sci A Polym Chem* 42:5695
113. Wang P-C, Chiu W-Y, Young T-H (2006) *J Appl Polym Sci* 100:4925
114. Brijmohan SB, Shaw MT (2007) *J Membrane Sci* 303:64
115. Xie G, Zhang Q, Luo Z, Wu M, Li T (2003) *J Appl Polym Sci* 87:1733
116. Kondo A, Fukuda H (1997) *J Ferment Bioeng* 84:337
117. Kondo A, Kamura H, Higashitani K (1994) *Appl Microbiol Biotechnol* 41:99
118. Khan A (2008) *Mater Lett* 62:898
119. Lee CF, Chou YH, Chiu WY (2007) *J Polym Sci A Polym Chem* 45:3062
120. Lee CF, Chou YH, Chiu WY (2007) *J Polym Sci A Polym Chem* 45:3912
121. Guan N, Liu C, Sun D, Xu J (2009) *Colloids Surf A Physicochem Eng Asp* 335:174
122. Jung S, Park S (2009) *Biotechnol Lett* 31:107
123. Pich A, Bhattacharya S, Ghosh A, Adler H-JP (2005) *Polymer* 46:4596
124. Stevens PD, Fan J, Gardimalla HMR, Yen M, Gao Y (2005) *Org Lett* 7:2085
125. Huang J, Pen H, Xu Z, Yi C (2008) *React Funct Polym* 68:332
126. Liu H, Guo J, Jin L, Yang W, Wang C (2008) *J Phys Chem B* 112:3315
127. Xu Z, Xia A, Wang C, Yang W, Fu S (2007) *Mater Chem Phys* 103:494
128. Li P, Zhu AM, Liu QL, Zhang QG (2008) *Ind Eng Chem Res* 47:7700
129. Pollert E, Knízek K, Marysko M, Záveta K, Lancok A, Boháček J, Horák D, Babic M (2006) *J Magn Magn Mater* 306:241
130. Horák D, Chekina N (2006) *J Appl Polym Sci* 102:4348
131. Horák D, Petrovský E, Kapicka A, Frederichs T (2007) *J Magn Magn Mater* 311:500
132. Qiu G-M, Xu Y-Y, Zhu B-K, Qiu G-L (2005) *Biomacromolecules* 6:1041
133. Guo N, Wu D, Pan X, Lu M (2009) *J Appl Polym Sci* 112:2383
134. Galperin A, Margel S (2007) *J Biomed Mater Res B Appl Biomater* 83B:490
135. Skaat H, Belfort G, Margel S (2009) *Nanotechnology* 22:5106
136. Boguslavsky Y, Margel S (2008) *J Colloid Interface Sci* 317:101
137. Yang Y, Tu C, Gao M (2007) *J Mater Chem* 17:2930
138. Tu C, Yang Y, Gao M (2008) *Nanotechnology* 19:105601/1
139. Montagne F, Mondain-Monval O, Pichot C, Elaissari A (2006) *J Polym Sci A Polym Chem* 44:2642
140. Xu H, Cui L, Tong N, Gu H (2006) *J Am Chem Soc* 128:15582
141. Cui L, Xu H, He P, Sumitomo K, Yamaguchi Y, Gu H (2007) *J Polym Sci A Polym Chem* 45:5285
142. Ding Y, Hu Y, Jiang X, Zhang L, Yang C (2004) *Angew Chem Int Ed Engl* 43:6369
143. Ding Y, Hu Y, Zhang L, Chen Y, Jiang X (2006) *Biomacromolecules* 7:1766
144. Wu Y, Guo J, Yang W, Wang C, Fu S (2006) *Polymer* 47:5287
145. Guo J, Wang C, Mao W, Yang W, Liu C, Chen J (2008) *Nanotechnology* 19:315605
146. Sacanna S, Philipse AP (2006) *Langmuir* 22:10209
147. Sacanna S, Philipse AP (2007) *Adv Mater* 19:3824
148. Sacanna S, Kegel WK, Philipse AP (2007) *Phys Rev Lett* 98:158301
149. Ge J, Hu Y, Zhang T, Yin Y (2007) *J Am Chem Soc* 129:8974
150. Nagao D, Yokoyama M, Saeki S, Kobayashi Y, Konno M (2008) *Colloid Polym Sci* 286:959
151. Deng YH, Yang WL, Wang CC, Fu SK (2003) *Adv Mater* 15:1729
152. Cai J, Guo J, Ji M, Yang W, Wang C, Fu S (2007) *Colloid Polym Sci* 285:1607
153. Ge J, Huynh T, Hu Y, Yin Y (2008) *Nano Lett* 8:931
154. Furusawa K, Nagashima K, Anzai C (1994) *Colloid Polym Sci* 272:1104
155. Du H, Zhang P, Liu F, Kan S, Wang D, Li T, Tang X (1997) *Polym Int* 43:274
156. Du H, Cao Y, Bai Y, Zhang P, Qian X, Wang D, Li T, Tang X (1998) *J Phys Chem B* 102:2329
157. Sauzedde F, Elaissari A, Pichot C (1999) *Colloid Polym Sci* 277:846
158. Sauzedde F, Elaissari A, Pichot C (1999) *Colloid Polym Sci* 277:1041
159. Sauzedde F, Elaissari A, Pichot C (2000) *Macromol Symp* 151:617
160. Gu S, Shiratori T, Konno M (2003) *Colloid Polym Sci* 281:1076

161. Gu S, Onishi J, Kobayashi Y, Nagao D, Konno M (2005) *J Colloid Interface Sci* 289:419
162. Lee J, Senna M (1995) *Colloid Polym Sci* 273:76
163. Sayar F, Güven G, Piskin E (2006) *Colloid Polym Sci* 284:965
164. Sun H, Yu J, Gong P, Xu D, Zhang C, Yao S (2005) *J Magn Magn Mater* 294:273
165. Candau F (1997) In: Lovell PA, El-Aasser MS (eds) *Emulsion polymerization and emulsion polymers*. Wiley, Chichester, p 723
166. Pichot C (2006) In: Pichot C, Daniel JC (eds) *Les latex synthétiques élaboration, propriétés, applications*. Lavoisier, Paris, p 207
167. Li X, Zhang L, Jin R (1999) *Polym Adv Technol* 10:90
168. Macková H, Králová D, Horák D (2007) *J Polym Sci A Polym Chem* 45:5884
169. Ménager C, Sandre O, Mangili J, Cabuil V (2004) *Polymer* 45:2475
170. Yang S, Liu H, Zhang Z (2008) *Langmuir* 24:10395
171. Hong RY, Feng B, Liu G, Wang S, Li HZ, Ding JM, Zheng Y, Wei DG (2009) *J Alloy Compd* 476:612
172. Liu H, Wang C, Gao Q, Chen J, Liu X, Tong Z (2009) *Mater Lett* 63:884
173. Ugelstad J, Berge A, Ellingsen T, Schmid R, Nilsen TN, Mørk PC, Stenstad P, Hornes E, Olsvik (1992) *Prog Polym Sci* 17:87
174. Ugelstad J, Ellingsen T, Berge A, Helgée B (1983) *Magnetic polymer particles and process for the preparation thereof*. WO 83/03920
175. Lindlar B, Boldt M, Eiden-Assmann S, Maret G (2002) *Adv Mater* 14:1656
176. Pich A, Bhattacharya S, Adler HJP (2005) *Polymer* 46:1077
177. Pich A, Bhattacharya S, Lu Y, Boyko V, Adler H-JP (2004) *Langmuir* 20:10706
178. Omer-Mizrahi M, Margel S (2009) *J Colloid Interface Sci* 329:228
179. Tapeinos C, Kartsonakis I, Liatsi P, Daniilidis I, Kordas G (2008) *J Am Ceram Soc* 91:1052
180. Suzuki D, Kawaguchi H (2006) *Colloid Polym Sci* 284:1443
181. Rubio-Retama J, Zafeiropoulos NE, Serafinelli C, Rojas-Reyna R, Voit B, Cabarcos EL, Stamm M (2007) *Langmuir* 23:10280
182. Zhang J, Xu S, Kumacheva E (2004) *J Am Chem Soc* 126:7908
183. Lee C-F, Lin C-C, Chien C-A, Chiu W-Y (2008) *Eur Polym J* 44:2768
184. Brugger B, Richtering W (2007) *Adv Mater* 19:2973
185. Conley RF (1996) In: *Practical dispersion – a guide to understanding and formulating slurries*. VCH, New York
186. Schofield JD (2002) *Prog Org Coat* 45:249
187. Hou WH, Lloyd TB, Fowkes FM (1992) In: Daniels ES, Sudol T, El-Aasser M (eds) *Polymer latexes: preparation, characterization and applications*, ACS symposium series 492. ACS, Washington DC, chap 25, pp 405–421
188. Sperry PR, Wiersema RJ, Nyi K (1978) *Dispersing paint pigments*. US Patent 4,102,843
189. Schofield JD (1982) *Dispersible inorganic pigment*. US Patent 4,349,389
190. Solc J (1983) *Colloidal size hydrophobic polymers particulate having discrete particles of an inorganic material dispersed therein*. US Patent 4,421,660
191. Martin RW (1984) *Polymer-encapsulated dispersed solids and methods*. Eur Patent Appl 0104498
192. Martin RW (1986) *Method of encapsulating finely divided solid particles*. US Patent 4,608,401
193. Solc J (1987) *Method for preparing colloidal size particulate*. US Patent 4,680,200
194. Hoy KL, Glancy CW, Lewis JMO (1990) *Micro-composite systems and processes for making same*. Eur Patent Appl 0392065
195. Martin RW (1992) *Encapsulating finely divided solid particles in stable suspensions*. US Patent 4,771,086
196. Hees U, Kluge M, Raulfs FW, Schoepke H, Siemensmeyer K, Van Gelder R, Weiser J, Heissler H, Adams S, Renz G, Simpson PA (2004) *Method for treating particulate pigments*. WO 2004113454
197. Templeton-Knight RL (1990) *J Oil Colour Chem Assoc* 73:459
198. Templeton-Knight RL (1990) *Chem Ind* 512



199. Lorimer JP, Mason TJ, Kershaw D, Livsey I, Templeton-Knight RL (1991) *Colloid Polym Sci* 269, 392
200. Hasegawa M, Arai K, Saito S (1987) *J Polym Sci Part A Polym Chem* 25:3117
201. Hasegawa M, Arai K, Saito S (1987) *J Appl Polym Sci* 33:411
202. Hoy KL, Smith OW (1991) *ACS Polym Mater Sci Eng Preprint* 65:78
203. Caris CHM, van Elven LPM, van Herk AM, German A (1998) 19th FATEPEC Conference Proceeding 3:341
204. Caris CHM, van Elven LPM, van Herk AM, German A (1989) *Brit Polym J* 21:133
205. Caris CHM, van Herk AM, German AL (1990) 20th FATEPEC Conference Proceedings 325
206. Caris CHM, Kuijpers RPM, van Herk AM, German AL (1990) *Makromol Chem Macromol Symp* 35/36, 535
207. Janssen EAWG, van Herk AM, German AL (1993) *ACS Div Polym Chem Polym Preprint* 34:532
208. Janssen RQF, van Herk AM, German AL (1993) *J Oil Colour Chem Assoc* 11:455
209. Janssen RQF, van Herk AM, German AL (1994) 22th FATEPEC Conference Proceedings 1:104
210. Caris CHM (1990) Polymer encapsulation of inorganic submicron particles in aqueous dispersion. Ph.D. Thesis, Eindhoven University of Technology, The Netherlands
211. Janssen RQF (1995) Polymer encapsulation of titanium dioxide. Efficiency, stability and compatibility. Ph.D. Thesis, Eindhoven University of Technology, The Netherlands
212. Yang M, Dan Y (2006) *J Appl Polym Sci* 101:4056
213. Haga Y, Watanabe T, Yosomiya R (1991) *Angew Makromol Chem* 189:23
214. Nguyen D, Zondanos HS, Farrugia JM, Serelis AK, Such CH, Hawke BS (2008) *Langmuir* 24:2140
215. Daigle JC, Claverie JP (2008) *J Nanomater* 609184
216. Charleux B, D'Agosto F, Delaitre G (2010) Preparation of hybrid latex particles and core-shell particles through the use of controlled radical polymerization techniques in aqueous media. *Adv Polym Sci* doi:10.1007/12\_2010\_64
217. Yu D-G, An JO, Bae JY, Lee YE, Ahn SD, Kang S-Y, Suh KS (2004) *J Appl Polym Sci* 92:2970
218. Yu D-G, An J-H, Bae JY, Ahn SD, Kang S-Y, Suh KS (2005) *J Appl Polym Sci* 97:72
219. Badila M, Brochon C, Hebraud A, Hadzioannou G (2008) *Polymer* 49:4529
220. Zhang P, Zhang HP, Li ZH, Wu YP, van Ree T (2009) *Polym Adv Technol* 20:571
221. Liu Y, Chen X, Wang R, Xin JH (2006) *Mater Lett* 60:3731
222. Chen T, Colver PJ, Bon SA (2007) *Adv Mater* 19:2286
223. Ai Z, Sun G, Zhou Q, Xie C (2006) *J Appl Polym Sci* 102:1466
224. Kondo Y, Yoshikawa H, Awaga K, Murayama M, Mori T, Sunada K, Bandow S, Iijima S (2008) *Langmuir* 24:547
225. Yang Su-C, Yang D-J, Kim J, Hong J-M, Kim H-G, Kim I-D, Lee H (2008) *Adv Mater* 20:1059
226. Chigane M, Watanabe M, Izaki M, Yamaguchi I, Shinagawa T (2009) *Electrochem SolidState Lett* 12:E5
227. Shiho H, Kawahashi N (2000) *Colloid Polym Sci* 278:270
228. Li GK, Zhang ZC (2004) *Mater Lett* 58:2768
229. Syoufian A, Inoue Y, Yada M, Nakashima K (2007) *Mater Lett* 61:1572
230. Wang P, Chen D, Tang F-Q (2006) *Langmuir* 22:4832
231. Imhof A (2001) *Langmuir* 17:3579
232. Caruso F, Shi X, Caruso RA, Susha A (2001) *Adv Mater* 13:740
233. Eiden S, Maret G (2002) *J Colloid Interface Sci* 250:281
234. Liu H, Ye H, Zhang Y (2007) *Appl Surf Sci* 253:7219
235. Liu H, Ye H, Zhang Y (2008) *Colloids Surfaces A Physicochem Eng Asp* 315:1
236. Karlsson PM, Esbjörnsson NB, Holmberg K (2009) *J Colloid Interface Sci* 337:364
237. Agrawal M, Pich A, Zafeiropoulos NE, Gupta S, Pionteck J, Simon F, Stamm M (2007) *Chem Mater* 19:1845
238. Chen JH, Cheng C-Y, Chiu W-Y, Lee C-F, Liang N-Y (2008) *Eur Polym J* 44:3271



239. Yang Y, Kong XZ, Kan CY, Sun CG (1999) *Polym Adv Technol* 10:54
240. Yu J, Yu J, Guo Z-X, Gao Y-F (2001) *Macromol Rapid Commun* 22:1261
241. Wu W, He T, Chen J-F, Zhang X, Chen Y (2006) *Mater Lett* 60:2410
242. Batzilla Th, Tulke A (1998) *J Coat Technol* 70:77
243. Alexandre M, Dubois P (2000) *Mater Sci Eng* 28:1
244. Ray SS, Okamoto M (2003) *Prog Polym Sci* 28:1539
245. Okada A, Usuki A (2006) *Macromol Mater Eng* 291:1449
246. Chen B, Evans JRG, Greewell HC, Boulet P, Coveney PV, Bowden AA, Whiting A (2008) *Chem Soc Rev* 37:568
247. Paulis M, Leiza JR (2009) In: Mittal V (ed) *Advances in polymer nanocomposites technology* Nova, New York, chap 5
248. Solomon DH, Rosser MJ (1965) *J Appl Polym Sci* 12:1261
249. Solomon DH, Loft BC (1968) *J Appl Polym Sci* 12:1253
250. Talapatra S, Guhaniyogi SC, Chakravarti SK (1985) *J Macromol Sci Chem A22*:1611
251. Bhattacharya J, Chakravarti SK, Talapatra S, Saha SK (1989) *J Polym Sci A Polym Chem* 27:3977
252. Lee DC, Jang LW (1996) *J Appl Polym Sci* 61:1117
253. Noh MW, Lee DC (1999) *Polym Bull* 42:619
254. Noh MW, Jang LW, Lee DC (1999) *J Appl Polym Sci* 74:179
255. Noh MW, Lee DC (1999) *J Appl Polym Sci* 74:2811
256. Tong X, Zhao H, Tang T, Feng Z, Huang B (2002) *J Polym Sci A Polym Chem* 40:1706
257. Pan M, Shi X, Li X, Hu H, Zhang L (2004) *J Appl Polym Sci* 94:277
258. Kim TH, Jang LW, Lee DC, Choi HJ, Jhon MS (2002) *Macromol Rapid Commun* 23:191
259. Bandyopadhyay S, Giannelis E, Hsieh, A (2000) *Polym Mater Sci Eng* 82:208
260. Diaconu G, Asua JM, Paulis M, Leiza JR (2007) *Macromol Symp* 259:305
261. Diaconu G, Paulis M, Leiza JR (2008) *Polymer* 49:2444
262. Laus M, Camerani M, Lelli M, Sparnacci K, Sandrolini F (1998) *J Mater Sci* 33:2883
263. Wang D, Zhu J, Yao Q, Wilkie CA (2002) *Chem Mater* 14:3837
264. Liu G, Zhang L, Li Z, Qu X (2005) *J Appl Polym Sci* 98:1010
265. Feng X, Zhong A, Chen D (2006) *J Appl Polym Sci* 101:3963
266. Yang W-T, Ko T-H, Wang S-C, Shih P-I, Chang M-J, Jiang GJ (2008) *Polym Comp* 29:409
267. Min H, Wang J, Hui H, Jie W (2006) *J Macromol Sci B Phys* 45:623
268. Qutubuddin S, Fu X, Tajuddin Y (2002) *Polym Bull* 48:143
269. Sedlakova Z, Plestil J, Baldrian J, Slouf M, Holub P (2009) *Polym Bull* 63:365
270. Choi YS, Wang KH, Xu M, Chung IJ (2002) *Chem Mater* 14:2936
271. Kim YK, Choi YS, Wang KH, Chung IJ (2002) *Chem Mater* 14:4990
272. Xu M, Choi YS, Kim YK, Wang KH, Chung IJ (2003) *Polymer* 44:6387
273. Choi YS, Xu M, Chung IJ (2005) *Polymer* 46:531
274. Li H, Yang Y, Yu Y (2004) *J Adhes Sci Technol* 18:1759
275. Greesh N, Hartmann PC, Cloete V, Sanderson RD (2008) *J Polym Sci A Polym Chem* 46:3619
276. Chen G, Ma Y, Qi Z (2001) *Scr Mater* 44:125
277. Chou CS, Lafleur EE, Lorah DP, Slone RV, Neglia KD (2005) *Aqueous nanocomposite dispersions: processes, compositions and uses thereof*. US Patent 6,838,507
278. Meneghetti P, Qutubuddin S (2004) *Langmuir* 20:3424
279. Li H, Yu Y, Yang Y (2005) *Eur Polym J* 41:2016
280. Negrete-Herrera N, Letoffe JM, Putaux JL, David L, Bourgeat-Lami E (2004) *Langmuir* 20:1564
281. Negrete-Herrera N, Persoz S, Putaux JL, David L, Bourgeat-Lami E (2006) *J Nanosci Nanotechnol* 6:421
282. Negrete-Herrera N, Putaux JL, Bourgeat-Lami E (2006) *Prog Solid State Chem* 34:121
283. Negrete-Herrera N, Putaux J-L, David L, De Haas F, Bourgeat-Lami E (2007) *Macromol Rapid Commun* 28:1567
284. Ruggerone R, Plummer CJG, Negrete-Herrera N, Bourgeat-Lami E, Manson J-AE (2009) *Eur Polym J* 45:621

285. Voorn DJ, Ming W, van Herk AM (2006) *Macromolecules* 39:4654
286. Voorn DJ, Ming W, van Herk AM (2006) *Macromol Symp* 245:584
287. Choi YS, Choi MH, Wang KH, Kim SO, Kim YK, Chung IJ (2001) *Macromolecules* 34:8978
288. Yeom EH, Kim WN, Kim JK, Lee S-S, Park M (2004) *Mol Cryst Liq Cryst* 425:85
289. Lin KF, Lin SC, Chien AT, Hsieh CC, Yen MH, Lee CH, Lin CS, Chiu WY, Lee YH (2006) *J Polym Sci A Polym Chem* 44:5572
290. Zhang J, Chen K, Zhao H (2008) *J Polym Sci A Polym Chem* 46:2632
291. Guillot S, Bergaya F, de Azevedo C, Warmont F, Tranchant J-F (2009) *J Colloid Interface Sci* 333:563
292. Voorn DJ, Ming W, Van Herk AM (2006) *Macromolecules* 39:2137
293. Alivisatos AP (1996) *Science* 271:933
294. Murphy CJ (2002) *Anal Chem* 520A
295. Tomczak N, Janczewski D, Han M, Vancso GJ (2009) *Prog Polym Sci* 34:393
296. Trindade T, O'Brien P, Pickett NL (2001) *Chem Mater* 13:3843
297. Murray CB, Norris DJ, Bawendi MG (1993) *J Am Chem Soc* 115:8706
298. Peng X, Wickham J, Alivisatos AP (1998) *J Am Chem Soc* 120:5343
299. Peng X, Manna L, Yang W, Wickham J, Scher E, Kadavanich A, Alivisatos AP (2000) *Nature* 404:59
300. Peng ZA, Peng X (2001) *J Am Chem Soc* 123:183
301. Peng X (2002) *Chem Eur J* 8:334
302. Spanhel L, Haase M, Weller H, Henglein A (1987) *J Am Chem Soc* 109:5649
303. Huang J, Sooklal K, Murphy CJ, Ploehn HJ (1999) *Chem Mater* 11:3595
304. Sherman RL Jr, Chen Y, Ford WT (2004) *J Nanosci Nanotech* 4:1032
305. Hines MA, Guyot-Sionnest P (1996) *J Phys Chem* 100:468
306. Dabbousi BO, Rodriguez-Viejo J, Mikulec FV, Heine JR, Mattoussi H, Ober R, Jensen KF, Bawendi MG (1997) *J Phys Chem B* 101:9463
307. Yang X, Zhang Y (2004) *Langmuir* 20:6071
308. Sherman RL Jr, Ford WT (2005) *Langmuir* 21:5218
309. Lee BH, Kwon K-W, Shim M (2007) *J Mater Chem* 17:1284
310. Yang Y, Wen Z, Dong Y, Gao M (2006) *Small* 2:898
311. Janczewski D, Tomczak N, Han M-Y, Vancso GJ (2009) *Macromolecules* 42:1801
312. Kuang M, Wang D, Bao H, Gao M, Möhwald H, Jiang M (2005) *Adv Mater* 17:267
313. Gong Y, Gao M, Wang D, Möhwald H (2005) *Chem Mater* 17:2648
314. Li J, Liu B, Li J (2006) *Langmuir* 22:528
315. Zhang J, Coombs N, Kumacheva E (2002) *J Am Chem Soc* 124:14512
316. Zhang J, Coombs N, Kumacheva E, Lin Y, Sargent EH (2002) *Adv Mater* 14:1756
317. Chu YC, Wang CC, Huang YH, Chen CY (2005) *Nanotechnology* 16:376
318. Wang C-C, Chen A-L, Chen IH (2006) *J Inorg Organomet Polym Mater* 16:31
319. Wang C-C, Chen A-L, Chen I-H (2006) *Polym Adv Technol* 17:598
320. Cheng X, Zhao Q, Yang Y, Tjong SC, Li RKY (2008) *J Colloid Interface Sci* 326:121
321. Xu S, Zhang J, Paquet C, Lin Y, Kumacheva E (2003) *Adv Funct Mater* 13:468
322. Wu W, Zhou T, Shen J, Zhou S (2009) *Chem Commun*:4390
323. Quaroni L, Chumanov G (1999) *J Am Chem Soc* 121:10642
324. Bao H, Chumanov G, Czerw R, Carroll DL, Foulger SH (2005) *Colloid Polym Sci* 283:653
325. Obare SO, Jana NR, Murphy CJ (2001) *Nano Lett* 1:601
326. Gu S, Onishi J, Mine E, Kobayashi Y, Konno M (2004) *J Colloid Interface Sci* 279:284
327. Ohnuma A, Cho EC, Camargo PHC, Au L, Ohtani B, Xia Y (2009) *J Am Chem Soc* 131:1352
328. Ohnuma A, Cho EC, Jiang M, Ohtani B, Xia Y. (2009) *Langmuir* 25:13880
329. Kim JH, Lee TR (2004) *Chem Mater* 16:3647
330. Kim JH, Lee TR (2004) *Polym Mater Sci Eng* 90:637
331. Wen F, Zhang W, Wei G, Wang Y, Zhang J, Zhang M, Shi L (2008) *Chem Mater* 20:2144
332. Hao E, Kelly KL, Hupp JT, Schatz GC (2002) *J Am Chem Soc* 124:15182
333. Mayer ABR, Grebner W, Wannemacher R (2000) *J Phys Chem B* 104:7278
334. Wang PH, Pan C-Y (2001) *Colloid Polym Sci* 279:171
335. Tamai H, Sakurai S, Hirota Y, Nishiyama F, Yasuda H (1995) *J Appl Polym Sci* 56:441

- 336. Tamai H, Hamamoto S, Nishiyama F, Yasuda H (1995) *J Colloid Interface Sci* 171:250
- 337. Tamai H, Sumi T, Nishiyama F, Yasuda H (1996) *J Appl Polym Sci* 60:1727
- 338. Wang PH, Pan CY (2000) *Colloid Polym Sci* 278:245
- 339. Wang PH, Pan C-Y (2000) *Colloid Polym Sci* 278:581
- 340. Wang PH, Pan CY (2002) *Colloid Polym Sci* 280:152
- 341. Warshawsky A, Upson DA (1989) *J Polym Sci A Polym Chem* 27:2963
- 342. Zhang J, Liu J, Wang S, Shan P, Wang Z, Ming N (2004) *Adv Funct Mater* 14:1089
- 343. Ou JL, Chang CP, Sung Y, Ou KL, Tseng CC, Ling HW, Ger MD (2007) *Colloids Surfaces A Physicochem Eng Asp* 305:36
- 344. Lu Y, Mei Y, Walker R, Ballauf M, Drechsler M (2006) *Polymer* 47:4985
- 345. Mei Y, Lu Y, Polzer F, Ballauff M (2007) *Chem Mater* 19:1062
- 346. Kumbhar A S, Chumanov G (2009) *Chem Mater* 21:2835
- 347. Kawahashi N, Persson C, Matijevic E (1991) *J Mater Chem* 1:577
- 348. Kawahashi H, Matijevic E (1991) *J Colloid Interface Sci* 143:103
- 349. Kawahashi N, Shiho H (2000) *J Mater Chem* 10:2294



# Preparation of Hybrid Latex Particles and Core–Shell Particles Through the Use of Controlled Radical Polymerization Techniques in Aqueous Media

Bernadette Charleux, Franck D’Agosto, and Guillaume Delaittre

**Abstract** The synthesis of hybrid and core–shell nanoparticles using controlled/living radical polymerization in aqueous dispersed systems is reviewed. The processes involve emulsion, miniemulsion, and dispersion polymerizations as well as grafting techniques, with the aim of producing submicrometric latex particles with well-defined morphologies that might not be accessible via classical radical polymerization. Those morphologies include organic/inorganic hybrids, nanostructured particles, (nano)capsules, and particles with a hydrophobic core and hydrophilic shell.

**Keywords** Controlled/living radical polymerization · Core–shell particle · Dispersion polymerization · Emulsion polymerization · Grafting from · Hybrid · Miniemulsion polymerization · Nanogel · Nanoparticle

## Contents

1	Introduction .....	128
2	Controlled/Living Radical Polymerization in Aqueous Dispersed Systems .....	128
2.1	Main Controlled/Living Radical Polymerization Methods .....	128
2.2	Controlled/Living Radical Polymerization in Aqueous Dispersed Systems .....	132

---

B. Charleux (✉) and F. D’Agosto  
Laboratoire de Chimie Catalyse Polymères et Procédés (C2P2), CNRS UMR 5265,  
CPE Lyon, Université de Lyon 1, Université de Lyon, 43 Bd du 11 novembre 1918,  
Villeurbanne, 69616, France  
e-mail: [charleux@lcpp.cpe.fr](mailto:charleux@lcpp.cpe.fr); [dagosto@lcpp.cpe.fr](mailto:dagosto@lcpp.cpe.fr)

G. Delaittre  
Institute for Molecules and Materials, Radboud University Nijmegen, Heyendaalseweg 135,  
Nijmegen, 6525ED, The Netherlands  
e-mail: [g.delaittre@science.ru.nl](mailto:g.delaittre@science.ru.nl)

3	Organic/Inorganic Hybrid Particles .....	134
3.1	Silica Nanoparticles .....	135
3.2	Iron Oxide .....	136
3.3	Other Metallic Oxides .....	138
3.4	Clays .....	141
4	(Nano)structured Particles .....	142
5	(Nano)capsules .....	145
5.1	Solid-Templated Synthesis .....	146
5.2	Oil-Templated Synthesis .....	147
6	Core-Shell Particles with Hydrophilic Shell and Hydrophobic Core via a Convergent Method .....	150
6.1	Reversible Transfer Methods .....	150
6.2	Reversible Termination Methods .....	162
7	Core-Shell Particles via a Divergent Method: Grafting of Polymer Brush at the Surface of Polymer Particles .....	170
7.1	Grafting from Technique .....	171
7.2	Grafting to Technique .....	178
8	Conclusion .....	178
	References .....	179

## Abbreviations

Cryo-TEM	Cryogenic-transmission electron microscopy
4VP	4-Vinylpyridine
AA	Acrylic acid
AAm	Acrylamide
AAUA	11-Acrylamidoundecanoic acid
ACPA	<i>N,N'</i> -Azobiscyanopentanoic acid
ADA	12-Acryloyloxydodecanoic acid
AGET	Activator generated by electron transfer
AIBN	<i>N,N'</i> -Azobisisobutyronitrile
ATRP	Atom transfer radical polymerization
BA	<i>n</i> -Butyl acrylate
BMA	<i>n</i> -Butyl methacrylate
BPMODA	Bis(2-pyridylmethyl)octadecylamine
CMC	Critical micelle concentration
CPADB	4-(Cyanopentanoic acid)-4-dithiobenzoate
CRP	Controlled/living radical polymerization
DEAAm	<i>N,N</i> -Diethylacrylamide
DEAEMA	Diethylaminoethyl methacrylate
DLS	Dynamic light scattering
DMAAm	<i>N,N</i> -Dimethylacrylamide
DMAEA	Dimethylaminoethyl acrylate

DMAEMA	Dimethylaminoethyl methacrylate
$DP_n$	Number-average degree of polymerization
DSC	Differential scanning calorimetry
FTIR	Fourier transform infra-red
HEMA	Hydroxyethyl methacrylate
HMTETA	1,1,4,7,10,10-Hexamethyltriethylene tetramine
ITP	Iodine transfer polymerization
LA	Lactide
LCST	Lower critical solution temperature
MA	Methyl acrylate
MAA	Methacrylic acid
MAETACl	2-(Methacryloyloxy)ethyl trimethylammonium chloride
Manh	Maleic anhydride
MBAAm	<i>N,N'</i> -Methylenebisacrylamide
Me <sub>6</sub> -TREN	Tris[2-(dimethylamino)ethylamine]
MMA	Methyl methacrylate
$M_n$	Number-average molar mass
$M_w$	Weight-average molar mass
NAM	<i>N</i> -Acryloylmorpholine
NaSS	Sodium styrene sulfonate
NIPAAm	<i>N</i> -Isopropylacrylamide
NMP	Nitroxide-mediated radical polymerization
PDI	Polydispersity index ( $M_w/M_n$ )
PEG	Poly(ethylene glycol)
PEGMA	Poly(ethylene glycol) monomethacrylate
PEO	Poly(ethylene oxide)
PMDETA	<i>N,N,N',N',N''</i> -Pentamethyldiethylenetriamine
RITP	Reverse iodine transfer polymerization
RAFT	Reversible addition–fragmentation chain transfer
ROMP	Ring-opening metathesis polymerization
S	Styrene
SDS	Sodium dodecyl sulfate
SEC	Size exclusion chromatography
SG1	<i>N-tert</i> -Butyl- <i>N</i> -(1-diethyl phosphono-2,2-dimethylpropyl) nitroxide
SI	Surface-initiated
SR&NI	Simultaneous reverse and normal initiation
TEMPO	2,2,6,6-Tetramethylpiperidinyl-1-oxy
TeRP	Organotellurium-mediated radical polymerization
TGA	Thermogravimetric analysis
TIPNO	<i>N-tert</i> -Butyl- <i>N</i> -[1-phenyl-2-(methylpropyl)] nitroxide
VAc	Vinyl acetate
XPS	X-ray photoelectron spectroscopy



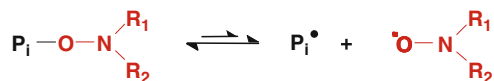
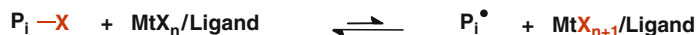
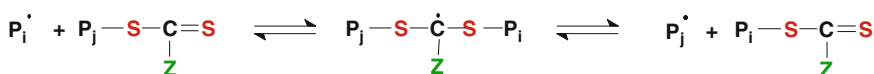
## 1 Introduction

Since the advent of controlled/living radical polymerization (CRP) methods and thanks to their compatibility with water, a huge amount of work has been performed on their implementation in aqueous dispersed systems, mainly for miniemulsion and emulsion polymerizations. As for homogeneous systems, the first goal was to achieve good control over molar mass, molar mass distribution, and chain architecture, e.g., for the synthesis of block or star copolymers in latex particles. With miniemulsion and emulsion polymerizations, another dimension can be readily controlled, namely particle morphology. The aim of this review article is to show how the development of CRP in aqueous media, including miniemulsion and emulsion polymerizations as well as grafting techniques, has opened a new field in the design of submicrometric particle morphology. We will focus on (a) organic/inorganic hybrid particles and will show the great potential of grafting techniques performed either in aqueous solution or in heterogeneous systems; (b) formation of (nano)structured particles via the design of block copolymers that induce internal phase separation; (c) (nano)capsules; and (d) particles with a hydrophobic core and hydrophilic shell produced via two different approaches – a convergent approach using hydrophilic or amphiphilic reactive polymers as precursors, and a divergent approach using grafting techniques and polymer colloids as substrate. Our purpose is to point out the advantage of CRP either for the design of new morphologies or for a better control over already known morphologies, together with potentially easier access to them.

## 2 Controlled/Living Radical Polymerization in Aqueous Dispersed Systems

### 2.1 Main Controlled/Living Radical Polymerization Methods

Free-radical polymerization [1] is a widely used process for industrial production and applications. This technique is relatively easy to perform because it does not require any stringent purification of the reagents and is tolerant to many functional groups. It generally leads to high molar mass polymers under relatively mild conditions. Many different processes can be applied, such as bulk, solution, suspension, or emulsion polymerizations. Moreover, a wide range of functional monomers are polymerized by radical mechanisms, and copolymerization provides a great variety of random copolymers with many structures and properties. However, the main drawback of radical polymerization is the lack of control over molar mass, molar mass distribution, chain-end functionalities, and macromolecular architecture. This is explained by the unavoidable, fast radical–radical terminations. For that main reason, the emergence of “living” or controlled radical polymerization (CRP) has opened a new era of research into this polymerization method [1, 2].

Nitroxide-mediated polymerization (NMP)Atom transfer radical polymerization (ATRP) (X = Cl, Br; Mt = Cu(I) and Cu(II))Degenerative transfer reactions (X = I, TeCH<sub>3</sub> ...)Reversible addition-fragmentation transfer (RAFT) (Z = activating group)

**Fig. 1** Main activation–deactivation equilibria in controlled/living radical polymerization. The first two are reversible termination reactions and the last two are reversible chain transfer reactions.  $P_i^\bullet$  stands for a macroradical with  $i$  monomer subunits. In the initial control agent, the polymer chain is replaced by a low molar mass leaving/initiating group, often referred to as  $R$

The CRP techniques can be divided into two groups according to their mechanism. They are based either on a reversible termination reaction or on a reversible chain transfer reaction (Fig. 1). In both cases, macromolecular radicals undergo reversible deactivation, i.e., successive activation–deactivation cycles. A very small fraction of chains are instantaneously active and can thus propagate. During the deactivation period, the chains are end-functionalized by a specific group and are called “dormant”. As a consequence of the dynamic activation–deactivation equilibrium, chains build up and grow simultaneously during the whole polymerization period. The main feature of CRP is that the number-average molar mass ( $M_n$ ) increases linearly with monomer conversion. The molar mass distribution is narrow, provided that a fast exchange occurs between active and dormant chains and that the chains can be further extended with either the same or another monomer. This opens the way to the synthesis of block copolymers and other more complex architectures.

### 2.1.1 Main Methods Operating via a Reversible Termination Mechanism

Nitroxide-mediated polymerization (NMP) [3] and atom transfer radical polymerization (ATRP) [4, 5] are the two main methods of CRP based on a reversible termination reaction. This corresponds to an equilibrium between the active macromolecular radical and a dormant covalent counterpart, which is either an alkoxyamine for NMP or an alkyl halide for ATRP (Fig. 1). Activation of the alkoxyamine is a thermal process and requires elevated temperatures, whereas in

ATRP a transition metal complex is needed for the activation of the alkyl-halide-ended macromolecules, and a wider range of temperatures can be applied. In both cases, the polymerization kinetics are governed by the activation–deactivation equilibrium and by the persistent radical effect [6]. The number-average degree of polymerization ( $DP_n$ ) is calculated by the ratio of the initial monomer concentration to the initiator (i.e., alkoxyamine or alkyl halide) concentration, multiplied by monomer conversion.

### Nitroxide-Mediated Controlled Radical Polymerization

Nitroxides are stable radicals that are able to trap carbon-centered radicals at a nearly diffusion controlled rate. At low temperatures, the formed alkoxyamine is stable and therefore the trapping reaction corresponds to an irreversible termination step. However, at elevated temperature, the C–O bond might undergo homolytic cleavage, leading back to the propagating radical and to the nitroxide. This equilibrium between propagating radical and inactive alkoxyamine is the key step in nitroxide-mediated CRP. Moreover, owing to the stability of their alkoxyamine end-group, the dormant macromolecules can be isolated and further used as macroinitiators for the polymerization of the same or another monomer. The main nitroxides are 2,2,6,6-tetramethylpiperidiny-1-oxyl (TEMPO) [3, 7], which was successfully applied for styrene and derivatives, and *N*-*tert*-butyl-*N*-(1-diethyl phosphono-2,2-dimethylpropyl) nitroxide (SG1) [8] and *N*-*tert*-butyl-*N*-[1-phenyl-2-(methylpropyl)] nitroxide (TIPNO) [9] (Fig. 2), which allowed the range of monomers to be very significantly expanded and the polymerization time to be reduced. The initiation step can be performed in two different ways by using either a bicomponent system with a classical radical initiator along with the free nitroxide deactivator, or a monocomponent system based on a preformed alkoxyamine. The latter is now the most popular method because it allows the kinetics and molar mass to be tuned very precisely.

### Atom Transfer Radical Polymerization

ATRP is based on the reversible transfer of a halogen atom between a dormant alkyl halide and a transition metal catalyst using redox chemistry. The alkyl halide is reduced to a growing radical and the transition metal is oxidized via an inner sphere electron transfer process. In the most studied reaction, the role of the activator is

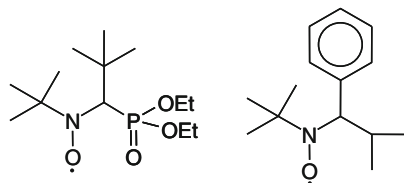


**Fig. 2** Structure of SG1 (left) and TIPNO (right)

played by a Cu(I) species complexed by a multidentate amine ligand, and the role of deactivator by the corresponding Cu(II) species. The initiation step can be performed in different manners, starting either from Cu(I) or from Cu(II). With the former, the process is called direct ATRP and employs an alkyl halide initiator. With the latter, there are multiple possibilities, among which one can cite the reverse ATRP process [4], which uses a classical radical initiator; the SR&NI method [10], which combines an alkyl halide along with a small fraction of a classical radical initiator [the latter produces radicals able to reduce Cu(II) into Cu(I)]; and the activator generated by electron transfer (AGET) technique [11], which uses an alkyl halide initiator along with a reducing agent to turn Cu(II) into Cu(I). ATRP can be successfully applied to a broad variety of monomers and can use a multitude of available mono- or multifunctional initiators and catalysts that enable the polymerization process and polymer characteristics to be finely tuned.

### 2.1.2 Main Methods Operating via a Reversible Transfer Mechanism

The activation–deactivation cycles are governed by a reversible chain transfer reaction, i.e., a bimolecular reaction between an active macromolecule and a dormant one, leading to the exchange of the functional end-group. It can be a direct exchange, like in the so-called degenerative transfer technique in which an iodine atom is exchanged (called the ITP method for iodine transfer polymerization, and RITP for reverse iodine transfer polymerization) [12–14]. The organotellurium-mediated CRP (TeRP) follows a similar principle [15], with the exchange of a terminal  $-\text{TeCH}_3$  group. The reaction proceeds via the two activation processes, namely thermal dissociation and degenerative transfer. However, when an external source of free radicals is used at low temperature, the reaction only proceeds via degenerative transfer. Another approach is the reversible addition–fragmentation chain transfer (RAFT) [16–20], in which case chains are end-functionalized by an unsaturated group (mainly a  $\text{C}=\text{S}$  bond from a dithioester, a dithiocarbonate, a dithiocarbamate, or a trithiocarbonate) that is exchanged through an addition–fragmentation process (Fig. 1). Technically, the polymerization system requires the use of a classical radical initiator in conjunction with a reversible chain transfer agent RX. The first step can be considered as a conventional transfer reaction to RX, creating new chains with a R group at one end and an X atom or functional group at the other end. The next step is the transfer of X from an end-functionalized chain to a propagating macroradical, which is a thermodynamically neutral, i.e., degenerative process. This second step does not create new chains but contributes to the extension of existing chains. If the initial concentration of radical initiator is small with respect to the initial concentration of transfer agent, a large majority of the macromolecules have the same expected end-group structure. The chain concentration becomes constant and close to the initial concentration of transfer agent once the latter has been completely consumed. At that stage only, and if the reversible transfer takes place, a linear increase in the  $M_n$  with monomer conversion can be observed ( $DP_n$  is calculated by the ratio of the initial monomer concentration to the chain transfer agent

concentration, multiplied by monomer conversion). The main requirement is that the rate constant of the transfer reaction to RX should be large, which is particularly the case in the RAFT process. The polymerization kinetics follow the classical steady-state assumption but, in some cases, especially with the dithiobenzoate-based RAFT agents, a significant rate retardation effect is often observed [21].

## **2.2 *Controlled/Living Radical Polymerization in Aqueous Dispersed Systems***

The developments of CRP in aqueous dispersed systems have been reviewed several times in the last 10 years [22–30]. Since an exhaustive description of the achievements in the field is not the main target of this article, the reader is invited to refer to those well-documented review articles. Only a brief overview will be given here and all references concerning miniemulsion and emulsion polymerizations (the main processes discussed in this review) can be found in the above-mentioned papers.

It should be mentioned, before starting this short description, that transposition of CRP from homogeneous systems (i.e., bulk or solution) to aqueous dispersed systems was far from being straightforward. Nevertheless, although challenging, the target was considered to be a particularly important one due the intrinsic qualities of those processes (high polymerization rates, low viscosity, environmentally benign conditions, broad application range, wide use in the industry, etc.). CRP was considered to offer additional advantages in controlling the polymer at the molecular level, in fine-tuning the particle composition and morphology, and in opening the door to well-defined hybrid nanocomposites for a variety of new potential applications.

### **2.2.1 Miniemulsion Polymerization**

In a first approach, CRP was mainly studied in miniemulsion polymerization [31–33] because the technique allows the complex nucleation and mass transport processes of an emulsion polymerization to be avoided. Consequently, the same recipes used in bulk could be employed, in particular the use of hydrophobic initiators and control agents. Many successful examples have been reported, and led to well-defined polymer chains and sometimes complex architectures in stable, sub-micrometric latex particles. Depending on the CRP technique, several requirements have to be considered.

In NMP, the nitroxide deactivator should be sufficiently oil-soluble to remain within the particles and participate in the activation–deactivation equilibrium. In case of favorable partitioning towards the aqueous phase or chemical degradation due to side reactions, an increase in the polymerization rate is observed at the expense of the molar mass distribution, which broadens. In ATRP, the transition metal complexes (mainly copper-based activator and deactivator) should be stable enough in the presence of water and should not interact with the various components of

the miniemulsion system, like the surfactant. For this reason, nonionic surfactants are preferred. Because Cu(I) can be easily oxidized in the presence of air, direct ATRP cannot be carried out under simple experimental conditions (the most delicate step being the ultrasonication). Reverse ATRP is well-suited but requires a large amount of catalyst. Recently, the best and most promising results were obtained using AGET ATRP [34–38]. With this method, the miniemulsion is prepared in the presence of the Cu(II) complex deactivator, which is not sensitive to air, along with a hydrophobic or amphiphilic alkyl halide initiator. The polymerization reaction is simply triggered by the addition of a water-soluble reducing agent, ascorbic acid for instance. In NMP and ATRP, the polymerization kinetics were studied in depth (both experimentally and theoretically) [39–44] and the compartmentalization effect was the subject of debate.

For polymerizations controlled by a reversible chain transfer mechanism, the key points to consider are the solubility and the reactivity of the chain transfer agent. In all cases, because the polymerization kinetics follow the classical steady-state assumption, enhanced polymerization rate with respect to homogenous systems is expected, owing to the compartmentalization effect. Concerning the reactivity (i.e., the value of the chain transfer constant), the effect on molar mass and molar mass distribution should be the same in miniemulsion as in homogeneous systems. The difference is thus mainly related to the solubility of the chain transfer agent and its partition coefficient between water and the monomer phase. The most hydrophobic transfer agents can be easily used in miniemulsion polymerization, without any potential exit of the primary radicals. Consequently, both the kinetics and the molar masses are well-controlled. For more hydrophilic control agents, exit of primary leaving radicals can be an issue and could lead to rate-retardation effects and poor control over molar masses. Despite colloidal stability problems encountered in some particular examples (mainly with ionic surfactants), the miniemulsion process was very successful for ITP and RAFT in aqueous dispersed systems, and allowed block copolymers to be synthesized with good control over molar mass, molar mass distribution, and chain structure.

### 2.2.2 Emulsion Polymerization

The development of true emulsion CRP processes was more challenging. Initially, only the RAFT method was applied with success, using moderately hydrophobic chain transfer agents with low chain transfer constants. In such a situation, the nucleation step was not altered with respect to a classical radical emulsion polymerization and the colloidal properties of the latexes were good. Generally, the batch process was employed, but a slow addition of the monomer was sometimes preferred in order to enhance transfer over propagation and lead to well-defined polymers. With more reactive RAFT agents, the emulsion polymerization was more difficult to achieve and the key to success was the use of an amphipathic macromolecular RAFT agent based on poly(acrylic acid) (PAA) in starved monomer conditions, without additional surfactant. More recently, poly(ethylene oxide) (PEO)-based amphiphilic

trithiocarbonate RAFT agents were employed in batch conditions, in a very simple surfactant-free, batch, *ab initio* emulsion polymerization process. This achievement was considered to be related to a judicious combination of the solubility and reactivity of the chain transfer agent. As those methods lead to hydrophilic–hydrophobic core–shell particles, they will be the subject of a particular section of this article (Sect. 6.1). It should also be mentioned here that a general difficulty of RAFT in aqueous dispersed systems, and particularly emulsion polymerization, is related to the need for a radical initiator in conjunction with the RAFT agent. Consequently, it is not always easy to control the locus where reversible transfer will take place, and this may have important and sometimes deleterious consequences on the control over molar mass and molar mass distribution.

Considering NMP and ATRP, the initial development of emulsion polymerization required the application of a two-step process. In the first step, a microemulsion-like system is employed with a minimum amount of monomer to swell the surfactant micelles and avoid the presence of large droplets. The latter are particularly detrimental to the colloidal stability of the latex, due to extensive droplet nucleation. This first step leads to a living polymer seed, containing end-functionalized oligomers, trapped inside stable particles. In a second step, the remaining monomer is added either in one shot or with a slow feeding rate, and the polymerization is resumed with simultaneous chain extension of the preformed oligomers and particle growth. This method is particularly effective for creating well-defined homopolymers and block copolymers within stable, submicrometric latex particles at high solids content. In NMP, water-soluble mono- or difunctional alkoxyamine initiators were used, whereas the alkyl halide initiator was hydrophobic in ATRP. Like in RAFT, further developments of NMP were based on surfactant-free recipes using water-soluble or amphiphilic macromolecular alkoxyamines. This method leads to the *in situ* formation of amphiphilic block copolymers that are able to self-assemble during the polymerization process, following a polymerization-induced micellization mechanism. Again, since the method leads to hydrophilic–hydrophobic core–shell particles similar to crew-cut micelles, it will be more extensively described later (Sect. 6.2.1).

### 3 Organic/Inorganic Hybrid Particles

Organic/inorganic hybrid particles are nanocomposites meant to combine the best attributes of the organic and the inorganic part. They can be defined as colloidal particles that contain both organic and inorganic domains either forming clearly distinguishable macroscopic phases or exhibiting some degree of mixing at the molecular level. They can be obtained (a) by assembling preformed organic and inorganic components, (b) by simultaneously reacting organic and inorganic precursors, or (c) by polymerizing *in situ* organic and/or inorganic precursors in the presence of their counterpart [45]. Because they require a structural order at the nanometer scale, a key issue is the creation of specific interactions at the interface of the organic and



inorganic components. This can be achieved by the incorporation onto inorganic particles of well-defined polymers that provide specific properties to the resulting hybrid via their functionality, composition, and dimensions.

A variety of CRP techniques have been employed to generate organic/inorganic hybrid particles including NMP, ATRP, and RAFT [46–52] but only a very small number of studies deal with organic/inorganic hybrid particles obtained via the use of CRP in aqueous medium. Those are mainly related to modification of silica, metallic oxides, or clays.

### 3.1 Silica Nanoparticles

Perruchot et al. [53] originally took advantage of successful poly(ethylene glycol) monomethacrylate (PEGMA) ATRP experiments directly performed in water [54] to graft a variety of methacrylate-based polymers from silica nanoparticles. The nanoparticles were first turned into ATRP initiators after reaction with 3-(dimethylethoxysilyl)propyl-2-bromoisobutyrate. Surface-initiated ATRPs of PEGMA and 2-(*N*-morpholino)ethyl methacrylate were then performed in water at 20°C. The presence of polymer chains on the resulting silica particles was shown by Fourier transform infra-red (FTIR) spectroscopy, elemental analyses and thermogravimetric analysis (TGA). Increasing amounts of polymers were grafted when the targeted molar mass was increased. The diameter of the resulting particles determined by dynamic light scattering (DLS) increased consistently. The authors mentioned that the livingness of the process should be assessed by size exclusion chromatography (SEC) analyses performed on the cleaved chains. In addition, they pointed out that a significant fraction of the polymer chains became detached from the silica surface due to hydrolysis of the single Si–O bonds, by which the polymer was linked to the particle.

Instead of covalently grafting small ATRP initiator molecules onto silica through a Si–O link, an alternative can be to strongly adsorb a polyelectrolyte containing ATRP initiator moieties. This strategy takes advantage of the charged surface of the silica particles (either positive or negative depending on the pH). Armes and coworkers investigated the synthesis of cationic [55, 56] and anionic [57] polyelectrolytes obtained by modification either of a preformed statistical copolymer of hydroxyethyl methacrylate (HEMA) and dimethylaminoethyl methacrylate (DMAEMA) or of polyHEMA obtained by ATRP, respectively. Cationic charges were obtained by quaternization of the tertiary amine of DMAEMA units with iodomethane, and anionic groups were introduced by partial esterification of the hydroxyl side groups of polyHEMA with 2-sulfobenzoic acid cyclic anhydride. Bromoisobutyrate ATRP initiators were introduced by esterification of the remaining hydroxyl groups. The resulting polyelectrolytes were then adsorbed onto anionic Monospher 100 or Ludox TM-40 silica sols and cationic Ludox CL silica sol. A range of hydrophilic monomers (nonionic and zwitterionic monomers) were then

successfully polymerized in water or in water/organic cosolvent mixtures from these modified silica surfaces. The success of the grafting reactions was shown by TGA,  $^1\text{H}$  NMR, FTIR, XPS, aqueous electrophoresis, DLS, and TEM. The livingness of the process was, however, only indirectly shown by the increased amount of grafted polymer with the increase in targeted molar mass.

The synthesis of hybrid materials conducted via a polymerization in organic or aqueous solution from a monolayer of initiators attached to the inorganic particle surface is a very popular strategy. ATRP has been the most widely used technique in this area, but gelation often occurred as a result of interparticle coupling reactions. In order to suppress this gelation, “grafting from” reactions are stopped at low monomer conversion and are usually conducted under high dilution, which greatly increases polymerization times. Gelation can also be avoided by addition of sacrificial initiator in the dispersing phase that produces free unbound polymer chains, which, however, need to be separated from the hybrid material. Bombalski et al. [58] proposed to take advantage of the miniemulsion process to create boundaries and force polymerization to occur inside very small compartmentalized monomer droplets. Although the microscopic gelation can occur inside the droplet, the macroscopic gelation could be efficiently avoided. For that purpose, the authors used modified silica nanoparticles carrying an ATRP initiator and obtained by reaction of (chlorodimethylsilyl)propyl 2-bromoisobutyrate with silica surface Si–OH groups [59]. These particles were dispersed in a *n*-butyl acrylate (BA) phase in the presence of CuBr as Cu(I) source, bis(2-pyridylmethyl)octadecylamine (BPMODA) as ligand, and hexadecane as hydrophobe. A miniemulsion was formed after sonication of this mixture with an aqueous solution of Brij98 as surfactant. However, reproducibility problems were encountered and attributed to the difficulty in homogeneously dispersing the silica nanoparticles, CuBr, and BPMODA inside the monomer droplets and in keeping the copper complex stable under sonication conditions. AGET ATRP in which Cu(I) was replaced by Cu(II) was found to be the right alternative. Because Cu(II) survives the sonication step much better than Cu(I), the polymerization was started at 80°C by addition to the miniemulsion of an aqueous solution of sodium ascorbate that reduces Cu(II) to Cu(I). Miniemulsions remained stable throughout the course of the polymerization, and the final latex particle sizes were very close to the starting droplet size (220 nm). In addition, molar mass evolutions showed a high initiation efficiency since narrowly distributed molar mass values (polydispersity index,  $\text{PDI} < 1.5$ ) were close to the theoretical ones. TEM analysis showed that the macroscopic gelation effect was effectively suppressed because individualized core–shell silica particles could be visualized after dissolution of the particles in tetrahydrofuran and drying of the final latex.

### 3.2 Iron Oxide

Due to the number of potential applications, particularly in biorelated fields, very intensive investigations have been conducted to look for new strategies for

preparation of magnetic nanoparticles with tailor-made properties through attaching appropriate functional moieties. In biorelated fields, water-dispersible nanoparticles are commonly required [60]. In the case of magnetic iron oxide particles, two routes have successfully ensured good control over size and size distribution: (a) the use of emulsions as nanoreactors to nucleate nanoparticles [61], which, however, does lead to magnetite exhibiting poor crystallinity; and (b) the nucleation of nanoparticles in organic solvents at high temperature [62] in the presence for example of oleic acid, thus leading to particles dispersible in nonpolar and low-polarity medium.

Lattuada et al. [63] used iron oxide nanoparticles synthesized at high temperature and carrying surface oleic acid ligand (Fig. 3) as a starting point for generation of a range of functionalized nanoparticles after ligand exchange. An ATRP initiator, namely 2-bromo-2-methyl propionic acid, was introduced at the surface of the particles. As this initiator was found to be incapable of providing sufficient stabilization of the particles in any solvent, citric acid was concomitantly employed in 1:5 molar ratio to ensure good stability in aqueous media. The same type of initiator was also incorporated at the surface of nanoparticles containing surface hydroxyl groups, obtained after ligand exchange with OH-containing ligands (ricinoleic acid and galactaric acid in Fig. 3), by reaction with 2-bromo-2-methyl propionyl bromide. These ATRP-initiator-containing nanoparticles were then used to grow hydrophilic polymer chains such as polyAA, polyMAA, polyHEMA, and polyDMAEMA using organic solvents such as dimethylformamide, dimethylsulfoxide, or dichlorobenzene. Of interest for the present review, poly (sodium styrene sulfonate) (polyNaSS) and poly(*N*-isopropylacrylamide) (polyNIPAAm) chains were grown at room temperature in a mixture of water and methanol (3:1 v/v)

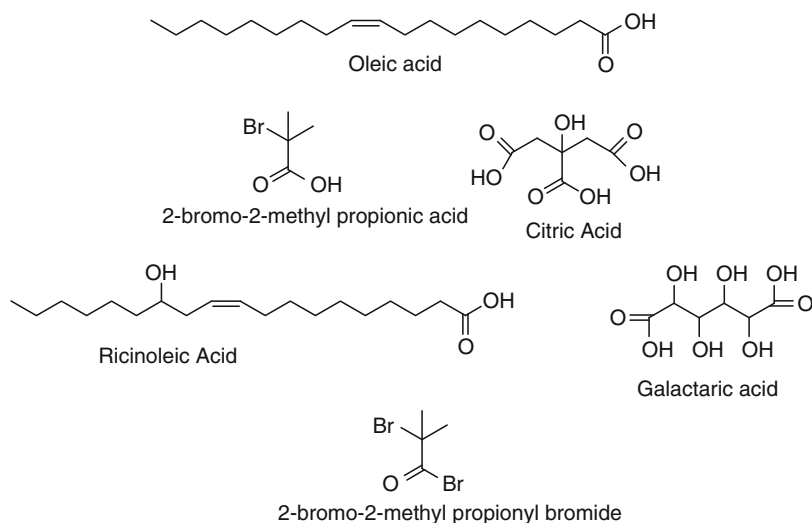


**Fig. 3** Different ligands used to coat iron oxide nanoparticles [63]

using CuBr as Cu(I) source and 1,1,4,7,10,10-hexamethyltriethylene tetramine (HMTETA) as copper ligand. However, no evaluation of the control of the polymerization was provided and although highly water-dispersible particles were obtained, stability issues assigned to the poor stabilization potential of the grafted polymeric layer were mentioned.

Using similarly synthesized oleic-acid-stabilized iron oxide nanoparticles, the same strategy was pursued by Hu et al. [64], who grafted an ATRP initiator onto the surface of the nanoparticles via a silane-based precursor, 4-[(chloromethyl)phenyl] trichlorosilane. The modified nanoparticles were characterized using FTIR, XPS, and TGA, which showed the success of the functionalization. A methacrylate macromonomer based on poly(ethylene glycol) (PEGMA) was then polymerized in water after a short sonication step. Polymerization was performed at 35°C using CuCl as a Cu(I) source and bipyridine as a ligand. Again, little information on the control of the polymerization was provided apart from the facts that characterizations such as FTIR and XPS showed that polyPEGMA chains were formed on the surface, and that the obtained nanoparticles were stable for several months in aqueous medium whereas pristine particles were dispersible in hexane only. The authors mentioned a linear increase with time of the weight loss calculated from TGA analyses of polyPEGMA-coated nanoparticles and claimed that the polyPEGMA grafted chains exhibited all the features of controlled chains. However, they also mentioned the formation of side homopolymer and a rapid increase in viscosity of the polymerization medium with time. This is consistent with a loss of control, probably arising from gelation due to interparticle coupling reactions, the elimination of which is one of the biggest challenges in this “grafting from” approach (see above) [65]. Finally, and as a bio-application, the authors showed that the uptake of magnetic nanoparticles by macrophage cells was greatly reduced after grafting of polyPEGMA chains using this strategy.

### 3.3 Other Metallic Oxides

Nguyen et al. [66] developed an original and generic method for the encapsulation of solid particulate material wherein living amphipathic copolymers are used to stabilize dispersions of inorganic pigments. These copolymers were obtained by the RAFT process and thus were carrying a thiocarbonylthio end-group (macroRAFT agents). This group can be reactivated for the polymerization of another monomer, e.g. a hydrophobic one. In aqueous medium, these copolymers can thus be grown on, to form an encapsulating hydrophobic shell. The authors used low molar mass ( $M_n$  less than  $2000\text{ g mol}^{-1}$ ) poly(AA-co-BA) obtained from RAFT copolymerization of BA and AA in dioxane solution. Because one key requirement for an efficient encapsulation of the pigments is that these copolymers do not form micelles when dispersed in the reaction medium, a random distribution of hydrophilic and hydrophobic units was necessary. As a result, a copolymer containing an average of

10 AA units and 5 BA units [poly(AA<sub>10-co</sub>-BA<sub>5</sub>)] was used under neutral to basic pH (5.5–8) conditions to disperse titanium oxide. After a sonication step, well-dispersed particles were obtained even when the zero charge point was reached (pH 8), suggesting a good level of adsorption of the macroRAFT agents even at this pH. By additionally testing poly(AA<sub>10-co</sub>-BA<sub>7.5</sub>) and poly(AA<sub>10-co</sub>-BA<sub>2.5</sub>), the authors also showed that the higher the hydrophobicity of the macroRAFT agent, the better its adsorption onto titanium oxide particles. Although these copolymers were more liable to form micelles in water, the authors assigned this result to the corresponding increasing surface activity of the copolymers. Encapsulation was performed at 70°C by slowly feeding the dispersed system with a mixture of hydrophobic monomers MMA and BA, using *N,N'*-azobiscyanopentanoic acid (ACPA) as a water-soluble initiator. The living ends of the macroRAFT agents further grew by adding hydrophobic monomer units and pulling the hydrophilic part of the newly formed block copolymers towards the water phase. As long as pH was maintained lower than 8, a very nice encapsulation of titanium oxide was obtained (size around 365 nm), as shown in Fig. 4. The authors observed the absence, as targeted, of non-encapsulated particles as well as the presence of a very low number of new polymer particles. This last result is directly related to the presence or not of macroRAFT agents in the water phase. The authors showed that although present in the water phase at the end of the encapsulation process (~75%) and still living, the macroRAFT agents can only add hydrophobic monomers when adsorbed onto the surface of the pigment (~19%). They remained trapped there for the rest of the process.

SEC analyses were performed on polymer formed during the encapsulation process, after treatment of the core–shell particles with a tetrahydrofuran/trifluoroacetic acid mixture to remove the inorganic part. Control of the polymerization was shown

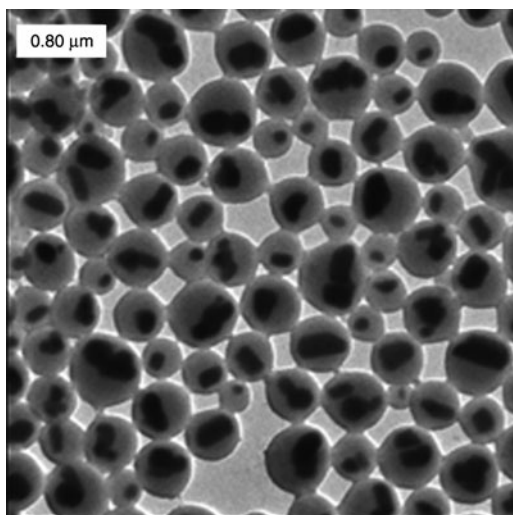


**Fig. 4** Encapsulated TiO<sub>2</sub> pigment particles with poly(BA-*co*-MMA) shell using poly(AA<sub>10-co</sub>-BA<sub>5</sub>) macroRAFT agent as dispersant. From [66], with permission from the American Chemical Society

by the linear increase in molar masses with the quantity of monomer mixture fed, while the PDI remained relatively low ( $<1.7$ ).

In a very similar approach, Daigle et al. [67] reported a general method for synthesis of hybrid core-shell nanoparticles. Instead of a copolymer incorporating hydrophobic and hydrophilic units, the authors used polyAA macroRAFT agents obtained by RAFT polymerization of AA performed in ethanol and using a trithiocarbonate as a control agent (according to previously published results [68]). The polyAA macroRAFT agent was used to stabilize and disperse in water a range of inorganic compounds such as oxides [ $\text{BaTiO}_3$ ,  $\text{TiO}_2$  (rutile and anatase),  $\text{Al}_2\text{O}_3$ ,  $\text{CuO}$ ,  $\text{ZrO}_2$ ], metals (Zn, Mo) and nitrides ( $\text{Si}_3\text{N}_4$ ). The polymerization of a hydrophobic monomer (styrene and/or BA) was then performed at  $80^\circ\text{C}$  using ACPA as a water-soluble initiator. However, in contrast to Nguyen's work [66], the monomer was introduced at the beginning of the process while a solution of initiator was fed over 4 hours. According to TEM analyses (Fig. 5), the inorganic materials were effectively encapsulated by a layer of hydrophobic polymer without formation of aggregates or partially encapsulated compounds. However, the presence of homopolymer particles was sometimes observed (Fig. 5b,  $\text{TiO}_2$ ). This phenomenon originated from polyAA macroRAFT agents adding hydrophobic monomer units and becoming amphiphilic enough to behave as surfactants, which were then able to nucleate a crop of polymer particles. Control of the polymerization was not really achieved, as attested by the high molar mass and the large PDI (2.2) obtained after SEC analyses of the soluble fraction of polymer in tetrahydrofuran. The authors, however, did not aim at controlling the polymerization but took advantage of the RAFT technique to reinitiate a dormant polyAA chain carrying a highly reactive trithiocarbonate end-group.

Compared to Nguyen's work [66], this strategy required the use of additional surfactant (SDS) in order to minimize secondary nucleation induced by both the presence of polyAA in the water phase – particularly emphasized in the case of inorganic compounds for which polyAA adsorption is weak – and the absence of monomer feed. However, the strategy appears simpler and more convenient for the preparation of a wide range of inorganic/organic hybrid nanoparticles.

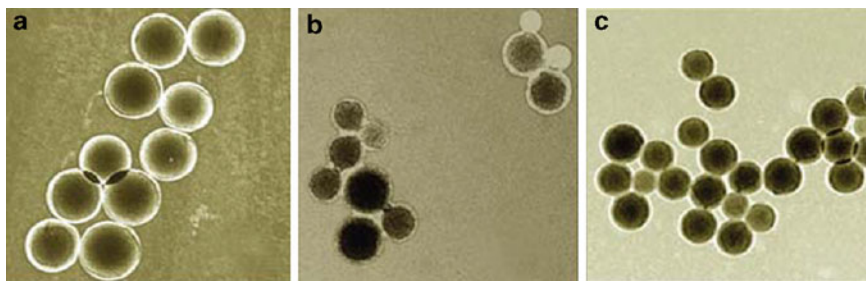


**Fig. 5** (a)  $\text{BaTiO}_3$ , (b)  $\text{TiO}_2$ , and (c)  $\text{Al}_2\text{O}_3$  encapsulated with a polystyrene shell using polyAA macroRAFT agent as dispersant. From [67], with permission from Hindawi Publishing Corporation

### 3.4 Clays

Investigating the use of functional surfactants for the modification of clay and the properties of the resultant polymer/clay nanocomposite, Hartmann's team [69, 70] used surface-active RAFT agents. The appropriate functionalization of these RAFT agents made their attachment to clay platelets possible. As a result, a controlled growth of polymer chains from the surface of the clay platelets was achievable. They extrapolated to miniemulsion for the first time [71] their studies on styrene polymerization performed in bulk [72] in the presence of Montmorillonite clay modified with PCDBAB and DCTBAB (Fig. 6).

Stable miniemulsions of styrene were obtained with hexadecane as a hydrophobe and SDS as a surfactant. Polymerizations were performed at 75°C using *N,N'*-azobisisobutyronitrile (AIBN) as an initiator and resulted in high conversion (>80%) in relatively short times (<3 h) compared to the bulk polymerization, as a result of the compartmentalization phenomenon. Consistent with a controlled process, an increase in clay loading (i.e., RAFT agents) resulted in a decrease in molar mass while keeping relatively low PDIs (around 1.6 and 1.4 for Montmorillonite-DCTBAB and Montmorillonite-PCDBAB, respectively). As observed for bulk polymerization [73] and as a result of the relatively high heterogeneity of the system, the PDI seemed to decrease as the clay loading was increased, with a threshold clay concentration of 2 wt%. Particle sizes were examined by DLS and TEM analyses and exhibited a fairly narrow distribution with a slight secondary particle nucleation. This was expected considering that the RAFT agents were electrostatically bound to the clay via their leaving/initiating group, which could not easily escape to the water phase. In addition, the physical barrier formed by the clay platelets made it difficult for growing radicals to escape to the water phase. Surprisingly, clay platelets were not visible by TEM in the raw final latex without drying the latex and embedding it into epoxy resin. The resulting nanocomposites were of partially exfoliated morphology as the clay loading increased, due to the decrease in molar mass of the bound polystyrene or poly(styrene-*co*-BA) [74] chains, as attested by thermo-mechanical studies.

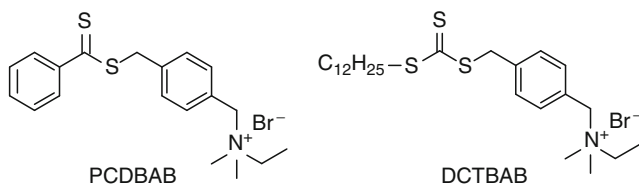


**Fig. 6** Structure of the surface-active RAFT agents *N,N*-dimethyl-*N*-(4-((phenyl carbonothiol)thio) methyl)benzyl)-ethyl ammonium bromide (PCDBAB) and *N,N*-dimethyl-*N*-(4-(((dodecylthio)carbonothioyl)thio)methyl)benzyl)-ethyl ammonium bromide (DCTBAB)



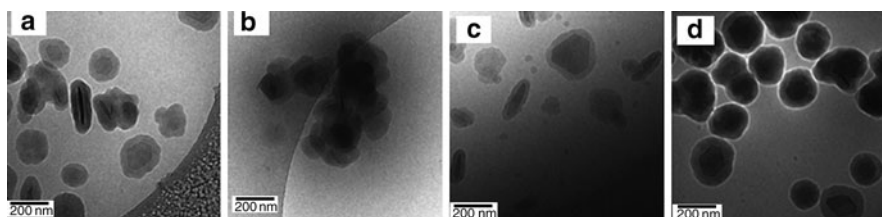


**Fig. 7** Encapsulated gibbsite with poly(MMA-*co*-BA) shell using (a) poly(AA<sub>10</sub>-*co*-BA<sub>5</sub>), (b) poly(AA<sub>10</sub>-*co*-BA<sub>2.5</sub>), (c) poly(AA<sub>10</sub>-*co*-BA<sub>7.5</sub>), and (d) poly(AA<sub>5</sub>-*co*-BA<sub>5</sub>) macroRAFT agents as dispersants. From [75], with permission from the American Chemical Society

Very recently, Ali et al. [75] extended Nguyen's strategy [66] to the encapsulation of gibbsite as model substrate for platelet-like colloidal substrates. Cationically charged gibbsite platelets were coated with random copolymers of AA and BA obtained by RAFT polymerization mediated by dibenzyltrithiocarbonate. These copolymers were previously treated with NaOH and added to gibbsite until charge inversion was observed by zeta-potential measurements. The gibbsite platelets, now stabilized by anionically charged poly(AA-*co*-BA) macroRAFT agents in water, were encapsulated using a feed of MMA and BA (10:1 w/w). This allowed chain extension of the macroRAFT agents and formation of a polymer shell around the platelets (Fig. 7). The influence of the hydrophobicity and of the chain length of the copolymers was studied by varying the BA/AA molar content and their molar masses, respectively. The corresponding data showed that these parameters had to be finely tuned in order to achieve efficient anchorage of the copolymers onto gibbsite through charge interactions, and also to favor the presence of free copolymers in water. Indeed, some of these RAFT copolymers in the aqueous phase became adsorbed on the growing surface and could further participate in the encapsulation process. As mentioned in the earlier works of Nguyen et al. [66], the random nature of the copolymers prevents them from self-assembling in the aqueous phase at the beginning of the polymerization. This reduces the possible early formation of a crop of gibbsite-free polymer particles. However, the authors noticed that during the polymerization, RAFT copolymers in the aqueous phase can still chain-extend, become amphiphilic, and potentially create a crop of new particles that will end up in the majority on the nanocomposite. It is worth mentioning the tremendous impact of the monomer feed composition, since the use of a MMA to BA ratio of 7:3 (w/w) led to a loss of control over the platelet orientation and additional armored morphologies were consequently obtained.

## 4 (Nano)structured Particles

As detailed in Sect. 2.2, the development of CRP in aqueous dispersed systems allowed new copolymer architectures to be synthesized in latex particles via miniemulsion or emulsion polymerization processes. Block copolymers and their

synthesis in such systems was quite a new development, as CRP is the main way to achieve such a goal via aqueous phase polymerization. In this review article, only the copolymers leading to phase separation and nanostructuration are considered. Two main types of morphology can be contemplated: the simple core–shell morphology and the multilayered or “onion-like” morphology.

One of the first reports on the synthesis of core–shell particles via the design of diblock copolymers in emulsion polymerization dealt with polystyrene-*b*-poly(*n*-butyl acrylate-*co*-acetoacetoxyethyl methacrylate) [76]. The first step consisted of the batch, *ab initio*, emulsion polymerization of styrene in the presence of 1-(*O*-ethylxanthyl) ethylbenzene, a RAFT agent of the dithiocarbonate (xanthate) family with a low transfer constant. The method led to latex particles with diameter of 30 nm. The polystyrene chain length was poorly controlled due to the low activity of the xanthate, but chains were still living because they exhibited the xanthate group at their end and could thus be further extended in a second step. This was actually performed via seeded-emulsion polymerization of a mixture of BA and acetoacetoxyethyl methacrylate, either in batch or under starved-feed conditions. The method allowed a diblock copolymer to be formed *in situ*, with 64.5% reinitiating efficiency in batch and 76.4% in the semi-continuous process. The final particle morphology was visualized by cryo-TEM and appeared to be of the core–shell type, with polystyrene in the core. In a second study, the authors started the polymerization from a non-controlled poly(MMA) seed latex in order to perfectly control the particle size and particle size distribution [77]. Then, the first polystyrene block was synthesized in the presence of *O*-ethylxanthyl ethyl propionate as a reversible chain transfer agent in batch conditions to target an end-functionalized, low molar mass polystyrene. The latter was further chain-extended via the slow addition of BA to form a diblock copolymer with high (>90%) crossover efficiency. In both works, a major difficulty was to prevent secondary particle nucleation, as the latter would lead to the formation of homopolymer without any control over the chain growth.

In a different approach, Herrera et al. [78] studied the effect of the presence of different amounts of a polystyrene-*b*-polyMMA block copolymer on the morphology of polystyrene/polyMMA composite latex particles prepared via miniemulsion polymerization. The block copolymers were produced *in situ* in the presence of SG1 as a nitroxide mediator. The simple end-capping of variable fractions of the polystyrene chains prepared in the first step, allowed chain extension to proceed upon the addition of MMA in the second step. No control of the polymerization was really targeted, but only the creation of a small fraction of block copolymers. A change of morphology was clearly observed upon variation of the amount of compatibilizing block copolymer in the particles. Indeed, as the amount of the block copolymer increased, the particle morphology changed from a hemisphere system (without any block copolymer) to core–shell morphology because of a decrease in the polymer–polymer interfacial tension.

When block copolymers with immiscible blocks are synthesized directly via (mini)emulsion polymerization, the particles might exhibit internal phase separation during the polymerization, without the need for a cosolvent to induce

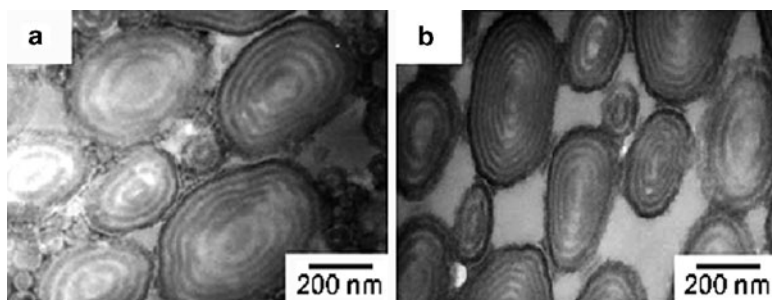


**Fig. 8** (a, b) TEM images of ultrathin cross-sections of latex particles with multilayered “onion-like” morphology composed of poly(*iso*-butyl methacrylate)-*b*-polystyrene diblock copolymer prepared via miniemulsion ATRP. From [79], with permission from Elsevier

the phenomenon. Such a situation was first shown by Okubo’s group [79] when they used ATRP in miniemulsion to produce a poly(*iso*-butyl methacrylate)-*b*-polystyrene diblock copolymer with a 1:1 weight ratio of the two blocks. Due to the thermodynamically stable lamellar structure, the particles exhibited a multilayered, onion-like morphology as shown in Fig. 8. The polymerization was performed in two steps, first the miniemulsion ATRP of *iso*-butyl methacrylate till high conversion (>93%), and then the seeded emulsion polymerization of styrene. The  $M_n$  of the diblock copolymers was close to  $50\text{ kg mol}^{-1}$ , with both blocks exhibiting  $M_n \sim 25\text{ kg mol}^{-1}$ . The final particle diameter was close to 300 nm and the layer thickness was  $\sim 19\text{ nm}$ .

The same phase separation process was also observed for polystyrene and polyBA diblock or triblock copolymers prepared via NMP in miniemulsion or in emulsion [80]. The synthesis started with the polyBA block using either a monofunctional or a difunctional water-soluble alkoxyamine initiator based on the nitroxide SG1. The second step was the introduction of styrene to create the diblock copolymer or the polystyrene-*b*-polyBA-*b*-polystyrene triblock copolymer, respectively. Because the polymerization of BA was stopped at incomplete conversion to avoid side reactions and to maintain a high degree of livingness of the so-formed polymer, the polystyrene segments were not pure and contained BA subunits. The study then focused on the effect of the composition of this polymer block on the phase separation behavior. The onion-like nanostructure within the particles was shown by TEM of films dried at room temperature (observations were performed on ultrathin sections cryo-microtomed at  $-70^\circ\text{C}$ ), as displayed in Fig. 9 for a diblock copolymer exhibiting  $M_n = 61\text{ kg mol}^{-1}$  with the following molar composition: polyBA<sub>232</sub>-*b*-poly(BA<sub>25</sub>-*co*-styrene<sub>267</sub>). The shape of the particles was clearly maintained, as shown in Fig. 9a, with an average diameter of 310 nm and a broad particle size distribution. After casting the film in a good solvent and drying at  $150^\circ\text{C}$ , well above the  $T_g$  of both blocks, a more classical lamellar phase separation was observed (Fig. 9b). Similar results were also obtained with polyMMA-*b*-polyBA-*b*-polyMMA triblock copolymers, even though the polymerization step leading to the external blocks was not controlled [80].

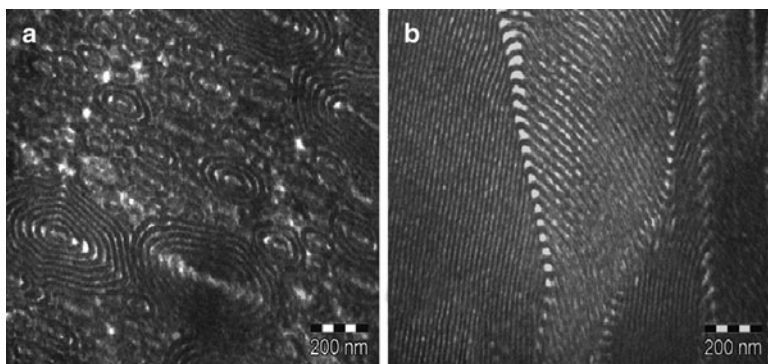


**Fig. 9** TEM images of the polymer films formed from the polyBA<sub>232</sub>-*b*-poly(BA<sub>25</sub>-*co*-styrene<sub>267</sub>) diblock copolymer latex particles (a) after drying at room temperature for 4 days, and (b) after solvent-casting in dichloromethane and drying at 15°C for 48 h

By combining CRP with another polymerization technique such as ring-opening metathesis polymerization (ROMP), Airaud et al. [81, 82] demonstrated that particles with unique morphology could be synthesized in a single polymerization step in miniemulsion or microemulsion. They performed simultaneous ATRP of MMA and ROMP of norbornene, with a single water-soluble ruthenium macrocatalyst to both initiate ROMP and mediate ATRP. The method led to the formation of two incompatible homopolymers that segregated within the particles into hemispheres, hence leading to “Janus-type” particles [83].

## 5 (Nano)capsules

Capsules are hollow spheres consisting of a thin (co)polymer membrane. Their advantage over other nanoparticles is that they can be used as nanocarriers, mainly for encapsulated hydrophobic molecules. The term “vesicle” is often used and corresponds to a particular class of capsules with a bilayered membrane that is composed of amphiphilic molecules or block copolymers [84]. Vesicles allow encapsulation of either hydrophilic molecules in their inner cavity or hydrophobic ones in their membrane. Considering the scope of this review article, CRP in aqueous dispersed systems usually leads to classical capsules, except in one case, which will be described in Sect. 6.2. However, only a few reports are actually devoted to this topic. Two main strategies can be distinguished. The first is the use of a solid template such as silica or metal particles on which surface-initiated polymerization is performed (see Sects. 3 and 7.1). The second strategy relies on a heterogeneous polymerization process (emulsion, miniemulsion, or even suspension) in the presence of an organic liquid (oil).

## 5.1 Solid-Templated Synthesis

In 2005, Duan et al. [85] used gold nanocrystals modified with ATRP initiators to create a shell of terpolymer comprising DMAEMA, diethylaminoethyl methacrylate (DEAEMA) and PEGMA subunits. They further crosslinked the DMAEMA units with 1,2-bis(2-iodoethoxy)ethane. The Au core was subsequently etched with an aqueous solution of potassium cyanide to produce hollow polymeric particles. Thanks to the DEAEMA and non-crosslinked DMAEMA units, the capsules were pH-sensitive. Depending on the proportion of crosslinked DMAEMA units (30 or 100%), the diameter of the capsules varied between 320 and 220 nm or 240 and 150 nm, respectively, when the pH was raised from 2 to 12. This behavior was exploited to encapsulate and release rhodamine dye using pH as a trigger. As a final feature, instead of integrally etching the gold template, only the Au–S bond linking the polymer to the metal particle was cleaved by a mild treatment to produce capsules with free Au cores, thought to behave as sensors.

Silica nanoparticles have also been employed as templates to produce nanocapsules, though the process used was slightly different from that used for Au nanocrystals. A Pickering aqueous emulsion of paraffin oil, stabilized by silica particles previously functionalized with ATRP initiators, was first formed [86]. Then the polymerization of HEMA was initiated using a CuCl/bipyridine catalytic system. Because HEMA is water-soluble and insoluble in paraffin, its polymerization could only occur in the water phase, leading to a sort of Janus silica particle. Because HEMA has a tendency to produce lightly crosslinked polymers when polymerized in water, a gel shell was formed around the stabilizing silica shell in place of true Janus particles. The authors did not try to remove the silica particles from the obtained hybrid capsules but showed that the shell of the so-called colloidosomes was semipermeable, depending on the nature of the solvent. In tetrahydrofuran or ethanol, in which polyHEMA is soluble, the shell swelled and diffusion of a small fluorescent molecule through it could be achieved. In hexane, in which polyHEMA is insoluble, no diffusion was observed.

Finally, another type of solid-templating technique was reported by Ting et al. [87] (Fig. 10). First, they synthesized an amphiphilic block copolymer of polylactide and poly(6-*O*-acryloyl- $\alpha$ -D-galactopyranose) by RAFT from a polylactide macro-RAFT agent and then assembled it in water. The nature of the RAFT agent was such (polylactide in the Z group) that the polymerization of another monomer in presence of the block copolymer would lead to insertion of the monomer units between the two blocks. The authors took advantage of this to insert monomer units between the polylactide core and the polysaccharide shell. The polymerization of hexanediol diacrylate was conducted, leading to the formation of a crosslinked polymeric layer around the polylactide core. The polylactide core was subsequently removed by aminolysis with hexylamine, giving rise to sugar-coated capsules. The further availability of thiol groups inside the capsules, usually arising from aminolysis of RAFT polymers, has not yet been demonstrated.

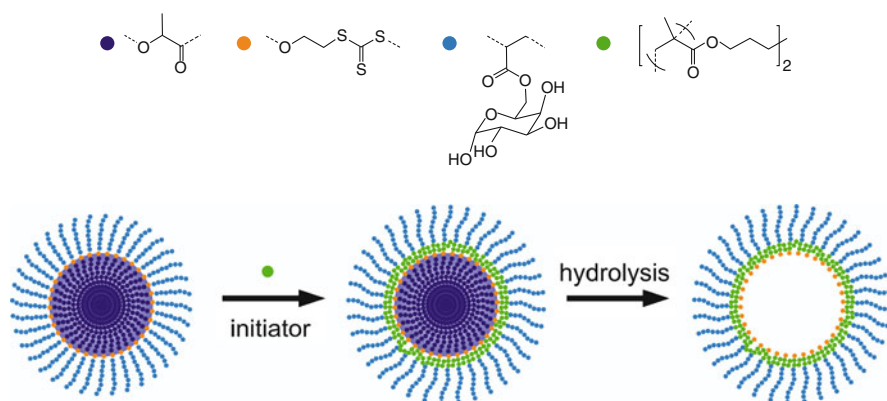


**Fig. 10** Synthesis of sugar hollow cages by RAFT intrashell crosslinking and subsequent core hydrolysis of poly(lactide-*b*-poly(6-*O*-acryloyl- $\alpha$ -D-galactopyranose) amphiphilic block copolymers [87]

## 5.2 Oil-Templated Synthesis

This technique is completely different from the previous method because it involves an oil-in-water emulsion. The system is typically based on the polymerization of a monomer that is (partially) soluble in the oil, giving a polymer that will migrate at the oil–water interface to result in an oil core surrounded by a polymeric shell. This technique has the particularity of generating capsules with their interiors already filled.

The first example of CRP applied to this technique concerns ATRP of MeO-PEGMA (PEGMA with a methoxy end-group) and MMA in diphenyl ether [88]. The method consists of three stages. First, the synthesis of poly(MMA-*co*-MeO-PEGMA) was initiated in the oil solution by toluenesulfonyl chloride in the presence of CuBr/4,4'-dinonyl-2,2'-dipyridyl. At 57% conversion, a crosslinker was injected and this oil phase was then transferred to an aqueous solution of poly(vinyl alcohol), where the polymerization proceeded in the formed droplets, hence producing particles with diameters of several microns. Because the nature of the polymer determines the interaction with the oil, the authors showed that the percentage of MeO-PEGMA in the copolymer had a strong influence on the morphology of the particles obtained. Indeed, when the ratio of MeO-PEGMA to MMA was low, the polymer was quite soluble in diphenyl ether and gave an inner matrix morphology. On increasing the MeO-PEGMA content, a few hollow particles among the matrix particles were formed, as well as macroporous particles. When the MeO-PEGMA content reached 31 mol%, microcapsules were obtained because the greater polarity of the crosslinked copolymer allowed its migration to the interface. This example perfectly illustrates the kinetic advantage of CRP because a slow propagation allows



the migration to occur – especially within micrometer-sized particles – whereas analogous conventional radical polymerization experiments only gave rise to matrix particles. Later, the same authors used hydroxy-terminated PEGMA and showed that the content of HO-PEGMA in the copolymer needed to achieve capsule formation could be decreased to 17 mol% thanks to the intrinsic higher polarity of the comonomer [89]. For a HO-PEGMA content of 24 mol%, two-layer capsules were obtained. The authors attributed this phenomenon to the possible polymerization at the interface due to the high hydrophilic nature of HO-PEGMA.

NMP was also recently used to produce crosslinked capsules of submicrometer size [90]. Miniemulsion copolymerization of styrene and divinylbenzene in the presence of a high proportion of hydrophobe was mediated by TEMPO at 125°C. When a toluene/tetradecane oil mixture was used, conventional nanogels were obtained because the crosslinked polymer was soluble. Even with a high content of tetradecane (50 vol%), no hollow particles formed. By contrast, with substitution of tetradecane by hexadecane (50 vol%), nanocapsules were achieved because of the higher incompatibility of this latter oil with the polymer. The authors also suggested that the nature of the surfactant could play a role in the formation of hollow structures because it influences the interfacial tension of the particles. For example, poly(vinyl acetate) (polyVAc) being only a steric stabilizer would favor the presence of the polymer at the interface, whereas an electrostatic stabilizer would minimize the driving force for migration. The miniemulsion process was also thought to be more prone to hollow particle formation because the distance of migration is reduced compared to processes involving bigger particles.

The third main CRP technique, the RAFT process, was also employed to obtain nanocapsules. Van Zyl et al. [91] used *iso*-octane as template for styrene miniemulsion polymerization in presence of a RAFT agent and a radical initiator. They showed that the formation of capsules was strongly dependent on the nature of these two species. When the polymerization was initiated in the organic phase by AIBN, only solid particles were obtained due to the absence of driving force for the migration of polymer to the interface of the particles. When potassium persulfate was used as a water-soluble radical initiator in conjunction with a dithioacetate RAFT agent, nanocapsules were observed in contrast to the same experiment with a dithiobenzoate. The different results arose from the different reactivities of the RAFT agents. Initially, the radicals are created in the water phase and, after addition of few monomer units, they diffuse to the monomer droplets to nucleate them. When a RAFT agent that gives no rate retardation (like dithioacetate) was employed, nanocapsules could be obtained because long polymer chains were rapidly formed and the viscosity at the interface increased quickly, hence locking the polymer chains in place. Even the non-charged species coming from transfer reactions did not seem to be able to diffuse inside the particles. Due to rate retardation, dithiobenzoate only led to short chains at the beginning of the polymerization, which were able to diffuse inside the particles.

Later, Luo et al. [92] reported a more versatile version of this technique, which was later highlighted by Klumperman [93]. With the help of an oligomeric surface-active RAFT agent [ammonolyzed poly(Manh-*co*-styrene)], not only the primary



radical species could be confined at the interface but also the chains initiated by the leaving/initiating group of the oligoRAFT agent. The process did not depend on the type of monomer and, thus, one can imagine that many different types of capsules could be produced by taking advantage of the versatility of the RAFT process. However, the first reported example was not perfect because a non-negligible amount of solid polystyrene particles was present. Investigations on the structure and hydrophilicity of the oligoRAFT agents were thus performed by employing different degrees of ammonolysis/hydrolysis of the Manh units and different compositions or structures. When a too-hydrophobic transfer agent (poor surface activity) was used, only solid particles were obtained. When the RAFT agent was too hydrophilic, its surface activity was also low and a high proportion of the agent was presumably dissolved in water, giving rise to homogenous nucleation. A majority of solid particles was also produced. Keeping a high degree of amphiphilicity combined to high molar mass of the macroRAFT agent could improve the encapsulation efficiency and thus decrease the proportion of solid particles. Finally, using a conventional surfactant such as SDS helped to obtain a very high fraction of capsules (98 wt%) because the degree of ammonolysis of the RAFT agent could be reduced while keeping a small initial droplet diameter. The last possible improvement was the precise control of the capsule structure (size, shell thickness, and symmetry). The authors addressed this issue by using an oligomeric polyAA<sub>2</sub>-*b*-polystyrene<sub>1-3</sub> RAFT agent together with SDS, and succeeded in getting capsules of about 110 nm in diameter with a shell thickness of 20 nm [94] and narrow size distributions (Fig. 11). The solid particles produced in parallel could be easily removed by centrifugation.

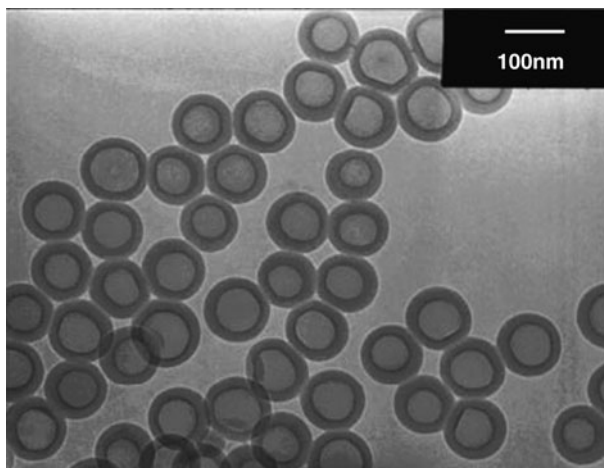


**Fig. 11** TEM image of the capsules obtained by RAFT miniemulsion of styrene in the presence of 20 wt% hexadecane (with respect to monomer), SDS, and a polyAA<sub>2</sub>-*b*-polystyrene<sub>1-3</sub> macroRAFT agent. From [94], with permission from Wiley InterScience

## 6 Core–Shell Particles with Hydrophilic Shell and Hydrophobic Core via a Convergent Method

Due to their size, macromolecular stabilizers (providing steric or electrosteric stabilization) show many advantages in emulsion and miniemulsion polymerizations over those of low molar mass, such as improving stability under freezing conditions or under high shear, or preventing diffusion issues during film formation. Macromolecular stabilizers that are strongly adsorbed onto the surface of the particles [95–98] or even anchored via a covalent bond are less inclined to desorb or migrate compared to conventional low molar mass surfactants like SDS. In some sense, the resulting latexes can be described as core–shell particles with a hydrophilic shell and hydrophobic core. In the context of this review article, we will not focus on the use of amphiphilic block copolymers as stabilizers but will examine in detail the situation where a covalent bond is created between the stabilizer (i.e., the hydrophilic shell) and the hydrophobic particle core.

To be covalently linked to the particles, the stabilizer must carry a group able to participate in one of the key steps of the free radical polymerization process (initiation, propagation, termination, or transfer reactions). According to the reaction in which they are involved, the reactive surfactants are referred to as *inisurf* (initiation), *surfmer* (propagation) or *transurf* (transfer). In these particular cases, the surfactant not only plays a key role in the formation of the particles and the functionalization of their surface, but also becomes an actor in the synthesis of the polymer chains that will form the particles.

With CRP techniques, one may envision new ways of incorporating the reactive surfactant, using either an attached reversible chain transfer group or a living initiator group. Considering macromolecular species, the technique is based on the use of a living, amphiphilic or water-soluble polymer, end-capped with an activatable functional group that is typical for the CRP method chosen for its synthesis or that is introduced via post-modification. During the aqueous polymerization of hydrophobic monomer, chain extension will proceed and lead to the formation of amphiphilic block copolymers, which will eventually self-assemble into particles. The following section describes this new technique according to the selected CRP method, and discusses the structure of the so-formed polymers and the morphology of the resulting particles.

### 6.1 *Reversible Transfer Methods*

Irreversible transfer reactions have been used in the past to generate block copolymers from hydrophilic or amphiphilic thiol molecules such as sodium 10-mercapto-1-decanesulfonate [99], or functionalized PEO [100] or poly(VAc-*co*-vinyl alcohol) [101]. In fact, the very efficient transferring nature of the thiol function leads to a high reactivity of the *transurf* in the dispersing phase. Although the *in situ* formation

of amphiphilic block copolymers (able to act as the proper surfactant and to stabilize the formed particles) takes place, the hydrophobic segment is not long enough to provide the block copolymers with sufficient surface activity. This leads to a poor anchorage of the surfactant at the surface of the particles.

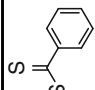
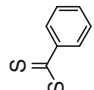
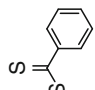
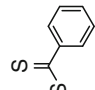
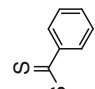
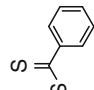
In the new approach, the use of reversible chain-transfer agent groups located at one end of a hydrophilic or amphiphilic macromolecule provides an interesting alternative for production of core–shell particles with a hydrophilic shell and hydrophobic core. One of the advantages (besides the classical ones for CRP) resides in the fact that chains grow continuously throughout the polymerization, hence overcoming the former drawback of the macromolecular chain-transfer agents with a thiol end-group. This strategy has very recently emerged and benefits from the unprecedented advances in CRP techniques; those based on degenerative transfer being the focus of this section. These techniques include the RAFT process, which relies on the use of thiocarbonylthio compounds of structure  $Z-C(=S)-SR$ , as well as TeRP and RITP. As a general overview, all the systems that will be described below are summarized in Table 1.

### 6.1.1 Reversible Addition–Fragmentation Chain Transfer Polymerization

#### From “Simple” Particles with Hydrophobic Core and Hydrophilic Shell

Tichagwa et al. [102] very briefly investigated the use of oligomers of 12-acryloyloxydodecanoic acid (ADA) and 11-acrylamidoundecanoic acid (AAUA) obtained by the RAFT process as possible stabilizers in batch emulsion polymerization of styrene. Polystyrene latexes were successfully obtained, although particle sizes were large. The RAFT moiety was expected to facilitate the control over molar mass and polydispersity, but the corresponding study was not provided in the paper. The first evidence that macroRAFT could effectively participate in the nucleation of particles through the RAFT chain-end in a batch emulsion polymerization was given by Manguian et al. [103]. They synthesized polyDEAEMA oligomers by RAFT polymerization performed in ethanol and mediated by 4-(cyanopentanoic acid)-4-dithiobenzoate (CPADB) as a RAFT agent. The resulting well-defined oligomers ( $M_n = 5200 \text{ g mol}^{-1}$ ,  $PDI = 1.31$ ) were then protonated with HCl and used as hydrophilic macroRAFT agents in emulsion polymerization of styrene. Stable and cationically charged polystyrene latexes (particle diameter of 112 nm) were obtained with a complete conversion in less than 3 h. The involvement of the dithiobenzoate chain-end in the nucleation of the particles was additionally shown by experiments performed with a well-defined polyDEAEMA obtained by ATRP. This polymer, carrying a bromine end-group (with low and non-reversible transfer reactivity), was used instead of the polyDEAEMA macroRAFT. Much longer polymerization times were required (6 h, 54% conversion) and much larger particles (diameter of 405 nm) were obtained. As no large particles were obtained that would have been generated by homogeneous nucleation, as expected in a surfactant-free emulsion polymerization, the possible nucleation mechanism proposed by the

**Table 1** Hydrophilic macromolecules carrying a reversible chain transfer agent end-group used in aqueous dispersed media for the synthesis of particles with hydrophilic shell and hydrophobic core

Hydrophilic chain transfer macroagents	Hydrophobic monomer	Polymerization process	Control of the polymerization	References
$\text{poly(ADA-co-AAUA)}-\text{S}-\text{C}(=\text{S})\text{Ph}$ 	Styrene	Batch emulsion	No	[102]
$\text{polyDEAEEMA}-\text{S}-\text{C}(=\text{S})\text{Ph}$ 	Styrene	Batch emulsion	No	[103]
$\text{PEO}-\text{S}-\text{C}(=\text{S})\text{Ph}$ 	Styrene	Batch emulsion	No	[104, 114]
$\text{PEO}-\text{S}-\text{C}(=\text{S})\text{Ph}$ 	Styrene	Miniemulsion	Yes	[118]
$\text{polyDMAEMA}-\text{S}-\text{C}(=\text{S})\text{Ph}$ 	Styrene	Miniemulsion	No	[108]
$\text{polyDMAEMA}-\text{S}-\text{C}(=\text{S})\text{Ph}$ 	Styrene	Batch emulsion	No	[104]

$\text{PEO-}b\text{-polyDMAEMA-S-C(=S)-C}_6\text{H}_5$	Styrene	Batch emulsion	No	[104]
$\text{Dextran-S-C(=S)-OCH}_2\text{CH}_3$	VAc	Batch emulsion	No	[105]
$\text{polyNAM-S-C(=S)-C}_6\text{H}_5$	BA	Dispersion	No	[107]
$\text{poly(AA-co-ABu)-S-C(=S)-C}_4\text{H}_9$	BA	Starved-feed emulsion	Yes	[109–111]
$\text{poly(AA-co-ABu)-S-C(=S)-C}_{12}\text{H}_{25}$	Styrene, BA	Starved-feed emulsion	Yes	
$\text{polyAA-}b\text{-polyS-S-C(=S)-C}_4\text{H}_9$	Styrene	Starved-feed emulsion	Yes	[112]
$\text{poly4VP-S-C(=S)-C}_{12}\text{H}_{25}$	Styrene/acrylonitrile	Starved-feed emulsion	Yes	[113]
$\text{PEO-S-C(=S)-C}_{12}\text{H}_{25}$	Styrene, BA, BA/MMA	Batch emulsion	Yes	[114, 115]

(continued)

Table 1 (continued)

Hydrophilic chain transfer macroagents	Hydrophobic monomer	Polymerization process	Control of the polymerization	References
$\text{polyAAm} - \text{S} - \overset{\text{S}}{\underset{\text{  }}{\text{C}}} - \text{S} - \text{C}_2\text{H}_5$	Styrene	Batch emulsion (sonication step)	Yes	[116]
$\text{polyMAA} - \text{S} - \overset{\text{S}}{\underset{\text{  }}{\text{C}}} - \text{C}_6\text{H}_5$	Styrene	Batch emulsion	–	[116]
$\text{polyDMAAm} - \text{S} - \overset{\text{S}}{\underset{\text{  }}{\text{C}}} - \text{S} - \text{C}_{12}\text{H}_{25}$	NIPAAm	Precipitation	Yes	[120, 121]
$\text{polyDMAAm} - \text{S} - \overset{\text{S}}{\underset{\text{  }}{\text{C}}} - \text{S} - \text{C}_4\text{H}_9$	NIPAAm	Precipitation	Yes	
$\text{PEO-}b\text{-polyDMAAm} - \text{S} - \overset{\text{S}}{\underset{\text{  }}{\text{C}}} - \text{S} - \text{C}_{12}\text{H}_{25}$	DEAAm	Precipitation	Yes	[122]
polyMAA-Te-CH <sub>3</sub>	BA	Batch emulsion	Yes	[123]
poly(AA-co-ABu)-I	BA	Batch emulsion	Yes	[125]

authors was that water-soluble oligoradicals reacted with the macroRAFT agent. The resulting chain extension led to the formation of amphiphilic block copolymers able to play the role of stabilizers.

These results were further exploited by Dos Santos et al. [104], who intended to sterically and electrostatically stabilize latex particles using a combination of hydrophilic macroRAFT agents. For that purpose, a PEO ( $M_n = 2000 \text{ g mol}^{-1}$ ) carrying a dithiobenzoate chain-end and a polyDMAEMA ( $M_n = 5730 \text{ g mol}^{-1}$ , PDI = 1.24), obtained by RAFT polymerization mediated by CPADB, were simultaneously used in a batch emulsion polymerization of styrene. However, although some of the PEO chains seemed to participate in the nucleation process, the corresponding amount was not enough to prevent the latex from flocculation under alkaline conditions. PEO macroRAFT agent was then used as control agent for the RAFT polymerization of DMAEMA in organic solvent. The resulting block copolymer was further successfully used in its protonated form as a double hydrophilic macroRAFT agent to form polystyrene latexes in a batch emulsion polymerization of styrene. The double stabilization of the latexes was confirmed by their stability for months under alkaline conditions and against freeze–thaw cycles.

Bernard et al. [105] used the same strategy to decorate polyVAc latex particles with a dithiocarbonate end-functionalized dextran (dextran-RAFT), well-suited for the CRP of non-activated vinyl esters such as VAc. Dextran-RAFT was obtained by Cu(I)-catalyzed Huisgen [3 + 2] dipolar cycloaddition [106] between an alkyne end-functionalized dextran and an azido-containing dithiocarbonate. The low functionalization yield (30%) was apparently not an impediment for the syntheses of stable polyVAc latex particles (diameters from 80 to 150 nm) via batch emulsion polymerization. The involvement of the dithiocarbonate end-group was corroborated by the retardation effect observed when the dextran-RAFT concentration was increased. In addition, a drastic effect on particle size was observed as compared to emulsion polymerization experiments performed with native or alkyne-functionalized dextran (particle diameter above 500 nm).

The above-mentioned examples show that the design of the hydrophilic shell can be adjusted either by chemical modification of preformed hydrophilic polymers (e.g., PEO, dextran) or by making the most of the RAFT process in terms of macromolecular architectural control (by using polyDMAEMA, polyDEAEMA, or PEO-*b*-polyDMAEMA). The RAFT process also allows the synthesis of well-defined  $\alpha$ -functionalized polymer, provided that the RAFT agent used to control the polymerization is designed accordingly. Bathfield et al. [107] performed the dispersion polymerization of BA in a mixture of ethanol and water in the presence of polyNAM that was previously prepared by RAFT polymerization. They first showed that polyNAM prepared by conventional free radical polymerization did not act as an efficient stabilizer under BA dispersion polymerization conditions since particles exhibiting diameters above 3000 nm were obtained in this case. The use of polyNAM carrying a dithiobenzoate chain-end as hydrophilic macroRAFT agent allowed the particle diameters to be drastically decreased down to 200 nm, and resulted in polyBA latexes that were stable for several months. Again, the success of the formation of a latex was explained by the in situ formation



of polyNAM-*b*-polyBA block copolymers that acted as stabilizers of the forming particles, although kinetic issues such as very long inhibition periods (more than 10 h) remained unexplained. The presence of a polyNAM hydrophilic shell was further shown by  $^1\text{H}$  NMR analyses performed directly on the latex. In addition, the visualization of the particles by TEM at room temperature was explained by the presence of a hairy hydrophilic layer of polyNAM of high  $T_g$  (420 K) that prevented any film formation of the soft hydrophobic polyBA core. Finally, polyNAM macroRAFT, containing a sugar moiety on the  $\alpha$ -end and obtained using the corresponding sugar-containing RAFT agent, was used in dispersion polymerization of BA. A stable latex (250 nm) was obtained and was decorated at the periphery of the hydrophilic polyNAM shell with sugar moieties.

Xiong et al. [108] performed miniemulsion polymerization of styrene or MMA in the presence of presynthesized polyDMAEMA macroRAFT agents and SDS. The authors claimed to obtain stable miniemulsions of hydrophobic monomer droplets. However, they did not present any kinetic data on the miniemulsion polymerization nor evidence for the formation of amphiphilic block copolymers that could stabilize the latex particles.

Taking advantage of the reactivity of the thiocarbonylthio end-group of hydrophilic (co)polymers (i.e., hydrophilic macroRAFT agents) for controlling the formation of the particles in batch emulsion, miniemulsion, and dispersion polymerizations seems to be an original and challenging approach to the production of core-shell particles with a hydrophilic shell and a hydrophobic core. However, in none of the above-mentioned examples, was the purpose of the authors to control the length and polydispersity of the polymer chains in the latex. They essentially aimed at creating the stabilizer *in situ* with a long hydrophobic block of the same kind as the polymer in the dispersed phase, and to design the hydrophilic shell of the produced latex by making the most of the best attributes of the RAFT process or of post-modifications of hydrophilic macromolecules. A further step towards a comprehensive control of particle structure was the use of macromolecular stabilizers capable of controlling the architecture of the polymer chains inside the particles as well as the structure of their surface.

### Via Controlled Self-Assemblies of Amphiphilic Block Copolymers under Hydrophobic Monomer Feed Control

Starved-feed conditions were first used to obtain a perfect control of the growth of the hydrophobic block throughout the course of the emulsion polymerization and to ensure a simultaneous self-assembly of the forming block copolymers. Ferguson et al. [109, 110] and Sprong et al. [111], originally performed the emulsion polymerization of BA using an amphiphilic polyAA macroRAFT agent. PolyAA was obtained by RAFT polymerization of AA mediated by a trithiocarbonate, namely 2-[[*tert*-butylsulfanyl]carbonothioyl]sulfanylpropanoic acid. The starved-feed conditions prevented the formation of hydrophobic monomer droplets and allowed the controlled growth of the hydrophobic block from the polyAA chains. The absence

of monomer droplets is required at least up to the point where the RAFT moieties are locked into particles, in order to avoid the macroRAFT agents migrating to the droplet surface and stabilizing the monomer droplet–water interface. The authors proposed that this resulted in the formation of trithiocarbonate-containing rigid micelles that functioned as seeds for further polymerization. The RAFT control of the molar mass was maintained throughout the course of the polymerization. Molar masses continued to increase (up to  $M_n = 50,000 \text{ g mol}^{-1}$ ) with the feed of BA, while PDI remained lower than 1.5. The particle size of the final latex was around 60 nm. It is worth mentioning that the polyAA hydrophilic macroRAFT agent employed here was a very short oligomer (5 AA repetitive units).

Armed with these first successful results, the same team expanded its work in an exhaustive mechanistic study of this system [110]. The authors calculated that, consistent with the very narrowly distributed and small particle sizes (<60 nm), around 2700 macroRAFT agents seemed to be present in each particle, which is much greater than the typical surfactant aggregation number. They thus called into question their original assumption that rigid micelles were formed, and suggested that diblocks were able to migrate to the surface of those micelles where polymerization was occurring, from those micelles where polymerization had not yet taken place. The authors discussed the inconsistency between the 60 nm particle size obtained and the chain dimension (block copolymer with  $M_n = 40,000 \text{ g mol}^{-1}$  and estimated radius of gyration of 12 nm). They concluded that the burying of a certain number of polyAA segments was possible. The excellent control over molar mass and the livingness of the chains that composed the particles allowed the authors to investigate the synthesis of novel core–shell particles (Fig. 12) [110]. Indeed, by switching from a BA feed to a styrene feed they showed that polyAA-*b*-polyBA-*b*-polystyrene triblock copolymers exclusively formed and that latex particles with a hydrophilic polyAA shell, a polyBA hydrophobic first core, and a polystyrene more hydrophobic center core were obtained, as evidenced by TEM.

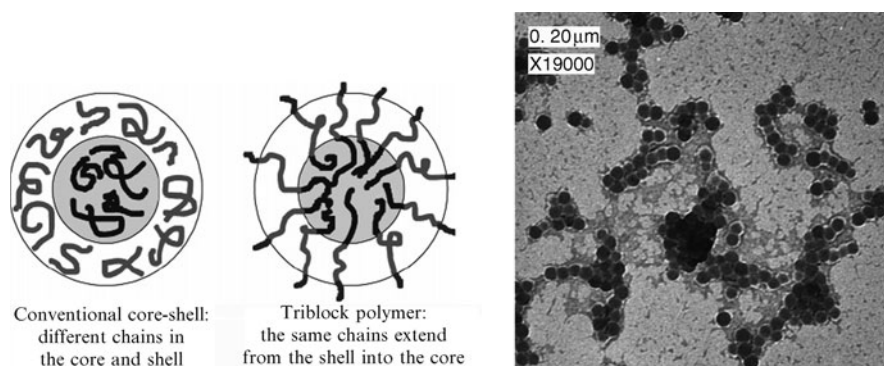


**Fig. 12** *Left:* Conventional core-shell particle from classical radical polymerization. *Middle:* PolyAA-*b*-polyBA-*b*-polystyrene core-shell particles obtained after switching from a BA to a styrene feed in emulsion polymerization using polyAA macroRAFT agent. *Right:* TEM image of polystyrene domains stained with ruthenium tetroxide. From [110], with permission from the American Chemical Society

Finally, the authors commented on the use of a starting trithiocarbonate having thiododecyl as an activating group, namely 2-[(dodecylsulfanyl)carbo thioyl] sulfanyl} propanoic acid. The more pronounced hydrophobicity of the polyAA obtained therefore required fewer BA units to be added before being insoluble in water. This resulted in smaller particle diameter (49.9 nm, 20% solid content) than with the original thiobutyl-containing trithiocarbonate (60.3 nm, 13% solid content).

A similar study [112] was then carried out by the same research team using preformed trithiocarbonate end-functionalized polyAA-*b*-polystyrene diblock copolymers (with 8 or 9 AA units and 10 or 5 styrene repetitive units) instead of pure polyAA and performing semicontinuous styrene emulsion polymerizations. Very little information on the characterization of these diblocks was provided. Indeed, the blocking efficiency of a polyAA macroRAFT agent towards styrene does not favor the formation of pure block copolymers, and the structural definition of the block copolymer used remains questionable. The mobility of the diblock copolymers was found to be largely dependent on their overall hydrophobicity. When used in emulsion polymerization, these block copolymers were able to migrate between micelles, the nucleation of which was possible provided that a sufficient radical flux was implemented. At low initiator concentrations, un-nucleated micelles could break up and the corresponding block copolymers could migrate to stabilize newly created particles until they grew sufficiently to remain trapped.

Following the same strategy, Božović-Vukić et al. [113] synthesized poly (4-vinylpyridine) (poly4VP) chains using (*S*-dodecyl-*S'*-isobutyric acid) trithiocarbonate in a mixture of toluene and ethanol under RAFT control. The obtained poly4VP macroRAFT agents were chain-extended with styrene and acrylonitrile in solution, but also under emulsion copolymerization conditions (which is of interest for this review). Under acidic conditions (pH 4–5), poly4VP macroRAFT agents are soluble in water and were exposed to a feed of styrene and acrylonitrile in a semicontinuous process. In agreement with the results of Ferguson et al. [110], the feed was carefully adjusted to avoid monomer droplets. Molar masses very nicely shifted toward high molar masses up to complete conversion of the monomers, showing the formation of particles almost exclusively composed of block copolymers. This was additionally confirmed by gradient elution chromatography analyses although no colloidal characterization such as particle size or TEM microscopy was provided.

This last example confirmed the usefulness of this novel approach for producing particles of hydrophilic shell and hydrophobic core that indeed consisted of self-assembled amphiphilic block copolymers. However, for the strategy to be successful, the authors underlined the prerequisite of avoiding monomer droplets and thus advised the use of slowly feeding the hydrophobic monomer.

### Towards Controlled Self-Assemblies of Amphiphilic Block Copolymers in Batch?

The obvious improvement was then to find conditions and/or reagents capable of producing amphiphilic block copolymers from hydrosoluble macroRAFT agents, ensuring such a self-assembly under batch conditions. This was indeed achieved by

Rieger et al. [114], who simply used a PEO macroRAFT agent ( $M_n = 2000 \text{ g mol}^{-1}$ ) as both stabilizer and control agent in ab initio batch emulsion polymerization of styrene and BA. This macroRAFT agent was obtained by esterification of a commercial  $\alpha$ -methoxy- $\omega$ -hydroxy PEO with (*S*-dodecyl-*S'*-isobutyric acid) trithiocarbonate. It exhibited a critical micelle concentration (CMC) of 0.5 mM, in the range of conventional PEO-based surfactants. First performing styrene emulsion polymerizations, experiments were stopped after 23 h (67% conversion) and stable latexes were obtained. According to SEC analyses, molar masses increased with conversion and the final latex exhibited a symmetric and narrow molar mass distribution. However, the chromatograms corresponding to lower conversions were asymmetric. Particle sizes in the range of 250 nm did not match the theoretical small sizes expected for a pure self-assembly of block copolymers (see beginning of this section) and indeed might reveal the complexity of the emulsion polymerization process that was occurring. However, due the very nice control over the molar mass and the stability of the obtained latex, the authors further evaluated the potential of their system using BA. Much larger polymerization rates were then achieved (100% conversion within 4 h). In addition, narrowly distributed molar masses were obtained that increased linearly with conversion throughout the course of the polymerization. Stable latexes exhibiting very narrow particle size distributions indicated a negligible impact of monomer droplets nucleation in this batch system.

The effect of the PEO macroRAFT agent molar mass (from 1000 up to  $5000 \text{ g mol}^{-1}$ ) was also studied [115]. This last parameter was shown to affect the particle size and the kinetics, and was advantageously used to tune the final particle size of the targeted latexes by mixing, in the same experiment, PEO macroRAFT agents of different molar masses. The macroRAFT agent with  $M_n = 2000 \text{ g mol}^{-1}$  was shown to provide a good control over the copolymerization of BA and MMA, up to a MMA content of 75%. Additionally, original morphologies assumed to result from block copolymer aggregation were obtained in this system.

In the same vein, Ji et al. [116] synthesized a living polyAAM using a 2-[[[(ethylsulfanyl)carbonothioyl] sulfanyl] butyric acid. This trithiocarbonate-functionalized polyAAM was used in a batch emulsion polymerization of styrene. A preliminary sonication step was performed to disperse the hydrophobic monomer into sufficiently small droplets. After 6 h of polymerization, the authors noted the formation of a stable latex composed of polymer chains, which were analyzed by FTIR, differential scanning calorimetry (DSC), and SEC. These characterizations showed the formation of polyAAM-*b*-polystyrene block copolymers. Particle sizes increased up to 58 nm during the polymerization, and the corresponding distribution remained narrow. The authors proposed that particles were mainly formed by nucleation of the very small monomer droplets formed after the sonication step and stabilized by polyAAM macroRAFT agents. Entry of oligoradicals, favored by the large surface offered by these small droplets, would lead to extension of the polyAAM macroRAFT agents into block copolymers under RAFT control. The same strategy was further applied by Wi et al. [117] using polyMAA macroRAFT agents carrying a dithiobenzoate chain-end. However, the provided data – both on the synthesis of polyMAA macroRAFT agent and on its further use in

batch emulsion polymerization of styrene – did not allow clear conclusions on the nucleation and polymerization mechanisms to be drawn.

Compared to emulsion polymerization, miniemulsion polymerization presents the advantage of avoiding the critical nucleation step by preforming nanometric monomer droplets that will act as nanoreactors as long as their stability is maintained throughout the polymerization. Miniemulsion can thus be regarded as an interesting tool for producing stabilized nanoreactors that can further generate particles with hydrophobic core and hydrophilic shell. Dos Santos et al. [118] investigated the use of a PEO carrying a dithiobenzoate end-group as both a stabilizer and a control agent to mediate the miniemulsion polymerization of styrene. After checking the ability of PEO macroRAFT agent to stabilize a miniemulsion of styrene in water, polymerizations were undertaken at 75°C using AIBN as an initiator. DSC measurements and molar mass determinations showed that the system was living, although polydispersity indices reached values up to 2.2. This rather broad molar mass distribution was assigned to the presence of different populations of controlled chain length arising from the partitioning of PEO macroRAFT agent between the aqueous phase, the droplets, and the water–droplet interface. This also led to a loss of miniemulsion features. Complex mechanisms induced by PEO macroRAFT agent partitioning were corroborated by the presence of holes, which were observed by TEM in the final latex when the PEO macroRAFT agent concentration was raised, and probably arose from the formation of buried PEO-*b*-polystyrene block copolymers.

Attempts to improve the molar mass distribution by varying the concentration and the nature of the initiator did not work. A decrease in polymerization temperature, in conjunction with the use of an adequate hydrophobic initiator, seemed to be the way to obtain a true miniemulsion polymerization system with a relatively constant particle diameter during the polymerization, while maintaining a good level of control. Pham et al. [119] proposed the use of amphipathic RAFT agents such as polyAA-*b*-polyBA and polyAA-*b*-polystyrene, to emulsify the dispersed phase, stabilize the particles, and control the molar mass of the polymer produced under styrene miniemulsion polymerization conditions. Although very little information on the characterization of the starting block copolymers was provided, they were sufficiently hydrophobic to be nonlabile, i.e., they were strongly adsorbed at the droplet surface and incapable of diffusing through the aqueous phase. The miniemulsion of styrene formed in their presence was stable over the timescale of the polymerization. This led to a stable latex, and a true miniemulsion polymerization process was indicated by DLS and TEM measurements that showed no evidence of new particle formation. Control of the polymerization was shown by the linear increase in molar masses with conversion and a narrowing of the corresponding molar mass distributions (PDI from around 2 down to 1.2) with an increasing initial amount of macroRAFT agents.

The success of the use of hydrophilic macroRAFT agents as both stabilizer and control agent for the polymerization of hydrophobic monomers in aqueous dispersed media was easily transposed to dispersion or precipitation polymerizations in which the monomer is completely soluble in the dispersing phase and the corresponding

polymer is not. An et al. [120] polymerized NIPAAm in water using hydrosoluble poly(*N,N*-dimethylacrylamide) (polyDMAAm) macroRAFT agents (polyDMAAm1 and polyDMAAm2) obtained using *S*-1-dodecyl-*S''*-2-(2,2'-dimethyl acetic acid) trithiocarbonate and *S*-3-(propionic acid)-*S''*-2-(2,2'-dimethyl acetic acid) trithiocarbonate as RAFT agents, respectively. Polymerization of NIPAAm being set at 70°C and thus above the lower critical solution temperature (LCST) of polyNIPAAm (32°C), the formation of block copolymers in water rapidly led to precipitation of the polyNIPAAm segment and formation of particles. The additional use of a crosslinker *N,N'*-methylenebisacrylamide (MBAAm) during the polymerization of NIPAAm allowed the particle integrity to be maintained once the latex was cooled down to room temperature. The polymerization being conducted under microwave conditions, polymerization times were short (10–30 min). The particle size distribution was narrower in the case of polyDMAAm2 (carrying a propionic acid end-group) than with polyDMAAm1 (carrying the dodecyl end-group). The use of the latter – exhibiting a CMC – could lead to both homogeneous and micellar nucleation and explain the broader particle size distribution mentioned earlier [110]. In both cases, however, a very good control over the molar mass of the polyNIPAAm block was obtained, as shown by the good agreement between theoretical and expected molar mass values obtained by SEC analyses ( $PDI < 1.2$ ). Further surface bioconjugation was performed by reaction of a fluorescein-labeled albumin with the surface carboxylic acid group of particles obtained with polyDMAAm2.

The same group [121] further expanded the potential of these nanostructured hydrogel materials by using polyDMAAm macroRAFT agents containing an azide  $\alpha$ -chain-end. Latex particles obtained after NIPAAm precipitation polymerization in water were thus decorated by azide surface functionalities. The hydrophilic shell was functionalized with an alkyne-containing dansyl molecule using Cu(I)-catalyzed Huisgen [3 + 2] dipolar cycloaddition [106]. The additional presence of the trithiocarbonate functionality inside the particles was advantageously used to functionalize the hydrophobic core. In the presence of ethanolamine, the trithiocarbonate was turned into a thiolate that could add onto an acrylate via 1,4-Michael addition. The hydrophobic core was then labeled according to this strategy using a fluorescein-containing acrylate. Finally, Rieger et al. [122] prepared hydrogels using the same PEO as the one successfully used in batch emulsion polymerization of styrene [114, 115]. They synthesized double hydrophilic block copolymers by first polymerizing DMAAm in solution using this PEO macroRAFT agent. Then, the direct synthesis of thermosensitive nanogel particles in aqueous dispersion was performed by using these double hydrophilic block copolymers for the polymerization of *N,N*-diethylacrylamide (DEAAm) in water. In the presence of a crosslinker for this step, thermoresponsive gel particles were obtained. The swelling/shrinking phenomena induced by temperature variations around the LCST of polyDEAAm were perfectly reversible. The resulting material consisted of original nanogels carrying a double hydrophilic PEGylated shell that might be further functionalized via copolymerization of the DMAAm with functional monomers.



### 6.1.2 Organotellurium-Mediated Radical Polymerization and Reverse Iodine Transfer Polymerization

Hydrophilic polymer chains obtained by TeRP carry a terminal carbon–Te bond that can be reactivated. These chains can be extended in water using a hydrophobic monomer to generate amphiphilic block copolymers in situ. The first and the only study in this area was performed by Okubo et al. [123], who used hydrosoluble polyMAA synthesized by TeRP, and thus carrying a  $-\text{TeCH}_3$  end-group, to synthesize polyBA latex particles. They showed that the polymerization was complete (16 h) and that a stable latex exhibiting small particle sizes (19 nm) was obtained. The molar masses were controlled, although 50% conversion had to be reached to fully activate and thus consume the polyMAA- $\text{TeCH}_3$  chains, leading to a PDI over 1.5. By increasing the stirring rate from 200 to 1000 rpm, polymerizations were much faster (100% conversion reached in 4 h) and particle sizes of 22 nm were obtained. A linear increase in molar masses with conversion was still observed with much narrower molar mass distributions ( $\text{PDI} < 1.5$ ), indicating a better control at this high stirring rate. Faster polymerizations at high stirring rates were explained by higher BA concentrations inside the particles, which were induced by a higher monomer diffusion through the water phase. Lower PDI and better control were explained by the corresponding lower polymer weight fraction at higher stirring rates (higher BA concentration in the particles), which favored the degenerative transfer between two polymer chains.

In RITP [124], molecular iodine is used to generate in situ iodinated transfer agents. Using RITP, Tonnar et al. [125] took advantage of the higher reactivity and solubility in water of AA compared to BA to produce poly(AA-*co*-BA) copolymers that became gradually richer in BA during the progress of polymerization in surfactant-free, batch, *ab initio* emulsion polymerization. The authors mentioned that these copolymers self-assembled to form particles in which the polymerization was resumed, although the particle sizes in the range of 200 nm were not commented upon. The livingness of the obtained latexes was shown by their successful reactivation (seeded emulsion polymerization) to form poly(AA-*co*-BA)-*b*-poly(BA-*co*-styrene) copolymer.

## 6.2 Reversible Termination Methods

For CRP based on a reversible termination process, the strategy was to synthesize water-soluble macroinitiators (with either an alkoxyamine or an alkyl halide chain-end) by direct CRP or by post-functionalization, before using them as both initiators and stabilizers in emulsion polymerization of a hydrophobic monomer.

### 6.2.1 Nitroxide-Mediated Radical Polymerization

The first results on the use of NMP macroinitiators were published by Wang et al. [126], who used a TEMPO-capped polyNaSS to initiate the polymerization of



styrene in water without surfactant. Although the polydispersity indexes for the synthesis of the polyNaSS macroalkoxyamine were rather low ( $1.2 < \text{PDI} < 1.3$ ), no data were provided concerning the polymerization. The same observation can be made for the kinetic and macromolecular characteristics of the emulsion polymerization. Stable dispersions were obtained, but the solid content did not exceed 5 wt%. The particle size distributions were quite broad and within the 50–200 nm range.

A few years later, Charleux's team developed a similar strategy using SG1-based macroalkoxyamine, after having thoroughly studied the use of water-soluble molecular alkoxyamines based on SG1 in both miniemulsion and seeded emulsion polymerizations [127–131]. First, the conditions for control of the polymerization of acrylic acid in solution with SG1 were determined and allowed the preparation of well-defined SG1-capped polyAA [132, 133]. After purification, a polyAA<sub>21</sub>-SG1 ( $\text{PDI} = 1.17$ ) was used to initiate the polymerization of styrene or BA in basic water at 120°C and 3 bar pressure, and with a typical solids content of 20 wt% [134] (Fig. 13).

Although the molar masses were significantly higher than the theoretical ones, they increased linearly with monomer conversion, and the PDIs were rather low for such a process ( $< 1.5$  at 80% conversion). Narrow particle size distributions were obtained at the end of the polymerization (conversion  $> 90\%$ ) and diameters below 100 nm could be reached, as demonstrated by DLS and TEM. The comparisons between results obtained by these two techniques allowed the authors to prove the existence of a core–shell morphology, measuring a shell thickness of 5–7 nm at high pH (i.e., hydrophilic polymer in extended conformation) in good agreement with the length of the polyAA<sub>21</sub> segment. The pH-responsive behavior of the shell was illustrated by DLS and showed a clear decrease in diameter when the pH was lowered (Fig. 14) [135]. These spherical aggregates could thus be defined as crew-cut micelles, according to Eisenberg's description [136], with a short hydrophilic stabilizing block and a long hydrophobic block in the particle core.

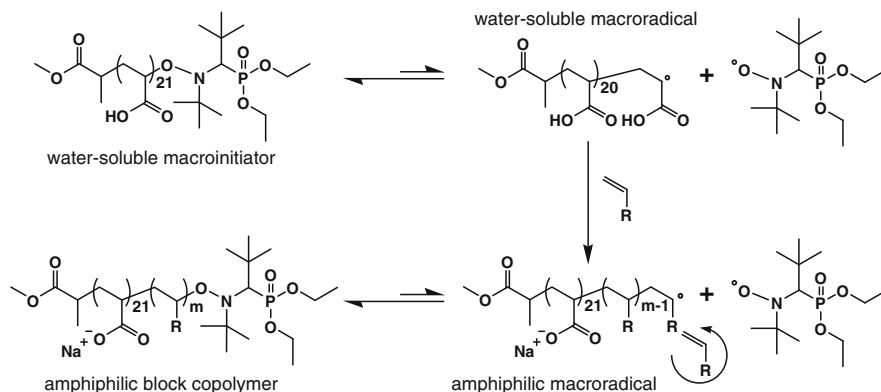


**Fig. 13** Chain extension via NMP of polyAA-SG1 by a hydrophobic monomer in water to form amphiphilic block copolymers in situ and to induce micellization by polymerization

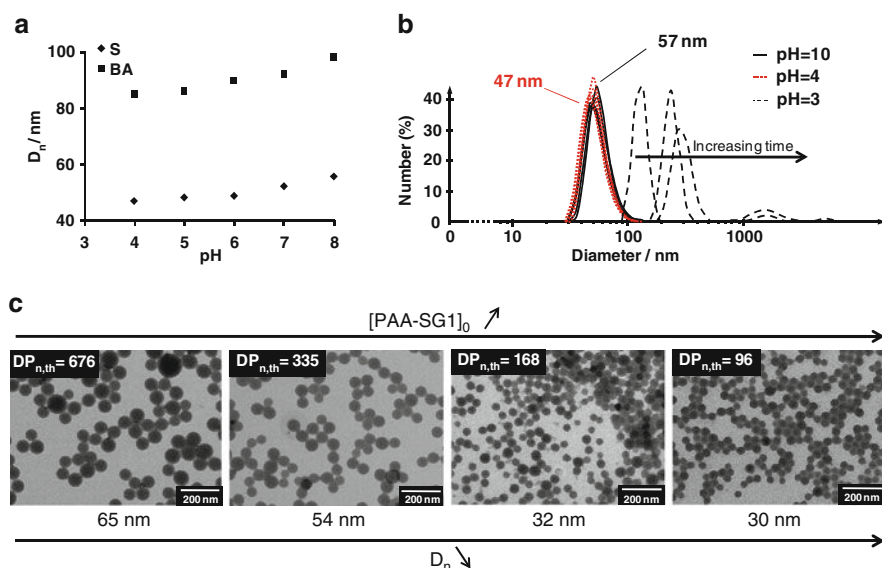


**Fig. 14** Colloidal characteristics of the polyAA-stabilized particles prepared by surfactant-free nitroxide-mediated emulsion polymerization of styrene: (a) pH-dependence of the diameters ( $D_n$ ), (b) stability of the polystyrene particles with pH, and (c) influence of the initial polyAA-SG1 concentration and of the target degree of polymerization,  $DP_{n,th}$ , on the particle diameter

Later, the influence of diverse experimental parameters such as the macroinitiator length, its concentration, the initial free nitroxide concentration, the solids content, and the concentration of an added electrolyte was evaluated and exploited to propose a mechanism for particle formation and growth of polymer chains [135]. For instance, it was demonstrated that the molar mass of the so-formed amphiphilic block copolymers and the particle diameter could be tuned by varying the initial macroalkoxyamine concentration (Fig. 14). Narrower molar mass distribution could also be reached ( $PDI = 1.3$  at 90% conversion), although complete and/or fast initiation could still not be achieved. To explain this, the importance of water-phase kinetics and slow initiation by the polyAA-based macroinitiator was pointed out [135, 137].

Solids contents that were rather high for such a batch, *ab initio*, emulsion polymerization process could be reached (i.e., up to 40 wt%) keeping an excellent colloidal stability [44]. With the chains being end-capped by an alkoxyamine, it was possible to resume the polymerization after removal of residual monomer and addition of a second load of monomer. When styrene was added to a polyAA-*b*-polyBA-based latex, polyAA-*b*-polyBA-*b*-polystyrene triblock copolymers were formed within polystyrene-polyBA-polyAA core-shell-corona particles [137]. Similar results were obtained when styrene was injected into the mixture during the polymerization of BA in a two-step semi-batch process. In this latter case, the third block was a poly(styrene-*co*-BA) random copolymer.

This polyAA-SG1 methodology was also employed in the dispersion polymerization of DEAAm at up to 40 wt% solids [137, 138]. The same polymerization kinetics and control over polymer chains as for styrene and BA polymerization were observed. Nanoparticles exhibiting similar structural features were also obtained [137]. The thermoresponsive nature of the polyDEAAm core-constituting block permitted the complete disassembly of the particles to release double hydrophilic diblock copolymers in water below its LCST (32°C). Upon heating above this temperature, particles could be reformed, though with different dimensions. This last feature was evidence for the out-of-equilibrium nature of the aggregates obtained by the polymerization-induced self-assembly process (*vide supra*). When a difunctional monomer like MBAAm was added to the recipe, the structures of the thermoresponsive particles could be locked by crosslinking of the inner block. Upon cooling of the sample, the colloids swelled with water and their diameter increased. However, macrogelation occurred when the molar fraction of crosslinker was higher than 0.05. This could be explained by the slow initiation process, which created radicals in the aqueous phase for a rather long period of time and prevented confinement of the crosslinking reaction inside the particles. This problem could be partially circumvented thanks to the living nature of the polymerization. Not to disturb the nucleation step, a semi-batch process was used to delay the introduction of the crosslinker, and the efficient crosslinking of the particles was achieved [138]. This technique allowed the complete decoupling of the nucleation and crosslinking processes. For example, for a certain polyAA-SG1 concentration and several crosslinker concentrations, particles with the same size at high temperature were obtained, but with differing abilities to swell. Nanogels ranging from 30 to 120 nm in their dry state could be produced, with volumic swelling ratios of up to 10 in some cases. As nanogels of small dimensions were previously impossible to obtain at high concentrations without surfactant, this work could be regarded as a significant step towards an industrial-scale production because the removal of surfactant and water-soluble species is avoided and particle morphology is well-controlled [139]. The nanogels retained the pH-sensitivity of the shell-constitutive polyAA and thus precipitated at high temperature and low pH [137]. Aiming at physically crosslinked nanogels, the authors carried out a two-step semi-batch dispersion/emulsion polymerization by adding styrene to a running DEAAm dispersion polymerization. Polystyrene-*b*-polyDEAAm-*b*-polyAA core–shell–corona structures were eventually obtained [137].

This macroalkoxyamine route is a very simple way of obtaining highly concentrated dispersions of crew-cut micelles in a batch, *ab initio*, emulsion polymerization process because few reagents are needed. It is noteworthy that a single molecule, *i.e.*, the polyAA-SG1 macroalkoxyamine, acts simultaneously as a stabilizer, an initiator, and a control agent in the complete absence of any other additional molecule (mainly radical initiator and surfactant). Moreover, the method enables the synthesis of out-of-equilibrium structures that are difficult to obtain under other conditions. For example, different morphologies like spherical or worm-like micelles, multi-compartmented or spherical vesicles (the latter being the most represented) have

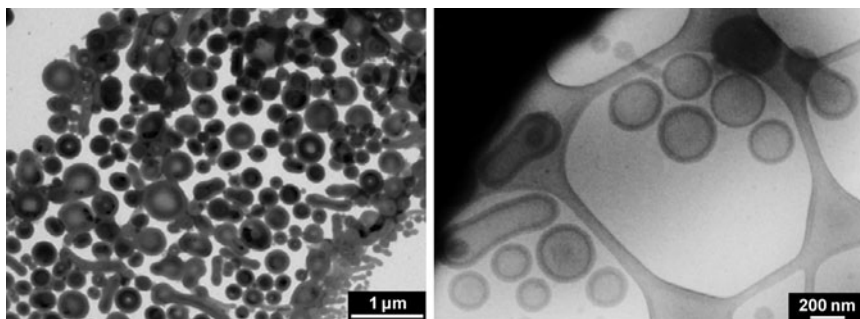


**Fig. 15** Classical (*left*) and cryo- (*right*) TEM images of the aggregates obtained by nitroxide-mediated emulsion polymerization of 4-vinylpyridine initiated by polyAA-SG1

been recently reported using 4VP as the core monomer and the same polymerization technique (Fig. 15) [140]. These structures were composed of well-defined block copolymers of AA and 4VP with a long hydrophobic block. The structures were found to solubilize with decreasing the pH owing to the basic nature of the poly4VP block. Re-assembling of the amphiphilic copolymers at basic pH gave rise to a monomodal 85-nm spherical micelle population. This proved the out-of-equilibrium structure of the initial aggregates.

With the incomplete and/or slow initiation by polyAA-SG1 being a recurring problem with regard to macromolecular control, Dire et al. [141] designed polyMAA-based macroalkoxyamines. They took advantage of the SG1-mediated copolymerization effect of methacrylate monomers with styrene reported by Charleux et al. [142, 143] to improve the initiating efficiency. A poly(MAA-*co*-styrene) macroinitiator with 8 mol% of styrene units was synthesized because it was shown that the so-formed alkoxyamine exhibited a methacrylate-styrene-SG1 terminal sequence that was able to dissociate at low temperature (70–90°C) [143]. Thanks to this new feature, the emulsion homopolymerization of MMA was carried out at very low temperature (40°C) and high solids content (20 wt%). A non-controlled mechanism was observed since a rather broad molar mass distribution was obtained. This was clearly explained by a slow consumption of the macroinitiator due to a low dissociation rate constant of the alkoxyamine bond at such a temperature, leading to the continuous creation of block copolymer chains throughout the polymerization process. Nevertheless, the obtained latex was stable and showed a very narrow particle size distribution. This provided a mild and simple method for synthesizing poly(MAA-*co*-styrene)-*b*-polyMMA amphiphilic block copolymer core-shell particles at a high solids content [144].

For the same reason as for bulk or solution synthesis of methacrylate-based macroalkoxyamines, a low percentage of styrene was needed to improve control of the emulsion polymerization [144]. Even for very low amounts (3 mol%), the polymerization could be controlled over a lower temperature range (60–80°C), though the polymerization rate was quite slow. Increasing the reaction temperature, together with increasing the amount of styrene to keep a good control, resulted in faster

polymerizations. It appeared clearly that the temperature was the main lever because high conversions were reached in more than 20 h at 65–80°C whereas a few hours (2–3 h) were sufficient at 85–90°C. The macromolecular features of the amphiphilic block copolymers formed in situ were highly improved by this method, and a 100% initiation efficiency was observed with good control over molar mass and very narrow molar mass distribution. The colloidal characteristics were, however, not as good as when polyAA-SG1 was used as a macroinitiator, though they remained largely acceptable owing to the more hydrophobic nature of the macroalkoxyamine.

The variety of the type of particles obtained by NMP in surfactant-free emulsion was finally extended to PEG-coated particles [145]. In this case, macroalkoxyamines composed of PEGMA and MAA units were synthesized according to the same procedure as described above, i.e., with a low amount of styrene. Two different reactive water-soluble polymers were used in emulsion, one with a large majority of MAA units and another with equal proportions of the two polar monomer units. When used to initiate the polymerization of MMA with a small percentage of styrene in surfactant-free emulsion at 85°C and 20 wt% solids content, the reaction proceeded very quickly and 90% of the monomer reacted in ca. 3 h. The molecular characteristics perfectly followed the trend of a CRP with a final PDI as low as 1.3 (Fig. 16). In all cases, small particles of 30–50 nm were produced. Nevertheless, some aggregates were present in the final latex. Moreover, the particle dispersion based on the highest amount of PEGMA stabilizing units exhibited quite a high viscosity, giving rise to a white cream. In this system, it seems that the steric stabilization was not sufficient to provide a very good stability to the particles and that an electrostatic stabilization was also required.

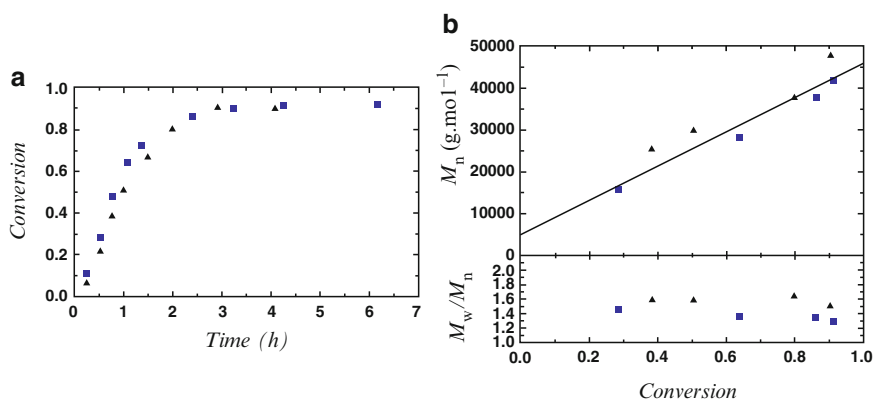


**Fig. 16** Overall conversion versus (a) time and (b) number-average molar mass,  $M_n$ , and polydispersity index,  $M_w/M_n$  (the line represents the theoretical  $M_n$ ) for the nitroxide-mediated surfactant-free emulsion copolymerizations of methyl methacrylate and styrene in the presence of poly(PEGMA-co-MAA-co-styrene)-SG1 macroalkoxyamines of different molar masses (triangles 9400, and squares 4400 g mol<sup>-1</sup>) [145]

## 6.2.2 Atom Transfer Radical Polymerization

The ATRP process has also been used to create hydrophobic–hydrophilic core–shell particles. All the published studies are related to the use of a PEG segment as the stabilizing block for the particles. Indeed, a charged hydrophilic block would interact with the catalytic system and disrupt its effect. In all cases, a commercial PEG was functionalized with a chlorine- or a bromine-based ATRP initiator via simple esterification of the PEG hydroxyl end-group. In the first report, a PEG<sub>44</sub>-Br was used to initiate the polymerization of NIPAAm at 50°C in water and very low concentration (> 0.5 wt%) using the CuBr/Me<sub>6</sub>-TREN catalytic system [146]. At this temperature, the polyNIPAAm block was insoluble so the reaction proceeded through a dispersion mechanism. The molar mass of the polyNIPAAm block was 7400 g mol<sup>-1</sup> with a PDI of 1.62 for the block copolymer. The authors did not provide any data on the colloidal characteristics of the dispersion. Later, they introduced a crosslinker to stabilize the particles and obtained a diameter of ca. 70 nm for the swollen nanogels at 25°C. An electron micrograph showed a rather broad size distribution. The authors also demonstrated that using an organic cosolvent like tetrahydrofuran during the reaction allowed the size of the aggregates to be increased.

PEG-based ATRP initiators were also used to polymerize hydrophobic monomers in an emulsion polymerization process. Xu et al. [147] used a PEG<sub>120</sub>-Cl to initiate the polymerization of styrene at 75°C in presence of CuCl/bipyridine and Tween-20 as catalyst and surfactant, respectively, at low theoretical solids content (4–8 wt%). Although the authors referred several times to the ATRP mechanism to explain the colloidal behavior of their system, they did not give precise details to prove the controlled character of the polymerization. A linear increase in the molar mass with monomer conversion was stated. When the monomer to macroinitiator ratio was decreased, the diameter of the particles increased. An increase in the catalyst concentration had the reverse effect. The diameter ranged from 30 to 90 nm in the given examples. Irradiating with microwaves during the reaction improved the colloidal features (smaller particles with lower polydispersity). It was proposed that, under such conditions, the catalytic system was more active and so the initiation step was faster and gave rise to many more particles of smaller size for the same mass content.

Stoffelbach et al. used another technique to obtain PEG-coated hydrophobic particles by ATRP [35]. They employed a miniemulsion process in which the surfactant was a reactive amphiphilic block copolymer. A PEG<sub>111</sub>-*b*-polystyrene<sub>33</sub> bearing a bromine atom at its hydrophobic end was first synthesized by ATRP of styrene from a PEG macroinitiator in homogeneous medium. Then, it was dispersed in water and mixed with a monomer solution containing hexadecane and a Cu(II) complex for AGET ATRP before being subjected to cooling, ultrasonication, and deoxygenation (Fig. 17). The polymerizations of *n*-butyl methacrylate (BMA), BA, and styrene were initiated by adding ascorbic acid and were conducted at 80 or 90°C to afford triblock copolymers. The polymerization of BMA was rather fast but initiation was slow, giving rise to slightly high PDIs. This could be improved by adding a small amount of styrene to slow the polymerization down. Polymerizations of BA

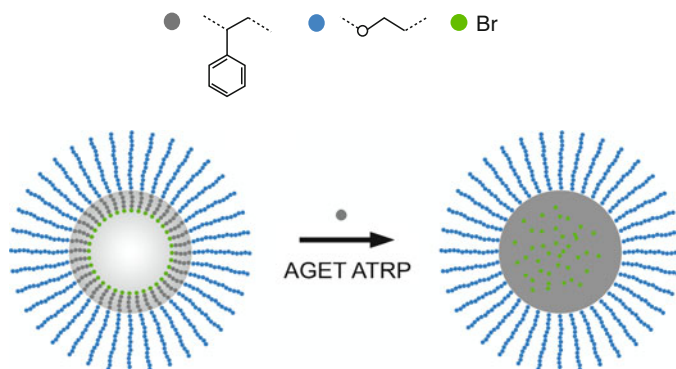


**Fig. 17** Synthesis of PEG-shell/polystyrene-core nanoparticles by AGET ATRP in miniemulsion from a PEG-*b*-polystyrene-Br macroinitiator [35]

and styrene were very slow. All these polymerizations gave a plateau at incomplete conversion after 1 or 2 h of reaction, which might be explained by hydrolysis of the bromine group or migration of the catalyst in the aqueous phase. In all cases, initial and final dispersions were found to be stable, even though their size distributions were rather broad. The diameters ranged from 130 to 230 nm and were smaller when the concentration of PEG-*b*-polystyrene-Br was increased. Because the reactive block copolymer acted as both an initiator and a stabilizer, the evolution of particle size could not be decoupled from the molar mass of the polymers.

Li et al. [37] published new results using the same approach by additionally introducing a hydrophobic molecular initiator together with the PEG-*b*-polystyrene-Br amphiphilic macroinitiator to control the macromolecular and colloidal characteristics independently. Thanks to this methodology, the amount of reactive surfactant could be reduced (while aiming at a similar degree of polymerization for the polymer formed) by keeping the overall initiator concentration constant. At the beginning of the polymerization, two different molar mass distributions could be observed owing to the presence of two initiators of different lengths. Progressively, a monomodal distribution was formed as the influence of the molar mass of the initiators became negligible. For a similar molar concentration of macroinitiator, when the degree of polymerization of the polystyrene block was increased, the stability of the latex was slightly affected. Nevertheless, this technique allowed the synthesis of triblock copolymers with  $M_n$  ranging from 10,000 to 25,000 g mol<sup>-1</sup> within particles of 200–390 nm in diameter. Finally in the same study, a PEG<sub>44</sub>-Br without any hydrophobic segment was also used to initiate and stabilize the miniemulsion ATRP. The initial monomer-in-water miniemulsion proved to be stable for at least 2 days at 70°C, with a slight increase in the droplet diameter compared to the initial value. Without additional initiator, the reaction was slow but controlled. A few dead PEG chains were formed at the beginning but stable particles of 140–200 nm were obtained. When a molecular ATRP initiator was used, a low  $M_n$  could be targeted without a huge quantity of PEG-Br and the same general features as in the case of the PEG-*b*-polystyrene-Br were obtained.



## 7 Core–Shell Particles via a Divergent Method: Grafting of Polymer Brush at the Surface of Polymer Particles

To create particles with a hydrophobic core and a hydrophilic shell, preformed hydrophobic polymer particles can be used as substrate for the covalent grafting of hydrophilic polymer chains. Aqueous emulsion polymerization is thus the method of choice for synthesis of core particles with submicrometric diameter (due to the scope of this review article, discussion will be restricted to aqueous emulsion polymerization, although some examples of particle substrates created via suspension polymerization exist; however, with much larger diameters). The grafting methods are very close to those used for the surface modification of inorganic materials, such as for instance silicon wafers or colloidal silica particles [46, 48–52]. Various strategies can be employed such as:

- *Grafting through* methods, via copolymerization of monomers with vinylic bonds attached at the surface
- *Grafting to* methods, using a preformed polymer able to react with co-reactive groups covalently bound to the surface
- *Grafting from* methods (also called surface-initiated polymerization), by which the polymer is grown from the surface via attached initiator or chain transfer agent

With the development of CRP the “grafting from” method has been extensively studied in the recent years. The main reason comes from the non-drastic experimental conditions and the versatility in terms of monomers and processes. In particular, CRP is tolerant to water and can thus be conducted in an aqueous environment. Thanks to the fast initiation step and simultaneous growth of all polymer chains, the surface-initiated CRP (SI-CRP) methods lead to high grafting densities and allow polymer brushes to be formed, with chain attached to the surface by a single point located at their extremity. All of these methods are very powerful for the synthesis of a broad variety of well-defined (co)polymers with controlled molar mass and narrow molar mass distribution. However, the number of articles reporting grafting reactions at the surface of polymer colloids is far lower than those on surface modification of inorganic particles. The majority of articles deal with surface-initiated ATRP (SI-ATRP), i.e., the “grafting from” methodology. In the context of this review article, the most relevant works concern grafting via aqueous ATRP of hydrophilic polymer from an initiator located at the particle surface [148–157] (Fig. 18). In some other examples, grafting via SI-ATRP was performed in an organic solvent after transferring the particles from the aqueous phase where they were first synthesized [158–164]. One article refers to surface-initiated NMP [165] and two others show the application of RAFT for the synthesis of end-functionalized polymer chains that were further grafted onto the surface of polymer particles [166, 167].

**Step 1.**

Synthesis of (crosslinked) latex particles via emulsion polymerization

**Step 2.**

Synthesis of functional latex particles via seeded-emulsion copolymerization: incorporation of a functional monomer bearing an alkyl halide initiating group for ATRP

**Step 3.**

Surface-initiated ATRP either in water or in organic solvent

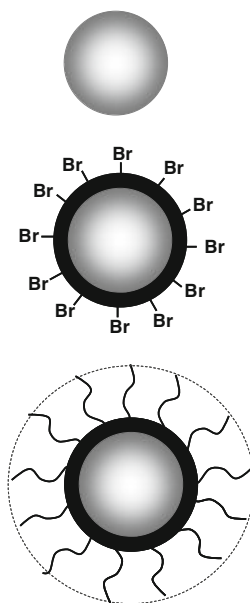


**Fig. 18** Three steps needed for performing a SI-ATRP reaction from the surface of a polymer latex particle

## 7.1 Grafting from Technique

### 7.1.1 Atom Transfer Radical Polymerization in Water

#### Synthesis of Functionalized Latex Particles

Surfactant-free batch emulsion polymerization initiated by a charged radical initiator was generally used to synthesize the latex particles constituting the hydrophobic core [149–156], which was composed of polystyrene in all of the published works. Such a method led to latexes of low solids content (below 5 wt%), with large particles exhibiting diameters above 500 nm. In a different way, Guerrini-Manuszak et al. [148] worked in more classical conditions with a mixture of cationic and non-ionic surfactants, and the resulting core particle diameter was significantly smaller (92 nm). Taniguchi et al. employed miniemulsion in the presence of a polymerizable surfactant [157]. Because SI-ATRP requires the synthesis of particles with appropriate reactive functions located at the surface, post-functionalization was performed by (co)polymerization with a monomer bearing an ATRP initiator group, i.e., an alkyl halide (except for miniemulsion, in which a single copolymerization step was employed [157]) (Fig. 19). For that purpose, the preformed particles were used as a seed, and various strategies were developed to target a thin, uniform reactive layer at the surface, to tune the surface density in functional groups, and to avoid secondary nucleation.

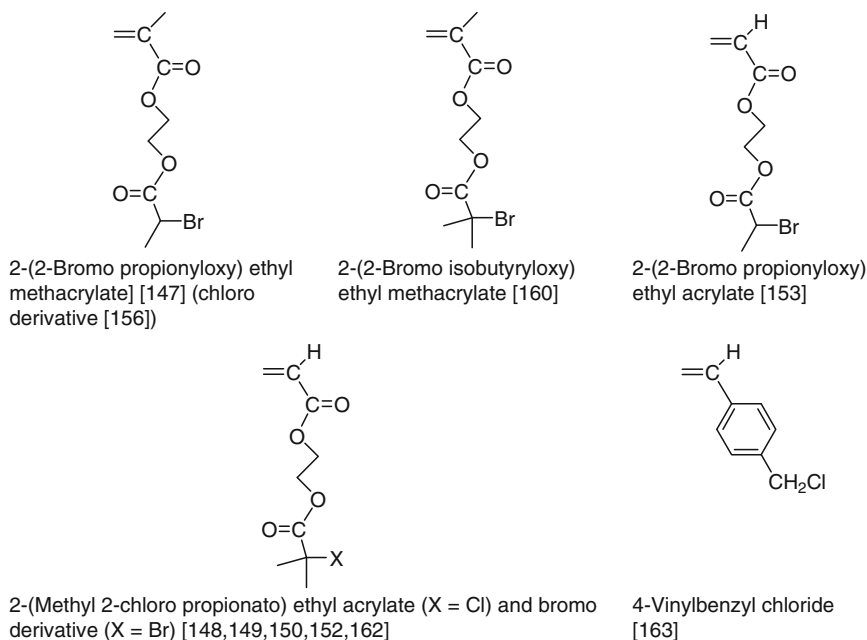


**Fig. 19** Monomers bearing an ATRP initiator group used in emulsion polymerization for the functionalization of latex particles

A complete study from Mittal et al. [154] aimed at finding the best conditions in the particular case of polystyrene core particles and an acrylate functional monomer. To enhance the compatibility between the core and the reactive shell and favor creation of core-shell particles instead of a second population of small particles, it was found appropriate to maintain unreacted monomer in the seed (incomplete conversion of 70%) and to introduce a crosslinker in both the core and the shell. Moreover, the presence of the latter had the advantage of improving the properties of the final particles by favoring the irreversible anchorage of the hydrophilic shell (further grown by SI-ATRP). Due to incomplete monomer conversion in the first step, the seed particles were soft, which favored the formation of a uniform shell. In addition, the way the functional monomer was introduced (shot or delayed addition; pure or mixed with styrene) also had an effect on the uniformity of the reactive layer. In the presence of a crosslinker, however, irregular morphologies were more difficult to avoid.

### Surface-Initiated Atom Transfer Radical Polymerization

The latex particles functionalized with the ATRP initiator were cleaned either by dialysis and/or by cycles of centrifugation and serum replacement to eliminate all water-soluble species (either initially present or generated during the latex synthe-

sis) and to better control the surface properties. For instance, the radical initiator had to be removed very carefully when ATRP was carried out at elevated temperature [148] in order to limit the initiation of free chains in the aqueous phase. Because the particles were electrostatically stabilized by the charged initiator fragments located at the chain-ends, the addition of the ATRP cationic catalyst could cause latex flocculation. This was not observed at low solids content and when a cationic initiator was chosen [148]. However, the problem was encountered with negatively charged latexes (persulfate initiator) and was fixed by the addition of a nonionic surfactant just before the ATRP reaction [149].

In the vast majority of the published examples, “grafting from” was carried out using a Cu(I) catalyst for direct ATRP (either CuBr alone [148] or a mixture of CuX/CuX<sub>2</sub>, with X = Cl or Br, and Cu powder [149–153, 155, 156]) with various multidendate amine ligands. For some reactions, a free ATRP initiator was added in the latex serum [149, 152, 153]. In one instance, the polymerization was performed at 70°C or 80°C [148], whereas in all the other works room temperature was applied. A single, very recent article reported the use of AGET ATRP with Cu(II) complex and ascorbic acid [157]. The hydrophilic monomers were 2-hydroxyethyl acrylate [148], 2-(methacryloyloxy)ethyl trimethylammonium chloride (MAETACl) [148], DMAAm [149–151], methoxyethylacrylamide [152], NIPAAm [152, 153, 155], methoxypoly(ethylene glycol)-based *N*-substituted acrylamide macromonomers [156] and a styrene derivative bearing a lactose residue [157].

Very little information has been reported on the SI-ATRP kinetics, but it appears that incomplete monomer conversions are reached even after a long polymerization time of 24 h [148, 153]; this can be ascribed to the persistent radical effect and the accumulation of Cu(II) deactivator in the aqueous phase [6].

By degrafting the polymer chains via hydrolysis of the ester function located at the initiator–particle junction, a complete characterization of the grafted chains (i.e., molar mass, molar mass distribution, mass of chains per unit area of latex, and radius of gyration,  $R_g$ ) was performed by Brooks and coworkers [149–153] as a function of various parameters such as the concentrations of monomer, latex particles, surface initiator, deactivator [Cu(II)], and external initiator. The system was mainly studied for the SI-ATRP of DMAAm at the surface of polystyrene latexes bearing negative charges [149, 151]. It was clearly seen that an increase in the initial monomer concentration (at constant grafted initiator concentration) led to an increase in  $M_n$  of the grafted chains (up to values as high as  $\sim 6 \times 10^5 \text{ g mol}^{-1}$ ) (Fig. 20) along with an increase in the grafting density. The latter could reach a value of 0.8 chains per nm<sup>2</sup>, which is particularly high. The ratio of the average distance between grafted chains to  $R_g$  was always below 2, indicating the formation of a polymer brush. This was confirmed by the linear increase in the hydrodynamic thickness of the hydrophilic polymer shell with  $M_n$  (Fig. 21), reaching 650 nm for  $M_n = 3.5 \times 10^5 \text{ g mol}^{-1}$ . This led to an increased viscosity of the latex due to the high particle volume fraction. Depending on the ligand, the control over the polymer chain growth was quite effective as the PDIs were relatively low, typically in the 1.2–1.6 range for the *N,N,N'*, *N',N''*-pentamethyldiethylenetriamine (PMDETA) and HMTETA ligands (Fig. 20). Moreover, as expected for a well-controlled ATRP, the addition of more Cu(II) de-

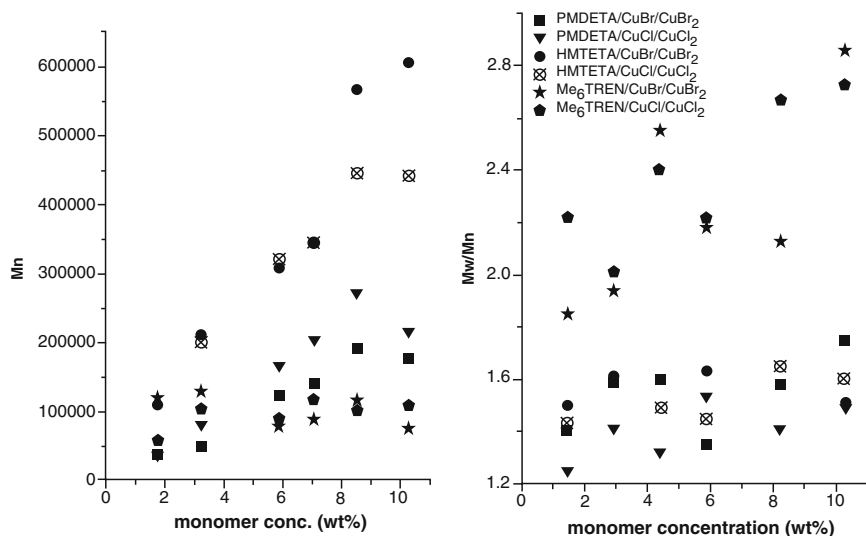
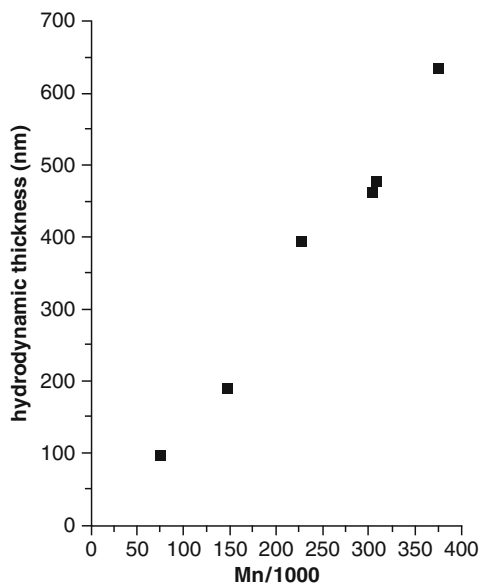


**Fig. 20** Typical evolution of  $M_n$  (left) and  $M_w/M_n$  (right) versus monomer concentration as a function of the ATRP catalytic system, for the SI-ATRP of DMAAm in water at 22°C from the surface of polystyrene particles. From [149], with permission from the American Chemical Society

**Fig. 21** Variation of the hydrodynamic thickness for the SI-ATRP of DMAAm in water at 22°C from the surface of polystyrene particles. From [149], with permission from the American Chemical Society



activator led to a decrease in the PDI, together with a decrease in  $M_n$  at similar polymerization time, due to a reduction of the polymerization rate. The addition of an external ATRP initiator, either hydrophilic or hydrophobic, led to a decrease in  $M_n$ , but did not improve control over the polymerization. In all reactions performed

in the absence of external initiator, free polymer chains were still found in the latex serum, most probably generated by chain transfer reactions to the ligand [149, 155]. Therefore, cleaning of the latex after grafting might be needed for further application. The effect of the surface ATRP initiator concentration was studied in detail [151], and its increase led to a great enhancement of the polymer grafting density. With a negatively charged latex, the positively charged catalyst was shown to be more concentrated in the surrounding of the particles than in the solution, but remained lower than the initiator concentration. Nevertheless, its local concentration depends on the charge surface density of the latex and on physico-chemical parameters, and is not easily controlled. It should be noted that it is an important parameter, which affects the rate of initiation and the initiator efficiency.

It can thus be concluded that the way of generating and controlling a well-defined hydrophilic polymer brush via SI-ATRP from polystyrene latex particles has been well-studied, and that the parameters affecting the most important outcomes (such as grafting density, chain length, and shell thickness) were correctly understood. These achievements became the foundation for targeting a variety of organic particles with hydrophobic core and hydrophilic shell. For instance, one of the goals was to cover the surface of the latex particles with a temperature-sensitive polymer shell composed of polyNIPAAm, (LCST at approximately 32°C) [153, 155]. The growth of the polyNIPAAm chains from the latex particle surface was studied in detail and results similar to those found for the SI-ATRP of DMAAm were found [153]. At 20°C, the hydrodynamic thickness of the grafted polyNIPAAm layer measured by DLS was proportional to  $DP_n^{0.66}$  at constant grafting density and continuously decreased with the increase in temperature from 22 to 36°C. The fully collapsed and hydrated dimensions of the core–shell particles were retained upon repeated cycles of heating and cooling [153]. The presence of a regular extended polymer layer was visualized by TEM after drying the latex at a temperature below the LCST [155]. At temperatures above the LCST, the shell was no longer visible because the polyNIPAAm chains collapsed onto the polystyrene surface and the particles tended to aggregate due to their enhanced hydrophobic character.

The possibility of grafting block copolymer chains via a two-step SI-ATRP was studied. The concomitant increase in molar mass and thickness of the hydrophilic layer proved both the living character of the polymer grafted in the first step and the efficient reinitiation in the second step [152]. An example of block copolymer used was polyDMAAm-*b*-polyNIPAAm, which exhibited a change in the chain conformation leading to a reduction of the hydrodynamic diameter of the particles upon an increase in temperature above the LCST, in a similar way as the polyNIPAAm homopolymer.

Hairy polymer colloids formed in this way might find application in several domains in the future. With a polymer brush exhibiting a LCST, the change of surface properties with temperature could be of high interest for applications based on adsorption–desorption processes, such as their use as stationary phases for bioseparation. Recently, PEG-based N-substituted acrylamide macromonomers were grafted via SI-ATRP from the surface of polystyrene latexes. These PEG-based surfaces showed good protection against nonspecific protein adsorption from

blood plasma compared to the bare surface [156]. A similar result was shown with polystyrene particles coated with lactose residues, which enhanced protection against adsorption of bovine serum albumin [157]. Although out of the scope of this review article, it is also interesting to mention the application of the SI-ATRP grafting method to “gigaporous” polymeric chromatography beads for the synthesis of polyDMAAm brushes, with the goal of creating tunable high-throughput size-exclusion chromatography media [168].

### 7.1.2 Atom Transfer Radical Polymerization in Organic Medium

Like the method described in the previous section, the first step of ATRP in an organic medium is the preparation of functionalized latex particles via aqueous (seeded) emulsion polymerization [158, 159, 161–164]. Synthesis of the core latex particles was not different from the above-mentioned recipes, except that the particles were stabilized against dissociation in the organic medium by crosslinking. In addition, the use of a surfactant to tune the particle size was not a problem as the particles were easily washed before being used as a substrate. In a particular example, the ATRP initiator was not introduced by copolymerization with a functional monomer but by using layer-by-layer deposition of polyelectrolytes, one of them containing halogenated functional groups [160]. The functionalized particles were then isolated, washed, and transferred into an organic solvent for subsequent SI-ATRP. In some sense, the technique is out of the scope of the present review article because the CRP (i.e., the grafting reaction) was not performed in aqueous medium. Depending on the solvent used for the ATRP, the experimental procedure was close to that of a surface-initiated polymerization (poor solvent for the core polymer) or close to that used in homogeneous conditions for the synthesis of grafted copolymers (good swelling solvent for the core polymer). The core polymer used was either polystyrene (either crosslinked with divinylbenzene [158, 159, 161, 162] or non-crosslinked [160]), poly(4-vinylbenzyl chloride) (also crosslinked with divinylbenzene) [164], or polyMMA (crosslinked with a trifunctional methacrylate) [163]. In parallel, the solvents were cyclohexanone [158], methanol [159, 161], isopropanol/water [159, 161], acetone/water [159, 161], tetrahydrofuran/methanol [162], toluene [163], or propanol [164]. The ATRP conditions were classical, using Cu(I)/Cu(II) catalyst, various aminated ligands, and either room temperature or more elevated temperature such as 75°C. The resulting polymers were examined in terms of molar mass (when degrafted) and layer thickness.

Generally, the conditions leading to a CRP system were found to yield a well-defined polymer shell. In some examples, the latter was a classical hydrophobic polymer such as polyMMA [158, 160], polyMA [158], polystyrene [163], poly(*tert*-butyl acrylate) [163], or polyBMA [163]. In one example, the grafted polymer was polyDMAEMA, which showed pH- and temperature-responsive behavior when the particles were further transferred to water [159]. The polyDMAEMA domains were used as nanoreactors to generate gold nanoparticles at the particle surface, the catalytic activity of which was effective in the reduction of 4-nitrophenol by NaBH<sub>4</sub>



[161]. In another study, a poly4VP layer was grafted, which was further activated in a  $\text{PdCl}_2$  solution followed by reaction with CO or  $\text{H}_2\text{S}$  to yield composite particles with metallic palladium or palladium sulfide nanoparticles in the shell.

### 7.1.3 Nitroxide-Mediated Radical Polymerization in Organic Medium

In recent years, nitroxide-mediated CRP (using SG1 in particular) has undergone important development due to the increase in the number of polymerizable monomers, and has hence become quite versatile for a variety of functional systems. It is thus of great interest to consider the technique for grafting polymer chains onto reactive substrates. The technique was used for grafting polyDMAEA, polystyrene-*b*-polyDMAEA and polyBA-*b*-polyDMAEA (co)polymers from polymer particles prepared via aqueous emulsion polymerization [165]. As described in the previous section, the grafting reaction was not performed directly in water but in dimethylformamide, although the use of water might be possible if one considers the successful development of NMP in aqueous dispersed systems (see Sect. 2.2). As for ATRP, the reaction requires the use of polymer particles functionalized with a proper NMP initiator at their surface. The latex was prepared via batch emulsion copolymerization of styrene and 4-vinylbenzyl chloride in the presence of a surfactant, to yield latex particles with an average diameter of 60 nm. The particles were then transferred to dimethylformamide, and water was further eliminated by evaporation. At this stage, the surface chloromethyl groups ( $-\text{CH}_2-\text{Cl}$ ) were turned into the corresponding SG1-based alkoxyamines ( $-\text{CH}_2-\text{SG1}$ ). Because of the need for copper catalyst in this reaction, the modified particles had to be thoroughly cleaned by cycles of centrifugation and serum replacement. Then, the “grafting from” reaction was performed in dimethylformamide in the presence of the selected monomers (DMAEA, styrene or BA), free nitroxide and, for some reactions, an additional free alkoxyamine initiator. Grafted block copolymers were synthesized in a two-step procedure, using the particles with the living chains as a “multifunctional macroinitiator”.

Compared to ATRP, the method is more straightforward because no catalyst is required, only a simple elevation of temperature to reversibly activate the surface alkoxyamine groups and start the polymerization. However, by comparison, the reaction temperature needs to be high ( $112^\circ\text{C}$ ), whereas SI-ATRP were mostly performed at room temperature. The polymerization kinetics and evolution of  $M_n$  of the free chains formed in solution were studied. The rate and  $M_n$  depended on the presence or not of free alkoxyamine initiator in the polymerization solution. When the initiator was present, the rate was enhanced but  $M_n$  was lower, as expected. In parallel, the free chains exhibited a very narrow molar mass distribution, which might also be the same for the grafted chains. In addition, the latter were still living because the reinitiation towards diblock copolymers was effective. An increase in the particle diameter was observed concomitant to the growth of the polymer chains at the surface (for instance, variation of the diameter was 18 nm when  $M_n$  of the polyDMAEA was  $25,000\text{ g mol}^{-1}$ ). Complete analyses of the particles confirmed

the creation of surface polymer brush. All particles modified by a polyDMAEA layer could be readily redispersed in water, which was not the case for the particles without the grafted hydrophilic shell.

## 7.2 *Grafting to Technique*

The “grafting to” technique has the great advantage of allowing the synthesis of a well-defined polymer before the grafting reaction, but it generally leads to low grafting densities. To date, only the RAFT method has been used in this way for coating preformed latex particles. By introducing a reactive function in the initiating and/or leaving group of the RAFT agent, the macromolecules can be attached via their  $\alpha$ -end while they maintain their living character (i.e., reactive  $\omega$ -end group) after the grafting reaction. Alternatively, the thiocarbonylthio  $\omega$ -end group can be easily turned into a thiol function for further attachment of biological molecules. In a first approach [166], a polystyrene latex was prepared via an emulsifier-free emulsion polymerization in the presence of a hydrophilic functional comonomer, aminoethyl-methacrylate hydrochloride, which creates a hydrophilic layer at the particle surface and yields primary amine groups in alkaline conditions. The hydrophilic polymer to be grafted was polyNAM prepared using a dithiobenzoate RAFT agent with a propionic acid leaving group, which was further modified into the corresponding activated ester. The amide linkage between the polymer chains and the latex surface was then created by reaction between the activated polyNAM chains and the surface amine groups. The reaction was performed at 40°C for 12 h. The other approach [167] was based on a crosslinked latex of poly(styrene-*co*-4-vinylbenzyl chloride), in which the surface chloromethyl groups were turned into azides via reaction with sodium azide. The hydrophilic polymer to be grafted was a poly[methyl ether oligo(ethylene glycol) methacrylate] synthesized via RAFT using a dithiobenzoate chain transfer agent with an ethynyl substituent on the leaving group. Grafting of the polymer onto the latex surface was performed via the Cu(I)-catalyzed Huisgen [3 + 2] dipolar cycloaddition between alkyne and azide [106], and the reaction was carried out overnight at 70°C. In both cases, the modified latex was further cleaned to remove all unattached polymer, and the presence of the hydrophilic shell was checked by various techniques, including particle size analysis.

## 8 Conclusion

After a long period of time devoted to the implementation and understanding of CRP in aqueous dispersed systems, a greater level of control has been achieved and will lead to the design of new systems and eventually new particle morphologies. Besides the classical target of control over chain structure, CRPs in miniemulsion or in emulsion along with grafting techniques offer exceptional tools for the design of new

nano-objects that were not accessible before via classical radical polymerization or that required many synthetic steps. We believe that this target will be the most important one for CRP in the future because not only will new types of particles emerge but also because more robust structures will be achieved via easier syntheses.

## References

1. Matyjaszewski K, Davis T (eds) (2002) Handbook of radical polymerization. Wiley, Hoboken, NJ
2. Braunecker WA, Matyjaszewski K (2007) *Prog Polym Sci* 32:93–146
3. Hawker CJ, Bosman AW, Harth E (2001) *Chem Rev* 101:3661–3688
4. Matyjaszewski K, Xia J (2001) *Chem Rev* 101:2921–2990
5. Kamigaito M, Ando T, Sawamoto M (2001) *Chem Rev* 101:3689–3745
6. Fischer H (2001) *Chem Rev* 101:3581–3610
7. Georges MK, Veregin RPN, Kazmaier PM, Hamer GK (1993) *Macromolecules* 26: 2987–2988
8. Benoit D, Grimaldi S, Finet J-P, Tordo P, Fontanille M, Gnanou Y (1998) In: Matyjaszewski K (ed) Controlled radical polymerization, ACS Symp Ser 685:225–235
9. Benoit D, Chaplinski V, Braslau R, Hawker CJ (1999) *J Am Chem Soc* 121:3904–3920
10. Gromada J, Matyjaszewski K (2001) *Macromolecules* 34:7664–7671
11. Jakubowski X, Matyjaszewski K (2005) *Macromolecules* 38:4139–4146
12. Tatemoto M, Nakagawa T (1978) Daikin Kogyo Co., Ltd. German Offenlegungsschrift 2729671
13. Matyjaszewski K, Gaynor SG, Wang JS (1995) *Macromolecules* 28:2093–2095
14. Tonnar J, Lacroix-Desmazes P (2008) *Angew Chem Int Ed* 47:1294–1297
15. Goto A, Kwak Y, Fukuda T, Yamago S, Iida K, Nakajima M, Yoshida J (2003) *J Am Chem Soc* 125:8720–8721
16. Chiefari J, Chong YK, Ercole F, Krstina J, Jeffery J, Le TPT, Mayadunne RTA, Meijs GF, Moad CL, Moad G, Rizzardo E, Thang SH (1998) *Macromolecules* 31:5559–5562
17. Charnot D, Corpart P, Adam H, Zard SZ, Biadatti T, Bouhadir G (2000) *Macromol Symp* 150:23–32
18. Barner-Kowollik C (ed) (2008) Handbook of RAFT polymerization. Wiley, Weinheim
19. Chiefari J, Mayadunne RTA, Moad CL, Moad G, Rizzardo E, Postma A, Skidmore MA, Thang SH (2003) *Macromolecules* 36:2273–2283
20. Chong YK, Krstina J, Le TPT, Moad G, Postma A, Rizzardo E, Thang SH (2003) *Macromolecules* 36:2256–2272
21. Barner-Kowollik C, Buback M, Charleux B, Coote ML, Drache M, Fukuda T, Goto A, Klumperman B, Lowe AB, McLeary JB, Moad G, Monteiro MJ, Sanderson RD, Tonge MP, Vana P (2006) *J Polym Sci A Polym Chem* 44:5809–5831
22. Qiu J, Charleux B, Matyjaszewski K (2001) *Prog Polym Sci* 26:2083–2134
23. Cunningham MF (2002) *Prog Polym Sci* 27:1039–1067
24. Monteiro M, Charleux B (2005) In: van Herk A (ed) Chemistry and technology of emulsion polymerization. Blackwell, Oxford, pp 111–139
25. Save M, Guillaeney Y, Gilbert RG (2006) *Aust J Chem* 59:693–711
26. Charleux B, Ganachaud F (2007) In: Matyjaszewski K, Gnanou Y, Leibler L (eds) Macromolecular engineering: from precise macromolecular synthesis to macroscopic materials properties and application, vol 1. Wiley, Weinheim, pp 605–642
27. McLeary JB, Klumperman B (2006) *Soft Matter* 2:45–53
28. Cunningham MF (2008) *Prog Polym Sci* 33:365–398
29. Zetterlund PB, Kagawa Y, Okubo M (2008) *Chem Rev* 108:3747–3794
30. Oh JK (2008) *J Polym Sci A Polym Chem* (2008) 46:6983–7001

31. Antonietti M, Landfester K (2002) *Prog Polym Sci* 27:689–757
32. Asua JM (2002) *Prog Polym Sci* 27:1283–346
33. Schork FJ, Luo Y, Smulders W, Russum JP, Butté A, Fontenot K (2005) *Adv Polym Sci* 175:129–255
34. Min K, Gao H, Matyjaszewski K (2005) *J Am Chem Soc* 127:3825–3830
35. Stoffelbach F, Belardi B, Santos JMRCA, Tessier L, Matyjaszewski K, Charleux B (2007) *Macromolecules* 40:8813–8816
36. Min K, Yu S, Lee H, Mueller L, Sheiko SS, Matyjaszewski K (2007) *Macromolecules* 40:6557–6563
37. Li W, Min K, Matyjaszewski K, Stoffelbach F, Charleux B (2008) *Macromolecules* 41:6387–6392
38. Stoffelbach F, Griffete N, Bui C, Charleux B (2008) *Chem Comm* 39:4807–4809
39. Butte A, Storti M, Morbidelli M (1998) *DECHEMA Monogr* 134:497–507
40. Charleux B (2000) *Macromolecules* 33:5358–5365
41. Zetterlund PB, Okubo M (2006) *Macromolecules* 39:8959–8967
42. Kagawa Y, Zetterlund PB, Minami H, Okubo M (2006) *Macromol Theory Simul* 15:608–613
43. Maehata H, Buragina C, Keoshkerian B, Cunningham MF (2007) *Macromolecules* 40:7126–7131
44. Delaître G, Charleux B (2008) *Macromolecules* 41:2361–2367
45. Bourgeat-Lami E (2007) In: Kickelbick G (ed) *Hybrid materials: synthesis, characterization and applications*. Wiley, Weinheim, pp 87–149
46. Pyun J, Matyjaszewski K (2001) *Chem Mater* 13:3436–3448
47. Bourgeat-Lami E, Duguet E (2006) In: Ghosh SK (ed) *Functional coatings*. Wiley, Weinheim, pp 85–152
48. Advincula RC, Brittain WJ, Caster KC, Rühle J (eds) (2004) *Polymer brushes*. Wiley, Weinheim
49. Radhakrishnan B, Ranjan R, Brittain WJ (2006) *Soft Matter* 2:386–396
50. Tsujii Y, Ohno K, Yamamoto S, Goto A, Fukuda T (2006) *Adv Polym Sci* 197:1–45
51. Ghannam L, Parvole J, Laruelle G, Francois J, Billon L (2006) *Polym Int* 55:1199–1207
52. Zou H, Wu S, Shen J (2008) *Chem Rev* 108:3893–3957
53. Perruchot C, Khan MA, Kamitsi A, Amres SP, von Werne T, Patten TE (2001) *Langmuir* 17:4479–4481
54. Wang XS, Lascelles SF, Jackson RA, Armes SP (1999) *Chem Commun* 18:1817–1818
55. Chen X, Armes SP (2003) *Adv Mater* 15:1558–1561
56. Chen XY, Armes SP, Greaves SJ, Watts JF (2004) *Langmuir* 20:587–595
57. Vo CD, Schmid A, Armes SP, Skai K, Biggs S (2007) *Langmuir* 23:408–413
58. Bombalski L, Min K, Dong H, Tang C, Matyjaszewski K (2007) *Macromolecules* 40:7429–7432
59. Pyun J, Jia S, Kowalewski T, Patterson GD, Matyjaszewski K (2003) *Macromolecules* 36:5094–5104
60. Lu AH, Salabas L, Schüth F (2007) *Angew Chem Engl Int Ed* 46:1222–1244
61. Pileni MP (1997) *Langmuir* 13:3266–3276
62. Sun SH, Zeng H (2002) *J Am Chem Soc* 124:8204–8205
63. Lattuada M, Hatton TA (2007) *Langmuir* 23:2158–2168
64. Hu F, Neoh KG, Cen L, Kang ET (2006) *Biomacromolecules* 7:809–816
65. Mori H, Seng DC, Zhang M, Mueller AHA (2004) *Prog Colloid Polym Sci* 126:40–43
66. Nguyen D, Zondanos HS, Farrugia JM, Serelis AK, Such CH, Hawke BS (2008) *Langmuir* 24:2140–2150
67. Daigle JC, Claverie J (2008) *J Nanomater* article ID 609184. doi:10.1155/2008/609184
68. Ladavière C, Dörr N, Claverie JP (2001) *Macromolecules* 34:5370–5371
69. Samakande A, Hartmann PC, Cloete V, Sanderson RD (2007) *Polymer* 48:1490–1499
70. Greesh N, Hartmann PC, Cloete V, Sanderson RD (2008) *J Colloid Interf Sci* 319:2–11
71. Samakande A, Sanderson RD, Hartmann PC (2008) *J Polym Sci A Polym Chem* 46:7114–7126

72. Samakande A, Juodaityte JJ, Sanderson RD, Hartmann PC (2008) *Macromol Mater Eng* 293:428–437
73. Di JB, Sogah DY (2006) *Macromolecules* 39:1020–1028
74. Samakande A, Sanderson RD, Hartmann PC (2009) *Polymer* 50:42–49
75. Ali SI, Heuts JPA, Hawket BS, Van Herk AM (2009) *Langmuir* 25:10523–10533
76. Monteiro MJ, de Barbeyrac J (2001) *Macromolecules* 34:4416–4423
77. Smulders W, Monteiro MJ (2004) *Macromolecules* 37:4474–4483
78. Herrera V, Pirri R, Asua JM, Leiza JR (2007) *J Polym Sci A Polym Chem* 45:2485–2493
79. Kagawa Y, Minami H, Okubo M, Zhou J (2005) *Polymer* 46:1045–1049
80. Nicolas J, Ruzette AV, Farcet C, Gérard P, Magnet S, Charleux B (2007) *Polymer* 48: 7029–7040
81. Airaud C, Héroguez V, Gnanou Y (2008) *Macromolecules* 41:3015–3022
82. Airaud C, Ibarboure E, Gaillard C, Héroguez V (2009) *J Polym Sci A Polym Chem* 47: 4014–4027
83. Walther A, Müller AHE (2008) *Soft Matter* 4:663–668
84. Discher DE, Eisenberg A (2002) *Science* 297:967–973
85. Duan H, Kuang M, Zhang G, Wang D, Kurth DG, Möhwald H (2005) *Langmuir* 21: 11495–11499
86. Chen Y, Wang C, Chen J, Liu X, Tong Z (2009) *J Polym Sci A Polym Chem* 47:1354–1367
87. Ting SRS, Gregory AM, Stenzel MH (2009) *Biomacromolecules* 10:342–352
88. Ali MM, Stöver HDH (2003) *Macromolecules* 36:1793–1801
89. Ali MM, Stöver HDH (2006) *J Polym Sci A Polym Chem* 44:156–171
90. Zetterlund PB, Saka Y, Okubo M (2009) *Macromol Chem Phys* 210:140–149
91. Van Zyl AJP, Bosch RFP, McLeary JB, Sanderson RD, Klumperman B (2005) *Polymer* 46:3607–3615
92. Luo Y, Gu H (2006) *Macromol Rapid Commun* 27:21–25
93. Klumperman B (2006) *Macromol Chem Phys* 207:861–863
94. Lu F, Luo Y, Li B (2007) *Macromol Rapid Commun* 28:868–874
95. Guyot A, Tauer K, Asua JM, Van Es S, Gauthier C, Hellgren AC, Sherrington, DC, Montoya-Goni A, Sjöberg M, Sindt O, Vidal F, Unzue M, Schoonbrood H, Shipper E, Lacroix-Desmazes P (1999) *Acta Polym* 50:57–66
96. Guyot A, Tauer K (2001) Polymerizable and polymeric surfactants. In: Texter J (ed) *Reactions and synthesis in surfactants systems*, vol 100. Marcel Dekker, New York, pp 547–576
97. Guyot A (2002) *Macromol Symp* 179:105–132
98. Riess G, Labbe C (2004) *Macromol Rapid Commun* 25:401–435
99. Fifield CC, Fitch RM (2003) *CR Chim* 6:1305–1312
100. Vidal F, Guillot J, Guyot A (1995) *Polym Adv technol* 6:473–479
101. Miyazaki H, Terada K, Sato T, Maruyama H, Okaya T (1996) *J Appl Polym Sci* 60: 2149–2157
102. Tichagawa L, Götz C, Tonge M, Sanderson R, Pash H (2003) *Macromol Symp* 193:251–260
103. Manguian M, Save M, Charleux B (2006) *Macromol Rapid Commun* 27:399–404
104. Dos Santos AM, Pohn J, Lansalot M, D’Agosto F (2007) *Macromol Rapid Comm* 28: 1325–1332
105. Bernard J, Save M, Arathoon B, Charleux B (2008) *J Polym Sci A Polym Chem* 46: 2845–2857
106. Kolb HC, Finn MG, Sharpless KB (2001) *Angew Chem Int Ed Engl* 40:2004–2021
107. Bathfield M, D’Agosto F, Spitz R, Charreyre MT, Pichot C, Delair T (2007) *Macromol Rapid Commun* 28:1540–1545
108. Xiong Q, Ni P, Zhnag F, Yu Z (2004) *Polym Bull* 53:1–8
109. Ferguson CJ, Hughes RJ, Pham BTT, Hawket BS, Gilbert RG, Serelis AK, Such CH (2002) *Macromolecules* 25:9243–9245
110. Ferguson CJ, Hughes RJ, Nguyen D, Pham BTT, Gilbert RG, Serelis AK, Such CH, Hawket BS (2005) *Macromolecules* 38:2191–2204
111. Sprong E, Leswin JSK, Lamb DJ, Ferguson CJ, Hawket BS, Pham BTT, Nguyen D, Such CH, Serelis AK, Gilbert RG (2006) *Macromol Symp* 231:84–93

112. Ganeva DE, Sprong E, de Bruyn H, Warr GG, Such CH, Hawket BS (2007) *Macromolecules* 40:6181–6189
113. Božović-Vukić J, Mañon HT, Meuldijk J, Koning C, Klumperman B (2007) *Macromolecules* 40:7132–7139
114. Rieger J, Stoffelbach F, Bui C, Alaimo D, Jérôme C, Charleux B (2008) *Macromolecules* 41:4065–4068
115. Rieger J, Osterwinter G, Bui C, Stoffelbach F, Charleux B (2009) *Macromolecules* 42:5518–5525
116. Ji J, Yan L, Xie D (2008) *J Polym Sci A Polym Chem* 46:3098–3107
117. Wi Y, Lee K, Lee BH, Choe S (2008) *Polymer* 49:5626–5635
118. Dos Santos AM, Le Bris T, Graillat C, D'Agosto F, Lansalot M (2009) *Macromolecules* 42:946–956
119. Pham BTT, Nguyen D, Ferguson CJ, Hawket BS, Serelis AK, Such CH (2003) *Macromolecules* 36:8907–8909
120. An Z, Shi Q, Tang W, Tsung CK, Hawker CJ, Stucky GD (2007) *J Am Chem Soc* 129:14493–14499
121. An Z, Tang W, Wu M, Jiao Z, Stucky GD (2009) *Chem Commun* 6501–6503
122. Rieger J, Grazon C, Charleux B, Alaimo D, Jérôme C (2009) *J Polym Sci A Polym Chem* 47:2373–2390
123. Okubo M, Sugihara Y, Kitayama Y, Kagawa Y, Minami H (2009) *Macromolecules* 42:1979–1984
124. Lacroix-Desmazes P, Severac R, Boutevin B (2005) *Macromolecules* 38:6299–6309
125. Tonnar J, Lacroix-Desmazes P (2008) *Soft Matter* 4:1255–1260
126. Wang L, Chuang W-R, Chiu W-Y, Cheng K-C (2002) *Polym Prepr* 43:297–298
127. Nicolas J, Charleux B, Guerret O, Magnet S (2004) *Macromolecules* 37:4453–4463
128. Nicolas J, Charleux B, Guerret O, Magnet S (2004) *Angew Chem Int Ed* 43:6186–6189
129. Nicolas J, Charleux B, Guerret O, Magnet S (2005) *Macromolecules* 38:9963–9973
130. Nicolas J, Charleux B, Magnet S (2006) *J Polym Sci A Polym Chem* 44:4142–4153
131. Charleux B, Nicolas J (2007) *Polymer* 48:5813–5833
132. Couvreur L, Lefay C, Belleney J, Charleux B, Guerret O, Magnet S (2003) *Macromolecules* 36:8260–8267
133. Lefay C, Belleney J, Charleux B, Guerret O, Magnet S (2004) *Macromol Rapid Commun* 25:1215–1220
134. Delaître G, Nicolas J, Lefay C, Save M, Charleux B (2005) *Chem Commun* 615–616
135. Delaître G, Nicolas J, Lefay C, Save M, Charleux B (2006) *Soft Matter* 2:223–231
136. Zhang L, Eisenberg A (1996) *J Am Chem Soc* 118:3168–3181
137. Delaître G (2008) Ph.D. Thesis Dissertation, University Pierre and Marie Curie, Paris
138. Delaître G, Save M, Charleux B (2007) *Macromol Rapid Commun* 28:1528–1533
139. Pelton R (2004) *Macromol Symp* 207:57–66
140. Delaître G, Dire C, Rieger J, Puteaux JL, Charleux B (2009) *Chem Commun* 2887–2889
141. Dire C, Charleux B, Magnet S, Couvreur L (2007) *Macromolecules* 40:1897–1903
142. Charleux B, Nicolas J, Guerret O (2005) *Macromolecules* 38:5485–5492
143. Nicolas J, Dire C, Mueller L, Belleney J, Charleux B, Marque S, Bertin D, Magnet S, Couvreur L (2006) *Macromolecules* 39:8274–8282
144. Dire C, Magnet S, Couvreur L, Charleux B (2009) *Macromolecules* 42:95–103
145. Dire C, Nicolas J, Brusseau S, Charleux B, Magnet S, Couvreur L (2009) In: Matyjaszewski K (ed) *Controlled/living radical polymerization: progress in RAFT, NMP & OMRP*. ACS Symp Ser, vol 1024. American Chemical Society, Washington DC, pp 303–318
146. Kim KH, Kim J, Jo W H (2005) *Polymer* 46:2836–2840
147. Xu Z, Hu X, Li X, Yi C (2008) *J Polym Sci A Polym Chem* 46:481–488
148. Guerrini-Manuszak M, Charleux B, Vairon JP (2000) *Macromol Rapid Commun* 21:669–674
149. Jayachandran KN, Takacs-Cox A, Brooks DE (2002) *Macromolecules* 35:4247–4257
150. Kizhakkedathu JN, Goodman D, Brooks DE (2003) *Am Chem Soc Symp Series* 854:316–330
151. Kizhakkedathu JN, Brooks DE (2003) *Macromolecules* 36:591–598
152. Kizhakkedathu JN, Kumar KR, Goodman D, Brooks DE (2004) *Polymer* 45:7471–7489

153. Kizhakkedathu JN, Norris-Jones R, Brooks DE (2004) *Macromolecules* 37:734–743
154. Mittal V, Matsko NB, Butte A, Morbidelli M (2007) *Polymer* 48:2806–2817
155. Mittal V, Matsko NB, Butte A, Morbidelli M (2007) *Eur Polym J* 43:4868–4881
156. Kizhakkedathu JN, Janzen J, Le Y, Kainthan RK, Brooks DE (2009) *Langmuir* 25:3794–3801
157. Taniguchi T, Kasuya M, Kunisada Y, Miyai T, Nagasawa H, Nakahira R (2009) *Colloid Surf B Biointerf* 71:194–199
158. Min K, Hu J, Wang C, Elaissari A (2002) *J Polym Sci A Polym Chem* 40:892–900
159. Zhang M, Liu L, Zhao H, Yang Y, Fu G, He B (2006) *J Coll Int Sci* 301:85–91
160. Fulghum TM, Patton DL, Advincula RC (2006) *Langmuir* 22:8397–8402
161. Zhang M, Liu L, Wu C, Fu G, Zhao H, He B (2007) *Polymer* 48:1989–1997
162. Ishizu K, Kobayakawa N, Takano S, Tokuno Y, Ozawa M (2007) *J Polym Sci A Polym Chem* 45:1771–1777
163. Jhaveri SB, Koyle D, Maschke D, Carter KR (2007) *J Polym Sci A Polym Chem* 45:1575–1584
164. Cheng Z, Zhang L, Zhu X, Kang ET, Neoh KG (2008) *J Polym Sci A Polym Chem* 46:2119–2131
165. Bian K, Cunningham MF (2006) *Polymer* 47:5744–5753
166. D'Agosto F, Charreyre MT, Pichot C, Gilbert RG (2003) *J Polym Sci A Polym Chem* 41:1188–1195
167. Breed DR, Thibault R, Xie F, Wang Q, Hawker CJ, Pine DJ (2009) *Langmuir* 25:4370–4376
168. Coad BR, Kizhakkedathu JN, Haynes CA, Brooks DE (2007) *Langmuir* 23:11791–11803





# Miniemulsion Polymerization as a Means to Encapsulate Organic and Inorganic Materials

Clemens K. Weiss and Katharina Landfester

**Abstract** The miniemulsion technique greatly enhances the possibilities for the preparation of hybrid nanomaterials by encapsulating molecular compounds, liquids, or solid material. Using this technique, a wide variety of novel functional nanocomposites can be generated that are not accessible with other techniques. After briefly introducing miniemulsions and the miniemulsion polymerization techniques for the preparation of polymeric nanoparticles, this review focuses on the preparation of functional nanostructures by encapsulation of organic or inorganic material in polymeric matrices. The examples presented highlight the possibility to either protect the encapsulated material (e.g., dyes, drugs, magnetite, or DNA) and create completely new properties that emerge in a synergistic manner from the components of the nanocomposites, or to perform reactions in polymer-enclosed vessels of submicrometer size.

**Keywords** Hybrid materials · Miniemulsion · Nanocomposites · Nanomaterials · Nanoparticles

## Contents

1	Introduction .....	186
2	Encapsulation of Material Soluble in the Dispersed Phase .....	187
2.1	Dyes .....	188
2.2	Metal Complexes .....	194
2.3	Functional Organic Molecules .....	195
3	Capsule Formation .....	198
3.1	Capsule Formation by Phase Separation .....	199
3.2	Capsule Formation by Polymerization From or at the Interface .....	201
3.3	Polymer Precipitation on Preformed Nanodroplets .....	206

4	Encapsulation of Material Insoluble in the Dispersed Phase .....	208
4.1	Organic Pigments and Carbon-Based Material .....	210
4.2	Inorganic Material .....	212
5	Summary .....	226
	References .....	227

## 1 Introduction

Novel applications in science and technology require highly efficient and, if possible, environmentally friendly methods and techniques for the generation of functional nanocomposite materials. Serving the environmental aspect, water-based formulation techniques that avoid the use of organic solvents are the focus of attention. Besides the well-known water-based emulsion and microemulsion polymerization processes, the miniemulsion polymerization technique is a highly versatile heterophase system that is suitable for the preparation of complex nanoparticles.

Miniemulsions are two-phase systems that consist of finely dispersed stable droplets in a second, continuous phase. The droplets are usually created by the application of high shear forces (ultrasound, high pressure homogenization, etc.) on a conventional emulsion formulated from two immiscible liquids. Direct (oil-in-water, o/w) as well as indirect (water-in-oil, w/o) miniemulsions can be prepared and stabilized with the appropriate surfactant. The droplets are in the submicrometer range and show a narrow size distribution. The ideal concept of individually acting nanoreactors is realized in miniemulsions because the droplets are stabilized from collisions and coagulation by a surfactant, and a costabilizer suppresses diffusional degradation. Cationic, anionic, and nonionic surfactants can be used for the formulation of a miniemulsion. The costabilizer, often called “(ultra)hydrophobe” (direct miniemulsion) or “lipophobe” (inverse miniemulsion), has to be a compound with an extremely low solubility in the continuous phase. For direct miniemulsions hexadecane is often used; for indirect miniemulsions a salt such as NaCl is usually used. The costabilizer creates an osmotic pressure inside the droplets, counteracting the Laplace pressure that is responsible for diffusional degradation (Ostwald ripening).

This has several implications on the reactions and on the products obtained from a miniemulsion process [1–3]. Ideally, the droplets do not change their identity during the whole miniemulsion process. This means that, without outer stimuli and low solubility in the continuous phase, the contents of the droplets remain inside and do not interact with droplets in the vicinity. The reaction volume is essentially limited to the volume of one droplet. Furthermore, as long as no product is created that is soluble in the continuous phase, the concentrations and relative amounts of the droplet contents are unchanged before and after the reaction.

Unlike in conventional emulsion polymerization processes, the droplets can be regarded as individually acting nanoreactors, suitable for a wide variety of different reactions. Organic reactions (esterifications) [4, 5], crystallization processes [6–9] and sol-gel reactions [10], to name only few, can be conducted in

mini-emulsions. However, the miniemulsion technique is especially of great interest for the preparation of (functional) polymeric nanoparticles. The nanoreactor concept, realized in miniemulsions, allows the independent polymerization of a large number of individually acting nanodroplets. Thus, not only radical homopolymerization can be performed, but also defined copolymerization for the generation of copolymer nanoparticles or the defined introduction of functional groups to the particle surface. Moreover, miniemulsion polymerization is not limited to free radical polymerization. The examples found in literature range from controlled radical polymerization, anionic and cationic polymerization, enzymatic polymerization, and polymerase chain reaction to polyaddition and polycondensation reactions, highlighting the versatility of the miniemulsion polymerization technique [1].

In addition to “simple” particle generation, the miniemulsion offers great opportunity for the encapsulation of small molecules, liquids, and solids in polymeric matrices or shells to generate functional hybrid nanomaterials for a wide variety of applications.

## 2 Encapsulation of Material Soluble in the Dispersed Phase

Compounds that are soluble in the dispersed monomer phase can be very easily integrated in a standard miniemulsion polymerization process, as illustrated in Fig. 1.

After dissolution of a desired amount of functional molecule, the two phase system is homogenized and subsequently polymerized. During the homogenization process, the added compound is homogeneously distributed among the generated droplets, ensuring that the concentration in the droplets is essentially the same concentration as in the bulk monomer phase before homogenization. Owing to the nanoreactor concept, the concentration remains at the adjusted value throughout the polymerization process. The final morphology of the nanocomposite is determined by the solubility of the added compound in the polymer. Full miscibility leads to

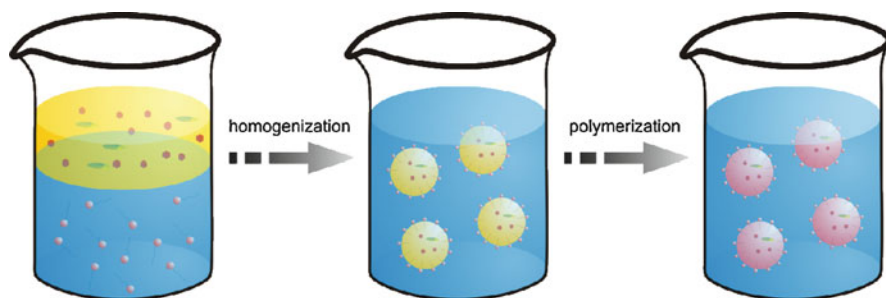


**Fig. 1** Miniemulsion polymerization process in the presence of additional compounds added to the monomer. *Left:* Two-phase system consisting of an aqueous surfactant solution (*lower phase*) and a monomer phase (*upper phase*) containing the costabilizer and the functional compound. *Middle:* Nanodroplets of same size containing the functional molecules. *Right:* Polymerized particles with the encapsulated component

a solid solution in which the compound is homogeneously distributed all over the polymeric matrix. If the component becomes insoluble in the polymer, phase separation occurs and leads to smaller or larger domains, which can be distributed as microdomains all over the matrix or assemble to form a core-shell structure.

## 2.1 Dyes

Dyes have not only been encapsulated for the generation of colored or dye-labeled beads or for protection of the dye, but also for investigation of the miniemulsion polymerization process, especially droplet nucleation and particle formation [11–16].

Musyanovych et al. [17] investigated the particle formation process in miniemulsions containing styrene plus an additional positively aminoethyl-methacrylate (AEMH) or negatively charged acrylic acid (AA) comonomer in the presence of the nonionic surfactant Lutensol AT50. The fluorescent dye *N*-(2,6-diisopropylphenyl)perylene-3,4-dicarboximide (PMI) was added to the monomer phase as probe. The authors observed that in contrast to pure polystyrene (PS) particles, the particles prepared with a high amount of functional comonomer result in bimodal size distribution. By evaluating the PMI content in the fractions of the large and the small particles, it was found that the dye concentration was the same in both fractions. Such a situation cannot be generated by monomer diffusion or secondary nucleation (see Fig. 2) because different PMI concentrations in the fractions are to be expected. Diffusion of monomer from smaller to larger particles without the diffusion of PMI would lead to a high PMI concentration in the smaller particles and a lower concentration in the larger particles because the amount of PMI remains the same and the amount of monomer changes. Particles generated by secondary nucleation should be free of dye. Only the so-called budding-effect can explain the equal dye concentrations found in both fractions.

The encapsulation of different types of fluorescent dyes gave evidence for the protection of encapsulated molecules from environmental influences by a polymeric shell. Although the particles are about 100–200 nm, which means that the actual barrier created by the polymeric shell is less than 100 nm, the protection against water or oxygen is highly efficient.

It is well known that the luminescence of lanthanide complexes is quenched by the presence of water, as  $\text{OH}^-$  vibrations can interact and thermally relax the excited lanthanide states [18]. After encapsulation of the europium- $\beta$ -diketonato complexes europium-(2-naphthoyl trifluoroacetone)<sub>3</sub>,  $\text{Eu}(\text{NTFA})_3$ , and europium-(2-naphthoyl trifluoroacetone)<sub>3</sub>(triethylphosphine oxide)<sub>2</sub>,  $\text{Eu}(\text{NTFA})_3(\text{TOPO})_2$ , in a PS matrix, the quantum yield observed for the encapsulated complex in the presence of water was significantly higher (about four times) than without the polymeric shell, indicating protection from environmental water [19].

Pyrene was used as a fluorescence probe by several authors [20–22]. Bradley et al. [20] used poly(methylmethacrylate) (PMMA) as matrix to prepare pyrene/

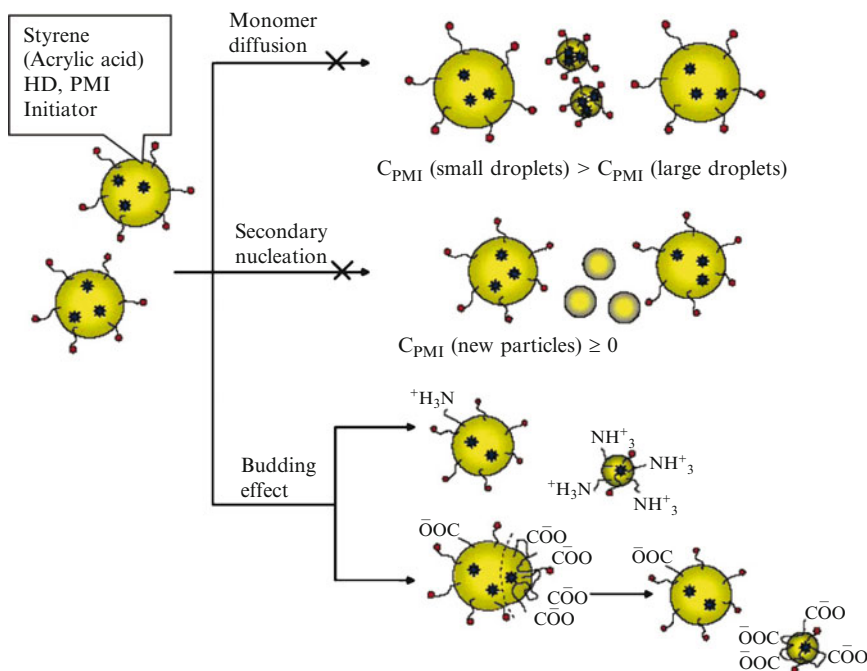


**Fig. 2** Mechanism for the emergence of a bimodal particle distribution after miniemulsion copolymerization of styrene with charged comonomers in the presence of Lutensol AT50

PMMA hybrid particles of less than 100 nm. The authors found that the lifetime of encapsulated pyrene was 520 ns, irrespective of the oxygen concentration (a quencher for pyrene fluorescence) in the dispersion. In solution, the lifetime of pyrene was 20 ns in air and increased to 118 ns in nitrogen atmosphere. Additionally, it could be shown that the fluorescent dye could be efficiently protected from water-based quenchers. Even in the presence of  $\text{Ti}_2\text{SO}_4$ , a highly efficient quenching agent for pyrene fluorescence, no reduction of the fluorescence lifetime was observed, which also indicates that no pyrene can be found on the particle surface. The incorporation of pyrene and some of its derivatives in a PS matrix showed comparable results [21, 22]. It is interesting that pyrene, as a molecularly dissolved component in the PS matrix, does not show excimer emission until high concentrations in the matrix are reached [21, 22]. This means that the molecules are efficiently separated by the phenyl rings of the PS matrix. Using a polymerizable pyrene-based comonomer in the same concentration as pyrene, excimer formation was observed, indicating less effective separation due to the introduction of the polymerizable group [22].

Colored latexes or nanocolorants have been proposed as a new class of colorants, in addition to conventional dyes and pigments, that combine the advantages of both classes while overcoming their disadvantages. Although dyes show excellent color saturation and contrast, their poor thermal and light stability and their low resistance against water limits their application as water-based inks. Pigments, on the other

hand, are generally highly stable against environmental influences but show low color brilliance and low image gloss. Additionally, the size of the pigment particles has to be reduced by means that consume energy and time, and thus money. Because nanocolorants are polymeric nanoparticles with encapsulated and protected dye, one can imagine that the advantages of both of the conventional colorants are indeed combined. Several dyes have been used for the preparation of colored latexes. Takasu et al used phthalocyanine dyes as well as styryl or azo dyes [23–25] to investigate the aggregation state of the dyes in the polymeric matrix and the “leaking” of the dyes as a function of their bulkiness. Diffusion from the composite particles into the aqueous phase of a nanocolorant dispersion can be limited by either using a bulky dye, thus increasing the stiffness of the polymeric matrix (e.g., by crosslinking), or by the introduction of an impermeable shell around the particles [23]. Here, a polyurea shell limited the leaking of the dye from the particles [24].

Sudan Black B, a dye insoluble in monomers could be encapsulated by mixing a 50 wt% Sudan Black B solution (methylisobutyl ketone) with styrene and subjecting the mixture (1:1) to subsequent miniemulsion polymerization. After polymerization and evaporation of the solvent, phase separation occurred and the dye was encapsulated by a polymeric shell, which effectively protects the dye from photodegradation induced by UV-activated oxygen [26].

Co-encapsulation (which is essentially limited to the miniemulsion technique) of a hindered amine acting as radical scavenger improved the photobleaching performance of the encapsulated dye [23].

With a modified miniemulsion technique using the encapsulated dye and preformed PS ( $M_w = 50,000 \text{ g mol}^{-1}$ ) as hydrophobic costabilizer, the dyes solvent green, solvent yellow, solvent blue, and solvent red could be encapsulated in a PMMA matrix [27, 28]. Depending on the concentration and the dye, phase separation occurred during the generation of the composite particles to form dye crystallites enclosed by a polymeric shell [27]. In the dispersed state, the dyes interact with the polymeric matrix, which is manifested by a small but significant bathochromic shift of the absorption maxima [28].

By copolymerizing a stimuli-responsive polymer/hydrogel layer around a colored nanoparticle of PS-*co*-PMMA, color-changing latexes could be prepared. The hydrogel can switch from a collapsed hydrophobic to a swollen hydrophilic layer around the central particle, changing the local refractive index and, consequently, the color intensity of the latex. Using poly(*n*-isopropylacrylamide) (PNIPAM) [29], the layer reacts to temperature changes, and using poly(2-(diethylamino)ethyl methacrylate) (PDEAEMA) [30], the layer reacts to changes in the pH of the aqueous continuous phase.

Photochromes are a special class of dyes. After irradiation with a specific wavelength, generally in the UV range, these dyes change their chemical structure (e.g., cyclization). The newly formed compound shows different spectral properties (“color”) to the original structure. After irradiating such dyes with a second characteristic wavelength, usually in the visible range, the structural change is reversed and the original chemical structure and, consequently, the original color is regenerated. Integrating these compounds in nanosized polymeric matrices allows, e.g., the formulation of color-changing inks.



Several photochromes of different structures (diarylethene and spirobenzopyran) were encapsulated in PS matrices to form composite nanoparticles with diameters between 70 and 150 nm [31]. TEM images did not show phase-separated dye crystals in the nanoparticles. Hybrid films were prepared by spin-coating and investigated for their photochromic properties. After UV irradiation, the films changed their color according to the embedded photochrome. The reversibility of this process was shown by irradiation with light of 500–650 nm, which reinstalled the original state.

The above-mentioned possibility for the co-encapsulation of two or more compounds in exact relative amounts enables the preparation of “photoswitches.” Furukawa et al. [32] co-encapsulated a boron-dipyrromethene (BODIPY)-based dye (top, Fig. 3) in combination with (*cis*-1,2-bis(2,4,5-trimethyl-3-trienyl)ethane (CMTE), a photochromic dye. CMTE changes from the two-ring structure (left, Fig. 3) to the condensed three ring structure (right, Fig. 3) through irradiation with UV light. By applying visible light of the correct wavelength (broad maximum at 518 nm), the change can be reversed. Before irradiation with UV light, the BODIPY dye exhibits its normal fluorescence properties: excitation at 488 nm and emission at 510 nm. After irradiation with UV light, the three-ring structure of CMTE efficiently quenches the fluorescence of the excited BODIPY dye as the energy is transferred by a Förster-type resonance effect. After energy transfer, the

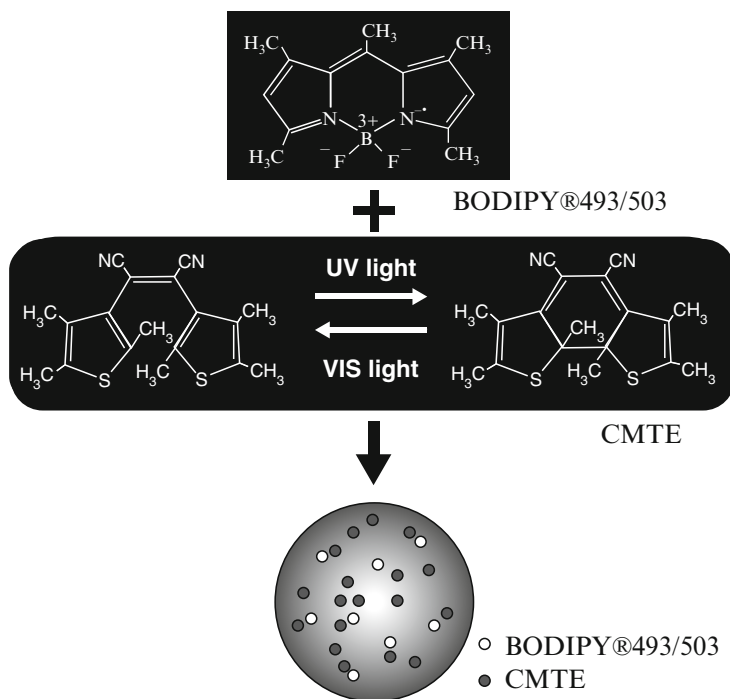


**Fig. 3** Co-encapsulation of BODIPY and CMTE [32]. Copyright Wiley-VCH Verlag GmbH & Co. KGaA. Reproduced with permission

two-ring form of CMTE is reformed and the excited BODIPY state is no longer quenched. The particles fluoresce as they did before UV irradiation. The switching efficiency is dependent on the distances between BODIPY and CMTE. Hence, at higher concentrations and, consequently, less distance, the energy transfer is more efficient.

Comparable photoswitchable fluorescent nanoparticles with other fluorescent dye/photochrome systems were prepared by Hu et al. [33, 34]. Here, a spirobenzopyran (BTF6) was co-encapsulated with solvent green 5, disperse yellow 184 [34] and solvent yellow 44 [34]. Due to the spectral overlap of the open-ring form of BTF6 with the emission wavelengths of the respective fluorescent dyes, the fluorescence emission could effectively be quenched and transferred to the encapsulated BTF6.

### 2.1.1 Biomedical Application of Dye-Labeled Nanoparticles

Polymeric nanoparticles have been proposed for several biomedical applications ranging from drug delivery to cell labeling [35]. As the polymeric particles are in the size range of 100 nm, detection is only possible via electron microscopy or particle labeling. Traditionally, nanoparticles are labeled with radioactive isotopes (e.g.,  $^{14}\text{C}$  [36],  $^{125}\text{I}$  [37]), which can easily be integrated in the polymeric matrix with conventional emulsion polymerization because the radiolabeled monomer is chemically identical to the non-radioactive compound. More popular and powerful is fluorescence labeling of bioactive molecules or particles because several dyes with different fluorescent colors can be applied. Introduction of a fluorescence label to nanoparticles via surface reactions, or particle coating with a fluorescent polymer (e.g., FITC-dextran [38]) is possible with preformed polymeric nanoparticles. Adsorbed dyes are prone to desorption and alter the surface of the nanoparticles, which might also affect the response of biological systems to the nanoparticles. The integration of markers in the particles can label them without alteration of the particle surface. Here, the miniemulsion polymerization technique offers the unique possibility of directly introducing hydrophobic fluorescent dyes into a polymeric matrix. Besides the possibility of applying a wide variety of monomers, the nanoparticles can be surface-functionalized in situ via the addition of functional co-monomer to the miniemulsion.

The ability of different cell lines to internalize polystyrene nanoparticles with different densities of amino or carboxy surface-functionalization was investigated quantitatively using fluorescence-activated cell sorting (FACS), and qualitatively using confocal laser scanning microscopy. Both techniques are based on the reliable and uniform distribution of the fluorescent dye among the nanoparticles [39, 40]. Here, the highly hydrophobic dye PMI is used. As the amount of dye in the nanoparticles is known and, as the nanoparticles are prepared with the miniemulsion technique, it can be assumed that each particle contains essentially the same amount of dye; therefore, quantification of particle uptake is possible. The experiments showed that especially the highly amino-functionalized nanoparticles

are favorably internalized in all of the investigated cell lines. Surface functionalization with carboxylic groups also slightly enhances the particle uptake compared to that of plain, non-functionalized PS nanoparticles. In order to investigate the actual uptake path into HeLa cells, positively and negatively charge PS nanoparticles of the same size were applied in combination with selective inhibitors for different uptake mechanisms [41]. By quantification of the incorporated fluorescent dye it could be shown that the uptake is energy-dependent and involves F-actin and dynamin, irrespective of the surface charge of the particles. Additionally, macropinocytosis seems to be important for the uptake of the positively charged nanoparticles.

Besides the above-mentioned experiments using PS-based nanoparticles, PMI could be successfully incorporated into phosphate-functionalized PMMA and PS [42], polyisoprene (PI), PS-*co*-PI [43], polyester [44], and poly(butylcyanoacrylate) (PBCA) [45, 46] matrices (Fig. 4) for the investigation of cellular response to these polymeric nanoparticles. It could be shown that the internalization in different cell lines depends on the cell line, the polymer, and the surface functionalization of the nanoparticles.

Moreover, PBCA nanoparticles were also applied to *in vivo* studies on their ability to permeate the blood–brain barrier (BBB). The results (Fig. 5) showed that, depending on the particle dose applied to rats, the particles are located in the brain blood vessels (45 mg) or can cross the BBB (200 mg). The results were confirmed through investigations of the blood–retina barrier (comparable to BBB) [45].

So-called dual-marker particles are functionalized with dye and magnetite simultaneously. Magnetite label can be detected *in vivo* by altering the contrast in magnetic resonance tomography experiments, while the location of the fluorescent dye can be investigated by fluorescence or confocal laser scanning microscopy [47–49].

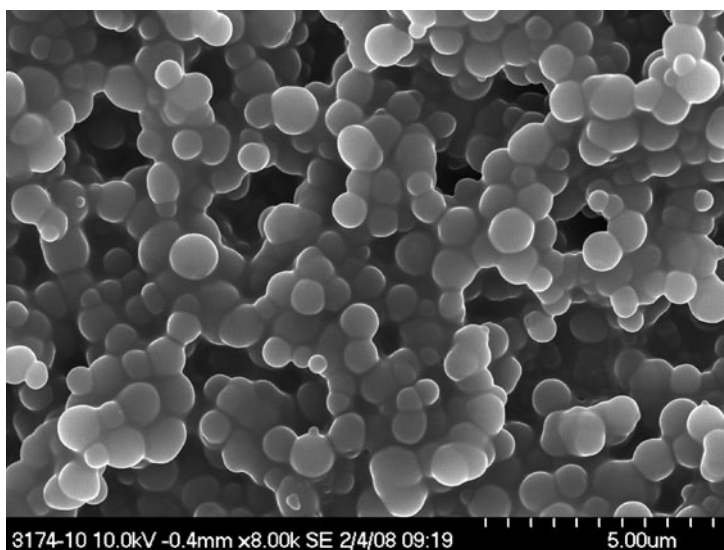


**Fig. 4** SEM image of PBCA nanoparticles with encapsulated fluorescent dye PMI

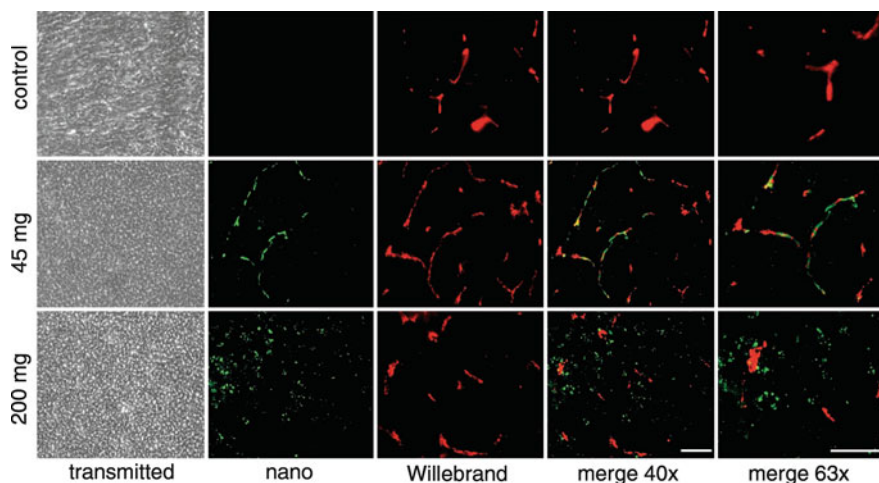


**Fig. 5** Cryosections of rat brain after administration of 45 and 200 mg of PBCA nanoparticles. *Transmitted*: optical transmission images of the sections (40 $\times$ ). *Nano*: green fluorescence created by the PMI-labeled nanoparticles. *Willebrand*: endothelial cells stained with red fluorescent antibody (von Willebrand factor primary and anti-IgG secondary antibody with fluorescent label). *Merge 40 $\times$*  and *merge 63 $\times$* : images merged from the green and red channels. *Scale bars*: 100  $\mu$ m [45]

Hydrophilic dyes were encapsulated in nanogels using the inverse miniemulsion polymerization method. The crosslinked poly[oligo(ethylene glycol) monomethyl ether methacrylate] (POEOMA) nanogel was prepared by using atom transfer radical polymerization (ATRP) in Span80-stabilized aqueous droplets. A polymeric dye [rhodamine isothiocyanate (RITC) dextran] [50] could be incorporated in the systems, as could rhodamine in combination with doxorubicin [51] or with bovine serum albumin and gold nanoparticles [52].

## 2.2 Metal Complexes

As mentioned above, organometal dyes, especially lanthanide-based dyes, have been used for the generation of dye-containing, colored latexes. Several other applications that do not exploit the optical properties of the metal complexes can also be found in literature.

Usually, the encapsulated compound is present in a finely dispersed state, distributed all over the polymeric matrix or in aggregates of different size, up to small crystallites (see above). Tetramethylheptadionate lanthanide ( $\text{Ln}(\text{tmhd})_3$ ) complexes, on the other hand, were found to generate spherical lamellar structures that resemble “nano-onions” [53] when used in a miniemulsion polymerization process with acrylate monomers. Although the exact mechanism of the layer formation and the exact composition of the layers remain the subjects of ongoing research, some facts have become evident. The special triangular-prismatic geometry of

the complex, which gives access to further coordination sites, seems to play a crucial role in structure formation because the corresponding octahedral  $\text{Al}(\text{2,2,6,6-tetramethylheptane-3,5-dione})_3$  complex did not induce structure formation. It has been speculated that either the complexes themselves assemble to the layer structures or that coordinative interactions between the carboxy functions of the acrylate monomers or sodium dodecyl sulfate (SDS) and the lanthanide ions generate entities that assemble to lyotropic subphases.

No structure formation was observed by Vancaeyzeele et al. [54] after the encapsulation of unsymmetrical lanthanide- $\beta$ -diketonato [lanthanide tris(4,4,4-trifluoro-1-(2-naphthyl)-1,3-butanedione)] complexes (where the lanthanide is Pr, Ho, La, Tb, or Eu) in crosslinked PS nanoparticles. Single-element as well as multi-element particles of different sizes could be prepared. The lanthanide content of the particles was investigated using inductively coupled plasma mass spectrometry (ICP-MS) and optical emission spectrometry (ICP-OES) and determined as 1000 complexes per particle. By evaluating the lanthanide content in the continuous phase after removal of the particles, they found that no complex leaks from the composite beads. With exact determination of the element combination and their relative amounts, an elemental signature can be attributed to one specific particle batch. Exploiting this feature, Vancaeyzeele and coworkers could monitor the amount of internalization of differently sized element-encoded particles in different, clinically relevant cell lines.

A novel approach for non-conventional nanolithography is also based on a miniemulsion process that includes the encapsulation of a hydrophobic metal complex [55, 56] in a polymeric matrix. Acetylacetonatoplatinum(II)-loaded PS nanoparticles of extremely narrow size distribution could be deposited in a highly ordered hexagonal array on hydrophilic Si substrates [55]. After deposition, the array was subjected to plasma and temperature treatment for removal of the polymer and annealing of the resulting metal particles, leading to a highly ordered array of platinum nanoparticles of ca. 10 nm, the size being dependent on the amount of Pt complex encapsulated in the PS beads. The Pt nanoparticles occupy the centers of the former composite particles and have interparticle distances that are determined by the size of the initial beads. Increasing or decreasing the initial particle size leads to larger or smaller distances between the Pt particles (Fig. 6). The size of the Pt particles can easily be adjusted by the amount of complex added to the monomer before polymerization. These arrays of perfectly ordered nanoparticles can be used to produce, e.g., arrays of silicon nanopillars or ordered arrangements of nanoholes in a Si substrate. Co-encapsulation of acetylacetonatoplatinum(II) and acetylacetonatoiron(III) in a stoichiometric ratio Fe:Pt of 1:1 led to the formation of a highly ordered array of FePt nanoparticles after the same treatment as described above.

### 2.3 Functional Organic Molecules

Sensitive or volatile substances such as drugs, initiators, or fragrances need to be encapsulated and protected for applications with a sustained demand of the respective

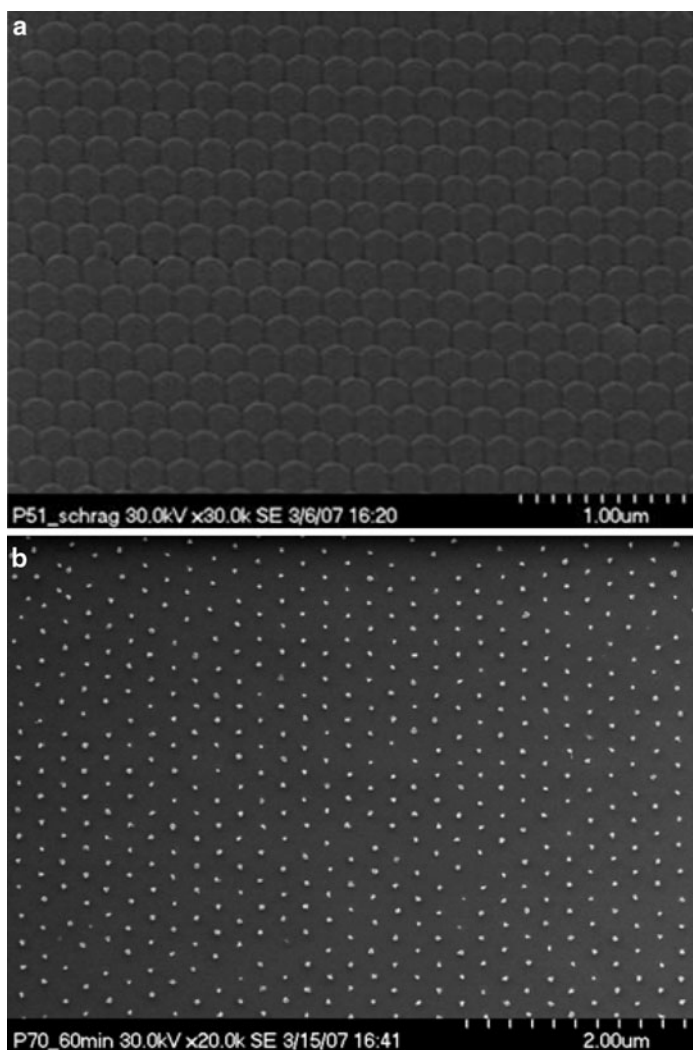


**Fig. 6** (a) Pt-containing latex after depositing a monolayer onto a silicon substrate. (b) Same substrate after exposing the deposited latex to an isotropic oxygen plasma for 2 h, and subsequently annealing the sample up to 850°C for a short period of time. The initial diameter of the latexes is 200 nm; the final diameter of the Pt nanoparticles is around 10 nm

compound. A further benefit of the polymeric shell is the possibility of controlling the release of the compound from the composite particles and, hence, its concentration in the environment.

By encapsulation in PMMA or PBA-*co*-PMMA, the acid-sensitive photoinitiator Lucirin TPO could effectively be shielded from acidic environments [57]. The hybrid particles are a typical example of a system in which a core-shell morphology (Fig. 7) is generated by phase separation during the polymerization process.

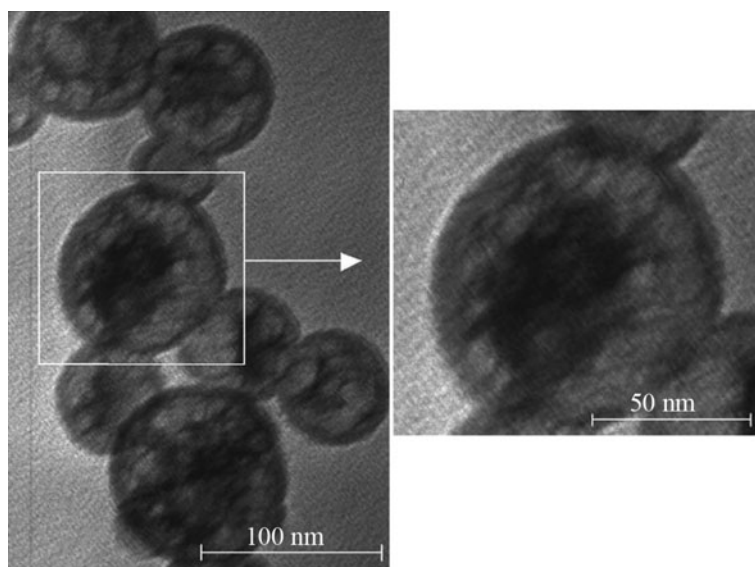


**Fig. 7** TEM images of encapsulated Lucirin TPO in polymer shells, clearly revealing core-shell morphology

Although the photoinitiator is readily soluble in the monomer(s), it is insoluble in the polymer. Thus, Lucirin TPO precipitates and forms an amorphous core surrounded by a polymeric shell. The encapsulation efficiency, which is the ratio of encapsulated material to material initially added to the system, was determined to be about 90%. The release of the initiator into the environment was investigated using isopropanol as solvent. Compared to a 50% release of Lucirin TPO after less than 1 min, the release from a crosslinked shell is significantly prolonged to about 5 min.

The encapsulation of a volatile fragrance was shown by Theisinger et al. [58]. The authors used 1,2-dimethyl-1-phenyl-butyramide (DMPBA) (bp 41°C) for encapsulation in PS, PMMA, poly(butylmethacrylate) (PBMA) and copolymers to adjust the  $T_g$  of the polymeric particles. Hybrid particles with a ratio of 1:1 DMPBA to polymer could be prepared. Calorimetric measurements revealed the altered polymerization kinetics after the addition of DMPBA to the monomer. Full conversion was reached after significantly longer reaction times (150 min compared to 25 min for pure monomer). Additionally, the molecular weight is reduced by an increased amount of added amine. The release, which was gravimetrically determined, can be controlled by the amount of encapsulated material and the environmental temperature. Generally, higher fragrance content leads to slower release, and if the material is released at temperatures above  $T_g$  the loss is faster and more complete compared to release at temperatures below  $T_g$ .

In contrast to sustained release, some applications might require the liberation of the entire encapsulated material during a very short period of time, initiated by an external stimulus as temperature. To achieve this goal, azoinitiators with high decomposition temperatures were encapsulated in polymeric matrices [59]. The idea



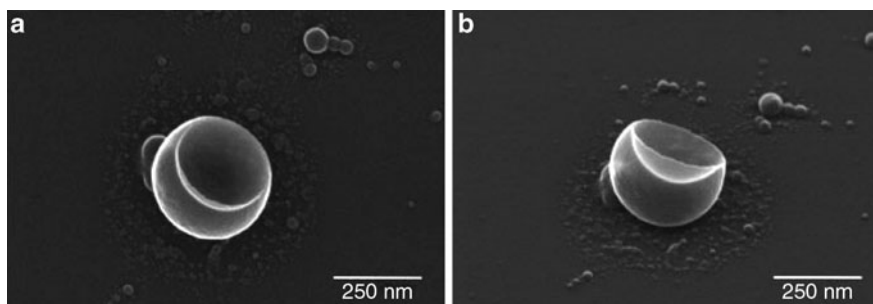


**Fig. 8** SEM image of nanoparticles with encapsulated azoinitiator after “nanoexplosion”: (a) top view, (b) plane tilted by 35°

is to decompose the encapsulated initiator very rapidly at elevated temperatures, producing a large volume of nitrogen that will literally blow up the nanoparticle and lead to a rupture in the particle wall – a “nanoexplosion” (Fig. 8). Encapsulated material would thus be released all at once, triggered by increased temperature. It is important that the decomposition temperature is chosen below the  $T_g$  of the polymer, otherwise the generated gas can escape from the particles without breaking the shell.

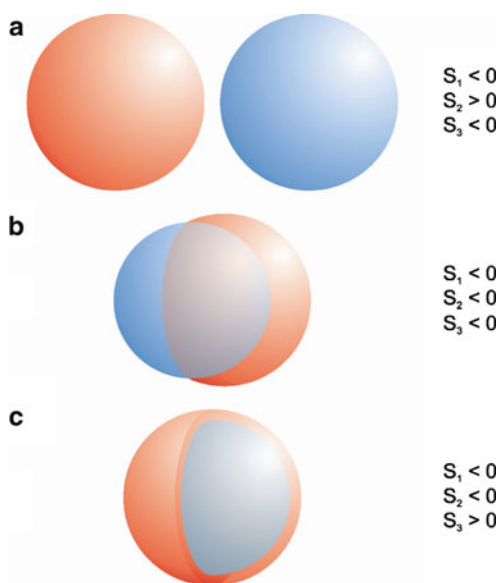
### 3 Capsule Formation

Particles with liquid (aqueous or organic) or hollow interior are generally termed capsules. In contrast to solid particles, capsules can, for example, accommodate and protect aqueous solutions of sensitive structures such as proteins or DNA. Additionally, thin capsule shells with adjusted material and porosity can guarantee rapid exchange of solvent with the capsule exterior but keep the (functional) encapsulated material in the interior. In addition to the well-known layer-by-layer approach, with or without the use of sacrificial cores [60, 61], the miniemulsion technique is an ideal candidate for capsule formation and provides several ways for the formation of polymeric capsules in the range of several hundred nanometers. The formation of inorganic capsules (e.g., [62]) by miniemulsion polymerization is also possible. For the formation of polymeric nanocapsules, three general techniques can be distinguished and will be discussed in detail:

1. Capsule formation by phase separation (Sect. 3.1; Fig. 10)
2. Generation of polymer at/from the interface (Sect. 3.2.2; Fig. 13)
3. Nanoprecipitation of polymer on preformed nanodroplets (Sect. 3.3; Fig. 18)

Irrespective of the technique applied for capsule formation, the resulting morphology delicately depends on thermodynamic and kinetic factors. The polymer used for the shell formation has to be sufficiently insoluble in the core liquid: if the solubility is too high, no phase separation can occur and homogenous structures are formed (i.e., particles or gels). If the phase separation cannot proceed “smoothly”

**Fig. 9** Equilibrium morphologies in a three-phase system. Phase 1, *blue*; phase 3, *red*; phase 2 is the continuous phase. (a) Non-engulfing, (b) partially engulfing, and (c) core-shell morphology



(e.g., when the viscosity of the system is too high, or in the case of restricted chain mobility by excessive crosslinking) the kinetics will determine the morphology of the resulting nanostructures (e.g., particles or multicore structures).

Thermodynamic considerations, based on the work of Torza and Mason [63], can predict the equilibrium morphology without the influence of kinetic factors. The studies were conducted with two immiscible organic liquids in water. Based on the interfacial tensions  $\gamma_{ij}$  and the respective spreading coefficients  $S_i$ , the equilibrium morphology could be predicted. The spreading coefficient  $S_i$  is defined as:

$$S_i = \gamma_{jk} - (\gamma_{ij} + \gamma_{ik})$$

Assuming that  $\gamma_{12} > \gamma_{23}$ , with subscripts 1, 2, and 3 denoting organic liquid 1, water, and organic liquid 2, respectively, the morphologies shown in Fig. 9 can be predicted.

Although the considerations give a general idea of the resulting morphology, surfactants that alter the interfacial tensions of the components are employed in miniemulsions, and at least one component is not a liquid but a high molecular polymer. Thus, more elaborate models have to be used for more accurate prediction of the equilibrium morphologies. These models are discussed in detail elsewhere [64].

### 3.1 Capsule Formation by Phase Separation

This technique is suitable for the encapsulation of hydrophobic liquids. The basic steps are shown in Fig. 10.

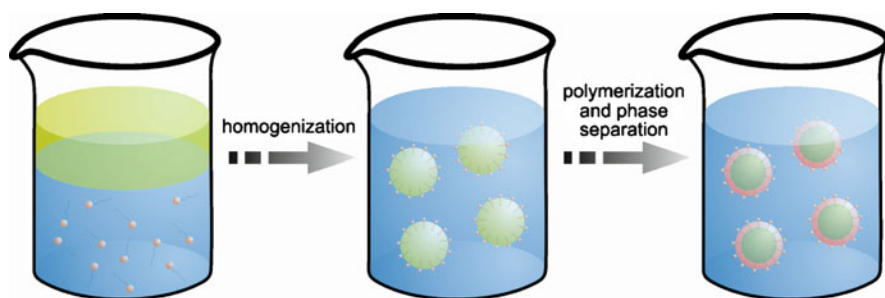


**Fig. 10** Capsule formation by phase separation. A solution of monomer and hydrophobic oil (*left*) is dispersed in an aqueous surfactant solution (*middle*). Phase separation between the growing polymer and the oil occurs, leading to core-shell morphology with encapsulated liquid (*right*)

Here, the disperse phase of the direct miniemulsion consists of an organic liquid (usually a long chain hydrocarbon or a triglyceride), which is a solvent for the monomer(s) but a nonsolvent for the emerging polymer. When the polymer has the proper hydrophilicity and interfacial tensions with the other phases, phase separation occurs in a way that the nonsolvent is engulfed by the growing polymeric shell, eventually leading to complete encapsulation of the organic liquid.

The importance of the polymer is underlined by the work of several authors [65, 66]. Generally it was found that an increase in the polymer's hydrophilicity favored the formation of capsules, while the application of hydrophobic polymer, such as PS, yielded a mixture of capsules and particles. The copolymerization of styrene with MMA, AA [65], methacrylic acid (MAA) [66] or NIPAM [67] led to the formation of a large fraction of capsules, but solid particles were still generated. Using MMA [65] as monomer, capsules are generated. Their properties such as size and shell thickness can be adjusted by changing the ratio of monomer to hexadecane (HD), which is encapsulated. In a conventional miniemulsion polymerization of MMA with HD as osmotic pressure agent (MMA : HD = 24 : 1) particles of 70 nm are generated. Increasing the ratio of MMA:HD to 1:5, nanocapsules with a liquid core and sizes up to 160 nm are formed. The shell thickness constantly decreases with the amount of added HD. As mentioned above, the surfactant is another crucial factor in determining the final morphology. Decreasing the amount of SDS used for stabilization of the droplets/capsules from 4.1 wt% (with respect to the dispersed phase) to 0.6 wt%, the morphology changes from capsules to bowl-like structures and fragments of capsules. Here, the increase in interfacial tension changes the morphology of the structures. The same can be observed for the application of Lutensol AT50 (Fig. 11). In this case, the structures have larger diameters (230 nm) but show the same bowl-like shape as observed with a low amount of SDS [65].

Capsule morphologies could also be obtained by applying the biodegradable surfactant lecithin and the eco-friendly hydrophobe Neobee M5 (triglyceride) [68] after copolymerization of styrene and divinyl benzene (DVB), controlled by 2,2,6,6-tetramethylpiperidine-1-oxyl (TEMPO) and stabilized by poly(vinyl alcohol) (PVA) [69].

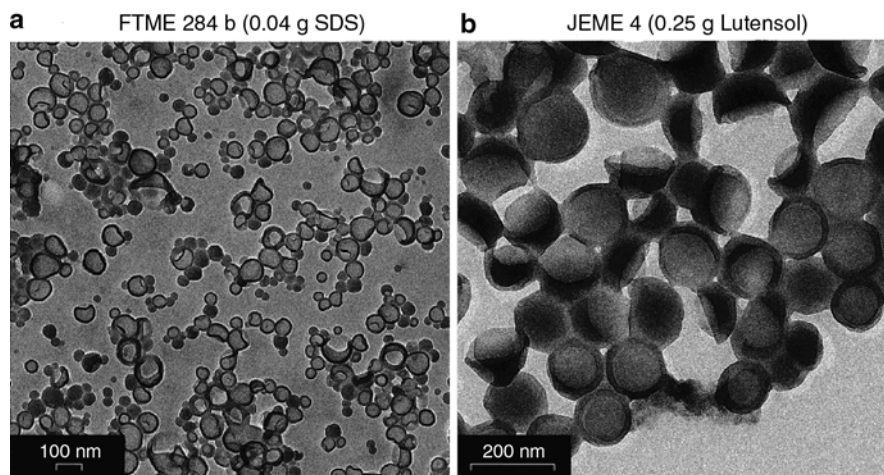


**Fig. 11** Coexistence of PMMA nanocapsules and capped particles in the presence of (a) low concentration of SDS and (b) Lutensol AT50 as stabilizer

### 3.2 Capsule Formation by Polymerization From or at the Interface

Another concept is to initiate the polymerization reaction from the interface to the center of the monomer-containing droplets, or to generate polymer at the interface. The first approach can be realized by interfacially active initiators or water-soluble initiators generating amphiphilic species that “anchor” the growing polymeric chain to the interface. Here, the monomer is only located in one phase. For the second approach, it is most convenient to have a hydrophilic monomer in the aqueous phase and a hydrophobic monomer in the organic phase – they only meet and react to polymer at the interface.

#### 3.2.1 Initiation at the Interface

In their effort to generate capsules from PS, Tiarks et al. [65] used the interfacially active initiator PEGA200, which increased the fraction of capsules in direct miniemulsions.

Ni et al. [70] generated organic/inorganic PS/silica shells around an inert hydrocarbon by copolymerizing styrene with methacryloxypropyltrimethoxysilane (MPS). The application of the hydrophilic comonomer MPS, potassium peroxydisulfate (KPS) as initiator, and a critical octane/monomer ratio led to the formation of polymeric shells. A subsequent condensation of ~40% of the silanol groups led to the formation of silica. The authors assign the capsule morphology to the presence of the hydrophilic comonomer favoring phase separation, with KPS being responsible for the above mentioned anchoring effect.

A detailed study, comparing the thermodynamic prediction for the equilibrium morphology with the experimental results, was performed using a system

comprising HD as core material, polybutylacrylate (PBA) as polymeric component, and KPS as anchoring initiator [71]. The thermodynamic model predicted an inverted core-shell structure with polymer engulfed by HD. The theoretical predictions stood in clear opposition to the experimental results. Although PBA is difficult to visualize due to its low  $T_g$ , evidence for core-shell structures with encapsulated hydrocarbon could be found. This difference is explained by kinetic factors, such as impaired diffusion, and most importantly by the initiation and propagation of the polymerization from the interface to the liquid droplet core.

Some insight into the kinetic requirements for the formation of polymeric capsules can be gained by the experiments of van Zyl et al. [72]. The authors investigated the controlled living polymerization of styrene for the encapsulation of isooctane. Two different RAFT agents (reversible addition fragmentation chain transfer) were employed in a miniemulsion polymerization process. Phenyl 2-propyl phenyl dithioacetate (PPPDTA) led to very fast polymerization reactions, whereas phenyl 2-propyl dithiobenzoate (CDB) retards the polymerization reaction. Again, KPS was used to fix one end of the polymer to the interface. The effect of KPS could clearly be shown in comparison to the application of *N,N*-azo-bis-(isobutyronitril) (AIBN). Using PPPDTA, a living polymerization with KPS and AIBN could be observed, but capsules were generated with only KPS. Initiation by using AIBN led to the formation of solid particles because no amphiphilic, anchoring species are generated, allowing the growing species to diffuse into the droplets. The combination of CDB and KPS could not generate capsules because the viscosity of the growing polymeric shell is not high enough to reduce the chain mobility sufficiently and also allow diffusion of the growing polymer into the droplet.

Living polymerizations can be restricted to the interface between an organic droplet and the water phase in a miniemulsion by using amphiphilic oligomeric RAFT agents. The thioester group was coupled to either PAA-*b*-PSS (polyacrylic acid-*block*-polystyrenesulfonate) oligomers [73] or SMA oligomers (styrene-maleic anhydride) [74, 75]. In the first case, NaOH solution is used to deprotonate the carboxylic acid groups, and in the second case ammonia is employed for ammonolysis/hydrolysis of the maleic anhydride, thus generating amphiphilic structures. The amphiphilic oligomers are also capable of stabilizing the miniemulsion droplets so that no additional surfactant is needed. Nevertheless, it could be shown that small amounts of SDS lead to the formation of a larger fraction of capsules.

Anionic polymerization of alkylcyanoacrylates (ACA) can also be performed at the interface between aqueous and organic phases. This reaction is suitable for the encapsulation of aqueous [76] as well as organic droplets [77]. Taking advantage of the fact that the polymerization is initiated by nucleophiles such as water, Musyanovych et al. [76] could form a shell of PBCA around droplets of an aqueous solution of DNA (790 base pairs). The droplets are generated by miniemulsification of the aqueous DNA solution in an inert continuous phase, which is miscible with the monomer BCA but is a nonsolvent for the polymer. As soon as the BCA is added to the inverse miniemulsion, polymerization is initiated at the droplet interface. Because the polymer is insoluble in the continuous phase and in the droplet phase, a shell around the droplets is formed. After completion of the polymerization, the

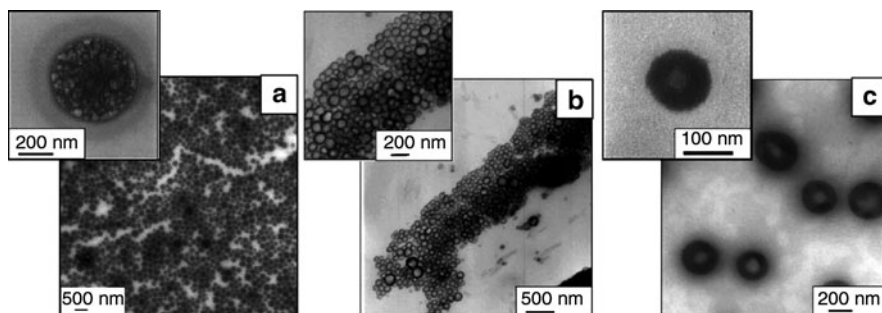


**Fig. 12** TEM images of PBCA capsules obtained in the presence of 5 wt% Span80 and different amounts of monomer butylcyanoacrylate: (a) 70, (b) 100, and (c) 200  $\mu$ L

capsules can be separated from the oil phase and redispersed in an aqueous solution of Lutensol AT50. The shell thickness (5–40 nm) and the morphology are dependent on the amount of monomer added (Fig. 12). The droplet/capsule size can be adjusted between 250 and 700 nm by the type and amount of stabilizer and the continuous phase. The least amount of coagulum and the most uniform capsules could be obtained using Miglyol 812N as continuous phase and a 2:3 mixture of Span80 and Tween80 as stabilizer. DNA could be encapsulated with 100% efficiency.

For the encapsulation of organic liquids, a solution of BCA in Miglyol 812N was dispersed in a methoxypoly(ethylene glycol) (MePEG)-containing aqueous phase [77]. MePEG bearing a hydrophilic OH group is capable of initiating anionic polymerization from the water phase, eventually generating the polymeric shell around the oil droplet. In the oil core, paclitaxel (for cancer therapy) could be encapsulated with 65% efficiency.

### 3.2.2 Generation of Polymer at the Interface: Polymerization and Polyaddition

Reports of interfacial radical copolymerization as well as of interfacial polyadditions can be found in the literature. Representatively, the formation of polymeric shells by interfacial reactions, the polyaddition in inverse miniemulsions, is shown in Fig. 13.

Interfacial copolymerization of hydrophilic vinyl ethers with hydrophobic maleates can be conducted in direct [79] and in inverse [80] miniemulsions, leading to encapsulation of organic liquids or water, respectively. The concept is based on two monomers that do not homopolymerize and are located in the organic and aqueous phase, respectively. The polymerization is initiated by an interfacially active azoinitiator. Regarding the system for encapsulation of organic liquids, thermal initiation (60°C) leads to coalescence and destabilization of the miniemulsion, and thus lower reaction temperatures (30°C) are required. UV initiation was also used for the generation of stable capsules.



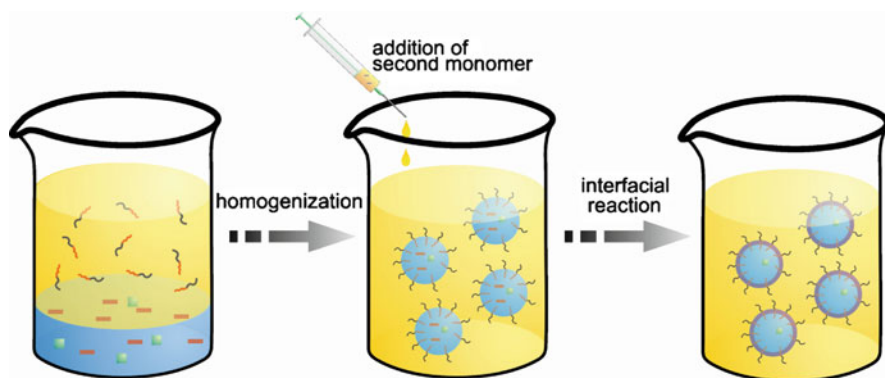


**Fig. 13** Formation of polymer shells by interfacial reactions, shown here with an inverse miniemulsion. *Left:* Aqueous dispersion containing a lipophile (which can also be a functional molecule, e.g., Gd(DTPA) [78]) and monomer A (e.g., diamine, diol) in an organic solvent (e.g., cyclohexane). *Middle:* Solution of monomer B (e.g., diisocyanate) in the same organic solvent used for preparation of the miniemulsion is added. *Right:* Polymeric shell is generated by interfacial polycondensation of monomers A and B

The inverse miniemulsion system was studied in more detail. It was found that the conversion is limited by the ability of the monomers to diffuse to and react with each other. Complete conversion could only be obtained at low monomer loadings of 2.5 wt% vinyl ether in the aqueous phase and an equimolar amount of maleate in the organic phase. Increasing the weight fraction of vinyl ether monomer to 10 wt% (maleate also adjusted), the total conversion drops to 40%. The addition of a crosslinker has the same effect, and also depresses the total conversion by restricting the monomer diffusion. Using hydrophilic maleate components, the total conversion can be increased from about 40% for dioctylmaleate to 100% for diethyl maleate. The more hydrophilic monomers can access the water phase, thus increasing the volume in which polymerization can take place. The authors could also show that the water-soluble dye Rhodamine B can be encapsulated and released from the capsules [80].

A more general approach without the need for highly specialized co-monomers is represented by the generation of polyurethane (PU) or polyurea (PUR) by interfacial polyaddition. Usually, the diol or diamine component is water-soluble, whereas the diisocyanate is hydrophobic and thus soluble in organic media. In analogy to the radical polymerization approach, polyadditions can be conducted in direct and inverse miniemulsions, giving rise to the possibility of encapsulating nonpolar and polar liquids. As mentioned before, the encapsulated liquids must not be a solvent for the generated shell if capsules are the desired morphology.

For direct miniemulsions, mostly isophorone diisocyanate (IPDI) [81, 82] was used because this compound slowly reacts with water, which is the main component of a direct miniemulsion. The reaction with water generates amine groups, which themselves can react with diisocyanates, leading to PUR as byproduct. Despite the application of slow-reacting diisocyanate, PUR is generally found in polymeric



shells generated by interfacial polyaddition in miniemulsion. The reactions can be performed with or without a catalyst [e.g., dibutyltin dilaurate (DBTDL)], in the organic phase. The diol component is added to the aqueous continuous phase, leading to capsules consisting of PU with urea units. In contrast to cationic or nonionic surfactants, anionic surfactants such as SDS were shown to be most suitable for stabilization of the capsules.

More interesting for biomedical applications is the encapsulation of aqueous (physiological) solutions. This can be accomplished by using the inverse miniemulsion technique [78, 83–85]. After stable aqueous droplets have been generated, the polymeric shell is generated by polyaddition, protecting the aqueous interior. Again, the hydrophilic diol or diamine is dissolved in the polar phase, while the diisocyanate is added via the organic phase. After the shell formation, it is possible to transfer the capsules to water for further applications. A wide variety of hydrophilic components can be used, ranging from diols and triols to polysaccharides as dextran or starch, and from diamines to an amine-bearing surfactant (Lubrizol U, a polyisobutylene-succinimide pentamine) that acts as a crosslinking surfmer [85]. The application of Lubrizol U for stabilization and crosslinking of PUR capsule shells leads to extraordinarily stable and water-impermeable nanoshells for the encapsulation of aqueous solutions of e.g., fluorescein (Fig. 14) [85].

Besides the application of water as dispersed phase in an inverse miniemulsion, it is also possible to disperse polar organic solvents such as dimethylsulfoxide, formamide, vinylpyrrolidone, or ethylene glycol in an inert hydrocarbon [e.g., cyclohexane, dodecane, or Isopar M (a mixture of several hydrocarbons)] [83]. Irrespective of the dispersed phase, the size can be controlled by the amount of the stabilizer. The lowest droplet/capsule size could be obtained for ca. 9% of the stabilizer poly[(ethylene-*co*-butylene)-*block*-ethylene oxide] [P(E/B-*b*-EO)], which has shown to be highly efficient at stabilizing any kind of inverse miniemulsion [86]. As the reaction of the diisocyanate with the diol or diamine is very fast, as confirmed by calorimetry, the mode of the diisocyanate addition to the reaction system is crucial. A quick addition leads to small capsules, resembling the size of the preformed droplets. Slow addition gives the components (with a low but recognizable solubility) in the polar droplets time to diffuse through the continuous phase, which leads to an increase in the droplet size. The thickness of the polymeric shell can be controlled by the total amount of reactants used. It could also be shown that reactions such as

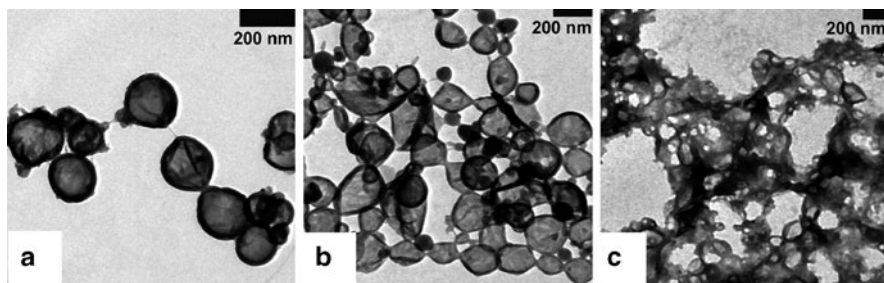


**Fig. 14** TEM images of polyurea capsules or frazzles prepared at different hexamethylenediamine/toluenyldiisocyanate molar ratios: (a) 1:2, (b) 1:1.5, and (c) 2:1 [85]

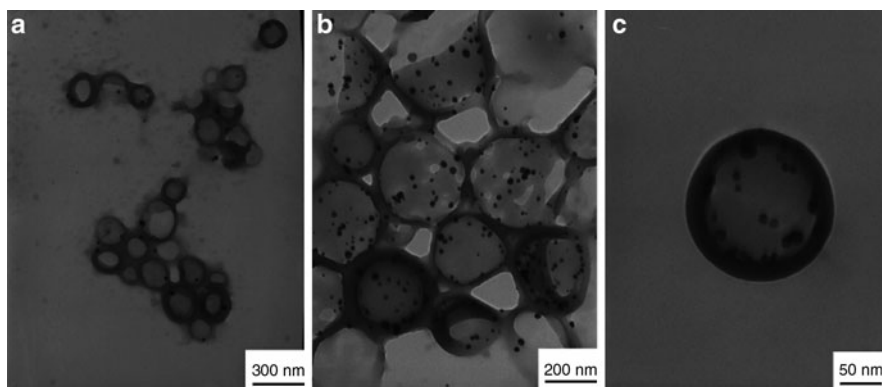


**Fig. 15** TEM micrographs of polyurea capsules loaded with different amounts of silver nanoparticles: (a) 30, (b, c) 120 mg  $\text{AgNO}_3$  in the aqueous phase

the reduction of  $\text{Ag}^+$  by hydrazine can be performed within the polymer enclosed area (see Fig. 15). The number of silver particles can be varied over a wide range.

The porosity of the particles could be shown by encapsulating an aqueous solution of a gadolinium-based magnetic resonance imaging (MRI) contrast agent [Gd-diethylenetriamine penta acetic acid (DTPA)]. As the Gd complex is still accessible by water from the capsule exterior, changing the water's proton relaxation time, it can be concluded, that the shell is porous and allows water to diffuse into the capsules, but restricts the complex to the interior [78].

A further step towards efficient biomedical application was shown by the work of Paiphansiri et al. [84]. Using a convenient carboxymethylation reaction with chloroacetic acid, it was possible to introduce carboxylic acid groups onto the PU/PUR particle surface (Fig. 16).

These groups allow physical and chemical immobilization of biologically active molecules as proteins. This could be shown by physically immobilizing gold-labeled IgG antibodies to the capsule surface (Fig. 17). Encapsulation of an aqueous solution of suforhodamine adds a fluorescent label for microscopic detection. By evaluating the capsule internalization in HeLa cells, it could be shown that negatively charged capsules are not taken up by the cells, and pristine capsules only to a very limited extent, whereas positively charged capsules [as obtained by adsorption of PAEMA or poly(ethylene imine) PEI on the surface] were very well internalized. These results are in good agreement with the data obtained from experiments with PS particles [35].

### 3.3 Polymer Precipitation on Preformed Nanodroplets

Nanoprecipitation can also be a very efficient method for the generation of polymeric shells encapsulating an aqueous core. The aqueous core is generated by miniemulsification and can be charged with the desired functional molecule, e.g.,

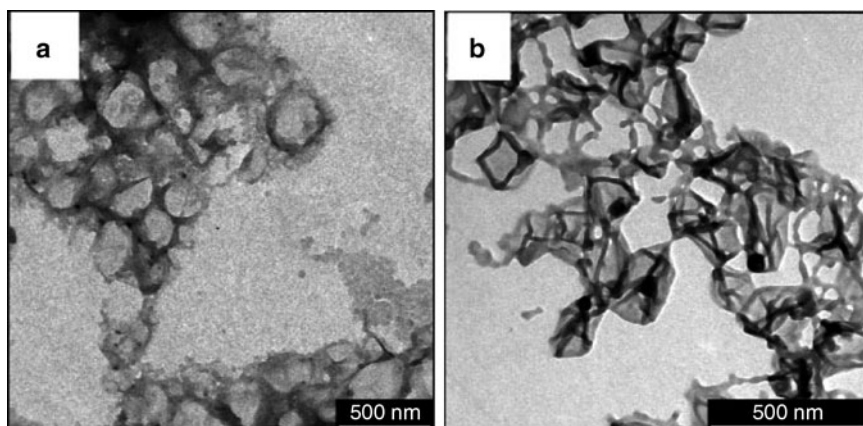


**Fig. 16** TEM micrographs of polyurethane nanocapsules prepared using hexadecane/toluenediisocyanate molar ratios of (a) 1:1.9 and (b) 1:2.25 from cyclohexane phase. The images were taken before the carboxymethylation reaction

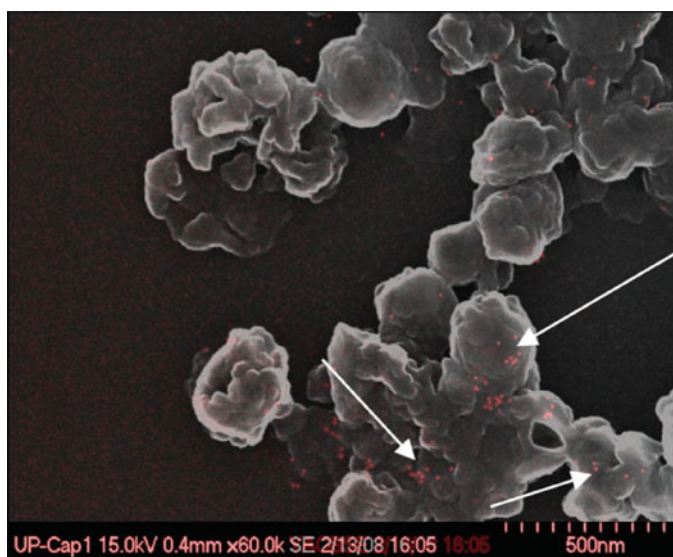


**Fig. 17** PAEMA-coated polyurethane capsules with physically adsorbed gold-IgG antibodies. Gold is visualized with the backscattered electron detector (indicated by arrows) in the SEM

the antiseptic chlorohexidine digluconate [87, 88]. The continuous phase of the miniemulsion consists of a mixture of a solvent (e.g., dichloromethane, DCM) and a nonsolvent (e.g., cyclohexane) for the polymer [e.g., PMMA, polycaprolactone PCL, or poly(methylacrylate) PMA]. After miniemulsification, the solvent is carefully evaporated and the polymer precipitates on the aqueous droplet (Fig. 18).

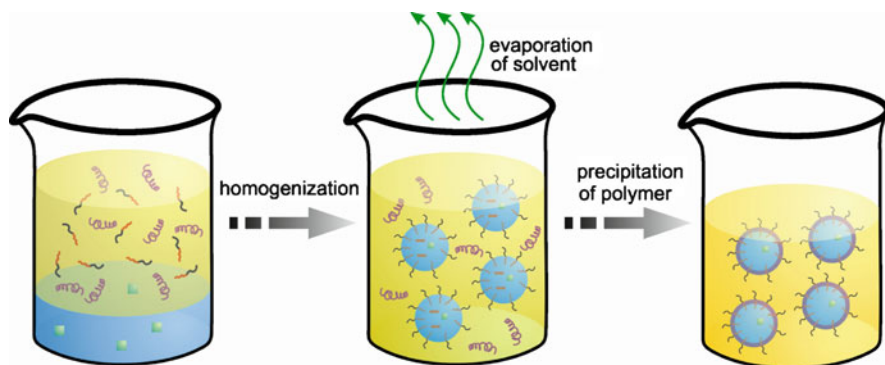


**Fig. 18** Formation of polymer capsules by polymer nanoprecipitation on preformed miniemulsion droplets. *Left:* An aqueous solution containing a lipophile (can also be a functional molecule, e.g., chlorohexidine digluconate [87, 88]) is dispersed in a solution of a polymer in a solvent/nonsolvent mixture. *Middle:* After homogenization, solvent is evaporated in a controlled manner. *Right:* The polymer precipitates on the aqueous droplets and eventually forms a polymeric shell

Irrespective of the molar mass of the precipitated polymer, the encapsulation efficiency of the aqueous core increases from 20% (100 mg polymer in 0.5 mL aqueous solution) to >90% (500 mg polymer in 0.5 mL aqueous solution). After redispersion in an aqueous SDS solution, it could be observed that the size increases, probably due to influx of water induced by osmotic pressure. After redispersion, the high molecular weight PMMA capsules ( $996,000 \text{ g mol}^{-1}$ ) retained their encapsulation efficiency, whereas the capsules prepared from lower molecular weight polymer ( $335,000$  or  $71,000 \text{ g mol}^{-1}$ ) lost some of their payload. The method is also suitable for other polymers (PCL, PMA). Although PCL encapsulation showed lower encapsulation efficiencies, PMA encapsulation led to an almost complete encapsulation of the chlorohexidine digluconate, but also to the formation of coagulum after nanoprecipitation (Fig. 19).

## 4 Encapsulation of Material Insoluble in the Dispersed Phase

Material insoluble in the dispersed phase includes inorganic crystallites such as iron oxide or titania, amorphous nanostructures (e.g., silica) with a size of 5–100 nm, organic pigments such as carbon black, or insoluble dyes. The main problem encountered during the encapsulation of such structures in polymer matrices is the interfacial tension between inorganic material, monomer/polymer and the continuous phase of the miniemulsion. Generally, inorganic structures are difficult to disperse in a typical organic monomer phase due to their hydrophilic character. Thus, the surface has to be made “compatible,” by hydrophobization. Typical examples are the coating of magnetic iron oxide nanoparticles with oleic acid, or

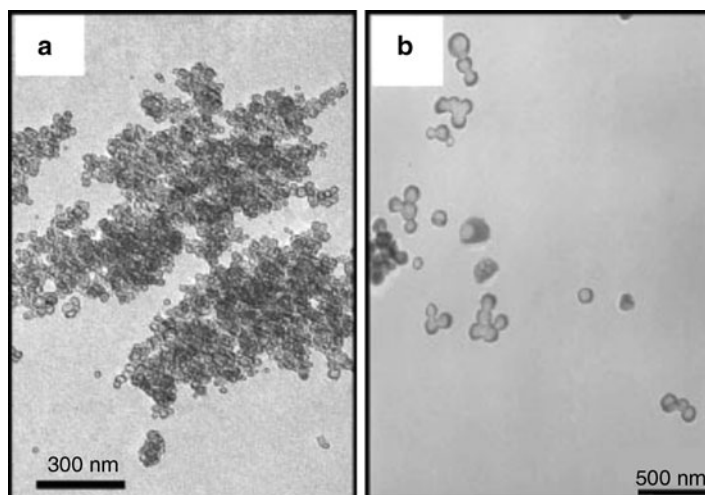


**Fig. 19** Capsule formation by nanoprecipitation with (a) PCL and (b) PMA [87]

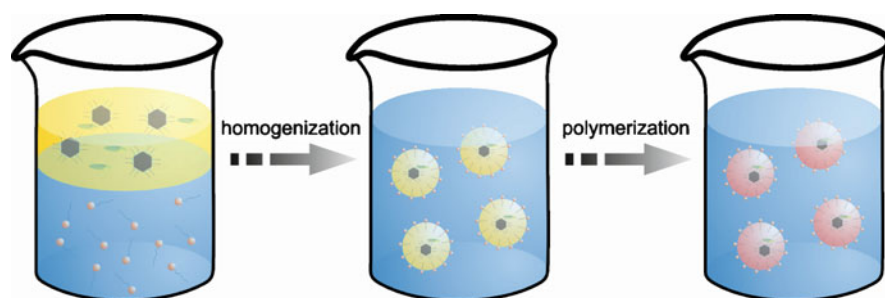


**Fig. 20** Encapsulation of insoluble material (*hexagons*) in miniemulsion. *Left*: The insoluble material is hydrophobized with a compatibilizer and dispersed in the monomer phase (with costabilizer). *Middle*: This dispersion is subsequently homogenized with an aqueous surfactant solution. *Right*: The composite particles can be generated by polymerization

the surface reaction of silica with alkylsilanes (see below). Such surface-modified inorganic structures can be dispersed in a monomer phase and successfully encapsulated by polymeric shells (Fig. 20). Nevertheless, with an increasing amount of the dispersed material in the monomer phase, the viscosity becomes too high for an efficient dispersion in order to generate a miniemulsion. To overcome this limitation, the so-called co-sonication process, which is suitable for, e.g., organic pigments or magnetite, was established. Several examples are presented here to illustrate the principle, the limitations, and the possibilities for the formation of homogenous hybrid nanoparticles.

## 4.1 Organic Pigments and Carbon-Based Material

Dyestuffs that are insoluble in the matrix are usually referred to as pigments. Besides inorganic pigments such as titania, organic pigments such as carbon black and phthalocyanines are widely used in industry. As the pigments are usually structures of sub-100 nm size, they tend to aggregate due to their high specific surface. For a successful application, the use of single, separated pigment particles, preferably in form of an aqueous dispersion, would be ideal. Encapsulation in polymeric nanoparticles presents a way to efficiently separate the structures from each other, and moreover to protect the encapsulated material. Formulating the systems in water-based miniemulsions leads to water-based dispersions.

Direct dispersion of carbon black or organic pigments in the monomer (e.g., styrene) leads to increased viscosity of the organic phase, making it difficult to disperse this phase in aqueous media. Thus, only less than 10 wt% [89, 90] of the pigment can be dispersed in styrene and formulated as a miniemulsion. A great improvement, with respect to the amount that can be encapsulated, is given by the so-called co-sonication process (Fig. 26). Initially developed for carbon black [91], this technique was also applied for other organic [92] or inorganic pigments [93, 94].

Instead of directly dispersing the pigment in the monomer, in the first step of the process, a dispersion of the respective pigment in water is generated by ultrasonic irradiation and the pigment particles are stabilized by a surfactant (ionic and nonionic surfactants can be applied) [92]. This dispersion is mixed (usually with the help of ultrasound) with a miniemulsion composed of the desired monomer dispersed in water and stabilized with the appropriate surfactant. During the incorporation of the pigment in the monomer droplets, surfactant desorbs from the pigment, a process that is monitored by surface tension measurements [91]. The generated ad-mini-emulsions (adsorbed-mini-emulsion) exhibit distinct reaction kinetics, depending on the encapsulated material as it interacts with the polymerization initiator [92]. Complete encapsulation of up to 80 wt% of pigment could be shown by TEM and, in the case of carbon black, with nitrogen sorption measurements. Because carbon black exhibits a high inner porosity, a successful encapsulation dramatically reduces the specific surface area that is accessible for nitrogen. After encapsulation, only the surface provided by solid nanostructures can be measured [91].

The costabilizer plays an important role in the encapsulation of hydrophobic pigments in polymeric matrices, especially if the pigment is directly dispersed in the monomer phase. In addition to its original task of establishing an osmotic pressure to avoid diffusional degradation, it serves as mediator between the pigment surface and the monomer and the polymer, respectively. For carbon black, the use of HD, Jeffamine M2070, and M1000 [89] as well as a oligourethane-derived costabilizer [91] led to stable dispersions with uniform particles. The encapsulated pigment is not an efficient costabilizer (to build up the osmotic pressure in the droplets) as the aggregates do not induce sufficiently high osmotic pressure. In the case of phthalocyanine-based pigments, HD or hexadecanol were shown to be efficient ultrahydrophobes, whereas the application of PS ( $M_n = 35,220 \text{ g mol}^{-1}$  and  $M_w = 65,600 \text{ g mol}^{-1}$ ) induced phase separation [90].



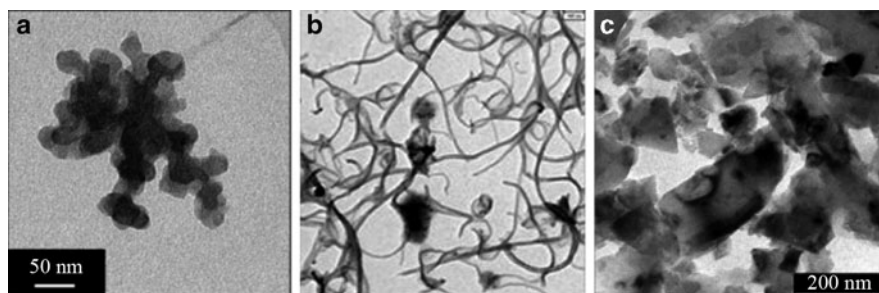


**Fig. 21** Carbon-based materials suitable for encapsulation in polymers: (a) carbon black, (b) carbon nanotubes, and (c) nanodiamond

Other carbon-based, hydrophobic materials used for the encapsulation in polymeric nanoparticles are nanodiamond (unpublished results from our laboratory) and single walled carbon nanotubes (Fig. 21).

Single-wall carbon nanotubes (SWNTs) are very promising materials for innovative electronic applications, like novel electrode materials and highly effective reinforcements for polymeric systems, because of their extremely high tensile strength. Despite the high potential, actual application is difficult because the nanotubes tend to aggregate due to their high surface area and  $\pi$ - $\pi$  interactions. A very simple, but not very effective and only temporary approach is the generation of a dispersion by separating the tubes by surfactants. More promising is coating of individual SWNTs with a polymer, creating a barrier that prevents aggregation of the nanotubes. Bearing in mind that polymeric nanoparticles prepared by the miniemulsion polymerization technique are in the range of few hundred nanometers, it seems to be obvious that the SWNTs (with a length of several micrometers) cannot be completely encapsulated in a polymeric nanoparticle generated in a miniemulsion. Nevertheless, the miniemulsion polymerization can provide a platform for coating the SWNTs with polymeric material of different kinds, mostly PS, PI, or their copolymers [95–98]. The structure is best described as a beaded-nanorod [97–99] (Fig. 22). Interestingly, SWNT dispersions prepared with anionic surfactants (SDS, 4-dodecylbenzenesulfonic acid SDBS) are reported to be unstable and thus not suitable for the miniemulsion process [95, 96] because the anionic surfactants tend to desorb from the carbon nanotubes in aqueous dispersion. In contrast, the application of cationic (e.g., cetyltrimethylammoniumbromide, CTAB) [95] or a combination of anionic and nonionic surfactants (SDS and Igepal DM-970) [98] leads to polymer-covered SWNTs. The resistance of carbon PS and PS-*co*-PI with dispersed (8.5 wt%) SWNT decreases to  $10^6 \Omega \text{cm}^{-1}$  compared to  $10^{16} \Omega \text{cm}^{-1}$  for the pristine polymer, indicating incomplete coverage of the SWNTs with polymer [95]. A similar effect was observed in a system of  $\text{LiClO}_4$ -doped polypyrrole (PPy)-coated SWNTs. An electrode from the composite material in Kynar FLEX showed higher conductivity than the pure polymer dispersed in Kynar [99].



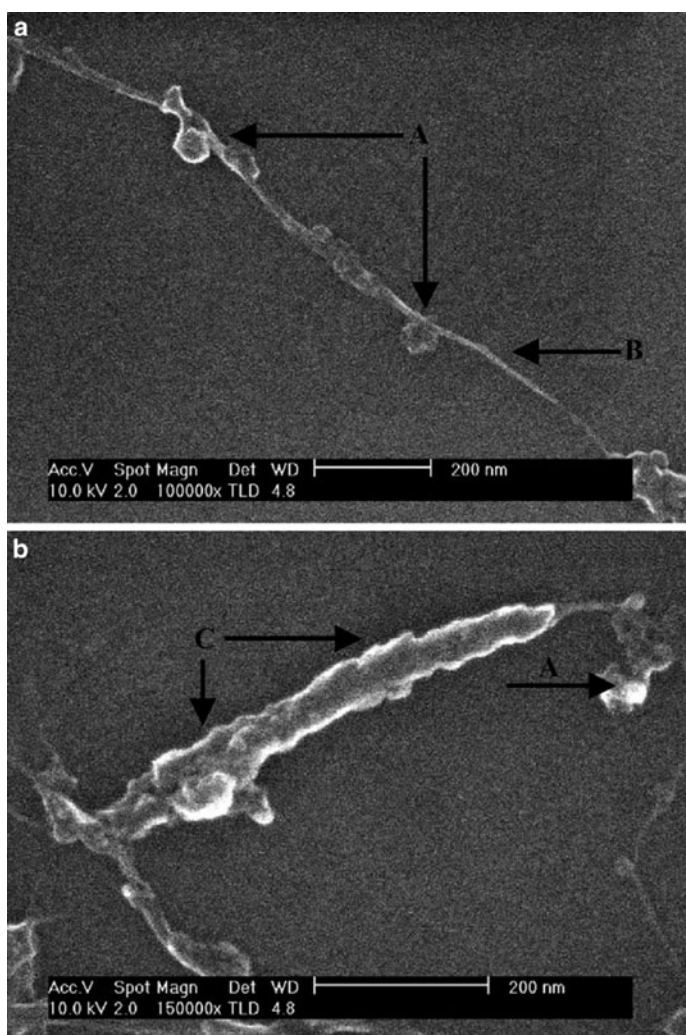


**Fig. 22** PPy-coated SWNT. (a) Beaded-nanorod morphology (A polymeric particles, B plain SWNT). (b) PPy film around SWNT (C PPy film). Reprinted from [99], copyright 2005, with permission from Elsevier

## 4.2 Inorganic Material

As mentioned above, inorganic surfaces are usually not compatible with nonpolar organic liquids as monomers. Thus, the crucial point in generating hybrid nanoparticles from polymer and inorganic (nano)structures is their surface modification for making the inorganics compatible to the organic monomer/polymer matrix. Most of the published work deals with silica, clay, and iron oxides, although some reports covering other inorganic material can be found (e.g., ZnO for UV-blocking

applications [100–102]). There are several reasons to incorporate inorganic material into polymeric matrices: protection of the encapsulated material [e.g., quantum dots (QDs)], protection of the environment from the encapsulated materials (e.g., Cd from CdS QDs), and the improvement of different properties of the polymer, among which the mechanical properties and gas diffusion properties have to be mentioned.

For the encapsulation in PS, the surface of calcium carbonate crystals was modified with stearic acid. With this modification, up to 5 wt% of the inorganic material could be directly dispersed in the monomer and subsequently encapsulated by miniemulsion polymerization [89]. For the encapsulation of alumina nanoparticles, oleic acid was used to generate hydrophobic surfaces [103]. Carbon-coated silver nanoparticles (0.5 wt%) could be incorporated in PMMA nanoparticles and increased the  $T_g$  by 14°C [104]. Another method for the generation of Ag/polymer hybrid nanoparticles was presented by Crespy et al. [105]. By using non-aqueous inverse miniemulsions with high-boiling solvents, it is possible to generate silver nanoparticles *in situ* by the reduction of silver nitrate via the polyol route. The dispersed phase, *N*-vinyl pyrrolidone (NVP), DMSO, 2-pyrrolidone, or ethylene glycol, can efficiently be stabilized by P(E/B-*b*-EO) alone or in combination with poly(vinylpyrrolidone) (PVP), despite temperatures of >150°C. Although droplet collisions and thus coalescence are highly favored at these temperatures, the droplets of, e.g., 2-pyrrolidone stabilized with the above-mentioned surfactant combination, retain their size of 180 nm for 20 h. The addition of silver nitrate and ethylene glycol to NVP can be used to simultaneously reduce the silver ions to metallic silver nanoparticles (reaction volume restricted to droplet) and polymerize NVP to generate a polymeric matrix around the metallic nanoparticles (Fig. 23).

Detailed studies were conducted on the encapsulation of hydrophilic and hydrophobic titania nanoparticles in PS. The inorganic nanoparticles were surface-modified with polybutylene succinimide diethyl triamine (OLOA370), which has been shown to be the most efficient surfactant for enabling the dispersion of titania in styrene [106–110]. After separation of the product particles by centrifugation in a density gradient, the encapsulation efficiency was calculated. Up to 89% of

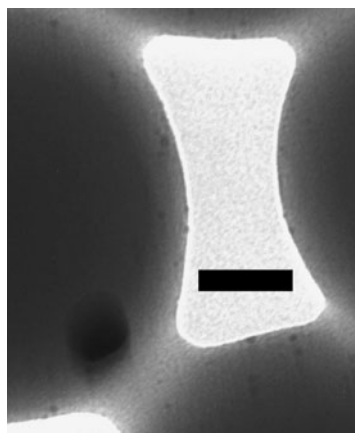


**Fig. 23** TEM micrograph of Ag/PVP hybrid nanoparticles prepared in inverse miniemulsion at high temperatures. Scale bar: 50 nm [105]

the titania could be encapsulated in 73% of the PS. This means that not all the titania was encapsulated and that pure PS particles were generated as well, most probably by secondary nucleation in the aqueous phase. Another efficient compatibilizer for titania is Solsperse 32,000, a polyamine/polyester. By modifying titania with this polymer, hybrid nanoparticles with PS and PS-*co*-PBA could be generated [111–114].

As already mentioned, the generation of fluorescent nanoparticles is of great interest for biomedical applications. An alternative to the widely used organic dyes are fluorescing nanocrystals, as lanthanide-based [115] or, more commonly, as semiconductor QDs. Because the QDs are generally composed of highly toxic elements such as cadmium, selenium, or tellurium, it is absolutely imperative that biological systems are protected from these materials. Thus, the encapsulation in polymeric matrices provides an excellent way to convert QDs into a more biotolerable form. CdS or CdSe QDs are generally prepared by a process that caps the nanocrystal with trioctylphosphine oxide (TOPO), generating a highly hydrophobic shell. This allows the direct dispersion of the QDs in the monomer and a subsequent miniemulsion polymerization procedure. Different coatings can be introduced (e.g., with vinylmercaptobenzene [116] or hexadecylamine [117]), but do not interfere with nor improve the integration into the polymer. Hybrid particles with PS [116–119] or PBA matrices [118, 120] could be prepared and characterized with respect to their photoluminescent properties. The radicals generated during the polymerization process seem to interact with the QDs because their emission frequency is shifted, indicating a changed size [118, 119]. Besides the commonly used CdX (X = S or Se) QDs, CdTe stabilized by 3-mercaptopropionic acid could be homogeneously incorporated in PS nanoparticles by the use of OV-DAC (octadecyl-*p*-vinylbenzyltrimethylammonium chloride) or DVMAC (didecyl-*p*-vinylbenzyltrimethylammonium chloride) as phase transfer agent [116]. These additives prevent the system from phase separation, which pushes the QDs to the outer region of the polymeric particles, where they might be prone to environmental influences (see, e.g., [117]). Another possibility for overcoming the inhomogeneous distribution of QDs in polymeric particles is to generate a second polymeric layer on the QDs/PS hybrid nanoparticles, which can be created by seeded emulsion polymerization [117]. The second shell further protects the QDs located in the outer parts of the primary hybrid nanoparticles protecting the QDs. These multilayer particles could be assembled to colloidal crystals, showing an angle-dependent fluorescence, according to the stop band of the photonic crystal. A polymerization from the QD surfaces was shown by Esteves et al. [121]. By coordinating a phosphine-oxide-modified ATRP starter to CdS QDs it was possible to generate a PBA shell around the nanocrystal. Performed in miniemulsion, the authors used the AGET (activator generated by electron transfer)–ATRP technique.

#### 4.2.1 Silica

Silica nanoparticles have been widely used for the generation of nanocomposite materials because they are easy to obtain, are available in variable sizes, and can be functionalized. Owing to their surface silanol groups, they can be very

easily covalently modified with trimethoxysilanes bearing a wide variety of different functionalities. Various studies, especially investigating the influence of the size and the surface properties, have been conducted by applying the miniemulsion polymerization technique.

Silica/polymer hybrid nanoparticles of different morphologies could be obtained after introducing 20 nm negatively charged silica particles into a miniemulsion polymerization process [122]. The morphologies obtained strongly depend on the surfactant added to the system, the pH of the continuous phase, and the (co)monomer composition. Only after complete surface coverage with cetyltrimethylammonium chloride (CTMA-Cl), a cationic surfactant that strongly interacts with the silica surface, could the particles be incorporated into a polystyrene-*co*-poly-4-vinylpyridine (PS-*co*-P4VP) matrix (Fig. 24). By applying different reaction conditions, such as other surfactants or changing the pH, several morphologies, like raspberry or hedgehog structures can be realized. Modifying this process by introduction of large (90 nm) silica particles with methacryloxy(propyl)trimethoxysilane (MPS)-hydrophobized surface, raspberry-like PS/silica hybrids with an additional large silica particle in the center could be prepared [123].

The influence of differently sized, MPS-modified silica nanoparticles on the morphology of PS/silica particles was investigated by Zhang et al. [124]. Using 45 nm silica (20 mM SDS), 200 nm multicore hybrids could be obtained. Reducing the particle size by increasing the amount of SDS led to the reduction of the number of encapsulated silica particles, eventually leading to a single core-shell morphology (40 mM SDS). Single core-shell hybrids could be obtained with 90 nm silica particles for any surfactant concentration (20–40 mM SDS); only the particle size (180–130 nm) and thus the shell thickness decreased. Silica particles of 200 nm led to raspberry-like structures with PS spheres attached to one silica bead. Comparable results were obtained in a system with PS/PBA copolymer matrix [125].

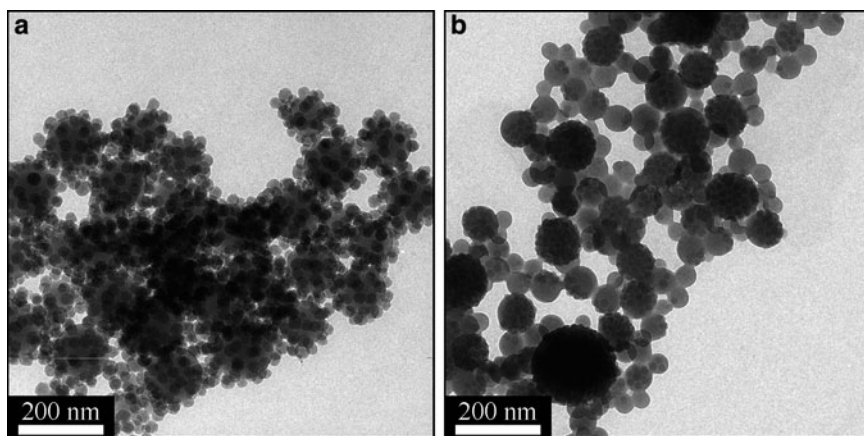


**Fig. 24** PS-*co*-P4VP/silica hybrid nanocomposites prepared with (a) non-hydrophobized silica, and (b) hydrophobized silica using CTMA-Cl as surfactant [122]

The protecting abilities of the polymeric shell around silica particle were shown by subjecting silica/PMMA-*co*-PBA hybrids to HF treatment. Nearly 90% of the silica was encapsulated and thus not prone to dissolution by HF [126].

The dispersion of 120 nm MPS-modified silica particles in styrene with a subsequent miniemulsion polymerization, initiated by AIBA (azodiisobutyramidine dihydrochloride) and stabilized by CTAB, led to cationic core-shell particles. Adding titanium tetraisobutoxide to the system generated a thin titania shell around the silica/PS nanocomposites [127].

Several efforts were made to prepare anisotropic hybrid particles. Lu et al. [128] formulated a miniemulsion with a dispersed phase containing tetraethylorthosilicate (TEOS), styrene, and MPS, stabilized by CTAB. After initiation of the styrene polymerization, a copolymer from styrene and MPS was formed. Addition of ammonia induces hydrolysis and condensation of TEOS to silica. The processes induce phase separation to a styrene droplet with the growing PS, and a TEOS droplet with the growing silica. The droplets are bridged by the PS-PMPS copolymer. Conducting the reaction without MPS generates separate silica and PS particles.

Asymmetric hybrids could also be generated by partial functionalization of silica beads with octadecyltrimethoxysilane (ODMS) at interfaces [129] or with MPS at defined aggregates of silica beads. With this technique, a great number of different morphologies could be realized by varying the ratio of monomer to silica [130] (Fig. 25).

Initiators for the controlled living radical polymerization could also be introduced to silica particles. Nitroxide-mediated polymerization (NMP) conducted with styrene in miniemulsion led to the generation of core-shell particles, with styrene grafted to the central silica particle [131]. PBA could be polymerized from 20 nm silica beads by attaching an ATRP agent to the silica surface and subsequent miniemulsion polymerization [132]. Confining the polymerization to miniemulsion droplets could avoid gel formation, which was observed in the bulk reaction. Due to the limited monomer diffusion, only 25–35% of conversion could be obtained in bulk.

Usually the silica/polymer composites are prepared with styrene, MMA, BA, or their copolymers. However, few reports cover experiments with less commonly used polymers such as poly(styrene sulfonic acid) (PSSA), poly(hydroxyethylmethacrylate) (PHEMA), poly(aminoethylmethacrylate) PAEMA [133], polyethylene (PE) [134], or polyamides [135]. Using a miniemulsion of nickel-based catalysts for the polymerization of ethylene, which is dispersed in toluene in the presence of hydrophobically modified silica particles, PE/silica hybrids could be prepared [134]. The ethylene is introduced into the system by bubbling through the miniemulsion. The hydrophobic moiety of the silica particles interacts with the growing polymer and leads to lentil-shaped or isotropic hybrids. Lentil-shaped particles are composed of semicrystalline PE, whereas the isotropic hybrids are composed of amorphous polymer. The crystallinity of the polymer is determined by the choice of polymerization catalyst. Silica/polyamide hybrid nanoparticles were prepared with 3-aminopropyl triethoxysilane (APS)-modified silica particles [135]. These particles were dispersed in sebacoylchloride and the solution miniemulsified in an aqueous

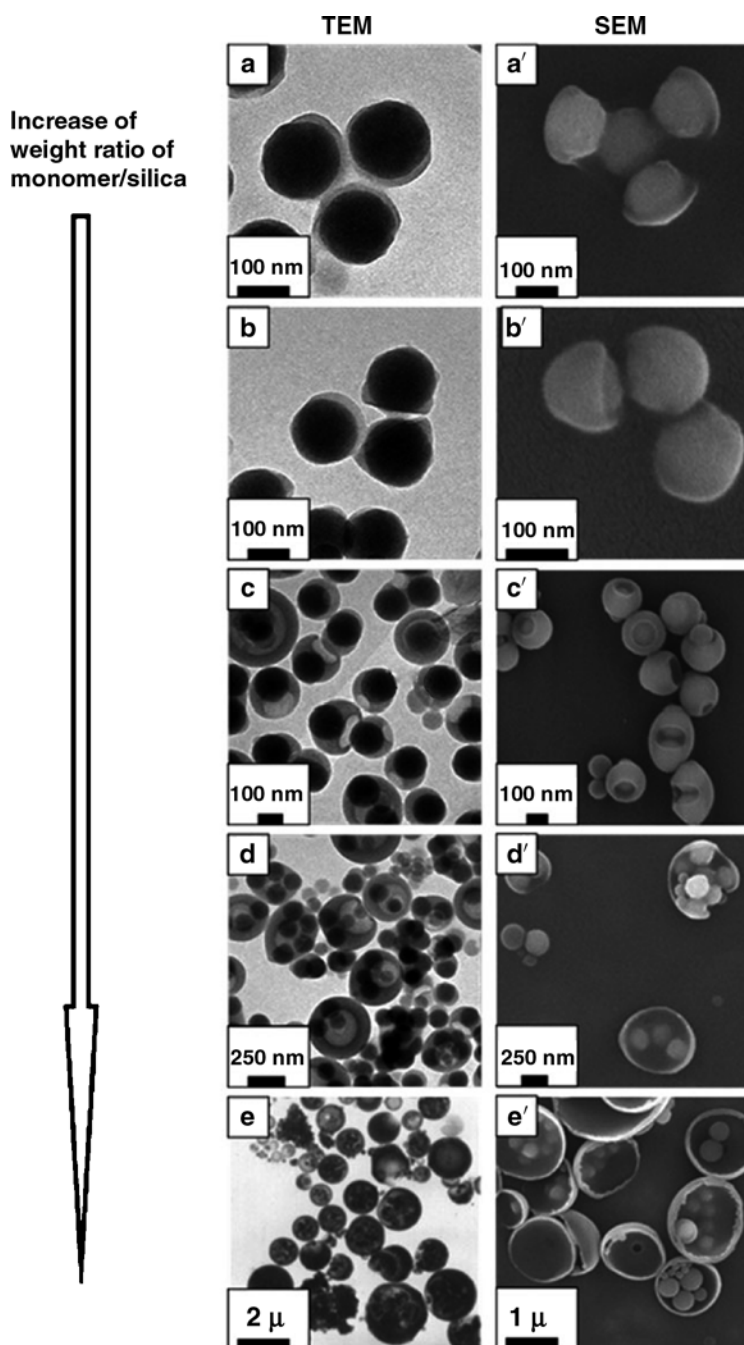


**Fig. 25** TEM (a–e) and SEM (a'–e') images of anisotropic PS/silica hybrid particles synthesized in the presence of w/o-silica. The weight ratio of monomer/silica was increased systematically in images (a–e) and (a'–e'): (a, a') 28:1, (b, b') 60:1, (c, c') 72:1, (d, d') 80:1, and (e, e') 100:1 [130]. Reproduced by permission of The Royal Society of Chemistry



SDS solution. The dropwise addition of hexamethylene diamine led to the formation of polyamide, covering the silica particles and resulting in 200 nm hybrid particles.

Asymmetric snowman-like PS/silica hybrids containing two different fluorescent labels and suitable for biomedical applications were reported by Wang et al. [136]. While the carboxy-functionalized PS part served as anchor for green fluorescing NHS-FITC, the amino-functionalized silica part was functionalized with red fluorescing TRITC. The asymmetric distribution was confirmed by confocal laser scanning microscopy.

#### 4.2.2 Clay

Clays are layered silicates. The layers usually have a thickness of 1 nm and several tens or hundreds of nanometers of lateral extension. The surfaces of these platelets are negatively charged and stacked by intercalated, positively charged metal ions. By exchanging the metal ions with hydrophobic quaternary ammonium salts (e.g., CTAB or CTMA-Cl), the single layers can be made hydrophobic, allowing organic solvents to swell and eventually exfoliate the silicate layers. Functional quaternary ammonium salts allow the introduction of, e.g., polymerizable groups (e.g., 2-methacryloyloxyethyl hexadecyldimethylammonium bromide, MA16 [137]) or groups that can act as initiator [138] for polymerization reactions. The integration of clay platelets into polymeric films is of high interest because the inorganic component improves the mechanical properties and, due to their flat disc-like shape, greatly reduces gas permeation through polymeric films. Most widely used are the naturally occurring montmorillonite [137, 139–143] or saponite [144, 145] minerals as well as commercially available Cloisite [137, 138, 146, 147] (organomodified montmorillonite) or the synthetic Laponite RD [148].

Organo-modified clay can be directly dispersed in monomers and subjected to miniemulsion polymerization. However, there is an upper limit for the application of this technique because the organo-modified clay dispersed in monomers forms thixotropic gels from concentrations of about 4% [144] or more. A monomer/clay dispersion with increased viscosity cannot be dispersed finely enough to generate a stable miniemulsion. However, Tong et al. [149] could successfully disperse 30 wt% of modified saponite in styrene. The clay was modified with (ar-vinylbenzyl)trimethylammonium chloride (VBTA), a small quaternary ammonium salt that is capable of copolymerizing with styrene or acrylates. The dispersion in styrene was of low viscosity and therefore suitable for the miniemulsification process. After polymerization, nanohybrids with 30 wt% of exfoliated organomodified clay could be obtained.

Macroinitiators or agents for controlled radical polymerizations (NMP, RAFT) could be immobilized on clay surfaces by modifying NMP [137, 138] or RAFT [142, 143, 150] agents with ammonium groups and subsequent ion exchange. This ensures close contact of the clay and the polymer, which is very important for highly enhanced properties [151]. Samakande et al. investigated the kinetics of RAFT-mediated living polymerization of styrene [143] and styrene/BA [142] mixtures in miniemulsion. The authors found that the molecular weight of the polymer is, as



expected, dependent on the amount of RAFT-agent-modified clay added to the dispersed phase of the miniemulsion. Increasing the amount of clay, meaning more RAFT agent, decreases the molecular weight. The clay morphology also changes with the amount added to the miniemulsion. While at low (1 wt%) clay loadings, the platelets are fully exfoliated, intercalated (platelets still stacked, but with increased distance) structures can be found at 5 wt% loading.

#### 4.2.3 Iron Oxides (Magnetic Nanoparticles)

Although there are a few reports of using the miniemulsion technique for preparation of magnetic nanohybrids that are not based on iron oxide [152, 153], most of the literature deals with superparamagnetic iron oxide. Superparamagnetism is a feature exhibited by single-domain nanoparticles of magnetite ( $\text{Fe}_3\text{O}_4$ ) or maghemite ( $\gamma\text{-Fe}_2\text{O}_3$ ), generally of a size of about 10 nm. Superparamagnetism is characterized as saturation magnetization of ferromagnetic material, but the material does not show remanent magnetization, which is typical for bulk ferro- and ferrimagnets. As the particles do not have a permanent magnetic dipole, they do not coagulate due to magnetic interactions. However, in a magnetic field they show a significant response due to their high saturation magnetization. Due to these extraordinary features, these nanoparticles give rise to several applications such as cell separation, hyperthermia, MRI contrast enhancement, or magnetic drug targeting. For these biomedical applications, the iron oxide nanoparticles have to be brought into the bloodstream of a target organism and must be shielded from the aqueous environment to protect them from being degraded and metabolized. Fast degradation in the organism might induce toxic effects.

#### Encapsulation in Inverse Miniemulsion

Commercial iron oxide nanoparticle-based formulations (e.g., Ferridex, Resovist) contain iron oxide nanoparticles encapsulated in hydrophilic dextran or modified dextran. The encapsulation of superparamagnetic iron oxide nanoparticles in hydrophilic polymer shells can very easily be accomplished by an inverse miniemulsion polymerization process. Although magnetite surface is hydrophilic, it is beneficial to coat the nanoparticles with hydrophilic polymer (e.g., PMAA) [154] or “double hydrophilic” block copolymer PEO-PMAA [155]. Interestingly, the magnetite nanoparticles precipitated in the presence of PEO-PMAA are significantly smaller (5 nm) than nanoparticles prepared in the presence of either PEO or PMAA, which are each about 10 nm. The PEO-PMAA-coated particles could easily be dispersed in hydroxyethylmethacrylate/acrylic acid (HEMA/AA). After miniemulsification of the ferrofluid in a P(E/B-*b*-EO)-decane solution, the monomer droplets were thermally polymerized to yield fairly monodispersed nanoparticles of 140–220 nm, according to the amount of stabilizer. The iron oxide saturation magnetization did not change during the encapsulation process and remained at about  $60\text{emu g}^{-1}$  iron oxide.

PMAA- or citrate-coated magnetite [154] or maghemite [156] nanoparticles could successfully be encapsulated in a crosslinked polyacrylamide matrix using an inverse miniemulsion process. Here, an inert hydrocarbon (cyclohexane or dodecane) was used as continuous phase and Span80 as stabilizer.

Xu et al. used the same process to encapsulate PMAA-coated magnetite in silica [157]. By adding TEOS to a miniemulsion of magnetite-PMAA/water dispersed in Span80/cyclohexane, silica/magnetite hybrid nanoparticles could be generated. About 19 wt% of magnetite could be incorporated in the silica matrix.

Thermoresponsive P(NIPAM-*co*-MAA) could be obtained using PAA-coated magnetite nanoparticles in an inverse miniemulsion polymerization process [158]. The superparamagnetic particles could change their size from 250 nm to 100 nm by changing the temperature from 20 to 70°C.

### Encapsulation in Direct Miniemulsion

Encapsulation of superparamagnetic iron oxide nanoparticles in hydrophobic matrices offers a better protection for the inorganic particles in aqueous medium, because the encapsulated material is less accessible for water in the hydrophobic polymer particle. It is of great importance to generate a highly hydrophobic iron oxide in order to achieve high contents in the hybrid particles for a strong magnetic response to external fields. With some exceptions, oleic acid was used for hydrophobization of the magnetite surface. A few attempts to covalently functionalize the magnetite surface with silanes (aminopropyltrimethoxysilane or 3-methacryloxypropyltrimethoxysilane) [159, 160] have been reported.

Magnetite coated with sodium 1,2-bis(2-ethylhexoxycarbonyl)ethanesulfonate (AOT) was directly dispersed in styrene, but led to an inhomogeneous distribution of magnetite in the hybrid system [161, 162]. Pure PS nanoparticles, as well as polymeric particles partially covered with magnetite, could be distinguished by TEM analysis. Although this can be regarded as a hybrid system, the actual encapsulation in polymer seems to be uncertain from the presented results.

Using a phosphate-based dispersant (Disperbyk 106, organic amine salt composed of the partly esterified phosphate and organic amine), Zhang et al. [159, 163] generated magnetic hybrid particles from PS and magnetite. The authors confirmed the presence of hybrid particles using TEM. Again, the magnetite distribution is inhomogeneous and the magnetite seems to be located on the polymer and not inside the particles. The magnetic properties were investigated with a SQUID magnetometer. The particles exhibited typical paramagnetic behavior, with an extremely high saturation magnetization of  $47 \text{ emu g}^{-1}$ .

A single-pot reaction of maghemite nanoparticles, fluorescent pigment, polyester resin, Tween80, Span80, AIBN, and styrene dispersed in an aqueous NaOH solution, led to the formation of ferromagnetic (hysteresis in vibrating sample magnetometry analysis) hybrid nanoparticles [164]. Magnetite compatibilization is ascribed to the application of polyester resin.

A more elaborate approach is based on covalent immobilization of the Y-shaped surfactant 12-hexanoyloxy-9-octadecenoic acid (HOA) on the iron oxide nanoparticles [165]. These surfactant-modified magnetite nanoparticles were subjected to a miniemulsion polymerization process. The polymerization was initiated by  $\gamma$ -irradiation, and the droplets stabilized with the above-mentioned Y-shaped surfactant. Detailed SEM and TEM studies revealed that the morphology and the magnetite location were strongly dependent on the reaction parameters. Without the addition of HD as hydrophobic costabilizer, the particle size distribution is broad and the magnetite inhomogeneously distributed, irrespective of the amount of surfactant added. Addition of small amounts of HD expectedly improves the particle size distribution. With this technique, nearly 60 wt% of magnetite could be encapsulated in polystyrene matrixes, yielding superparamagnetic hybrid nanoparticles.

Most of the processes described in literature employ oleic acid for hydrophobization of the magnetite surface.

The uniform incorporation of larger amounts of magnetite into polymeric particles is the most crucial point in order to obtain a strong and uniform response from the magnetic hybrid nanoparticles. Based on the co-sonication process (Fig. 26) described earlier, a three-step process was used for the generation of aggregates of primary magnetite nanoparticles and their subsequently encapsulation in a polystyrene matrix [93, 94]. In the first step, magnetite nanoparticles are co-precipitated from

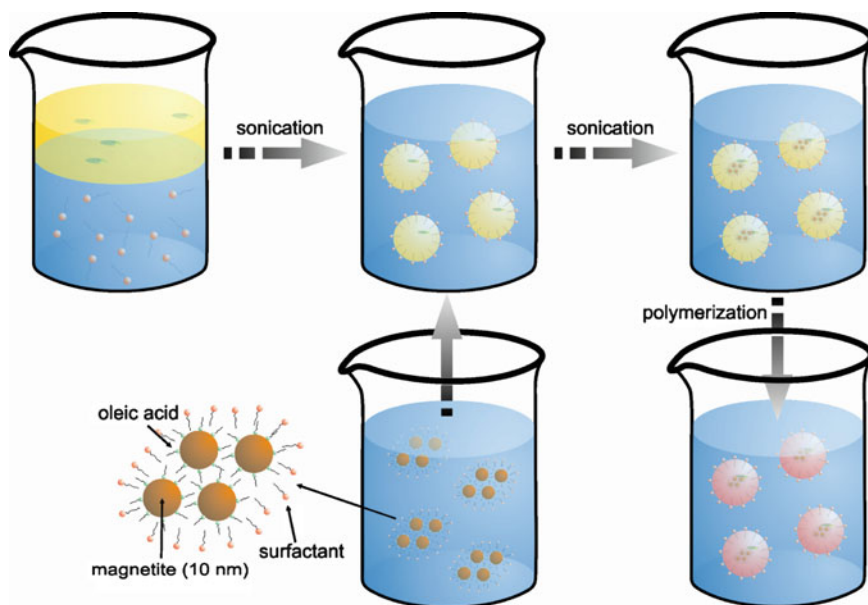


**Fig. 26** The co-sonication process, representatively shown for magnetite aggregates. A dispersion of magnetite is mixed with a preformed monomer miniemulsion (*middle*). Magnetite aggregates are engulfed by the monomer droplets after sonicating the mixture of both dispersions (*upper right*). After subsequent polymerization, the hybrid nanoparticles are obtained (*lower right*)

ferrous and ferric chloride to yield magnetite particles of about 10 nm in diameter. After hydrophobization of the primary superparamagnetic magnetite crystallites, the ferrofluid (hydrophobized magnetite in octane) was dispersed in an aqueous SDS solution by ultrasound. From this miniemulsion, octane was evaporated and a stable dispersion of SDS-stabilized aggregates of hydrophobized magnetite remained. In the last step, the magnetite dispersion and a styrene miniemulsion were mixed by co-sonication and, after subsequent polymerization, magnetic polystyrene nanoparticles could be obtained (Fig. 26).

Using this process, more than 40 wt% of magnetite could be encapsulated in polystyrene. Although the initial saturation magnetization of  $87 \text{ emu g}^{-1}$  iron oxide decreased to  $53 \text{ emu g}^{-1}$ , there was still significant magnetic response. This decrease, which was also observed by several other authors [166–168], might be caused by partial oxidation or by a change in the crystal structure on the surface of the magnetite nanoparticle. By adding comonomers to styrene, surface-functionalized magnetic PS nanoparticles could be obtained [47, 48]. Styrene copolymerized with a defined amount of acrylic acid creates carboxy functions on the particle surface, which could subsequently be covalently functionalized by lysine or by physical adsorption of the commercial transfection agent poly(L-lysine) (PLL). It could be shown that lysine-functionalized particles are highly efficiently internalized by cells. The extent of cellular uptake even exceeds the internalization of PLL-functionalized particles. The incorporated magnetite offers an easy and reliable assay for quantification of the internalized nanoparticles by generating Prussian blue. The co-incorporation of a fluorescent marker (e.g., PMI, or QDs [169]) into the magnetic PS particles offers the additional possibility of optical particle tracking using fluorescence microscopy.

Carboxy functions for further bioconjugation could also be introduced in magnetic poly(ethylmethacrylate) (PEMA) by copolymerization of EMA with acrylic acid [170, 171], or by using 4,4'-azo-bis(4-cyanopentanoic acid) (ACPA) as initiator [172].

In contrast to the homogenous magnetite distribution by the three-step process, the dispersion of hydrophobized magnetite in styrene/MAA [173] or a toluene-based ferrofluid [174] in styrene, followed by a miniemulsion polymerization process, leads to magnetite/polymer particles with inhomogeneous iron oxide distribution.

Further investigations of the magnetite distribution within PS/magnetite hybrid particles by electron microscopy tomography showed that the choice of initiator is decisive in the investigated system [175]. Using the water-soluble initiator KPS, magnetite is homogeneously distributed in the polymeric matrix (Fig. 27a). Apparently, no magnetite is located on the particle surface. The addition of AIBN does not change the distribution pattern (Fig. 27b). Using only AIBN, however, a hemispherical aggregate of magnetite is created, which is located at the particle surface and indicates an incomplete encapsulation (Fig. 27c). The authors attribute these observations to the fact that KPS initiates polymerization from the aqueous phase, confining the magnetite in the droplet. AIBN (see anchoring effect for the generation of polymeric capsules, Sect. 3.2), on the other hand, initiates the polymerization from within the droplets, leading to a microphase separation between the polymer and the hexane-based ferrofluid.

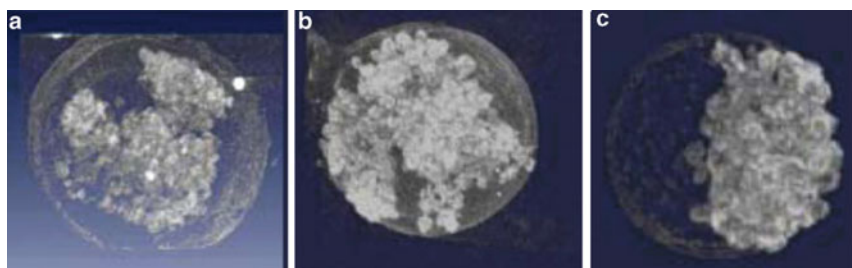


**Fig. 27** Three-dimensional tomograms of magnetic particles using various initiators: (a) KPS, (b) KPS + AIBN, and (c) AIBN. Reprinted from [175], copyright 2007, with permission from Elsevier

A study using an SDS-stabilized miniemulsion of oleic-acid-coated magnetite in octane as a “magneto template” identified the chain mobility of the generated polymer within the miniemulsion droplet as a possible reason for microphase separation and the subsequent non-uniform distribution of magnetite within the hybrid particles. In contrast to the application of pure styrene, the addition of DVB, leading to highly crosslinked polymer structures, produced hybrid particles with more homogenous magnetite distribution. The authors attribute the observation to hindered diffusion in crosslinked structures, which prevents the magnetite particles from phase-separating to the droplet surface [176].

Nonspherical, surface-imprinted magnetic PMMA (see Fig. 28) nanoparticles could be prepared by Tan et al. [177, 178]. A miniemulsion process was used to prepare magnetite/PMMA nanoparticles on which proteins were either immobilized by adsorption (RNase A) [178] or covalently (bovine serum albumin, BSA) [177]. After creating a shell of PMMA, the proteins were removed, leaving cavities on the particles surface. The BSA-imprinted nanoparticles showed superparamagnetic properties and exhibited a high rebinding capacity for BSA.

Crosslinked, magnetic PMMA nanoparticles were prepared by Liu et al. using a hexane-based ferrofluid [179]. The authors could incorporate less than 8 wt% of magnetite, yielding particles with a saturation magnetization of about  $4 \text{ emu g}^{-1}$ . X-ray photoelectron spectroscopy (XPS) was used to prove that no iron oxide is present on the particle surface. By treatment with sodium methoxylate the methyl ester groups were hydrolyzed and subsequently esterified with poly(ethylene glycol), which could be further functionalized with a reactive dye (Cibacron Blue F3G-A).

Another way to create specifically functionalized magnetic polymeric nanoparticles was recently presented by Qian et al. [180]. The authors introduced anchor groups by copolymerizing styrene with vinyl acetate and subsequently treated the system with ethanolic NaOH for the hydrolysis of the ethyl ester groups. The conjugation of mercaptotnicotinic acid with divinylsulfone introduced a highly specific ligand for the recognition of IgG antibodies. After magnetic separation of the magnetic nanoparticles from IgG-containing serum, the antibody could be isolated with >99% bioactivity purity.

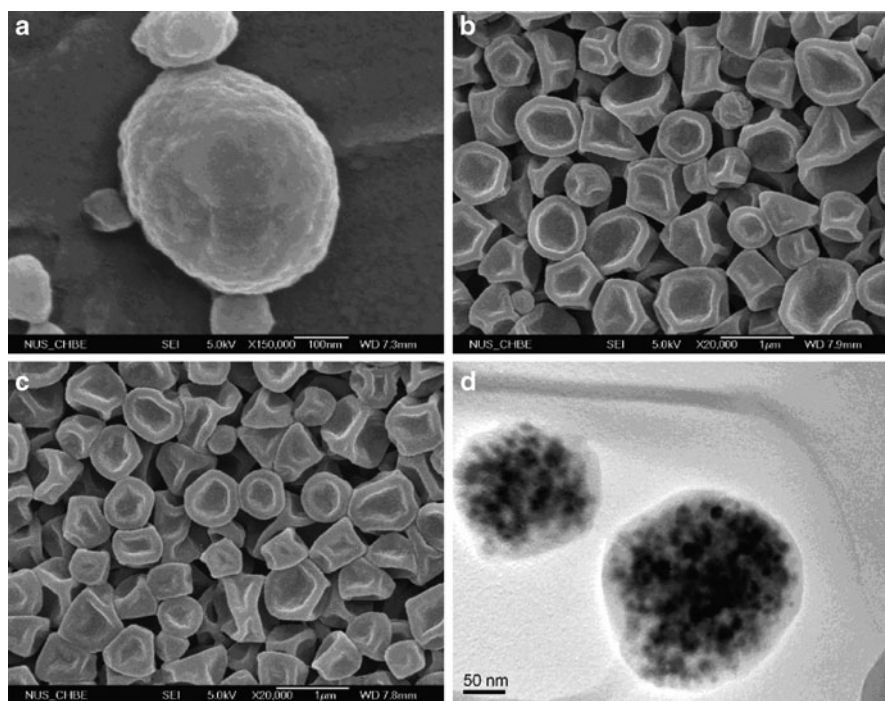


**Fig. 28** Microscopic observation of prepared surface-imprinted magnetic PMMA nanoparticles. Field emission SEM images of (a) support particles, (b) imprinted particles, and (c) non-imprinted particles. (d) TEM images illustrating the successful encapsulation of  $\text{Fe}_3\text{O}_4$  magnetite. Reprinted with permission from [177]. Copyright 2008 American Chemical Society

A further proof for the complete encapsulation and protection of magnetite nanoparticles by a polymeric shell was delivered by Zheng et al. [181], who treated magnetite/PS particles with 1 M HCl solution and found no evidence for dissolved iron in the solution.

Ultrasonic initiation of styrene polymerization was investigated by Qiu [182, 183]. Although hybrid particles could be obtained, plain polymer nanoparticles were found in the system as well.

Emulsifier-free miniemulsion polymerization was also used for the encapsulation of oleic acid/magnetite nanocrystals in styrene [184, 185] or chloromethyl-styrene for further functionalization [186]. For this approach, it is necessary to use a cationic ionizable initiator [2, 2-azobis (2-amidinopropane) dihydrochloride (V-50)], which contributes to the particle stabilization. The use of KPS did not lead to stable systems. Almost no encapsulated magnetite could be found by the authors performing conventional emulsion polymerization, using comparable conditions to the miniemulsion polymerization [185]. In the approach of Lu et al. [187], the stabilizer is formed during the polymerization of sodium styrene sulfonate added to the system. Here, hybrid nanoparticles with about 10 wt% of magnetite and a saturation magnetization of  $2 \text{ emu g}^{-1}$  could be prepared.



To improve the encapsulation efficiency, the hydrophobicity of oleic-acid-coated magnetite was increased by depositing the oleic acid in form of a monolayer with free hydrocarbon chains [188]. To ensure this, oleic-acid-coated magnetite particles (10 nm) were washed with ethanol, which is a better solvent for oleic acid than water, to remove excessive layers of oleic acid. After this treatment, the magnetite nanoparticles are more hydrophobic than particles purified with water. The contact angle of a dried film of coated magnetite against water changed from 70° (washed with water only) to 120° (washed with ethanol). The monolayer-coated magnetite could be homogeneously incorporated in polystyrene, whereas the encapsulation of the conventionally treated magnetite was incomplete and pure PS nanoparticles could be observed.

Extremely high magnetite contents of 86 wt% in styrene particles could be achieved by preparing the hybrid particles with a combined miniemulsion/emulsion system [189]. Initially, a miniemulsion of a ferrofluid consisting of magnetite coated with oleic acid and undecylenic acid in octane was prepared. A styrene “macroemulsion,” which was prepared by membrane emulsification using a SPG-membrane (Shirasu porous glass), was added dropwise to the previously prepared miniemulsion. The larger styrene droplets act as a reservoir, from which the monomer can diffuse to the miniemulsion droplets and polymerize there.

Shao et al. reported the preparation of all-inorganic magnetic hybrid nanoparticles by encapsulating oleic-acid-coated magnetite in silica [190]. First, a ferrofluid consisting of hydrophobized magnetite in TEOS was prepared, which was subsequently miniemulsified in water. Hydrolysis and condensation of TEOS to silica was initiated by the addition of ammonia to the miniemulsion, leading to the formation of amorphous silica particles with up to 30 wt% magnetite content. The nanocomposites were successfully used for DNA separation under high ionic strength solutions. The plasmids readily adsorb to the silica surface, while the magnetite enables magnetic separation.

The generation of magnetite polymer hybrid nanoparticles can not only be accomplished by the miniemulsion polymerization technique but also by a combination of miniemulsion and solvent evaporation. This opens the way to the preparation of composite particles consisting of polymer not generated by radical polymerization. Using this technique, biodegradable poly-L-lactide (PLLA) nanoparticles containing a fluorescent dye and iron oxide (25 or 10 nm) could be prepared. First, the primary magnetite nanoparticles were modified with oleic acid for compatibilization and dispersed in an SDS/water solution. This dispersion is mixed by co-sonication with a miniemulsion consisting of a solution of PLLA and the fluorescent dye in chloroform. Subsequently, the organic solvent is evaporated and the polymer precipitates around the magnetite particles and the fluorescent dye. The homogeneity of the iron oxide distribution depends on the size and on the amount of magnetic nanoparticles introduced in the formulation and is most homogenous for 25 nm particles in concentrations of 20 and 50 wt% (Fig. 29). As already observed with pure PLLA nanoparticles, the molecular weight of the polymer is reduced during the sonication treatment [49].



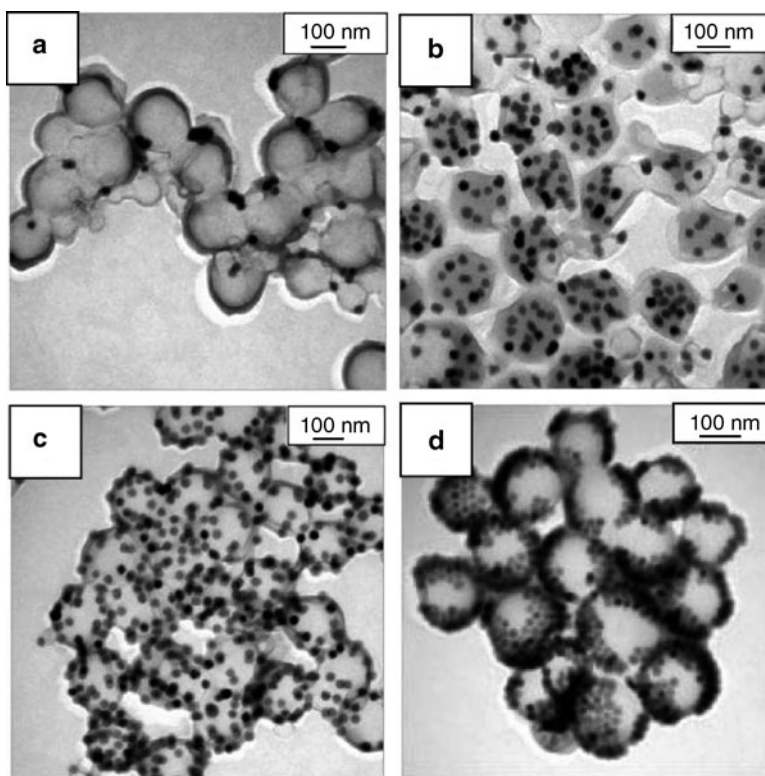


**Fig. 29** TEM images of PLLA particles with different encapsulated amounts of iron oxide (25 nm): (a) 6.7, (b) 20, (c) 50, and (d) 100 wt% related to PLLA [49]

Related to the generation of nanocapsules discussed above, is the appearance of rings or particles with single holes in hybrid system consisting of hydrophobic iron oxide, organic solvent, and polymer, probably in combination with KPS as initiator (see anchoring effect, Sect. 3.2). The emergence of these non-equilibrium structures is attributed to a delicate interplay of phase separation, viscosity, and solvent evaporation [191, 192].

## 5 Summary

The examples of a great variety of nanocomposites presented in this review underline the versatility of the miniemulsion process for the encapsulation of a wide variety of many different materials and compounds in a great number of different (functional) polymeric shells. Compounds that are soluble in a monomer can very easily be integrated in the miniemulsion polymerization process. The material can be incorporated to serve as label (e.g., fluorescence) or to be released from the poly-

meric nanoparticles (e.g., drugs). Capsules, hollow or liquid-filled particles, can be generated by several mechanisms, all relying on the miniemulsion technique. Phase separation and interfacial reactions (radical, polyaddition) were applied for the encapsulation of organic liquids. Aqueous solutions could be provided with a shell by precipitating polymer on preformed aqueous droplets and also by interfacial reactions. Solid, nanoscaled material, insoluble in the monomer phase, has to be made compatible with the polymer used for encapsulation. The required hydrophobic moiety can be introduced by physical adsorption of surfactants (e.g., oleic acid) or by covalently functionalizing the surface of the encapsulated material with hydrophobic siloxanes.

We are certain that many more functional materials for a wide field of applications can be created by the miniemulsion process, allowing the formation of complex hybrid materials.

## References

1. Landfester K (2009) Miniemulsion polymerization and the structure of polymer and hybrid nanoparticles. *Angew Chem Int Ed* 48:4488–4507
2. Schork FJ, Luo Y, Smulders W et al (2005) Miniemulsion polymerization. *Adv Polym Sci* 175:129–255
3. Asua JM (2002) Miniemulsion polymerization. *Prog Polym Sci* 27:1283–1346
4. Aschenbrenner EM, Weiss CK, Landfester K (2009) Enzymatic esterification in aqueous miniemulsions. *Chem Eur J* 15:2434–2444
5. de Barros DPC, Fonseca LP, Cabral JMS et al (2009) Synthesis of alkyl esters by cutinase in miniemulsion and organic solvent media. *Biotechnol J* 4:674–683
6. Taden A, Landfester K, Antonietti M (2004) Crystallization of dyes by directed aggregation of colloidal intermediates: a model case. *Langmuir* 20:957–961
7. Taden A, Landfester K (2003) Crystallization of poly(ethylene oxide) confined in miniemulsion droplets. *Macromolecules* 36:4037–4041
8. Montenegro R, Antonietti M, Mastai Y et al (2003) Crystallization in miniemulsion droplets. *J Phys Chem C* 107:5088–5094
9. Montenegro R, Landfester K (2003) Metastable and stable morphologies during crystallization of alkanes in miniemulsion droplets. *Langmuir* 19:5996–6003
10. Rossmann R, Weiss CK, Geserick J et al (2008) Porous anatase nanoparticles with high specific surface area prepared by miniemulsion technique. *Chem Mater* 20:5768–5780
11. Chern CS, Chen TJ, Liou YC (1998) Miniemulsion polymerization of styrene in the presence of a water-insoluble blue dye. *Polymer* 39:3767–3777
12. Chern CS, Liou YC, Chen TJ (1998) Particle nucleation loci in styrene miniemulsion polymerization using alkyl methacrylates as the reactive cosurfactant. *Macromol Chem Phys* 199:1315–1322
13. Chern C-S, Chang H-T (2002) Particle nucleation and growth mechanisms in miniemulsion polymerization of styrene. *Polym Int* 51:1428–1438
14. Chern C-S, Liou Y-C (1998) Effects of mixed surfactants on the styrene miniemulsion polymerization in the presence of an alkyl methacrylate. *Macromol Chem Phys* 199:2051–2061
15. Chern C-S, Liou Y-C (1999) Kinetics of styrene miniemulsion polymerization stabilized by nonionic surfactant/alkyl methacrylate. *Polymer* 40:3763–3772
16. Chern C-S, Liou Y-C (1999) Styrene miniemulsion polymerization initiated by 2,2'-azobisisobutyronitrile. *J Polym Sci Part A: Polym Chem* 37:2537–2550

17. Musyanovych A, Rossmanith R, Tontsch C et al (2007) Effect of hydrophilic comonomer and surfactant type on the colloidal stability and size distribution of carboxyl- and amino-functionalized polystyrene particles prepared by miniemulsion polymerization. *Langmuir* 23:5367–5376
18. Watarai H, Ogawa K, Suzuki N (1993) Formation of fluorescent complexes of Eu(III) and Sm(III) with [beta]-diketones and trioctylphosphine oxide in oil-water microemulsions. *Anal Chim Acta* 277:73–78
19. Ando K, Kawaguchi H (2005) High-performance fluorescent particles prepared via miniemulsion polymerization. *J Colloid Interface Sci* 285:619–626
20. Bradley M, Ashokkumar M, Grieser F (2003) Sonochemical production of fluorescent and phosphorescent latex particles. *J Am Chem Soc* 125:525–529
21. Tamai T, Watanabe M, Maeda H et al (2008) Fluorescent polymer particles incorporating pyrene derivatives. *J Polym Sci Part A: Polym Chem* 46:1470–1475
22. Taniguchi T, Takeuchi N, Kobaru S et al (2008) Preparation of highly monodisperse fluorescent polymer particles by miniemulsion polymerization of styrene with a polymerizable surfactant. *J Colloid Interface Sci* 327:58–62
23. Takasu M, Shiroya T, Takeshita K et al (2004) Improvement of the storage stability and photostability of colored latex prepared by miniemulsion polymerization. *Colloid Polym Sci* 282:740–746
24. Takasu M, Kawaguchi H (2005) Preparation of colored latex with polyurea shell by miniemulsion polymerization. *Colloid Polym Sci* 283:805–811
25. Takasu M, Shiroya T, Takeshita K et al (2003) Preparation of colored latex containing oil-soluble dyes with high dye content by mini-emulsion polymerization. *Colloid Polym Sci* 282:119–126
26. Zhao X, Zhou S, Chen M et al (2009) Effective encapsulation of Sudan black B with polystyrene using miniemulsion polymerization. *Colloid Polym Sci* 287:969–977
27. Hu ZK, Xue MZ, Zhang Q et al (2007) Controlled preparation of nanocolorants via a modified miniemulsion polymerization process. *J Appl Polym Sci* 104:3036–3041
28. Hu Z, Xue M, Zhang Q et al (2008) Nanocolorants: A novel class of colorants, the preparation and performance characterization. *Dyes Pigm* 76:173–178
29. Yuan B, Wicks DA (2007) Thermotropic color changing nanoparticles prepared by encapsulating blue polystyrene particles with a poly-N-isopropylacrylamide gel. *J Appl Polym Sci* 105:446–452
30. Yuan B, States J, Sahagun C et al (2008) Effects of three cross-linkers on colored pH-responsive core-shell latexes. *J Appl Polym Sci* 107:4093–4099
31. Han M, Lee E, Kim E (2002) Preparation and optical properties of polystyrene nanocapsules containing photochromophores. *Opt Mater* 21:579–583
32. Furukawa H, Misu M, Ando K et al (2008) Light-controlled on-off switch of a fluorescent nanoparticle. *Macromol Rapid Commun* 29:547–551
33. Hu Z, Zhang Q, Xue M et al (2007) Fluorescent photoswitchable nanohybrids based on photochromism. *J Phys Chem Solids* 69:206–210
34. Hu Z, Zhang Q, Xue M et al (2008) Spirobenzopyran-based photochromic nanohybrids with photoswitchable fluorescence. *Opt Mater* 30:851–856
35. Mailänder V, Landfester K (2009) Interaction of nanoparticles with cells. *Biomacromolecules* 10:2379–2400
36. Ambruosi A, Khalansky AS, Yamamoto H et al (2006) Biodistribution of polysorbate 80-coated doxorubicin-loaded [14C]-poly(butyl cyanoacrylate) nanoparticles after intravenous administration to glioblastoma-bearing rats. *J Drug Target* 14:97–105
37. Singer JM, Adlersberg L, Hoenig EM et al (1969) Radiolabelled latex particles in the investigation of phagocytosis in vivo: clearance curves and histological observations. *J Reticuloendothel Soc* 6:561–589
38. Alyautdin RN, Reichel A, Löbenberg R et al (2001) Interaction of poly(butylcyanoacrylate) nanoparticles with the blood-brain barrier *in vivo* and *in vitro*. *J Drug Target* 9:209–221

39. Holzapfel V, Musyanovych A, Landfester K et al (2005) Preparation of fluorescent carboxyl and amino functionalized polystyrene particles by miniemulsion polymerization as markers for cells. *Macromol Chem Phys* 206:2440–2449
40. Lorenz MR, Holzapfel V, Musyanovych A et al (2006) Uptake of functionalized, fluorescent-labeled polymeric particles in different cell lines and stem cells. *Biomaterials* 27:2820–2828
41. Dausend J, Musyanovych A, Dass M et al (2008) Uptake mechanism of oppositely charged fluorescent nanoparticles in HeLa cells. *Macromol Biosci* 8:1135–1143
42. Ziegler A, Landfester K, Musyanovych A (2009) Synthesis of phosphonate-functionalized polystyrene and poly(methyl methacrylate) particles and their kinetic behavior in miniemulsion polymerization. *Colloid Polym Sci* 287:1261–1271
43. Lorenz MR, Kohnle MV, Dass M et al (2008) Synthesis of fluorescent polyisoprene nanoparticles and their uptake into various cells. *Macromol Biosci* 8:711–727
44. Musyanovych A, Schmitz-Wienke J, Mailaender V et al (2008) Preparation of biodegradable polymer nanoparticles by miniemulsion technique and their cell interactions. *Macromol Biosci* 8:127–139
45. Weiss CK, Kohnle M-V, Landfester K et al (2008) The first step into the brain: uptake of NIO-PBCA nanoparticles by endothelial cells in vitro and in vivo, and direct evidence for their blood-brain barrier permeation. *ChemMedChem* 3:1395–1403
46. Weiss CK, Lorenz MR, Landfester K et al (2007) Cellular uptake behavior of unfunctionalized and functionalized poly(n-butylcyanoacrylate) particles prepared in a miniemulsion. *Macromol Biosci* 7:883–896
47. Holzapfel V, Lorenz M, Weiss CK et al (2006) Synthesis and biomedical applications of functionalized fluorescent and magnetic dual reporter nanoparticles as obtained in the miniemulsion process. *J Phys Condens Matter* 18:S2581–S2594
48. Mailaender V, Lorenz Myriam R, Holzapfel V et al (2008) Carboxylated superparamagnetic iron oxide particles label cells intracellularly without transfection agents. *Mol Imaging Biol* 10:138–146
49. Urban M, Musyanovych A, Landfester K (2009) Fluorescent superparamagnetic polylactide nanoparticles by combination of miniemulsion and emulsion/solvent evaporation techniques. *Macromol Chem Phys* 210:961–970
50. Oh JK, Siegwart DJ, Matyjaszewski K (2007) Synthesis and biodegradation of nanogels as delivery carriers for carbohydrate drugs. *Biomacromolecules* 8:3326–3331
51. Oh JK, Siegwart DJ, Lee H-i et al (2007) Biodegradable nanogels prepared by atom transfer radical polymerization as potential drug delivery carriers: synthesis, biodegradation, in vitro release, and bioconjugation. *J Am Chem Soc* 129:5939–5945
52. Siegwart DJ, Srinivasan A, Bencherif SA et al (2009) Cellular uptake of functional nanogels prepared by inverse miniemulsion ATRP with encapsulated proteins, carbohydrates, and gold nanoparticles. *Biomacromolecules* 10:2300–2309
53. Ramírez LP, Antonietti M, Landfester K (2006) Formation of novel layered nanostructures from lanthanide-complexes by secondary interactions with ligating monomers in miniemulsion droplets. *Macromol Chem Phys* 207:160–165
54. Vancaeyzeele C, Ornatsky O, Baranov V et al (2007) Lanthanide-containing polymer nanoparticles for biological tagging applications: nonspecific endocytosis and cell adhesion. *J Am Chem Soc* 129:13653–13660
55. Manzke A, Pfahler C, Dubbers O et al (2007) Etching masks based on miniemulsions: a novel route towards ordered arrays of surface nanostructures. *Adv Mater* 19:1337–1341
56. Schreiber E, Ziener U, Manzke A et al (2009) Preparation of narrowly size distributed metal-containing polymer latexes by miniemulsion and other emulsion techniques: applications for nanolithography. *Chem Mater* 21:1750–1760
57. Volz M, Ziener U, Salz U et al (2007) Preparation of protected photoinitiator nanodepots by the miniemulsion process. *Colloid Polym Sci* 285:687–692
58. Theisinger S, Schoeller K, Osborn B et al (2009) Encapsulation of a fragrance via miniemulsion polymerization for temperature-controlled release. *Macromol Chem Phys* 210:411–420

59. Volz M, Walther P, Ziener U et al (2007) Nano-explosions of nanoparticles for sudden release of substances by embedded azo-components as obtained via the miniemulsion process. *Macromol Mater Eng* 292:1237–1244
60. Johnston APR, Cortez C, Angelatos AS et al (2006) Layer-by-layer engineered capsules and their applications. *Curr Opin Colloid Interface Sci* 11:203–209
61. Wang Y, Angelatos AS, Caruso F (2007) Template synthesis of nanostructured materials via layer-by-layer assembly. *Chem Mater* 20:848–858
62. zu Putlitz B, Landfester K, Fischer H et al (2001) The generation of “armored latexes” and hollow inorganic shells made of clay sheets by templating cationic miniemulsions and latexes. *Adv Mater* 13:500–503
63. Torza S, Mason SG (1970) Three-phase interactions in shear and electrical fields. *J Colloid Interface Sci* 33:67–83
64. Musyanovych A, Landfester K (2007) Core-shell particles. In: Matyjaszewski K, Gnanou Y, Leibler L (eds), *Macromolecular engineering. Precise synthesis, materials properties, applications*, vol 2. Wiley-VCH, Weinheim, pp 1209–1247
65. Tiarks F, Landfester K, Antonietti M (2001) Preparation of polymeric nanocapsules by miniemulsion polymerization. *Langmuir* 17:908–918
66. Luo YW, Zhou XD (2004) Nanoencapsulation of a hydrophobic compound by a miniemulsion polymerization process. *J Polym Sci Part A: Polym Chem* 42:2145–2154
67. Cao Z, Shan G (2009) Synthesis of polymeric nanocapsules with a crosslinked shell through interfacial miniemulsion polymerization. *J Polym Sci Part A: Polym Chem* 47:1522–1534
68. Romio AP, Sayer C, Araújo PHH et al (2009) Nanocapsules by miniemulsion polymerization with biodegradable surfactant and hydrophobe. *Macromol Chem Phys* 210:747–751
69. Zetterlund PB, Saka Y, Okubo M (2009) Gelation and hollow particle formation in nitroxide-mediated radical copolymerization of styrene and divinylbenzene in miniemulsion. *Macromol Chem Phys* 210:140–149
70. Ni KF, Shan GR, Weng ZX (2006) Synthesis of hybrid nanocapsules by miniemulsion (co)polymerization of styrene and gamma-methacryloxypropyltrimethoxysilane. *Macromolecules* 39:2529–2535
71. van Zyl AJP, Sanderson RD, de Wet-Roos D et al (2003) Core/shell particles containing liquid cores: morphology prediction, synthesis, and characterization. *Macromolecules* 36:8621–8629
72. van Zyl AJP, Bosch RFP, McLeary JB et al (2005) Synthesis of styrene based liquid-filled polymeric nanocapsules by the use of RAFT-mediated polymerization in miniemulsion. *Polymer* 46:3607–3615
73. Lu F, Luo Y, Li B (2007) A facile route to synthesize highly uniform nanocapsules: use of amphiphilic poly(acrylic acid)-*block*-polystyrene RAFT agents to interfacially confine miniemulsion polymerization. *Macromol Rapid Commun* 28:868–874
74. Luo YW, Gu HY (2006) A general strategy for nano-encapsulation via interfacially confined living/controlled radical miniemulsion polymerization. *Macromol Rapid Commun* 27:21–25
75. Luo Y, Gu H (2007) Nanoencapsulation via interfacially confined reversible addition fragmentation transfer (RAFT) miniemulsion polymerization. *Polymer* 48:3262–3272
76. Musyanovych A, Landfester K (2008) Synthesis of poly(butylcyanoacrylate) nanocapsules by interfacial polymerization in miniemulsions for the delivery of DNA molecules. In: Auernhammer GK, Butt H-J, Vollmer D (eds), *Surface and interfacial forces – from fundamentals to applications. Progress in colloid and polymer science*, vol 134. Springer, Berlin, Heidelberg, pp 120–127
77. Zhang Y, Zhu SY, Yin LC et al (2008) Preparation, characterization and biocompatibility of poly(ethylene glycol)-poly(n-butyl cyanoacrylate) nanocapsules with oil core via miniemulsion polymerization. *Eur Polym J* 44:1654–1661
78. Jagielski N, Sharma S, Hombach V et al (2007) Nanocapsules synthesized by miniemulsion technique for application as new contrast agent materials. *Macromol Chem Phys* 208:2229–2241
79. Scott C, Wu D, Ho CC et al (2005) Liquid-core capsules via interfacial polymerization: a free-radical analogy of the nylon rope trick. *J Am Chem Soc* 127:4160–4161

80. Wu D, Scott C, Ho CC et al (2006) Aqueous-core capsules via interfacial free radical alternating copolymerization. *Macromolecules* 39:5848–5853
81. Torini L, Argillier JF, Zydowicz N (2005) Interfacial polycondensation encapsulation in miniemulsion. *Macromolecules* 38:3225–3236
82. Johnsen H, Schmid RB (2007) Preparation of polyurethane nanocapsules by miniemulsion polyaddition. *J Microencapsulation* 24:731–742
83. Crespy D, Stark M, Hoffmann-Richter C et al (2007) Polymeric nanoreactors for hydrophilic reagents synthesized by interfacial polycondensation on miniemulsion droplets. *Macromolecules* 40:3122–3135
84. Paiphansiri U, Dausend J, Musyanovych A et al (2009) Fluorescent polyurethane nanocapsules prepared via inverse miniemulsion: surface functionalization for use as biocarriers. *Macromol Biosci* 9:575–584
85. Rosenbauer E-M, Landfester K, Musyanovych A (2009) Surface-active monomer as a stabilizer for polyurea nanocapsules synthesized via interfacial polyaddition in inverse miniemulsion. *Langmuir* 25:12084–12091
86. Landfester K (2006) Synthesis of colloidal particles in miniemulsions. *Annu Rev Mater Res* 36:231–279
87. Paiphansiri U, Tangboriboonrat P, Landfester K (2006) Polymeric nanocapsules containing an antiseptic agent obtained by controlled nanoprecipitation onto water-in-oil miniemulsion droplets. *Macromol Biosci* 6:33–40
88. Paiphansiri U, Tangboriboonrat P, Landfester K (2007) Antiseptic nanocapsule formation via controlling polymer deposition onto water-in-oil miniemulsion droplets. *Macromol Symp* 251:54–62
89. Bechthold N, Tiarks F, Willert M et al (2000) Miniemulsion polymerization: applications and new materials. *Macromol Symp* 151:549–555
90. Lelu S, Novat C, Graillat C et al (2003) Encapsulation of an organic phthalocyanine blue pigment into polystyrene latex particles using a miniemulsion polymerization. *Polym Int* 52:542–547
91. Tiarks F, Landfester K, Antonietti M (2001) Encapsulation of carbon black by miniemulsion polymerization. *Macromol Chem Phys* 202:51–60
92. Steiert N, Landfester K (2007) Encapsulation of organic pigment particles via miniemulsion polymerization. *Macromol Mater Eng* 292:1111–1125
93. Ramírez LP, Landfester K (2003) Magnetic polystyrene nanoparticles with a high magnetite content obtained by miniemulsion processes. *Macromol Chem Phys* 204:22–31
94. Landfester K, Ramírez LP (2003) Encapsulated magnetite particles for biomedical application. *J Phys Condens Matter* 15:S1345–S1361
95. Barraza HJ, Pompeo F, O'Rear EA et al (2002) SWNT-filled thermoplastic and elastomeric composites prepared by miniemulsion polymerization. *Nano Lett* 2:797–802
96. Ha MLP, Grady BP, Lolli G et al (2007) Composites of single-walled carbon nanotubes and styrene-isoprene copolymer latices. *Macromol Chem Phys* 208:446–456
97. Ham HT, Choi YS, Chee MG et al (2006) Singlewall carbon nanotubes covered with polystyrene nanoparticles by in-situ miniemulsion polymerization. *J Polym Sci Part A: Polym Chem* 44:573–584
98. Lu HF, Xin JH, Fei B et al (2007) Synthesis and lubricating performance of a carbon nanotube seeded miniemulsion. *Carbon* 45:936–942
99. Ham HT, Choi YS, Jeong N et al (2005) Singlewall carbon nanotubes covered with polypyrrole nanoparticles by the miniemulsion polymerization. *Polymer* 46:6308–6315
100. Lu HF, Fei B, Xin JH et al (2006) Fabrication of UV-blocking nanohybrid coating via miniemulsion polymerization. *J Colloid Interface Sci* 300:111–116
101. Luo YD, Dai CA, Chiu WY (2008) Synthesis of P(AA-SA)/ZnO composite latex particles via inverse miniemulsion polymerization and its application in pH regulation and UV shielding. *J Polym Sci Part A: Polym Chem* 46:8081–8090
102. Zhang JJ, Gao G, Zhang M et al (2006) ZnO/PS core-shell hybrid microspheres prepared with miniemulsion polymerization. *J Colloid Interface Sci* 301:78–84



103. Mahdavian A, Sarrafi Y, Shabankareh M (2009) Nanocomposite particles with core-shell morphology III: preparation and characterization of nano  $\text{Al}_2\text{O}_3$ -poly(styrene-methyl methacrylate) particles via miniemulsion polymerization. *Polym Bull* 63:329–340
104. Lopez-Martinez EI, Marquez-Lucero A, Hernandez-Escobar CA et al (2007) Incorporation of silver/carbon nanoparticles into poly(methyl methacrylate) via in situ miniemulsion polymerization and its influence on the glass-transition temperature. *J Polym Sci Part B: Polym Phys* 45:511–518
105. Crespy D, Landfester K (2009) Synthesis of polyvinylpyrrolidone/silver nanoparticles hybrid latex in non-aqueous miniemulsion at high temperature. *Polymer* 50:1616–1620
106. Erdem B, Sully Y, Sudol ED et al (2000) Determination of miniemulsion droplet size via soap titration. *Langmuir* 16:4890–4895
107. Erdem B, Sudol ED, Dimonie VL et al (2000) Encapsulation of inorganic particles via miniemulsion polymerization. III. Characterization of encapsulation. *J Polym Sci Part A: Polym Chem* 38:4441–4450
108. Erdem B, Sudol ED, Dimonie VL et al (2000) Encapsulation of inorganic particles via miniemulsion polymerization. II. Preparation and characterization of styrene miniemulsion droplets containing  $\text{TiO}_2$  particles. *J Polym Sci Part A: Polym Chem* 38:4431–4440
109. Erdem B, Sudol ED, Dimonie VL et al (2000) Encapsulation of inorganic particles via miniemulsion polymerization. I. Dispersion of titanium dioxide particles in organic media using OLOA 370 as stabilizer. *J Polym Sci Part A: Polym Chem* 38:4419–4430
110. Erdem B, Sudol ED, Dimonie VL et al (2000) Encapsulation of inorganic particles via miniemulsion polymerization. *Macromol Symp* 155:181–198
111. Al-Ghamdi GH, Sudol ED, Dimonie VL et al (2006) Encapsulation of titanium dioxide in styrene/*n*-butyl acrylate copolymer by miniemulsion polymerization. *J Appl Polym Sci* 101:3479–3486
112. Al-Ghamdi GH, Sudol ED, Dimonie VL et al (2006) High PVC film-forming composite latex particles via miniemulsification, part 3: optical properties. *J Appl Polym Sci* 101:4526–4537
113. Al-Ghamdi GH, Sudol ED, Dimonie VL et al (2006) High PVC film-forming composite latex particles via miniemulsification, part 2: efficiency of encapsulation. *J Appl Polym Sci* 101:4517–4525
114. Al-Ghamdi GH, Sudol ED, Dimonie VL et al (2006) High PVC film-forming composite latex particles via miniemulsification, part 1: preparation. *J Appl Polym Sci* 101:4504–4516
115. Kim H, Daniels ES, Li S et al (2007) Polymer encapsulation of yttrium oxysulfide phosphorescent particles via miniemulsion polymerization. *J Polym Sci Part A: Polym Chem* 45:1038–1054
116. Yang Y, Wen Z, Dong Y et al (2006) Incorporating CdTe nanocrystals into polystyrene microspheres: towards robust fluorescent beads. *Small* 2:898–901
117. Fleischhaker F, Zentel R (2005) Photonic crystals from core-shell colloids with incorporated highly fluorescent quantum dots. *Chem Mater* 17:1346–1351
118. Esteves ACC, Barros-Timmons A, Monteiro T et al (2005) Polymer encapsulation of CdE ( $E = \text{S}, \text{Se}$ ) quantum dot ensembles via in-situ radical polymerization in miniemulsion. *J Nanosci Nanotechnol* 5:766–771
119. Joumaa N, Lansalot M, Theretz A et al (2006) Synthesis of quantum dot-tagged submicrometer polystyrene particles by miniemulsion polymerization. *Langmuir* 22:1810–1816
120. Peres M, Costa LC, Neves A et al (2005) A green-emitting CdSe/poly(butyl acrylate) nanocomposite. *Nanotechnology* 16:1969–1973
121. Esteves ACC, Bombalski L, Trindade T et al (2007) Polymer grafting from CdS quantum dots via AGET ATRP in miniemulsion. *Small* 3:1230–1236
122. Tiarks F, Landfester K, Antonietti M (2001) Silica nanoparticles as surfactants and fillers for latexes made by miniemulsion polymerization. *Langmuir* 17:5775–5780
123. Qiao XG, Chen M, Zhou J et al (2007) Synthesis of raspberry-like silica/polystyrene/silica multilayer hybrid particles via miniemulsion polymerization. *J Polym Sci Part A: Polym Chem* 45:1028–1037
124. Zhang SW, Zhou SX, Weng YM et al (2005) Synthesis of  $\text{SiO}_2$ /polystyrene nanocomposite particles via miniemulsion polymerization. *Langmuir* 21:2124–2128



125. Zhou J, Zhang SW, Qiao XG et al (2006) Synthesis of SiO<sub>2</sub>/poly(styrene-*co*-butyl acrylate) nanocomposite microspheres via miniemulsion polymerization. *J Polym Sci Part A: Polym Chem* 44:3202–3209
126. Qi DM, Bao YZ, Weng ZX et al (2006) Preparation of acrylate polymer/silica nanocomposite particles with high silica encapsulation efficiency via miniemulsion polymerization. *Polymer* 47:4622–4629
127. Zhou J, Chen M, Qiao XG et al (2006) Facile preparation method of SiO<sub>2</sub>/PS/TiO<sub>2</sub> multi-layer core-shell hybrid microspheres. *Langmuir* 22:10175–10179
128. Lu W, Chen M, Wu L (2008) One-step synthesis of organic-inorganic hybrid asymmetric dimer particles via miniemulsion polymerization and functionalization with silver. *J Colloid Interface Sci* 328:98–102
129. Qiang W, Wang Y, He P et al (2008) Synthesis of asymmetric inorganic/polymer nanocomposite particles via localized substrate surface modification and miniemulsion polymerization. *Langmuir* 24:606–608
130. Ge X, Wang M, Yuan Q et al (2009) The morphological control of anisotropic polystyrene/silica hybrid particles prepared by radiation miniemulsion polymerization. *Chem Commun* 2765–2767
131. Bailly B, Donnenwirth AC, Bartholome C et al (2006) Silica-polystyrene nanocomposite particles synthesized by nitroxide-mediated polymerization and their encapsulation through miniemulsion polymerization. *J Nanomater* 2006 Article ID 76371
132. Bombalski L, Min K, Dong H et al (2007) Preparation of well-defined hybrid materials by ATRP in miniemulsion. *Macromolecules* 40:7429–7432
133. Toepfer O, Schmidt-Naake G (2007) Surface – functionalized inorganic nanoparticles in miniemulsion polymerization. *Macromol Symp* 248:239–248
134. Monteil V, Stumbaum J, Thomann R et al (2006) Silica/poly ethylene nanocomposite particles from catalytic emulsion polymerization. *Macromolecules* 39:2056–2062
135. Boutti S, Bourgeat-Lami E, Zydowicz N (2005) Silica/polyamide nanocomposite synthesis via an original double emulsification process in miniemulsion. *Macromol Rapid Commun* 26:1860–1865
136. Wang Y, Xu H, Qiang W et al (2009) Asymmetric composite nanoparticles with anisotropic surface functionalities. *J Nanomater* 2009 Article ID 620269
137. Diaconu G, Asua JM, Paulis M et al (2007) High-solids content waterborne polymer-clay nanocomposites. *Macromol Symp* 259:305–317
138. Diaconu G, Micusik M, Bonnefond A et al (2009) Macroinitiator and macromonomer modified montmorillonite for the synthesis of acrylic/MMT nanocomposite latexes. *Macromolecules* 42:3316–3325
139. Moraes RP, Santos AM, Oliveira PC et al (2006) Poly(styrene-*co*-butyl acrylate)-Brazilian montmorillonite nanocomposites, synthesis of hybrid latexes via miniemulsion polymerization. *Macromol Symp* 245/246:106–115
140. Bouanani F, Bendedouch D, Hemery P et al (2008) Encapsulation of montmorillonite in nanoparticles by miniemulsion polymerization. *Colloids Surf A Physicochem Eng Asp* 317:751–755
141. Moraes RP, Valera TS, Demarquette NR et al (2009) Influence of granulometry and organic treatment of a Brazilian montmorillonite on the properties of poly(styrene-*co*-*n*-butyl acrylate)/layered silicate nanocomposites prepared by miniemulsion polymerization. *J Appl Polym Sci* 112:1949–1958
142. Samakande A, Sanderson RD, Hartmann PC (2009) Rheological properties of RAFT-mediated poly(styrene-*co*-butyl acrylate)-clay nanocomposites [P(S-*co*-BA)-PCNs]: Emphasis on the effect of structural parameters on thermo-mechanical and melt flow behaviors. *Polymer* 50:42–49
143. Samakande A, Sanderson RD, Hartmann PC (2008) Encapsulated clay particles in polystyrene by RAFT mediated miniemulsion polymerization. *J Polym Sci Part A: Polym Chem* 46:7114–7126
144. Tong ZH, Deng YL (2006) Synthesis of water-based polystyrene-nanoclay composite suspension via miniemulsion polymerization. *Ind Eng Chem Res* 45:2641–2645

145. Tong ZH, Deng YL (2008) Kinetics of miniemulsion polymerization of styrene in the presence of organoclays. *Macromol Mater Eng* 293:529–537
146. Diaconu G, Paulis M, Leiza JR (2008) High solids content waterborne acrylic/montmorillonite nanocomposites by miniemulsion polymerization. *Macromol React Eng* 2:80–89
147. Mirzataheri M, Mahdavian A, Atai M (2009) Nanocomposite particles with core-shell morphology IV: an efficient approach to the encapsulation of Cloisite 30B by poly (styrene-*co*-butyl acrylate) and preparation of its nanocomposite latex via miniemulsion polymerization. *Colloid Polym Sci* 287:725–732
148. Sun QH, Deng YL, Wang ZL (2004) Synthesis and characterization of polystyrene-encapsulated laponite composites via miniemulsion polymerization. *Macromol Mater Eng* 289:288–295
149. Tong ZH, Deng YL (2007) Synthesis of polystyrene encapsulated nanosaponite composite latex via miniemulsion polymerization. *Polymer* 48:4337–4343
150. Samakande A, Juodaitis JJ, Sanderson RD et al (2008) Novel cationic RAFT-mediated polystyrene/clay nanocomposites: Synthesis, characterization, and thermal stability. *Macromol Mater Eng* 293:428–437
151. Alexandre M, Dubois P (2000) Polymer-layered silicate nanocomposites: preparation, properties and uses of a new class of materials. *Mater Sci Eng R Rep* 28:1–63
152. Martins MA, Neves MC, Esteves ACC et al (2007) Biofunctionalized ferromagnetic CoPt<sub>3</sub>/polymer nanocomposites. *Nanotechnology* 18:7
153. van Berkel KY, Piekarski AM, Kierstead PH et al (2009) A simple route to multimodal composite nanoparticles. *Macromolecules* 42:1425–1427
154. Xu ZZ, Wang CC, Yang WL et al (2004) Encapsulation of nanosized magnetic iron oxide by polyacrylamide via inverse miniemulsion polymerization. *J Magn Magn Mater* 277:136–143
155. Wormuth K (2001) Superparamagnetic latex via inverse emulsion polymerization. *J Colloid Interface Sci* 241:366–377
156. Ménager C, Sandre O, Mangili J et al (2004) Preparation and swelling of hydrophilic magnetic microgels. *Polymer* 45:2475–2481
157. Xu ZZ, Wang CC, Yang WL et al (2005) Synthesis of superparamagnetic Fe<sub>3</sub>O<sub>4</sub>/SiO<sub>2</sub> composite particles via sol-gel process based on inverse miniemulsion. *J Mater Sci* 40:4667–4669
158. Lin CL, Chiu WY, Don TM (2006) Superparamagnetic thermoresponsive composite latex via W/O miniemulsion polymerization. *J Appl Polym Sci* 100:3987–3996
159. Zhang QY, Zhang HP, Xie G et al (2007) Effect of surface treatment of magnetic particles on the preparation of magnetic polymer microspheres by miniemulsion polymerization. *J Magn Magn Mater* 311:140–144
160. Chen ZJ, Peng K, Mi YL (2007) Preparation and properties of magnetic polystyrene microspheres. *J Appl Polym Sci* 103:3660–3666
161. Betancourt-Galindo R, Saldivar R, Rodriguez-Fernandez OS et al (2004) Preparation and characterization of magnetic latexes using styrene monomer. *Polym Bull* 51:395–402
162. Betancourt-Galindo R, Saldivar-Guerrero R, Rodriguez-Fernandez OS et al (2004) Preparation of magnetic latexes using styrene monomer. *J Alloys Compd* 369:87–89
163. Zhang QY, Xie G, Zhang HP et al (2007) Encapsulation of magnetic particles via miniemulsion polymerization of styrene. II. Effect of some parameters on the polymerization of styrene. *J Appl Polym Sci* 105:3525–3530
164. Baharvand H (2008) Preparation and characterization of fluorescent polymer magnetic particles. *J Appl Polym Sci* 109:1823–1828
165. Qian Z, Zhicheng Z, Yun C (2008) A novel preparation of surface-modified paramagnetic magnetite/polystyrene nanocomposite microspheres by radiation-induced miniemulsion polymerization. *J Colloid Interface Sci* 327:354–361
166. Joumaa N, Toussay P, Lansalot M et al (2007) Surface modification of iron oxide nanoparticles by a phosphate-based macromonomer and further encapsulation into submicrometer polystyrene particles by miniemulsion polymerization. *J Polym Sci Part A: Polym Chem* 46:327–340

167. Mahdavian AR, Ashjari M, Mobarakeh HS (2008) Nanocomposite particles with core-shell morphology. I. Preparation and characterization of  $\text{Fe}_3\text{O}_4$ -poly(butyl acrylate-styrene) particles via miniemulsion polymerization. *J Appl Polym Sci* 110:1242–1249
168. Mahdavian AR, Sehri Y, Salehi-Mobarakeh H (2008) Nanocomposite particles with core-shell morphology II. An investigation into the affecting parameters on preparation of  $\text{Fe}_3\text{O}_4$ -poly (butyl acrylate-styrene) particles via miniemulsion polymerization. *Eur Polym J* 44:2482–2488
169. Tu C, Yang Y, Gao M (2008) Preparations of bifunctional polymeric beads simultaneously incorporated with fluorescent quantum dots and magnetic nanocrystals. *Nanotechnology* 19:105601
170. Nunes JS, De Vasconcelos CL, Cabral FAO et al (2006) Synthesis and characterization of poly(ethyl methacrylate-co-methacrylic acid) magnetic particles via miniemulsion polymerization. *Polymer* 47:7646–7652
171. Nunes JS, de Vasconcelos CL, Dantas TNC et al (2008) Preparation of acrylic latexes with dispersed magnetite nanoparticles. *J Dispersion Sci Technol* 29:769–774
172. Zheng WM, Gao F, Gu HC (2005) Carboxylated magnetic polymer nanolatexes: Preparation, characterization and biomedical applications. *J Magn Magn Mater* 293:199–205
173. Lu SH, Forcada J (2006) Preparation and characterization of magnetic polymeric composite particles by miniemulsion polymerization. *J Polym Sci Part A: Polym Chem* 44:4187–4203
174. Csetneki I, Faix MK, Szilagyi A et al (2004) Preparation of magnetic polystyrene latex via the miniemulsion polymerization technique. *J Polym Sci Part A: Polym Chem* 42:4802–4808
175. Mori Y, Kawaguchi H (2007) Impact of initiators in preparing magnetic polymer particles by miniemulsion polymerization. *Colloids Surf B Biointerfaces* 56:246–254
176. Gong T, Yang D, Hu J et al (2009) Preparation of monodispersed hybrid nanospheres with high magnetite content from uniform  $\text{Fe}_3\text{O}_4$  clusters. *Colloids Surf A Physicochem Eng Asp* 339:232–239
177. Tan CJ, Chua HG, Ker KH et al (2008) Preparation of bovine serum albumin surface-imprinted submicrometer particles with magnetic susceptibility through core-shell miniemulsion polymerization. *Anal Chem* 80:683–692
178. Tan CJ, Tong YW (2007) Preparation of superparamagnetic ribonuclease a surface-imprinted submicrometer particles for protein recognition in aqueous media. *Anal Chem* 79:299–306
179. Liu XQ, Guan YP, Ma ZY et al (2004) Surface modification and characterization of magnetic polymer nanospheres prepared by miniemulsion polymerization. *Langmuir* 20:10278–10282
180. Qian H, Lin ZY, Xu HM et al (2009) The efficient and specific isolation of the antibodies from human serum by thiophilic paramagnetic polymer nanospheres. *Biotechnol Prog* 25:376–383
181. Zheng WM, Gao F, Gu HC (2005) Magnetic polymer nanospheres with high and uniform magnetite content. *J Magn Magn Mater* 288:403–410
182. Qiu GH, Wang Q, Wang C et al (2007) Polystyrene/ $\text{Fe}_3\text{O}_4$  magnetic emulsion and nanocomposite prepared by ultrasonically initiated miniemulsion polymerization. *Ultrason Sonochem* 14:55–61
183. Qiu GH, Wang Q, Wang C et al (2006) Ultrasonically initiated miniemulsion polymerization of styrene in the presence of  $\text{Fe}_3\text{O}_4$  nanoparticles. *Polym Int* 55:265–272
184. Faridi-Majidi R, Sharifi-Sanjani N, Agend F (2006) Encapsulation of magnetic nanoparticles with polystyrene via emulsifier-free miniemulsion polymerization. *Thin Solid Films* 515:368–374
185. Faridi-Majidi R, Sharifi-Sanjani N (2007) Emulsifier-free miniemulsion polymerization of styrene and the investigation of encapsulation of nanoparticles with polystyrene via this procedure using an anionic initiator. *J Appl Polym Sci* 105:1244–1250
186. Faridi-Majidi R, Sharifi-Sanjani N (2007) Preparation of magnetic latexes functionalized with chloromethyl groups via emulsifier-free miniemulsion polymerization. *J Magn Magn Mater* 311:55–58
187. Lu S, Ramos J, Forcada J (2007) Self-stabilized magnetic polymeric composite nanoparticles by emulsifier-free miniemulsion polymerization. *Langmuir* 23:12893–12900

188. Yan F, Li J, Zhang J et al (2009) Preparation of  $\text{Fe}_3\text{O}_4$ /polystyrene composite particles from monolayer oleic acid modified  $\text{Fe}_3\text{O}_4$  nanoparticles via miniemulsion polymerization. *J Nanopart Res* 11:289–296
189. Cui L, Xu H, He P et al (2007) Developing a hybrid emulsion polymerization system to synthesize  $\text{Fe}_3\text{O}_4$ /polystyrene latexes with narrow size distribution and high magnetite content. *J Polym Sci Part A: Polym Chem* 45:5285–5295
190. Shao D, Xia A, Hu J et al (2008) Monodispersed magnetite/silica composite microspheres: Preparation and application for plasmid DNA purification. *Colloids Surf A Physicochem Eng Asp* 322:61–65
191. Sun Y, Wang B, Wang HP et al (2007) Controllable preparation of magnetic polymer microspheres with different morphologies by miniemulsion polymerization. *J Colloid Interface Sci* 308:332–336
192. Cui LL, Gu HC, Xu H et al (2006) Synthesis and characterization of superparamagnetic composite nanorings. *Mater Lett* 60:2929–2932

# Organic–Inorganic Hybrid Magnetic Latex

Md Mahbubor Rahman and Abdelhamid Elaissari

**Abstract** The preparation of magnetic hybrid latex, consisting of inorganic magnetic iron oxide nanoparticles and organic polymer, in dispersed media is reviewed. The aim of this chapter is to highlight the recent advances of research into the synthesis of hybrid magnetic latex preparation in dispersed media. Although the term “organic–inorganic hybrid composite/latex” covers a wide range of materials, this review will principally focus on the preparation methods, emphasizing emulsion polymerization in the presence of inorganic iron oxide magnetic particles. However, some relevant hybrid polymer latexes of other metal oxides and their synthetic methods will be highlighted. Furthermore, some applications and properties of magnetic latex, polymerization parameters and the shortcomings of preparation methods will be reviewed.

**Keywords** Core–shell morphology · Dispersion polymerization · Emulsion polymerization · Ferrofluids · Hybrid latex · Magnetic latexes · Magnetic nanoparticles

## Contents

1	Introduction .....	239
2	Applications of Magnetic Particles .....	241
2.1	Biomedical Applications of Magnetic Latex .....	241
3	Iron Oxide Magnetic Nanoparticles .....	245
3.1	Mechanical Size Reduction Method .....	246
3.2	Chemical Methods .....	246
4	Synthesis of Magnetic Latex .....	251
4.1	Magnetic Latex Fabrication in Preformed Polymers .....	251
4.2	In Situ Synthesis .....	253
4.3	Polymerizations of Monomer in the Presence of Magnetic Nanoparticles .....	257
5	Concluding Remarks .....	276
	References .....	277

## Abbreviations

μ-TAS	Micro total analysis system
AA	Acrylic acid
AAEM	Acetoacetoxyethyl methacrylate
ACPA	4,4-Azobis(4-cyanopentanoic acid)
ACVA	4,4-Azobis(4-cyanovaleric acid)
AEM	2-Aminoethylmethacrylate
AIBA	2,2-Azobis(2-isobutyramidine)
AIBN	Azobis(isobutyronitrile)
AM	Acrylamide
APS	Ammonium persulphate
ATRP	Atom transfer radical polymerization
CA	Cetylalcohol
DVB	Divinylbenzene
EA	Ethylacrylate
EDA	Ethylene diamine
EGDM	Ethylene glycol dimethacrylate
GLYMO	[3-(Glycidyloxy)propyl] trimethoxysilane
GMA	Glycidyl methacrylate
IgepalCO-520	Poly(oxyethylene nonylphenylether)
KPS	Potassium persulphate
LBL	Layer-by-layer
MAA	Methacrylic acid
MBA	<i>N,N</i> -methylene bis acrylamide
MMA	Methyl methacrylate
MPDMS	Methacryloxypropyl dimethoxysilane
MPSA	3-Mercapto-1-propane sulfonic acid
MPTMS	[3-(Methacryloxy)propyl]trimethoxysilane
MRI	Magnetic resonance imaging
NIPAM	<i>N</i> -Isopropyl acrylamide
NVP	<i>N</i> -Vinyl pirolidone
Oligo-dT	Oligodeoxythymidylic acid
P(DMAEMA-EGMA)	Poly(2-dimethyl aminoethyl methacrylate–ethylene glycol dimethacrylate)
PAA	Poly(acrylic acid)
PAMPS	Poly(2-acrylamido-2-methyl-1-propanesulphonic acid)
PCL	Poly( $\epsilon$ -caprolactone)
PEG	Poly(ethylene glycol)
PEO	Poly(ethylene oxide)
PEI	Poly(ethylene imine)
PEOAM	Poly(ethylene oxide acrylamide)
PEOVB	Poly(ethylenoxide) vinylbenzene

PGMA	Poly(glycidyl methacrylate)
PHEMA	Poly(2-hydroxyethyl methacrylate)
PLGA	Poly(D,L-lactide- <i>co</i> -glycolide)
PLLA	Poly(L-lactide)
PMA	Poly(methacrylic acid)
PMAMVE	Poly(maleic anhydride- <i>alt</i> -methyl vinyl ether)
PMI	<i>N</i> -(2,6-Diisopropylphenyl)-perylene-3, 4-dicarbonacidimide
PMMA	Poly(methyl methacrylate)
PPO	Poly(propylene oxide)
PVA	Poly(vinyl alcohol)
SDS	Sodium dodecyl sulphate
SEM	Scanning electron microscopy
St	Styrene
TEM	Transmission electron microscopy
TEOS	Tetraethyl orthosilicate
TGA	Thermogravimetric analysis
Triton X-405	Poly(oxyethylene) isooctylphenylether
V-59	2,2-Azobis(2-methylbutyronitrile)
VA-057	2,2-Azobis[ <i>N</i> -(2-carboxyethyl)-2-methyl- propionamidine]
VSM	Vibrating sample magnetometry

## 1 Introduction

Composite or hybrid materials are materials consisting of organic materials (i.e. polymers) and inorganic materials. The latter can be composed of a metal oxide such as iron oxide, silica, gold particles or quartz powder. Magnetic latex is a hybrid material consisting of polymer-encapsulated magnetic particles. The discussion in this chapter will be confined to iron oxide magnetic nanoparticles.

Currently, an enormous amount of magnetic particles are produced, and outstanding research is performed due to their promising applications. Research into magnetic latex at the smaller nano- and microlevels is of great interest. The special behaviour of these nano/micromaterials points to a very promising future in the area of biomedical applications [1, 2].

The size of nanoparticles permits access to the area of quantum behaviour. It is in this size range that a lot of progress has been made in different scientific areas such as chemistry, physics and, principally, in biotechnology [3]. By changing the size of the nano/microparticles or using different kinds of materials, the relaxation time of magnetic particles can also be changed. Magnetic nanoparticles have been (and will be in the future) a very useful tool in various kind of applications, from



biomedical to information carriers and data storage systems. Even the micro total analysis system ( $\mu$ -TAS) has been developed using magnetic particles as magnetic fluid stimuli-responsive carriers [4].

Metal oxides can show a variety of interesting magnetic, electronic and optical properties that can be used in many applications. For instance, when metal oxides like  $\text{TiO}_2$  are incorporated into hybrid materials, they act as pigments to enhance the appearance and durability of polymeric films. Properties such as wettability, solubility, corrosion resistance, modulus, strength, gas permeability, heat resistance and flammability can also be tuned by combining inorganic materials with polymers. Magnetic polymers can even be used in hostile environments such as seawater and petroleum [5].

Profound attention has been given to the magnetic latexes because of their special properties like superparamagnetism, high field irreversibility, high saturation field and extra anisotropy contribution. These properties are, for example, controlled by size and surface type.

Among the magnetic particles, iron oxides such as magnetite ( $\text{Fe}_3\text{O}_4$ ) or its oxidized form maghemite ( $\gamma\text{-Fe}_2\text{O}_3$ ) are mostly preferred in biomedical applications because they are superparamagnetic and biocompatible [6]. There are many other highly magnetic materials like cobalt and nickel oxides but they are usually toxic and prone to oxidation.

The encapsulation and/or surface modification of magnetic nanoparticles by polymers protects particles from oxidation, and improves toxicity, dispersability and colloidal stability. In the paint industry, the encapsulation of pigments and other fillers with polymers is sometimes applied. A pigment like titanium dioxide is introduced in paints to achieve opacity, which depends on light absorption as well as light scattering. The latter is related to the particle size and to the distance between particles. Agglomeration of pigments can occur by flocculation during drying and reduces the scattering effectiveness of the dispersed pigment particles. The polymer coating of pigments can solve the above problem, preventing flocculation of particles in the paint film [7]. Besides chemical and block resistance, better adhesion and protection from ambient unwanted materials are the advantages of the encapsulation of pigments with polymers.

In the biomedical field, the role of polymers in the preparation of magnetic composites and latexes is generally to protect the inorganic part and to induce reactive chemical functions capable of immobilizing biomolecules via chemical reactions. The chemical reaction between magnetic polymers and biological species may occur by the formation of covalent bonds or hydrogen bonding. The presence of magnetic materials endows the polymer particles with additional properties [8]. For instance, iron oxides and ferrites are used to produce conducting polymers [9], in magnetic polymer composites for radiowave-absorbing materials [10], to modify the optical properties of films [11], and for inks used in printers based on magnetism [12] where the specific magnetic properties of iron oxides are utilized.

## 2 Applications of Magnetic Particles

There is a broad range of applications of polymer-coated magnetic particles in different industrial sectors. The particles are interesting for the preparation of paint, ink, pharmaceuticals, cosmetic formulations and catalyst carriers, and are used in the paper industry and for chromatographic separation, water treatment, waste management etc. [13–17]. Moreover, magnetic particles are of interest in some other industries, e.g. for recording media and magnetic seals in motors. Magnetic particles are used extensively in pharmacy, biology and medicine to transport biological compounds. Biomolecules can be separated quickly from a complex medium by fixing them to magnetic particles. They can be used not only *in vitro* for diagnostic applications but also for *in vivo* therapeutic applications. The magnetic latex must have the following characteristics, regardless of the application in the biomedical field:

- Colloidal and chemical stability in different conditions and media
- No or very low magnetic remanence that affects the dispersability of the particles after removing the external magnetic field
- In cases where no remanence occurs, no magnetic interactions among the particles remain; with low remanence it is easy to disperse particles after switching off the applied magnetic field
- No leaching of iron oxide in the case of biomedical applications
- The small size renders a large surface area for adsorption and/or interaction of biomolecules and a low sedimentation rate in comparison to the magnetic separation process
- Capable of complete and rapid separation
- Biocompatible surface
- Good response to the applied external magnetic field, because with a better response, the necessary intensity of the applied magnetic field can be lower and leads to a better process rate
- Easy production and low cost

For the magnetic particles to be biocompatible, the particles must be coated with biocompatible polymers in order to prevent the formation of large aggregates, geometry change and biodegradation when exposed to a biological system.

### 2.1 *Biomedical Applications of Magnetic Latex*

#### 2.1.1 **In Vivo Applications**

The magnetic latex can be utilized in therapeutic processes, for example magnetic resonance imaging (MRI) [18], targeted drug delivery [19, 20] and hyperthermia [21].

## MRI Contrast Agents

The intensity of human body tissue proton(s) is measured in a particular magnetic field using the MRI technique. Normally, the difference of the proton signal intensity between healthy tissue and affected tissue is not sufficient to be useful for diagnostic assessment [22]. As a contrast agent, magnetic particles bearing superparamagnetic iron oxides can play a pivotal role in amplifying the signal intensity difference between healthy and affected tissue in MRI. The magnetic particles within tissue help to obtain a significantly larger signal from the MRI scanner. In medicine, MRI is used to demonstrate pathological or other physiological alterations of living tissues. In an MRI examination under a magnetic field, the magnetic particles localized in the tumour can be detected. The effect of the magnetic nanoparticles in the MRI sequence can be attributed to the resulting magnetic field heterogeneity around these particles, through which water molecules diffuse and induce a modification of proton relaxation. Some researchers combined drug delivery and MRI approaches in a one-design system [23]. For example, in clinical oncology, magnetic MRI-guided delivery of drug-loaded nanoparticles administered by an intratumoral injection, (or intravenously) can result in remarkably better treatment efficiency [18, 23].

## Controlled Drug Delivery

The typical procedure for drug administration, in which drugs are injected intravenously or orally for general systemic distribution, is accompanied by some problems. Some examples are non-specificity to the target site, the need to use high doses to get the required result, side effects and toxicity to normal cells. Different types of drug delivery approaches have been scouted to resolve the above-mentioned problems and to increase the amount of uptake drugs into lesion (wound) cells. The use of magnetic micro- or nanoparticles as a carrier for drugs has the potential to mitigate the side effects and to control the drug distribution on the target site [24]. In this technique, drugs immobilized on magnetic particles can be transported in a controlled manner to target sites through applying an external high magnetic field gradient. However, it is less effective in the interior of the human body because of the lower magnetic field strength at a larger distance [25]. This problem can be overcome by implanting magnets close to the target site within the body [26]. It is also interesting that magnetic particles accumulate not only at the required site but also throughout the cross-section from the external source to the depth marking the effective field limit [27]. In a recent review, the interaction of nanoparticles with cells has been discussed [28]. Superparamagnetic iron oxide nanoparticles encapsulated with different polymers have been explored for targeted and controlled drug delivery. Gang et al. [29] reported the preparation of tetraheptylammonium-capped  $\text{Fe}_3\text{O}_4$  magnetic nanoparticles to study the accumulation of anticancer drug in target cancer cells and revealed that magnetic nanoparticles enhance the interaction of anticancer drugs with leukaemia cells, which resulted in a higher uptake of the drug by cancer cells. Recently, multilayered magnetic composites consisting of a magnetic

core and two coating shells made up of poly(*N*-isopropyl acrylamide) (PNIPAM) and poly(D,L-lactide-*co*-glycolide) (PLGA) have been prepared for controlled drug delivery [30]. Magnetic particles, for example embedded in poly(ethylene glycol) (PEG) [31], thermally sensitive hydrogel [20, 21] or liposomes [32, 33] are also used in drug delivery.

## Hyperthermia

Hyperthermia is an approach in which heat is applied to a definite tissue site containing malevolent cells in order to reduce the viability of cancer cells and increase their sensitivity to chemotherapy and radiation [34]. In hyperthermia, magnetic particles are used to kill affected cells by producing heat and elevating the body temperature due to the action of an external magnetic field with limited effect on the healthy cells. Magnetic particles guided by an external electromagnetic field emit energy in the form of heat, which raises the temperature to such a level (42–45°C) that pernicious tissues can be destroyed or paralyzed [35]. Cationic magnetic liposomes, which can be used as heating mediator for application in local hyperthermia, have been developed [36]. Different clinical applications of magnetic particles for hyperthermia are summarized in [37].

### 2.1.2 In Vitro Applications

#### Magnetic Separation

In biomedical diagnostics, the use of magnetic latex can replace the time-consuming and laborious steps of centrifugation or filtration [38]. The separation technique is associated with the binding of magnetic particles to biomolecules that have specific affinity to target molecules for separation or analysis. Since magnetic supports can be separated from solutions containing other species like suspended solids, cell fragments and contaminants, the magnetic affinity separation is useful for crude samples [39, 40]. Direct and indirect methods of separation are frequently used in biomedical diagnostics, such as for detecting disease with magnetic particles and for specific interaction between biological molecules (e.g. antibody/antigen or nucleic acids). In the direct method, the magnetic particles carrying antibodies are mixed with the sample containing the target molecules and then the mixture is kept for incubation. During the incubation, an immunological reaction takes place between the molecules immobilized on the particles and the target molecules. Then, by applying a magnetic field, the particles are separated. In the case of indirect methods, the target molecule in the sample is recognized by a specific molecule (first molecule), which is capable of reacting with another second molecule that is immobilized on the magnetic particles. The indirect method is more specific than the direct method [41].

## Immunoassay

The process by which the concentration or the amount of any analyte in solution is determined through an interaction between the antibody and the targeted antigen, is called an immunoassay. Generally, either the antibody or antigen is immobilized onto a solid support, which can be magnetic particles to make the immunoassay easier. Superparamagnetic particles are used in sandwich or competitive binding immunoassay. In a sandwich immunoassay, target antigens that have two binding sites to an antibody immobilized on magnetic particles can be physically separated from a mixture containing analyte (antigen). Labelled antibodies (using radiolabels, fluorescent dyes, enzymes or chemiluminescent molecules) are used to measure the bound target. On the other hand, antigens having a single binding site (to antibody) are measured by a competitive immunoassay [42]. Magnetic beads seem to be one of the most effective methods for removing tumour cells from bone marrow [43]. It should be mentioned that magnetic latexes, which have a large surface area in combination with functional group(s) on the surface for binding of biomolecules, have been tested for many different immunological applications for their easy separation from any medium [44, 45].

## Magnetic Latex for Nucleic Acids

The use of magnetic particles as a solid support in the separation, isolation and purification of nucleic acid is indispensable in the biomedical field. It offers benefits over conventional methods like phenol extraction or ethanol precipitation methods [46]. Specific DNA isolation and extraction (to obtain purified nucleic acid) without using any organic solvent is required in biomedical diagnostic tests and is possible with magnetic particles. Polymeric magnetic particles linked to oligodeoxythymidylic acid (oligo-dT) are also used to purify mutated RNA (e.g. polyadenylated RNA) for identifying genes, cDNA synthesis and subtracting hybridization [41]. Other magnetic colloidal particles (e.g. cationic, gelatin-coated and silica-coated particles) are used as solid support for nucleic acid extraction and concentration [47–50].

Magnetic latex for protein and enzyme isolation, separation and purification is widely used in the field of biotechnology. One of the advantages of using magnetic particles is that the denaturation of proteins can be prevented [51]. Protein or enzymes are subject to lower shear stresses in magnetic separation than in centrifugation, filtration or chromatographic separations. The magnetic latex consisting of an iron oxide magnetic core and a polymeric shell can be easily adapted to immobilize antibodies [52], proteins [53] and enzymes [54, 55]. The magnetic polymer particles usually need to be sufficiently hydrophobic to allow a relatively strong physical adsorption of antibodies via hydrophobic interaction. On the other hand, the immobilization of biomolecules is sensitive to different parameters like temperature, pH, ionic strength and viscosity of the medium. For this reason, the presence of

different kinds of reactive functional groups on the surface of the magnetic particles can be used for chemical covalent grafting instead of physical hydrophobic interaction with biomolecules [56].

### Virus and Bacteria Capture

Magnetic particles have been investigated in labelling processes like accelerated agglutination [57] and accelerated sedimentation. Besides the above applications, magnetic latex is very suitable for extraction or concentration of viruses and bacteria. Recently, some work has been done using magnetic beads for virus detection and concentration [58, 59]. In the study of Satoh et al. [58], some DNA and RNA viruses were concentrated more than 100 and 1000 times, respectively, using poly(ethylene imine) (PEI)-conjugated magnetic beads. Elaissari et al. [59] developed functionalized magnetic beads with low-diameter and high iron oxide content to obtain a large reactive surface area and rapid magnetic separation, and to develop tools for generic virus extraction and purification.

The bacteria tested for most often in the food industry are *Salmonella*, *Escherichia coli* and *Listeria*. Numerous detection processes use magnetic particles to give faster results, with a detection limit that is the same as or lower than that of conventional techniques [60, 61].

### Miscellaneous Uses

Recently developed systems attempt to use magnetic particles in the so-called magnetic twisting cytometry (MTC) [62]. The extensive use of magnetic nano/microparticles in biotechnology is also described in the literature [63].

Taking into account all of the above mentioned applications, the synthesis of magnetic latex will be discussed in two parts: first, the preparation of iron oxide nanoparticles and, second, the preparation of magnetic latex. Depending on the aim of researchers, many polymerization techniques are applied such as suspension, dispersion, emulsion, microemulsion and miniemulsion polymerization in combination with controlled radical polymerization techniques like atom transfer radical polymerization (ATRP), reversible addition-fragmentation chain transfer (RAFT) and nitroxide-mediated radical polymerization (NMP). The preparation of hybrid magnetic latex by emulsion polymerization will be the focus of this review.

## 3 Iron Oxide Magnetic Nanoparticles

The stable colloidal dispersion of iron oxide nanoparticles in a liquid carrier medium is known as magnetic ferrofluid. The iron oxides mostly used are magnetite  $\text{Fe}_3\text{O}_4$  and maghemite  $\gamma\text{-Fe}_2\text{O}_3$ . The carrier medium can be chosen to be aqueous or organic, depending on the application. The stability of the ferrofluids is the main

quality that determines the possibility for exploitation in different industrial and biomedical applications. To obtain stable ferrofluids, particles are coated with a stabilizing dispersing compound such as a polymer or surfactant and, obviously, the choice of polymer or surfactant depends on the liquid carrier medium. This fluid acts as a single-phase system that responds to a magnetic field but completely demagnetizes in the absence of a magnetic field. For this unique combination of fluid and magnetic properties, ferrofluids have been used in a vast range of areas [64].

There are two basic methods for the preparation of iron oxide magnetic nanoparticles: the mechanical size reduction method and the chemical method.

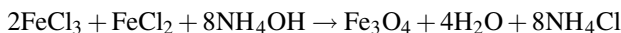
### ***3.1 Mechanical Size Reduction Method***

The idea of this method was proposed by Papell [65] and improved by other authors, including Rosenweing [66]. In this method, bulk magnetic iron oxide is mixed with a liquid organic solvent in the presence of huge amount (10–20 vol%) of surfactants like oleic acid [66] and poured into a crushing ball mill to grind for a period of a few weeks. The role of the surfactant is not only to prevent the particles from re-agglomeration but also to enhance the grinding process of the particles. Since the obtained particles have a broad size distribution, the method is not very cost-effective. It is also time-consuming, so the method is less used than chemical methods.

### ***3.2 Chemical Methods***

#### **3.2.1 Chemical Coprecipitation Method**

The chemical coprecipitation method is most widely used to prepare nanosized magnetic particles. Various procedures have been introduced to reach this goal [67–70]. Generally, all these procedures begin with a mixture of  $\text{FeCl}_3$  and  $\text{FeCl}_2$  solution in water and then coprecipitation is performed by the addition of base, typically ammonium or sodium hydroxide. The reaction can be written as follows:



The method is affected by different parameters like the type and concentration of salts, temperature, pH and the addition rate of ammonia. After coprecipitation by the addition of a basic medium, the system is subjected to different purification steps like magnetic separation, filtration and washing. It should be mentioned here that a rapid pH increase (from 8.5 to 10), and not using strong bases like  $\text{LiOH}$  or  $\text{NaOH}$ , are important to avoid the precipitation of nonmagnetic hydroxides of iron [71]. Nanosized iron oxide magnetic particles dispersed in aqueous or organic medium can be directly produced by this wet chemical method.



Ferrofluids synthesized by chemical coprecipitation may be surfactant-stabilized ferrofluids or ionic ferrofluids. Surfactant ferrofluids are iron oxide nanoparticles coated by stabilizers or surfactant layer(s) for colloidal stability. The coating agents are polymers and surfactants, be they polar, non-polar or non-ionic. Fatty acid derivatives are most often used to stabilize these iron oxide nanoparticles either in organic or aqueous medium. If the particles are dispersed in an aqueous medium, a double layer of surfactant is needed to form a hydrophilic layer. On the other hand, if the particles are dispersed in an organic non-polar medium, one layer of surfactant forms a hydrophobic layer on the surface of the particles.

For instance, Khalafalla et al. prepared stable magnetic particles both in organic and aqueous media. First of all, addition of excess ammonia in a mixture of the aqueous solution of ferrous and ferric salts precipitates magnetic particles. Then, oleic acid is added to the system and reacts with the ammonium groups to form ammonium oleate. A hydrophobic coating is formed around the particles. The aggregated particles are separated by a magnet and then subjected to dispersion in an organic solvent [67]. The authors also showed that a stable colloidal dispersion of magnetic particles in an aqueous system is possible by just replacing the oleic acid by the more hydrophilic dodecanoic acid [68].

Elaissari et al. [69] prepared oil-in-water (O/W) magnetic emulsions by following the Khalafalla method. A ferrofluid was obtained that was composed of superparamagnetic maghemite nanoparticles with a diameter below 10 nm (Fig. 1), stabilized in octane by a surrounding oleic acid layer. This magnetic fluid was then emulsified in SDS-water in order to obtain stable ferrofluid droplets [69]. Another research group [70] published a different method: magnetic nanoparticles were prepared from an iron sulphate solution, which was oxidized by a sodium nitrate solution before being precipitated by concentrated ammonia. The obtained magnetic

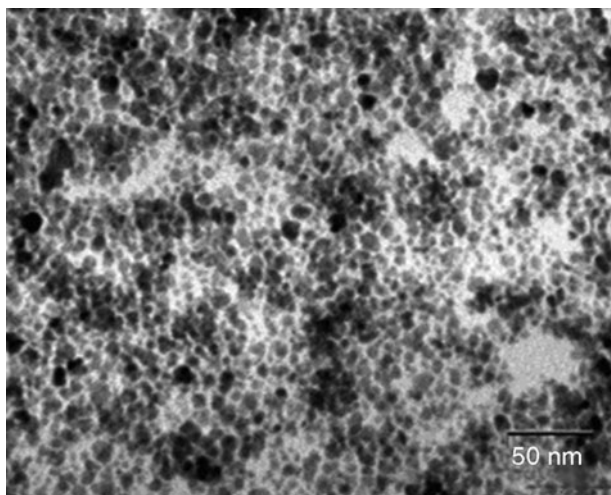


**Fig. 1** TEM image of magnetic nanoparticles prepared by the Khalafalla coprecipitation method. Reprinted from [68] with permission (copyright © IEE)

particles were dispersed in an aqueous solution containing fatty acid surfactants such as oleic acid; the addition of hydrochloric acid induced the colloidal aggregation of the magnetic particles. After eliminating water, the hydrophobic particles were dispersed in toluene. The particle sizes ranged from 4 to 70 nm, depending on the quantity of the sodium nitrate used to oxidize the iron sulphate.

A surfactant-free ionic ferrofluid preparation was accomplished in water by Massart [71]. The electrical charges (either positive or negative) on the surface of magnetic iron oxide nanoparticles create electrostatic repulsion between the particles. This repulsion keeps the colloidal system stable. The sign of the charge on the particles depends on the pH of the solution. Below pH 7 the particles are positively charged, whereas above pH 7 the particles are negatively charged. The experimental parameters under which reaction takes place, such as the initial molar ratio between the ferrous and ferric salts, the type of base used, the temperature, the pH, or the type and concentration of cations present, all strongly influence the size, yield and the magnetic properties of the formed iron oxide nanoparticles [72]. Low polarizing ions, tetramethylammonium cations, perchlorate anions, citrate or nitrate ions are used to impart the colloidal stability of the dispersion. Aqueous suspensions of magnetite nanoparticles (Fig. 2, size 9 nm) have been prepared by this group [73].

The binding of surfactants to the surface of the particles can be done through electrostatic interaction or complexation with metal ions; the surfactants molecules should have a complexing (chelating) groups in the latter case. Ferrofluids can also be stabilized by various low molecular weight compounds such as fatty acids, saccharides and the polymers polyvinyl alcohol (PVA), PEG, dextran, polyacrylamide,

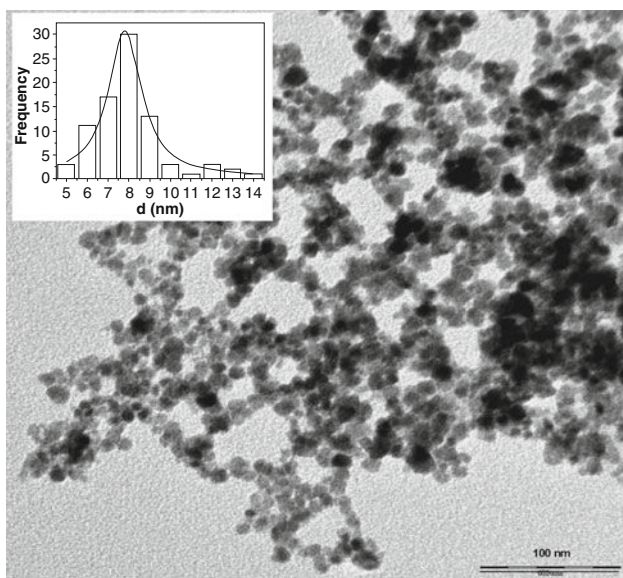


**Fig. 2** TEM image of magnetic particles prepared by the Massart method. Reprinted from [73] with permission

poly(methacrylic acid) (PMA), poly(ethylene oxide)-*co*-poly(propylene oxide) (PEO-*co*-PPO) bisphosphonates, etc. Of them, PEG is most suitable for use in biomedical applications because of its biocompatibility [74].

### 3.2.2 Thermal Decomposition Method

Besides the chemical coprecipitation method, iron oxide magnetic particles can be prepared by thermal decomposition of organometallic compounds such as iron pentacarbonyl and by hydrothermal reaction of mixed oxides or hydroxides of iron. In this method, usually oxides or hydroxides of iron are treated at high temperature (above 200°C) and pressure (more than 2000 psi), known as the supercritical conditions for water. The size, size distribution and morphology of the particles depend on the presence and concentration of surfactant, the temperature, residence time, pH of the reaction system, and on the concentration of the precursor (such as ferric nitrate) [75] (Fig. 3). Water acts as a hydrolytic reactant. The main chemical processes involved are hydrolysis, oxidation and neutralization of mixed metal hydroxides. The amount and size of the magnetic particles are increased with a long reaction time and high water content in the reaction medium [76]. As a precursor, an iron chloride salt or iron acetylacetonate can also be used for example (instead of iron pentacarbonyl) and the resulting particles are dispersible in organic solvents [77, 78].

### 3.2.3 Polyol Method

The method deals with the preparation of magnetic particles in polyol (ethylene glycol, diethylene glycol, propylene glycol etc) as solvent. Inorganic materials are dissolved in polyol and the reaction can be carried out at a wide range of

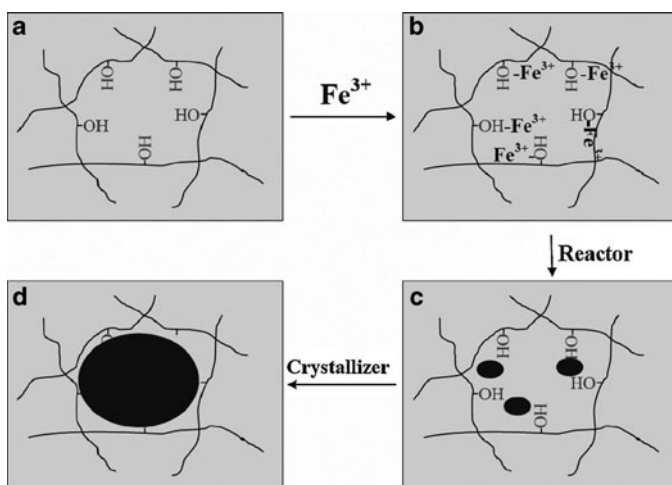


**Fig. 3** (a–d) Mechanism of iron oxide nanoparticle formation in PVA by a hydrothermal process. Reprinted with permission from [75]

temperatures due to the high boiling point of the polyol. The polyol has a multiple role: as a solvent, as a stabilizer, as a ligand and, finally, as a reducing agent [79]. In a typical reaction, precursor metal hydroxides or metal salts are dispersed in polyol and the temperature is raised. In the course of the reaction, the metal precursor forms an intermediate that is reduced to form metal nuclei, which then form metal particles.

### 3.2.4 Aerosol Method

The synthesis of magnetic particles by the aerosol or vapour method deals with the chemical reaction that takes place in confined droplets of reactant that are dispersed in an inert gas. The aerosol collides with the vapour of co-reactants and turns into solid particles [80]. High production rate is the main advantage of this continuous chemical process. There are two routes in the aerosol technique: spray pyrolysis, in which ferric salt is reduced by organic compounds; and laser pyrolysis, in which iron pentacarbonyl is decomposed in the presences of an energy transfer agent with air as an oxidant to form maghemite nanoparticles [81]. The latter method is more favourable for preparation of less-aggregated particles.

### 3.2.5 Microemulsion Method

To control the size and size distribution, synthesis of magnetic nanoparticles in a W/O microemulsion has been reported. The presence of surfactant molecules results in the formation of different sizes (1–10 nm) of micelles. The surfactant molecules organize themselves with the polar end inside in the water phase and the non-polar end in the oil phase. The micelles/droplets contain the aqueous solution of iron salts. The concentration and type of surfactants and metal ions, the pH, reducing agents and co-surfactants can all affect the particle growth and, consequently, the particle size distribution (Fig. 4) [82, 83].

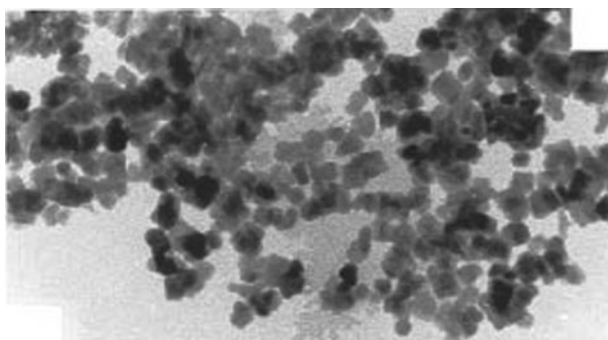


**Fig. 4** TEM image of magnetic particles prepared in microemulsion. Reprinted from [82] with permission

## 4 Synthesis of Magnetic Latex

### 4.1 *Magnetic Latex Fabrication in Preformed Polymers*

#### 4.1.1 Solvent Evaporation Process

This is one of the easier processes for synthesis of magnetic polymer microspheres. The magnetic component is dispersed in an organic phase (a suitable solvent) containing polymer (PLLA, Polybutyral, PCL) and then it is emulsified in an aqueous solution of stabilizing polymeric surfactants (PVA, SDS, Pluronic PE6800) to form an O/W emulsion. The evaporation is accomplished by vigorous stirring of the emulsion at room temperature. The prepared particles are usually polydisperse and large in size. Using the solvent evaporation method, Homoudeh et al. [84, 85] have demonstrated incorporation of a large amount of magnetite in poly(lactic acid)-based nanoparticles, and high magnetic saturation values in poly( $\epsilon$ -caprolactone) (PCL)-based microparticles. The particles can be used as a contrast agent in MRI. Here, magnetic components are dispersed in a dichloromethane phase containing the dissolved polymer. This organic phase is then subjected to emulsification in an aqueous phase containing PVA to form an O/W emulsion. The evaporation of dichloromethane enables the precipitation of the dissolved polymer onto magnetite-loaded polymeric particles. The magnetite nanoparticles are simply mechanically entrapped during the polymer precipitation process.

Tanyolac et al. [86] also prepared magnetic microbeads by applying the solvent evaporation method. They used chloroform as organic phase and polybutyral as polymeric material. The range of produced particle size was 125–250  $\mu\text{m}$ .

Here, it is also worth mentioning that the solvent diffusion method (also known as the phase separation method) is used to prepare magnetic nanoparticles. The method consists of using a partially water-miscible solvent like ethyl acetate as an organic solvent. This solvent is emulsified in an aqueous solution of a stabilizing agent, followed by dilution of the internal phase with an excess of water to induce the precipitation of polymer. Applying the method, 90–180 nm size particles with a good magnetic loading of PLGA were reported by Lee et al. [87]. At first, iron-oxide–PLGA-containing saturated ethyl acetate phase in the Pluronic-containing aqueous phase was emulsified with a high speed homogenizer. Then, excess water was added to the O/W emulsion while applying ultrasound. The subsequent addition of water dilutes the solvent concentration in water and extracts solvent from the organic solution, which leads to the nanoprecipitation of polymer matrix, entrapping iron oxide nanoparticles.

The modification of the surface of iron oxides by hydrophilic macromolecules such as PVA and proteins is also reported [88–90]. For instance, Lee et al. [90] carried out a coprecipitation of iron salts in an aqueous solution of PVA to form a stabilized dispersion. They reported a decreasing crystallinity of iron oxide particles with an increase in the concentration of PVA, while the morphology and particles

size remained the same. Chatterjee et al. [88] studied the encapsulation of individual iron oxide nanoparticles or small clusters by human serum albumin using the heat stabilization method.

Another work of Chatterjee et al. [89] describes the incorporation of magnetic particles in a biocompatible polymer gel using PVA. The obtained magnetic gel was dried to form a biocompatible magnetic film. The authors reported efficient crosslinked magnetic nanoparticles in the polymer network with superparamagnetic properties. In very recent work, iron oxide nanoparticles were loaded by the micelles of amphiphilic block copolymer of poly(NIPAM-*co*-AM)-*block*-PCL using the solvent evaporation method. The resulting thermally responsive magnetic micelles were used for simultaneous magnetic hyperthermia and drug delivery [21].

#### 4.1.2 Sol–Gel Method

The sol–gel method can be associated with the transformation of a homogeneous solution (sol) of a metal oxide or alkoxide precursor to a crosslinked three-dimensional solid (gel) [91]. At room temperature, the precursor undergoes multistep hydrolysis and polymerization reactions to form a colloidal dispersion and the particles turn into a new “gel” phase. Controlled bulk properties and microstructure of the materials, and synthesis of optically transparent materials, are the advantages of the sol–gel method. However, there is a problem in controlling the sol–gel mixture composition because the outcome depends on many factors like pH, temperature, nature of the solvent, ratio of water and precursor, and concentration. The superparamagnetic Fe<sub>3</sub>O<sub>4</sub> nanoparticles were coated with silica by dispersing iron oxide particles in a 2-propanol/water mixture using ultrasonication for about 10 min. Then, ammonium hydroxide and tetraethyl orthosilicate (TEOS) were consecutively added to the reaction mixture under continuous stirring at room temperature for 12 h. Alternatively, the surface of the particles was modified by [3-(glycidyloxy)propyl] trimethoxysilane (GLYMO) and iminodiacetic acid [92].

#### 4.1.3 Layer-by-Layer Process

Spontaneous electrostatic attraction between oppositely charged polymer chains is used to synthesize magnetic latex in a layer-by-layer process (LBL). The LBL method can produce coated latex of different shapes and sizes, and with uniform and controlled thickness of the layer without using high cost equipment.

It is also possible to incorporate various functional groups on the surface of the particles to produce multifunctional magnetic latex [93, 94]. The LBL adsorption of polyelectrolyte onto the colloidal particles is a well-recognized method for magnetic nanoparticle encapsulation and functionalization [95, 96].

Sauzedde et al. [93] reported the synthesis of monodisperse magnetic latex, combining anionic iron oxide nanoparticles (5–10 nm) and cationic core–shell polymer particles containing polystyrene core–shell PNIPAM, poly(St-*co*-NIPAM) and poly(NIPAM-*co*-MBA) functionalized with 2-aminoethyl methacrylate (AEM). The negatively charged iron oxide particles were adsorbed onto the seed particles by electrostatic interaction. Adsorption of iron oxide onto pure cationic PNIPAM latex was strongest. Elaissari et al. [97] studied the encapsulation and functionalization of O/W magnetic emulsions using sequential adsorption of oppositely charged polyelectrolytes via the LBL process. In the encapsulation process, at first, polyelectrolyte was adsorbed onto negatively charged magnetic particles using PEI. After that, the obtained cationic magnetic particles were introduced into the solution of a high concentration of polyanion poly(maleic anhydride-*alt*-methyl vinyl ether) (PMAMVE). The average diameter and magnetic content of the final particles were 240 nm and 60% (wt/wt), respectively.

## 4.2 *In Situ Synthesis*

### 4.2.1 Incorporation of Iron Oxide by the Precipitation Process

Magnetic polymer microspheres can be prepared by coprecipitation of iron salts inside the polymer matrix. Ugelstad et al. [98] synthesized monodisperse magnetic polymer microspheres using a multistep procedure that is based on four steps:

1. Synthesis of porous polymer particles as a seed latex with diameters in the range 2–4  $\mu\text{m}$  and a very narrow size distribution
2. Diffusion of iron oxide salts into the porous latex particles
3. Precipitation of Fe(II) and Fe(III) salts inside the porous latex by the addition of a base like ammonium hydroxide or sodium hydroxide
4. Encapsulation of the magnetic iron oxides inside the porous latex particles by a seeded polymerization process

The porous latex seed particles are obtained via the dynamic swelling method followed by an emulsion polymerization process. A volatile solvent that has no tendency to take part in the polymerization is used in the swelling process and is followed by evaporation to prepare the porous microspheres [99]. The monodisperse particles can be swollen up to 50–1000 times with respect to their initial volume by a vinyl monomer solution, sometimes in combination with other reactants such as a porogen solvent. All reactants are present inside the swollen particles before polymerization.

One of the most widely used magnetic beads was prepared by Ugelstad et al. [100]. In the preparation of magnetic polymer particles, hydrophobic polymers of styrene (St) or styrene-*co*-divinylbenzene (St-*co*-DVB) are used, which have a large



tendency for non-specific binding to proteins. The second polymer encapsulation layer can be chemically modified by reactive functional groups (e.g. amine, carboxylic, thiol, epoxy and aldehyde groups) for the introduction of specific affinity ligands or biomolecules.

Synthesis of hydrophilic magnetic particles with an average size of  $2.6\mu\text{m}$  and PDI 1.02, and a 24.3% iron oxide content was carried out by Ma et al. [101]. She used coprecipitation of iron oxide inside an amino functional polymer matrix. The total process involves three steps: (a) preparation of poly(glycidyl methacrylate) (PGMA) seed particles by a dispersion polymerization, (b) functionalization of the seed PGMA particles with ethylene diamine (EDA), and (c) impregnation of iron salts and precipitation with ammonium hydroxide solution inside the functional polymers matrix.

The synthesis of core-shell magnetic nanoparticles from polyacrylic acid (PAA) graft copolymers containing side chains of PEO and PPO (Fig. 5) was demonstrated by Hatton et al. [102]. Using a mixture of the polymers at a temperature of  $180^\circ\text{C}$ , amine-terminated PEO and PPO were coupled onto the PAA via amidation. Superparamagnetic polymer-coated nanoparticles were synthesized by the hydrolysis and condensation of Fe(II) and Fe(III) chloride salts in the presence of PPO- or PEO-modified PAA copolymers. The extraction of organic compounds from aqueous media towards the copolymer shell of hydrophobic PPO segments can be applied in the field of water purification.

Homogeneous distribution of magnetic particles in the polymer matrices can be obtained using polyacrylamide-based microgel particles swollen with water. The amount of ferric and ferrous salts contained in the microgel and the quantity of water depends on the crosslinking density. Fe(II) and Fe(III) salts are transformed into iron oxide nanoparticles inside the hydrogel, by raising the pH and temperature. However, the application of ultrasound to disperse the prepared magnetic microgel may desorb or release the iron oxide from the microgel latex. Consequently, the prepared

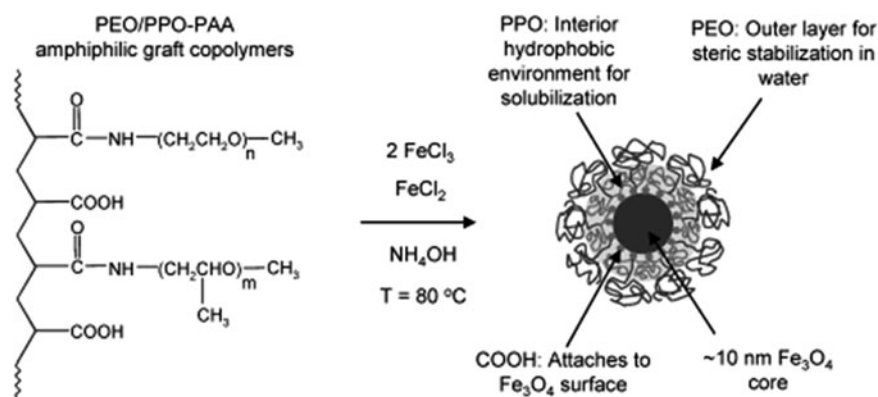


**Fig. 5** Magnetic fluid synthesis in an aqueous solution of PEO/PPO-PAA graft copolymer. Reprinted from [102] with permission

magnetic microsphere may have a more porous surface, which is not suitable for use as a solid support in immunoassay. A similar approach was proposed by Kawaguchi et al. [103], who prepared a magnetic microgel in the following way: acrylamide (AM), methacrylic acid (MAA) and bisacrylamide are dispersed in a solution of Fe(II) and Fe(III) salts, which are then precipitated by addition of ammonium hydroxide. Dextran is used to limit the precipitation in the aqueous phase. Dextran can also enhance the dispersability of ferrite particles, preventing aggregation in the dispersion medium and improve biocompatibility of the particles. Finally, the magnetic composite microspheres are coated by a layer of epoxy functional PGMA to protect any release of the magnetic particles in the course of the application or post-application periods. The average diameter of the final particles is 400 nm and magnetic content is 20–25%.

Recently, Sahiner et al. [104] reported the preparation of anionic hydrogels (Fig. 6) of poly(2-acrylamido-2-methyl-1-propane sulphonic acid) (PAMPS) with different amounts of crosslinking agent for use in in situ synthesis of magnetic and metal particles. Different size metal particles were prepared inside the polymeric matrices by the adsorption of the metal ions from their aqueous salt solution into the preformed polymer network by the aid of the ion-exchange ability of the pH-sensitive hydrogel and subsequent reduction of the metals using strong reducing agents. Transmission electron microscopy (TEM) and thermogravimetric analysis (TGA) analysis demonstrated that the (PAMPS) content of hydrogel has a great effect on both the metal ion loading capacity as well as particle size.

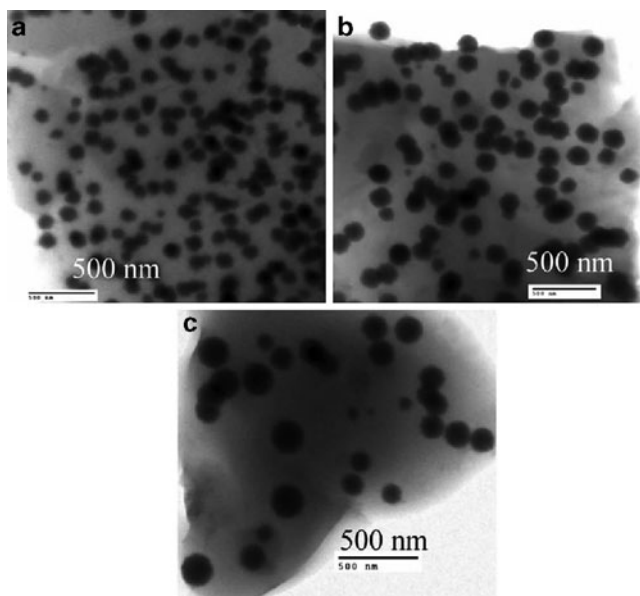


**Fig. 6** (a–c) TEM images at different magnifications of composite-PAMPS-co-PAMPS hydrogels containing iron oxide particles. Reprinted from [104] with permission

Another appealing approach to the synthesis of superparamagnetic latex has been taken by Wormuth [105]. The method proceeds in two steps: first, the in situ precipitation of iron oxide in the presence of a double hydrophilic block copolymer (PEO-*block-co*-PMA), which dictates the nucleation, controls growth, and sterically stabilizes the magnetic particles. Then, this is followed by a miniemulsion polymerization technique to encapsulate the magnetic particles, utilizing hydroxyethyl methacrylate (HEMA) and MAA monomers. TEM, DLS, TGA and XRD magnetic measurements were used to analyse the produced magnetic latex. Iron oxide particles of 5 nm were present inside the magnetic latex particles, having a diameter of 140–220 nm. The magnetic latex contained 18% magnetic iron oxide.

In order to prepare core-shell magnetic microspheres for use as an MRI contrast agent, “double hydrophilic” block copolymers of PEO-*block*-PGA have also been investigated by another research group [106].

The preparation of dendrimer-coated magnetic nanoparticles was reported by Douglas et al. [107]. In the preparation process, Fe(II) salt precursor using  $(\text{CH}_3)_3\text{NO}$  was reduced and this was done in the presence of COOH-terminated poly(amidoamine) dendrimers; 20–30 nm sized particles were formed.

#### 4.2.2 Deposition of Magnetic Metals

In order to have magnetic properties, iron, cobalt and nickel metals can be used to prepare magnetic polymer particles. The preparation of well-defined cobalt magnetic nanoparticles was reported by Thomas [108]; in this method, the cobalt metal is deposited into the polymer matrix in the presence of a random terpolymer poly(MMA-EA-NVP) by thermolysis of the cobalt carbonyl precursor  $\text{Co}_2(\text{CO})_8$  in toluene. The terpolymer stabilizes the magnetic cobalt particles. Tuning the ratio of the metal precursor and surfactants, core-shell nanoparticles with controllable size can be obtained. One of the major features of this method is the organization of ferromagnetic cobalt nanoparticles into one-dimensional nanoparticle chains when cast from the solution onto TEM grids.

The method of preparing superparamagnetic particles developed by Charmot [109] uses hydrophobic non-porous polystyrene seed particles of narrow size distribution. A seeded polymerization is carried out to increase the particle size ( $1.35\text{ }\mu\text{m}$ ) and a terpolymer is formed around the seed particles by a dispersion polymerization of styrene, DVB and 4-vinylpyridine in toluene. The toluene containing cobalt precursor swells the latex particles, which results in a homogeneous distribution of the metal precursor. A thermolysis reaction is conducted in the presence of 4-vinylpyridine, and the release of carbon monoxide indicates the decomposition of the metal salt into cobalt. The main problem of this method is the particle surface deformation during the evolution of carbon monoxide. The amount of crosslinker, however, cannot be reduced below a certain level without significantly modifying the properties of the particles.

Takahashi et al. [110] studied the synthesis of magnetic core and polymeric shell particles, taking carboxylic-acid-containing copolymers as stabilizer. The

copolymerization of an allyl-terminal PEO macromonomer with maleic anhydride is carried out, followed by basic ring-opening that produces carboxylic functional copolymer. Due to the presence of this copolymer, ferrite salts are oxidized by hydrogen peroxide to form superparamagnetic nanoparticles. Finally, the adsorption of lipase onto the polymer-coated magnetic particles renders a catalytically active support for esterification.

### ***4.3 Polymerizations of Monomer in the Presence of Magnetic Nanoparticles***

For the preparation of hybrid magnetic latexes, different monomers can be polymerized in heterogeneous reaction systems in the presence of magnetic particles. Several polymerization techniques, namely suspension, dispersion, emulsion, microemulsion and miniemulsion are prevalent.

#### **4.3.1 Suspension Polymerization**

Suspension polymerization is one of the heterogeneous polymerization methods for magnetic latex preparation in which water-insoluble monomers, magnetic particles and monomer soluble initiator are dispersed as a droplet in a continuous aqueous phase. The droplets are stabilized sterically by surfactants or stabilizers, and vigorous stirring takes place during polymerization to prevent aggregation or coalescence of these droplets. The target in suspension polymerization is the formation of a uniform dispersion of polymerized monomer droplets in the aqueous phase. These droplets are subjected to polymerization by direct conversion of the droplets to corresponding magnetic polymer particles of about the same size. The range of the particle size distribution depends on the initial droplet size, which is influenced by the concentration of surfactant, the interfacial tension, the degree of agitation and the design of the stirrer/reaction system [111]. The dynamic equilibrium between coalescence and break-up, which depends on the above-mentioned parameters, drives the final droplets size [112].

Synthesis of hydrophobic magnetic latex was reported in a patent [113]; magnetic particles are dispersed in organic phase consisting of water-insoluble initiator and vinyl aromatic monomers. The obtained dispersion is then mixed with an aqueous solution of surface-active agent and the mixture is emulsified. The size of the produced magnetic polymer lattices ranges from 0.03 to 5  $\mu\text{m}$ . Another group, Lee et al. [114], prepared magnetic microspheres using St and DVB. The dispersed phase consists of oleic-acid-coated magnetic particles (size less than 5  $\mu\text{m}$ ) dispersed in organic phase containing St and DVB. Oil-soluble initiator azobis(isobutyronitrile) (AIBN) is used. After stirring for 1 h at room temperature, the dispersed phase is then transferred into the continuous aqueous phase in which PVA is dissolved, and is stirred for 16 h at 70°C under nitrogen atmosphere. The average diameter

of the prepared magnetic microsphere is  $219\mu\text{m}$ . Using almost the same recipe, Maria et al. [115] produced a range of  $65\text{--}300\mu\text{m}$  particles with 2–7% iron oxide. Another illustration of suspension polymerization is the use of St and DVB in the presence of magnetic powder to prepare magnetic latex with large diameters in the region of  $100\text{--}300\mu\text{m}$ . Magnetic particles of  $20\mu\text{m}$  are dispersed in an organic phase by applying ultrasound. The mixture is then dispersed in an aqueous phase and polymerized, initiated by a peroxide at  $80^\circ\text{C}$ . The prepared particles are functionalized by photo-oxidation using UV radiation and used for covalent coupling of biomolecules such as enzymes [116].

Oxidation of the polystyrene shell results in the presence of carbonyl groups ( $\text{C=O}$ ), as indicated by FTIR. The incorporation of iron oxide in the polymer is very low at about 1.25% of the monomer mass.

To achieve a narrow size distribution and smaller particle size, modified suspension polymerization is also reported [117] for preparation of magnetic poly(methyl methacrylate) (PMMA)-DVB-GMA microspheres (Fig. 7). The magnetic particle is functionalized by the reaction of the epoxy groups with ammonia solution to provide amino group on the surface, and is activated by glutaraldehyde for protein adsorption. The average size of the obtained particles is  $6.4\mu\text{m}$ . Three modifications in the approach can be made. First, polymerization is conducted under enhanced mechanical agitation to form uniformly sized monomer droplets. Second, the reaction temperature is increased with a controlled rate, resulting in smaller droplets. The

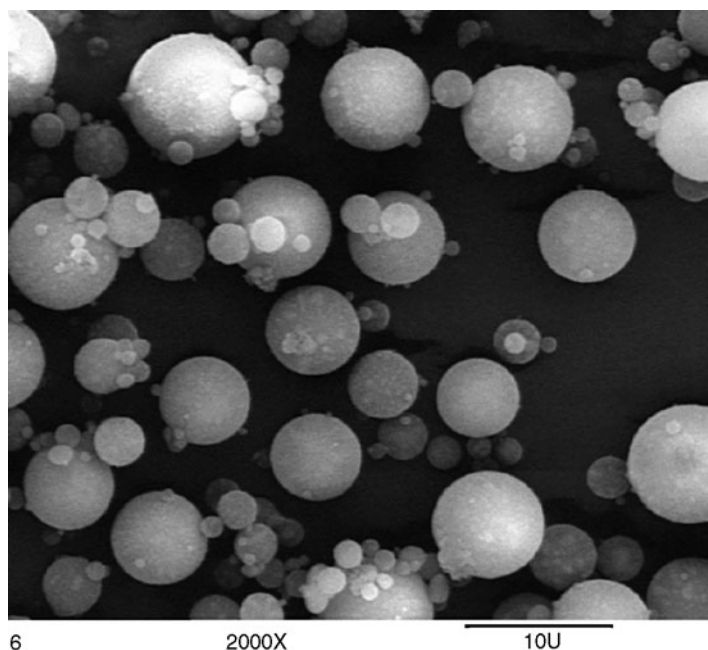


**Fig. 7** SEM micrograph of magnetic P(MMA-DVB-GMA) microspheres. Reprinted from [117] with permission (copyright Wiley-Interscience)

resulting particles have a higher magnetic content. Third, the use of high levels of surfactant, (20% PVA relative to monomer) leads to a narrower size distribution of particles.

In addition, magnetic latex with hydrophilic polymer can be produced by inverse suspension polymerization using a W/O suspension. Müller-Schulte et al. reported [118] the preparation of hydrophilic thermally sensitive magnetic polymer particles for an *in vivo* contactless controlled drug release by using inverse suspension polymerization (Fig. 8). A ferrofluid and initiator ammonium persulphate

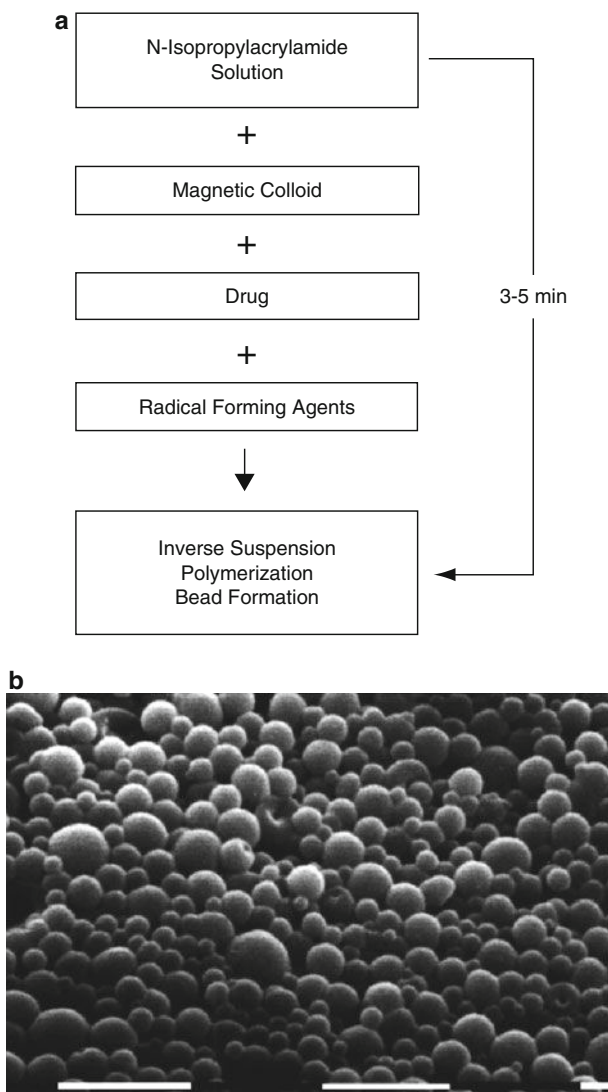


**Fig. 8** Flow diagram of NIPAM bead preparation (a) and SEM image of NIPAM microbeads (b). Reprinted from [118] with permission

(APS) were added to a monomer phase consisting of NIPAM, poly(oxyethylene nonylphenylether) (IgepalCO-520) and, as a crosslinker, *N,N*-methylene bis acrylamide (MBA). The mixture was treated for 30 s in an ultrasonic bath (as drug-like substances, methylene blue or rhodamine B were used) and dispersed in oil phase containing Span 80, Brij 72 and Prisorine. Spherical micron-sized magnetic polymer particles with a size of 10–200  $\mu\text{m}$  were obtained, depending on stirring speed. It is also possible to prepare spherical nanoparticles using an oil phase consisting of F 127, Aerosol or Span 60.

Moreover, a magnetic molecularly imprinted polymer of 4-divinylpyridine and EGDMA particles was synthesized by inverse suspension polymerization [119]. The reaction was carried out in silicon oil as a dispersion phase, and in the presence of 2,4-dichlorophenoxyacetic acid and MPTS. The advantages of the silicon oil as a continuous phase are a low polarity and immiscibility with the monomer mixture. The prepared particle average size is 20  $\mu\text{m}$  and the magnetic content is very low, at around 1 wt%.

Using the suspension polymerization approach, Lu et al. [120] also described the preparation of molecularly imprinted  $\text{Fe}_3\text{O}_4$ /poly(St-DVB) composite beads for amino acid recognition using MAA and AM as functional monomer, stearic acid as porogen, and PEG 4000 as dispersant. The diameter of the composite particles was 400–450  $\mu\text{m}$  and the magnetic content was 3.78%. Tyrosine and phenylalanine were both used as templates and comparative molecules for studying molecular recognition selectivity.

#### 4.3.2 Dispersion Polymerization

Dispersion polymerization is an appealing method due to the inherent simplicity and non-tedious single-step process in attaining monodisperse micron-sized polymer particles. In a typical dispersion polymerization process, monomer(s) and initiator are soluble in the continuous phase but the produced polymers are not soluble in the dispersion medium. The oligomer chains formed in the dispersion medium coalesce to form nuclei and, at the same time, adsorb stabilizers from the medium to form stable primary particles containing magnetic cores. At the stage where sufficient nuclei are formed, nuclei formation stops and the number of particles is constant from there on. The reason is that the surface area of the particles is sufficient to capture newly formed oligomers and insoluble polymer chains. Further particle growth takes place by polymerization inside the particles, which are swollen with the monomer [121–123]. It should also be mentioned that the solvent polarity in the dispersion polymerization is one of the important factors [124].

Horak et al. prepared magnetic PGMA latex by dispersion polymerization of glycidyl methacrylate (GMA) in the presence of magnetic iron oxide in a water/alcohol mixture. The polymerization was carried out using oil-soluble AIBN as an initiator and PVP as stabilizer [125]. Moreover, Horak et al. also demonstrated the synthesis of magnetic poly(2-hydroxyethyl methacrylate) (PHEMA) in the presence



of different geometrical or morphological structured (needles or cubes) iron oxide particles in an organic continuous medium [126]. The resultant particles (Figs. 9 and 10) produced by this method contain 15 wt% iron oxide.

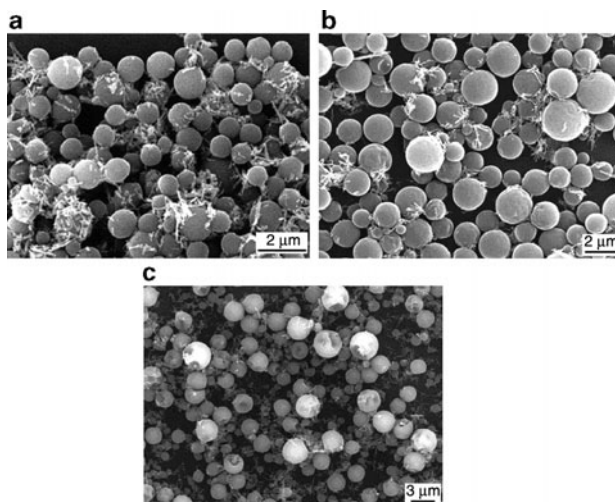


**Fig. 9** SEM images of (a) magnetic PGMA microspheres. Polymerization conditions: 68 g ethanol, 12 g GMA, 2 g  $\text{Fe}_2\text{O}_3$ , 4.5 wt% PVP (based on polymerization mixture), and 2 wt% AIBN (based on monomer). (b, c) crosslinked magnetic PGMA microspheres. Polymerization conditions: (b) 66 g ethanol, 2 g water; (c) 62 g ethanol, 6 g water; 11.04 g GMA, 0.96 g EDMA, 1 g  $\text{Fe}_2\text{O}_3$ , 2.25 wt% PVP (relative to the polymerization mixture), and 2 wt% AIBN (relative to the monomers). Reprinted from [125] with permission

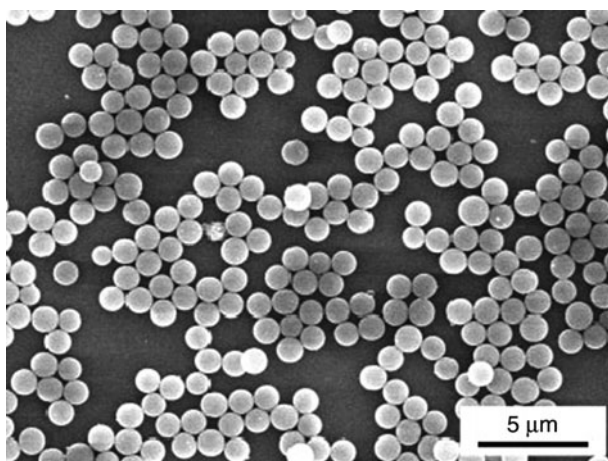


**Fig. 10** SEM micrograph of magnetic poly(HEMA-co-GMA) (1/1 w/w) microspheres prepared in a polymerization mixture containing 38.2/29.8 (g/g) toluene/2-methylpropan-1-ol, 2 wt% BPO (relative to the monomers), 1 g of an oleic-acid-stabilized ferrofluid, and 5 wt% EC. Reprinted from [126] with permission

Thermally sensitive magnetic poly(*St-co*-NIPAM) with particle sizes of 5–100  $\mu\text{m}$  and magnetic amphiphilic poly(*St-co*-PEOAM) particles of 5–80  $\mu\text{m}$  were synthesized by Ding et al. [127, 128] through dispersion polymerization. Amphiphilic magnetic poly(*St-co*-PEOVB) was also reported by the same group [129]. The aim of the synthesis of magnetic amphiphilic polymer microspheres, which have homogeneous catalytic property, is to use them as a catalyst carrier. In both cases, particle size distribution and magnetic content were not satisfactory. The phase transition behaviour (at about 31°C) and adsorption behaviour of emulsifier and trypsin on the magnetic PS/P(DMAEMA-EGMA) prepared by dispersion polymerization were investigated [130].

Recently, work has also been published by Zhang et al. [131] regarding the synthesis of magnetic poly(*St*-GMA) microspheres using dispersion polymerization. Different instrumental analyses like Fourier transform infrared (FTIR) spectrometry, X-ray diffraction (XRD), TEM, TGA and vibrating sample magnetometry (VSM) were performed to characterize the obtained microspheres. A high content (about 70 wt%) of iron oxide has been claimed to be present in the (0.5–1  $\mu\text{m}$  size) polymer microspheres. However, as shown in the TEM micrograph, a matter of concern is that the magnetic iron oxide particles are not fully encapsulated by polymer. The resulting particles will be of questionable use in biomedical applications.

The method was used by Park et al. to prepare polymer-coated carbonyl iron magnetic composites particles [132]. The carbonyl iron was encapsulated by PMMA macromolecules via dispersion polymerization. The prepared polymer-coated magnetic particles were further crosslinked with ethylene glycol dimethacrylate (EGDM) to improve the mechanical properties of PMMA for use as a dispersed phase for magnetorheological fluids in industry. Besides, Sun et al. [133] investigated the synthesis of nonporous and spherical magnetic beads by dispersion polymerization of GMA crosslinked with DVB. Further amino functionalization was accomplished so that the particles could be used as anion exchangers to capture plasmid DNA.

### 4.3.3 Emulsion Polymerization

Emulsion polymerization is the polymerization technique that starts with emulsified monomer in the continuous aqueous phase. Polymer formation takes place in the micelles and is initiated by water-soluble initiators. The monomers are insoluble or sparingly soluble in water. Emulsion polymerization is used very frequently in order to perform encapsulation of inorganic particles with polymers where water-based coatings are required. For the encapsulation of inorganic particles, seeded emulsion polymerization is performed; hydrophobic inorganic particles are dispersed with normal surfactants or protective colloids in the aqueous phase. As polymerization on the surface of inorganic particles is always in competition with secondary particle formation, the concentration of the surfactants should be lower than their critical micelle concentration. However, homogeneous nucleation can also occur, which

is more dominant for more water-soluble monomers. Therefore, the chance for secondary nucleation is higher and the resulting encapsulation will be poorer. The efficiency of encapsulation thus depends on the water solubility of monomers [134].

The required properties of the hybrid particles can only be obtained when the magnetic particles are dispersed as single particles in the matrix. So, initially the magnetic particles (stabilized by surfactants or protective colloids) should be well-dispersed in the aqueous phase and aggregation should be avoided during the polymerization. Additionally, in combination with surfactants, ultrasound can be used to make well-dispersed particles.

An interesting approach has been developed by Elaissari et al. [135] to prepare magnetic latex via free radical emulsion polymerization of the hydrophobic monomer St and the crosslinking agent DVB in the presence of submicronic magnetic droplets dispersed in water. The particle size distribution was controlled by the size distribution of the initial magnetic emulsion. In this case, oleic-acid-coated iron oxide magnetic nanoparticles in octane were emulsified with an aqueous solution of amphiphilic copolymer or the nonionic surfactant poly(oxyethylene) isooctylphenylether (Triton X-405) to form ferrofluid magnetic droplets in water. Then, St and DVB were added to the mixture and stirred at room temperature to diffuse the monomers into the ferrofluid droplets. The polymerization was initiated by either AIBN or potassium persulphate (KPS). The influence of different reaction conditions, for instance initiator type, level of DVB and adsorption of carboxylic-containing amphiphilic copolymers, was investigated in terms of polymerization kinetics and latex particle morphology.

It was demonstrated that the homogeneous encapsulation of iron oxide nanoparticles was possible when amphiphilic copolymer was used with 60:40 wt% ratio of St to DVB and KPS as initiator (Fig. 11). The use of only St and AIBN as initiator

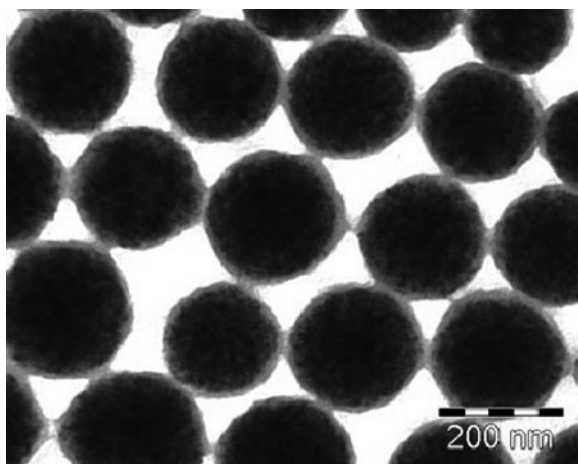


**Fig. 11** TEM image of latex prepared with St, DVB and KPS (40 wt% DVB) obtained from ferrofluid droplets stabilized with a functional polymeric surfactant. Reprinted from [135] with permission

produced an asymmetric hemisphere-like morphology. The particles were characterized by TEM, scanning electron microscopy (SEM) and TGA. Particles of 200 nm, with a highly magnetic content (60%) and high carboxylic surface charge were claimed.

Earlier, oleic-acid- or sodium dodecyl sulphate (SDS)-stabilized ferrofluid encapsulation with EGDM was reported, where 4,4'-azobis (4-cyanovaleric acid) (ACVA) was used as initiator and particles were further functionalized with MA [136]. The emulsion polymerization of GMA in the presence of dextran-coated sterically stabilized iron oxide magnetic particles using various emulsifiers (Disponil AES 60, Tween 20, Triton X-100) and initiators (APS and ACVA) was carried out [137]. Disponil AES 60 and ACVA were considered suitable emulsifiers and initiators, respectively, due to the hydrolysis of epoxy groups (originated from GMA) in the course of APS-initiated polymerization. The obtained particles were polydisperse and almost spherical, as shown by SEM (Fig. 12). Similar work with different initiators and surfactants was reported [138, 139].

However, the use of water-soluble monomer in emulsion polymerization is more complicated. A potential example is the synthesis of thermally sensitive magnetic microspheres using water-soluble NIPAM, using the combination of emulsion polymerization and then seeded precipitation polymerization [140, 141]. Lee et al. [140] conducted the synthesis of magnetic latex by a two-stage process: at the first

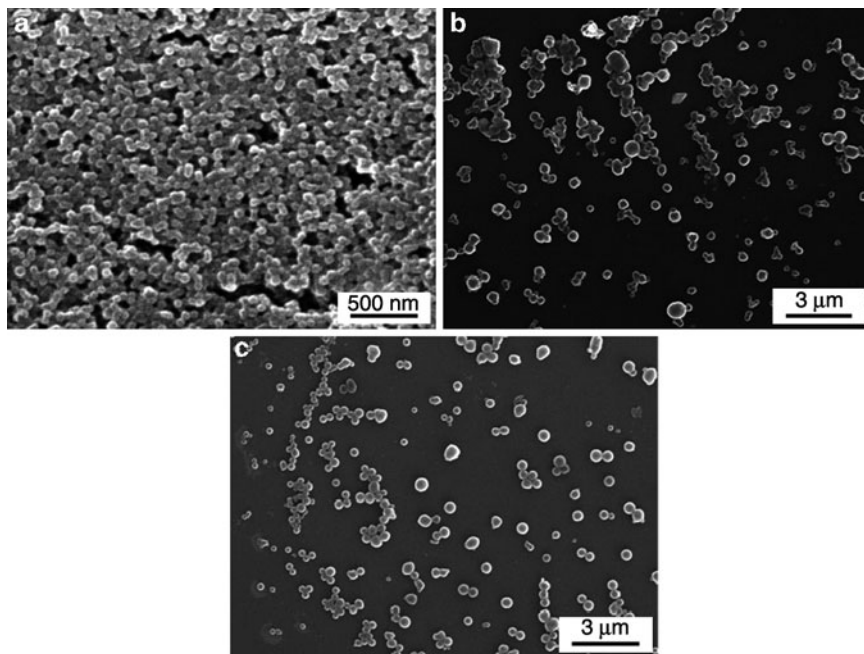


**Fig. 12** SEM of magnetic PGMA microspheres obtained by emulsion polymerization in the presence of 0.75 wt% of (a) Disponil AES 60, (b) Tween 20 and (c) Triton X-100 in water. Polymerization conditions: 0.26 wt% ACVA (relative to feed), dextran-coated iron oxide/GMA–0.33. Reprinted from [137] with permission

stage, magnetic polystyrene seed particles were synthesized, which were then used as seed for second stage seeded emulsion polymerization with NIPAM and MAA. As observed in TEM, the morphology of the particles was not uniform core–shell, and secondary nucleation was also found. Another approach to the synthesis of magnetic latex was pointed out by Shang et al. [142]. An O/W emulsion of a ferrofluid was prepared by replacing the SDS with oleic-acid–SDS-coated iron oxide particles, and then forcing the emulsion through a membrane with highly uniform micrometer (2 or 5  $\mu\text{m}$ ) pore size. The emulsion-templated free radical polymerization of acrylic acid (AA) was performed in the presence of oleic acid and propenyl polyethylate alcohol (RN-10)-coated iron oxide particles and initiated by UV light, with benzophenone as initiator. In another research study, Shamim et al. [143] performed emulsion polymerization [144] for the synthesis of a PNIPAM shell on magnetic particles using iron oxide nanoparticles coated with the polymerizable surfactants thidiglycolic acid (TDGA) and 4-vinylaniline. The thiol group (-SH) and carboxylic group (-COOH) of TDGA can be attached to magnetic particles and to the amine group (-NH<sub>2</sub>) of vinylaniline, respectively. The preparation process is described in Fig. 13.

Margel and Boguslavsky prepared DVB-coated magnetic latex in emulsion polymerization to form air-stable carbon-coated nanoparticles containing crystalline iron. They also studied the influence of DVB on the particle size and size distribution, and revealed that above a certain concentration of DVB (nearly 2%) the size distribution becomes wider [145]. It is very interesting to note that a similar result was found by another research group: in their case, more than 2% of DVB monomer led to less uniform magnetic core–polymeric shell, with secondary particle formation [139]. Recently, Margel et al. [146] reported the preparation of PGMA/polystyrene core–shell micron-sized particles (Fig. 14) prepared by emulsion polymerization, which were subsequently covered with iron oxide nanoparticles.

The use of DVB in emulsion polymerization for the preparation of functional magnetic microsphere was described by Zhao et al. [147].

More recently, the fabrication of multihollow superparamagnetic magnetite/polystyrene nanocomposite particles via water-in-oil-in-water (W/O/W) double emulsions (Fig. 15) was demonstrated [148].

When amphipathic magnetic particles having hydrophilic hydroxyl and hydrophobic oleic ester groups on the surface are mixed with St in water, the magnetic particles reside on the interface of water and oil. At reaction temperature (70°C) and specific stirring conditions, the magnetic particles can pull water inside the oil phase, resulting in the formation of a W/O/W double emulsion. The presence of the more amphipathic magnetic particles at the interface of water and oil enhances the possibility of easier formation of double emulsions [148]. The effect of the amount of magnetic particles present in the reaction system, in combination with stirring and temperature, were studied. KPS as initiator at a temperature of 70°C and proper stirring conditions provided multihollow particles (Fig. 16c–i) at moderate concentration (0.50–1 g) of magnetic particles, whereas the presence of .25 g magnetic particles caused either hollow or multihollow particles (Fig. 16b).

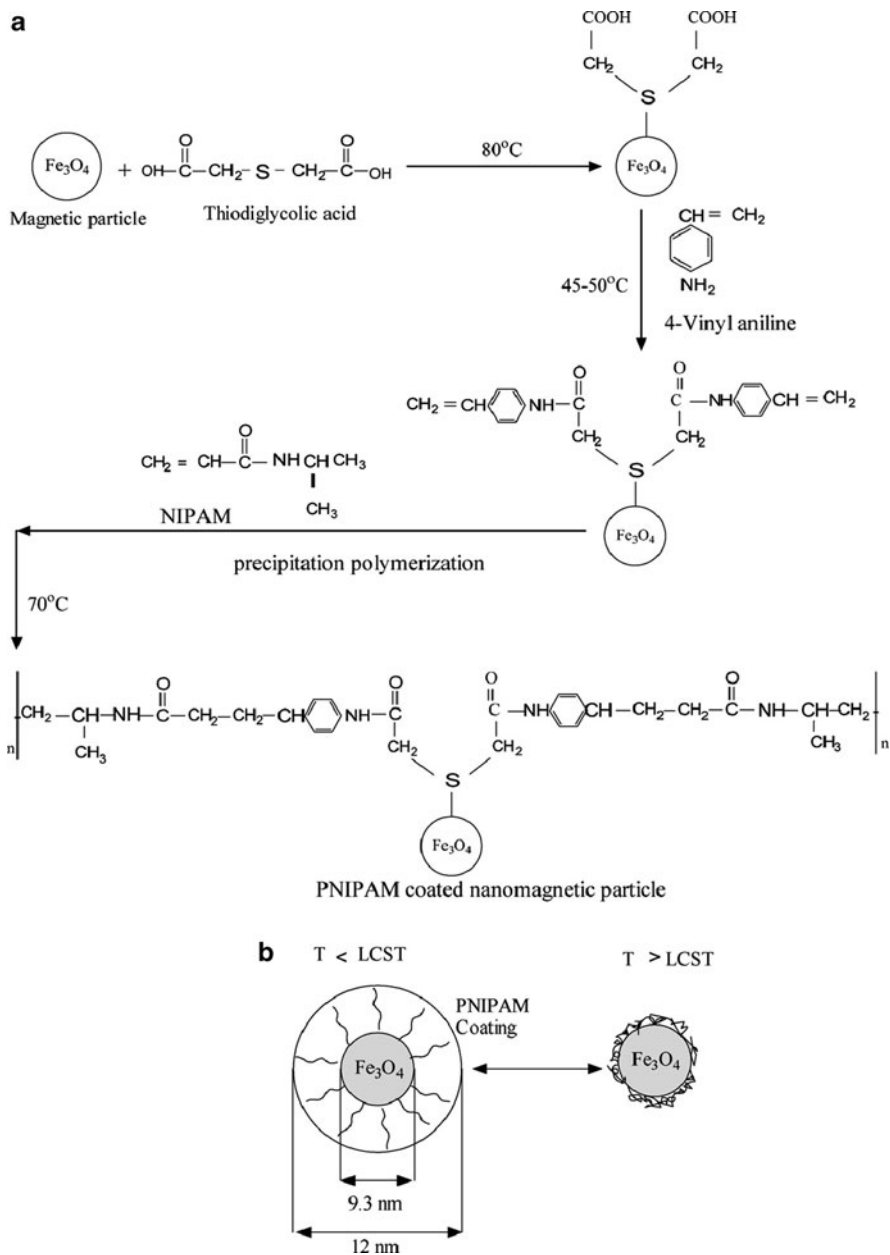


**Fig. 13** (a) Preparation of thermally sensitive PNIPAM-coated nanomagnetic particles. (b) Illustration of PNIPAM-coated nanoparticles. Reprinted from [143] with permission



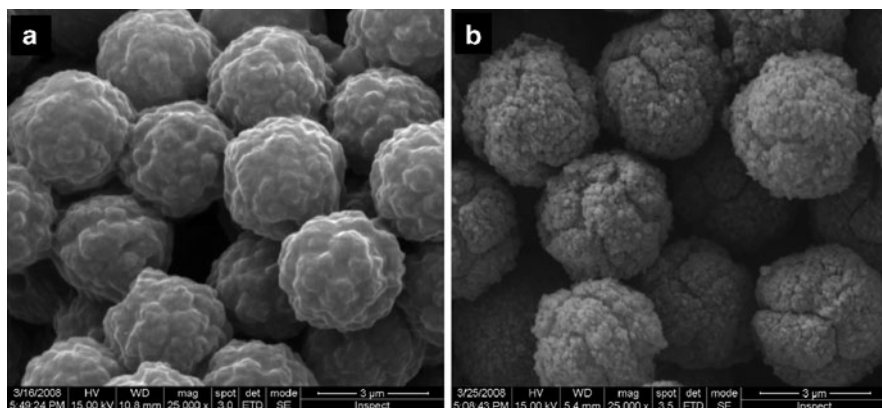


**Fig. 14** SEM images of (a) PGMA/PS and (b) magnetic PGMA/PS particles. Reprinted from [146] with permission

Elaissari and coworkers recently reported the synthesis of hydrophilic aminodextran containing magnetic latex using the combination of seeded and miniemulsion-like polymerization processes. The characterization of the latex demonstrated that the particles were cationically charged, hydrophilic, and have a high colloidal stability irrespective of the aminodextran immobilization process [149].

Polymerization in disperse media (dispersion, suspension or emulsion) is always accompanied by some problems, for example, non-uniform encapsulation and secondary particle formation. The new approach of using “inverse emulsion polymerization” is promising to resolve the problems mentioned above. Pioneering work on inverse emulsion was done by Vanderhoff et al. [150]. Menager et al. [151] synthesized magnetic latex using inverse emulsion (W/O) polymerization of AM with MBA in dodecane. Citrate-coated iron oxide magnetic particles were placed in an aqueous dispersion of the monomers. This aqueous mixture, stabilized by Span 80, was added to the oil (dodecane) phase under stirring. The polymerization was initiated with 2,2-azobis(2-isobutyramidine) (AIBA). Radiation by a  $^{60}\text{Co}$   $\gamma$ -ray source, at a dose rate of  $103.9\text{ Gy min}^{-1}$ , initiated an inverse emulsion polymerization to produce superparamagnetic magnetite/PS composite particles [152].

Many efforts have been devoted to the synthesis of magnetic latex using a special type surfactant-free emulsion polymerization technique (Fig. 17a). This technique was a substantial breakthrough in preparing polymer latex without using surfactants. An example of soap-free emulsion polymerization is the polymerization (initiated by KPS) of St in presence of surface-modified iron oxide magnetic particles, where silane-coupling reagents like [3-(methacryloxy)propyl]trimethoxysilane (MPTMS) and methacryloxypropyldimethoxysilane (MPDMS) were used. The produced magnetic latex particles were characterized routinely and revealed that the use of the di-functional coupling reagent MPDMS is suitable for production of monodisperse and spherical magnetic latex [153] (Fig. 17b). However, with the magnetic particles in the outer shell of the latex, the possibility of iron oxide leaching and interaction with target molecules in biomedical applications is high.



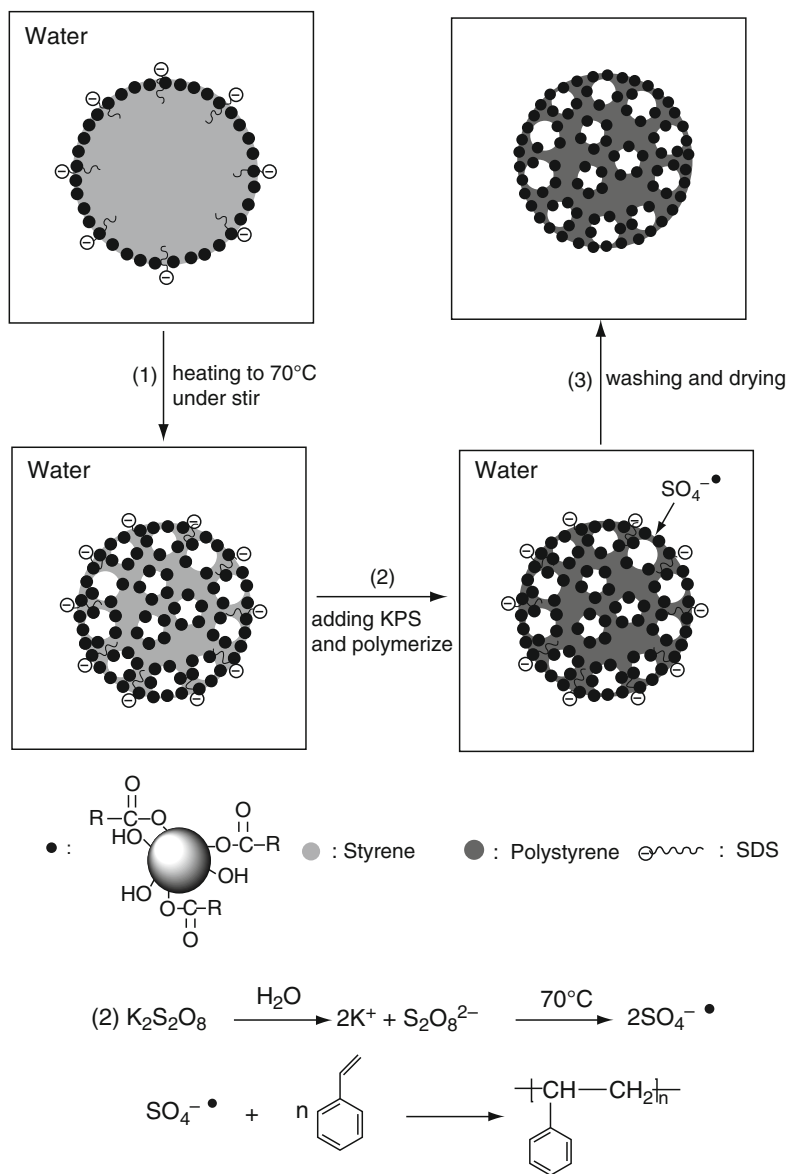


**Fig. 15** Fabrication of multihollow superparamagnetic magnetite/polystyrene nanocomposite particles via W/O/W double emulsions. Stages 1–3 and the reaction scheme are shown. Reprinted from [148] with permission

Similar work has been done by Gu et al. [154] on improving on the colloidal stability of the magnetic latex produced. Sodium *p*-styrene sulfonate (NaSS) was added in the course of the polymerization reaction. Very recently, silica-coated magnetic silica particles were encapsulated by a fluorescent polymeric shell of styrene and

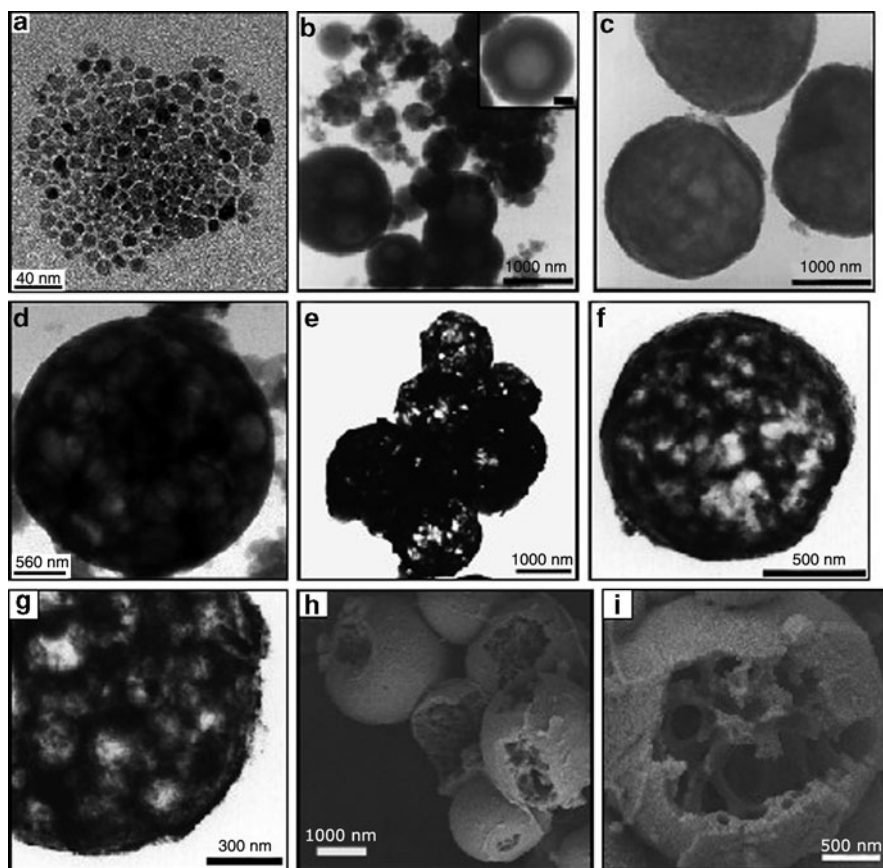


**Fig. 16** TEM images of (a) oleic-acid-coated magnetic particles, (b) hollow or multihollow and (c–g) multihollow magnetic particles. (h, i) SEM images of multihollow magnetic polymeric particles. Reprinted from [148] with permission

pyrene using soap-free emulsion polymerization initiated by the amphoteric initiator 2,2-azobis[*N*-(2-carboxyethyl)-2-methylpropionamidine] (VA-057) (Fig. 18). The important advantages of using the amphoteric initiator are to control the electrostatic surface potential of polymer particles to such a range that it can stabilize the particles without producing new particles, and to impart carboxyl groups that make it easier to attach other functional groups on the surface of the composite particles. The surface of the prepared magnetic composite was amphoteric in nature, as indicated by the zeta potential [155].

In a quest for different applications various numbers of polymers have been chosen to prepare encapsulated and functionalized magnetic particles by soap-free emulsion polymerization. Examples are amide- and carboxyl-functionalized magnetic latex for protein immobilization [156], and thermally sensitive and carboxyl-functionalized particles for antibody purification [157], bioprocesses



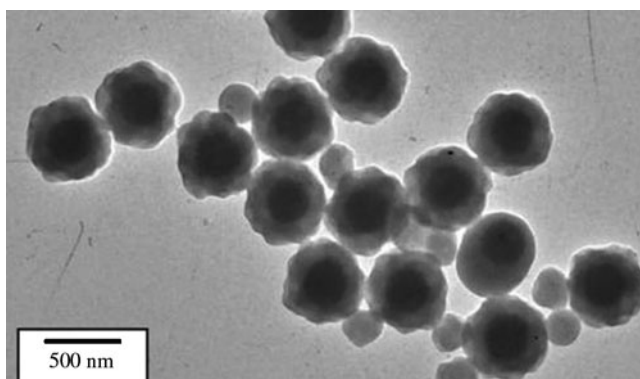
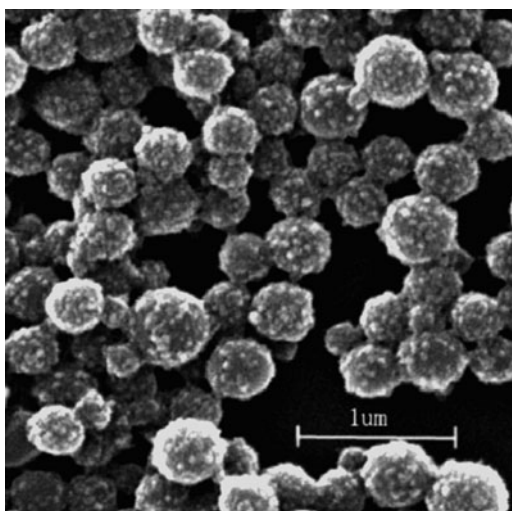


**Fig. 18** TEM image of magnetic core–polymeric fluorescent shell particles. Reprinted from [155] with permission

**Fig. 19** TEM image of raspberry-like magnetic polystyrene particles. Reprinted from [160] with permission



NIPAM, GMA and MBA were copolymerized with different feed ratios in a soap-free aqueous medium using V-50 as initiator, resulting in particles with a PGMA-rich core and PNIPAM-rich shell. The obtained template particles were allowed to react with the sodium salt of 3-mercaptopropionic acid (MPSA), 2-aminoethanethiol (AET) and mercaptoacetic acid to introduce functional groups to the particles. Magnetic iron oxide particles were precipitated inside the template particles by the use of  $\text{FeSO}_4 \cdot 7\text{H}_2\text{O}$  and  $\text{NH}_4\text{OH}$  solution. The resulting hybrid core–shell particles contain 33% magnetic nanoparticles in the core. Philipse et al. [163] prepared magnetic PMMA hybrid latex exhibiting field-induced colloidal crystallization. The magnetic emulsion of iron oxide particles coupling with silane agent was used as seed in the soap-free emulsion polymerization of MMA with

KPS as initiator [163]. Liu et al. [164] started with bilayer oleic-acid-coated iron oxide nanoparticles and applied the combination of soap-free and seeded emulsion polymerization (Fig. 20a) to produce GMA-functionalized magnetic poly(MMA-DVB-GMA) microspheres. This was followed by modification of the PGMA shell with EDA to introduce amino groups that can react with the organic dye fluorescein isothiocyanate and that impart multifunctional, photoluminescence, superparamagnetic and pH-responsive properties to the particles (Fig. 20b).

#### 4.3.4 Microemulsion Polymerization

A microemulsion is defined as a thermodynamically stable, isotropic and optically transparent dispersion of two immiscible liquids prepared in the presence of a stabilizing system, which can be a single surfactant, a mixture of surfactants, or mixture of a surfactant and a cosurfactant [165]. Liu et al. [166] reported the synthesis of polymer-coated magnetic microspheres using direct microemulsion polymerization. They produced 1–5  $\mu\text{m}$  sized magnetic polymer particles from oleic-acid-coated 10 nm iron oxide magnetic particles. A microemulsion was formed by dissolving the magnetic nanoparticles in different monomers like St, DVB, MAA and AM in the presence of SDS and cetylalcohol (CA); benzoylperoxide or KPS was used, respectively, as initiator for the polymerization.

Preparation of iron oxide magnetic nanoparticles and their encapsulation with polymers in W/O, i.e. inverse microemulsion polymerization, was also applied by O'Connor et al. [167]. Inverse microemulsion polymerization was used to prepare submicron hydrophilic magnetic latex containing 5–23 wt% iron oxide. AM and crosslinker MBA were added to an aqueous suspension of previously synthesized iron oxide nanoparticles (6 wt%); this aqueous phase was dispersed in a aerosol OT (sodium 1,4-bis(2-ethylhexoxy)-1,4-dioxobutane-2-sulfonate) (AOT)-toluene solution to form a W/O microemulsion, followed by polymerization with AIBN or V-50 as initiator. The particle size (80–180 nm) was controlled by tuning the concentration of the water-soluble crosslinker agent as well as the amount of surfactant with respect to water [168].

#### 4.3.5 Miniemulsion Polymerization

The aqueous dispersions of thermodynamically unstable O/W droplets that are prepared by using high mechanical shear (ultrasound, high speed homogenizers) are known as miniemulsions. Depending on the conditions, the droplet diameter is in the range of 20–500 nm and they are kinetically stable from hours to days. The droplets are stabilized against Ostwald ripening by low molecular weight costabilizers known as hydrophobes, which are highly water-insoluble but soluble in the dispersed phase. A very frequently used hydrophobe is hexadecane, which remains in the dispersed phase, suppresses Ostwald ripening, and retards monomer diffusion from smaller droplets to larger droplets. Anionic, cationic or nonionic surfactants dissolved in the continuous aqueous phase can be used to prevent the coalescence of droplets [169, 170].

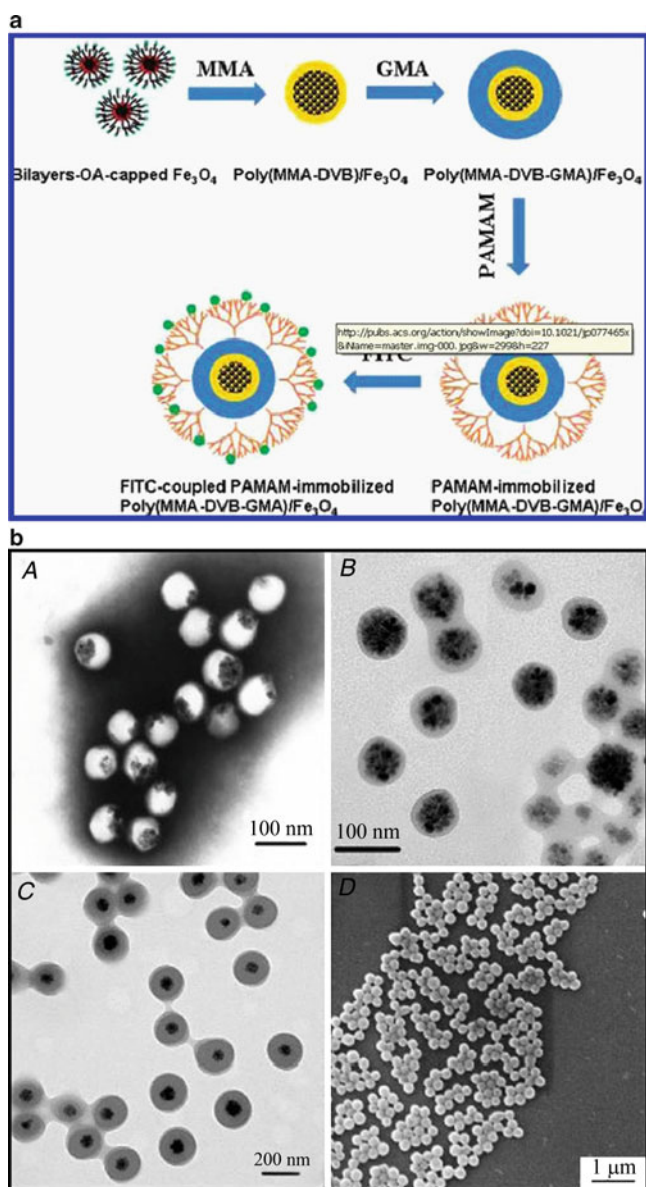


**Fig. 20** (a) Preparation of dendritic polyamidoamine-immobilized magnetic poly(MMA-DVB-GMA) microspheres with coupling FITC. (b) TEM images of the magnetic PMMA microspheres coating the bilayer-oleic-acid-stabilized magnetite nanoparticles (A), the magnetic poly(MMA-DVB) microspheres (B), and the magnetic poly(MMA-DVB-GMA) microspheres (C). SEM image of magnetic poly(MMA-DVB-GMA) microspheres (D). Reprinted with permission from [164]

Ramírez et al. encapsulated double-layer (oleic acid and SDS) surfactant-coated magnetite into polystyrene particles by miniemulsion polymerization [171]. In the three-step process, oleic-acid-coated magnetite and oleic acid/SDS double-coated magnetite were prepared in the first and second step, respectively. The third step consists of the preparation of a miniemulsion by stirring 1 h for pre-emulsification, followed by ultrasonication for 2 min using St as monomer with hexadecane and SDS in water. The encapsulation of magnetite was accomplished by cosonication of an St miniemulsion and SDS-stabilized magnetite nanoparticles. The polymerization was initiated by KPS at 80°C.

A similar approach was used by Holzapfel et al. to produce a magnetic latex (45–70 nm) that had both magnetic and fluorescent properties [172]. The magnetite (10 nm) was encapsulated with poly(St-co-AA) in the presence of a fluorescent organic dye *N*-(2,6-diisopropylphenyl)-perylene-3,4-dicarboxylic diimide (PMI). 2,2'-azobis (2-methylbutyronitrile) (V-59) was used as initiator. The final particles were further functionalized by poly-L-lysine onto the surface of the magnetic latex.

Using miniemulsion polymerization, Gu et al. reported the synthesis of magnetic polystyrene latex and carboxylated magnetic polymer latex [173, 174]. In the latter, carboxyl end groups were provided on the surface of the latex directly from the initiator 4,4'-azobis (4-cyanopentanoic acid) (ACPA). The average size of the final magnetic particle was 250 nm.

The preparation of magnetic latexes and the investigation of the effect of different parameters on the particle morphology, size, size distribution and miniemulsion polymerization kinetics were discussed by various research groups [175–177]. Zhang et al. [176] showed that a higher amount of KPS and sonication time increased the polymerization rate at the beginning period. On the other hand, an increase in iron oxide made the reaction rate slower and resulted in less monodisperse particles.

The effect of the amount of surfactant SDS, hydrophobe hexadecane, iron oxide magnetic particles, MAA and non-ionic cellulose ether, hydroxyethylcellulose, on the magnetic latex morphology, surface quality and size distribution was studied by Forcada et al. for the encapsulation of magnetic particles by miniemulsion polymerization of St. Optimal conditions were 2–3% of SDS, 9–12% of hexadecane, 10% of iron oxide and 2% of HEC, relative to the total amount of St and iron oxide [177].

Mori and Kawaguchi reported the preparation of magnetic polystyrene particles containing 30 wt% of magnetite. Magnetic polystyrene particles of 300 nm were produced and easily separated when persulphate, KPS or APS initiator was used. Conversely, due to high colloidal stability, the latex prepared by oil-soluble initiator (for instance AIBN) was not easy to separate, and the magnetite nanoparticles were located on the surface of the polystyrene latex. A mixture of initiators resulted in intermediate properties compared to individual systems [170].

The synthesis of magnetic PMMA by miniemulsion polymerization was also illustrated [178, 179]. Hong et al. prepared particles in the range of 100–150 nm and 15–26 wt% magnetite content by miniemulsion polymerization. They also studied the effect of initiator AIBN and monomer MMA dosages on the polymerization



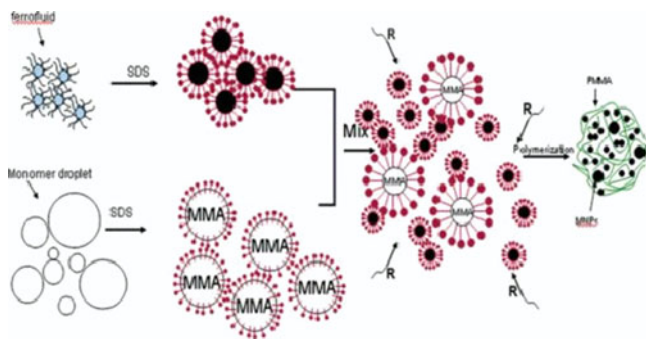


**Fig. 21** Reaction scheme for the preparation of magnetic PMMA. Reprinted from [178] with permission

kinetics in the presence of magnetic particles (Fig. 21), where a higher amount of initiator and a lower amount of monomer enhanced the polymerization rate [178].

Liu et al. prepared magnetic poly(MM-DVB) latex following the same process. Benzoyl peroxide, CA and hexane were used as initiator, cosurfactant and hydrophobe, respectively. Additionally, the surface of the magnetic latex was modified with PEG to be coupled to the affinity dye, Cibacron blue F3G-A (CB) [179].

Thermosensitive magnetic latex was reported to produce on/off switching-controlled polymer membranes; miniemulsion polymerization was applied to obtain magnetic polystyrene seed, which was further used for functionalization with PNIPAM [180]. Membrane fabrication was accomplished by the mixing of MPS-PNIPAM microgel latex with a 8 wt% solution of PVA containing glutaric aldehyde as a crosslinking agent. The crosslinking reaction of PVA was induced by lowering the pH of the solution to 2 by the addition of HCl solution. The mixture was poured into a square mould with a thickness of 1.5 mm and width of 4 cm. The layer was placed perpendicularly to the direction of a static uniform magnetic field for 5 h. Due to the mutual interaction between the magnetic gel beads, a pearl chain structure develops. The crosslinking reaction locks the chainlike structure in the gel, aligned along the direction of the field. The chains of core-shell MPS-PNIPAM particles form channels in the PVA matrix.

Inverse miniemulsion polymerization was used by Wormuth to prepare superparamagnetic poly(HEMA-*co*-MAA) latex. Double hydrophilic diblock copolymer (PEO-*b*-PMA) was not only used as a stabilizer but also as a structure-directing agent by which particle nucleation and growth could be influenced. The obtained particle size was in the range 140–220 nm and the magnetic content was 18% [181].

Recently, Qiu et al. synthesized magnetic polystyrene latex by polymerizing St in the presence of iron oxide nanoparticles and using ultrasound to initiate the reaction [182]. More recently, Teo et al. reported the use of ultrasound for initiating the polymerization of *n*-butyl methacrylate in the presence of magnetic nanoparticles [183].

Following the emulsifier-free miniemulsion polymerization route, Forcada et al. illustrated the synthesis of self-stabilized magnetic latex. Ionic NaSS was taken as a stabilizer as well as comonomer (Fig. 22). Photon correlation spectroscopy (PCS)

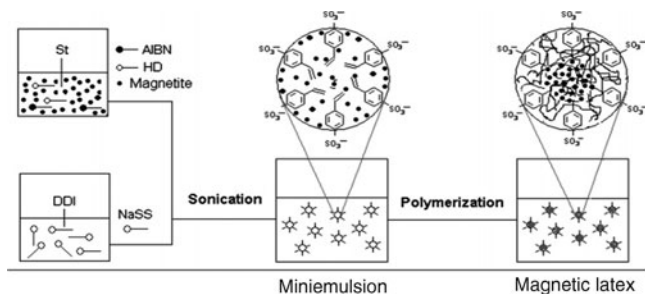


**Fig. 22** Stabilization mechanism for the self-stabilized magnetic polymeric composite nanoparticles obtained by emulsifier-free miniemulsion polymerization. Reprinted from [184] with permission

was applied to determine the surface hairy layer and colloidal stability in the presence of various electrolytes. The presence of higher amounts of NaSS improved the encapsulation and PSD, and decreased the particle size. The optimum amount of NaSS was found to be 20 wt% with respect to the total amount of St and magnetite [184]. A similar approach has been reported by Reza et al., who prepared magnetic poly(St-*co*-DVB-chloromethyl styrene) via emulsifier-free miniemulsion polymerization [185].

## 5 Concluding Remarks

Hybrid latex, consisting of a magnetic inorganic part and a polymeric organic part, is an important material both in research and for applications in chemistry, biochemistry, colloid science and environmental science. Every day, new aspects of magnetic latexes are being developed due to the demand for magnetic latexes in different forms in areas like separation techniques, drug delivery, MRI contrast agents, cancer therapy, ink, paint, cosmetic industries etc.

In the last few years, many efforts have been given to the preparation of magnetic latexes in dispersed media using suspension, precipitation, dispersion, emulsion, miniemulsion and microemulsion polymerizations. In this review chapter, the synthesis and functionalization of magnetic core-shell polymer particles in dispersed media have been reviewed with the main focus on emulsion polymerization.

Some new approaches, using for example ATRP, RAFT and NMP, are emerging for the synthesis of well-controlled structures of hybrid magnetic materials. The chapter of Charleux et al. [186] covers this area and also includes the preparation of magnetic latex.

**Acknowledgments** This work has been achieved within the frame of ADNA (Advanced Diagnostics for New Therapeutic Approaches), a program dedicated to personalized medicine, coordinated by Institut Mérieux and supported by research and innovation aid from the French public agency, OSEO.

## References

1. Hood JD, Bednarski M, Frausto R, Guccione S, Reisfeld RA, Xiang R Cheresch DA (2002) *Science* 296:2404–2407
2. Grainger DW, Okano T (2003) *Adv Drug Deliv Rev* 55:311–313
3. Elaissari A (ed) (2008) *Colloidal nanoparticles in biotechnology*. Wiley, New Jersey
4. Stone HA, Stroock AD, Ajdari A (2004) *Annu Rev Fluid Mech* 36:81–411
5. Tuichiev Sh, Rashidov V, Esfidary A (2003) *Electromagn Mater*:213–216. doi:10.1142/9789812704344 0042
6. Schwertmann T, Cornell RM (1991) *Iron oxides in the laboratory: preparation and characterization*. Wiley, Weinheim
7. Van Herk AM (1997) In: Asua JM (ed) *Polymeric dispersions: principle and application*, vol 335. Kluwer, Netherlands, pp. 435–450
8. Wilson JL, Poddar P, Frey NA, Srikant H, Mohamed K, Harmon JP, Kotha S, Wachsmuth J (2004) *J Appl Phys* 95:1439–1443
9. Yan F, Xue G, Chen J, Lu Y (2001) *Synth Met* 123:17–20
10. Lapotin AV, Kazantseva NE, Kazantsev YN, D'yakonova OA, Vilcàková J, Saha P (2008) *J Commun Technol Electron* 53:487–496
11. Sohn BH, Cohen RE (1997) *Chem Mater* 9:264–269
12. Helseth LE (2007) *Appl Phys Lett* 90:093501
13. Deetz DJ (1998) US patent 5843329
14. Duran JDG, Arias JL, Gallardo V, Delgado AV (2008) *J Pharm Sci* 97:2948–2983
15. Feyen M, Heim E, Ludwig F, Schmidt AM (2008) *Chem Mater* 20:2942–2948
16. Polasek P, Mult S (2002) *Water SA* 28:69
17. Cumbal L, Greenleaf J, Leun D, Sengupta AK (2003) *React Funct Polym* 54:167–180
18. Pauser S, Reszka R, Wagner S, Wolf KJ, Buhr HI, Berger G (1997) *Anticancer Drug Des* 12:125–135
19. Torchilin VP (2000) *Eur J Pharm Sci* 11:81–91
20. Brazel CS (2009) *Pharmaceut Res* 26:644–656
21. Kim DH, Elena R, Rajh T, Bader SD, Novosad V (2009) *Nanotechnology* 2:294–297
22. Tanimoto A (2001) In: Arshady R (ed) *Radiolabeled and magnetic particulates in medicine & biology*. MML series, vol 3. Citus Books, London, p 525
23. Zielhuis SW, Nijssen JF, Seppenwoolde JH, Zonnenberg BA, Bakker CJ, Hennik WE, Rijk VPP, Van Schip AD (2005) *Curr Med Chem Anticancer Agents* 5:303–313
24. Dobson J (2006) *Drug Dev Res* 67:55–60
25. McBain SC, Yiu HP, Dobson J (2008) *Int J Nanomedicine* 3:169–180
26. Benjamin BY, Zachary GF, Derek SH, Gregory F, Kenneth AB, Michael C, Robert L, Gary F (2005) *J Magn Magn Mater* 293:647–654
27. Arruebo M, Fernández-Pacheco R, Ibarra R, Santamaria J (2007) *Nanotoday* 2:22–32
28. Mailander V, Landfester K (2009) *Biomacromolecules* 10:2379–2400
29. Gang L, Fang H, Xuemei W, Feng G, Gen Z, Tao W, Hui J, Chunhui W, Dadong G, Xiaomao L, Baoan C, Zhongze G (2008) *Langmuir* 24:2151–2156
30. Koppolu BP, Rahimi M, Nattama SP, Wadajkar A, Nguyen K (2009) *Nanomedicine: NBM* 20:1–7
31. Gupta AK, Wells S (2004) *IEEE Trans NanoBioscience* 3:66–73
32. Kubo T, Sugita T, Shimose S, Nitta Y, Murakami T (2000) *Int J Oncol* 17:309–316
33. Shinkai M, Suzuki M, Ijima S, Kobayashi T (1995) *Biotechnol Appl Biochem* 21:125–137
34. Chan DCF, Kirpotin DB, Bunn PA Jr (1997) In: Hafeli U, Schutt W, Teller J, Zborowski M (eds) *Scientific and clinical application of magnetic carriers*. Plenum, New York, pp. 607–617
35. Hergt R, Andra W, d'Ambly CG, Hilger I, Kaiser WA, Richter U, Schmidt H-G (1998) *IEEE Trans Magn* 34:3745–54
36. Motoyama J, Hakata T, Kato R, Yamashita N, Morino T, Kobayashi T, Honda H (2008) *BioMagn Res Technol* 6:4
37. Thiesen B, Jordan A (2008) *Int J Hyperthermia* 24:467–74

38. Gupta AK, Gupta M (2005) *Biomaterials* 26:3995–4021
39. Chegnon MS, Groman EV, Josephson L, Whithead RA (1995) *Adv Magn Inc EP* 0125995
40. Chen H, Ebner AD, Bockenfeld D, Ritter JA, Kaminski MD, Liu X, Remfer D, Rosengart AJ (2007) *Phys Med Biol* 52:6053–6072
41. Elaissari A (ed) (2004) *Colloidal biomolecules, biomaterials, and biomedical applications. Surfactant series*, vol 116. Marcel Dekker, New York, p 1
42. Meza M (1997) In: Hafeli U, Schutt W, Teller J, Zborowski M (eds) *Scientific and clinical application of magnetic carriers*. Plenum, New York, pp. 303–309
43. Haik Y, Cordovez M, Chen C-J, Chatterjee J (2002) *Eur Cell Mater* 3:41–44
44. Tokoro H, Nakabayashi T, Fujii S, Zhao, H, Hafeli U (2009) *J Magn Magn Mater* 321:1676–1678
45. Ugelstad J, Berge A, Ellingsen T, Auno O, Kilaas L, Nilsen TN, Schmid R, Stenstad P, Funderud S, Kvalheim G, Nustad K, Lea T, Vartdal F, Danielsen H (1998) *Macromol Symp* 17:177–211
46. Obata K, Segawa O, Yakabe M, Ishida Y, Kuroita T, Ikeda K, Kawakami B, Kawamura Y, Yohda M, Matsunaga T, Tajima H (2001) *J Biosci Bioeng* 91:500–503
47. Elaissari A, Rodrigue M, Meunier F, Herve F (2001) *J Magn Magn Mater* 225:127–133
48. Yoza B, Arakaki A, Matsunaga T (2003) *J Biotechnol* 101:219–228
49. Intoraso S, Srirung R, Intoraso A, Ngamratana-paiboon S (2009) *Anal Biochem* 386:291–292
50. Taylor JJ, Hurst CD, Davies MJ, Sachsinger N, Bruce IJ (2000) *J Chromatogr A* 890:159–166
51. Safarik I, Safarikova M (2004) *BioMagn Res Technol* 2:7
52. Kondo A, Kamura H, Higashitani K (1994) *Appl Microbiol Biotechnol* 41:99–105
53. Huang X, Meng X, Tang F, Li L, Chen D, Liu H, Zhang Y, Ren J (2008) *Nanotechnology* 19:445101
54. Varlan AR, Suls J, Jacobs P, Sansen W (1995) *Biosens Bioelectron* 10:15–19
55. Koneracká M, Kopčanský P, Timko M, Ramchand CN, Saiyed ZM, Trevan M, de Sequeira A (2006) In: Guisan JM (ed) *Immobilization of enzymes and cells. Methods in biotechnology*, vol 22. Humana, Totowa, NJ, pp. 217–228
56. Pichot C (2004) *Colloid Interface Sci* 9:213–221
57. Haukanes BI, Kvam C (1993) *Bio/Technology* 11:60–63
58. Satoh K, Iwata A, Murata M, Hikata M, Hayakawa T, Yamaguchi T (2003) *J Virol Methods* 114:11–19
59. Veyret R, Elaissari A, Marianneau P, Alpha Sall A, Delair T (2005) *Anal Biochem* 346:59–68
60. Esteve F, Amiral J, Padula C, Solinas I (1999) *WO* 9504279. Societe Diagnostica-Stago
61. Ugelstad J, Olsvik O, Schmid R, Berge A, Funderud S, Nustad K (1993) In: Ngo TT (ed) *Molecular interactions in bioseparation*. Plenum, New York, pp. 229–244
62. Mijailovich SM, Kojic M, Zivkovic M, Fabry B, Fredberg JJ (2002) *J Appl Physiol* 93:1429–1436
63. Renault NJ, Martelet C, Chevolot Y, Cloarec JP (2008) In: Elaissari A (ed) *Colloidal nano particles in biotechnology*. Wiley, New Jersey, p 169
64. Bacry JC, Perzynski R, Salin D (1987) *Recherche* 170:232
65. Papell S (1965) *US patent* 3,215,572
66. Rosensweig RE (1997) *Ferrohydrodynamics*. Dover, New York
67. Khalafalla SE, Reimers GW (1973) *US Patent* 3,764,540,
68. Khalafalla SE, Reimers GW (1980) *IEEE Trans Magn* 16:178
69. Montagne F, Mondain-Monval O, Pichot C, Mozzanega H, Elaissari A (2002) *J Magn Magn Mater* 250:302–312
70. Shinkai M, Honda H, Kobayashi T (1991) *Biocatal Biotransformation* 5:61–69
71. Massart RC (1980) *R Acad Ser C* 291:1
72. Massart R, Cabuil VJ (1987) *Chem Phys* 84:967
73. Viota JL, Duran JDG, Gonzalez-Caballero F, Delgado AV (2007) *J Magn Magn Mater* 314:80–86

74. Răcuciu M, Creangă DE, Bădescu V, Sulitanu N (2007) *J Magn Magn Mater* 316:e772–e775
75. Chunbao Xu, Teja AS (2008) *J Supercrit Fluids* 44:85–91
76. Laurent S, Forge D, Port M, Roch A, Robic C, Elst EV, Muller RN (2008) *Chem Rev* 108:2064–2110
77. Jana NR, Chen Y, Peng X (2004) *Chem Mater* 16:3931–3935
78. Wan J, Cai W, Feng J, Meng X, Liu E (2007) *Chem Commun* 47:5004
79. Viau G, Fievet-Vincent F, Fiévet F (1996) *J Mater Chem* 6:1047–1053
80. Gonzalez-Carreno T, Morales MP, Gracia M, Serna CJ (1993) *Mater Lett* 18:151–155
81. Veintemillas-Vendaguer S, Bomati-Miguel O, Morales MP, Di Nunzio PE, Martelli S (2003) *Mater Lett* 57:1184–1189
82. Feltin N, Pileni MP (1997) *Langmuir* 13:3927–3933
83. Pileni MP (2001) *Adv Funct Mater* 11:323–333
84. Hamoudeh M, Al Faraj A, Canet-Soulas E, Besueille F, Leonard D, Fessi H (2007) *Int J Pharm* 338:248–257
85. Hamoudeh M, Fessi H (1996) *J Colloid Interface Sci* 300:584–590
86. Tanyolac D, Ozdural AR (2000) *React Funct Polym* 43:279–286
87. Lee SL, Jeong JR, Shin SC, Kim JC, Chang YH, Lee KH, Kim JD (2005) *Colloids Surf A Physicochem Eng Asp* 255:19–25
88. Chatterjee J, Haik Y, Chen CJ (2001) *Colloid Polym Sci* 279:1073–1081
89. Chatterjee J, Haik Y, Chen CJ (2004) *Biomagn Res Tech* 2:4
90. Lee J, Isobe T, Senna M (1996) *J Colloid Interface Sci* 177:490–494
91. Brinker CJ (1994) In: Bergna HE (ed) *The colloid chemistry of silica advances in chemistry series*, vol 234. American Chemical Society, Washington, DC, p 359
92. Ma Z, Guan Y, Liu H (2006) *J Magn Magn Mater* 301:469–477
93. Sauzedde S, Elaissari A, Pichot C (1999) *Colloid Polym Sci* 277:846–855
94. Kim HS, Sohn BH, Lee W, Lee JK, Choi SJ, Kwon SJ (2002) *Thin Solid Films* 419:173–177
95. Caruso F, Lichtenfeld H, Donath E, Möhwald H (1999) *Macromolecules* 32:2317
96. Caruso F, Susha AS, Giresig M, Möhwald H (1999) *Adv Mater* 11: 950–953
97. Veyret R, Delair T, Elaissari A (2005) *J Magn Magn Mater* 293:171–176
98. Ugelstad J, Ellingsen T, Berge A, Helgee B (1986) *European Patent* 0 106,873
99. Ugelstad J, Mork PC, Schmid R, Ellingsen T, Berge A (1993) *Polym Int* 30:157–168
100. Ugelstad J, Killas L, Aune O, Bjorgum J, Herje R, Schmid R, Stenstad P, Berge A, Uhlén M, Hornes E, Olsvik O (1994) In: Uhlén M, Hornes E, Olsvik O (eds), *Advances in biomagnetic separation*. Eaton, Stockholm, p 1
101. Ma Z, Guan Y, Liu H (2005) *J Polym Sci A Polym Chem* 43:3433–3439
102. Moeser GD, Roach KA, Green WH, Laibinis PE, Hatton TA (2002) *Ind Eng Chem Res* 41:4739–4749
103. Kawaguchi H, Fujimoto K, Nakazawa Y, Sagakawa M, Ariyoshi Y, Shidara M, Okazaki H, Ebisawa Y (1996) *Colloids Surf A Physicochem Eng Asp* 109:147–154
104. Sahiner N (2006) *Colloid Polym Sci* 285:283–292
105. Wormuth K (2001) *J Colloid Interface Sci* 241:366–377
106. Thuenemann AF, Schuett D, Kaufner L, Pison U, Möhwald H (2006) *Langmuir* 22:2351–2357
107. Strable E, Bulre WM, Moskowitz B, Vivekannandan K, Allen M, Douglas T (2001) *Chem Matter* 13:2201–2209
108. Thomas JR (1996) *J Appl Phys* 377:2914–2915
109. Charmot D (1989) *Prog Colloid Polym Sci* 79:94–100
110. Takahashi K, Tamaura Y, Koderia Y, Mihama T, Saito Y, Inada Y (1987) *Biochem Biophys Res Comm* 142:291–296
111. Vivaldo-Lima E, Wood Philip E, Hamielec AE, Penlidis A (1997) *Ind Eng Chem Res* 36:939–965
112. Yuan HG, Kalfas G, Ray WH (1991) *Rev Macromol Chem Phys C* 21:215–299
113. Daniel JC, Schuppiser JL, Tricot M (1981) *US patent* 4,358,388
114. Lee Y, Rho J, Jung B (2003) *J Appl Polym Sci* 89:2058–2067

115. Maria LCD, Leite MCAM, Costa MAS, Ribeiro JMS, Senna LF, Silva MR (2003) *Eur Polym J* 39:843–846
116. Iman M, Celebi SS, Ozdzural R (1992) *Reac Polym* 17:325–330
117. Zhiya M, Guan Y, Liu X, Liu H (2005) *Polym Adv Technol* 16:554–558
118. Müller-Schulte D, Schmitz- Rode T (2006) *J Magn Magn Mater* 302:267–271
119. Wang X, Ding X, Zheng Z, Hu X, Cheng X, Peng Y (2006) *Macromol Rapid Commun* 27:1180–1184
120. Lu S, Cheng G, Pang X (2003) *J Appl Polym Sci* 89:3790–3796
121. Richard J, Sophe V (1999) US patent 5,976,426
122. Li X, Sun Z (1995) *J Appl Polym Sci* 58:1991–1997
123. Horák D, Babic M, Macková H, Beneš J M (2007) *J Sep Sci* 30:1751–1772
124. Tao Z, Yang W, Zhou H, Wang C, Fu S (2000) *Colloid Polym Sci* 278:509–517
125. Horák D (2001) *J Polym Sci A Polym Chem* 39:3707–3715
126. Horák D, Semenyuk N, Lednický F (2003) *J Polym Sci A Polym Chem* 41:1848–1863
127. Ding X, Sun, Z, Wan G, Jiang Y (1998) *React Funct Polym* 38: 11–18
128. Liu X-Y, Ding X-B, Zheng Z-H, Peng Y-X, Long X-P, Wang X-C, Chan ASC, Yip CW (2003) *J Appl Polym Sci* 90:1879–1884
129. Ding X-B, Li W, Zheng Z-H, Zhang W-H, Deng J-G, Peng Y-X, Chan ASC, Li P (2001) *J Appl Polym Sci* 79:1847–1851
130. Ahmad H, Rahman MA, Miah MAJ, Tauer K (2008) *Macromol Res* 16:637–643
131. Zhang J, Yu D, Chen W, Xie Y, Wan W, Liang H, Min C (2009) *J Magn Magn Mater* 321:572–577
132. Park BJ, Park CW, Yang SW, Kim HM, Choi HJ (2009) *J Phys Conf Ser* 149:012078
133. Zhang HP, Bai S, Xu L, Sun Y (2009) *J Chromatogr B* 877:127–133
134. Van Herk AM, Janssen RQF, Janssen EAWG, German AL (1993) In: *Proceedings of the XIX international conference in organic coatings science and technology*. Athens, Greece, pp. 219–224
135. Montagne F, Mondain-Monval O, Pichot C, Elaissari A (2006) *J Polym Sci A Polym Chem* 44:2642–2656
136. Khng HP, Cunliffe D, Davies S, Turner AN, Vulfson EN (1998) *Biotechnol Bioeng* 60:419–424
137. Horak D, Chekina N (2006) *J Appl Polym Sci* 102:4348–4357
138. Mes' Shikova AY, Shabsel's BM, Skurkis YO, Inkin KS, Chekina NA, Ivanchev SS (2007) *Russ J Gen Chem* 77:354–362
139. Braconnot S, Hoang C, Fessi H, Elaissari A (2008) *Mater Sci Eng C* 29:624–630
140. Lee CF, Chou YH, Chiu WY (2007) *J Polym Sci A Polym Chem* 45:3062–3072
141. Zhang F, Wang CC (2009) *Langmuir* 25:8255–8262 doi:10.1021/1a9004467
142. Shang H, Chang WS, Kan S, Majetich SA, Lee GU (2006) *Langmuir* 22:2516–2522
143. Shamim N, Hong L, Hidajat K, Uddin MS (2007) *Colloids Surf B Biointerfaces* 55:51–58
144. Van Herk AM (1997) In: Asua JM (ed) *Polymeric dispersion: principles and applications*. NATO ASI series, applied science, vol 335. Kluwer, Dordrecht, pp. 435–450
145. Boguslavsky Y, Margel S (2008) *J Colloids Interface Sci* 317:101–114
146. Omer-Mizrahi M, Margel S (2009) *J Colloids Interface Sci* 329:228–234
147. Zhao J, Han Z, Song Q, Wang Y, Sun D (2008) *Front Chem China* 3:81–87
148. Yang S, Liu H, Zhang Z (2008) *Langmuir* 24:10395–10401
149. Mouaziz H, Braconnot S, Ginot F, Elaissari A (2009) *Colloids Polym Sci* 287:287–297
150. Vanderhoff JW, Branford EB, Tarkowski HL, Schaffer JB (1962) *Adv Chem Ser* 34:32
151. Menager C, Sandre O, Mangili J, Cabuil V (2004) *Polymer* 45:2475–2481
152. Chen Y, Qian Z, Zhang Z (2008) *Colloids Surf A Physicochem Eng Asp* 312:209–213
153. Gu S, Shiratori T, Konno M (2003) *Colloids Polym Sci* 281:1076–1081
154. Gu S, Onishi J, Kobayashi Y, Nagao D, Konno M (2005) *J Colloids Interface Sci* 289:419–426
155. Nagao D, Yakoyama M, Yamauchi N, Matsumoto H, Kobayashi Y, Konno M (2008) *Langmuir* 24:9804–9808
156. Guo N, Wu D, Pan X, Lu M (2009) *J Appl Polym Sci* 112:2383–2390
157. Kondo A, Kamura H, Higashitani K (1994) *Appl Microbiol Biotechnol* 41:99–105

158. Kondo A, Fukuda H (1999) *Colloids Surf A Physicochem Eng Asp* 153:435–438
159. Lee CF, Lin CC, Chien CA, Chiu WY (2008) *Eur Polym J* 44:2768–276
160. Xu Z, Xia A, Wang C, Yang W, Fu S (2007) *Mater Chem Phys* 103:494–499
161. Pich A, Bhattacharya S, Ghosh H, Adler JP (2005) *Polymer* 46:4596–4603
162. Suzuki D, Kawaguchi H (2006) *Colloids Polym Sci* 284:1443–1451
163. Sacanna S, Philipse A P (2006) *Langmuir* 22:10209–10216
164. Liu H, Guo J, Jin L, Yang W, Wang C (2008) *J Phys Chem B* 112:3315–3321
165. Larpent C (2003) In: Elaissari A (ed) *Colloid polymers: synthesis and characterization*. Marcel Dekker, New York, pp. 145–187
166. Liu ZL, Yang XB, Yao KL, Du GH, Liu ZS (2006) *J Magn Magn Mater* 302:529–535
167. O'Connor CJ, Lee Y-S, Tang J, John VT, Kommareddi NS, Tata M, McPherson GL, Akkara JA, Kaplan DL (1994) *IEEE Trans Magn* 30:4954–4956
168. Deng Y, Wang L, Yang W, Fu S, Elaissari A (2003) *J Magn Magn Mater* 257:69–78
169. Landfester K (2003) In: Elaissari A (ed) *Colloid polymers: synthesis and characterization*. Marcel Dekker, New York, pp. 225–243
170. Mori Y, Kawaguchi H (2007) *Colloids Surf B Biointerfaces* 56:246–254
171. Ramírez LP, Landfester K (2003) *Macromol Chem Phys* 204:2–31
172. Holzapfel V, Lorenz M, Weiss CK, Schrezenmeier H, Landfester K, Mailänder V (2006) *J Phys Condens Matter* 18:2581–2594
173. Zheng W, Gao F, Gu H (2005) *J Magn Magn Mater* 288:403–410
174. Zheng W, Gao F, Gu H (2005) *J Magn Magn Mater* 293:199–205
175. Csetneki I, Kabai Faix M, Szilagyí A, Kovacs AL, Németh Z, Zrinyi M (2004) *J Polym Sci A Polym Chem* 42:4802–4808
176. Zhang Q, Xie G, Zhang H, Zhang J, He M (2007) *J Appl Polym Sci* 105:3525–3530
177. Lu S, Forcada J (2006) *J Polym Sci A Polym Chem* 44:4187–4203
178. Hong RY, Feng B, Cai X, Liu G, Ding J, Zheng Y, Wei DG (2009) *J Appl Polym Sci* 112:89–98
179. Liu X, Guan Y, Ma Z, Liu H (2004) *Langmuir* 20:10278–10282
180. Csetneki I, Filipcsei G, Zrinyi M (2006) *Macromolecules* 39:1939–1942
181. Wormuth K (2001) *J Colloids Interface Sci* 241:366–377
182. Qiu G, Wang Q, Wang C, Lau W, Guo Y (2007) *Ultrason Sonochem* 14:55–61
183. Teo BM, Chen F, Hatton T, Grieser F, Ashokkumar M (2009) *Langmuir* 25:2593–2595
184. Lu S, Ramos J, Forcada J (2007) *Langmuir* 23:12893–12900
185. Reza F-M, Naser S-S (2007) *J Magn Magn Mater* 311:55–58
186. Charleux B, D'Agosto F, Delaittre G (2010) Preparation of hybrid latex particles and core-shell particles through the use of controlled radical polymerization techniques in aqueous media. *Adv Polym Sci* doi:10.1007/12\_2010\_64. Springer, Heidelberg





# Index

## A

Acetoacetoxyethyl methacrylate (AAEM) 270  
 Acetylacetonatoplatinum(II)-loaded PS 195  
 2-Acrylamido-2-methyl-1-propanesulfonic acid (AMPS) 98  
 11-Acrylamidoundecanoic acid (AAUA) 151  
 Acrylic acid (AA) 44, 65, 163, 188, 222, 265  
 Acrylonitrile–butadiene–styrene 98  
 12-Acryloyloxydodecanoic acid (ADA) 151  
 Activator generated by electron transfer (AGET) technique 131  
 Addition–fragmentation chain transfer polymerization 151  
 Admicellar polymerization 74  
 Ag nanoparticles 84, 110  
 Ag/PS 111  
 AIBN 30, 80, 141, 202, 222, 257  
 Alkyd resin 2  
 Alkylcyanoacrylates (ACA) 202  
 Aluminosilicates 57  
 2-Aminoethanethiol (AET) 271  
 Aminoethyl methacrylate (AEMH) 188  
 Antibodies 223  
 Atom transfer radical polymerization (ATRP) 129, 130, 168  
   surface initiated 172  
 Au-(PS-PEO)<sub>n</sub> nanoparticles 27  
 Avidin–biotin recognition 31  
 Azo dyes 190  
 Azobis[N-(2-carboxyethyl)-2-2-methylpropionamidine] (VA-057) 269  
 Azobis(2-isobutyramidine) (AIBA) 267  
 Azobis(2-isobutyronitrile) (AIBN) 30, 80, 141, 202, 222, 257  
 Azobis(2-methylbutyronitrile) (V-59) 274  
 Azobis(4-cyanopentanoic acid) (ACPA) 222, 274  
 Azobis(4-cyanovaleric acid) (ACVA) 264

## B

Bacteria capture 245  
 Bentonite 97  
 Biotin 31  
 Bis(2-ethylhexoxycarbonyl)ethanesulfonate 220  
 (*cis*-1,2-Bis(2,4,5-trimethyl-3-trienyl)ethane 191  
 Blood–brain barrier (BBB) 193  
 Boron-dipyrromethene (BODIPY) 191  
 2-Bromo-2-methyl propionic acid 137  
 Budding-effect 188  
*N-tert-Butyl-N*-(1-diethyl phosphono-2, 2-dimethylpropyl) nitroxide (SG1) 130  
*N-tert-Butyl-N*-[1-phenyl-2-(methylpropyl)] nitroxide (TIPNO) 130

## C

Cadmium selenide (CdSe) 38, 57, 103, 214  
 Cadmium sulfide (CdS) 57, 108, 110, 213  
 Calcium carbonate 56, 89, 93, 94, 213  
 Capsules 33, 39, 125, 145  
   formation 198  
 CdS 57, 108, 110, 213  
 CdSe 38, 57, 102, 214  
 Chitosan 79, 81  
 Chromium(III) oxide sols 21  
 Cibacron Blue F3G-A 223, 275  
 Clays 15, 53, 141, 218  
 Cloisite 218  
 Cobalt ferrite 74  
 Colloidosome 3, 44  
 Colloids 2, 19, 61  
   metal 109  
 Controlled/living radical polymerization (CRP) 125  
 Core–shell particle/morphology 56, 125, 237

Critical micelle concentration (CMC) 6, 159, 161  
 CS–PMAA magnetic particles 82  
 4-(Cyanopentanoic acid)-4-dithiobenzoate (CPADB) 151

## D

DCTBAB 141  
 Dextran-RAFT 155  
 Diethylacrylamide (DEAAm) 161  
 Diethylaminoethyl methacrylate (DEAEMA) 146  
 N-(2,6-Diisopropylphenyl)perylene-3, 4-dicarbonacidimide (PMI) 188, 274  
 1,2-Dimethyl-1-phenyl-butylamide (DMPBA) 197  
 Dimethylaminoethyl methacrylate (DMAEMA) 84, 135  
 Disperbyk 106 220  
 Dispersion polymerization 125, 237, 260  
 Divinylsulfone 223  
 DLVO theory 21  
 DNA encapsulation 103, 184, 198, 203  
   grafting 29  
   isolation/extraction 225, 244  
   strand recognition 31  
 Dodecylmethacrylate 9  
 Doxorubicin 194  
 Drug delivery 242  
 Dual-marker particles 193  
 DVMAC (didecyl-*p*-vinylbenzylmethylammonium chloride) 214  
 Dyes 188

## E

Emulsion paints 11  
 Emulsion polymerization 1, 5, 53, 125, 133, 237  
 Encapsulation 1, 3, 56  
   direct miniemulsion 220  
   dispersed phase 187  
   DNA 103, 184, 198, 203  
   efficiency 14  
   inorganic particles 10  
   inverse miniemulsion 219  
   pigments 75  
   quantum dots 103  
 Ethylene glycol dimethacrylate (EGDM) 262  
 Europium- $\beta$ -diketonato complexes 188  
 Europium-(2-naphthoyl trifluoroacetone)<sub>3</sub> 188

## F

Ferrofluids 237  
 Fluorescent magnetite colloid particles (FMCPs) 79  
 Free-radical polymerization 128

## G

Galactaric acid 137  
 Gd-diethylenetriamine penta acetic acid (DTPA) 206  
 Gibbsite 142  
 Glycidyl methacrylate (GMA) 260  
 Grafting from 125, 170  
 Grafting to 170, 178

## H

Hemimicelle 13  
 Heteroadagulation 20  
 Heterocoagulation 3, 19, 85, 113  
 Hexamethyltriethylene tetramine (HMTETA) 138  
 12-Hexanoyloxy-9-octadecenoic acid (HOA) 221  
 HHF theory 21  
 Hybrid latex 1, 237  
 Hybrid materials 125, 185  
 Hydrogen bonding 30  
 2-Hydroxyethyl acrylate 173  
 Hydroxyethylmethacrylate (HEMA) 69, 135  
   / acrylic acid (HEMA/AA) 219  
 Hydroxypropyl celluloses (HPCs) 22  
 Hyperthermia 243

## I

Immunoassay 244  
 Initiators, cationic 67  
 Inverse emulsions 15  
 Iron oxides 53, 136, 219, 240, 245  
   nanoparticles 74  
   superparamagnetic 87  
 Iron salts 73  
 Isopar M 205  
 Isophorone diisocyanate (IPDI) 204  
*N*-Isopropylacrylamide (NIPAM) 76

## J

Janus particles/colloids 61

## L

Lanthanide-based dyes 194  
 Laponite 24, 40, 57, 100, 218

Layer-by-layer (LbL) 33, 252  
Lecithin 200  
Lucirin TPO 196  
Ludox silica nanoparticles 69  
LutensolAT50 188, 200

## M

Macroalkoxyamine 165  
Macroinitiators 130, 162, 177, 218  
Maghemite 73, 219, 240  
Magnetic latexes 72, 237, 241  
Magnetic nanoparticles 237  
Magnetic twisting cytometry (MTC) 245  
Magnetite 73, 219, 240  
MeO-PEGMA 147  
3-Mercapto-1-propane sulfonic acid (MPSA) 271  
Mercaptonicotinic acid 223  
Metal oxides 240  
  metals 57  
Metal/polymer hybrid 110  
Metallic latex particles 109  
Metallic particles, encapsulation 109  
Metallic shells 110  
Metals 53, 57, 110  
Methacryloxy propyl methyl dimethoxy silane (MPDMS) 86, 267  
Methacryloxy propyl trimethoxy silane (MPTMS) 59, 201, 267  
2-(Methacryloyl) ethyl 66  
2-(Methacryloyloxy)ethyl trimethylammonium chloride (MAETACl) 173  
Methoxypoly(ethylene glycol) (MePEG) 203  
 $\alpha$ -Methoxy- $\omega$ -hydroxy PEO 159  
Methylenebisacrylamide (MBAAm) 161  
Methylmethacrylate (MMA) 62  
Microemulsion polymerization 5, 9, 272  
Miglyol 812N 203  
Miniemulsion polymerization 1, 80, 125, 132, 185, 272  
Montmorillonite 16, 24, 42, 57, 96, 141, 217  
MRI contrast agents 242

## N

Nanocomposites 1, 19, 56, 185  
Nanoexplosion 198  
Nanogels 125  
Nanomaterials 185  
Nano-onions 194  
Nanoparticles 125, 185  
Nanosynthons 1, 2  
Neobee M5 200

Nitroxide-mediated polymerization (NMP) 129, 162, 177, 216, 245  
Non-oxide semi-conductors 57  
Nucleation 6  
Nucleic acids, magnetic latex 244

## O

Octadecyltrimethoxysilane (ODMS)  
Oleic acid (OA) 65, 137, 224  
Onion-like morphology 143, 194  
Opacity 90  
Organic/inorganic composite colloids 53  
Organic/inorganic hybrid particles 134  
Organoclays 98  
Organotellurium-mediated radical polymerization 162  
Ostwald ripening 9, 103, 186, 272  
OVDAC (octadecyl-*p*-vinylbenzyltrimethylammonium chloride) 214

## P

P(E/B-*b*-EO) 205, 219  
P(MMA-DVB-GMA) 258  
P(NIPAM-*co*-MAA), thermoresponsive 220  
PAA-*b*-PSS 202  
Paclitaxel 203  
Palladium nanoparticles 110, 113, 177  
Particle lithography 44  
Particle morphology 53  
PCDBAB 141  
PEGA200 201  
Pentamethyldiethylenetriamine (PMDETA) 173  
PEO-*block-co*-PMA 256  
PEO-PMAA 219  
Persulfate-derived radicals 7  
Phenyl 2-propyl dithiobenzoate 202  
Phenyl 2-propyl phenyl dithioacetate (PPPDTA) 202  
Photochromes 190  
Photopolymerization 3  
Phthalocyanine dyes 190  
Pickering polymerization 15, 38, 100  
Pickering stabilization 19, 34, 92, 102  
Pigment encapsulation 75  
Pigments 53, 89, 210  
PMMA 22, 62, 200, 223, 274  
PMMA/MMT 97, 101  
PMMA/PMPTMS 62  
PNIPAM 76, 86, 137, 243  
Polyacrylate/silica latexes 70

- Polyacrylic acid (PAA) 255  
 Polyamides 216  
 PolyBA-*b*-polyDMAEA 177  
 Polybutylacrylate (PBA) 202  
 Polybutylene succinimide diethyl triamine (OLOA370) 213  
 Polyethylene (PE) 216  
 PolyHEMA 135, 146  
 Polylactide 146  
 Polylactide-*b*-poly(6-*O*-acryloyl- $\alpha$ -D-galactopyranose) 147  
 Poly-L-lysine 71  
 Polymer latex 19  
 Polymer precipitation, preformed nanodroplets 206  
 Polymer/Laponite 100  
 Polymer-clay nanocomposites (PCNs) 95  
 Polymer-silica nanocomposite 58  
 PolyMMA-*b*-polyBA-*b*-polyMMA 144  
 PolyNAM 155  
 PolyNaSS 137, 162  
 PolyPEGMA 138  
 Polystyrene (PS) 23, 29, 188  
     latex 22, 33, 38, 40, 94, 151, 173, 174  
 Polystyrene-*block*-poly(ethylene oxide) 26  
 Polystyrene-*b*-polyBA-*b*-polystyrene 144  
 Polyurea (PUR) 204  
 Polyurethane (PU) 204, 207  
 Poly(AA-*co*-BA) 138  
 Poly(2-acrylamido-2-methyl-1-propane sulfonic acid) (PAMPS) 255  
 Poly(acrylic acid) (PAA) 135  
 Poly(6-*O*-acryloyl- $\alpha$ -D-galactopyranose) 146  
 Poly(aminoethylmethacrylate) (PAEMA) 216  
 Poly(BA-*co*-AA)/MMT 98  
 Poly(BA-*co*-MMA) 139  
 Poly(BA-*co*-MMA)/MMT 98  
 Poly(BA-*co*-MMA-*co*-MPTMS) 71  
 Poly(butylcyanoacrylate) (PBCA) 193  
 Poly(butylmethacrylate) (PBMA) 24, 197  
 Poly(diallyldimethylammonium chloride) (PDADMAC) 33  
 Poly(2-(diethylamino)ethyl methacrylate) (PDEAEMA) 190  
 Poly[2-(dimethylamino)ethyl methacrylate] (PDMAEMA) 101  
 Poly(divinyl benzene) (PDVB) 79  
 Poly(ethyl acrylate-*co*-ethyleneglycol dimethacrylate-*co*-methacrylic acid) 24  
 Poly(ethylene glycol dimethacrylate-*co*-acrylic acid) 30  
 Poly(ethylene glycol) (PEG) 79, 243  
 Poly(ethylene glycol) monomethacrylate (PEGMA) 44, 64, 134, 138  
 Poly(ethylene oxide) 133  
     macromonomer 64  
 Poly(ethylmethacrylate) (PEMA) 222  
 Poly(glycidyl methacrylate) (PGMA) 255  
 Poly(HEMA-*co*-GMA) 261  
 Poly(HEMA-*co*-MAA) 275  
 Poly(hydroxyethylmethacrylate) (PHEMA) 216, 260  
 Poly(D,L-lactide-*co*-glycolide) (PLGA) 243  
 Poly(L-lysine) (PLL) 222, 225  
 Poly(maleic anhydride-alt-methyl vinyl ether) (PMAMVE) 253  
 Poly(methylmethacrylate) (PMMA) 22, 62, 188  
 Poly(MMA-*co*-BA) 107  
 Poly(MMA-*co*-GMA) 88  
 Poly(MMA-*co*-MAA) 87, 107, 110  
 Poly(MMA-DVBGMA) 273  
 Poly(MMA-EA-NVP) 256  
 Poly(MM-DVB) 275  
 Poly(N,N-dimethylacrylamide) 161  
 Poly(*n*-butyl acrylate) 69  
 Poly(NIPAM-*co*-4VPy) 106  
 Poly(NIPAM-*co*-AA) 106, 110  
 Poly(NIPAM-*co*-GMA) 89  
 Poly(NIPAM-*co*-MBA) 253  
 Poly(N-isopropylacrylamide) (PNIPAM) 76, 86, 137, 243  
 Poly(N-isopropylacrylamide-*co*-acrylamide-*co*-phenyl boronic acid) 108  
 Poly[oligo(ethylene glycol) monomethyl ether methacrylate] (POEOMA) 194  
 Poly(oxyethylene nonylphenylether) (IgepalCO-520) 260  
 Poly(sodium styrene sulfonate) (polyNaSS) 137  
 Poly(St-*co*-DVB-chloromethyl styrene) 276  
 Poly(St-*co*-NIPAM) 253, 262  
 Poly(St-*co*-PEOAM) 262  
 Poly(St-GMA) 262  
 Poly(styrene sulfonic acid) (PSSA) 216  
 Poly(styrene-*co*-BA) 68  
 Poly(styrene-*co*-BA)/MMT 99  
 Poly(styrene-*co*-BA-*co*-AA) 86  
 Poly(styrene-*co*-DMAEMA) 108  
 Poly(styrene-*co*-DVB-*co*-NaSS) 110  
 Poly(styrene-*co*-GMA-IDA) 107  
 Poly[styrene-*co*-(N-isopropylacrylamide)] 86  
 Poly(styrene-*co*-MAA) 109  
 Poly[styrene-*co*-(methacryloyloxyphenyl-dimethylsulfonium methylsulfate)] 26

Poly(styrene-*co*-NIPAM) 86  
 Poly[styrene-*co*-MMA-*co*-sodium styrene sulfonate (NaSS) 75  
 Poly(styrene-*co*-4-vinylbenzyl chloride) 178  
 Poly(styrene-*co*- 4VPy)/Pd 111  
 Poly(VAc-*co*-vinyl alcohol) 150  
 Poly(vinylidene chloride) 24  
 Poly(4-vinylpyridine) [poly(4VPy)] 66, 158  
 Poly(vinylpyrrolidone) (PVP) 72, 213  
 Potassium peroxodisulfate (KPS) 201  
 PS/MMT 97  
 PS/P(DMAEMA-EGMA) 262  
 PS/PGMA core-shell 88  
 PS-*co*-P4VP/silica 215  
 Pt nanoparticles 110, 195  
 Pyrene 83, 188

## Q

Quantum dots (QDs) 53, 56, 213  
   encapsulation 103  
   tagged latex particles 102

## R

Raspberry-like morphologies 7, 23, 30, 39, 63, 67, 77, 214, 270  
 Reverse iodine transfer polymerization 162  
 Reversible addition-fragmentation chain transfer (RAFT) 131  
 Reversible termination 129  
 Reversible transfer 150  
 Rhodamine isothiocyanate (RITC) 194  
 Ricinoleic acid 137

## S

Seeded emulsion polymerization 7  
 Self-assembly 19  
 Silica 53, 214  
   particles 58  
 Silica/PMMA raspberry-like colloids 66  
 Silica/polystyrene 60  
   raspberry-like colloids 64  
 Silicates 218  
 Silver nanoparticles 84, 110  
 Single-wall carbon nanotubes (SWNTs) 211  
 Smith-Ewart nucleation model 6  
 Soap-free latexes 68, 100  
 Sodium 10-mercapto-1-decanesulfonate 150  
 Sodium oleate 86  
 Sodium *p*-styrene sulfonate (NaSS) 75, 86, 104, 109, 268, 275  
 Spirobenzopyran (BTF6) 192

Stöber process 59  
 Styrene 130  
 Styrene/MAA 222  
 Styrene/MMA 98  
 Styrene-*co*-divinylbenzene (St-*co*-DVB) 253  
 Styryl dyes 190  
 Sudan Black B 190  
 Superparamagnetism 73, 84, 219, 240, 242  
 Supracolloidal structures 19  
 Surface modification 53  
 Surfactant bilayer 74  
 Suspension polymerization 257  
 Synthons 2

## T

Tetraethylorthosilicate (TEOS) 59, 216  
 Tetramethylheptandionato lanthanide 194  
 Tetramethylpiperidiny-1-oxyl (TEMPO) 130, 200  
 Titanium dioxide/titania 11, 89, 210  
 Titanium(IV) bis(ammonium lactate) dihydroxide (TALH) 93  
 Trimethyl ammonium chloride (MTC) 66  
 Trioctylphosphine oxide (TOPO) 214

## U

Ureido(tetrahydroimidizalone) 31

## V

Vesicles 3, 15, 145, 165  
 1-Vinyl imidazole (1VID) 66  
 Vinylbenzyl dimethyl dodecyl ammonium chloride (VDAC) 98  
*N*-Vinylcaprolactam (VCL) 88  
 4-Vinylpyridine (4VPy) 66  
 Virus capture 245

## W

Widom-Rowlinson (WR) fluid 37

## Y

Yttrium 113  
 Yttrium hydroxide nanotube 28

## Z

Zinc oxide 57, 93  
 Zirconium 10, 56, 113